PUBLICATIONS of the EARTH PHYSICS BRANCH

volume 41

DEPARTMENT OF ENERGY, MINES AND RESOURCES

OTTAWA, CANADA 1972

TABLE OF CONTENTS
Volume 41

PUBLICATIONS of the EARTH PHYSICS BRANCH

VOLUME 41 – NO. 1

bibliography of fluxgate magnetometers

F. PRIMDAHL

DEPARTMENT OF ENERGY, MINES AND RESOURCES

OTTAWA, CANADA 1970

bibliography of fluxgate magnetometers

F. PRIMDAHL *

The following bibliography lists papers on fluxgate magnetometers and closely related devices, by the name of the first author in the order of the English alphabet. Most of the references include a short description of the contents under the following headings:

1) Type of sensor
2) Theoretical calculations
3) Experimental data
4) Instrument design and description.

The list is not claimed to be complete, but it is believed to cover the major developments in the field from the early 1930s to the present.

Adams, Charles Q. A simple field detector for a dc permeameter. *Rev. Sci Instr.*, 31, pp. 1119-1120, 1960.

1) Two parallel rods.
2) No.
3) Sensitivity 25 μa/moe, range 1 moe – 10 oe.
4) Design data are given for the sensor as well as a simple circuit diagram for the measuring bridge.

Adams, G.D., R.W. Dressel, and F.E. Towsley. A small milligaussmeter. *Rev. Sci. Instr.*, 21, pp. 69-70, 1950.

1) Ring-core with airgap and a single coil.
2) No.
3) Biased and unbiased hysteresis loops are shown together with the corresponding current and voltage waveforms. Calibration curve-sheet for measurements by nulling the field and by using the output voltage directly. Range 10 mgauss to 100 gauss.
4) Design data for the sensor are given and a description of the bridge using a search, and a comparison probe.

Afanas'yev, Yu. V., V.P. Lyulik, and G.D. Alekseyeva. Magnetometric equipment of the Luna-10 and Venera-4 space stations. *Kosmicheskiye Issledovaniya*, 6, pp. 772-781, 1968.

(This paper is quoted in *Foreign Science Bull.*, 5, pp. 84-88, 1969.)

1) Two parallel rods.
2) Short description of the principle.
3) Sensitivity threshold 0.3 γ. Calibration accuracy 0.4 γ. Measuring range ±50 γ. Temperature coefficient less than 0.1 per cent per °C. A graph of the zero offset drift during six days is shown. The zero offset is obtained by comparison with a D-variometer.
4) Detailed descriptions of sensor and electronics are given.

Ageyev, M.V. Approximate theory of magnetically modulated detectors. *Automation and Remote Control*, 17, pp. 827-843, 1956.

1) Two parallel rods.
2) The hysteresis loop is approximated with an average B-H curve and it is shown that the output voltage wave shape is equal to the shape of the derivative $\frac{d\mu}{dt}$, where $\mu = \frac{dB_{eff}}{dH}$ taking the demagnetization into account. B_{eff} is approximated by an arctan curve and from this the output voltage is calculated, the average rectified, and the second harmonic voltage is derived; and formulae for the optimum excitation and for the sensitivity are given. The null output voltage is explained as a "residual transformer" action.
3) From the measured B-H curve is derived $B = \frac{1}{\pi} \times 13000 \arctan 0.42H$ giving optimum sensitivity of 247 mv/oersted for 56.8 ma excitation current; the experimental values were 244 mv/oersted and 55 ma. The sensitivity may be increased by using a certain amount of positive feedback.
4) Design data on the sensor is given together with a description of the electronics.

Aleksanyan, L.M., E.G. Eroshenko, L.N. Zhuzgov, and U.V. Fastovskii. Magnetometric equipment on board the space laboratory "Elektron 2" *Kosmicheskie Issledovaniya,* 4, pp. 302-310, 1966.

*National Research Council postdoctorate fellow, on leave from the Meteorological Institute, Copenhagen, Denmark.

1) Two parallel rods.
2) No.
3) Measuring range ±120 γ for sensitive and ±1200 γ for coarse instrument. Sensitivity without feedback 0.3 – 0.6 v/γ. Measuring threshold 2-3 γ and 20-30 γ respectively. Linearity 2-3 per cent, temp. coeff. 0.2 γ/deg. and 0.7 γ/deg. BW: dc – 0.2 hz and 0.3 hz. Average error on computed total intensity ±2γ and ±20γ respectively. In flight zero corrections 4-12 γ and 35-40 γ (curve sheet). Zero drift per day 2-3 γ (curve sheet).
4) Block diagram and a detailed description of the system is given

Alldredge, L.R. Magnetometer *U.S. Patent, 2,856,581,* Oct. 14, 1958.
1) Tubular ferrite core and ferromagnetic conducting-wire core, both orthogonally gated.
2) A Fourier series describing the output voltage is obtained by assuming the magnetization curve to be a series in odd powers of h, where h is the resultant applied field.
3) No.
4) Detailed descriptions of sensor designs and means of adjustment are given together with a block diagram of a simple magnetometer.

Antranikian, H. Magnetic field direction and intensity finder. *U.S. Patent, 2,047,609,* July 14, 1936.
1) Two rods, parallel or perpendicular to each other, one rod the two halves of which are opposingly magnetized.
2) The operation is explained by assuming that the working point on the common hysteresis curve describing the magnetic state of the two cores splits up into two points when a dc bias field is applied to the sensor.
3) No.
4) Detailed descriptions of the sensors and block diagrams of the electrical circuit is given.

Armstrong, L.D. The use of high permeability materials in magnetometers. *Can. J. Phys.,* 25, *Sec. A,* pp. 124-133, 1947.
1) Two parallel rods.
2) Assuming that the flux variation in a biased transformer contains only fundamental, second harmonic, and third harmonic terms it is shown that the output from the two-core sensor consists of a second harmonic voltage proportional to the bias field. The difference in height of the actual positive and negative output peaks is explained by hysteresis.
3) Waveforms of magnetization circuit core flux, and output voltages are shown. Sensitivity level 10^{-5} gauss.
4) Short description of the sensor design.

Aschenbrenner, H., and G. Gaubau. Eine Anordnung zur Registrierung rascher magnetischer Stoerungen. *Hochfrequenztechnik und Elektroakustik,* 47, pp. 177-181, 1936.
1) Ring-core and two parallel rods.
2) Assuming a magnetization curve of the form $B = a.H - b.H^3$ and a sine wave excitation it is shown that the secondary output is a second harmonic voltage proportional to the applied earth's field.
3) Several recordings with full scale deflection 10γ is shown. The instrument is suited for registration of field variations with periods between 10 min and 1/20 sec. Noise level and reproductibility 1/3 γ.
4) Description of the ring-core sensor and field-gathering devices is given together with electronic circuit diagrams and operation principles of the oscillator and the second harmonic tuned amplifier.

Bailey, Ralph. Canadian aerial magnetic surveys (M.A.D.). *Can. J. Res.,* 26, *Sec. F,* pp. 523-539, 1949.
Description of Canadian use of essentially the same instrument as described by J.R. Balsley.

Balsley, James R. Aeromagnetic surveying. *Advances in Geophysics,* 1, edited by H.E. Landsberg, pp. 313-349, Academic Press, New York, 1952.
1) Single rod and two parallel rods.
2) Short explanation of the principle.
3) No.
4) Block diagrams of second harmonic and of "all even harmonics" magnetometers.

Beck, F.J., and J.M. Kelly. Magnetization in perpendicularly superposed direct and alternating fields. *J. Appl. Phys.,* 19, pp. 551-562, 1948.
For long cylindrical specimens curves are measured of the longitudinal magnetic induction for a steady longitudinal magnetic field vs. transverse magnetic induction from an alternating current through the cylinder.

Bendix Aviation Corporation. Electromagnetic induction device. *British Pat., 592,394,* Sept . 17, 1947.
1) Single rod, two parallel rods, three rods in a triangle, six rods in a star, combination of three orthogonally positioned two-rod sensors.
2) The principle of even harmonics generation in a biased core is explained, and it is claimed that the linearity of the device is poor because of the highly nonlinear B-H curve. However, an improvement is suggested by using a two-rod open core to linearize the B-H curve.
3) Detailed investigations of the magnetic materials and calculations of the expected linearity has been carried out.
4) Detailed descriptions of sensor designs.

Bershtein, I.L. A new type of magnetometer. *Izv. Akademii Nauk, Phys. Series,* 8. No. 4, pp. 189-193, 1944.
Based on the findings by Gorelik *et al.* the author has developed a magnetometer using an orthogonally gated sensor.

Blackett, P.M.S. On a negative experiment relating to magnetism and the earth's rotation. *Phil. Trans. Roy. Soc.*, A **245**, pp. 309-370, 1952.
1) Two parallel rods.
2) No.
3) Noise level 0.1 γ; compensates earth's field to within 0.2γ.
4) No.

Brandstaetter, F. Entwicklung und Anwendung einer magnetischen Feldmessonde zur Untersuchung von Ferromagnetika. *Oesterreichisches Ingenieurarkiv,* **6**, pp. 20-30, 1951, Vienna.
1) Two parallel rods.
2) The operation is explained by the superposition of two biased hysteresis-loops.
3) Several graphs of output voltage vs. ambient field is given with excitation current as a parameter. Range ±80 moe.
4) Design data are given for the sensor as well as for the electronic circuits.

Buckley, O.E. Detection of large magnetic bodies. *U.S. Patent, 2,415,808,* Feb. 18, 1947.
1) Two parallel rods.
2) No.
3) No.
4) Description of the sensor and of the electronics.

Carden, R., *et al.* Final engineering report. Prototype surveyor fluxgate magnetometer, Model ML 125-1. *JPL Contract 950156, ML/TN-2000.70,* Marshall Laboratories, 3530 Torrance Boulevard, Torrance, Calif., U.S.A., 14 June 1962. Clearinghouse Accession No. N65-17213, NASA CR 60762.
1) Two parallel rods.
2) No.
3) Sensitivity 10 μV/γ. 0.25 γ offset after exposure to ±1 oersted. Stability within ± 2γ 25°F to 125°F.
4) Detailed description and circuit diagrams of the magnetometer is given.

Chapman, S. and J. Bartels. Magnetic observations. *Geomagnetism,* **1**, Chap. II, 11, pp. 59-60, Clarendon Press, Oxford, 1940. Quotation of Aschenbrenner's and Goubau's paper. *Hochfrequenztechnik,* **47**, 1936.

Coleman, Paul J. Jr. An analysis of the operation of the fluxgate magnetometer. *Space Technology Laboratories,* Los Angeles 45, Calif., U.S.A., Report No. 7320.2-14, June 20, 1959.
1) Single rod.
2) Using a simplified, parallelogram-shaped, two-zone magnetization curve as a transfer function for the sine wave excitation current the author develops the Fourier series for the distorted output wave, and shows that the second harmonic component depends in amplitude on the ambient DC-field H, the permeability μ, the saturation field H_s, the maximum excitation field H_o, the half-width of the hysteresis loop δ, and on the frequency f. The phase of the second harmonic component depends on H_s, H_o, and δ. A change in H_s or in the shape of the hysteresis curve because of temperature is thus expected to change the phase of the second harmonic.
3) No.
4) No.

Dolginov, S. Sh., L.N. Zhuzgov, and V.A. Selyutin. Magnetometers in the third Soviet earth satellite. *Artificial Earth Satellites,* **2**, pp. 358-396, Plenum Press, New York, 1961.
1) Two parallel rods.
2) The directional sensitivity of the sensor is explained by the difference in demagnetization factors along and perpendicular to the core axis.
3) Mean zero deviation 10 γ /day. Temperature coeff. 2-6 γ/deg.
4) Design data are given for the sensor as well as a complete description of the electronic circuits.

Drozhzhina, V.I., *et al.* The theory of ferro-probes with longitudinal symmetrical excitation. *Fiz. metal. Metalloved.,* **10**, pp. 359-366, 1960. (English translation in *Physics of Metals and Metallography,* **10**, pp. 45-52, 1960.)
If the core is not driven well into the saturation regions by the excitation field it is shown that the superposition of a dc field $H\rho$ on the excitation field causes the working point to follow a minor hysteresis loop slightly different from the loop followed when $H\rho = 0$.
Crossing the apex of the minor hysteresis loop, biased or unbiased, the differential permeability goes through a discontinuity.

Fearon, R.E. Magnetic gradient measurement. *U.S. Patent, 2,520,677,* Aug. 29, 1950.
1) Two parallel rods.
2) The principle of using two different excitation frequencies F_1 and F_2 is explained. One of the modulation products, e.g. $F_1 - F_2$, is used to detect the magnetic field.
3) An accuracy of 0.1 γ is reported.
4) The sensor and the electronical circuits are described.

Felch, E.P., *et al.* Airborne magnetometers for search and survey. *AIEE Trans.,* **66**, pp. 641-651, 1947.

1) Single rod.
2) Neglecting hysteresis by taking a magnetization curve of the form $B = b_1 h + b_3 h^3 + b_5 h^5 + \ldots$ and substituting for h by $H_o \cos pt + H$ where H_o is the max. excitation field and H is the earth's field, the author develops a Fourier series representing the output voltage, where the coefficients to even multiples of pt are odd functions of H. Using a simplified two-zone B-H curve the sensitivity is obtained. A better approximation to the B-H curve, $B = \tan^{-1}(h/a)$, is reported to yield results not much different, and an analysis based on a double characteristic to account for the hysteresis is reported not to affect the foregoing results.
3) Magnetization curve and sensitivity vs. excitation level is shown. Sensitivity 10 $\mu v/\gamma$. Noise 0.25 γ.
4) Design data are given for the sensor as well as block diagrams for the electronics.

——— and J.L. Potter. Preliminary development of a magnettor current standard. *AIEE Trans.*, 72 Part 1, pp. 525-531, 1953.
The field from a permanent magnet is cancelled by a constant-current-carrying solenoid using a fluxgate sensor as null-field detector.
The residual second harmonic output in null field is reported to be in quadrature (cosine component) to the field-generated second harmonic (sine component). The quadrature output is dependent on the degree of inhomogeneity of the permanent magnet field.
A stability of ±0.01 per cent for a few days was obtained in constant temperature and for a 30°C temperature change the stability was ±0.05 per cent.

Foerster, F. Ein Messgeraet zur schnellen Bestimmung magnetischer Groessen. *Z. Metallkde,* 32, pp. 184-190, 1940.
This paper describes an instrument developed by the author to investigate magnetic properties of iron samples. The principle used here is very close to the fluxgate principle; but it was only later (autumn 1941) that the modified instrument was used to measure magnetic fields (see F. Foerster, *Z. Metallkde,* 46, pp. 358-370, 1955).

——— Ein Betriebsgeraet zur schnellen und genauen Messung der Koerzitivkraft sowie ihrer Temperaturabhaengigkeit. *Z. Metallkde.,* 46, pp. 297-302, 1955.
Description of the use of fluxgates for measuring the coercive force of small samples.

——— Ein verfahren zur Messung von magnetischen Gleichfeldern und Gleichfelddifferenzen und seine Anwendung in der Metallforschung und Technik. *Z. Metallkde,* 46, pp. 358-370, 1955.
1) Two parallel rods.
2) The operation is explained by the superposition of two biased hysteresis loops. Using a B-H curve made of three straight lines joined by a quarter of a sine wave the author calculates the second harmonic output voltage.
3) Biased and unbiased hysteresis loops are shown.
4) Short descriptions of the sensor and a block diagram of the electronics are given.

Frei, E.H., S. Shtrikman, and D. Treves. A transducer using crossed magnetic fields. *Bulletin of the Research Council of Israel,* 3, pp. 443-444, 1953,
1) Tubular, orthogonally gated sensor.
2) No.
3) No.
4) Short description suggesting the use of the principle as a magnetometer.

Fromm, W.E. The magnetic airborne detector. *Advances in Electronics,* 4, pp. 257-299, 1952.
1) Single rod, two parallel rods, ring-core.
2) Qualitative explanation of the principle.
3) No.
4) Descriptions of sensors and of the electronics are given. The paper is primarily intended as an introduction, and a survey over the subject.

Gans, F. Fonctionnement et applications des sondes électromagnétiques. *La Recherche Aéronautique,* 1, pp. 29-39, 1948.
1) Single rod and two parallel rods.
2) The appearance of second harmonic voltages by applying a dc-field is explained by Fourier analysis using the general properties of B-H curves.
3) Spectral distribution of the harmonics of the output voltage from a single rod sensor is shown.
4) A number of theoretical and practical considerations valuable for the sensor design are given.

Gebhardt, R.E. An induction magnetometer, constructions and tests. *Trans. Am. Geophys. Union,* 27, pp. 53-58, 1946.
1) Four parallel rods. The DC excitation current is chopped manually by a snap-switch.
2) No.
3) Mounted on a theodolite for use as an absolute magnetometer, the instrument has a deviation of $+3\gamma$ to -6γ in H and $+9\gamma$ to $+1\gamma$ in Z.
4) Design data are given for the sensor and for the electrical circuit.

Gerard, V.B. A simple, sensitive, saturated-core recording magnetometer. *J. Sci. Instr.,* 32, pp. 164-166, 1955.
1) Two parallel rods.
2) No.
3) Recording shown together with observatory magnetogram. Frequency response 0-20 hz. Max. sensitivity at output 4 γ per ma.

4) Design data of sensor is given. Very detailed description is given of the electronic circuit together with filter frequence response curve and circuit diagrams.

Germain-Jones, D.T. Post-war developments in geophysical instrumentation for oil prospecting. *J. Sci. Instr.*, 34, pp. 1-3, 1957.
1) Two parallel rods.
2) No.
3) Graphs of hysteresis curve and sensor output voltages shown.
4) Simple sketch of sensor is given.

Geyger, W.A. Self-balancing fluxgate magnetometers, *AIEE Trans.*, 77, pp. 213-216, 1958.
1) Two parallel rods and closed core sensor.
2) The principle is explained and the similarity to magnetic amplifiers is emphasized.
3) Linearity error of the order of 0.1 per cent.
4) The principle of the sensor is shown and a magnetometer is constructed using only ring-core magnetic amplifier circuits for amplification, frequency doubling, and signal detection.

———The ring-core magnetometer, a new type of second-harmonic fluxgate magnetometer. *AIEE Trans.*, 81, pp. 65-73, 1962.
1) Ring-core.
2) The principle is explained and the similarity to magnetic modulators is emphasized.
3) Oscillograms of excitation current and sensor output voltages are shown. Sensor output current vs. direction of magnetic axis with respect to the applied field is shown. Sensitivity 1 volt per oersted.
4) Design data are given for the sensor as well as simple diagrams of the electronic circuit.

———New type of fluxgate magnetometer. *J. Appl. Phys.*, suppl. to 33, pp. 1280-1281, 1962.
1) Ring-core.
2) A simple explanation of the principle is given.
3) Sensitivity 1 volt per oersted.
4) Design data are given for the sensor together with a simple magnetometer circuit.

———Fluxgate magnetometer uses toroidal core. *Electronics*, 35, pp. 48-52, 1962.
1) Ring-core.
2) A simple explanation of the principle is given.
3) Sensitivity 1 volt per oersted.
4) Design data are given for the sensor together with several simple magnetometer circuits.

Gold, T. Manual for fluxgate ferrite magnetometer. *Report No. CRSR 172,* Center for Radiophysics and Space Research, Cornell Univ., Ithaca, New York, June 1964, Clearinghouse Accession No. N64-28989, NASA CR 58342.
1) Tubular ferrite core. Orthogonally gated.
2) Discussion of design aspects.
3) Typically 40γ offset for 1 per cent sec. harm. in excitation. Sec. harm. of less than 0.01 per cent necessary if drift below 0.4γ is wanted.
4) Sensor and electronics are described.

———Four ferrite core magnetometers. *Final Status Report to NASA, NASA Contract NASr-46,* October 1, 1963 through May 15, 1964, Center for Radiophysics and Space Research, Cornell Univ., Ithaca, New York, Report No. CRSR174, NASA CR 58344, Clearinghouse Accession No. N64-28991.
1) Tubular ferrite core orthogonal sensor.
2) No.
3) Drift and noise within ±0.3γ. Power consumption 0.6–0.9 watts.
4) No.

Gordon, D.I., R.H. Lundsten and R.A. Chiarodo. Factors affecting the sensitivity of gamma-level ring-core magnetometers. *IEEE Trans., Mag.-1*, pp. 330-337, 1965, and *ibid, Mag.*-2, pp. 773-774, 1966
1) Ring-core.
2) Using a simplified, two-zone, parallelogram-shaped magnetization curve the authors derive the transfer function – i.e. induction in the secondary winding vs. excitation field – and use this to obtain the output voltage for constant-current and constant-voltage excitation. The attenuation of the input signal because of demagnetization is emphasized.
3) Experimental curves are given showing sensitivity vs. area and vs. effective length-to-diameter ratio of the cores, and compared to calculated curves. Additionally are given curves of sensitivity vs. dc initial permeability and vs. ac differential permeability.
4) A few design data are given together with suggestions of improvements.

——— **and H.H. Helms.** A fluxgate sensor of high stability for low field magnetometry. *IEEE Trans. Mag.-4,* pp. 397-401, 1968.
1) Ring-core.
2) No.
3) Stability performance curves are given showing zero-offset vs. time under temperature changes. Offset fluctuations ±0.10 γ in 24 hours at constant temperature and noise 0.10 to 0.20 γ p-p, dc to 10 hz. Difference between offsets at 60°C and −30°C is 0.35γ.
4) Descriptions and design data are given for the sensor.

Gorelik, G., X. Goronina, and I. Joukova. Sur les courbes d'aimantation longitudinale d'un fil ferromagnétique par-

couru par un courant continu. *Comptes Rendus (Doklady) de l'Académie des Sciences de l'URSS*, **44**, pp. 235-237, 1944.

The longitudinal permeability of a ferromagnetic wire carrying a dc current is investigated. When the longitudinal field Hx is small, the corresponding longitudinal induction Bx is expressed by the saturation induction Bs for the material and by Hy the transverse induction in the wire from the dc current,

$$\mu_x = \frac{Bx}{Hx} = \frac{Bs}{Hy} \text{ (Hy > Hs >> Hx).}$$

Graham, R.L., and J.S. Geiger. The application of a fluxgate magnetometer to an automatic electronic degaussing system. *Can. J. Phys.*, **39**, pp. 1357-1368, 1961.

1) Two parallel rods.
2) No.
3) Less than 0.2 per cent harmonic distortion in drive oscillator. Less than 10^{-4} gauss long-term drift. Zero error 5.10^{-5} gauss.
4) Electronic circuit diagrams are given together with a detailed discussion of the possible sources of zero drift and errors.

Greiner, J. Feldmessungen nach dem Oberwellenverfahren, Theoretische Betrachtungen. *Nachrichtentechnik*, **9**, pp. 173-180, 1959.

——— Feldmessungen nach dem Oberwellenverfahren, Methodische Untersuchungen. *Nachrichtentechnik*, **10**, pp. 123-126, 1960.

——— Feldmessungen nach dem Oberwellenverfahren, Sieb- und Differenzsonden. *Nachrichtentechnik*, **10**, pp. 156-162, 1960.

——— Feldmessungen nach dem Oberwellenverfahren, Winkelsonden. *Nachrichtentechnik*, **10**, pp. 495-498, 1960.

1) Single rod, double rod, and ring-core sensors (parallel gated). Wire, tubular, and plate sensors (orthogonally gated).
2) A qualitative explanation is given based on a two-zone B-H curve and a triangular excitation wave. Quantitative calculations are carried out assuming an arctan shaped B-H curve and a sine wave excitation. The theoretical curves of second harmonic output vs. excitation level are given for parallel as well as for orthogonal gating and it is concluded that there is no significant difference in performance of the various types of sensors.
3) Experimental curves of sensitivity vs. excitation level and vs. excitation frequency as well as of other investigations are given for the six different types of sensors. Mumetal and ferrite is used as core material.
4) Detailed descriptions of the various types of sensors are given.

Hancock, J.D. Engineering report on the evaluation of DLK 101A1 fluxgate magnetometer sensor. *Honeywell*, Boston, Mass., USA, Sept. 9, 1964.

1) No.
2) No.
3) Sensitivity: 15 $\mu v/\gamma$. Drift: ±0.5 γ over 24 hours. Minimum second harmonic output less than 2 γ. Temperature drift 0.18 γ per degree Celcius. Noise less than 0.6 γ p-p for 0.01 hz to 10 hz. Curve sheets are shown from which the quoted and other data are derived.
4) Block diagrams of the test setups are shown.

Hess, H. Aufbau und Theorie eines Geraetes zur Messung der Magnetischen Horizontal-feldstaerke auf See mit der Foerster-sonde. *Deutschen Hydrographischen Zeitschrift*, **16**, pp. 15-43, 1963.

1) Two parallel rods.
2) Short description based on the superposition of two biased two-zone B-H curves.
3) No.
4) Sketch of sensor and a block diagram of the electronics are given.

Hine, A., and H.L. Hitchins. Apparatus for measuring and detecting magnetic fields. *Brit. Patent, 619,525*, March 10, 1949.

1) Two parallel rods.
2) The sensor is modulated by a low frequency alternating field superposed on the dc field to be measured. The demodulated output voltage contains a fundamental component of the modulation frequency proportional to the dc field.
3) No.
4) Block diagrams of the electronical circuits are given.

——— *Magnetic Compasses and Magnetometers*, pp. 47-72, 77, 143-154, 304-316, and 375-388, University of Toronto Press, Toronto, 1968.

This book is a basic source of information on magnetometers. Nearly all types of sensors are treated theoretically, and examples of practical magnetometer circuits are given covering among others peak-detector, second harmonic, and high frequency modulated systems.

Hood, P., and S.H. Ward. Airborne geophysical methods. *Advances in Geophysics*, **13**, pp. 1-41, 1969.

A survey of some Russian, Canadian and American airborne fluxgate magnetometers is given.

Hull, A.W. Magnetic field gradient meter. *U.S. Patent, 2,379,716*, July 3, 1945.

1) Two parallel rods with field gathering devices.
2) Short description of the principle. The unbalance between the two inductors is detected by means of a

nonlinear resistor. ("peak detector" or "fundamental reference" system.)

3) No.
4) Drawing of the sensor and of the electrical circuit is given.

Johnes, J.H. A proposed method of measuring the derivatives of the earth's magnetic field. *Geophysics*, 8, pp. 23-31, 1943.

1) Two parallel rods.
2) Using a sine wave excitation field the core flux vs. time is expressed as a Fourier series and for reasons of symmetry only odd harmonics are generated even when hysteresis is taken into consideration. A small dc field superposed on the excitation is shown to generate even harmonics, and assuming a third degree polynomial approximation to the B-H curve it is estimated that the instrument should be able to detect a field difference of 10^{-7} oersteds.
3) No.
4) Block diagram of the sensor and of the associated electronical equipment is given.

Joukova, I.S. About the EMF-spectrum of transverse induction. *Doklady Akademii Nauk SSSR*, 65, pp. 151-154, 1949.

A ferromagnetic, ac-current-carrying wire surrounded by an axial solenoid is magnetized along the axis by a small dc field Hx. The axial induction Bx is shown to be a dual series in powers of Hx, of the transverse ac-field Hy, and of the stress σ, (established by twisting one end of the wire with respect to the other). The voltage induced in the axial solenoid contains even harmonics proportional to $Hx(1 + a\sigma^2)$ and odd harmonics proportional to $\sigma(1 + bH_x^2)$, where a and b are constants. The results are verified experimentally.

Kato, Y., Z. Abe, and A. Sakurai. The visual magnetic variometer (Tohoku University type) used for the measurement of the effect of 20 June 1955. *Science Reports of the Tohoku Univ., Ser. V, Geophysics, Vol. 7, Suppl.* March 1956, pp. 15-20, Faculty of Science, Tohoku Univ.

1) Two parallel rods.
2) Based on a simplified two-zone B-H curve it is shown that the integrated output from the sensor contains positive and negative pulses of different amplitude with the difference proportional to the applied dc-field.
3) Drift ±1 γ per several days. Noise about 1 γ. Temperature dependency within ±1 γ from 20°C to 40°C. Response time 3 sec. per 10 γ.
4) Design data are given for the sensor together with a block diagram of the electronics.

Kerbnikov, F.I., and M.A. Rozenblat. Magnetic modulators with perpendicularly superposed magnetic fields. *Avtomat. i Telemekh.*, 19, pp. 836-848, 1958. (English translation in *Automation and Remote Control*.)

The principle of orthogonal gating, here used in magnetic modulators, is described theoretically using an arctan shaped B-H curve and the results are shown to fit the experimental data well.

Kerwin, W.J., R.M. Munoz, and M.J. Prucha. An improved magnetometer for deep space use. *IEEE/AIAA National Aerospace Electronics Conf.*, solar wind measurement techniques, Part 1, pp. 73-81, Dayton, Ohio, 1964.

1) Ring-core modified to an elongated toroid.
2) No.
3) Several high sensitivity recordings are shown from which the following data are derived. Noise 0.1 γ p-p, 1 hz BW. Offset after exposure to 2 gauss is less than 0.1 γ. Offset caused by second harmonic content in excitation is less than 0.05 γ.
4) Circuit diagrams and a detailed description of the electronics is given.

Kobayashi, R., *et al.* Mariner A fluxgate magnetometer. Final Engineering Report, Model ML 100-1, *JPL contract 950036, ML/TN-2000.43*, 22 February 1962, Marshall Laboratories, 3530 Torrance Blvd., Torrance, Calif., U.S.A., Clearinghouse Accession No. N65-18096, NASA CR 57081.

1) Two parallel rods.
2) Short description of principle.
3) Sensitivity 10μV/γ.
4) Extensive description of circuits and performance tests are given.

——— and D. Sassa. Mariner R fluxgate magnetometer. Final Engineering Report, *JPL contract 950185, ML/TN 2000.47*, 16 March 1962, Marshall Laboratories, 3530 Torrance Blvd., Torrance, Calif., U.S.A., Clearinghouse Accession No. N65-18099, NASA CR 57080.

The report contains detailed technical discussions related to electrical design, test, and calibration process. Sensor analysis (based on a two-zone B-H curve) is presented in an appendix.

Krumhansl, J.A., and R.T. Beyer. Barkhausen noise and magnetic amplifiers. I. Theory of magnetic amplifiers, II. Analysis of the noise. *J. Appl. Phys.*, 20, pp. 432-436, and pp. 582-586, 1949.

It is shown analytically that a magnetic amplifier becomes unstable if the secondary is tuned to an even harmonic and the damping is sufficiently low. The behaviour in the vicinity of the harmonic is analogous to a voltage generator supplying the open-circuit output voltage to a four terminal network whose transfer characteristic is similar to that of a tuned L-C circuit except for an additional negative term in the denominator.

Kuehne, R. Magnetfeldmessung mit Eisenkern-Magnetometer nach dem Oberwellenverfahren. *Archiv fuer Technisches Messen, V 392-1,* pp. 175-178, 1952.

1) Single rod, two parallel rods.
2) The second harmonic output voltage vs. excitation level is derived from a simplified two-zone B-H curve.
3) Second harmonic output voltage vs. dc-field is shown for large fields and for very small fields. Sensor sensitivity 1 mv/moe.
4) Design data for the sensor is given together with a block diagram of the electronic circuit.

La Pierre, C.W. Direct current indicator. *U.S. Patent, 2,053,154,* Sept. 1, 1936.

1) Rectangular closed core with field gathering devices.
2) Superposition of any dc flux on the core makes the output wave unsymmetrical and introduces even harmonics.
3) No.
4) Many types of second harmonic fluxmeters with closed core is shown intended for magnetic field measurement or dc current measurement.

Lauche, Hans. Entwicklung einer Apparatur zur digitalen Registrierung erdmagnetischer Variationen. *Diplomarbeit, Institut für Geophysik und Meteorologie der Technischen Hochschule,* Braunschweig, 1967.

A digital feedback system for a fluxgate magnetometer is described.

Lawrence, L.G. Elektronik fuer die Geophysik. *Elektronik, Heft 11,* 5 Messtechnik, Messung nichtelektrischer Groessen, pp. 323-327, 1964.

1) Rectangular closed core, T-shaped core.
2) No.
3) No.
4) Electronic circuit diagrams of a magnetometer with T-sensor is shown together with a block diagram of the general principle.

Ledley, B.G. Magnetometers for space measurements over a wide range of field intensities. *Proc. of the URSI Conf. on Weak Magnetic Fields of Interest in Geophysics and Space,* May 1969, Paris.

A review is given on recent development work on a satellite fluxgate magnetometer. The design goal is to measure field components of up to 60,000 γ in a temperature range of $-150°C$ to $+50°C$ with an accuracy of 0.01 per cent. A highly stable current source has been developed and a pair of coaxial bucking coils with ceramic structure has been constructed to give less gradients over the sensor and less disturbance on the environment.

Ling, S.C. A fluxgate magnetometer for space application. *AIAA Summer Meeting,* Paper No. 63-187, June 27, 1963.

1) Tubular ferrite sensor, orthogonally gated.
2) By expressing the hysteresis loop as a bi-valued function it is shown that the second harmonic output is a linear function of the ambient dc-field. Any stress in the core material will, together with a second harmonic content in the excitation, give a 'false' second harmonic output. Other aspects of the sensor design are treated theoretically as well.
3) The waveforms of excitation field and induction are shown together with apparent permeability and damped output voltage. The axial apparent permeability vs. excitation field strength is shown and compared to the theoretically derived expressions.
4) Detailed sensor design data and electronic circuit diagrams are given.

——— Improved magnetometer uses toroidal gating coil. *NASA Tech. Brief, 65-10103,* Goddard Space Flight Center, GSFC – 249, 1965.

1) Tubular sensor, orthogonally gated.
2) No.
3) Detecting level about 0.1 γ. Sensor sensitivity when tuned to second harmonic is 1 mV/γ.
4) A multitude of suggestions to improve the sensor design is given together with detailed descriptions of an actual sensor.

Linlor, W.I., R.M. Munoz, and M.J. Prucha. Stability measurements of fluxgate magnetometers. *Space Magnetic Exploration and Technology, Symp.,* pp. 198-234, University of Nevada, Reno, 1967.

1) Flattened ring-core and ring-core.
2) No.
3) Sensitivity 25 $\mu v/\gamma$. Oscillograms of excitation voltage and current, of induced voltage waveform in the core, and of total null output are shown. Total null output 0.3 volt p-p. Second harmonic feed through is less than 1 γ equivalent with 2.5×10^{-4} sec. harmonic in the excitation. Noise is less than 0.3 γ p-p dc to 10 hz measured for 1 minute. The effect of stress in the core material is investigated. A number of graphs of the offset vs. time under temperature changes are shown. Offsets are from 0.4 γ (18°C to 44°C) to 1.6 γ (−6°C to 20°C).
4) Detailed description of the sensor and a block diagram of the electronics is given.

Lokken, J.E. Instrumentation for receiving electromagnetic noise below 3,000 cps. *Natural Electromagnetic Phenomena below 30 kc/s,* Editor D.F. Bleil, pp. 373-429, Plenum Press, 1964.

A survey of fluxgate magnetometers is given. The operation principle is explained by assuming an odd power series approximation to the B-H curve. Examples of a single rod, two parallel rods, and ring-core sensors are given with block diagrams and detailed descriptions of the electronics. Peak voltage, second harmonic, and saturation time difference systems are described.

Lutz, H. Magnetfeldmessung mit Foerstersonden und Hallgeneratoren. *Elektronik,* 17, pp. 247-250, 1968.
1) Two parallel rods.
2) Short description of the principle based on a simplified two-zone B-H curve.
3) Sensor noise is typically 0.1 γ for 2-20 hz BW. Offset after exposure to 1 oersted is from 0.1 γ to 0.5 γ. Sensor second harmonic null in zero field is 5 to 50 γ equivalent. The temperature coefficient of this offset is about 0.1 γ/°C.
4) Short description of the sensor and a block diagram of the magnetometer is given.

MacNichol, E.F. Jr., *et al.* Servo system employing direct current resolvers. *U.S. Patent, 2,697,808,* Dec. 21, 1954.
1) Two parallel rods.
2) Short description of the principle.
3) No.
4) Detailed description of the sensor with and without feedback, and of the electronics is given.

Mager, A. Ueber ein empfindliches Magnetsfeldmessgeraet nach dem Oberwellenverfahren, *Experim. Techn. Physik,* 1, pp. 109-120, 1953.
1) Ring-core, two parallel rods.
2) Qualitative explanation of the principle based on a two-zone B-H curve, and calculation of the sensitivity vs. excitation level based on an arctan shaped B-H curve.
3) Sensitivity level about 10^{-5} oersted.
4) Design data are given for the sensor as well as a complete circuit diagram for the magnetometer.

Marshall, S.V. An analysis of the ring-core fluxgate. *Proc. Nat'l. Electronics Conf.,* 22, pp. 133-138, 1966.
1) Ring-core.
2) For "constant voltage" excitation is shown that the instantaneous output voltage is proportional to the second derivative of the magnetization curve.
3) The apparent permeability of various ring cores is plotted vs. a normalized geometrical ratio and an empirical formula is given. Oscilloscope photographs of input and output waveforms are shown, together with an experimentally derived curve of the incremental permeability $\Delta B/\Delta H$ vs. dc-bias field.
4) Design data for the ring-core are given.

———An analysis of the fluxgate magnetometer. *U. of Missouri, Columbia,* Ph.D. thesis, 1967, Avail.: University Microfilms, Clearinghouse Accession No. N68-36303.

———An analytic model for the fluxgate magnetometer. *IEEE Trans., Mag-3,* pp. 459-463, 1967.
1) Single rod, two parallel rods, ring-core, and tubular sensor.
2) The even harmonic output from the single rod, the double rod, and the ring-core sensors is shown to be proportional to the second derivative of the B-H curve. For the orthogonally gated tubular sensor it is claimed that the permeabilities orthogonal and parallel to the gating field are equal and thus the same expression as above is valid for the output voltage. However, this is, not in accordance with earlier works (J. Greiner, T.M. Palmer, S.C. Ling).
3) Oscilloscope pictures are shown of output voltage vs. excitation field together with excitation and output voltages for square wave excitation and ramp excitation. An empirical formula for the output voltage vs. excitation field is derived.
4) The construction principle of the various sensors is shown.

Maxwell, A. III – Electronic recording of the transient variations in the earth's magnetic field. *Ann. IGY,* 4, pp. 281-286, 1957.
1) Two parallel rods.
2) Short description of the principle.
3) Range ± 500 γ, noise 0.1 γ dc 1 hz.
4) Block diagram of the electronics is given.

McCurley, E.P., and C. Blake. Simple null indicating saturable core magnetometer for the detection of static magnetic fields. *Rev. Sci. Instr.,* 31, pp. 440-443, 1960.
1) Single rod.
2) Short description of the principle.
3) Second harmonic content in the excitation is 73 dB below the fundamental. Changes in ambient field of less than 0.1 m oersted is readily observed.
4) Design data of the sensor is given together with a detailed description of the electronics.

McNish, A.G. An induction magnetometer. Principle of operation. *Trans. Am. Geophys. Union,* 27, pp. 49-51, 1946.
1) One long permalloy wire, the two halves of which are magnetized opposingly by the excitation current.
2) The dc-excitation current is chopped manually by a snap-switch and the output pulses are explained by superposing two biased hysteresis loops.
3) No.
4) Block diagram is given of the instrument, which involves no electronics.

Mee, C.D., and R. Street. An improved precision permeameter. *Proc. Instn. Electrical Engrs.,* 101, Part 2, pp. 639-642, 1954.
1) Two parallel rods.

2) No.
3) Noise and stray fields 0.3×10^{-3} oersted.
4) Design data of the sensor is given together with a block diagram of the electronics.

Meek, J.H., and F.S. Hector. A recording magnetic variometer. *Can. J. Phys.*, 33, pp. 364-368, 1955.
1) Two parallel rods.
2) No.
3) Noise level less than 0.5 γ. Range 1000 γ. Drift because of nulling field less than 10 γ in 24 hours. Temperature drift less than 10 γ for 5°F.
4) Detailed description of the sensor and of the electronics.

Meyer, O., and D. Voppel. Ein Theodolit zur Messung des erdmagnetischen Feldes mit der Foerstersonde als Nullfeldindikator. *Deutschen Hydrographischen Z.*, 7, pp. 73-77, 1954.
1) Two parallel rods.
2) No.
3) An accuracy of ±0.5′ in D, ±0.2′ in I, and ±1.7 γ in H is obtained.
4) Description of the mounting of the sensor on the theodolite and of the measuring procedure is given.

Mikhailovskii, V.N., and Iu. I. Spektor. Certain problems in the theory of magnetic amplifiers and magneto-modulation probes of the "second harmonic" type. *Automation and Remote Control*, 18, No. 8, pp. 771-777, 1957.
1) Two parallel rods.
2) Based on a parallelogram-shaped hysteresis loop it is shown that the second harmonic output voltage has a quadrature (cosine) component besides the sine component, both dependent on the dc-bias field. The cosine component is proportional to the area of the hysteresis loop. If the field to be measured or the compensation field is inhomogeneous it is shown that simultaneous cancellation of both sine and cosine component is not possible, thus explaining the observed residual quadrature second harmonic output voltage.
3) Measurements of the second harmonic output voltage and phase angle vs. bias field with excitation level as a parameter is shown to fit the theoretical curves well.
4) Description of the sensor is given together with a block diagram of the electronics.

Mocheshnikov, N.I., V.F. Ivanov, and V.V. Petrenko. Adjusting double frequency saturated magnetic probes. *Pribory i Tekhnika Eksperimenta*, 4, pp. 147-148, 1960. (English translation in *Instrum. Exper. Tech.*, 4, pp. 671-672, 1960.)
A simple method of determining the zero offset of a fluxgate is described.

Morris, R.M., and B.O. Pedersen. Design of a second harmonic fluxgate magnetic field gradiometer. *Rev. Sci. Instr.*, 32, pp. 444-448, 1961.
1) Two parallel rods.
2) Short description of the principle.
3) Less than 0.5 per cent second harmonic in the excitation. Differential temperature coefficient 1 γ/°C. A 40-hour stability test showed less than 10 γ drift.
4) Several gradiometer systems are discussed, the construction of the detector mounting is described, and a block diagram of the electronics is given.

Muffley, G. The airborne magnetometer. *Geophysics*, 11, pp. 321-334, 1946.
1) Two parallel rods.
2) Short description of the principle.
3) No.
4) A sketch of the sensor is shown together with a block diagram of the electronics. This paper contains mainly a historical survey of the development of American airborne magnetometers.

Munoz, R. The Ames magnetometer. *Proc. Nat'l. Telemetering Conf.*, Paper AA-3.3, pp. 77-80, 1966.
1) Flattened ring-core.
2) No.
3) Second harmonic distortion in excitation is less than 0.001 per cent. Accuracy ±0.2 γ. Long term stability of ±0.2 γ possible.
4) Description of the sensor is given together with a block diagram of the electronics.

Munoz, Robert M. Computer aided analysis and design of space instrument systems. *Symposium on Space Magnetics Exploration and Technology*, Editor Ernest J. Iufer, pp. 133-154, Reno, Nevada, 1967, Clearinghouse Accession No. N69-33962, CR73350.
As an example of computer aided design the development of the Ames fluxgate magnetometer is described in considerable detail.

Nahrgang, S. Contribution à la théorie du magnétomètre (sonde électromagnétique) à noyau de haute perméabilité alimenté par un courant alternatif. *La Recherche Aéronautique*, No. 16, pp. 11-18, 1950.
1) Single rod.
2) Three approximations to the B-H curve are used. A power series containing only odd powers, the Feldtkeller approximation, i.e. the B-H curve is built up of three straight lines joined by two segments of sine curves, and an approximation by a series of sine curves. If a second alternating field besides the excitation field is imposed on the core it is shown that the output contains only odd harmonics of the excitation field plus all possible combinations of sums and differences

of the fundamental and harmonics of the excitation and of the second alternating field. The cases of an ac or a dc field disturbed by an alternating field is treated and the possibilities for eliminating the disturbance is discussed.
3) No.
4) No.

Ota, M. (Editor). The three component airborne magnetometer. *Report on Aeromagnetic Survey in Japan*, pp. 21-32, World Data Center C2 for Geomagnetism, Kyoto University, Japan, 1966.
1) Single rod.
2) No.
3) Overall error of the system including orientation error of the stabilized platform and residual fields from the aircraft is ±50 γ.
4) Circuit diagram of the electronics is given.

Palmer, T.M. A small sensitive magnetometer. *Proc. Instr. Electrical Engrs.*, **100**, Part II, pp. 545-550, 1953.
1) Ferromagnetic wire carrying the excitation current.
2) Based on the earlier works by Gorelik and by Joukova the author shows, neglecting hysteresis, that for small axial fields the second harmonic output is proportional to the axial field. An expression for large fields is derived too assuming constant saturation of the core by either the axial or the excitation field.
3) Experimental curves of second harmonic output vs. axial dc-field show a close fit to the theoretical curve. Sensor zero offset vs. excitation current after exposure to an axial field of 100 oersteds is given. Fields from less than 5γ has been measured.
4) Detailed description of the sensor design is given together with descriptions of the electronic circuits.

———— A battery-operated magnetometer. *Symposium on precision electrical measurements,* Paper No. 9, 17th-20th November, 1954.
1) Ferromagnetic wire carrying the excitation current.
2) Short description of the principle.
3) Wave shape of the excitation current is given together with second harmonic voltage vs. ambient field, sensitivity vs. excitation current, and zero offset vs. excitation current after exposure to large fields. A recording is shown with ±8 γ calibration field and a noise level of about 2γ p-p.
4) Sensor design data and detailed description of the electronics is given.

Pearlstein, B.A., *et al.* Magnetometer sensor development program. *Honeywell Radiation Center,* Boston, Mass., U.S.A. Final report to NASA, Contract NAS2-2070, December, 1964.
Sensors with 0.2 – 0.3 γ noise in 0-10 hz BW has been produced and the second harmonic feedthrough has been cancelled by a voltage derived from an extra winding of about 30 turns on top of the excitation winding. This is based on the assumption that the sensor null output is due to a residual transformer action (suggested by J.D. Hancock). Several recordings of the sensor noise are shown.

———— **and D.E. Ratcliff.** AIMP-D and E fluxgate magnetometer experiment. *Honeywell Document HRC 67-62, NASA CR 73161,* 153 pp., October, 1967.
Final engineering report on a space magnetometer with test data and complete electronic circuit diagrams. No information is given on the sensor type. Second harmonic feedthrough $< 0.8\ \gamma$, absolute null offset $< 0.7\ \gamma$, noise $< 0.4\ \gamma$, long term drift $< 0.2\ \gamma$, repeatability $< 1.4\ \gamma$, and null change from room temperature to $-40^\circ C < 1.1\ \gamma$, and from room temperature to $+70^\circ C < 1.7\ \gamma$.

Primdahl, F. The fluxgate mechanism. *IEEE Trans. Mag.,* **Mag.-6**, pp. 376-383, 1970.
1) Parallel and orthogonally gated sensors.
2) It is shown that the main difference in gating mechanism between the two sensor types is that parallel gating is due to changes in dB/dH whereas orthogonal gating is due to changes in $B/(H-H_c)$.
3) Gating curves of the two types of sensors are shown.
4) Design data for the experimental sensors are given.

———— A ferrite core fluxgate magnetometer. *Publications of the Earth Physics Branch,* **Vol. 40**, No. 1, Department of Energy, Mines & Resources, Ottawa, Canada, 1970.
1) Ferrite tube, orthogonally gated.
2) No.
3) Long term stability ±3.5γ over 60 days in 58,600γ field, time constant 0.3 sec., noise 0.1-0.3γ p-p, sensor zero offset 2-7γ, temperature coefficient in 58,600γ field less than 0.18γ/°C.
4) Detailed description of the sensor and of the electronics is given.

Ringhiopol, I. Un magnétomètre de grande sensibilité avec des applications dans la spectroscopie magnétique nucléaire. *Nuclear Instrum. Methods,* **35**, pp. 309-312, 1965.
1) Two parallel rods.
2) Short explanation of the principle.
3) Sensitivity threshold 2×10^{-5} oersted. Sensitivity 1.4 v/oe. Linearity range 10^{-5} oersted to 10^{-1} oersted. Relative measuring accuracy 0.001 per cent.
4) Detailed descriptions are given of the sensor and the toroidal field nulling coil together with a block diagram of the electronics.

Rose, D.C., and J.N. Bloom. A saturated core recording magnetometer. *Can. J. Res.,* 28, *Sec. A,* pp. 153-163, 1950.
1) Single rod.

2) Using an odd power series approximation to the B-H curve the authors show that the even harmonics generated by the excitation field are proportional to the dc-bias field.
3) Excitation oscillator contains less than 1 per cent second harmonic, which in turn is attenuated 80 dB by filtering. 80 dB + 30 dB attenuation is provided for the fundamental in the second harmonic amplifier. Sensitivity 25 μV/ γ second harmonic. A curve of sensitivity vs. excitation level is shown.
4) Detailed descriptions are given of the sensor and of the electronics.

Rozenblat, M.A. The theory and calculation of a magnetic modulator operating on the second harmonic principle. *Radiotekhnika*, **11**, pp. 36-51, 1956.
Based on an Arctan-shaped B-H curve the output voltage vs. excitation level and the sensitivity of a balanced magnetic modulator is derived. The effect of unbalance, of noise and of zero drift is investigated together with the influence of demagnetization and of inhomogeneous fields.

———Magnetic modulators with second harmonic sine wave output voltage. *Avtomat. i Telemekh.*, 22, pp. 1386-1400, 1961. (English translation in *Automation and Remote Control.*)
For magnetic modulators having parallel or orthogonal gating it is shown that by adjusting the shape of the excitation current wave it is possible to get a pure sine wave second harmonic output which greatly increases the signal-to-noise ratio of the device.

Rumbaugh, L.H., and L.R. Alldredge. Airborne equipment for geomagnetic measurements. *Trans. Am. Geophys. Union*, **30**, pp. 836-849, 1949.
1) Single rod, two parallel rods.
2) Using an odd power series approximation to the B-H curve the authors show that the coefficients of the even harmonics in the output are odd functions of the bias field, and that the odd harmonics are even functions of the bias field.
3) Signal-to-noise ratio of ten at a sensitivity of one gamma for the double rod sensor, and detection of fields less than one gamma with the single rod sensor is reported. A curve of sensitivity vs. excitation level is shown.
4) Description of the sensor principle and a block diagram of the electronics is given. This paper is primarily intended as a survey of airborne magnetometers.

Scearce, C.S. Magnetic field experiment. Pioneers 6, 7 and 8. *Laboratory for Space Sciences,* NASA-Goddard Space flight center, Extraterrestrial Physics Branch Preprint Series, X-616-68-370, September, 1968.
1) Helical core.
2) Short discussion of fluxgate types and possible sources of error.
3) Magnetic noise 0.13 to 0.35 γ. Zero calibration is made in flight by flipping the sensor 180° with an accuracy of ±0.25 γ. Graphs of zero calibration and of frequency response are shown.
4) A description of the helical core sensor is given together with circuit diagrams of the electronics.

Schmitt, O.H. Unbalanced magnetometer. *U.S. Patent, 2,560,132,* July 10, 1951.
1) Two parallel rods.
2) The method of detection described here is of the "peak difference" type. Basically this is a phase sensitive detector using the fundamental of the excitation wave as a reference, instead of the second harmonic. The fundamental reference voltage is here fed to the detector via the sensor by destroying the sensor balance.
3) No.
4) Detailed description of the sensor.

Schonstedt, E.O. Saturable measuring device and magnetic core therefor. *U.S. Patents, 2,981,885* and *2,916,696,* 1961 and 1959.
1) Helical core, single spiral, two parallel spirals, and double spiral.
2) Short explanation of the principle.
3) No.
4) Detailed descriptions of the sensor designs.

Serson, P.H., and W.L.W. Hannaford. A portable electrical magnetometer. *Can. J. Tech.*, **34**, pp. 232-243, 1956.
1) Two parallel rods.
2) Based on a two-zone B-H curve the time varying core-permeability is developed as a Fourier series. The sensor is loaded by a tuning capacitance and a damping resistance, and it is shown that for certain values of the circuit parameters it is possible to obtain large amplification of the second harmonic in the sensor.
3) Used as an absolute magnetometer by mounting the sensor on a theodolite the accuracy is ±0.3′ in declination and ±0.2′ in inclination corresponding to ±3 γ. The probable error of a single observation of the total intensity is from 10 γ to 50 γ.
4) Detailed description is given of the sensor as well as of the electronics.

———An electrical recording magnetometer. *Can. J. Phys.*, 35, pp. 1387-1394, 1957.
1) Two parallel rods.
2) The field at the sensor is nulled by a feedback system. The second order differential equation describing the frequency response is given and from this the system parameters are chosen.

3) Noise and drift tests show 3γ p-p noise dc-1 hz and maximum drift 10 γ in 10 hours.
4) Design data are given for the sensor as well as a complete description of the electronic circuits together with a discussion of the sources of errors.

Snare, R.C., and C.P. Benjamin. A magnetic field instrument for the OGO-E spacecraft. *IEEE Trans.*, **NS-13**, pp. 333-339, 1966.
1) Two parallel rods.
2) Short description of the principle.
3) Telemetry resolution 1/16 γ. Calibration fields of ±8 γ and ±32 are provided during flight.
4) Short description of the sensor and a block diagram of the electronics are given.

Street, R., J.C. Woolley, and P.B. Smith. Magnetic viscosity under variable field conditions. *Proc. Phys. Soc.*, **B 65**, pp. 679-696, 1952.
1) Two parallel rods.
2) No.
3) With negative feedback the linearity is better than 1/4 per cent.
4) Design data for the sensor is given.

Tenani, M. Nuovo metodo di misura della declinazione e della inclinazione magnetica. *La Ricerca Scientifica*, **20**, pp. 1135-1140, 1941.
1) Closed rectangular core with field-gathering devices.
2) Short explanation of the principle. The sensor is taken from a fluxgate compass and mounted on a theodolite for D and I measurements.
3) The standard deviation on a declination measurement is 5″ (inclination at the site is approx. 60°).
4) Block diagram of the electrical circuit is given.

Thellier, E. Enquête sur les appareils enregistreurs des variations rapides du champ magnétique terrestre. *Ann. IGY*, **4**, Geomagnetism, Part II, pp. 225-280, 1957.
Short description of the fluxgate principle and a discussion of its use as an instrument for recording variations in the earth's magnetic field.

Thomas, H.P. Direction responsive system. *U.S. Patent, 2,016,977*, October 8, 1935.
1) Closed rectangular core and single rod with field-gathering devices.
2) Short explanation of the principle.
3) No.
4) Detailed description of the sensor and the electrical circuit. The even harmonic content is detected by the dc current flowing through a symmetrical nonlinear resistor connected to the output. This is equivalent to the "peak detector" or the "fundamental reference" detector system. The patent was filed in 1931 and is one of the earliest descriptions of fluxgates.

Tolles, W.E. Applications of the saturable-core magnetometer. *Proc. Nat'l. Electronics Conf.*, **3**, pp. 504-513, 1947.
1) Single rod.
2) Short explanation of the principle.
3) Noise level about 0.03 γ dc – 1 hz BW. Sensitivity from 10 μv/γ to 2000 μv/γ. Linear response from zero to 1000 γ or 10,000 γ. Temperature coefficient 0.1 per cent/°C.
4) Some data on sensor design are given. The paper is mainly intended as a survey of development and applications of the fluxgate.

Tucker, J.W. Magnetic amplifier noise limitations. *Naval Research Laboratories*, Washington, Rept. No. 3779, Dec. 29, 1950.
An equivalent input noise of 0.7×10^{-6} volts is reported for 1 hz BW, this corresponds to an input magnetic signal of 0.009 γ.

Vacquier, V.V. Apparatus for responding to magnetic fields. *U.S. Patent, 2,406,870*, Sept. 3, 1946.
1) Two parallel rods.
2) The principle is explained qualitatively from the hysteresis curves of the core material and from the phase difference in the otherwise similar output voltages from the two open core transformers because of the applied dc field.
3) Intensity changes of 20×10^{-5} oersteds are readily detected. Higher sensitivities are obtainable.
4) Detailed descriptions of the sensor and of the electronics are given.

——— Apparatus for responding to magnetic fields. *U.S. Patent, 2,407,202*, Sept. 3, 1946.
A gradiometer is described using the invention by the author in *U.S. Patent, 2,406,870.*

Vacquier, V., R.F. Simons, and A.W. Hull. A magnetic airborne detector employing magnetically controlled gyroscopic stabilization. *Rev. Sci. Instr.*, **18**, pp. 483-487, 1947.
1) Two parallel rods, single rod with opposingly magnetized halves.
2) Short description of the principle.
3) Noise level 0.2 γ.
4) Some design data are given of the sensor together with block diagrams of the electronics.

Vasiliu, Gh., N. Calinicenco, and C. Onu. Magnetometru cu sonda de saturatie. *Stud. Cerecetari Stiint., Fiz. Stiint. Tehn.*, **14**, pp. 341-348, 1963. Rumania.
1) Single rod and two parallel rods.

2) Calculation of second harmonic output and sensitivity based on a simplified two-zone B-H curve.
3) No.
4) Description of the sensor and electronic circuit diagram.

Weiner, Melvin M. Magnetostrictive offset and noise in fluxgate magnetometers. *IEEE Trans. Mag.*, Mag.-5, No. 2, pp. 98-105, 1969.
1) Elongated ring-core.
2) Theoretical analysis of the effect of magnetostriction.
3) Second harmonic output (magnetostrictive offset) vs. excitation voltage, and second harmonic output fluctuations (magnetostrictive noise) vs. excitation voltage are shown together with frequency spectra of the offset and noise.

Whitham, K. Measurements of the geomagnetic elements. *Methods and Techniques in Geophysics,* 1, editor S.K. Runcorn, pp. 134-147 and 165-167, Interscience, London, 1960.
This book contains a survey of saturable core magnetometers with information on core designs, performance data, theoretical analysis, and descriptions of the different types of electronical magnetometer circuits.

Williams, F.C., and S.V. Noble. The fundamental limitations of the second harmonic type of magnetic modulator as applied to the amplification of small dc signals. *Proc. Inst. Electrical Engrs., II 97,* pp. 445-459, 1950.
The theoretical and experimental results given in this paper are in most cases applicable to fluxgate devices. The noise which is attributed to Barkhausen jumps is equivalent to an input signal of 10^{-3} γ, the zero drift is ± 5 X 10^{-3} γ. These results are valid for a closed magnetic path; in applying them to an open core device as the fluxgate the input attenuation because of demagnetization will mean an increase in noise and drift of the order of 10^2.

Wurm, M. Beitraege zur Theorie und Praxis des Feldstaerkedifferenzmessers fuer magnetische Felder nach Foerster. *Z. Agew. Phys.*, 2, pp. 210-219, 1950.
1) Two parallel rods.
2) A qualitative explanation of the principle is given, based on a simplified two-zone B-H curve. Based on the actual hysteresis-loop for the core it is shown that, compared to a B-H curve without hysteresis, a phase shift of the second harmonic is introduced. This phase shift is proportional to the area of the hysteresis loop. Theoretical curves of second harmonic vs. excitation level are given and the possibilities of balancing the sensor by external impedances are investigated.
3) Balancing impedances are plotted for a number of cores compared to a standard core, and a null-field output of 5 γ to 20 γ, not further reducible, is reported. By using selected cores instead of external balancing, null-field outputs of less than 2 γ was obtained.
4) Some design data of the sensors are given.

Wyckoff, R.D. The Gulf airborne magnetometer. *Geophysics,* 13, pp. 182-308, 1948.
1) Two parallel rods, rectangular closed core.
2) No.
3) Many oscilloscope photographs explaining the operation of the sensor are shown.
4) A sketch of the sensor principle is shown together with a circuit diagram of the differential peak detector. This paper is intended as a survey of the airborne magnetometer development.

Yanus, R.I. Theory of ferro-probe magnetometers for non-uniform magnetic fields. *Fiz. Metal. Metalloved.*, 14, pp. 336-373, 1962. (English translation in *Phys. Metals Metallography,* 14, pp. 41-46, 1962.)
It is shown analytically that a fluxgate sensor in an inhomogenous field will measure the average field over its length.

Zatsepin, N.N., *et al.* Problem of the measurement of non-uniform magnetic fields by means of ferroprobes. *Fiz. Metal. Metalloved.*, 14, pp. 30-34, 1962. (English translation in *Physics of Metals and Metallography,* 14, pp. 29-32, 1962.)
In moderately inhomogenous fields it has been found that the fluxgate measures the average field along the sensor length. In highly non-uniform fields there is a considerable difference between the magnetometer indications and the average field, the magnitude and sign of which is dependent on the position of the sensor in the field.

PUBLICATIONS of the EARTH PHYSICS BRANCH

VOLUME 41 – NO. 2

the strong motion seismograph network in western canada, 1970

G. C. ROGERS, W. G. MILNE and M. N. BONE

DEPARTMENT OF ENERGY, MINES AND RESOURCES

OTTAWA, CANADA 1970

Cat. No.: M70-41/2

Contents

the strong motion seismograph network in western canada, 1970

G. C. ROGERS, W. G. MILNE and M. N. BONE

Abstract. A program to install strong motion seismographs in the active seismic regions in western Canada was initiated in 1961. A total of 14 accelerographs and 48 seismoscopes are now installed along the coast of British Columbia. The seismoscopes and eight of the accelerographs are instruments of United States Coast and Geodetic Survey design manufactured in Canada. The remaining six accelerographs have been purchased in the United States. The strong motion instruments are distributed in buildings on varied geological and local soil formations in a program to determine ground motion and its variation with soil type in the vicinity of earthquake epicentres.

Résumé. Un programme d'installation de séismographes à fortes secousses a été amorcé en 1961 dans les secteurs d'activité séismique prononcée de l'Ouest du Canada. Quatorze accélérographes et quarante-huit séismoscopes sont déjà en place le long de la côte de la Colombie-Britannique. Les séismoscopes et huit des accélérographes ont été fabriqués au Canada selon un modèle mis au point par le *Coast and Geodetic Survey* des États-Unis. Les six autres accélérographes ont été achetés aux États-Unis. Les séismographes à fortes secousses ont été installés dans des bâtiments sur divers genres de sols et de formations géologiques afin de permettre de déterminer le mouvement du sol et ses variations selon le type de sol aux environs de l'épicentre des séismes.

Introduction

Scientists of the United States Coast and Geodetic Survey developed, in the early 1930s, a seismograph system for the study of the response of buildings and different soils to the large accelerations which occur near the epicentres of large earthquakes (Ulrich, 1935). The units have proven successful in producing good records, although the original design has been modified several times. The accelerogram from the United States Coast and Geodetic Survey instrument near the El Centro earthquake of 1942 has been used for many earthquake engineering studies. Many of the early instruments were placed in California, but the most recent list of the United States strong motion seismographs shows that, at the present time, there are new stations being added in all the earthquake zones in the United States. A new series of instruments have appeared on the market to meet the demand. Japanese seismologists have also developed strong motion seismographs. There are many sites in Japan where strong motion instruments are located, and many records have been obtained. New Zealand seismologists have developed instruments for distribution in earthquake zones. Similar programs are in progress in Russia, India, Chile, Mexico and other countries.

In 1961, when Canadian seismologists first took an active interest in engineering seismology, there were no commercial manufacturers of strong motion seismographs in North America. A strong motion seismograph was borrowed from the U.S.C.G.S. site at Tacoma, Washington, and tenders were called for making blueprints and building units similar to it. Fairey Aviation of Victoria was the successful bidder, and have since built eight of the units for use in western Canada. The United Electro Dynamics Corporation of Pasadena, now a Teledyne Company, designed and produced the AR-240, a more compact and up-dated version of a strong motion seismograph. This unit lacks the displacement meters incorporated in the U.S.C.G.S. model, but otherwise retains similar basic instrumental constants. Six of these instruments have been purchased for use in western Canada. The price for one unit of either the Fairey model, or the AR-240 is approximately $4,000. Since these instruments have been purchased, new designs of strong motion instruments have appeared on the market at a greatly reduced price.

Several versions of a low-cost strong motion seismograph have been designed in various countries. The United States model is called the Wilmot-Survey type seismoscope. Fairey Aviation, and United Engineering, both Victoria firms, have each built 25 seismoscopes of this design for the Dominion Observatory. Many of these more limited units can be installed because the cost is low—approximately $200 each.

The aim of the strong motion program on the west coast of Canada is to obtain basic ground motion data on varied geological and soil formations during large earthquakes. In an effort to restrict measurements to that of true ground motion (and not building motion), the instruments have been placed in the basement of buildings. The buildings are low and have a relatively small mass to minimize the influence of the building on the true ground motion. The coastal region of British Columbia is part of the circum-Pacific earthquake zone, and earthquakes may occur throughout the region. Instruments are distributed along the coast from Prince Rupert to Victoria. There is a greater concentration of strong motion instruments in the more heavily populated southern section. In this section, because of the complex recent geological history (Armstrong 1956, 1957; Fyles 1960, 1963), there are areas where instruments may be installed on many different types and thicknesses of soil, relatively close to each other.

Instrumentation

Fairey Aviation strong motion accelerograph (U.S. Coast and Geodetic Survey standard design). Figure 1 is a photograph of an instrument in this series. This unit contains three mutually perpendicular accelerometers, and two displacement meters. Accelerometer and displacement meter response together with time marks are recorded on 12-inch wide photographic paper at a speed of approximately 2 cm/sec. The instrument operates from a 12-volt battery, maintained in fully-

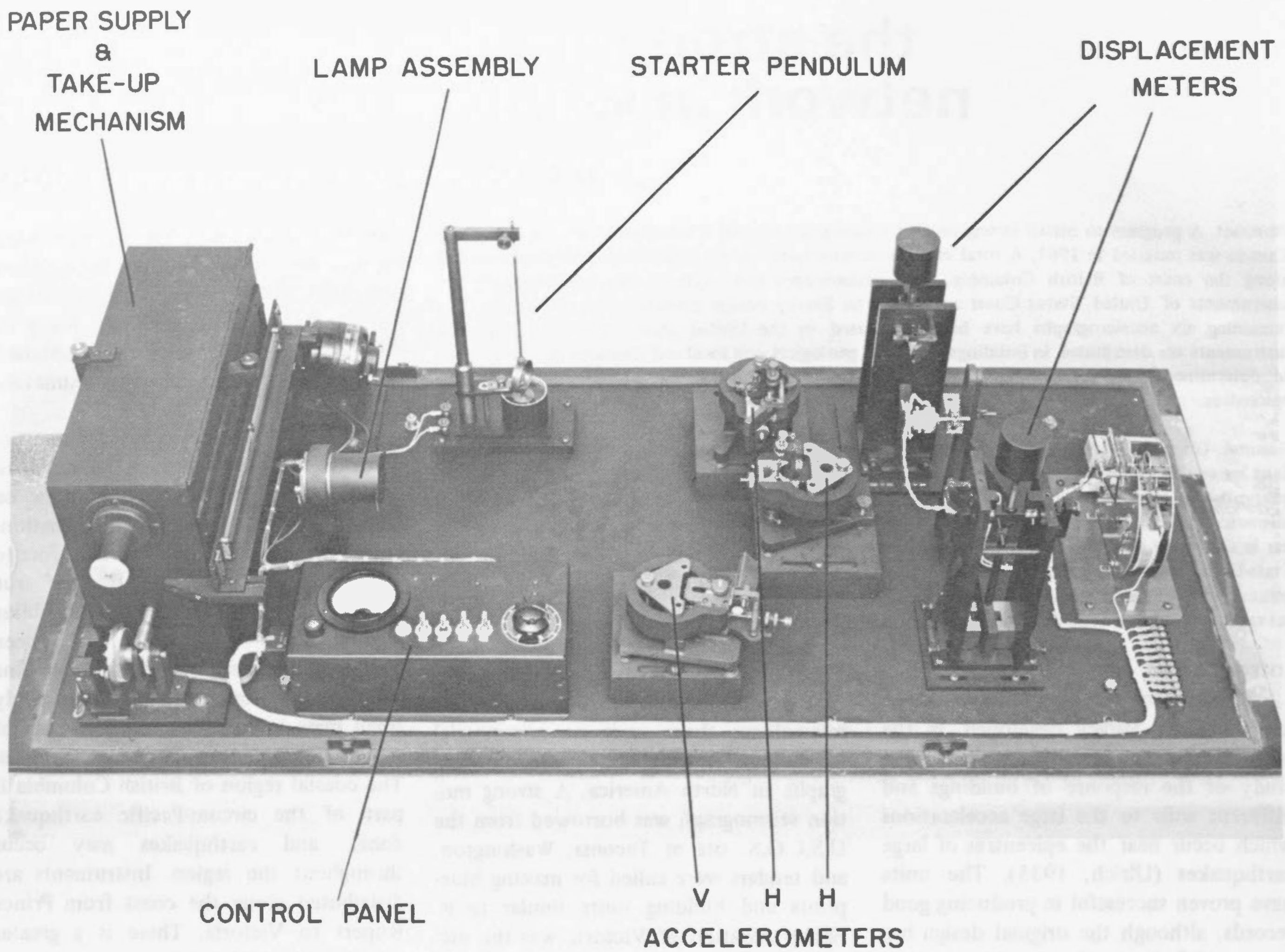

Figure 1. Photograph of accelerograph (U.S.C.G.S. design).

charged condition by a continuous trickle-charge. Recorder operation in the presence of large ground motion is initiated by closure of contacts on a starter pendulum that responds to horizontal ground motion. Sensitivity of the starter is adjustable by varying the spacing of the contacts. This starter pendulum has a natural period of approximately 1 second, and 30 per cent critical damping is obtained with a dash pot of oil. The gap between contacts on the starter is set at 0.6 mm. This will be closed by an earthquake with intensity of IV or greater at the site.

Momentary closure of the starter pendulum contacts de-energizes a holding relay. Release of the holding relay then initiates operation of an 8-day mechanical clock movement to provide half-second time interval marks, turns on the recording lamp and the paper drive motor. Once started, the unit operates for 90 seconds after which it is turned off and the holding relay is again energized. Additional 90-second operation cycles will occur whenever the ground motion is sufficient to produce closure of the starter pendulum contacts. A maximum of 10 such cycles can occur before a final stop switch is closed. The room must be darkened to remove or change the record.

The torsion-pendulum type accelerometers have a natural period of approximately 0.06 second, damping of 60 per cent critical, acceleration magnification of approximately 120, corresponding to a sensitivity of approximately 12 mm trace amplitude for an acceleration of 0.1 gravity. The normalized response curve for an accelerometer is shown in Figure 2 (after U.S.C.G.S.).

The Carder displacement meters have a natural period of approximately 3 seconds, damping of 60 per cent critical (eddy-current damping), and a magnification of 1. The response curve for a displacement meter is shown in Figure 3.

The U.E.D. AR-240 strong motion accelerograph. The AR-240 strong motion accelerograph of the U.E.D. Earth Sciences Division (Figure 4) was marketed in late 1963. The instrument contains three mutually perpendicular accelerometers with a natural period of approximately 0.06 second and 60 per cent critical electromagnetic damping. These torsion seismometers have a sensitivity of 7.6 mm trace amplitude for 0.1 gravity

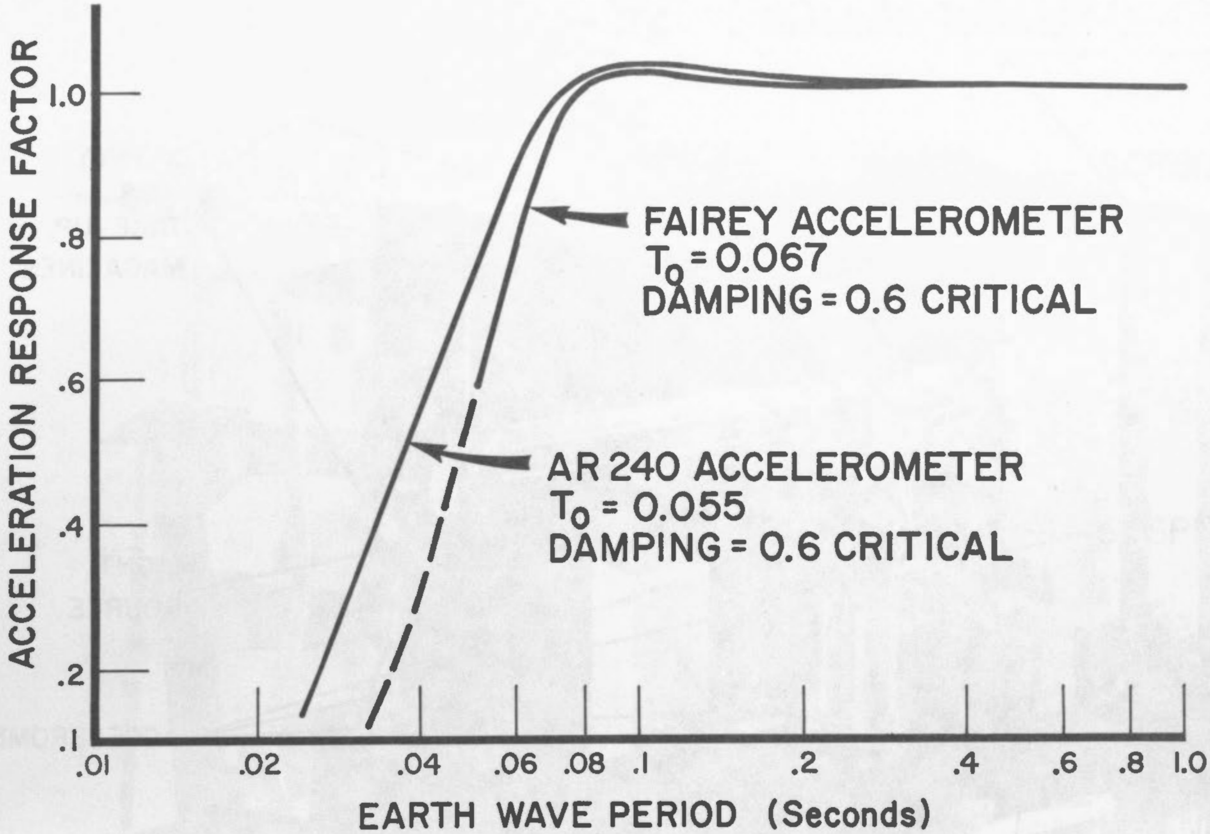

Figure 2. Response curve of accelerometers.

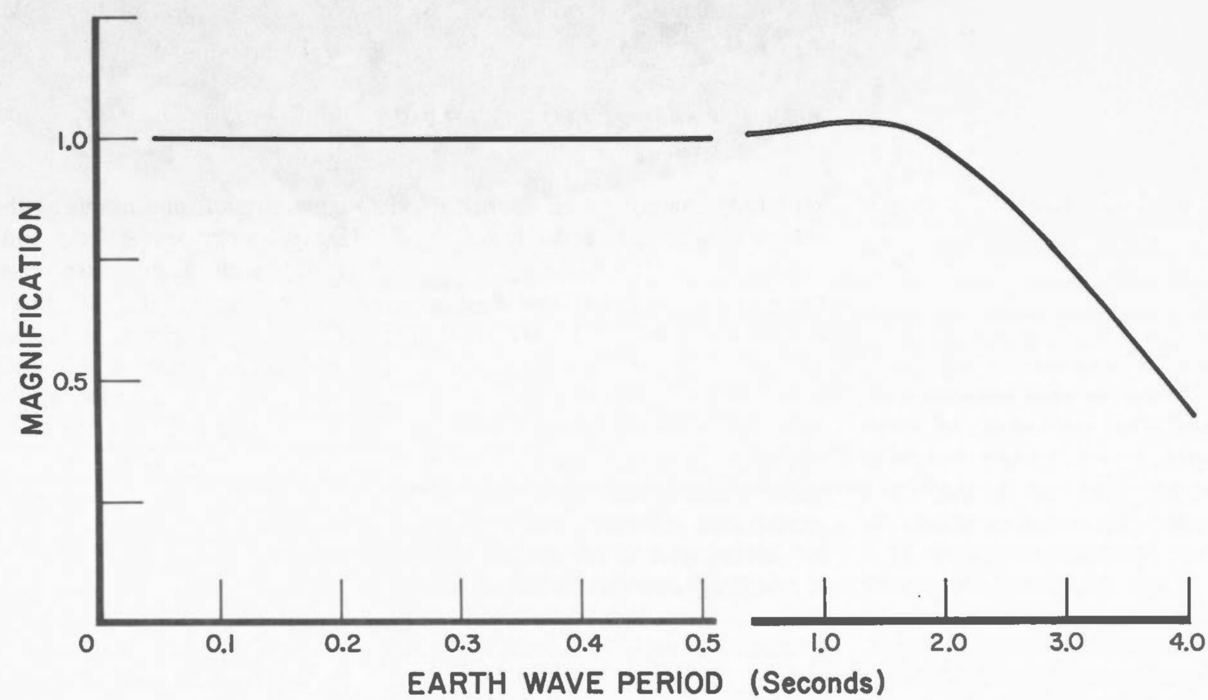

Figure 3. Response curve of Carder-type displacement meter.

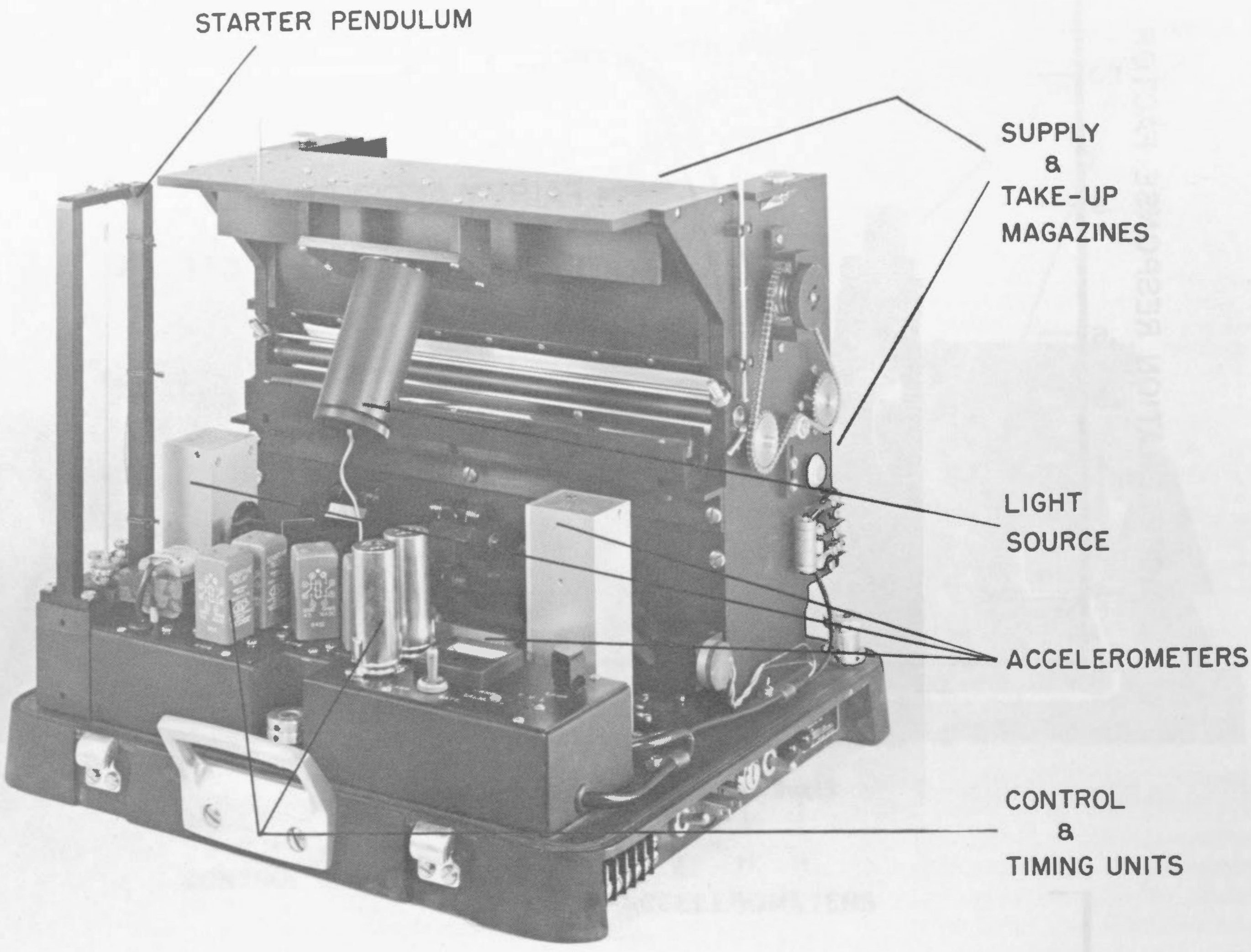

Figure 4. Photograph of U.E.D. AR-240.

acceleration. Their response curve is shown in Figure 2.

The AR-240 is self-triggering with a critically magnetic damped starter pendulum that has a natural period of one second and is sensitive to horizontal motion. The gap between contacts is set to 0.6 mm. The unit shuts off seven seconds after the last contact closure of the starter pendulum and is ready for a new operation. The recording is done on 12-inch-wide photographic paper at a speed of 2 cm. per second. Recording paper is carried in magazines which can be changed without darkening the room. Time marks are controlled by an electronic timing module and are put on the record every half second. The unit is operated from a 12-volt battery that is kept fully charged by an internal trickle charger connected to available A.C.

Fairey Aviation and United Engineering seismoscopes (Wilmot Survey type). The seismoscope (Figure 5) is a conical pendulum that includes a smoked glass plate upon which a scriber rides. The instrument does not measure either the displacement or the acceleration of the ground, but provides a direct record on the smoked glass of the velocity response of an average structure to ground motion. That is, it records a particular point, defined by its period and damping, on the velocity response spectrum (Hudson 1956).

The seismoscopes made by Fairey Aviation and United Engineering have the same physical dimensions as the Wilmot Survey instrument (Cloud and Hudson 1961) with slight alterations to the scriber support and damping magnets. They have a period of approximately 0.75 second and variable eddy-current damping. The Fairey instruments have a maximum damping of about 5 per cent critical at one centimetre amplitude.

A deflection of 1 cm at 5 per cent damping is the equivalent to a maximum velocity response of 0.45 ft/sec for a structure with 10 per cent damping and period of 0.75 sec. Because of their more powerful magnets, the United Engineering instruments have a wider range of damping values available and have been set at approximately 10 per cent critical for 1 cm of deflection. With this series of

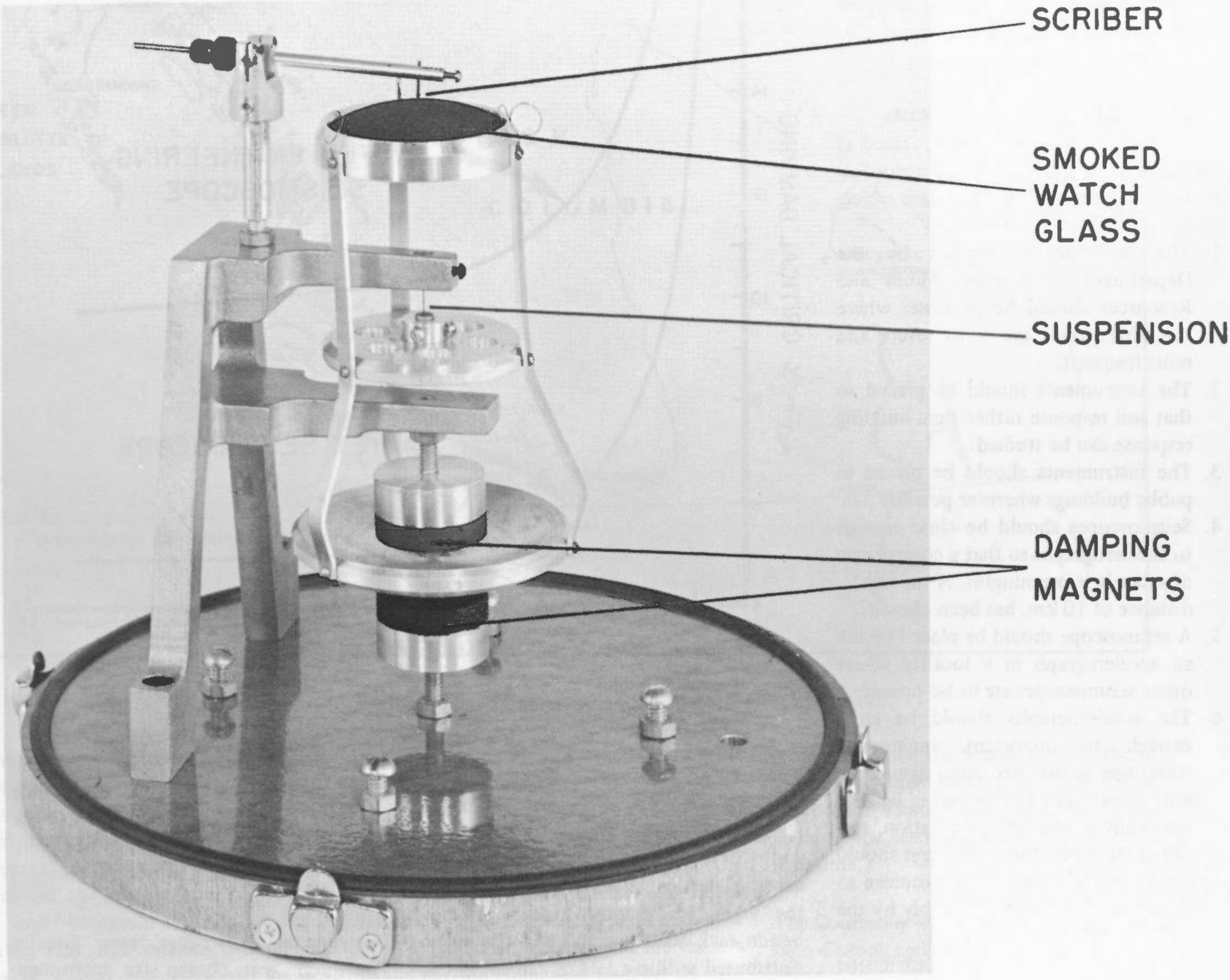

Figure 5. Photograph of seismoscope (Wilmot Survey type).

instruments, a deflection of 1 cm at 10 per cent damping is the equivalent to a maximum velocity response of 0.64 ft/sec for a structure with 10 per cent damping and period of 0.75 sec. Typical damping versus amplitude curves are shown for each model in Figure 6.

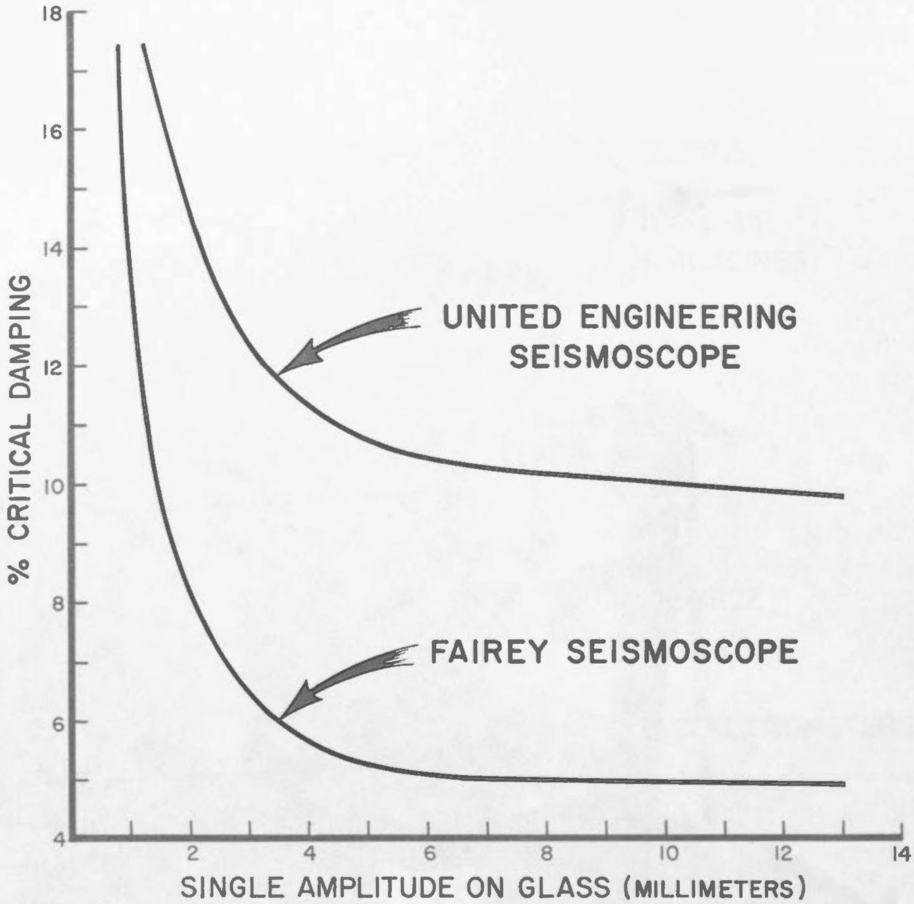

Figure 6. Seismoscope damping versus amplitude.

The distribution of instruments

The instruments have been placed at various sites in western Canada according to certain rules and with certain objectives:

1. The instruments supplied by the Department of Energy, Mines and Resources should be in zones where the earthquakes are most severe and most frequent.
2. The instruments should be placed so that soil response rather than building response can be studied.
3. The instruments should be placed in public buildings wherever possible.
4. Seismoscopes should be close enough to accelerographs so that a comparison of records is meaningful. A maximum distance of 10 km. has been chosen.
5. A seismoscope should be placed beside an accelerograph in a locality where other seismoscopes are to be operated.
6. The accelerographs should be close enough to important engineering structures so that structural damage or non damage can be assessed in light of the known ground acceleration recorded. However, the instrument should not be so close to a large structure so that it is influenced appreciably by the motion of the structure itself.

The 14 accelerographs are distributed as shown in Figure 7. Their distribution is a compromise between nearness to previous earthquake epicentres (Figure 8) and nearness to population centres where information gained can be most usefully applied. Several accelerographs have been located by themselves with the major factor in their site selection being proximity to a possible epicentre. The remaining accelerographs are accompanied by networks of seismoscopes and are located in and around population areas where construction on different types of foundation conditions is common. The seismoscopes are distributed so as to measure the response of these different conditions.

Presently there are four areas of the west coast where the accelerographs are accompanied by seismoscopes. In each of the areas, one seismoscope is located beside each accelerograph and the others distributed within a 10-km radius. In this way the records of all the seismoscopes can be compared more readily to the three component acceleration record by observing the record on the adjacent seismoscope. Also, in each area, one seismoscope is located on bedrock. This distribution provides a basis with which to compare areas and to form intensity interpretations of different microzones in a particular area.

Most of the seismoscopes have been located in schools. In this manner, by consulting with a single authority in an area, installation arrangements have been simplified and the coverage of many different types of soils and foundation conditions in that area have been made possible. Also, the school buildings are usually one or two storey structures minimizing any serious interaction between the building and the soil condition.

The greater Vancouver area. Greater Vancouver was chosen for instrumentation because it is the major city on the west coast of Canada, and most of the industry and major buildings of the west coast are located there. The original network inside the city limits has been expanded and is still under expansion outwards from Vancouver because of the different types of soils in the area. The deposits of three glaciations, intervening marine and glaciofluvial deposits, plus the deposits of the Fraser River and its large delta, offer many varying foundation conditions. The area is sufficiently industrialized so that there are buildings on almost every type of soil available.

Figure 7. Distribution of strong motion instruments in western Canada.

The instrument network presently consists of five accelerographs and 26 seismoscopes as shown in Figure 9. Two lines of instrument sites, A and B, appear as a general pattern. The A line begins on bedrock on the north shore of Burrard Inlet, and continues south to Point Roberts. This line crosses the varying depths of glacial and glacio-marine deposits upon which the city of Vancouver stands. It then crosses the Fraser River delta and ends upon glacial till at its southern end. The B line begins on the deep interglacial sandy deposits of Point Gray, and proceeds east across Vancouver to where it meets the silts of the Fraser River. It is planned to extend this line eastward to Abbotsford across the varying depths of marine, glacio-marine, and glaciofluvial deposits that have not been preloaded by glacial ice.

The one exception to the soil response study orientation of this strong motion program is in the 21 storey B.C. Hydro Building in Vancouver. During the Seattle earthquake (April 1965), motions that were imperceptible at ground level and did not trigger the strong motion unit located in the basement, caused a considerable amount of alarm on the upper floors of the building. A unit has now been installed on the roof and the starters of the two are connected together.

The greater Victoria area. The Victoria area was chosen for instrumentation because it is the second largest city on the Canadian west coast, and because it is the nearest city in Canada to epicentres located in the Puget Sound region. The major factor in choosing the distribution of sites in and around the city was the existence of an exact drilling record of soil information to bedrock. The network consists of two accelerographs and 11 seismoscopes distributed as shown in Figure 10. The accelerograph located on deep soil on the University of Victoria campus was triggered during the Seattle earthquake of 1965. The unit located on bedrock in downtown Victoria did not trigger. (The seismoscope network was not in place at that time.)

The Courtenay–Comox area. The Courtenay–Comox area was chosen for instrumentation because of its proximity to the large earthquake of 1946 (Hodgson 1946). The present network consists of one accelerograph and six seismoscopes distributed as shown in Figure 11.

The Alberni area. The Alberni Valley was chosen for instrumentation because in this area earthquakes throughout the region are experienced with a greater intensity than might be expected. The fluvial deposits of the Somass River intersect with the glacial and marine deposits of the area giving a variety of soil conditions on which construction exists. The present network consists of one

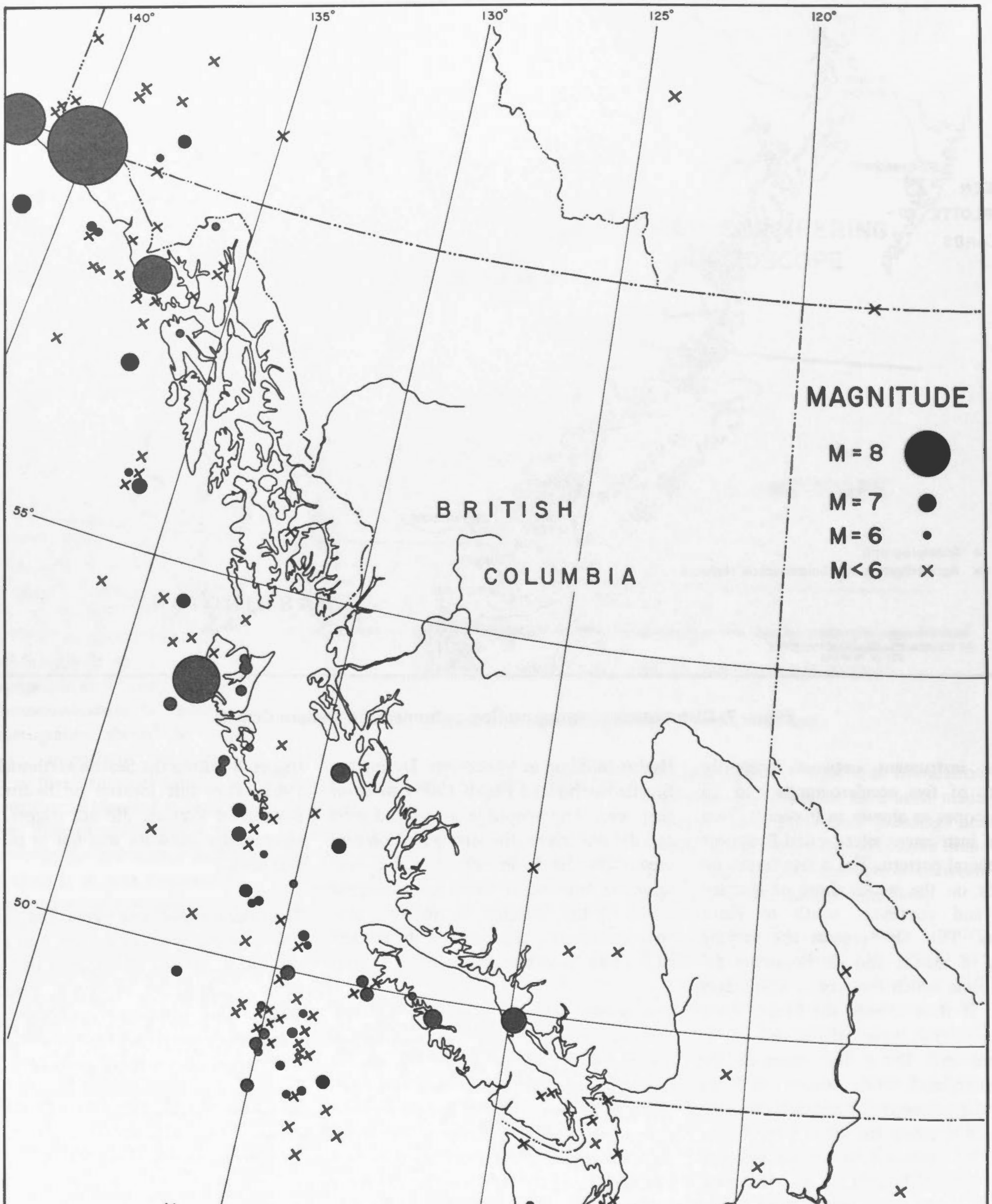

Figure 8. Epicentres of earthquakes in western Canada greater than magnitude 5 (1899-1966).

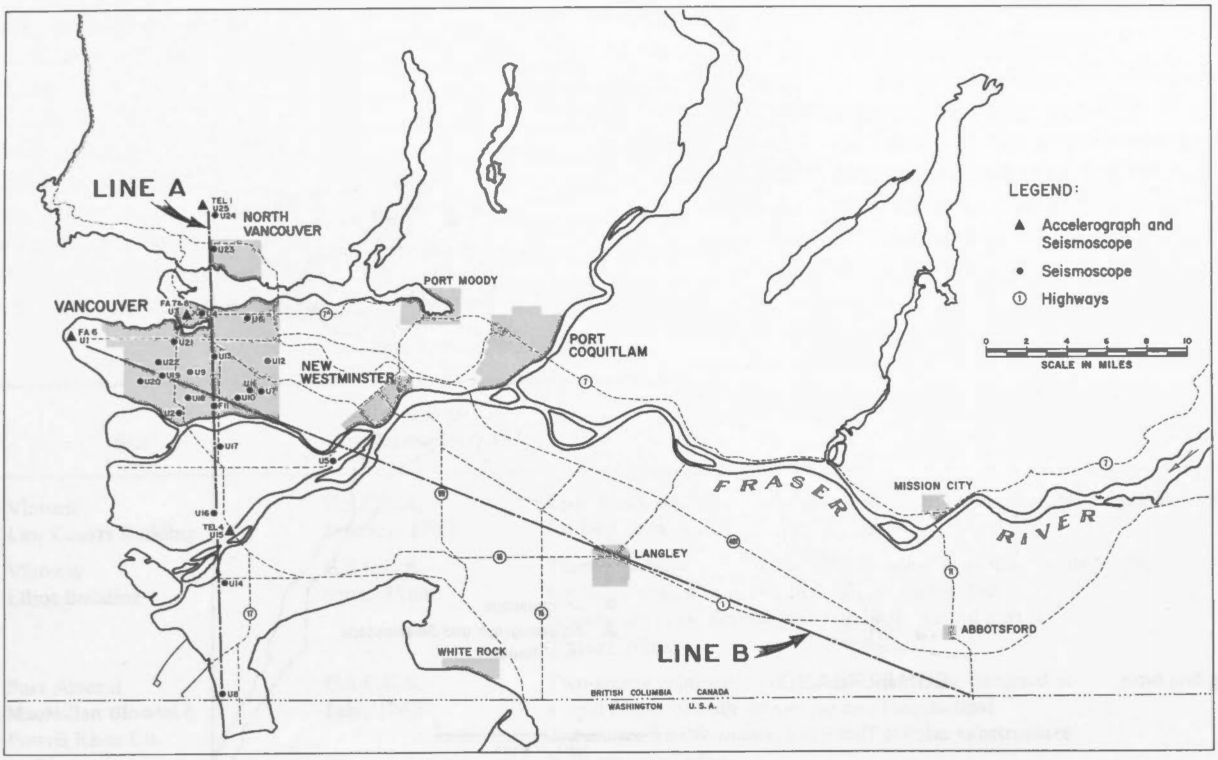

Figure 9. Distribution of strong motion instruments in the Vancouver area.

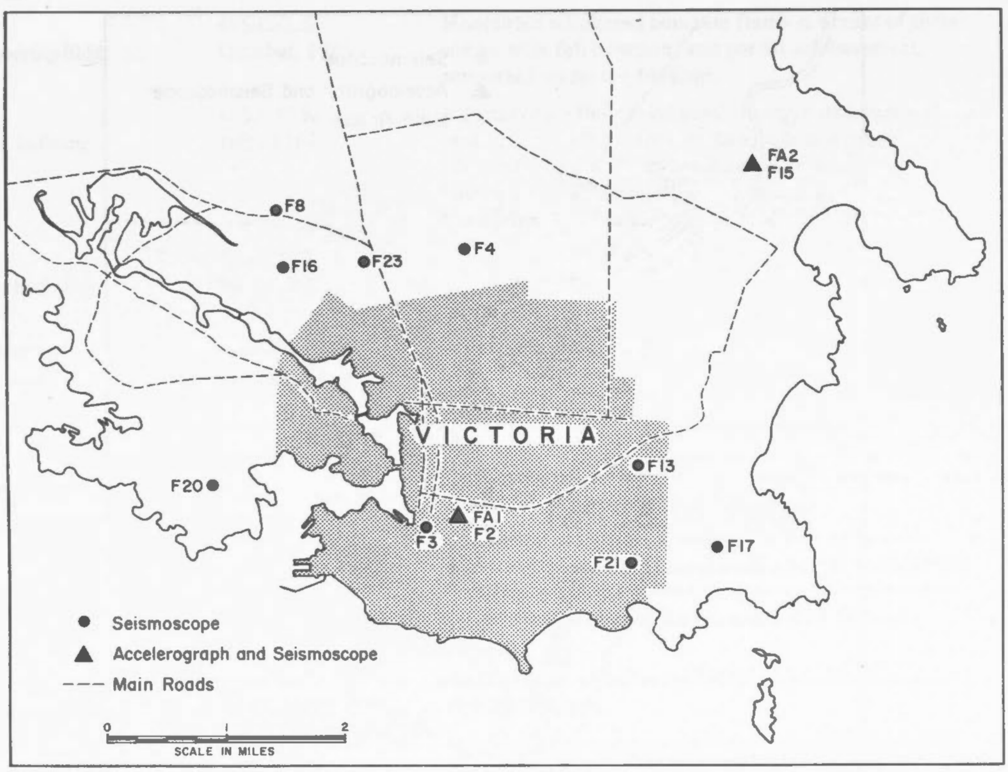

Figure 10. Distribution of strong motion instruments in the Victoria area.

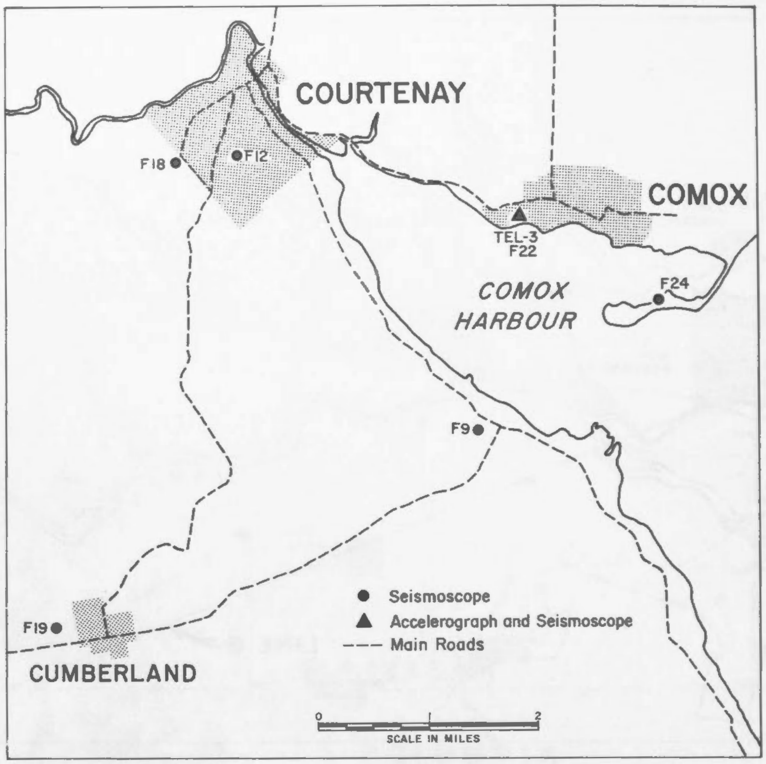

Figure 11. Distribution of strong motion instruments in the Courtenay-Comox area.

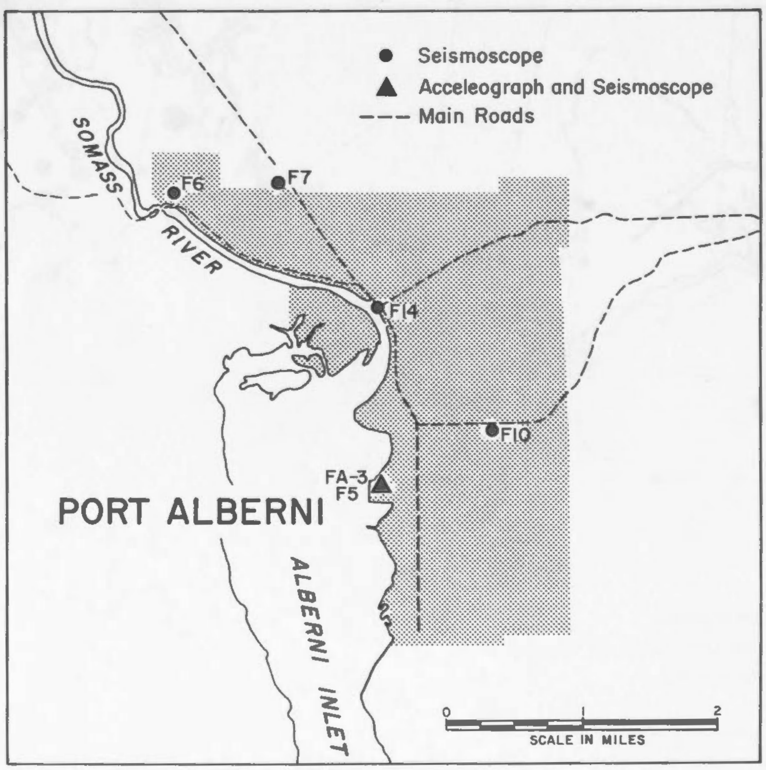

Figure 12. Distribution of strong motion instruments in the Port Alberni area.

accelerograph and five seismoscopes distributed as shown in Figure 12.

The strong motion network of western Canada is intended to be a continuing and growing network. It now consists of 14 accelerographs and 48 seismoscopes. The present policy is to continue this project as far and as rapidly as funds will permit. It is expected that private funds will permit the instrumenting of specific buildings or projects within this network. As far as possible, seismologists of the Earth Physics Branch will assist with the installation and maintenance of any private site provided any records obtained are in the public domain for earthquake engineering purposes. An example of this is the two seismoscopes which have been placed at positions near the Mica Creek Damsite by B.C. Hydro and Caseco Consultants.

Table I provides the details of the accelerograph sites and Table II provides the details of the seismoscope sites. The plans of the buildings, and the soil conditions as far as they are known are on file for each strong motion site for possible use in the future.

Table I. Information on accelerograph sites

Number	Site	Instrument and Installation Date	Building Description	Soil Type
FA-1	Victoria Law Courts Building	U.S.C.G.S. January, 1963	Five-storey reinforced concrete building with shear walls for transmission of horizontal forces.	granitic rock
FA-2	Victoria Elliot Building	U.S.C.G.S. Sept., 1964	Three-storey reinforced concrete building with shear walls for transmission of horizontal forces. Part of the foundation is reinforced concrete footings and part is 'Franki' piles.	clay
FA-3	Port Alberni MacMillan Bloedel & Powell River Co.	U.S.C.G.S. July, 1965	Two-storey reinforced concrete construction designed as a rigid frame in both transverse and longitudinal directions. The foundation is a stiff cellular substructure built on wood piles.	sand and gravel
FA-4	Campbell River Ladore Dam	U.S.C.G.S. July, 1965	A concrete gravity dam, 140 feet high.	granitic rock
FA-5	Port Hardy Seismic Vault	U.S.C.G.S. March, 1968	The instrument is on a pier in a standard underground seismic vault.	granitic rock
FA-6	Vancouver Civil Engineering Bldg.	U.S.C.G.S. October, 1965	Monolithic reinforced concrete frame structure of three stories with full basement and partial sub-basement, supported on spread footings.	sand and gravel
FA-7	Vancouver B.C. Hydro Building	U.S.C.G.S. July, 1963	A twenty-two floor reinforced concrete structure with the central core as the main structural element resisting horizontal forces. There are cross walls in the two basements to achieve complete hull action of the basements. The foundation is a modified raft design.	sandstone
FA-8	Vancouver B.C. Hydro Building (penthouse)	U.S.C.G.S. July, 1966	as above	as above
TEL-1	North Vancouver Cleveland Dam	AR-240 January, 1968	A concrete gravity dam, 300 feet high.	granitic rock
TEL-2	Duncan North Cowichan Hospital	AR-240 October, 1967	Reinforced concrete shear wall structure varying from one to six stories. Foundations are spread footings.	sand
TEL-3	Comox St. Joseph's Hospital	AR-240 August, 1967	Reinforced concrete shear wall structure four stories high. Foundations are spread footings.	glacial till
TEL-4	Richmond Massey Tunnel	AR-240 September, 1967	The tunnel has a cross section of 78 ft X 24 ft and is composed of six 344-ft reinforced concrete sections held together by clamps and rubber gaskets. It rests on a 4-ft bed of sand in a partial trench dredged in the river bottom.	sand and silt
TEL-5	Sandspit Airport Terminal Bldg.	AR-240 September, 1967	Single storey wood frame building. Foundations are a poured concrete.	sandy gravel
TEL-6	Prince Rupert Columbia Cellulose	AR-240 July, 1967	A 60-ft high two-storey steel box frame building with a concrete basement.	gravel

FA – Fairey Aviation strong motion accelerograph.
TEL – U.E.D. AR-240 strong motion accelerograph.

Table II. Information on seismoscope sites

Number	Site	Date	Soil Type
U1	Vancouver Civil Engineering Bldg., U.B.C.	October, 1965	sand and gravel
U2	Vancouver Lloyd George Elementary School	July, 1967	glacial till
U3	Vancouver B.C. Hydro Building	September, 1966	sandstone
U4	Vancouver Vancouver Vocational Institute	July, 1967	shale
U5	Richmond Hamilton Elementary School	October, 1967	boggy peat and sand
U6	Vancouver Templeton Junior Secondary School	September, 1966	glacial till
U7	Vancouver Killarney Secondary School	September, 1966	glacial till
U8	Delta English Bluff Elementary School	October, 1967	glacial till
U9	Vancouver Eric Hamber Secondary School	September, 1966	glacial till
U10	Vancouver David Thompson Secondary School	September, 1966	glacial till
U11	Vancouver Waverley Elementary School	July, 1967	muskeg
U12	Vancouver Windermere Secondary School	July, 1967	glacial till
U13	Vancouver Sir Charles Tupper Secondary	September, 1966	silt and gravel
U14	Delta Delta Secondary School	October, 1967	soft wet sand
U15	Richmond Massey Tunnel	September, 1967	sand and silt
U16	Richmond Daniel Woodard Elementary School	October, 1967	clay
U17	Richmond Mitchell Elementary School	October, 1967	clay
U18	Vancouver Churchill Secondary School	September, 1966	glacial till
U19	Vancouver Point Grey Jr. Secondary School	September, 1966	dense sand and silt
U20	Vancouver Kerrisdale Elementary Annex	September, 1966	sand, gravel and clay
U21	Vancouver School Board Administration Bldg.	September, 1966	glacial till
U22	Vancouver Prince of Wales Secondary School	July, 1967	bedrock
U23	North Vancouver Prince Charles School	October, 1967	glacial till
U24	North Vancouver Canyon Heights Elementary School	October, 1967	glacial till
U25	North Vancouver Cleveland Dam	January, 1968	bedrock
F2	Victoria Law Courts	September, 1965	bedrock

Table II. Information on seismoscopes sites (cont'd)

Number	Site	Date	Soil Type
F3	Victoria Bus Depot	October, 1967	clay and silt
F4	Victoria Cloverdale School	September, 1965	bedrock
F5	Port Alberni M.B. & P.R. Pulp Mill	May, 1965	sand and gravel
F6	Port Alberni River Bend Elementary School	September, 1969	firm sandy soil
F7	Port Alberni Seismic Station	February, 1968	bedrock
F8	Victoria Colquitz School	September, 1965	stiff brown clay
F9	Royston Royston Elementary School	September, 1967	gravel
F10	Port Alberni Calgary Elementary School	September, 1969	glacial till
F11	Vancouver Moberley Elementary Annex "A"	October, 1967	glacial till
F12	Courtenay Courtenay Elementary School	September, 1967	strongly bedded shale
F13	Victoria Bank Street School	September, 1965	dense glacial till
F14	Port Alberni Regional District of Alberni-Clayoquot office	November, 1969	sand and silt
F15	Victoria Elliot Building, Univ. of Victoria	September, 1965	clay
F16	Victoria Tillicum School	September, 1965	stiff brown clay
F17	Victoria Monterey School	September, 1965	stiff brown clay
F18	Courtenay Lake Trail Jr. Secondary School	September, 1967	sandy loam
F19	Cumberland Cumberland Junior Secondary School	September, 1967	sandstone
F20	Victoria McCauley School	September, 1965	stiff brown clay
F21	Victoria Margaret Jenkins School	September, 1965	stiff brown clay
F22	Comox St. Joseph's Hospital	August, 1967	glacial till
F23	Victoria Tolmie School	September, 1965	stiff brown clay
F24	Comox Goose Spit	November, 1968	sand

U – United Engineering seismoscopes.
F – Fairey Aviation seismoscopes.

Record of the earthquake of April 29, 1965. The Fairey accelerograph at the University of Victoria was triggered by this Seattle earthquake. The epicentre was 170 kms. from this site; the magnitude of the earthquake was 6.5 and the depth of focus was 57 kms. Intensities in Victoria varied from IV to V. A copy of the record is shown in Figure 13. Maximum acceleration is approximately 0.03 g. Dr. S. Cherry, at the University of British Columbia, produced the Fourier spectra curve for us which is shown in Figure 14. The response curve peaks at frequencies of 0.2 Hz and 3 Hz.

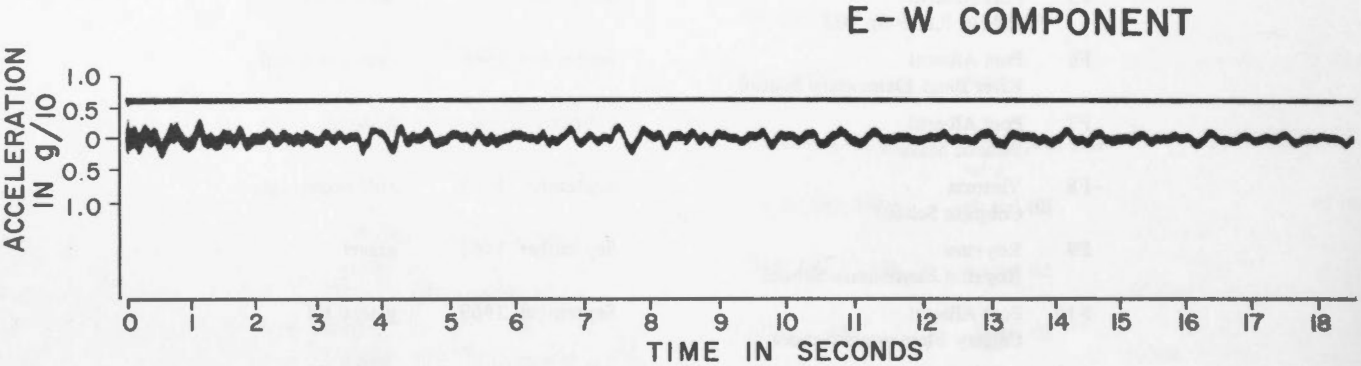

Figure 13. Record of April 29, 1965 earthquake.

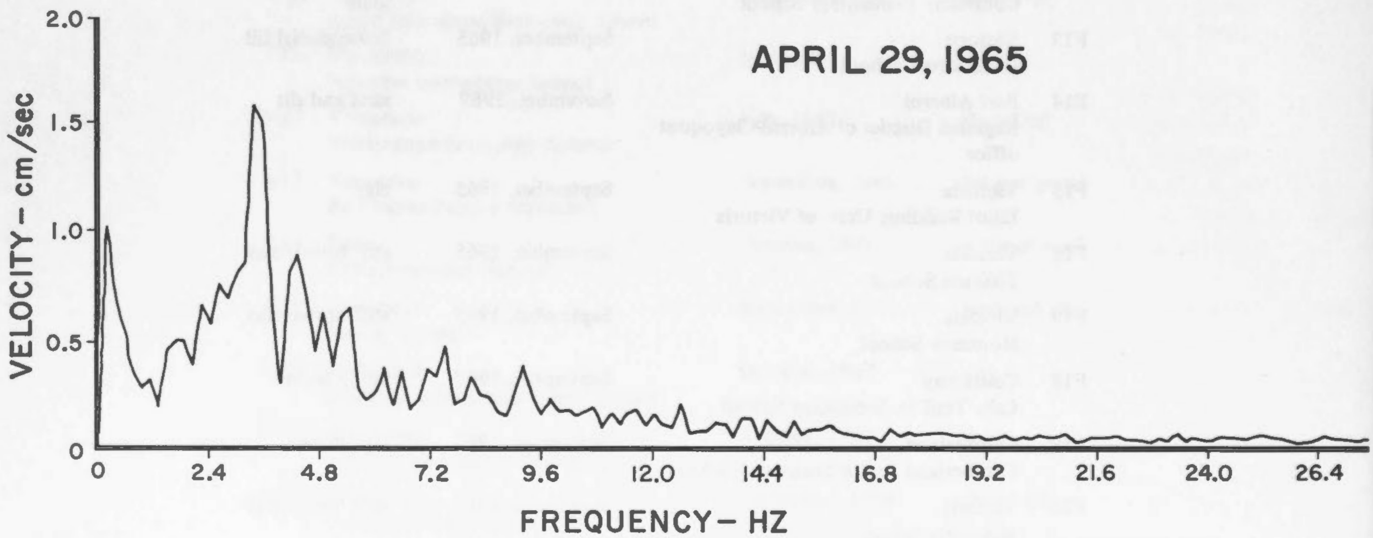

Figure 14. Spectra of April 29, 1965 earthquake.

Acknowledgments

The United States Coast and Geodetic Survey generously loaned one of their instruments for copying in order to get the program started. William K. Cloud of their San Francisco office has been most helpful. A. Camelford of the former Sidney office of Fairey Aviation is responsible for much of the effort to make the first Canadian instrument. There have been many suggestions from private individuals concerning engineering and geological details of sites. Those who have been especially helpful are H. Nasmith of R.C Thurber and Associates of Victoria, and Reid, Jones and Christofersen of Vancouver. Dr. S. Cherry of the Civil Engineering Department, U.B.C and D.A. Matheson of the Vancouver City Building Department have made many suggestions concerning sites in greater Vancouver.

The following organizations have permitted the installation of instruments at their respective sites, and have been very helpful in supplying many details of their structures:

University of Victoria and Public Works Dept. of B.C. – Elliot Building.

Public Works Department of British Columbia – Law Courts in Victoria.

Canadian Pacific Hotels – bus depot in Victoria.

School Board of District 61 – Greater Victoria.

Cowichan District Hospital – Duncan.

MacMillan, Bloedell, and Powell River Company – Alberni.

School Board of District 70 – Alberni.

St. Joseph's Hospital – Comox.

School Board of District 71 – Courtenay.

B.C. Hydro and Power Authority – Ladore Dam and Administration Building.

Department of Transport – Airport Manager – Sandspit.

Columbia Cellulose – Prince Rupert.

School Board of District 39 – Vancouver.

School Board of District 38 – Richmond.

School Board of District 37 – Delta.

School Board of District 44 – North Vancouver.

Greater Vancouver Water District.

University of British Columbia.

Department of Highways of British Columbia.

Department of National Defence – H.M.C.S. Quadra.

City of Port Alberni – Regional District of Alberni-Clayoquot Office.

References

Armstrong, J.E. 1956. Surficial geology of Vancouver area British Columbia. *G.S.C.* Paper 55-40.

__________1957. Surficial geology of New Westminster map-area British Columbia. *G.S.C.* Paper 57-5.

__________1959. Surficial geology of the Sumas map-area British Columbia. *G.S.C.* Paper 59-9.

Cloud, W.K. and D.E. Hudson. 1961. A simplified instrument for recording strong motion earthquakes. *B.S.S.A.*, Vol. 51, No. 2, pp. 159-174.

Fyles, J.G. 1963. Surficial geology of Horne Lake and Parksville map-areas, Vancouver Island, British Columbia. *G.S.C.* Memoir 318.

__________1960. Surficial geology of Comox area. *G.S.C.* Map No. 32.

Halverson, H.T. 1965. The strong motion accelerograph. *Proc. Third World Conference on Earthquake Engineering.*

Hodgson, E.A. 1946. British Columbia earthquake, June 23, 1946. *J.R.A.S. Can.*, Vol. 50, 1946.

Hudson, D.E. 1956. Response spectrum techniques in engineering seismology. *Proc. World Conference on Earthquake Engineering*, Earthquake Research Institute, Berkeley.

Ulrich, F.P. 1935. The California strong-motion program of the United States Coast and Geodetic Survey. *B.S.S.A.*, Vol. 25.

PUBLICATIONS of the EARTH PHYSICS BRANCH

VOLUME 41 – NO. 3

a magnetogram reading machine

B. CANER and K. WHITHAM

DEPARTMENT OF ENERGY, MINES AND RESOURCES

OTTAWA, CANADA 1970

Cat. No.: M70-41/3

Contents

a magnetogram reading machine

B. CANER
Victoria Magnetic Observatory, R.R. 7, Victoria, B.C.
K. WHITHAM
Earth Physics Branch, Ottawa, Ontario.

Abstract. A hybrid analogue/digital device has been designed for semi-automatic processing of records from magnetic observatories. The machine produces hourly and daily mean values in final form (i.e. multiplied by scale factor and with baseline correction added), in a single operation. Output is either on printed sheets suitable for direct photo-offset reproduction, or on punched cards, or on both simultaneously. The machine features high reliability (no errors caused by equipment malfunction or operator mistakes), and moderate accuracy (±1 per cent ±1 gamma). A significant saving in manpower is achieved by its use; three component data for an observatory for one year can be completely processed in about six weeks. One unit has been in operational use at Victoria since 1962, and seven years of data have so far been successfully processed by this method.

Résumé. Un ordinateur hybride à représentation analogique et numérique a été mis au point pour assurer le traitement semi-automatique des données enregistrées par les observatoires magnétiques. L'appareil produit en une seule opération des valeurs moyennes horaires et quotidiennes dans leur forme définitive, c'est-à-dire en tenant compte du facteur d'échelle et des corrections en fonction de la ligne de base. Les sorties sont portées soit sur feuilles imprimées prêtes à la reproduction par procédé photo-offset, soit sur cartes perforées, ou simultanément sous les deux formes. L'appareil est extrêmement sûr en ce qu'il n'est pas faussé par le mauvais fonctionnement de son mécanisme ou les erreurs des préposés, et il est relativement précis (±1 p. 100 ± 1 gamma). L'emploi de cet ordinateur permet de réaliser d'importantes économies de personnel; les données à trois composantes fournies par un observatoire pendant une année entière peuvent être traitées en six semaines environ. Un de ces appareils est en usage à Victoria depuis 1962 et a déjà traité avec succès des données enregistrées au cours d'une période de sept ans.

Introduction

The machine described in this paper is used to process "standard" magnetograms, to provide the hourly mean values in a single operation. Although "on-line" digital magnetographs are in use at a few locations (for example Alldredge and Saldukas, 1964; Hultquist *et al.*, 1962; Andersen, 1969), the majority of magnetic observatories still record their data in analogue form. A major part of the work at each observatory therefore consists in the manual reduction of these data; at its worst, this consists of four steps: a) scaling in mm by making a visual estimate of the hourly mean value; b) multiplication by scale factor; c) addition of baseline correction; d) typing. The typed sheets are subsequently reproduced for publication in a standardized form. Step (b) can usually be eliminated by the use of gamma-graduated scales, provided the scale factors are sufficiently stable to warrant the manufacture of permanent gauges; even step (c) can sometimes be eliminated by the use of more complicated add and multiply scales, but this increases the probability of errors. Altogether, the entire process uses about 4-6 man-months for three orthogonal components of magnetic data recorded in one year.

It is clear that "on-line" digital systems, i.e. recording systems with direct digital output, are the ideal answer to this problem. However, their technical complexity inevitably results in lower reliability than can be obtained for photographic variographs; typically, a standard magnetograph may have one failure (bulb replacement) every 2 - 3 years. The use of digital recording systems will therefore be limited to locations where technical facilities for servicing are readily available. Even if all their technical disadvantages are overcome to the point where they would be used for all new installations, it is unlikely that funds for retroactive modification of all existing installations would be available. At present, and in the foreseeable future, standard magnetographs will therefore continue to be used by most observatories; some "off-line" processing machine is therefore needed for two reasons: a) to cut down the processing time for the production of hourly mean values and thereby free personnel for more productive interpretation work; b) to provide the data in computer-compatible form in order to facilitate the increased use of automatic processing.

Since the "off-line" processing machine need not be located at the observing site, its technical complexity is not an obstacle, nor does its reliability have to be very high. The recording equipment can be kept technically simple and reliable, and processing for one or several stations can be carried out at some convenient central location. It should be pointed out that use of a processing machine is not necessarily the best solution in all cases. It is certainly justifiable in countries where relatively high-priced technical or scientific personnel are used for the manual processing. However, the machine has no inherent scientific advantage (other than better manpower utilization) over manual processing. If low-cost reliable labour is available, it may well be more efficient to do duplicate manual processing with cross-checking, followed by manual keypunching (again in duplicate) if computer-compatible data is required. The purchase or construction of a complex processing machine (and this applies to "on-line" systems as well) must be carefully weighed in terms of the particular economic situation–such as for example the availability of a low-cost clerical labour pool, or the use of prison labour at no cost for punching of data (Malin, 1969).

The most common approach to "off-line" processing involves digitizing of the traces, with subsequent computer processing to obtain the hourly mean values. Machines used for this purpose range from standard commercial X-Y digitizers to a highly complex computer-guided automatic machine using optical scanning (Lenners, 1966). A practical compromise between these two extremes is a specially designed Y-digitizer with manual guiding (Nelson, 1967) which is being used by the Coast and Geodetic Survey in the U.S.A. This machine is available commercially at a cost of about $22,000.

The alternative approach, used in the design described in this paper, is a machine which provides the hourly mean values directly, without the use of a digital computer. By aiming for realistic accuracies (1 - 1.5 per cent) such a machine, using internal analogue computation with digital output, can be built more economically–about $10,000 - $12,000 for a commercial version. The choice between digitizers and such a machine depends on the specific application and facilities of the user. The main advantage of the "magnetogram reader" is that final results are obtained without the need for a computer. Although this is becoming progressively less important as computers become more easily accessible, it is still a significant consideration for installations which are not located near a computer facility. Other than this, the distinction between the two types of system is mainly the obvious distinction between any "special-purpose" and "general-purpose" system. To state the obvious, the special-purpose system is usually more efficient (initial cost, operating time, convenience) for the particular purpose for which it was designed, but it lacks the flexibility of the "general-purpose" system. Specifically, we feel that our magnetogram reader is preferable if print-out of hourly mean values is the primary objective, with or without computer-compatible output as well. However, if higher time-resolution output of all or most of the data is required as well, or if a digitizer can actively be used for other purposes within the organization, then a digitizer/computer system may be preferable.

Design of the magnetogram reader and construction of a prototype unit were carried out at Victoria and completed in 1962; preliminary results have been reported by Caner and Whitham (1962). The prototype unit was "home-made", using surplus and other cheaply available components. The 1962 and 1963 data from the Victoria magnetic observatory were successfully processed on this machine and a commercial version

Figure 1. Overall view of magnetogram reader with keypunch and printer, shown set up for left-handed operator.

was ordered from a local manufacturer. The new version was built to higher engineering standards, and also incorporated modifications which were suggested by operational use of the prototype. Since then a further five years of data have been processed: 1964-1965 with printer output only (see for example Auld and Andersen, 1966, for the 1964 data), and 1966-1967-1968 with punched card output as well (for example Auld and Andersen, 1968). Accuracy and reliability have been maintained at the specified level; the present publication describes technical details of the final design, which has been thoroughly evaluated in operational use as indicated above.

Basic design considerations

The magnetogram reader is designed specifically to provide hourly mean values from standard magnetograms (15 or 20 mm/hr). Output is directly on printed sheets in final form, and of a quality adequate to permit direct photo-offset reproduction in observatory publications. A secondary output is available for digital data in computer-compatible form (punched cards or tape); this output can be used in addition to (or instead of) the printed output.

The main emphasis in the design has been on reliability, ease of operation, and service-free long lifetime. Little emphasis has been placed on the more usual criteria of electronic design, such as compactness, low weight, and power consumption. It was designed for simplicity of operation, to permit use by unskilled personnel with a minimum of supervision and checking. It is liberally equipped with interlock circuits of the "fail-safe" type which would stop operation (rather than give a false read-out) in case of incorrect operation or equipment failure.

The nominal accuracy of the process has been specified as ±1 per cent of ordinate ±1γ in the mean hourly value. Although this compares unfavourably with the accuracy which can be obtained in theory from digitizer systems, particularly the complex optical scanning type of Lenners (1966), it is quite acceptable for this particular application, both from the point of view of data usage and the point of view of the accuracy of the original data (i.e. variograph calibration accuracy, baseline stability, and dimensional stability of the photographic paper). This accuracy applies to magnetogram time-scales of 15 or 20 mm/hr; since the machine operates on a cumulative principle, the accuracy becomes progressively worse when used over shorter intervals, and better for longer intervals; for example an accuracy of 0.1 per cent ±0.1γ can be obtained in the daily mean.

The range of output values is ±9999 (four-digit counter); the ordinate range is 175 mm on either side of the baseline. The scale-factor range is 0 - 15γ/mm for a time scale of 20 mm/hr, with a setting resolution of 0.005 γ/mm. The scale-factor range and setting resolution can be modified at each others expense, for example 0 - 30 γ/mm with 0.01 resolution. Declination is being handled in the same ranges, defining 0.1′ as the basic unit, i.e. scale factor range 0 - 1.5′/mm at 20 mm/hr. The decimal point is subsequently inserted in the output format.

The machine is bi-directional; traces above or below the baseline are respectively added or subtracted. A toggle switch reverses the above pattern, to select upward or downward directions of increase for the particular component. The baseline (i.e. zero reference line) can be positioned anywhere on the magnetogram. Baseline corrections to be added to the scanned value can also be either positive or negative; they are entered by digital thumb-switches to the nearest integer unit (1γ or 0.1′). The final output, printed and/or punched, is the correct algebraic value: (mean hourly ordinate) × (scale factor) + (baseline correction).

Principles of operation

The magnetogram reader is a hybrid analogue/digital device; its operating principle is outlined schematically in Figure 2; optional components are shown in dashed lines. Mechanical analogue methods (ball and disc integrators with suitable gearing) are used to integrate the motion of the hand-guided pointer which follows the trace, and to multiply this integrated value by the scale factor. Analogue-to-digital conversion is performed by a rotating slotted disc and photo-cell. The digital output is accumulated on an electronic counter, where the baseline correction is added as well (by starting the count from a preset value rather than from zero). The counter is bi-directional, i.e. counts are added or subtracted according to the position of the pointer with respect to the baseline.

The accumulated counter reading (i.e. final hourly mean value) is transferred to a decimal storage relay matrix at the end of each hourly interval, and the counter automatically resets to the "baseline correction" value. The output devices can then operate off the storage relays while scanning of the next hourly interval is in progress. Two independent outputs are provided, which can be used separately or simultaneously: an IBM Type 82 Output Writer (electric typewriter with solenoid-actuation of numeric and function keys), and an IBM Type 526 Summary Punch (keypunch with facilities for remote input-output). Both output devices retain their non-specialized functions, as typewriter and manual keypunch, when not in use as the output stage of the magnetogram reader.

The magnetogram is taped to a plate which is driven laterally by a lead-screw at a variable rate controlled by foot-pedal. The operator tracks the trace by means of a pointer which is free to move in the vertical direction; the guiding can be done by directly holding the pointer (useful for following large-amplitude deflections), or more usually by a rotary handle. Since the lead-screw is geared to the integrator "time" input, the integrated output ("ordinate" with respect to "time") is correct whatever the rate of scan, allowing a wide range of scanning speeds as well as mid-scan pauses. The system is completely reversible; algebraically correct values are obtained when retracing backwards after overshoot.

In addition to the basic *hourly mean* system, an optional parallel system accumulates the *daily mean* value to the nearest 1/10 unit (0.1γ or 0.01′), which is then printed (and/or punched) at the end of the 24th hour. Apart from saving some

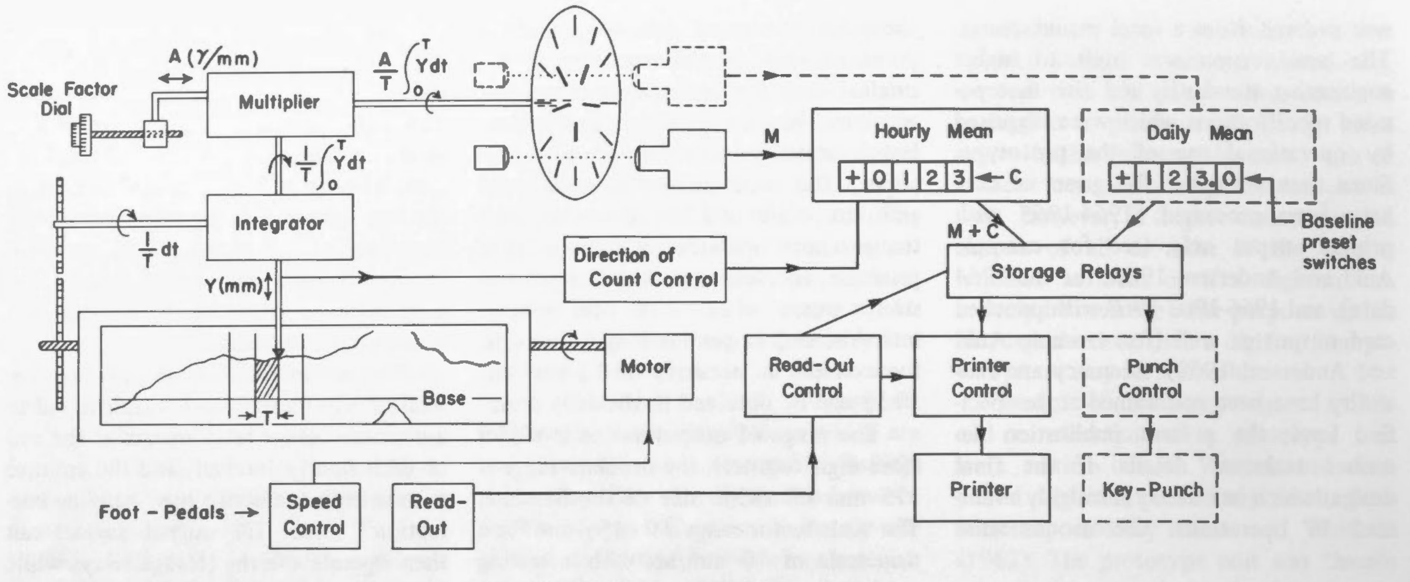

Figure 2. Block diagram of basic principle.

computations, this provides a double-check on the entire electronic and read-out system, since the two channels are processed independently. Since the mechanical system is inherently error-proof (short of actual physical damage), the overall output reliability is therefore very high. In fact no "random" errors which could be attributed to equipment were observed over the entire five-year period.

No line voltage stabilization is necessary, and there are no critical adjustments or alignments which can drift with time. Once zero reference, scale-factor, baseline correction, and direction of increase of the component have been entered, the operator needs to use only the "drive" and "read-out" foot-pedals.

Full technical details of the separate sub-systems (mechanical, control, output) are given in the next three sections. A discussion of accuracy and operating reliability is given at the end of the paper.

Mechanical system

The mechanical system is shown in Figure 3. The magnetogram is taped to the carriage plate (1), using the baseline (zero) setting bar (2) to determine its position; the setting bar itself can be moved up or down over the hinged rod (3), to accommodate different types of magnetogram layout. Once the magnetogram has been positioned, the setting bar is swivelled out of the way, to give unimpeded view of the entire magnetogram. The carriage itself consists of a heavy (0.5-in. thick) aluminum plate; it is driven by a 0.875-in. diameter lead-screw (4), but its weight rests on two 1.125-in. diameter polished steel bars (5) along which it can slide on linear-motion (ball-slide type) bearings. This provides minimum wear on the lead-screw mechanism. The entire system is sufficiently massive, and the motor (6) sufficiently geared down (54 in.-lb output torque), to permit the operator to rest his arm on the plate and "travel along" with the carriage, for maximum comfort and minimum fatigue. The operator can also do work on the carriage while it is moving, such as for example exchange magnetograms during the carriage return.

The free end of the lead-screw is geared (7) to the time input (8) of the first ball and disc integrator (9); this provides the "time-scale" (dt) input to the system. The carriage can therefore be driven at variable speed, to accommodate different degrees of trace disturbance or operator competence. The speed is controlled by a foot-pedal which varies (via a control circuit) the armature voltage of the 1/8 HP DC motor (6), providing smooth variation from virtually motionless creep to a maximum speed of about 5 mm/sec. A switch built into the foot-pedal also provides "dynamic braking" of the motor, to provide instantaneous stop without coasting. The motor can be reversed for backing up in case of overshoot or tracking error; since counting direction is reversed by the same circuit, the overshoot error is corrected if the operator retraces over the same path, i.e. correct algebraic reading is maintained.

The pointer itself consists of a small black dot engraved on the underside of a plexiglass disc (10) fixed to the pointer bar (13). The disc slides just above the magnetogram, providing a parallax-free optical system without the need for rigidly fixed location of the operator's eyes. This permits the use of auxiliary lighting or visual aids to suit the particular operator's convenience and eyesight, such as the ring-lighted magnifying lens shown in Figure 1. The pointer is normally guided to follow the trace by means of a rotary handle (11), at a rate of 3 mm per turn. However, it can also be guided directly by hand if the trace excursions are very steep or if it otherwise suits the operator's convenience. The guide crank box (12) containing the transmitter synchro is removable and can be relocated for maximum operator convenience; in particular it can be located to the left of the pointer bar (as shown in Figure 1) for use by a left-handed operator. This provides a significant increase in operating efficiency and accuracy when used by left-handed operators (about 10 per cent of the population)–a point often overlooked in the design of equipment of this type. The synchro-receiver is geared to the rack of the

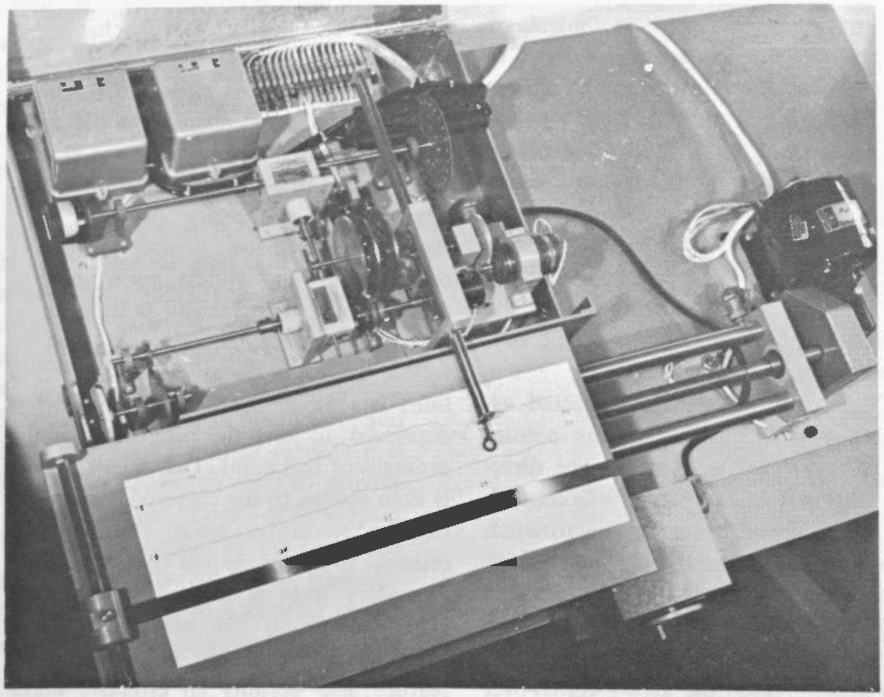

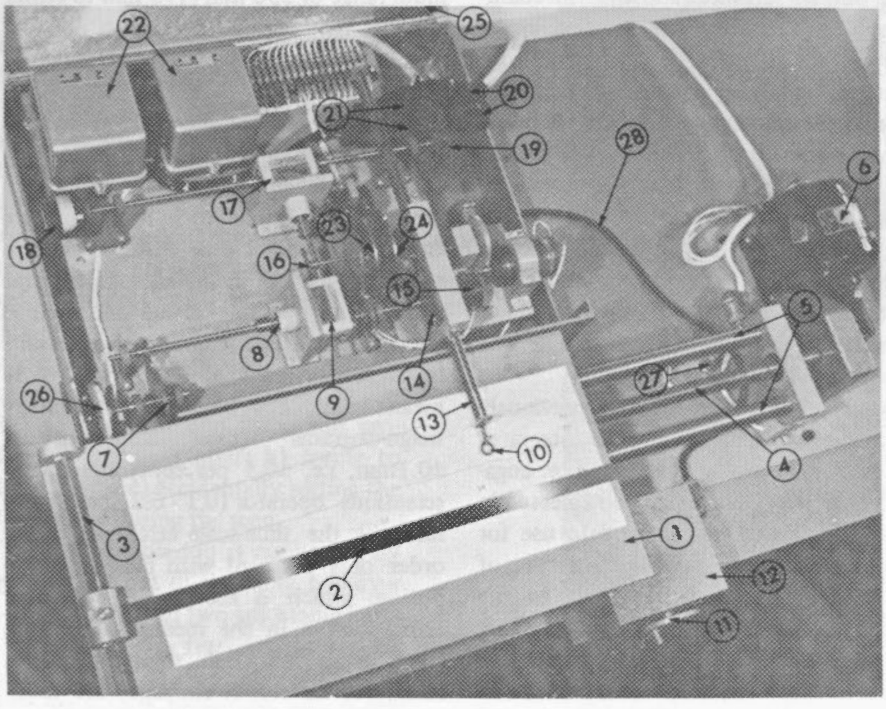

(1) Carriage plate
(2) Base-line setting bar
(3) Hinged rod
(4) Lead-screw
(5) Support bars
(6) Carriage motor
(7) Gear linkage to lead-screw
(8) Time-scale input of integrator
(9) Ball and disc integrator
(10) Pointer dot
(11) Guide crank
(12) Guide crank box (shown mounted for right-handed operator)
(13) Pointer bar
(14) Input gear of clutch
(15) Clutch
(16) Ordinate input of integrator
(17) Ball and disc multiplier
(18) Scale-factor dial
(19) Rotating disc
(20) Light sources
(21) Photo-cells
(22) Photo-cell amplifiers
(23) Cam, direction of count control
(24) Cam, integrator limit alarm
(25) Hinged metal cover
(26) Time-scale cam
(27) Carriage return microswitch
(28) Servo linkage, guide crank

Figure 3. Mechanical (analogue) system of magnetogram reader. Component numbers are referred to in text.

pointer bar, rather than directly to the input of the integrator; this means that the servo linkage and gearing need not be particularly tight or accurate, as long as it drives the pointer with acceptably low slippage. The gearing needs to be backlash-free only between the pointer bar and the integrator input.

The pointer bar (13) consists of two parallel rods spaced 1 in. apart, riding in two sets of linear-motion bearings in a 5.5-in. wide bracket. This prevents rotation or sideways motion of the pointer which would reduce tracking accuracy. The lower shaft is a 0.375-in. diameter round-stock rack, which rides directly over the input gear (14) of an electrically-operated clutch (15). The output shaft (inner concentric) of the clutch drives the linear-motion (y-ordinate) input (16) of the integrator through a gear and pinion/rack set. The output of the integrator is directly linked to the input of the second ball and disc integrator (17), which is used as a multiplier. The multiplying factor is entered by a 4-digit, 100-turn, digital dial (18) with locking brake. The dial rotation is converted to the linear motion of the ball slide by a pinion/rack drive within the integrator. With the chosen gear-ratios and other parameters, the dial setting is twice the desired scale-factor for a time-scale of 20 mm/hr; it can be set to within 0.005 units of scale factor, although 0.01 units is generally adequate. For example, dial setting 1602 represents 8.01γ/mm or 0.801′/mm. The dial range is 0000 - 3000, i.e. scale-factor ranges 0 - 15γ/mm or 0 - 1.5′/mm. Lower sensitivities (i.e. higher scale factors) can be accommodated by increasing the number of holes in the output disc (see farther on), with a corresponding decrease in setting resolution.

For magnetogram time-scales other than 20 mm/hr, an appropriate proportionality factor has to be applied to the dial settings. For example, if T = 15 mm/hr, a speed common in La Cour magnetographs, a dial setting of (20/15) X 1602 = 2136 would be required to obtain a scale factor of 8.01γ/mm. The machine can readily be used with acceptable accuracy (1 - 2 per cent) to about 10 mm intervals, but for shorter intervals it becomes progressively less satisfactory.

The output of the multiplier directly drives a light-weight fibre disc (19); with such minimal inertial loading the accuracy and lifetime of the ball and disc integrators is very high. The analogue-to-digital conversion is performed by the rotation of this disc between a light-source (20) and photo-cell (21). An outer ring of 24 holes drives a photo-cell at 24 counts per rotation, to provide the accumulated hourly mean value on a totalizing counter, in integer units (gammas, or minutes of arc for declination). A second ring of 10 holes can be used to drive a separate photo-cell, to provide an accumulated daily mean value, to the nearest 1/10 unit (0.1γ or 0.01′). The use of two independent channels permits a double check of the complete following, electronic, control, and read-out system.

The output of the photo-cells is processed by amplifiers (22) which provide uniform-width pulses regardless of the rate of rotation of the disc. The output of the amplifiers is fed directly (DC coupling, and with no intervening controls or reversals) to the inputs of two separate bi-directional counters. The amplifiers provide large-amplitude (24-volt) pulses at very low impedance (under 100-ohm); the counter input impedance and sensitivity can therefore be kept very low (and shunted by large capacitors), to provide immunity from noise pick-up, in spite of the heavy transients originating in the electromechanical components (the key-punch in particular).

Counts are added or subtracted according to the position of the pointer with respect to the baseline. The direction of count of the counters is controlled by a low-differential microswitch riding on a 4-in. diameter cam (23) which is geared to the y-ordinate system. The cam is fixed to its shaft by means of an adjustable hub-clamp. Coincidence between the "electrical zero" (cross-over from add to subtract) and the "mechanical zero" (stationary position, i.e. cross-over from clockwise to anti-clockwise rotation) is carried out on initial installation by adjustment of this hub. A second microswitch and cam (24) on the same shaft operate an alarm buzzer to indicate that the travel limit of the integrator is being approached. Although end-stops are provided as well, this alarm protects against possible distortion of components by forcing against the end stops.

The clutch (15) mentioned previously connects the pointer bar to the integrator input. It is normally energized (i.e. engaged) and its existence can be neglected in normal operation. It comes into use for two special functions: a) initial setting of the "zero" of the mechanism to the magnetogram baseline, and b) tracking secondary (off-scale) traces without loss of continuity. The zero setting needs to be carried out only once at the start of each day's run, or after any power-line interruption. The pointer is moved until zero is reached, as indicated by an audible click of the relay which operates on crossing between "add" and "subtract" (see relay L_{15} of Figure 5a). The clutch foot-pedal is then depressed, disconnecting the pointer from the mechanism. The clutch is of the "spring brake" type, i.e. the output shaft is locked when the input shaft is disconnected. The mechanism is therefore "frozen" in the zero position, the "free" pointer is moved to the baseline on the magnetogram, and the foot-pedal is released to re-engage the clutch. Coincidence of the baseline and mechanism "zero" is thereby obtained, and remains set until the operator or a power cut releases the clutch again. Setting accuracy and repeatability is 0.2 mm or better. A similar procedure is used to follow off-scale traces: when the trace limit is reached the clutch foot-pedal is depressed, locking the mechanism at the ordinate of this point. The "free" pointer is then moved to the corresponding point on the secondary trace, the pedal is released to re-engage the clutch, and the secondary trace is tracked in the usual way. Return to the primary trace is achieved by the same procedure. This feature also permits an effective maximum range of 350 mm (175 mm to either side of the baseline), in excess of the actual 300 mm mechanical travel range of the pointer bar.

The accuracy of the analogue system is limited almost entirely by the accuracy of the time scale, since the output is directly proportional to it. Any departure from the nominal time scale, whether a real irregularity in magnetogram time scale or an operator-caused one such as uncorrected over- or under-shoot, results in a proportional error in the hourly mean value. For standard observatory magnetograms (time scale usually ±0.1mm, i.e. ±0.5 per cent) and a conscientious operator (0.1 - 0.2 mm "resolution"), the time-scale errors are of the order of 1 per cent with random distribution, which is acceptable. All other error sources in the mechanical system (such as gear backlash, shaft distortions, integrator or clutch slippage) are negligible compared to the above figure. For records obtained from portable instruments and other magnetograph installations with irregular time scales, or for careless operators, the time-scale error could become prohibitive. An optional "time-scale interlock" has therefore been incorporated, to block read-out if the time scale is incorrect. A microswitch is operated by a notched cam (26) geared to the carriage lead-screw; the counts are accumulated on an electromechanical counter with decimal read-out contacts. This reading is a measure of the carriage travel. The counter is bi-directional, the direction of count being switched when the direction of carriage travel is reversed; the time-scale counter therefore provides a true measure of net carriage travel, regardless of reversals. The counter is automatically reset to zero during each hourly-mean print-out. With a 15-notch cam, 20 mm of carriage travel provide 94.5 counts; the cam is removable, and when processing 15 mm/hr records it is replaced by a 20-notch cam to provide the same count per "hour" of time scale.

The decimal output of the time-scale counter (nominally 94.5 per magnetogram hour) is wired to a control circuit which inhibits the read-out command if the reading differs by more than a specified percentage from the nominal value. The percentage can be set by a front-panel switch (see Figure 4) to 1, 2, 3, or 4 per cent. For example, with the switch set to 1 per cent, read-out cannot be obtained unless the time-scale counter reading is 93, 94, or 95; for 2 per cent the allowable range is 92 - 96. Use of the time-scale interlock therefore provides protection not only against inaccuracies caused by magnetogram time-scale irregularities or operator carelessness in overshooting the time-mark, but also against major operational errors such as: a) forgetting to read out one value and proceeding to the next hour; b) trying to read out twice; c) accidentally hitting the read-out pedal during the scan.

The entire table-top is connected by hinges to the front of the table, and by a lead-screw crank and two adjustable locking brackets at the rear. Its tilt can be adjusted to suit the operator's size and convenience, from horizontal to a maximum of 45°; about 30° is found to be the most comfortable position in most cases. Since the pointer moves just above the trace, i.e. is virtually parallax-free, the operator can use any lighting or vision aids he chooses, either permanently or occasionally. He can use just the general room lighting, or an additional fluorescent lamp clamped to the table, or (as

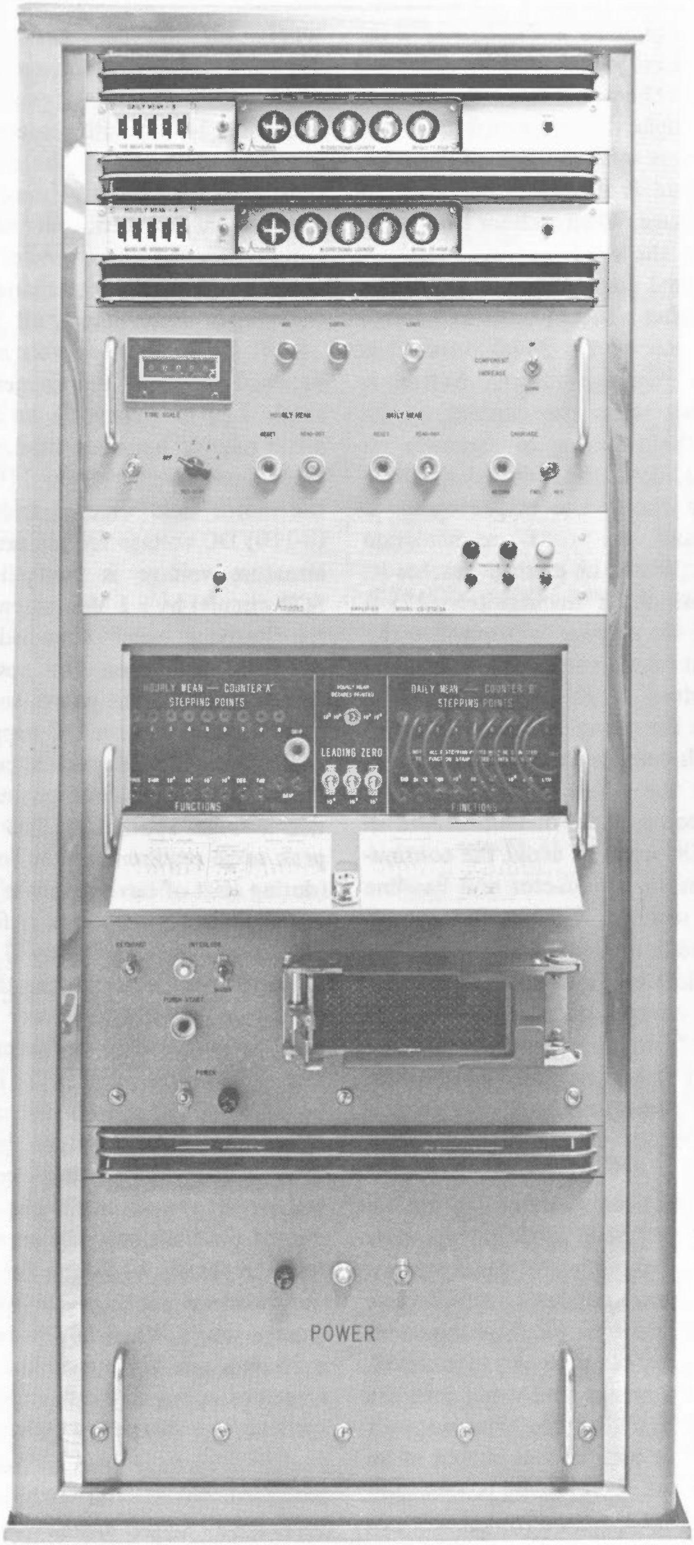

Figure 4. Control assembly, containing (from top to bottom): daily mean counter, hourly mean counter, main control unit, storage relays, print control unit (shown with opened access door to patch-board), punch control and power supply.

shown in Figure 1) a ring-lighted 5-in. diameter magnifying lens, which can be swung out of the way if not required.

Actual operation is very simple: the zero-set bar is swivelled out of the way, and the speed foot-pedal is depressed to run the carriage. When an hour time-mark is reached, the read-out foot-switch is depressed, and scanning continues to the next hour after a short (∿ 0.1 sec) delay. When the end of the 24-hour record is reached, a "carriage return" button is pressed; this starts the carriage on its return, without having to manually reverse or hold down the foot-pedal. During this return travel, the magnetogram is removed and the next magnetogram positioned. When the carriage reaches its "start" position, a microswitch (27) is struck and the carriage is stopped, ready for the next record's scan. The time taken for the return is 90 seconds, which is ample time for changing of the magnetograms. Each component is processed separately for the whole year, rather than the three components of each record in sequence, in order to avoid the continuous changes in scale-factor and baseline correction settings. If the magnetograms are recorded from 0 to 24 U.T. (as is the case for Victoria), a toggle switch at the rear of the control unit can be pre-set to "automatic"; in this case the carriage return cycle is automatically triggered by the "daily mean" read-out. No further controls need be used in normal operation.

An experienced operator can process comfortably, without particular pressure, an average of about eight magnetograms (one component) per hour. An effective rate of well over one month/component per working day can easily be maintained, even if some breaks and other jobs are interspersed to reduce the monotony of the work. The total annual output of an observatory can therefore be processed in about 6 - 7 weeks—a considerable saving in time over manual methods.

Main control assembly

A) Power and count control circuits (Figure 5a). The power supply is mounted on a separate chassis and consists of: a) two unregulated 24-volt–3-amp DC supplies, and b) a modular variable-speed supply for the DC motor. The two 24-volt supplies are connected in series with centre grounding, providing +24-volt and −24-volt with respect to ground (denoted as 0 volt in the drawings), as well as 48 volts. Most of the components operate on 24 volts, but 48 volts are required for the output writer circuits. In order to maintain interchangeability of the plug-in components, all relays have 24-volt coils; where 48-volt operation is imposed by circuit requirements (for example L_{30} on Figure 6), an appropriate series resistor has been used. The motor controller provides fixed 110 VDC for the motor field winding and a variable (0-110) DC voltage for the armature; the armature voltage is controlled (via an SCR circuit) by a 1 Meg potentiometer in the "carriage speed" foot-pedal. A main ON-OFF switch on the power supply chassis switches the power to the entire system, i.e. the above DC supply units as well as the AC loads such as counters and typewriter motor. Total power consumption averages about 150 - 200 watts, with peak surge requirements up to 300 watts (during start of carriage return).

The armature voltage is fed through the "forward-reverse" relay (L_{11}), which is normally not energized, to the "power" relay (L_{10}); with the power relay energized it is then fed to the motor armature. The power relay (L_{10}) is energized by 24 volts either from the microswitch in the foot-pedal, or from the "carriage return" relay (L_{17}); however, the relay coil circuit 0 volt end is cut a) if either one of the limit switches on the carriage frame is struck, b) during the transfer of the counter readings to the read-out storage relays. When L_{10} is de-energized, a 10-ohm resistor is switched across the armature, acting to dynamically brake the carriage to a sharp stop without coasting.

The "carriage reverse" relay L_{11} is energized by 0 volt either from the FWD-REV toggle switch on the front panel, or from the "carriage return" relay L_{16}. It reverses a) the direction of rotation of the motor (by reversing the armature voltage polarity), and b) the direction of count of the main counters.

Relays L_{16} and L_{17} are energized and self-locked either by the manual RETURN push-button on the front panel, or (if the rear mode control switch is on "automatic") by a pulse from the "daily mean read-out" cycle. These two relays perform the following functions: a) energize L_{11} to reverse the carriage travel direction; b) energize L_{10} to provide carriage power; c) switch the speed control from the foot-pedal potentiometer to a fixed-setting locking potentiometer on the rear panel. They also energize an auxiliary "carriage return" relay L_{21}, which locks the counters at their preset reading, and which has delayed release by means of a 120-mfd capacitor across the coil. All three relays remain locked until the carriage return microswitch is struck, opening the 0 volt line to the upper ends of L_{16} - L_{17} and releasing these two relays to stop the carriage travel. The release of L_{16} also de-energizes L_{21}, which releases with a time delay of about 0.1 second. This ensures that the carriage has come to a complete stop before the GRD is removed from the counter RESET inputs, so that the counters remain accurately at the preset (baseline correction) setting, ready to start scanning of the next record.

The counting direction control lines (115 VAC from the microswitch on the mechanical assembly) can be reversed either by the "carriage reverse" relay L_{11}, and/or by a front-panel toggle switch which is set for the direction of component increase on the magnetogram (UP or DOWN). If the counter function is ADD, only the "add" pilot light is energized. If the function is SUBTRACT, relay L_{14} is energized in addition to the "subtract" pilot light. In order to maintain maximum lifetime for the low-differential microswitch, all switching is carried out on the AC line, with subsequent rectifying to operate the DC relay L_{14}. A small (0.01-mfd) capacitor provides additional protection for the contacts. This "subtract" relay (L_{14}) applies the bias voltage (+25 VDC) from the counters to the "direction control" terminals of the counters, thereby switching the counters into the "subtract" mode. When these terminals are open-ended or grounded, the counters remain in the normal "add" mode. The counters fea-

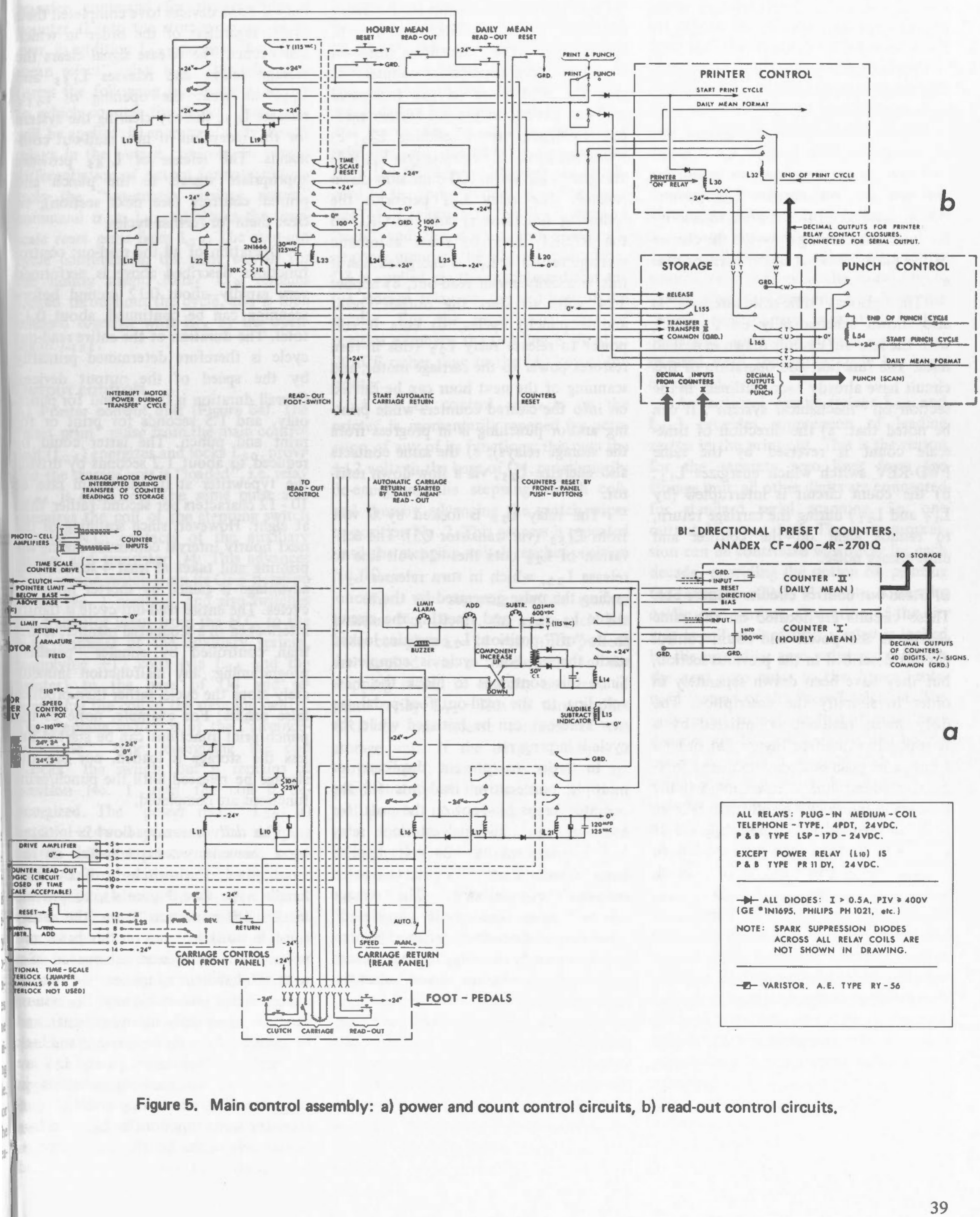

Figure 5. Main control assembly: a) power and count control circuits, b) read-out control circuits.

ture automatic internal reversal when counting through zero, e.g. 5, 4, 3, 2, 1, 0, −1, −2, −3. . . .

The subtract relay L_{14} also energizes L_{15}. This is a relay of the general-purpose type which is very noisy in its operation. It is not used as a load-carrying relay, but it provides a loud audible click when energized or released, i.e. on cross-over between add and subtract. This permits the operator to set the baseline to zero by ear instead of having to watch the change of the pilot lights out of the corner of his eye.

The optional "time-scale interlock" is also shown schematically on Figure 5, with the relevant circuits drawn in dashed lines. The function and operation of this circuit have already been outlined, in the section on "mechanical system". It can be noted that: a) the direction of time-scale count is reversed by the same FWD-REV switch which energizes L_{11}; b) the count circuit is interrupted (by L_{17} and L_{21}) during the carriage return, to reduce wear on the counter and unnecessary noise.

B) Read-out control circuits (Figure 5b). These circuits are located on the same chassis as the power and count control circuits described in the previous section, but they have been drawn separately in order to simplify the description. The daily mean read-out is initiated by a foot-pedal switch (see Figure 5a), or by a front-panel push-button switch; the foot-pedal read-out line is interrupted if the time-scale interlock is activated (Figure 5a). Provided both L_{23} and L_{25} are at rest, +24 volts is thereby applied to energize L_{22}. This relay is self-locked, and also a) cuts power to the coil of L_{10}, i.e. the carriage cannot be driven; b) energizes L_{12}. L_{12} in turn applies GRD to the "transfer I" terminal of the storage unit; the reading from counter I is thereby transferred to the storage relay matrix. A control relay on the storage unit (L_{155}) is also energized and a) releases L_{12}, thereby stopping the transfer command; b) energizes L_{23} (via transistor Q5). The pair of relays L_{23} - L_{24} (with assistance from L_{25}) forms a monostable (single-shot) circuit which provides a single pulse of duration 0.1 second.

The relay L_{23} performs the following functions: a) applies GRD from L_{24} to the counter RESET terminals (directed by L_{19} to the appropriate counter); b) cuts the +24 volts to the foot-pedal read-out switch, to prevent further read-out commands from reaching L_{22}; c) resets the time-scale counter (via L_{19}); d) energizes L_{24} via a 100-ohm slow-down resistor. The relay L_{24} performs the following functions a) cuts the GRD to the RESET lines; b) starts automatic carriage return if L_{19} is energized, i.e. if this is a *daily* mean read-out; c) applies +24 volts to start the output (print and/or punch) cycles; d) cuts 0 volt power to release relay L_{22} (this in turn restores power to the carriage motor, and scanning of the next hour can be carried on into the cleared counters while printing and/or punching is in progress from the storage relays); e) the same contacts also energize L_{25}, via a slow-down resistor.

The relay L_{25} is locked by 0 volt from L_{155} (via transistor Q5). The activation of L_{25} cuts the +24-volt line to release L_{23}, which in turn releases L_{24}, ending the pulse generated by the monostable L_{23}/L_{24} and resetting the circuit to its "off" position. L_{25} remains locked until the read-out cycle is completed. Since this continues to block the +24-volt line to the read-out foot-pedal, no new read-out can be initiated while the cycle is in progress.

In order to prevent duplicate or multiple consecutive read-outs (if the operator keeps his foot on the pedal for too long), an additional interlock relay L_{20} is energized by +24 volts applied from a second set of contacts on the read-out foot-pedal switch. The "storage release" pulse (i.e. "cycle completed" signal) from the output device(s) is interlocked through this relay; no release can occur and L_{25} remains locked unless the foot-pedal has been lifted.

Once the output device(s) have completed their cycle (see next section), GRD is applied to the RELEASE terminal of the storage unit. A switch at the rear of the control unit selects the mode of operation: print only, punch only, or print and punch simultaneously. In the latter mode, the release signal is applied only if *both* devices have completed their cycle, regardless of the order in which this occurs. The release signal clears the storage relays and releases L_{155} and L_{165} as well; the opening of L_{155} releases L_{25}, thereby clearing the system for the reception of new read-out commands. The release of L_{165} provides appropriate signals to the punch and printer controls (see next section), to clear them for further cycles.

Operation of all the read-out control functions described above is performed very rapidly–about 0.12 second before scanning can be continued, about 0.15 total. The duration of the entire read-out cycle is therefore determined primarily by the speed of the output devices. Overall duration is 0.3 second for punch only, and 1.5 seconds for print or for print and punch. The latter could be reduced to about 1.2 seconds by driving the typewriter at its maximum rate of 10 - 12 characters per second rather than at eight. However, since scanning of the next hourly interval continues during the printing and takes at least 4 seconds, no advantage is gained by shorter print-out cycles. The entire read-out cycle is tightly interlocked in a sequential manner, rather than controlled by simpler "parallel" programming; any malfunction immediately stops the cycle, rather than produce false results. For example, none of the punch/print functions can be started unless the storage is loaded, nor can the storage be released until the punch/print functions are completed.

The *daily* mean read-out is initiated by a momentary-contact switch on the front panel; the switch is of the bat-handle type (see Figure 4), to provide tactile differentiation from the other (push-button) switches on this panel and prevent accidental read-out instead of a reset. This switch: a) applies +24 volts to energize the interlock relay L_{20} (same function as in daily mean read-out), and b) applies +24 volts to energize and lock L_{18} and L_{13} (provided L_{23} and L_{25} are at rest, i.e. no read-out cycle is in progress). The relays L_{18} and L_{13} perform the same functions as L_{22} and L_{12} respectively in the hourly mean read-out, i.e. initiation of read-out controls and transfer command for the reading of counter II into the storage relays. However, in addition L_{18} energizes the "daily mean select" relay L_{19}. This relay performs the following functions: a) selects to which counter the "reset" from L_{23} will be applied; b) energizes "daily mean" relays in the output controls, to permit differentiation of output formats; c) controls the "automatic carriage return" command from L_{24}; d) blocks the time-scale reset pulse from L_{23}. The read-out cycle continues in the same way as for the hourly mean. Relay L_{19} remains locked throughout the cycle, and is then released together with L_{25} by the opening of L_{155}.

Output controls

A) Printer control unit (Figure 6a). The "start print" pulse from the main control unit (L_{24}) energizes and locks L_{30}, provided the storage unit is "loaded", i.e. relay L_{165} is energized. The same pulse also energizes the coil of the stepping switch via the N.C. contacts of the auxiliary springs and transistor Q4. This advances the stepping switch from its OFF position to the No. 1 position, and also switches the transistor input from the N.C. to the N.O. terminal of the auxiliary springs, reapplying +12 volts (via L_{34} and the printer) to the base of Q4 and re-energizing the coil of the stepping switch. The stepping switch is of the "advance-on-release" type: energizing the coil "cocks" the switch, but it remains at position No. 1 until the coil is de-energized. The "power relay" L_{30}: a) applies +24-volt power to the stepping switch coil, the printer solenoid "common", and other circuits; b) switches on the oscillator circuit Q_1 - Q_2. The output pulses of the oscillator are of about 0.030 second duration (controlled by R_2) and with a repetition rate of about eight pulses per second (controlled by R_1); neither of these parameters is critical, and variations over a wide range (±30 - 40 per cent) do not disrupt performance.

The pulses from the oscillator are applied through transistor Q3 and relay L_{31} to the wiper of one of the stepping switch decks. With L_{31} at rest they are applied to the hourly mean deck; if L_{31} is energized they are applied to the daily mean deck. The stepping switch points (1 to 9) are wired to a patchboard-panel, which can be wired by plug-in cords to control the desired print-out format: space or tab functions, insertion of decimal points, line return after daily mean print-out, etc. The pulse is thus applied from the No. 1 point through the patch-cord to the appropriate function or "scan line". For example, if "No. 1" is wired to "sign" and the storage unit contains a negative number, the -24-volt pulse from Q3 is applied via the patchboard and the (-) storage relay to the (-) key of the printer. For the more usual case of positive numbers, the (+) line is wired to SPACE rather than to the (+) key of the printer.

A set of control contacts on the printer is momentarily opened by actuation of any of its functions; this cuts the +12 volts to the base of Q4, momentarily de-energizing the stepping switch coil, and thereby advancing the switch wiper to position No. 2. This process is repeated until the stepping switch reaches position No. 10.

When the stepping switch reaches position No. 10, i.e. the print cycle has been completed, -24 volts (not pulsed) are applied via a third deck on the stepping switch to energize the "end of print" relay L_{32}. This in turn applies GRD to the release terminal of the storage unit. If the output function is "print only", this release signal is applied directly; if the function is "print and punch", the release signal originating from the punch unit is taken through the normally-open upper contacts of L_{32}, i.e. release cannot occur until both output devices have completed their cycle. The release signal clears the storage unit; L_{165} is released as well, de-energizing L_{30}. This in turn cuts the +24-volt power of the stepping switch coil, thereby advancing the switch from No. 10 to its OFF position, ready for the next cycle.

Again, the entire cycle is interlocked in a serial sequence for reliable fail-safe control. If for any reason a pulse failed to operate the typewriter function (for example, if only a fraction of the pulse duration was applied on the first pulse), the printer control contacts would fail to open and the stepping switch would not advance; it would not move to the next position until the next (or any) pulse had fulfilled the function required at this position. This in turn means that performance is not critically affected by reasonable changes in parameters such as mechanical condition of the stepping switch or printer, or oscillator pulse length and repetition rate. Similarly, any data gap (failure of a decade digit in the counter or of a relay in the storage unit) would stop the stepping switch in the "blank" position and prevent all further operation, since the storage cannot be released until the entire cycle has been completed.

An optional circuit (relays L_{36} and L_{37}) provides suppression of leading zeroes in the print-out. This is the reason for the separate zero lines from the storage unit; all other digits are connected for standard serial scanning, i.e. one output line per digit. The zero suppression can be controlled separately for each decade, providing the option of printing for example 00.3, 0.3, or .3 in the declination output. Operation of the circuit is self-explanatory; a relay is locked by the preceding zero pulse and redirects the next zero pulse to the "space" solenoid instead of the "zero" solenoid. The only point to note is that if only three decades are being scanned in the hourly mean, the relay L_{36} is locked by -24 volts via the toggle switch and L_{31}, i.e. a dummy first-decade zero is assumed.

B) Punch control unit (Figure 6b). The Type 526 Summary Punch has internal scanning and logic, so that the control circuits need to provide only through-wiring from the storage unit to the punch terminals and basic controls. The "start punch" pulse energizes L_{53}, which initiates the punch cycle. An interlock relay, L_{55}, is normally energized; it is released by punch failures such as power off, empty input card hopper, or over-full output card stacker. When de-energized, it operates an alarm buzzer, and also blocks the "start punch" pulse from reaching L_{53}.

A "scan end" signal to the keypunch

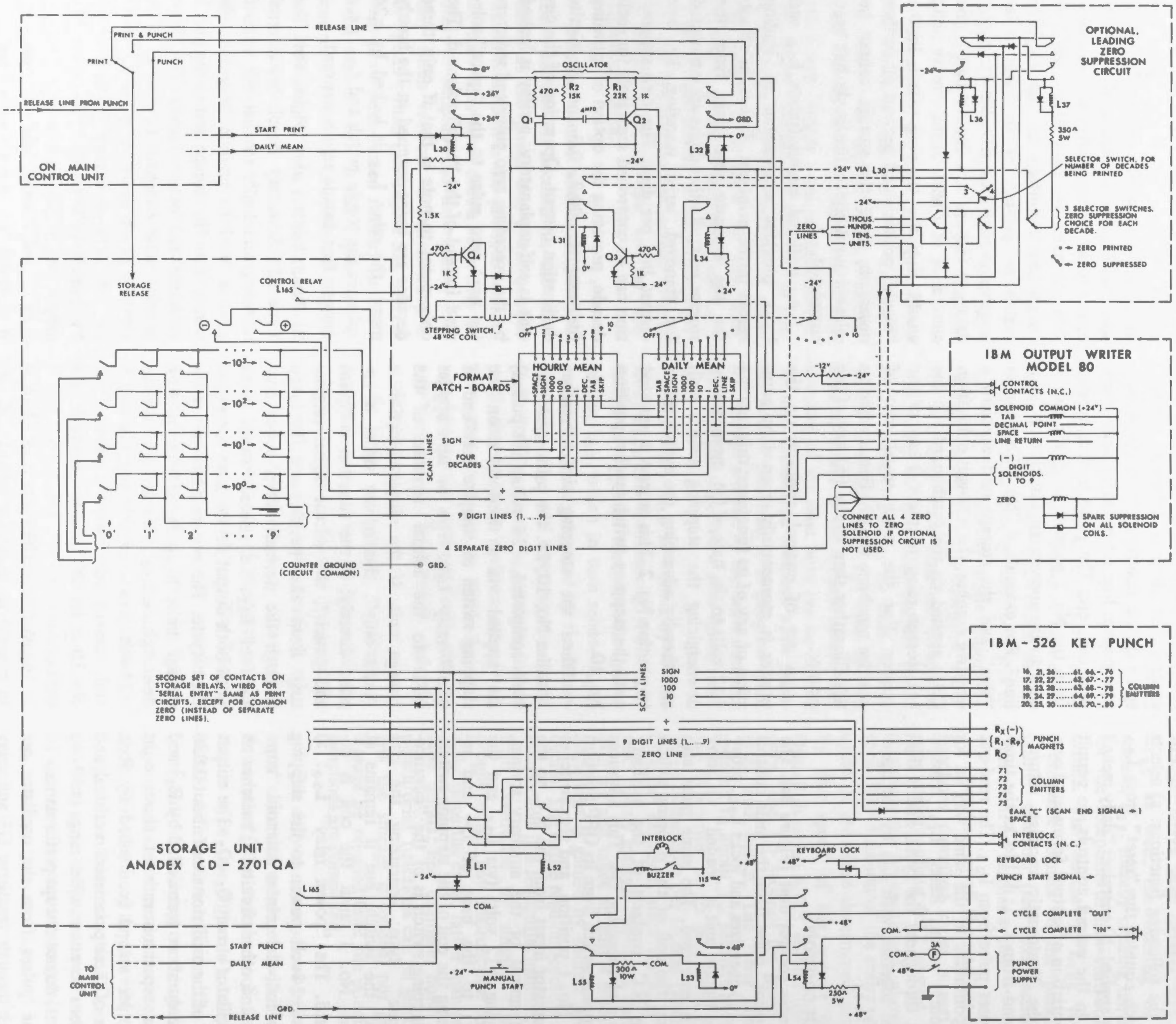

Figure 6. Output control circuits for a) printer and b) card punch.

is initiated by wiring the "units" scan line to the EAM–C hub; an internal "cycle complete in" signal is thereby generated within the punch to energize L_{54}, which is locked via L_{165} in the storage unit. This "cycle completed" relay, L_{54}, performs two functions: a) it disconnects the +48-volt line from the "cycle complete out" terminal of the punch, thereby terminating the cycle and preventing further punching; b) applies GRD to the release terminal of the storage unit; this clears the storage and opens L_{165}, which in turn releases L_{54} to leave the punch ready for its next cycle.

The punch keyboard is automatically locked during the cycle (see diode connection between the "punch start" and "keyboard lock" terminals). It can also be locked continuously by a toggle switch on the control unit, to prevent accidental manual punching by the operator, or unauthorized manual use during the operator's absence. The latter is particularly important because the data is entered into card decks which are pre-punched with date and serial numbers.

The unit was wired for five-digit fields (sign and four decades); the layout of these fields on the card can be controlled by the plug-in patch-cords on the control panel and by the standard program card of the punch. At present columns 16-80 of each card are used for the data, leaving columns 1-15 for non-data information (station and component identification, date, sequential card serial numbers). During daily mean read-out, relays L_{51} and L_{52} are energized, and change the output format by skipping five columns (71 - 75 in this case) before punching the daily mean (in columns 76 - 80). This permits easy visual identification of the daily mean on the card, and also clearly differentiates between the first and second card of each day.

The entire output deck is subsequently computer-processed in two steps. At present the printer output sheets are not used for the Victoria publications; these are now produced from the computer print-outs. The first-pass program performs two functions: a) checks the card order (sequence of serial numbers), and b) computes the daily mean from the 24 hourly means, compares it to the punched daily mean, and provides a warning print-out if they differ by more than a specified limit (usually set to 0.25 or 0.30 gamma). In the second-pass program, all auxiliary computations are carried out: means of the hour for each month, summary means (for all days, Q-days, and D-days) by month and season, and various cross-checks. The final results are output-printed in a format suitable for direct photo-offset reproduction in publications (for example Auld and Andersen, 1968).

Reliability and accuracy

As mentioned at various points in the description of the circuits, the primary consideration in the design has been high reliability, both in terms of service-free operation and in terms of data output. It is hoped that this reliability can be maintained over the lifetime of the machine (estimated at well over 200 observatory-years of data), as all components have been carefully selected to operate well within their rated capabilities. The mechanical components of the analogue system operate at very slow speeds under virtually no-load conditions and should last indefinitely without wear-caused inaccuracies. The two ball/disc integrators are the critical components of the system. Their lifetime expectancy of 5,000 - 10,000 hours of operation at the rated 0.05 per cent accuracy, i.e. about 20 observatory-years of data, is available only for high-speed (400 rpm) full-load conditions; at the actual speeds used (variable from 0 to 60 rpm maximum) and virtually no-load conditions, the rated accuracy should be maintained for at least 10 times that long.

The electromechanical components should similarly maintain their reliability for a long time. The control relays are of the medium-coil telephone type, with bifurcated twin contacts rated 4 amps at 28 VDC. They operate very quietly and feature very long lifetime: 10^8 mechanical operations minimum, contact life estimated at over 5×10^6 cycles with the loading and spark suppression used, i.e. at least 200 observatory-years of data for the hourly mean relays, indefinitely for all others. Trouble-free operating life can be lengthened by an interchange between the more frequently operated relays (hourly mean read-out) and the daily mean relays; since the relays are plug-in types such exchanges can be easily carried out. Similar specifications apply to the other electromechanical components such as stepping switch and storage relays.

The electronics are all solid-state, and so far have not caused any servicing problems. The two counters are identical, so that operation can continue on the basic hourly mean system if one of the counters is removed for servicing. The light-bulbs for the photo-cell actuation are operated well below their ratings and have so far not required replacement. In fact the only difficulties which have developed over the last three years of operation concerned peripheral equipment: routine servicing of the printer, key-punch, and counter, and failures in the speed foot-pedal. In the foot-pedal case, the original pulley system has been replaced by a commercial foot-pedal with a gear-driven potentiometer.

As far as the data output is concerned, "high reliability" simply means the absence of *large* (random or consistent) errors caused by either equipment malfunction or by operator carelessness. This is ensured by the fail-safe type of interlock circuitry, and by the automatic double-check provided by the two separate channels. No large errors have so far been detected in any of the data processed on this machine; this is in contrast to manually processed data where such errors occur with embarassing regularity, the most usual being reading or copying errors of one digit in a particular decade, i.e. 1, 10, or even 100 gammas.

Accuracy of the machine is limited primarily by two factors: a) time-scale inaccuracies, and b) digital resolution. The time-scale inaccuracies include genuine irregularities in magnetogram time scale as well as operator-caused ones such as uncorrected over or under-shoot of the hour mark. For observatory-quality magnetograms (time scale usually ±0.1 mm, i.e. ±0.5 per cent) and a conscientious operator (0.1 - 0.2 mm resolution), the combined time-scale errors are of the order of 1 per cent, with a maximum of 1.5 per cent. It should be noted that this error is strictly proportional to the ordinate. In most cases magnetograms are laid out so that each trace runs near its baseline, i.e. mean ordinate usually under 100 - 200 gammas; the percentage error of 1 per cent is therefore acceptably low when expressed in gammas. However, for magnetogram layouts where the traces are distant from the baseline, the percentage error could become prohibitive, in contrast to manual processing where the scaling accuracy is independent of amplitude. On the other hand, the accuracy of the magnetogram reader is independent of the degree of disturbance; this contrasts with manual scaling where the accuracy of the visual hourly mean estimate deteriorates markedly for disturbed periods.

The time-scale errors are not cumulative; an overshoot in one hour means an equivalent reduction in the next hour, so that the average value over any group of hours is correct to a much higher percentage accuracy. In the daily mean for example, a time-scale accuracy of 0.1 per cent can readily be achieved. Consistent time-scale differences in magnetograms from a particular observatory, i.e. *mean* time scale differing from the nominal 20 mm/hr, can of course be corrected for by an appropriate adjustment in the scale-factor dial setting, leaving only the superimposed random irregularities.

The digital resolution error of the system, i.e. a potential error of one unit (1 gamma or 0.1′), is inherent in the analogue-to-digital conversion. If the rotating disc is stopped for an hourly read-out just before a hole reaches the light-beam, the output value can be too low by almost one unit (e.g. true analogue value 10.9, digital output 10). Again, these errors are not cumulative; if the disc is stopped just below a hole on one hour, it will tend to give a correspondingly higher reading on the next hour. The maximum resolution error in the average of a group of n hours is therefore only 1/n. In the daily mean channel, in which the unit is 0.1 gamma or 0.01′, the resolution error is entirely negligible.

Potential accuracy of the entire process is therefore ±1 per cent of mean ordinate ±1 unit. For a medium-latitude observatory such as Victoria, with scale-factors of 3 - 4 gammas/mm and mean ordinates around 100 gammas, this means errors of ±1 - 2 gammas in individual hourly means (independent of the degree of disturbance). Additional errors of the order of 1 gamma can be expected occasionally, caused by operator tracking inaccuracies. The actual accuracy achieved in operational use is discussed in the next section.

Operational performance

A detailed test was carried out on three months of data in two components, i.e. 4,400 hourly mean values. A comparison was made between a data set which had been previously processed by hand, and the same data processed on the machine without the operator's knowledge that a test was involved. All values which differed by 3 gammas or more were checked out in detail; in most cases it was found that the difference was "split", i.e. a 1 - 2-gamma error in the machine values and a 1 - 2-gamma error of opposite sign in the manual values added up to a ⩾3-gamma difference. The remaining discrepancies have been summarized in Table I below, showing the percentage of the hourly values which were in error by the stated amounts.

All the ±4-gamma errors and all except one of the ±5-gamma errors in the machine-processed data correspond to time-scale irregularities in the magnetogram. Nevertheless, the accuracy which was obtained for the individual hourly means (3 per cent of values in error by ±3 gammas) was lower than could be expected from the theoretical design considerations. Some "legitimate" causes were recognized: curved baselines and minor time-scale irregularities. However, a significant residue of the 3-gamma errors can only be ascribed to operator causes, i.e. careless tracking. It is an unfortunate fact that no amount of circuit design care and other safeguards can protect such processing from careless operation, and the same applies to manual scaling and processing. This is perhaps the strongest argument in favour of fully automatic systems. Operational discipline has since been tightened up (by periodic spot checks), and generally only 2 per cent or less of the machine-processed values are now in error by ±3 gammas.

The most striking difference between the results of the two processes is the absence of large errors in the machine data, i.e. high data reliability. By comparison, the magnitude of the errors in the manually-processed data (26 errors larger than 4-gamma, out of 4,400 values) came as an unpleasant surprise, and impressed us with the need for duplicate processing rather than just spot-checking of manual data. Eighteen of these errors were very large (> 10-gamma), and at least some of them would probably have been noticed as "out of place" by simple visual inspection of the monthly sheets (for example a 100-gamma copying error in the addition of the baseline correction). The rest of the errors included some "legitimate" scaling errors during very disturbed sections, several 10-gamma copying errors, one 65-gamma error caused by use of the wrong baseline, a 75-gamma cross-over tracking error during minor disturbance, a 30-gamma copying error (writing 15 instead of −15) and a 45-gamma copying error (writing 5 instead of 50).

The comparative performance of the two methods is outlined in Table II.

Table I

Error (Gammas)	Percentage of Values a) Machine	b) Manual
±3	2.90	0.50
±4	0.91	0.23
±5	0.18	0.14
±6–9	0	0.04
±>10	0	0.41

Table II. Comparison of different magnetogram processing methods

		Manual processing	Duplicate manual processing	Magnetogram reader
Theoretical accuracy		resolution (±0.5γ)	resolution (±0.5γ)	1 per cent ±1γ
Potential	K = 0–2	±1γ	±1γ	±1–2γ
practical	K = 3–5	±1–3γ	±1–2γ	±1–2γ
accuracy	K ≥ 6	±2–10γ	±2–5γ	±1–2γ
Achieved	K = 0–2	±1γ	±1γ	K = 0–9:
practical	K = 3–5	±1–3γ	±1–3γ	any value ±1–2γ
accuracy	K ≥ 6	±2–10γ	±2–5	< 3 per cent of values ±3γ (random distribution)
Reliability: number of large errors (>10γ) in one year		variable, typical: 12 (10–100γ)	Nil	Nil
Daily mean value accuracy		±0.5γ	±0.5γ	±0.5γ
Time (man-months) to process one year in three components completely ready for publication		4 - 6	8 - 12	2
Output also available on cards or tape?		No (Unless manually punched)	No	Yes

Based on records from a mid-latitude observatory (Victoria, 54°N geomagnetic), scale factors 3–4γ/mm, variograph time scale reliable ±1 per cent, mean ordinates usually under 100γ.

Briefly summarized, duplicate manual processing provides the most accurate and reliable results, provided one can afford the manpower. Single manual processing is still more accurate than machine processing (0.5 per cent of values ±3-gamma, compared to 2 - 3 per cent). However, it is far less reliable; the machine data contains no large errors. Accuracy of the daily mean value is about the same for both methods, except in manual processing during the few days which contain the aforementioned large errors. The salient point is of course the saving in manpower with the machine processing.

Alternative versions

The basic feature of the machine is the mechanical analogue system; it can naturally be adapted to work into different digital output systems. For example, if digital recording facilities are already available, the output from the photo-cell amplifiers can be fed into any other equivalent counters (bi-directional with preset capability) which would be compatible with the available digital recorders. In particular, a complete range of commercial output processors is available to link BCD outputs from counters to a variety of output devices–magnetic tape or punched tape as well as punched cards or printers.

At the other extreme, a low-cost version can be built with electromechanical counters such as the Whittaker/Neuron Type 7005-D24-AS which is presently used for the time-scale interlock. This counter is bi-directional and has decimal contact-closure outputs which can operate the typewriter or key-punch directly, without the need for a relay storage unit; the one-second wait for the print-out is not prohibitive. The operating speed of these counters (40 counts per second) is adequate for scanning, although the clicking noise at high speeds could become objectionable. The main limitation on the use of this system is the fact that no instantaneous reset to a dialed-in "preset" value is available; reset to the baseline correction therefore has to be obtained by first resetting to zero and then counting up to the desired value (with the counting pulses gated by an output from the decimal contact closures). This method has been successfully used for the *daily* mean channel in the original home-made prototype; the counting time for the baseline reset was irrelevant since it could be carried out during the carriage return. However, for the hourly mean system this reset-by-counting would cause a prohibitive slowing-down of the entire process; for example, 1.2 seconds for print-out plus 4 seconds for reset to a baseline correction of 150 gammas. Nevertheless, if cost is an overriding consideration, such a low-cost version should be investigated in more detail. In particular, bi-directional counters with decimal read-out are now becoming available in single-decade modules. By disconnecting the "carry" between decades during reset, such a system could be rapidly reset by counting each decade separately to its desired value. Such an entirely electromechanical version would provide acceptable (though somewhat noisy) low-cost equivalence to the hybrid electromechanical/electronic system described in this paper.

Acknowledgments

We should like to acknowledge the original suggestion of D.H. Andrews of the Dominion Astrophysical Observatory, on the use of ball/disc integrators for this particular purpose. We should also like to thank R.G. Madill, former Chief of the Division of Geomagnetism, for his encouragement of the project during its start and earlier years, and Dr. P.H. Serson for his subsequent support. Mr. A. Camelford, formerly with the Fairey Aviation Company, assisted with engineering details of the mechanical system of the commercial version, and G.R. Ball, of Ball and Shemilt Electronics Ltd., with design and construction of the electronic system.

References

Alldredge, L.R., and I. Saldukas. 1964. An automatic standard magnetic observatory, *J. Geophys. Res.*, Vol. 69, pp. 1963-1970.

Andersen, F. 1969. An automatic magnetic observatory (abstract only), *Int. Assoc. Geomagnetism and Aeronomy Bull.* No. 26, p. 106.

Auld, D.R. and P.H. Andersen. 1966. Record of observations at Victoria magnetic observatory for 1963-1964, *Dom. Obs. Pub.*, Vol. XXXII, No. 8.

——————————1968. Record of observations at Victoria magnetic observatory for 1966, *Dom. Obs. Pub.*, Vol. XXXVII, No. 3.

Caner, B. and K. Whitham. 1962. A semi-automatic magnetogram reader, *J. Geophys. Res.*, Vol. 67, pp. 5362-5364.

Hultquist, B., A. Thunberg, S. Lindell, and K.E. Heikila. 1961. An automatic digital recording and reducing system for geomagnetic standard data, *Arkiv f. Geofysik*, Vol. 4, pp. 1-23.

Lenners, D. 1966. Eine programmgesteuerte Anlage zur Auswertung mehrspuriger Registrierungen, Deutsche Akad. Wiss., Geomagn. Institut Potsdam, Abh. No. 38.

Malin, S.R.C. 1969. World magnetic archive. Report on progress in United Kingdom, *IAGA News* No. 8 (Sept. 1969), p. 19.

Nelson, J.H. 1967. Magnetogram scaling machine, unpublished report, U.S. Coast and Geodetic Survey, ESSA, Rockville, Maryland.

PUBLICATIONS of the EARTH PHYSICS BRANCH

VOLUME 41–NO. 4

the Canadian pendulum apparatus, design and operation

H. D. VALLIANT

DEPARTMENT OF ENERGY, MINES AND RESOURCES

OTTAWA, CANADA 1971

Cat. No.: M70-41/4

Contents

Frontispiece. Author holding pendulum prior to opening pendulum case.

the Canadian pendulum apparatus, design and operation

H. D. VALLIANT

Abstract. A bi-pendulum apparatus which uses bronze quarter-metre pendulums has recently been developed by the Earth Physics Branch (formerly the Dominion Observatory) for relative gravity measurements. Variable factors such as temperature, pressure, humidity, amplitude, and time, are precisely controlled to minimize the corrections required to reduce the periods to identical conditions.

Rigorous testing of the equipment under laboratory and simulated field conditions disclosed that systematic errors in measuring gravity differences would not exceed 0.06 mgal and random errors would not exceed 0.20 mgal r.m.s.

Tests under complete field conditions along the North American Calibration Line resulted in a mean difference between gravimeter and pendulum values of 0.04 mgal and an r.m.s. difference of 0.06 mgal. It was expected that the random error would decrease, as a result of the effects of desiccating the pendulum storage box. Agreement with absolute measurements is within the error bounds estimated for these two instruments.

Résumé. Un dispositif à double pendule, constitué de pendules en bronze d'un quart de mètre, a été mis au point par la Direction de la physique du Globe (anciennement l'Observatoire fédéral) pour effectuer des mesures de gravité relative. Les facteurs variables, comme la température, la pression, l'humidité, l'amplitude et le temps, sont contrôlés avec une grande précision afin de réduire au minimum les corrections requises pour amener les périodes à des conditions identiques.

Des essais très précis de ce dispositif, effectués en laboratoire et dans des conditions simulées, ont révélé que les erreurs systématiques dans la mesure des différences de gravité ne dépasseraient pas 0.06 mgal et les erreurs aléatoires 0.20 mgal (erreur quadratique moyenne).

Les essais effectués sur le terrain même, le long de la Ligne d'étalonnage nord-américaine, ont révélé une différence moyenne de 0.04 mgal entre les valeurs indiquées par le gravimètre et le pendule, et une différence de 0.06 mgal dans l'erreur quadratique moyenne. On pense pouvoir réduire l'erreur aléatoire par assèchement de la boîte où est conservé le pendule. La comparaison avec les mesures absolues donne un résultat qui ne dépasse pas la marge d'erreur prévue pour ces deux instruments.

Introduction

General remarks. The Canadian pendulum apparatus is an instrument for the precise measurement of differences in gravity between two or more locations consisting of six bronze pendulums and ancillary equipment. This apparatus has recently undergone extensive redevelopment to increase its precision to a level equal to or exceeding present day standards. Descriptions of specific aspects of the design, construction and testing of this new apparatus has been published in appropriate engineering or geophysical journals (Valliant, 1965, 1967a and b, 1969a and b). The purpose of this paper is to co-ordinate the individual research reports, to provide a complete description of the Canadian pendulum apparatus and to summarize the results of nearly two years of testing.

History of the Canadian pendulum apparatus. The history of the Canadian pendulum apparatus dates back to the turn of the century when Mendenhall (Swick, 1921) designed a pendulum apparatus for the United States Coast and Geodetic Survey (USCGS). In 1902 the Dominion Observatory procured a pendulum apparatus and three bronze quarter-metre pendulums which were modelled after the 1890 Mendenhall design. Also included with the equipment was an air-tight chamber housing a single pendulum and "flash apparatus" for measuring the periods.

Gravity measurements were made with the original apparatus by Miller, Innes and other observers until around 1948 when pendulums were largely supplanted by gravimeters for geophysical surveying.

In 1954 Thompson (1959) began reconstructing the equipment with a view to converting it to a bi-pendulum apparatus with a high level of environmental control. In a bi-pendulum apparatus two pendulums are swung exactly out of phase in the same plane to eliminate motions of the support induced by the pendulums. At this time Thompson also acquired a second set of three bronze pendulums from USCGS.

Subsequent to the completion of these modifications, the equipment underwent three seasons of field observations from 1957 to 1959 (Thompson, 1959; Winter and Valliant, 1960; Winter, Valliant and Hamilton, 1961). Analyses of these results indicated that the apparatus only performed satisfactorily under stable laboratory conditions at Ottawa. Field measurements were subject to large systematic errors, affecting all six pendulums at any one location, and discrepancies as large as two milligals were sometimes noted.

Consequently a second attempt to develop a high precision pendulum apparatus using the original pendulums was begun late in 1959. By April 1965 the new apparatus which is the subject of this paper was essentially completed. The period from April 1965 until June 1966 was occupied by testing and improving the overall system, in measuring the stability of the temperature control and generally in assuring that all parts of the apparatus were functioning according to design parameters. During this time field procedures for the new apparatus were also established. From June 1966 until September 1967 a series of measurements of Δg between a field station at Almonte, Ontario and the base station at Ottawa, Ontario was made to determine the overall accuracy of the apparatus. The Almonte tests disclosed that the length of the pendulums (Valliant, 1969a) were altered by changes in humidity and steps were taken to control this effect.

In a dual effort to make a contribution to the establishment of the First Order World Gravity Network and to compare the accuracy of the Canadian pendulums with those of other countries, measurements along the North American calibration line at College, Alaska; Edmonton, Alberta; Denver, Colorado and Mexico City, Mexico were undertaken between September 1967 and September 1968 (Valliant, 1969b). At the present time the Canadian pendulum apparatus is being deployed to establish a network of pendulum stations at selected sites throughout Canada (see Appendix I).

The new Canadian pendulum apparatus

Description. The heart of the Canadian pendulum apparatus is a group of six bronze pendulums which are allowed to swing two at a time on agate knife edges. The knife edges are mounted on a common support so that the two pendulums oscillate in the same plane. While in use the pendulums are housed inside a vacuum chamber, where pressure and temperature may be maintained at a constant value. In operation the pendulums are first deflected by a mechanical device protruding through the wall of the vacuum chamber and suddenly released so that they oscillate freely in opposing phase. Anti-phase operation essentially decouples the pendulums from their support (Vening-Meinesz, 1929). The mean period of two nearly identical pendulums swinging in anti-phase on a common support may be thought of as the period of a fictitious pendulum (hereafter called the "fictitious period" for simplicity) swinging on a stationary support.

The fictitious period, which is approximately 1 second, must be determined to within 100 ns in order to achieve a 0.2 mgal accuracy in gravity. This precision is achieved by obtaining the average period for a large number of oscillations of the pendulum.

To simplify the description, the apparatus may be subdivided into the following sub-systems:

1. Pendulums.
2. Pendulum case.
3. Environmental control systems:
   a) Temperature control.
   b) Pressure control.
   c) Humidity control.
4. Data acquisition system:
   a) To measure and record pendulum periods.
   b) To measure and record phase and amplitude of oscillation.
   c) To measure and record environmental conditions such as pendulum temperature and operating pressure.

Pendulums. The pendulums approximate simple pendulums having a lenticular bob attached to a thin stem approximately 25 cm long. They are constructed from aluminum bronze and were gold plated in 1954 to prevent tarnishing. A complete description of the original form of the apparatus and the pendulums was given by Swick (1921). For relative gravity measurements accurate to 0.1 mgal it is required that the lengths of the pendulums remain constant to within 250 Å. The achievement of such a high degree of dimensional stability is hampered by the relatively large coefficient of linear expansion (17 ppm/degree C), the arrangement of the knife edges and the construction of the pendulums which are made from five separate pieces rivetted together. Because the knife edges are fixed to the pendulum case, it is essential that they engage the flats on the pendulums at the same location for each observation. Otherwise, errors are introduced because the effective length of the pendulum is altered. A rotation of the pendulum about its vertical axis also generates errors in the amplitude determination as described later.

On the other hand it is to be expected that the age of the pendulums may contribute significantly to the dimensional stability of the material of their construction. As it was felt that the advantages of using the old pendulums outweigh the disadvantages, in particular the disadvantage of providing a constant temperature environment, Thompson (1959) decided in 1954 to build a pendulum apparatus using the old Mendenhall pendulums. It should also be emphasized that the characteristics of the old pendulums were well established whereas the construction of new pendulums would create a completely new set of characteristics and problems some of which might have proved to be as severe as the limitations with the bronze pendulum.

Pendulum case. Since the pendulum case functions as an integral part of each of the sub-systems it is possibly the most critical component of the apparatus. It provides:

1. Support for two pendulums.
2. Primary insulation and heat source for the temperature control system.
3. The optical bench for the data acquisition system.
4. Means to accurately level the knife edges.
5. Means to deflect and release, raise and lower the pendulums.
6. The temperature sensors for the data acquisition system.
7. A vacuum chamber for pressure control and thermal insulation.

The construction details of the pendulum case are shown in Figure 1. The base of the pendulum case consists of a sixteen-sided aluminum vacuum "collar" constructed with a solid bottom. Twelve ports through the side of the base plate provide entry to the vacuum chamber for external mechanical and electrical controls. Three adjustable legs and two levels are mounted on the outside of the case to permit initial levelling of the pendulum apparatus. Precise levelling is accomplished with the aid of the adjustable legs and a striding-level resting on one of the knife edges. A glass bell jar, gold plated on its inner surface surmounts the base and completes the vacuum chamber. The gold plating helps prevent heat loss through radiation.

The oven which is located directly inside the vacuum chamber is constructed from thin sheet aluminum and has a highly polished outer surface to further reduce heat loss. A heating element is attached to the oven's inner surface with silicone rubber and arranged to supply an

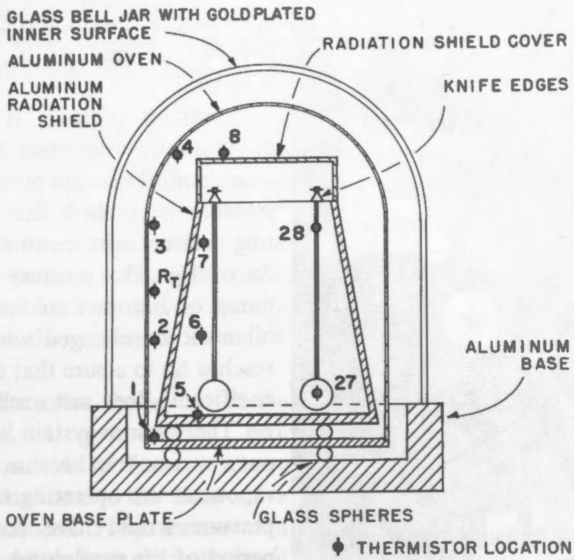

Figure 1. Schematic diagram of pendulum case showing approximate location of thermistors (1-28). To minimize heat loss, the major components are separated by glass spheres arranged in a kinematic mounting system.

even distribution of heat over its surface. Thin material is used in the construction of the oven to permit its temperature to respond quickly to changes in ambient temperature. The oven may be easily separated from its base to provide access to insert or remove the pendulums. The radiation shield which is located inside the oven carries the knife edges. It also prevents the direct transfer of radiant energy from the heaters to the pendulums. The surfaces of the radiation shield are dull to encourage heat transfer from the oven through the shield to the pendulums. As the mounting for the knife edges, the radiation shield ideally must provide a stationary support. Although two pendulums are operated in antiphase, their periods cannot be perfectly matched, nor can they be started exactly out-of-phase so that some force is, in practice, coupled to the support. To completely eliminate forced vibrations the support must be either perfectly rigid or its mass must be infinite. Consequently the radiation shield was made as heavy as practical by constructing it from $^3/_4$-in.-thick aluminum.

The massive nature of the radiation shield is also compatible with the requirements of the temperature control system. The radiation shield must have a large thermal capacity to average out rapid fluctuations in the oven temperature. Also the thickness of its walls permits rapid heat flow to all parts preventing the establishment of temperature gradients.

Conductive heat losses are minimized by supporting the oven on $^3/_8$-in.-diameter glass spheres. These spheres are held in position by three conoidal depressions located in the oven base plate and by a "slot-cone-plane" arrangement in the base of the vacuum chamber. The radiation shield is separated from and supported by the oven base plate in a similar manner. As the temperature of the radiation shield is nominally the same as the oven temperature little or no heat is conducted from the oven to the radiation shield by the supports thereby eliminating the establishment of temperature gradients in the radiation shield because of thermal heat sinking. Evacuating the entire assembly to below 10μ of Hg virtually eliminates heat loss through conduction and convection. All shafts leading outside the vacuum chamber are either retractable or insulated with nylon sections to prevent heat flow along the shafts.

Operation of the pendulum case as part of the temperature control and measuring systems may be stated as follows. The pendulums are completely surrounded by the radiation shield which functions as a black-body enclosure having a uniform wall temperature. Under these conditions radiant energy flows between the pendulums and the heat shield until any temperature differential is eliminated. The temperature of the pendulums, which can not be measured directly, may be obtained after equilibrium is established by measuring the radiation shield temperature.

Figure 2 is a view of the completed pendulum case showing some of the mechanical and electrical devices attached to the outer base plate. The mechanism for deflecting and releasing both pendulums simultaneously is contained in the small aluminum box attached at the left side of the case. One of the two mechanisms for raising and lowering the pendulums is operated by the retractable knob located at the right. An interior view of the pendulum case is given in Figure 3 showing the radiation shield after the bell jar and oven have been removed.

The success of the pendulum case has been proven by three years of continuous trouble free operation. Tests have shown (Valliant, 1967a) that the temperature gradient in the radiation shield does not exceed 0.02°C and that changes in the pendulum's temperature may be measured with an accuracy of 0.01°C. While the flexibility of the pendulum case is considerably larger than for either the Gulf or Cambridge pendulum apparatus the resulting flexure is within acceptable limits.

The environmental control system. Three facets of environment control–temperature, pressure and humidity–are applied to the Canadian pendulums.

The function of the pendulum case as part of the temperature control system has already been described. The electronic thermostat which maintains a nominal temperature of 40°C and the electronic thermometer for measuring the temperature of the radiation shield have been described in detail (Valliant, 1967a). Tests indicate that the maximum temperature variation over a wide range of ambient conditions is about 0.025°C even when the pendulum case is opened at regular intervals to change pendulums

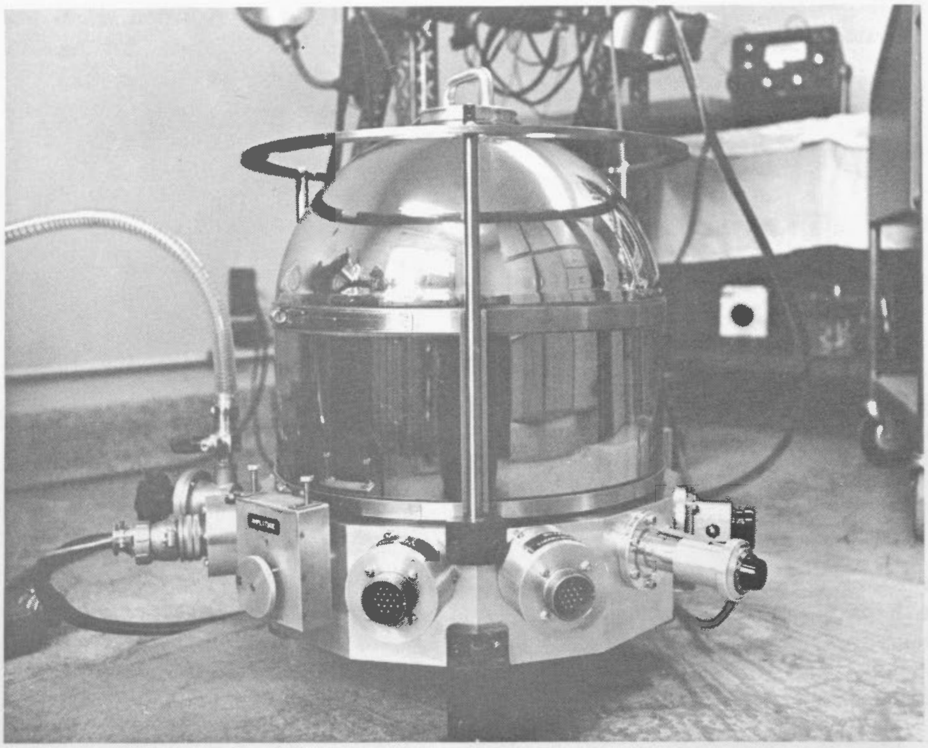

Figure 2. View of pendulum case showing vacuum sealed parts for electrical connections and mechanical devices for starting and lifting the pendulums.

and that a thermostatic coefficient of between 22 and 25 X 10^{-4} has been achieved.

Constant pressure is maintained by continuously evacuating the bell jar with a mechanical vacuum pump until terminal pressure is reached. The nominal operating pressure with continuous pumping is 3μ of Hg. The pressure increases if the pump oil becomes contaminated and the oil must be changed when the pressure reaches 6μ to assure that the thermostatic coefficient does not exceed 25 X 10^{-4}.

The vacuum system is operated without a vapour trap because even pure water vapour at the operating temperature and pressure would have no effect on the period of the pendulums. However, water absorbed by the agate flats and absorbed on the surface of the pendulums, while they are being stored, influences the effective length of the pendulums (Valliant, 1969a). The storage box for the pendulums must therefore be desiccated to maintain a constant humidity. By changing desiccant every two weeks the

Figure 3. View of the pendulum apparatus, with the bell jar and oven-cover removed, showing the radiation shield.

relative humidity in the storage box is maintained between 10 and 20 per cent thereby rendering the effect of moisture negligible.

Data acquisition system

The optics. The purpose of the optics is to generate an exact electrical analog of the pendulum's motion. This is accomplished by projecting a beam of light, after reflection from a mirror on the pendulum, onto the surface of a suitable photodetector.

Figure 4 illustrates the layout of the optical system. A quartz-iodine, projection lamp and slit S form a source which is focussed onto the face of a differential photocell P by means of a lens L. The light path is folded several times by reflection from mirrors M_1, M_2, M_3, M_p, M_3, M_2, and M_4 in that order. The mirror M_P is attached to and rotates with the pendulum so that the beam plies back and forth across the face of the photocell as the pendulum oscillates.

The photodetector consists of two selenium photocells each measuring 0.5 X 0.75 in., which are mounted closely together end to end. The optical slit is adjusted so that the width of the image is 0.75 in. When the pendulum is vertical both photocells are 50 per cent illuminated and the difference in their output voltage is zero. As the light traverses the face of the photocell arrangement, the differential output is a one Hz sinusoid which is the exact electrical analog of the pendulum's motion.

As the optical system also provides amplification it functions as a low noise preamplifier for the data acquisition system. The optical leverage or gain of this system is such that a displacement of the pendulum of 0.003 radian displaces the light beam 0.375 in. providing the full output from one photocell.

Amplitude and phase determination. The amplitude of the pendulum's motion is measured directly by comparing the amplified photodetector output with a variable calibrated voltage. In practice this device is calibrated before and after each day's observations by allowing the pendulum to swing with sufficient amplitude for the light beam to deflect past the ends of the photodetector. The photodetector output is then a truncated sinusoid whose peak-to-peak amplitude corresponds to a pendulum rotation of .00625 radian. After calibration the amplitude of the pendulum is reduced to normal and the output from the photodetector is again determined. The pendulum's amplitude is then given by the ratio of the normal to truncated amplitudes times .00625 radian.

Correction to the period for variations in amplitude are applied according to the following equation:

$$T = To\,(1 - \frac{\alpha^2}{16})$$

α = half amplitude in radians

To = observed period.

The magnitude of the amplitude correction varies between observations but usually amounts to 50 X 10^{-8} sec and never exceeds 200 X 10^{-8} sec. Thus an accuracy of 1 per cent in the amplitude measurement is required for a 0.1 mgal accuracy in gravity. This implies that the reference (amplitude of the truncated waveform) must be obtained with equal accuracy. While the voltage measurement is performed with an accuracy of 0.1 per cent the reference value varies with time as well as with the position of the pendulum on the knife edge.

Long term or daily drift in the value of the reference measurement is primarily due to variations in the light intensity because of aging of the lamp. Recent installation of a quartz-iodine lamp powered from a regulated supply has much alleviated this problem. Total variation in the reference value during the course of a day's observations rarely exceeds 10 per cent. To minimize this problem the mean of two determinations of the reference, one taken at the beginning and one at the end of each day's

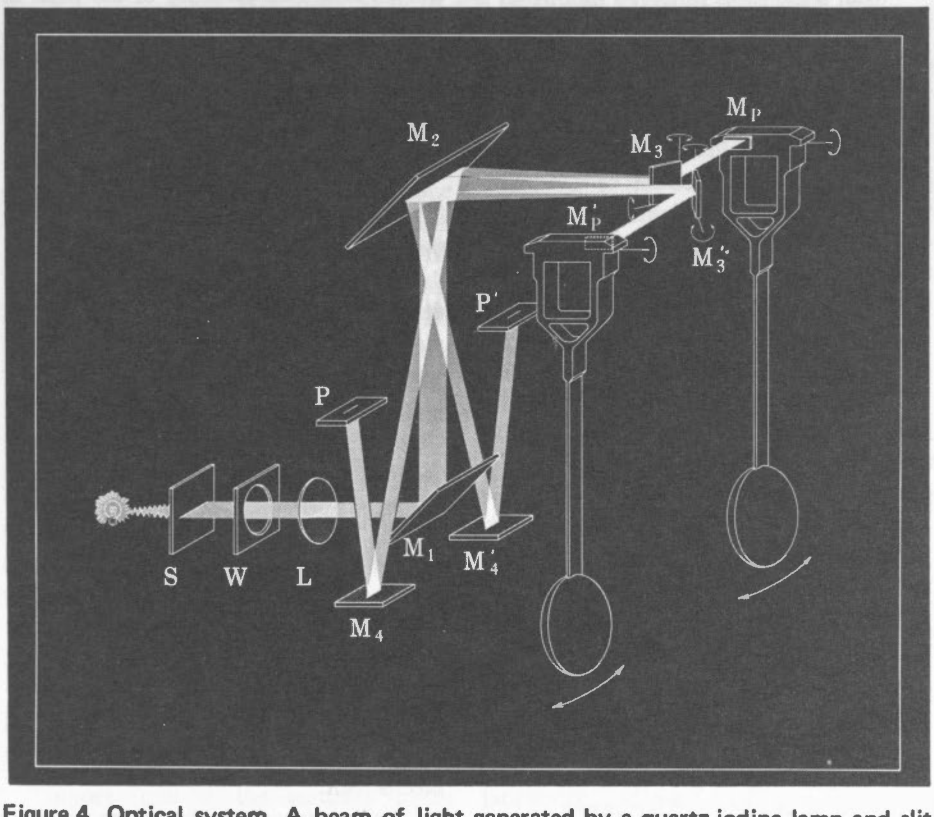

Figure 4. Optical system. A beam of light generated by a quartz-iodine lamp and slit (S) enters the vacuum chamber through a vacuum sealed window (W) and is focused on two photocells (P and P') by a lens (L). Two adjustable mirrors M_3 and M_3' divide the beam in two, one half for each pendulum.

observation, is used. If the long term drift in illumination is linear the error in the mean fictitious period for a day's observations is unaffected by the drift in the reference value.

An additional problem involves the rotation of the pendulum about a vertical axis as it is lowered onto the knife edge. Such a rotation causes a transverse displacement of the light beam across the photodetector. As the illumination of the light beam is not uniform along its length, but is brightest at the centre, lateral displacement of the beam alters the illumination of the photodetector and changes the reference value. The amount of rotation of the pendulum varies for each individual observation and depends on the degree of gentleness and uniformity, from observation to observation, with which the pendulum is lowered onto the knife edge. Changes in the reference of up to 20 per cent from this cause have been noted when a pendulum was rapidly lowered onto a knife edge.

The obvious solution–to measure the reference before and after each 15-minute observation–proves unwieldy in practice. It is more practical for the observer to *gently* lower the pendulum to the knife edge using a consistent technique to avoid rotating the pendulum about a vertical axis. Also if the amplitude of a pendulum is noted to change significantly after lowering to the knife edge, the pendulum is raised and lowered a second time before the observation is made. With these precautions the magnitude of this effect can be kept below 1 per cent of the total amplitude correction. Furthermore, as rotations of the pendulum in this sense are random, the effect on the mean fictitious period would be reduced by the square-root of the number of observations.

To observe the phase relation between the two pendulums concurrently with the observations, the amplified output from the two photodetectors, one for each pendulum, are displayed with a double beam oscilloscope. The pendulums are started so that their initial phase difference never falls outside the range of $\pi \pm 0.03$ radian. The maximum phase change for the poorest matched pair of pendulums during a 900-second observation is 0.125 radian.

Period measurement. A block diagram of the sub-system for measuring the pendulum periods is given in Figure 5. The primary time source is a James Knight frequency standard having a drift rate of better than 5 parts in 10^{10} per day. A "clock" pulse, 10 microseconds wide, is formed by the control and clock pulse generator every 20 seconds. The clock pulses are stored in a binary accumulator where they provide a measure of elapsed time and the resolution of a time interval measurement is ±1 count or 20 microseconds. A series of control pulses each spaced exactly between two clock pulses is also provided by the pulse generator. The control pulses regulate the operation of the print-out circuit so that the binary accumulator is interrogated only when it is dormant.

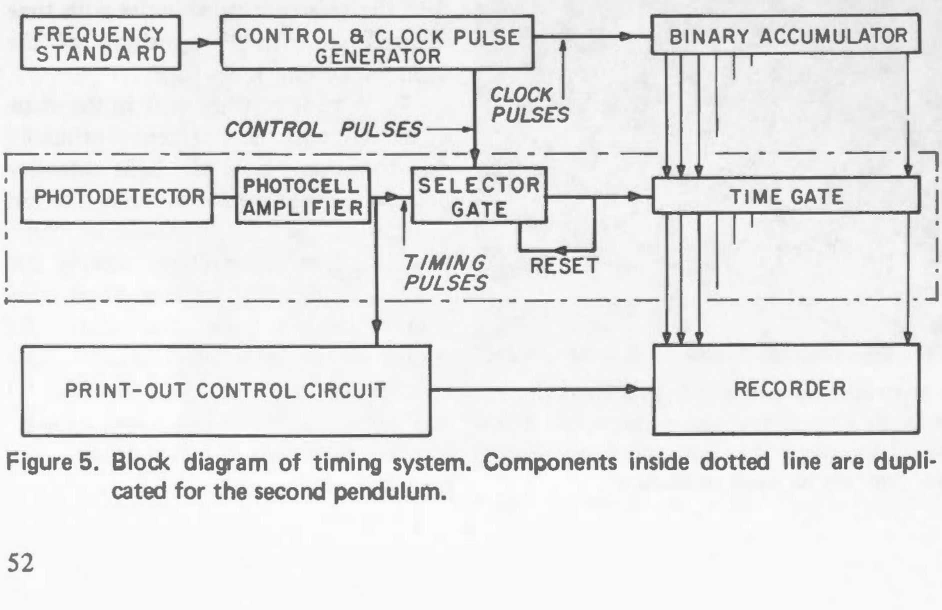

Figure 5. Block diagram of timing system. Components inside dotted line are duplicated for the second pendulum.

A timing pulse, generated at the zero-crossings of the photodetector signal, opens the selector gate so that a control pulse is applied to the time gate which consists of a series of transmission gates. As this control pulse also closes the selector gate only a single pulse is chosen. The transmission gates are arranged to provide a non-destructive readout of the instantaneous state of the binary accumulator. All gates connected to binaries in the one state are open, while those connected to binaries in the zero state are closed. The selected control pulse is then transmitted through the open gates to a specially designed digital recorder (Valliant, 1965).

Operation of the Canadian pendulum apparatus

Limitations of the temperature control system

Data acquisition rate. It has been pointed out that the environmental control system provides sufficient temperature control to assure an accuracy of 0.3 mgal in measuring g. Furthermore by measuring the temperature and applying a small correction to the pendulum's period errors because of temperature variations are reduced to below 0.1 mgal.

The chief drawback with this system is the excessive time required to establish temperature equilibrium after a pendulum change. Figure 6 shows empirically determined heating curves for both gold plated and tarnished bronze pendulums. These curves include the influence of heat transfer by radiation from the oven through the radiation shield to the pendulum, of pumping out the vacuum system concurrently with heating the pendulums, and heat transfer from the radiation shield through the pendulums via the lifting mechanism which supports the pendulums in their raised position. It is evident from the temperature gradient in the pendulum before temperature equilibrium is established that much of the heat transfer is through the lifting mechanism.

Approximately 35 hours are required to achieve temperature equilibrium with the gold plated pendulums. Since five hours are normally required to make the

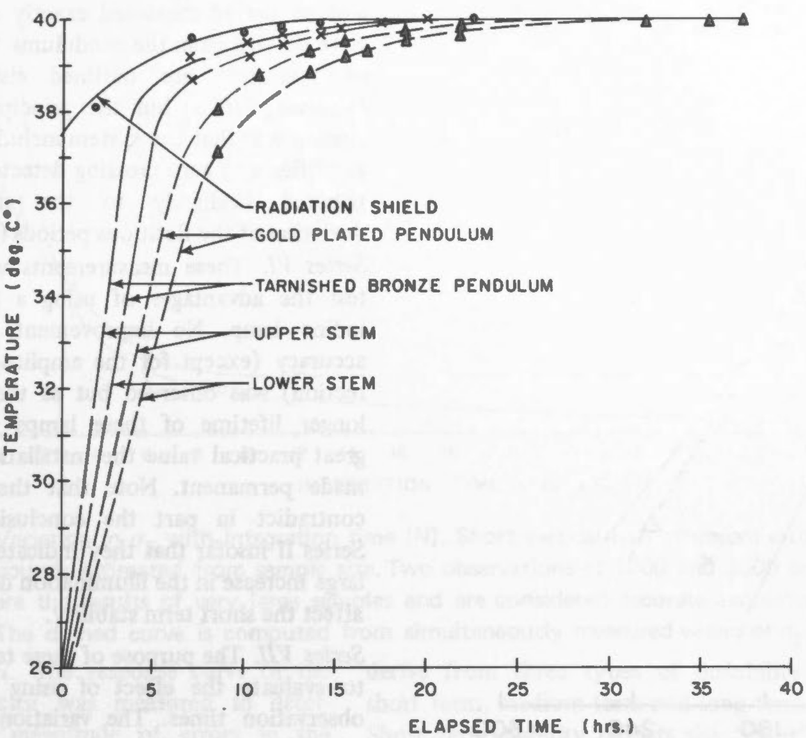

Figure 6. Pendulum heating curves. The temperature gradient between the upper and lower stem of the pendulum indicates downward heat flow from the lifting mechanism.

observations the turnaround time for one set of observations with one pair of pendulums amounts to 40 hours. As a 40-hour day is inconvenient the normal practice is to observe on a 48-hour schedule. The data acquisition rate could be doubled by the simple expedient of blackening the surface of the pendulums; equilibrium is established in under 20 hours with tarnished pendulums permitting a 24-hour schedule to be adopted. The pendulums have not as yet been blackened however, for fear of destroying their dimensional stability in so doing. Such a major modification of the pendulums would also introduce a singularity into the analysis of long-term drift in pendulum periods for which data has been accumulated since 1966.

Testing the pendulum apparatus

Tests were conducted essentially in three phases:

1. Laboratory tests to determine an upper limit to the accuracy under stable environmental conditions.
2. Simulated field tests to determine the reduction in accuracy as a result of transporting the apparatus.
3. Actual field tests to determine the accuracy of measurements under complete field conditions.

Laboratory tests. Eight series of tests were performed under a variety of conditions to determine the operational accuracy that could be achieved with stable conditions. Initially, the tests were concerned with adjusting the data acquisition system for optimum performance. As the tests proceeded more emphasis was placed on the determination of the performance of the complete system. In addition a series of temperature tests were carried out to insure adequate operation of the environmental control system. As field tests indicated that further knowledge of the influence of magnetic fields was required, this effect was briefly investigated in the laboratory.

Series I. These tests consist of the first observations made with the pendulum apparatus and were mainly to determine if the instrument functioned properly and to optimize the photodetector and associated amplifier circuitry. From these tests it was decided to use photo-voltaic cells rather than photo-conductive cells and to employ a.c. coupled electronics to alleviate the effect of drift in the photodetector response, amplifier d.c. levels and variations in illumination.

Series II. This series constituted a study of 60 samples of 100 individually measured pendulum periods which were observed during a 5-day interval. Various parameters were altered throughout the test in an attempt to determine the influence of these parameters on the short term stability (i.e. σ_S – the standard deviation of individual periods) of the measurements.

It was found that σ_S for knife edge 2 is always between 34 and 100 microseconds smaller than knife edge 1 (see Figure 20). As interchanging pendulums and/or the amplifiers has no effect it was concluded that this difference was due to differences in the behaviour of the two photodetectors. An attempt was made to differentiate between pendulum and photocell derived noise with three sets of observations. Firstly, the change in σ_S was observed as the pendulum amplitude was altered while the illumination remained constant. Secondly, the change in σ_S was observed as the illumination was reduced while the pendulum amplitude remained constant. Thirdly, the change in σ_S was observed as the pendulum amplitude was reduced with the output of the photocell maintained constant by increasing the illumination. The results of these tests are given in Figure 7. Interpretation of these data proves difficult. The lateral displacement between curves A and B appears to represent the reduction of noise with nighttime observations. The slope of these curves might be explained as the increase in error with reduced signal level due to the zero-crossing detector. It might also be explained if the pendulums and photocells contribute equally to the noise level. As curve C was derived with a constant signal level, zero crossing errors are excluded from these measurements and as the slope nearly equals that for curves A and B one might suggest that the pendulum is the sole contributor to the short term noise level. Obviously these two conclusions are contradictory and the contributions to the overall short

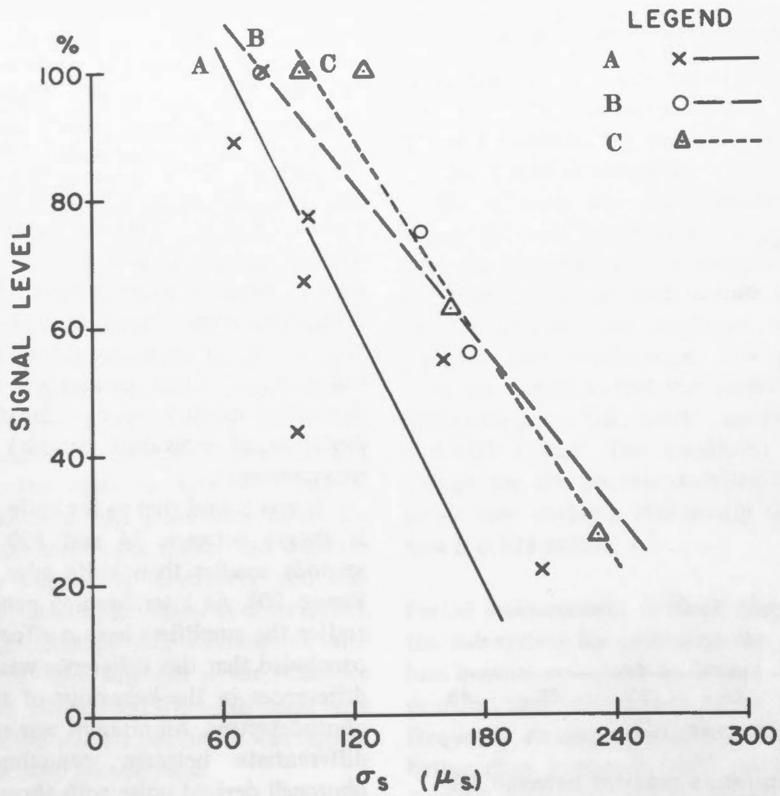

Figure 7. Series II test results.

term noise level of these two sources are not adequately explained. Although further tests made during Series VII also suggest that the photocells are not contributing significantly to the noise level a change of photocells during a field trip in 1969 resulted in a significant increase in σ_S. It will be shown later, however, that the existing short term noise level does not contribute significantly to the overall error for observation times exceeding approximately 200 seconds.

Series III. Following Series II a matched set of selenium photodetectors was permanently installed. The operational amplifier was reconnected to provide a differential input with an amplification of approximately 200. A device to permit the gain to be automatically increased in the vicinity of the zero crossing was included but discarded later as a result of these tests.

Series III was essentially a repeat of Series I to test the new amplifier configuration. The effect of changing pendulums on a routine basis was also observed and it was ascertained that a 24-hour warm up was insufficient. These tests further disclosed that the first of each day's observation was in error by approximately −10 ppm and that this error could be reduced or nearly eliminated by allowing the pendulums to swing for a 10-minute warm-up period before starting observations. This warm up has subsequently been increased to 20 minutes for routine observations. Tests to determine the time required to establish temperature equilibrium were begun as a result of these observations.

Series IV. These tests were performed to study the feasibility of using a photo-pot* instead of the selenium photodetectors. It was found that self heating of the photo-pot disrupted the temperature control system and this device could not as a result be employed.

Series V. Series V was conducted to test the complete electronic system exclusive of photocells. A 65 mv triangular waveform was generated by integrating the output of the binary accumulator to simulate the output of the photodetector. This signal was applied to both amplifiers and its period measured exactly as if it were derived from the pendulums. Details of this test are outlined elsewhere (Valliant, 1967b) but the principal conclusion was that the system including the amplifier and zero crossing detector contributed negligibly to the standard deviation of the fictitious periods (σ_F).

Series VI. These measurements were to test the advantages of using a quartz-iodine lamp. No improvement in the accuracy (except for the amplitude correction) was observed but as the much longer lifetime of these lamps was of great practical value the installation was made permanent. Note that these tests contradict in part the conclusions of Series II insofar that they indicate that a large increase in the illumination does not affect the short term stability.

Series VII. The purpose of these tests was to evaluate the effect of using various observation times. The variation in σ_F with observation time is plotted in Figure 8. The value of σ_F can be calculated from a knowledge σ_S as follows:

$$\sigma_F = \sigma_S/N\sqrt{7}$$

$$= \sigma_S{}'/\sqrt{7}$$

N = number of oscillations of pendulum.

It is interesting to note that the measured value of σ_F does not vary as 1/N but is nearly flat from 1,200 to 3,000 sec observations. Thus σ_F is influenced by sources of error other than σ_S such as the relative location of the knife edge and flat, errors in amplitude correction and errors because of seismic activity.

The integration time may be chosen to minimize the standard deviation of the mean fictitious period ($\sigma_{\bar{F}}$):

$$\sigma_{\bar{F}} = \sigma_F/\sqrt{n}$$

n = number of observations contributing to the mean.

Allowing five minutes to raise and lower the pendulums between observations and remembering that a total time limit of four hours is imposed by the heating effect of the projection lamp the optimum integration time is found to be 900 seconds. This allows 12 observations to be taken in the four-hour time interval and leads to a value of σ_F of approximately 350 ns.

*Registered trademark, Gianni Corp.

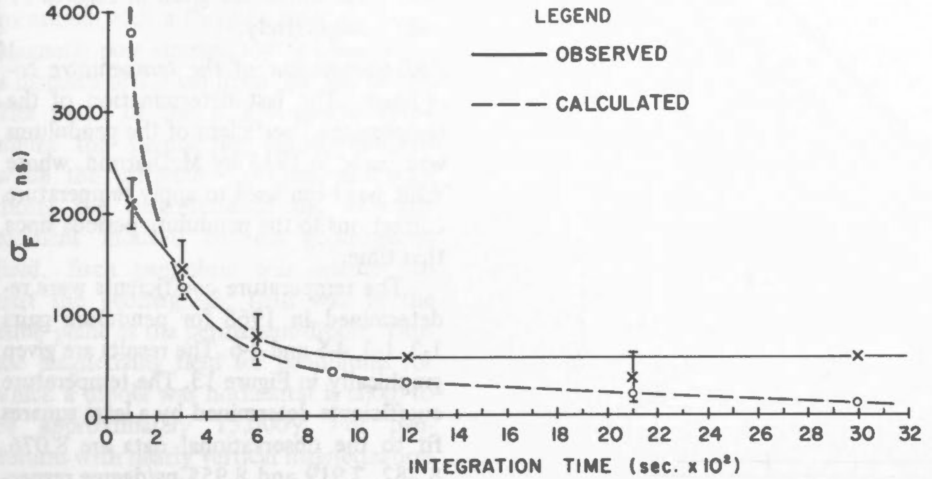

Figure 8. Variation in σ_F with integration time (N). Short vertical bars represent error bounds estimated from sample size. Two observations at 1200 and 3000 sec are the results of very large samples and are considered accurate estimates. The dashed curve is computed from simultaneously measured values of $\sigma_S{}'$.

Table I. Sources of error

A. Factors affecting short term stability (characterized by σ_S – standard deviation of individual periods).

1. Phase stability of pendulums, photocells, and amplifiers.
2. Electronic noise.
3. Zero-crossing detector errors.
4. Rapid changes in illumination.

B. Factors affecting medium term stability (characterized by σ_F – standard deviation of fictitious period on daily basis).

1. Ground motion.
2. Temperature errors.
3. Amplitude measurement errors.
4. Photocell and amplifier drift.
5. Rapid variation in pendulum's apparent length.
6. Knife edge effects.
7. Pressure changes.
8. Errors in flexure correction.

C. Factors affecting long term stability (characterized by σ_M – standard deviation of mean fictitious periods).

1. Temperature drift.
2. Changes in pendulum's length.
3. Levelling errors.
4. Humidity.
5. Secular change in gravity.

Series VIII. The response curve of the photodetector was measured to determine the magnitude of errors in the amplitude determination because of nonlinearity in the photodetector response. In Figure 9 the output of the photodetector is plotted versus the angle of elongation of the pendulum. The peak-to-peak amplitude, however, is used to compute the amplitude correction factor; the response to peak-to-peak measurements is shown in Figure 10. Comparison of Figures 9 and 10 indicate that for peak-to-peak measurements the nonlinearities of each half of the photodetector compensate improving the accuracy of the amplitude measurement. Also included in Figure 10 is the experimentally determined linear approximation to the response curve which is used to calculate the pendulum amplitude from the reference amplitude. The error in this approximation which amounts to about 13 per cent is systematic for all stations and tends to be cancelled out when differences in gravity are measured. Of greater importance is the change in this error with different amplitudes giving rise to a random error in the amplitude correction. This variation amounts to about 3 per cent over the range of amplitudes normally employed.

Sources of error. The factors contributing to the errors may be considered to derive from three types of instability: short term, medium term and long term. Short term stability reflects the "jitter" in the analog signal from the photodetector and is characterized by the distribution of individual period measurements. Medium term stability is characterized by the distribution of the fictitious periods on a daily basis. This distribution is found to be normally distributed with an expected standard deviation (σ_F) of 400 ns. Long term stability is characterized by the distribution of mean fictitious periods (averaged on a daily basis). The mean fictitious periods are found to be normally distributed about a

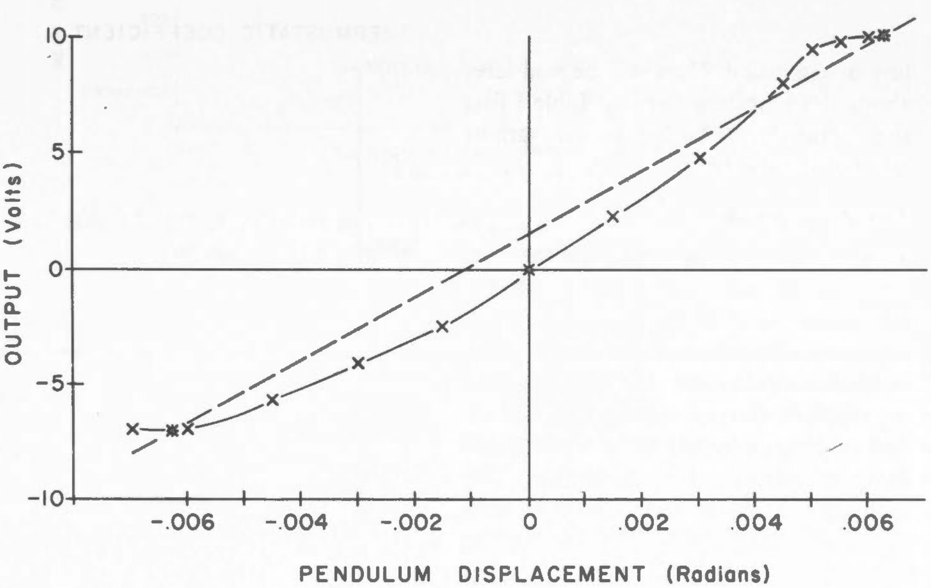

Figure 9. Photodetector calibration curve. The dotted line represents the empirical linear fit.

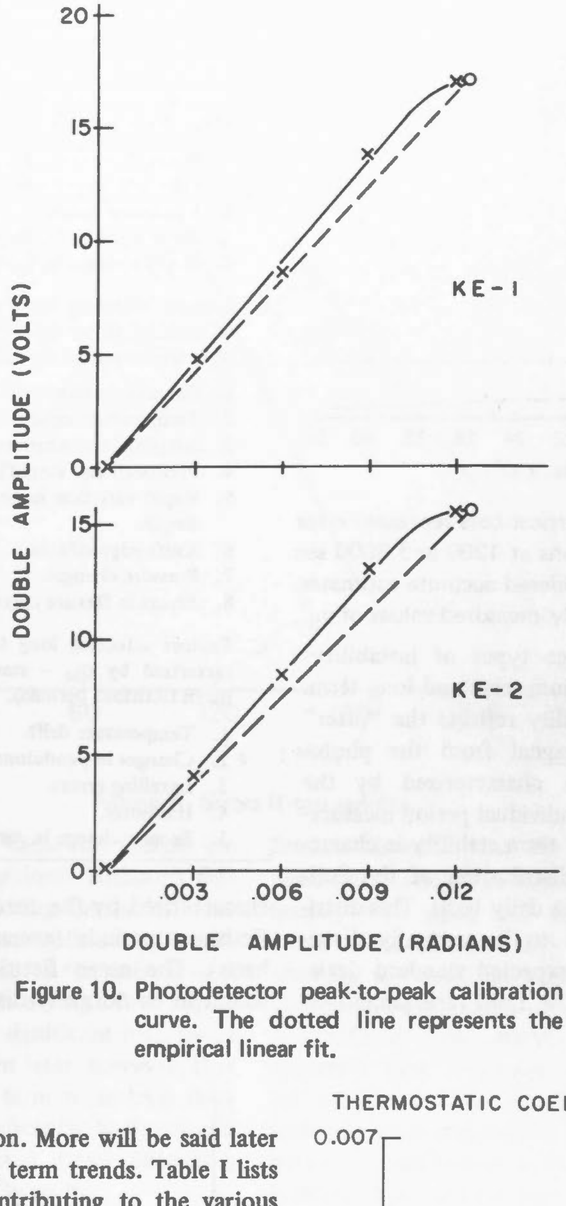

Figure 10. Photodetector peak-to-peak calibration curve. The dotted line represents the empirical linear fit.

line of regression. More will be said later about the long term trends. Table I lists the factors contributing to the various levels of instability.

Temperature tests

Temperature control. Temperature tests were carried out concurrently with the laboratory tests of the data acquisition system to determine if the temperature control was adequate, the time required to establish thermal equilibrium, the effect of pressure variations on temperature and to calibrate the thermostat. The highlights of these tests are given elsewhere (Valliant, 1967a) and the heating curve of the pendulums are reproduced in Figure 6. The variation of the thermostatic coefficient with pressure and the

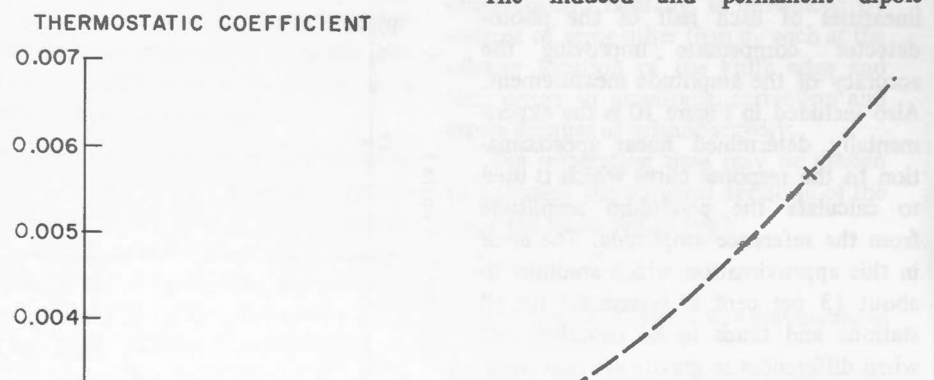

Figure 11. Variation of thermostatic coefficient with pressure.

calibration curve are given in Figures 11 and 12 respectively.

Redetermination of the temperature coefficient. The last determination of the temperature coefficient of the pendulums was made in 1915 by McDiarmid, whose value has been used to apply temperature corrections to the pendulum periods since that time.

The temperature coefficients were redetermined in 1968 for pendulum pairs 1-2, 1-3, 4-5 and 4-6. The results are given graphically in Figure 13. The temperature coefficients determined by a least squares fit to the observational data are 8,076, 8,282, 7,919 and 8,955 ns/degree respectively. The mean coefficient for pendulum pairs 1-2 and 1-3 (8,179 ns/degree) agrees to within 3 per cent of McDiarmid's value of 8,380 ns/degree. Temperature corrections for all measurements subsequent to the NACL observations will be computed using the value 8,179 for the set comprising pendulums 1, 2 and 3 and 8,440 for the set comprising pendulums 4, 5 and 6. The use of McDiarmid's coefficient does not introduce appreciable error as it is within 2 per cent of the mean temperature coefficient for all pendulums and the maximum temperature correction seldom exceeds 800 ns.

Magnetic tests

Magnetic properties of the pendulums. The induced and permanent dipole moments of each pendulum was measured with a fluxgate magnetometer. Magnetic pole strengths were observed at a distance of 1.9 cm from the pendulums. The mean of the pole strengths determines the permanent dipole moment while the difference in these values indicate the magnitude of the magnetic moment induced by the geomagnetic field. Each pendulum was oriented so that the geomagnetic field was in the same plane as the permanent dipole. Thus the magnetizing field for pendulums for which a dipole was horizontal is taken to be approximately 15,000γ. For pendulums with nearly vertical magnetization the magnetic field is considered to be 55,000γ.

Although no magnetic field could be observed in the vicinity of the stem or stirrup, the bobs of all the pendulums were found to be slightly magnetized. The observed dipole always lay in a plane perpendicular to the plane of oscillation of the pendulums. The dipole for different pendulums was found to be oriented within this plane through an angle ranging from nearly horizontal to nearly vertical. The permanent dipole moment, induced dipole moment, the pole separation and direction of magnetization are tabulated in Table II. It can be seen that the permanent and induced moments appear to be from 40 to 100 times larger for pendulums 4, 5 and 6.

Effect of the observed properties. The effect of a dipole moment on the pendulums period was determined by Bullard (1933):

$$\delta s = -\frac{So}{2mgh}(MoZ + aZ^2)$$

where:

So = unperturbed half period

h = distance from centroid to fulcrum

m = mass of pendulum

z = magnetic field strength

Mo = permanent magnetic movement

aZ = induced magnetic movement

The first term in the brackets represents the effect of the permanent dipole whereas the second represents the effect of the

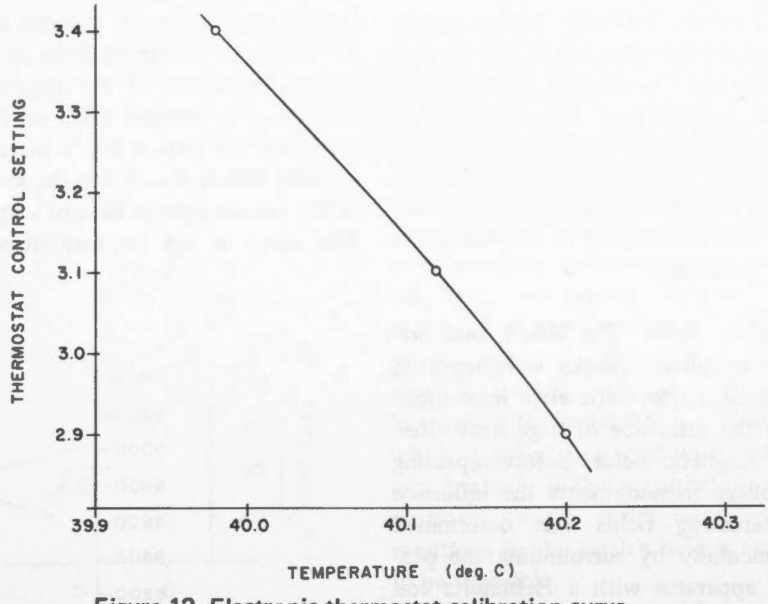

Figure 12. Electronic thermostat calibration curve.

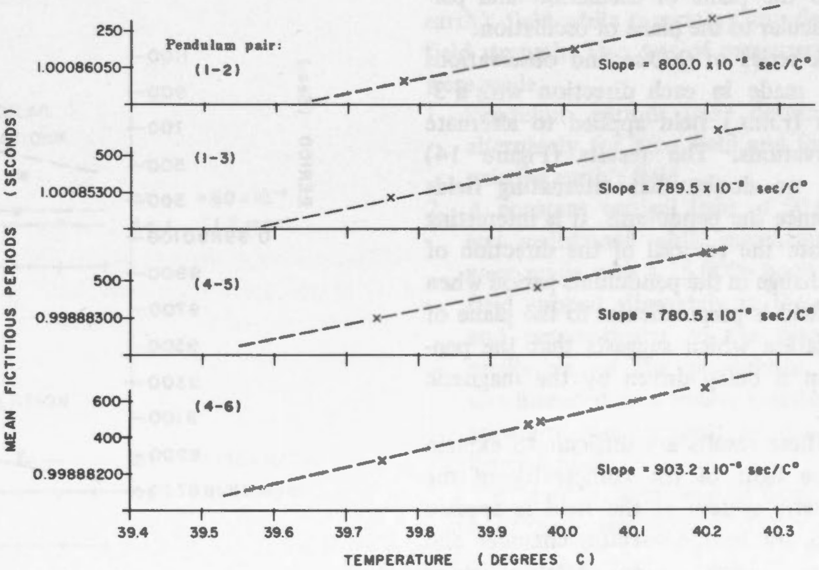

Figure 13. Effect of temperature change on the periods of the fictitious pendulums. The dotted lines represent a least-squares linear fit.

Table II. Magnetic properties of the pendulums

Pendulum	Permanent Moment (amp. m^2)	Induced Moment (amp. m^2)	Approximate Pole Separation (metres)	Orientation of Dipole
1	0.04×10^{-4}	0.03×10^{-4}	0.05	15° from horizontal
2	0.06×10^{-4}	0.01×10^{-4}	0.08	near vertical
3	0.07×10^{-4}	0.01×10^{-4}	0.04	horizontal
4	3.5×10^{-4}	2.4×10^{-4}	0.04	horizontal
5	2.7×10^{-4}	2.0×10^{-4}	0.04	horizontal
6	2.6×10^{-4}	0.3×10^{-4}	0.08	near vertical

induced dipole. Applying values representative of the Canadian pendulums we find that the magnetic moment either permanent or induced may not exceed 60 X 10^{-4} amp. m^2 if the error is to be maintained below 0.1 mgal. Table II makes it clear that any observed magnetic effects can not be due to magnetization of the pendulums.

Alternating fields. The NACL measurements at College, Alaska were repeated because of a systematic error introduced due to the influence of large stray alternating magnetic fields. Before repeating the College measurements the influence of alternating fields was determined experimentally by surrounding the pendulum apparatus with a Helmholtz coil and applying a known alternating field. The field was applied sequentially in the three principal directions–vertical, parallel to the plane of oscillation and perpendicular to the plane of oscillation.

A series of 900-second observations were made in each direction with a 3-gauss (r.m.s.) field applied to alternate observations. The results (Figure 14) leave no doubt that alternating fields influence the pendulums. It is interesting to note the reversal of the direction of the change in the pendulums period when the field is perpendicular to the plane of oscillation which suggests that the pendulum is being driven by the magnetic field.

These results are difficult to explain in the light of the complexity of the magnetic system as the field is applied externally to the vacuum chamber and the pendulums are completely shielded by three metal chambers including the gold plated bell jar. Also complicating the analysis is the irregular shape of the pendulums themselves. The increase in period for two field directions might well be due to eddy-current braking. As the power line frequency is about 120 ppm greater than the 60th harmonic of the pendulum's frequency the decrease in the period when the field is perpendicular may possibly be because of a resonance phenomenon.

The effect in changing the amplitude of the applied field in a plane parallel to the plane of oscillation is shown in Figure 15 where the observed error is plotted against the square of the magnetic field strength. The obvious linear relation suggests that the error is due to magnetically induced effects (i.e. it has the same form as the second term in Bullard's equation). This result is not inconsistent with the idea that eddy currents are the causative factor.

Obviously a much more extensive program is required to determine the cause of the anomalous behaviour due to alternating magnetic fields. However, these measurements indicate the existence and magnitude of such errors and

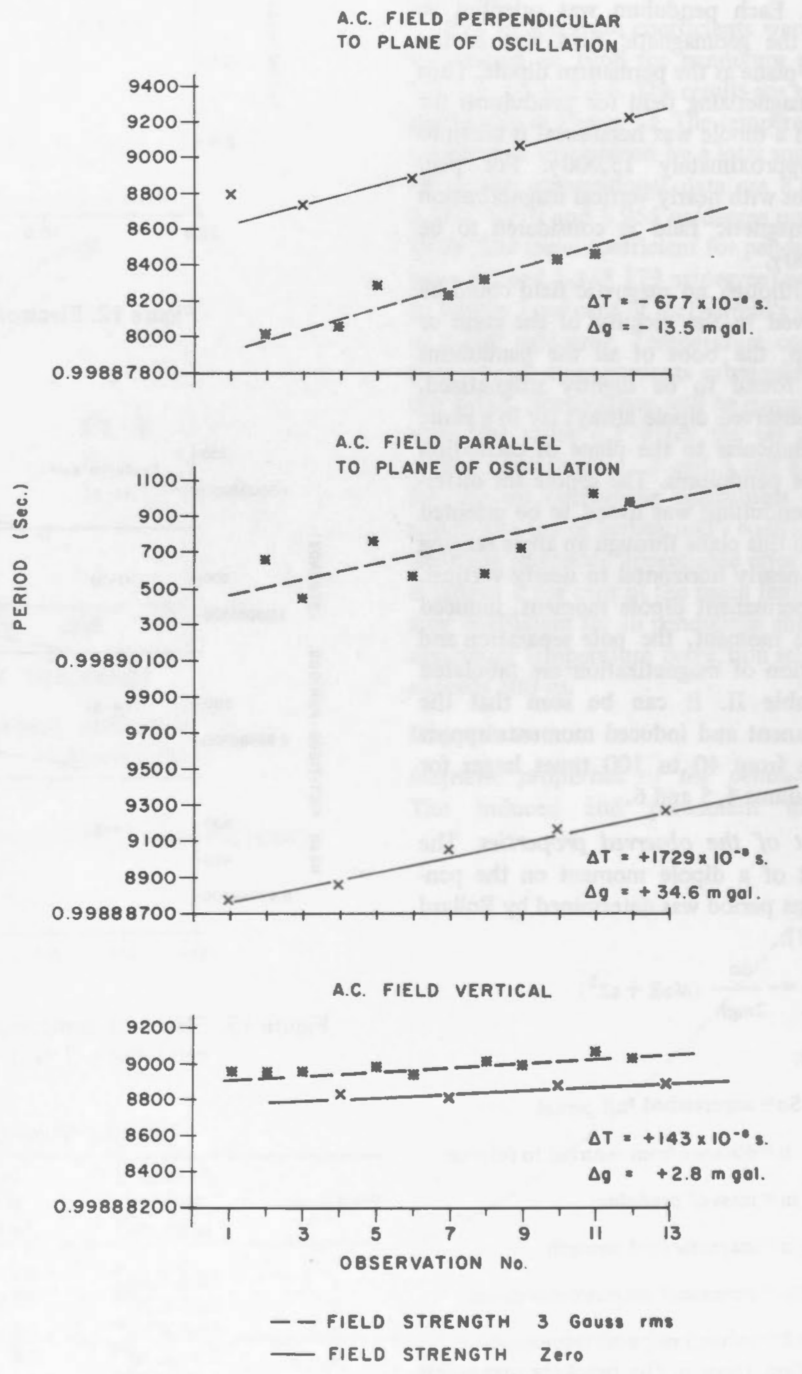

Figure 14. Effect of alternating magnetic fields applied in the three principle planes.

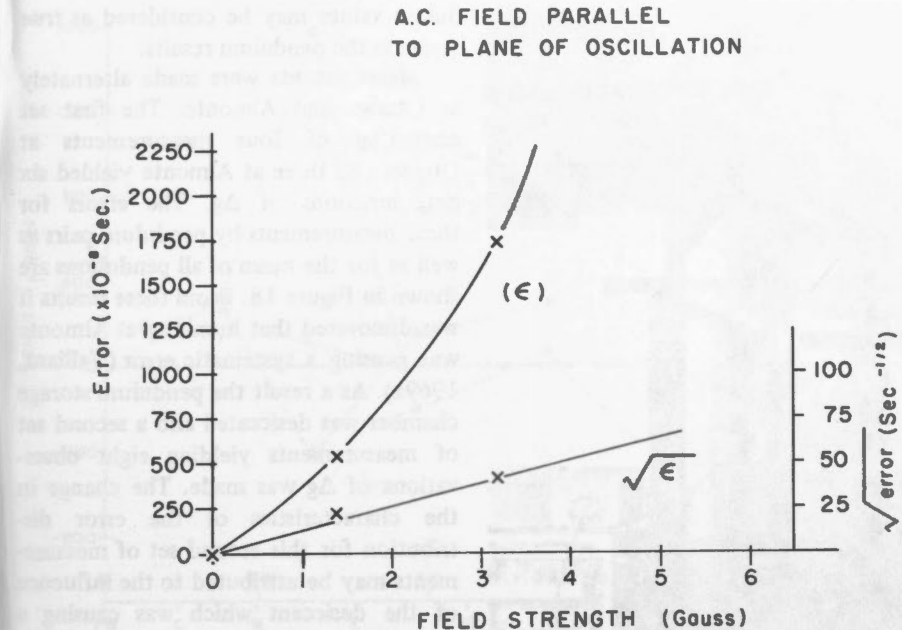

Figure 15. Variation of the effect of alternating magnetic fields with field strength.

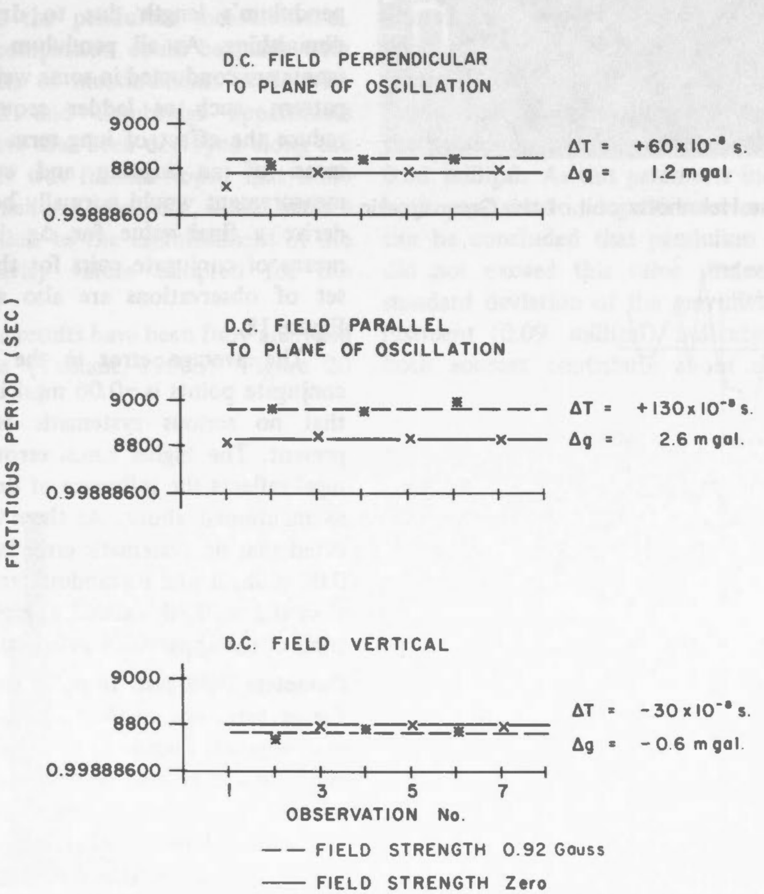

Figure 16. Effect of steady-state magnetic fields applied in the three principle planes.

the solution to this problem is to avoid locating the apparatus in areas subject to large alternating fields.

Direct fields. The effect of a direct or steady state field was also briefly investigated using the same Helmholtz coils. A field of nearly one gauss was applied in three principal directions as before. The net field, influencing the pendulum's motion, is of course the vector sum of the geomagnetic and applied fields. In every case (Figure 16) the error was found to increase with increasing field strength, which is again consistent with eddy current braking. If the perturbation is proportional to β^2 errors introduced by variations in the earth's field is expected to be negligible.

This was further tested by mounting the vacuum case inside large Helmholtz coils as shown in Figure 17. These coils are equipped to automatically null the earth's field while generating any desired field strength. Two sets of measurements were made:

1. Pendulum periods were determined alternately for zero field and for the existing earth's field.
2. A constant vertical field of 50,000γ was maintained while measurements were made with a 15,000γ horizontal field applied alternately in the plane and perpendicular to the plane of oscillation of the pendulums. This was intended to simulate rotating the apparatus with respect to the geomagnetic field.

No detectable effect was observed for either of these tests.

Simulated field tests. The effects of moving the apparatus during field operations was tested by making a series of measurements between the national reference pier in Ottawa and a typical field site located at Almonte, Ontario (a town 35 miles distant from Ottawa). As environmental conditions were carefully controlled at Ottawa, errors in the measured Δg would reflect the combined effects of transportation and environment at Almonte. The Δg was also measured with gravimeters and since this value is small (Δg = 32.15 milligal) differences between the gravimeter and pen-

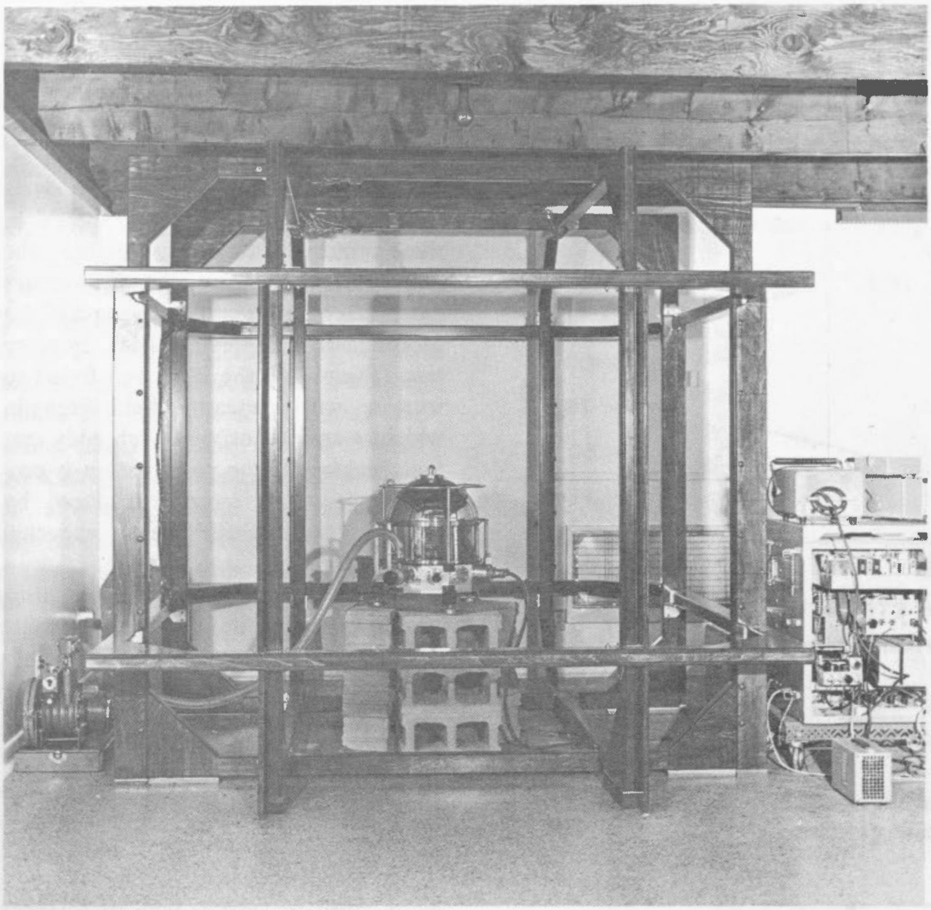

Figure 17. The pendulum apparatus installed in the Helmholtz coil of the Geomagnetic Division of the Earth Physics Branch.

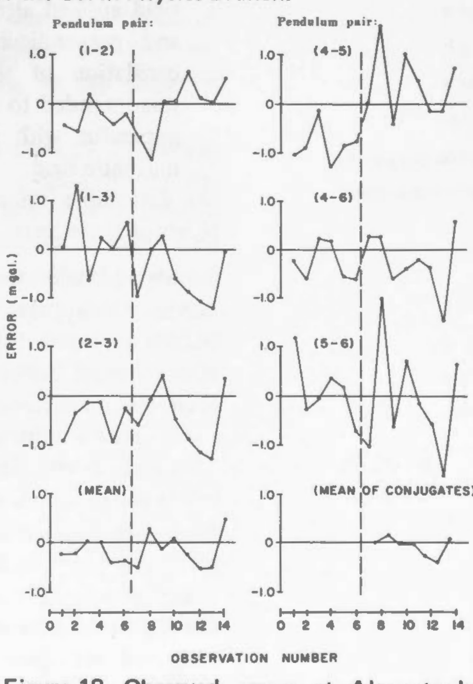

Figure 18. Observed errors at Almonte by pendulum pairs and grand means.

dulum values may be considered as true errors in the pendulum results.

Measurements were made alternately at Ottawa and Almonte. The first set consisting of four measurements at Ottawa and three at Almonte yielded six determinations of Δg. The errors for these measurements by pendulum pairs as well as for the mean of all pendulums are shown in Figure 18. From these results it was discovered that humidity at Almonte was causing a systematic error (Valliant, 1969a). As a result the pendulum storage chamber was desiccated and a second set of measurements yielding eight observations of Δg was made. The change in the characteristics of the error distribution for this second set of measurements may be attributed to the influence of the desiccant which was causing a monotonic change in the pendulum length due to continued drying. It was believed and later confirmed (Valliant, 1969a) that the rate of change in the pendulum's length due to drying was diminishing. As all pendulum measurements are conducted in some well defined pattern, such as ladder sequence, to reduce the effect of long term drift, the mean of an ingoing and outcoming measurement would normally be used to derive a final value for Δg. Thus the means of conjugate pairs for the second set of observations are also shown in Figure 18.

The average error in the mean of conjugate points is −0.06 mgal indicating that no serious systematic errors are present. The higher r.m.s. error of 0.20 mgal reflects the influence of desiccation as mentioned above. As these tests indicated that no systematic error larger than 0.06 milligal and no random errors larger than 0.2 milligal existed complete field trials of the apparatus was begun.

Complete field test. In order to evaluate the performance of the Canadian pendulum apparatus under actual field conditions, measurements were performed at selected sites along the North American Calibration Line (NACL). As the sites have been well connected with gravimeter measurements a comparison between gravimeter and pendulum derived values would indicate the magnitude of random

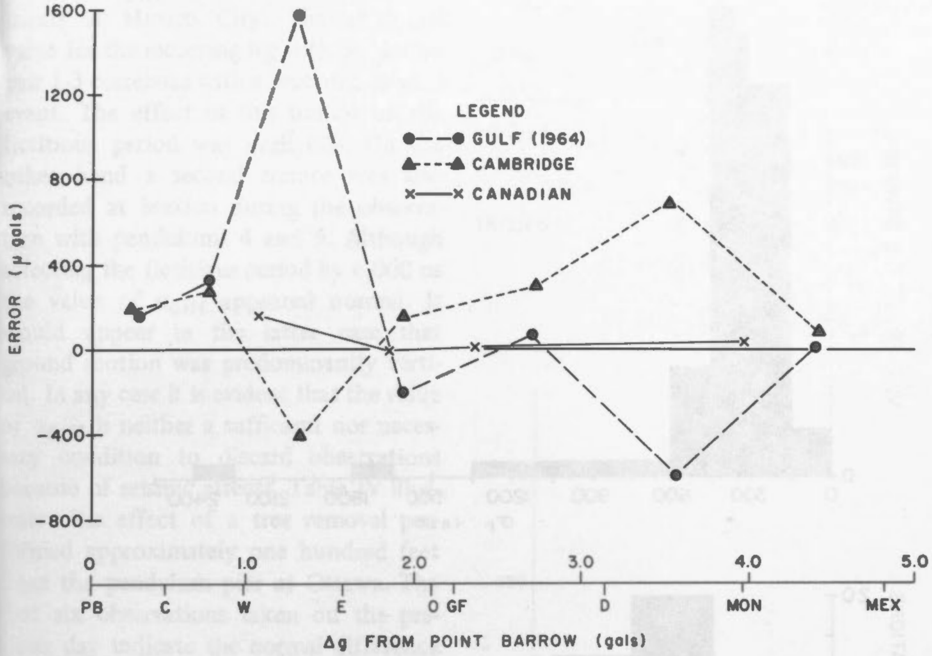

Figure 19. Observed errors for measurements on the North American calibration line compared with errors for the Gulf and Cambridge pendulums.

errors in the pendulum measurements. Also a comparison could be made with the results of measurements made with the Gulf and Cambridge apparatuses which have also been deployed along the NACL. It was further hoped that these measurements if successful, would make a contribution to the establishment of the final gravity values adopted for the NACL.

These results have been fully analyzed elsewhere (Valliant, 1969b). Figure 20 reproduces the comparison between the various pendulum measurements and gravimeter values. In summary it was found that the r.m.s. difference between the pendulum and gravimeter results was 0.08 milligal. As this parameter includes both pendulum and gravimeter errors it can be concluded that pendulum errors did not exceed this value. Indeed the standard deviation of the gravimeter adjustment (0.09 milligal) indicates that both sources contribute about equally to the error distribution and therefore the r.m.s. error of the pendulums alone amounted to about 0.06 milligal ($0.08/\sqrt{2}$). As was expected from the Almonte tests, the effects of continued drying of the pendulums was much diminished. The mean difference between gravimeter and pendulum values amounted to +0.04 milligal which is similar to that found in the Almonte tests. As the gravimeter analysis was based upon the European standard this is equivalent to a difference in scale of approximately 35 ppm between the Canadian pendulum and European standard.

Recently measurements on the NACL with the "Faller laser-interferometer free-fall apparatus" have been completed. Absolute measurements were made at the exact sites of the pendulum observations at College and Denver. The results tabulated below indicate agreement within the estimated error bounds:

*Δg from absolute measurements
− 2637.24 ±0.07 mgal.

Δg from pendulum measurements
− 2637.38 ±0.10 mgal

Difference
0.14 ±0.12 mgal

*Recently completed measurments from College, Alaska to Ottawa, Ont. combined with gravimeter ties from Ottawa to Boston agree with the absolute Δg from College to Boston to within .04 mgal.

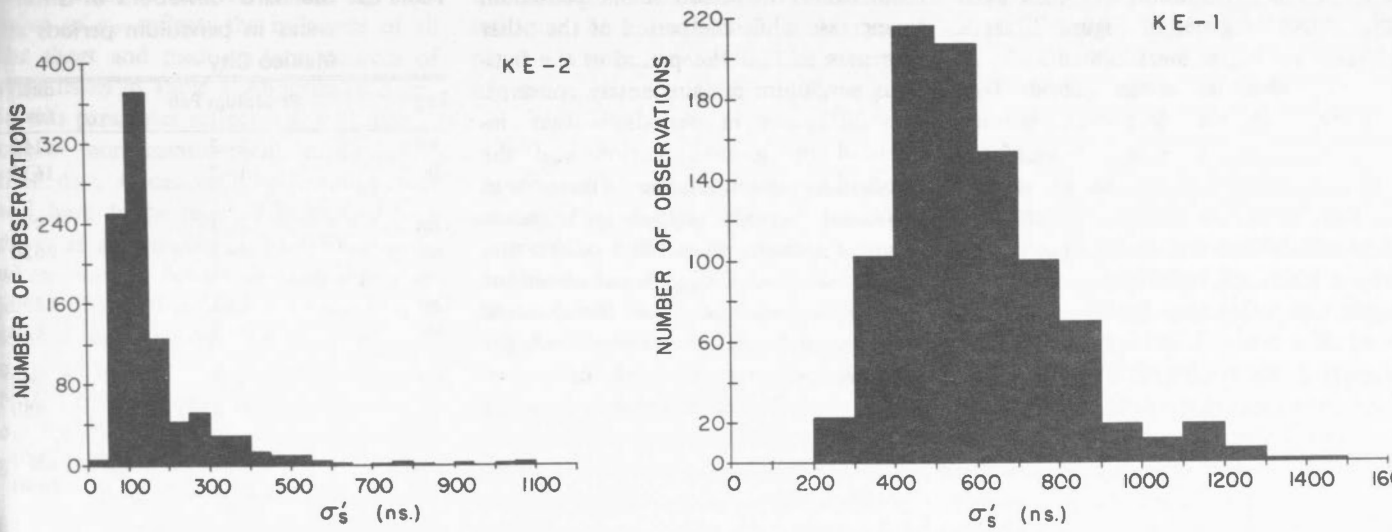

Figure 20. Distribution of σ_s' for knife-edges one and two for NACL results.

With the successful completion of these tests the Canadian pendulum apparatus is considered fully operational for gravity measurements in regions where gravity values are not closely controlled.

Normal test parameters. Several parameters are normally calculated in the complete analysis of pendulum data. Forty-nine measurements of the average period for each observation is obtained by taking all possible differences of the seven initial and final zero-crossing measurements. Their standard deviation σ_S' is a measure of the short term stability and is related to the standard deviation of individual periods by: $\sigma_S' = \sigma_{S/N}$ (where N is the number of oscillations of the pendulum, usually 900). This parameter indicates the proper functioning of the data acquisition system. It also serves as an indicator of sources of malfunction in the binary accumulator, transmission gates, or recorder as a fault associated with a particular binary level produces a well defined value of σ_S'. For example, an error in the 2^{+11} binary level yields a σ_S' in a small range centred around 16,000 ns; a σ_S' of 32,000 ns corresponds to an error in the 2^{+12} binary and $\sigma_S' = 8{,}000$ ns corresponds to an error in the 2^{+10} binary. If the 49 observed periods are listed in a suitable array, the offending binary counter can be quickly determined because it produces an error that affects all elements in either a row or a column. The distribution of σ_S' for both knife edges is given in Figure 20 as a reference for future measurements.

The individual mean periods (i.e. the mean of the 49 average periods for each pendulum) is also determined. This parameter yields information regarding the effect of ground motion and, when pendulums are swung together in sets, a study of individual periods can isolate the offending pendulum in the event of a tare (i.e. sudden unexplicable changes in the length of the pendulum). Note, however, that no significant tares have been observed with the Canadian pendulum apparatus during any of the laboratory tests or field trials.

In the bi-pendulum method horizontal ground motion in the plane of oscillation causes the period of one pendulum to increase while the period of the other decreases so that the period of the fictitious pendulum remains nearly constant. The difference in periods is then influenced by ground motion and the standard deviation of the differences in individual periods (σ_{diff}) is to some extent a measure of stability of the site. Hence the value of σ_{diff} is calculated for each day's observations (i.e. the standard deviation of the difference in periods for the twelve observations made on an observing day). The distribution of σ_{diff} for the NACL measurements is given in Figure 21 for reference purposes.

The influence on σ_{diff} of three isolated events are worth discussing in greater detail. Table III lists the observed

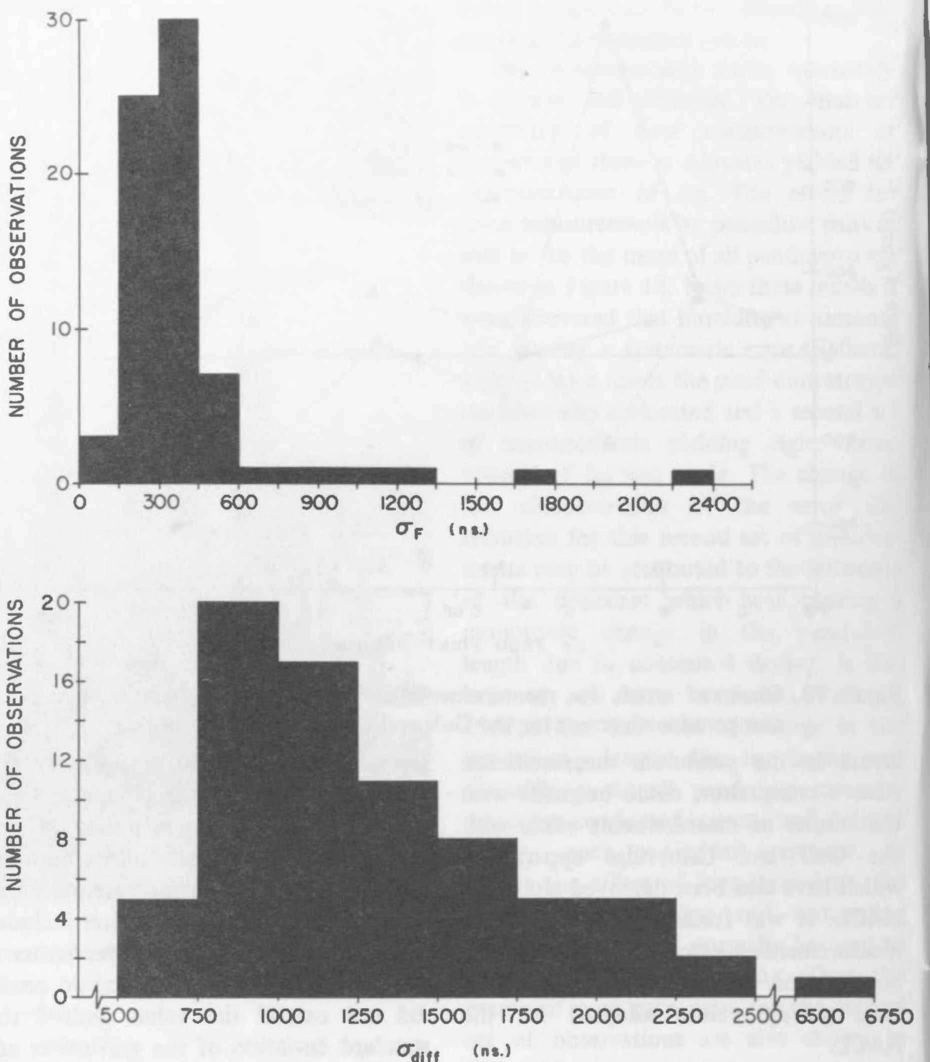

Figure 21. Distributions of σ_F and σ_{diff} for NACL results.

Table III. Standard deviations of differences in pendulum periods at Mexico City

Leg	Pendulum Pair	diff. (ns.)
Out	1–2	1110
In	1–2	1630
Out	1–3	990
In	1–3	6620
Out	2–3	1340
In	2–3	830
Out	4–5	990
In	4–5	980
Out	4–6	1350
In	4–6	1100
Out	5–6	1170
In	5–6	1250

value of σ_{diff} for the NACL measurements at Mexico City. The abnormal value for the incoming leg with pendulum pair 1-3 correlates with a recorded seismic event. The effect of this tremor on the fictitious period was negligible. On the other hand a second tremor was also recorded at Mexico during the observation with pendulums 4 and 5. Although affecting the fictitious period by 6,000 ns the value of σ_{diff} appeared normal. It would appear in the latter case that ground motion was predominantly vertical. In any case it is evident that the value of σ_{diff} is neither a sufficient nor necessary condition to discard observations because of seismic effects. Table IV illustrates the effect of a tree removal performed approximately one hundred feet from the pendulum pier at Ottawa. The first six observations taken on the previous day indicate the normal difference in periods for that particular pair of pendulums. The change in the difference in periods is striking on the second day. The main trunk of the tree was felled during observation 2 accounting for the exceptionally large value of ΔT for this observation. Note that although there was a significant increase in the value of σ_{diff} for all other observations the value of the fictitious period was not disturbed except for observation of 2.

The fictitious periods, the mean of the fictitious periods and their standard deviation (σ_F) is also prepared on a daily basis. The mean of the fictitious periods are used directly in determining Δg. The value of σ_F reflects the influence of all the short and medium term sources of error listed in Table I. Abnormal changes in this parameter reflect a disturbance in one or more measurements made during that day. Occasionally a measurement will have to be rejected because it produces an abnormally high σ_F. Frequently when seismic records are available a rejected observation can be correlated with seismic activity that has not affected σ_{diff} as in the example cited from the NACL observations. The distribution of σ_F for the NACL measurements is also given in Figure 21 for reference purpose.

The correlation between σ_F and σ_{diff} is given in Figure 22. A least squares linear fit is also plotted and a correlation coefficient of 0.16 was determined. Although large values of σ_{diff} indicate the influence of ground motion this parameter is a poor criterion for the rejection of data because of the influence of seismic activity.

Table IV. Effect of tree removal on differences in period

Date	Observation No.	Period Pend. 1 (sec)	Period Pend. 2 (sec)	Fictitious Period (sec)	ΔT (μs)
16/2/66	1	1.0008639	1.0008649	1.0008644	+ .13
	2	1.0008646	1.0008643	1.0008644	- 0.3
	3	1.0008635	1.0008659	1.0008647	+ 2.4
18/2/66	1	1.0008573	1.0008680	1.0008627	+ 10.7
	2	1.0003137	1.0008673	1.0005905	+553.6
	3	1.0008572	1.0008684	1.0008628	+ 11.2
	4	1.0008594	1.0008685	1.0008639	+ 9.1
	5	1.0008580	1.0008689	1.0008634	+ 0.9

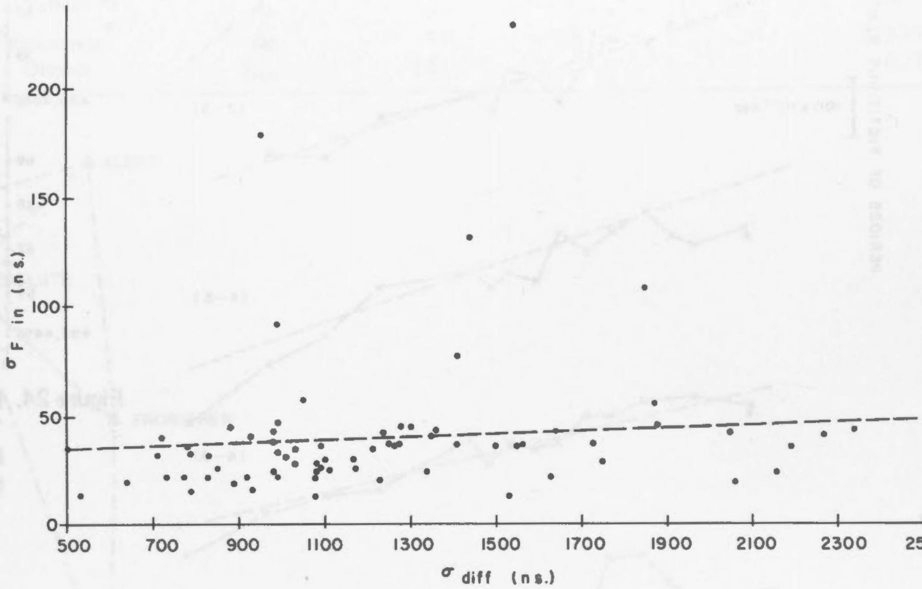

Figure 22. Correlation of σ_F with σ_{diff}. The dotted line represents a least-squares linear fit.

Long term trends in the pendulum periods. Factors affecting the long term characteristics of the distribution of fictitious periods are listed in Table I. All these appear negligible except for the long term drift in the effective length of the pendulums. Drift in the pendulum's apparent length may be due to creep effects, simple mechanical slippage at the joints of their component parts, or secular variation in gravity. Any or all of these factors may contribute to the distribution of fictitious periods shown in Figure 23.

A least squares linear fit to the time curves for each of the pendulum pairs is also shown. The statistics of the straight line fit is given in Table V. As can be seen there is a remarkable degree of linear correlation as well as a remarkable similarity in the slopes of all the curves. The average drift amounts to 3.3 ns per day which is equivalent to a monotonic shortening of the pendulums of about 2.4 ppm per year or in terms of gravity 2.4 mgal per year.

Hamilton (1961) published a similar graph (Figure 24) for pendulums 4, 5 and 6 for the years of 1957 to 1959 inclusive. Unfortunately the introduction of a new environmental control system introduces a singularity in the curves between 1959

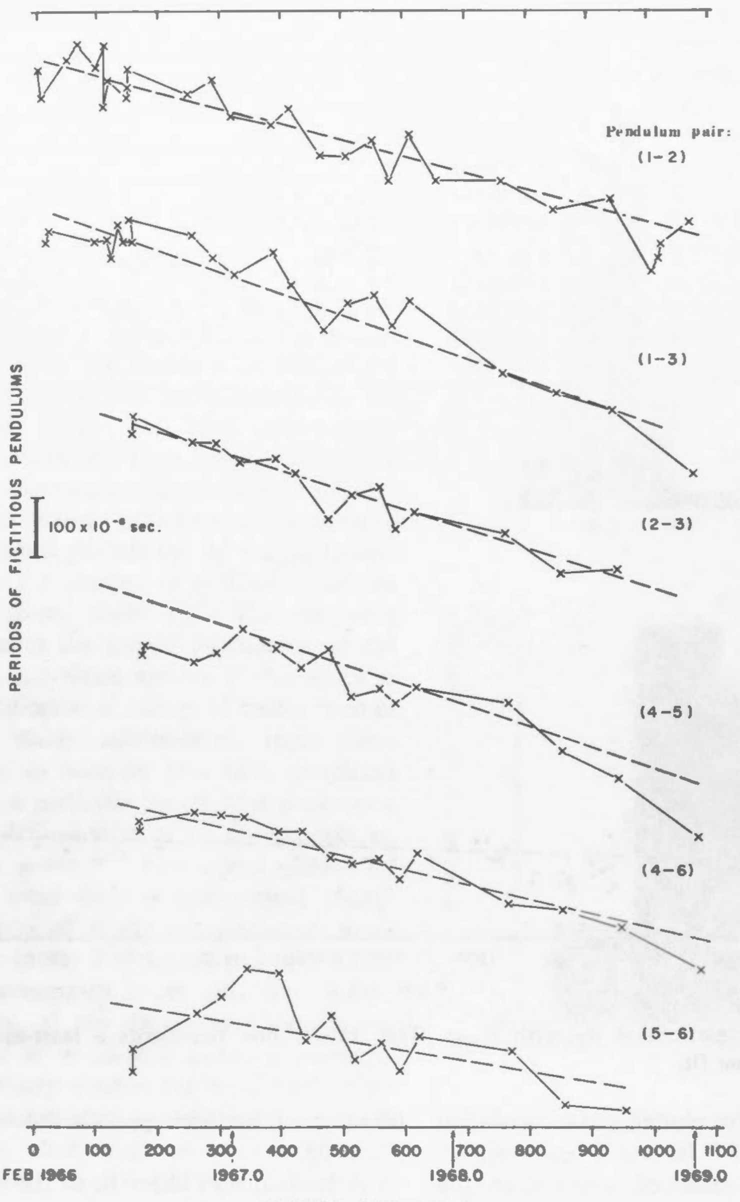

Figure 23. Long term trend in pendulum periods (effective length) from 1966 to 1969. The dotted lines represent a least-squares linear fit.

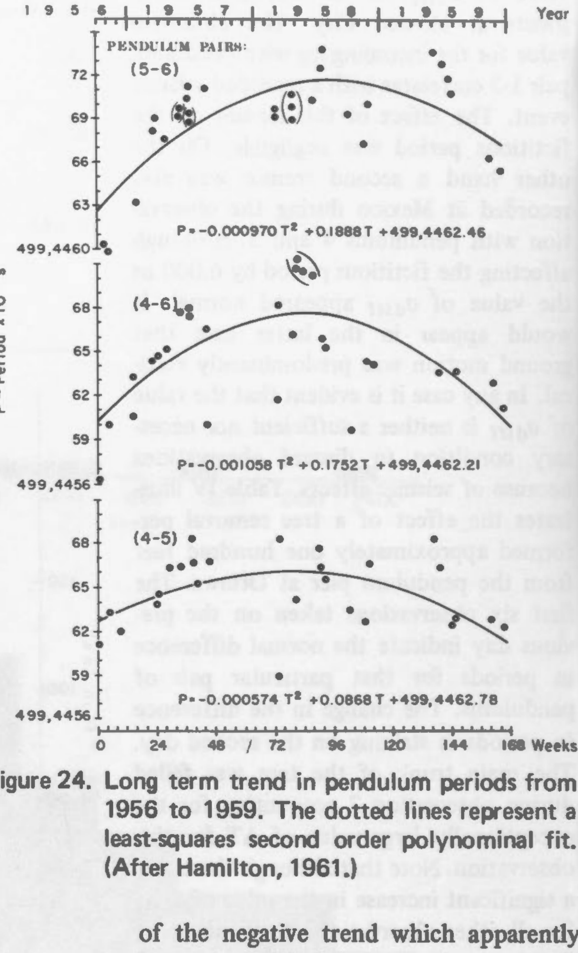

Figure 24. Long term trend in pendulum periods from 1956 to 1959. The dotted lines represent a least-squares second order polynominal fit. (After Hamilton, 1961.)

Table V. Statistics of long term drift analysis

Pendulum	Slope (ns/day)	Correlation Coefficient	Standard Deviation (ns)
1–2	−2.68	−0.92	328
1–3	−3.39	−0.95	303
2–3	−3.34	−0.96	236
4–5	−2.69	−0.91	306
4–6	−2.51	−0.95	208
5–6	−1.73	−0.60	573

and 1966 so that the two portions of the trend curves cannot be compared directly. The earlier data are also subject to large errors because of inadequate temperature control. It is further suggested by Saito (1963) that fitting a quadratic curve to these data is not statistically justified. Nevertheless comparison of the slopes of two sets of curves suggests that the present drift, having the same direction but greater magnitude than the slope in 1959, is a continuation of the negative trend which apparently began in 1958. It is interesting to postulate from these curves that the length of the pendulums (or gravity) is varying cyclically with a period in the order of 40 years and a half amplitude amounting to about 16 ppm in gravity. Notwithstanding the fact that the pendulums are all maintained in the same environment it is a remarkable coincidence that the behaviour of all six pendulums is nearly identical. There is no *a priori* reason to expect that two sets of pendulums which were constructed at different times, subject to widely different early histories, exhibit different magnetic properties, have a slightly different design and period, to exhibit identical long term drift characteristics.

Hysteresis in the thermal expansion curve is one possible explanation of the long term trend. In this case the pendulums do not attain their original length, but are slightly shorter after the temperature has been cycled from warm to cool

Table VI. Canadian network pendulum results

Interval	Parameter	Outgoing leg (mgal)	Incoming leg (mgal)	Difference (mgal)	Mean (mgal)
Resolute-	$\overline{\Delta g}$	839.54	839.72	0.18	839.63
Yellowknife	$\sigma_{\overline{\Delta g}}$	0.25	0.16		0.15
Yellowknife-	$\overline{\Delta g}$	855.90	855.92	0.02	855.91
Edmonton	$\sigma_{\overline{\Delta g}}$	0.84	0.27		0.44
Edmonton-	$\overline{\Delta g}$	232.61	231.98	−0.63	232.29
Vancouver	$\sigma_{\overline{\Delta g}}$	0.88	0.20		0.45
Winnipeg-	$\overline{\Delta g}$	59.94	59.40	−0.54	59.67
Vancouver	$\sigma_{\overline{\Delta g}}$	0.33	0.31		0.23
Vancouver-	$\overline{\Delta g}$	372.89	373.22	0.33	373.05
Ottawa	$\sigma_{\overline{\Delta g}}$	0.51	0.19		0.27

and back to the original temperature. The pendulums are kept at constant temperature, however, even in their storage container, and the only temperature cycling occurs when they are transferred from storage to the vacuum chamber. The long term trend was also analyzed as a function of observation number (rather than time), and it was found that the fit to linear regression was poorer. This suggests that the drift is more properly considered a time dependent process which excludes thermal hysteresis as a possibility. Also the effect of thermal hysteresis is not in accord with Figure 24. As observations were carried out on a daily basis from 1957 to 1959 one would expect the slope to be greater for this period if hysteresis is the causative factor.

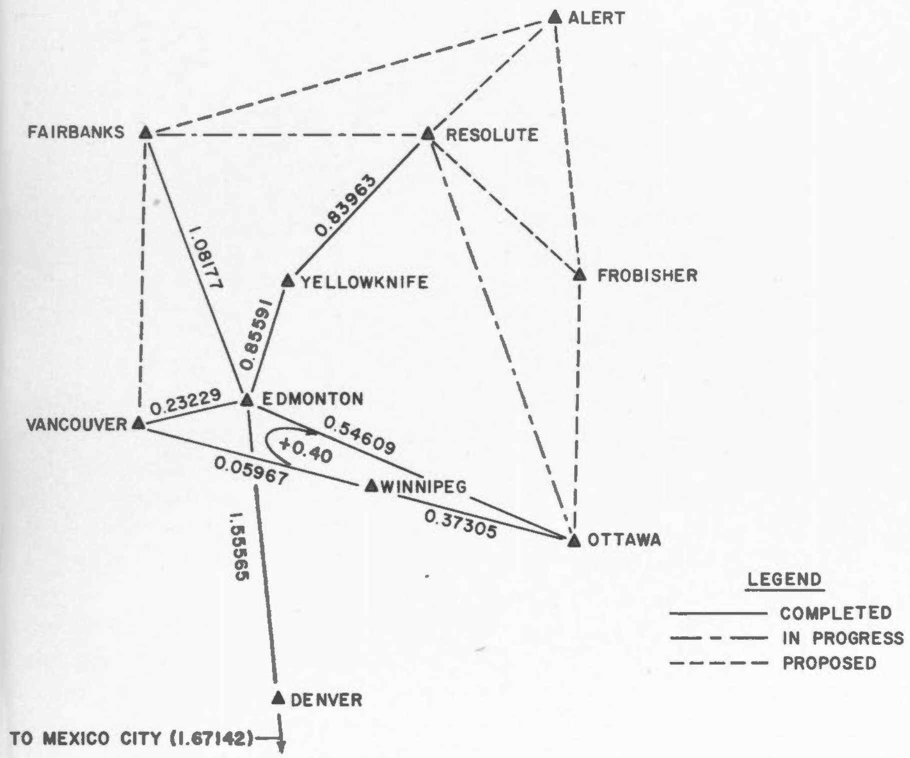

Figure 25. Network of pendulum stations in Canada.

Appendix I

Canadian Network of Pendulum Stations

Pendulum measurements at selected sites according to Figure 25 are being carried out. Measurements between Ottawa, Resolute Bay and Fairbanks were unsatisfactory because of an abnormally high apparent drift rate and are presently being repeated. The results of completed measurements are summarized in Table VI. A complete analysis of these results is expected to provide the subject of a future paper.

References

Bullard, E.C. 1933. The effect of a magnetic field on relative gravity determinations with invar pendulums. *Proc. Roy. Soc. A*, 141, 233.

Hamilton, A.C. 1961. Evaluation of the Dominion Observatory bronze pendulum apparatus. *Contr. Dom. Obs.*, 5, 3-21.

McDiarmid, F.A. 1915. *Gravity. Pub. Dom. Obs.*, 2, 202-269.

Saito, T. 1963. Statistical analysis of pendulum observations. *Boll. Geofs. teor. appl.*, 19, 217-234.

Swick, C.H. 1921. Modern methods for measuring the intensity of gravity. Dept. of Commerce, U.S. Coast and Geodetic Survey, special publication No. 29, 1-96.

Thompson, L.D.G. 1959. An improved bronze pendulum apparatus for relative gravity determination. *Publ. Dom. Obs.*, 3, 145-176.

Valliant, H.D. 1965. A digital recorder for pendulum measurements. *IEEE.*, GE-3, 2-6.

__________ 1969a. A temperature control system for the Canadian pendulum apparatus. *IEEE.*, GE-5, 84-89.

__________ 1967b. An electronic system for measuring pendulum periods. *IEEE.*, GE-5, 79-83.

__________ 1969a. The effect of humidity on the length of invariable pendulums. *Geophys. J.R. Astr. Soc.*, 17, 327-332.

__________ 1969b. Gravity measurements on the North American calibration line with the Canadian pendulum apparatus. *Geophys. J.R. Astr. Soc.*, 17, (in press).

Vening-Meinesz, F.A. Theory and practice of pendulum observations at sea. *Publ. Neth. Geod. Comm.*, Delft, The Netherlands.

Winter, P.J., Valliant, H.D. 1960. Relative gravity measurements in the Prairie Provinces with the Dominion Observatory bronze pendulum apparatus. *Contr. Dom. Obs.*, 3, 1-16.

Winter, P.J., Valliant, H.D., Hamilton, A.C. 1961. Pendulum observations at Ottawa, Gander, Teddington, Paris, Rome, and Bad Harzburg. *Contr. Dom. Obs.*, 3, 1-16.

PUBLICATIONS of the EARTH PHYSICS BRANCH

VOLUME 41 - NO. 5

a solid-state electrical recording magnetometer

D. F. TRIGG, P. H. SERSON AND P. A. CAMFIELD

DEPARTMENT OF ENERGY, MINES AND RESOURCES

OTTAWA, CANADA 1971

Cat. No.: M70-41/5

Contents

Figure 1. The solid-state, 3 component magnetometer.

a solid-state electrical recording magnetometer

D. F. TRIGG, P. H. SERSON AND P. A. CAMFIELD

Abstract. A solid-state, three-axis recording magnetometer using fluxgate-type magnetic detectors is described. Design theory, circuit details, performance data and operating instructions are provided. Instrument specifications include an output sensitivity of 1 volt per 100 gammas, a -3 db gain roll-off at 3.5 Hz and less than 4 watts power consumption. A comparison of instrument performance when using tuned magnetic detectors with performance when using untuned detectors indicates the superiority of the latter mode of operation.

Résumé. Nous donnons la description d'un magnétomètre enregistreur entièrement transistorisé dont les trois sondes magnétiques placées orthogonalement sont des solénoides à noyau saturable. La théorie, la construction, l'opération et le rendement sont donnés en détail. Les spécifications de l'instrument comprennent une sensibilité de rendement de 1 volt par 100 gammas, un niveau de -3 db à 3.5 Hz et une consommation de puissance de moins que 4 watts. Une comparaison de rendement entre instruments employant des sondes magnétiques syntonisées ou non-syntonisées démontre la supériorité de la dernière méthode d'opération.

Introduction

Three-axis recording magnetometers using fluxgate-type magnetic detectors were used extensively in Canada starting with the International Geophysical Year in 1957. Although these units were intended to be used chiefly at magnetic observatories, applications soon arose in which these magnetometers were transported frequently during research programs, often to inaccessible locations having no indigenous power source. With these problems of transportation and power in mind, the staff of the Geomagnetic Division proceeded to design a solid-state counterpart of the original electrical recording magnetometer described by Serson (1957). The result was the portable, solid-state magnetometer which appears in Figure 1 and is described in detail in the accompanying text. The magnetic detectors now in use are identical with those detailed by Serson (1957), and the magnetometer output is still in the form of three analog voltages proportional to three orthogonal components of magnetic field at a scale of 1 volt per 100 gammas.

Part I of this paper deals with general design information and data and Part II provides all detail necessary to those who must operate and test these instruments.

Part I – Theory of operation

The theory of operation of the magnetometer has been presented by Serson (1957) in a time-domain analysis. A similar analysis in the frequency domain leads rather naturally to analytic expressions for magnetometer response as a function of frequency, and will be presented here for the sake of completeness and continuity of the discussion.

A block diagram of one channel of the magnetometer currently in use by the Earth Physics Branch appears in Figure 2. The oscillator, frequency doubler and tuned amplifier characteristics do not enter directly into the calculations of system response, and are shown only for completeness. The oscillator amplitude will determine the second-harmonic signal voltage available from the fluxgate secondary coil, per Oersted of input magnetic field (Serson and Hannaford, 1956; Primdahl, 1970). A second-harmonic reference signal of sufficient amplitude and purity to ensure proper operation of the phase-sensitive detector is all that is required of the doubler and tuned amplifier. The output of the fluxgate is a second-harmonic signal e_5, proportional to the total axial magnetic field H_T, which is the sum of the earth's ambient magnetic field H_a and the magnetic fields H_f and H_b produced in the fluxgate secondary coil. H_f is generated by the system feedback current I_f, and H_b is the result of bias current I_b. The phase-sensitive detector output e_1 is a d.c. voltage proportional to the amplified fluxgate signal e_6, which is an a.c. voltage. The output of the low-pass filter consisting of R_2 and C_2 is the d.c. voltage e_2, which is integrated to produce the system output voltage e_3. It is assumed in the analysis that the integrator does not load the low-pass filter.

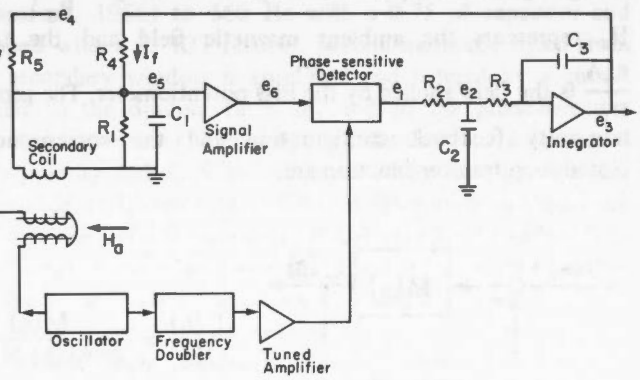

Figure 2. Block diagram of one channel of the magnetometer.

The transfer function F(s) of each element of the block diagram in Figure 2 can be obtained by the methods of control theory (Harrison and Bollinger, 1963). In particular, the transfer function of an element is defined as the ratio of the Laplace transform of the output to the Laplace transform of the input with the assumption that all initial conditions are zero. Listed below are the transfer functions of each element of Figure 2:

1. Fluxgate output: $e_5(s)/H_T(s) = G_1$
2. Fluxgate solenoid: $[H_f(s)+H_b(s)]/[I_f(s)+I_b(s)] = A$
3. Fluxgate signal amplifier: $e_6(s)/e_5(s) = G_2$
4. Phase-sensitive detector: $e_1(s)/e_6(s) = G_3$
5. Low-pass filter: $e_2(s)/e_1(s) = [1/R_2C_2][1/(s+1/R_2C_2)]$
6. Integrator: $e_3(s)/e_2(s) = 1/R_3C_3s$
7. Feedback resistor R_4: $I_f(s)/e_3(s) = 1/R_4$
8. Bias resistor R_5: $I_b(s)/e_4(s) = 1/R_5$

If the reference signal and e_6 are exactly in phase, $G_3=1$. For any other phase relationship $G_3<1$, and at 90° phase difference $G_3=0$.

A block diagram of these transfer functions appears in Figure 3. This diagram can be simplified to the form of Figure 4 by repeated application of the following rules:

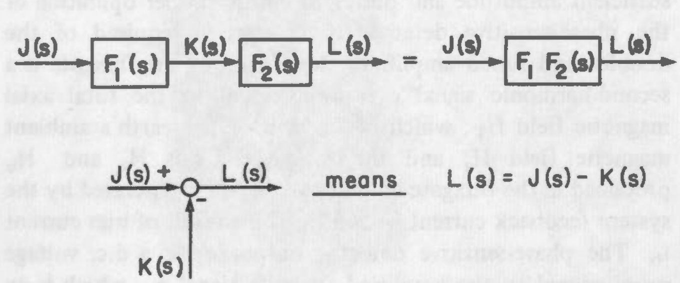

The block diagram of Figure 4 represents the magnetometer as a non-unity feedback system in which the output is the d.c. voltage e_3 and the input is the magnetic field $H_a - \frac{e_4A}{R_5}$, where H_a represents the ambient magnetic field and the term $\frac{e_4A}{R_5}$ is the field applied by the bias potentiometer. The general non-unity feedback configuration and the corresponding closed-loop transfer function are:

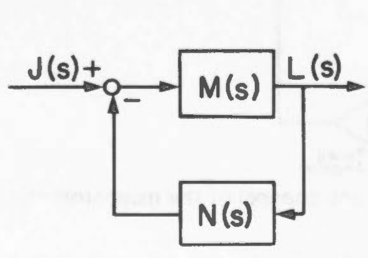

$$\frac{L(s)}{J(s)} = \frac{M(s)}{1+M(s)\,N(s)}$$

Applying this rule to the magnetometer system of Figure 4 gives:

$$\frac{e_3(s)}{H_a(s) - \frac{e_4(s)A}{R_5}} = \frac{\frac{G_1G_2G_3}{R_2C_2R_3C_3(s^2+s/R_2C_2)}}{\frac{G_1G_2G_3}{R_2C_2R_3C_3(s^2+s/R_2C_2)}\cdot\frac{A}{R_4}+1}$$

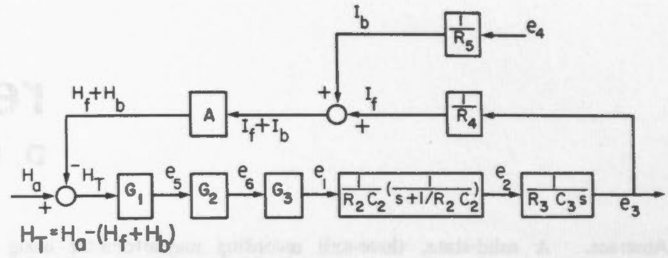

Figure 3. Transfer function block diagram, one channel.

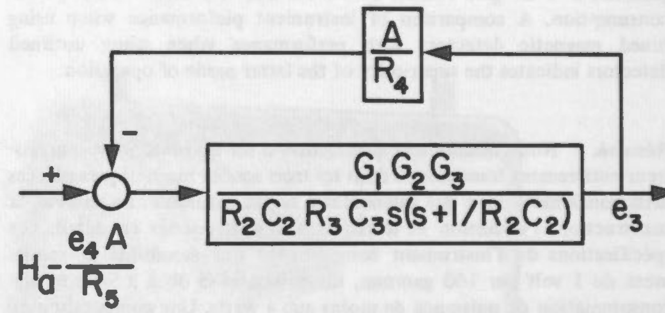

Figure 4. Simplified block diagram, one channel.

which reduces to:

$$\frac{R_2C_2R_3C_3R_4}{G_1G_2G_3A}s^2e_3(s) + \frac{R_3C_3R_4}{G_1G_2G_3A}se_3(s) + e_3(s) = \frac{R_4}{A}H_a(s) - \frac{R_4}{R_5}e_4(s) \quad \ldots\ldots (1)$$

The inverse Laplace transform of equation (1) gives the system differential equation in familiar form:

$$\frac{R_2C_2R_3C_3R_4}{G_1G_2G_3A}\ddot{e}_3 + \frac{R_3C_3R_4}{G_1G_2G_3A}\dot{e}_3 + e_3 = \frac{R_4}{A}H_a - \frac{R_4}{R_5}e_4 \quad \ldots\ldots (2)$$

By comparison of equation (1) with the general second order equation $\frac{s^2 f}{\omega_n^2} + \frac{2\delta}{\omega_n}sf + f = K$, in which ω_n is natural frequency and δ is damping ratio, it is seen that for the magnetometer of Figure 2,

$$\omega_n^2 = \frac{G_1G_2G_3A}{R_2C_2R_3C_3R_4} \quad \text{and} \quad \delta^2 = \frac{R_3C_3R_4}{4R_2C_2G_1G_2G_3A}$$

The output sensitivity of the instrument is determined by letting all derivative terms of equation (2) equal zero (steady-state conditions) and assuming the bias field to be constant. In this case $e_3 = \frac{R_4}{A} H_a$, or output sensitivity $\frac{e_3}{H_a} = \frac{R_4}{A}$ volts/oersted. The values actually used for these constants are R_4 = 340,000 ohms and A = 340 oersted/amp., giving a magnetometer output of 1 volt per 100 gammas.

Frequency response

An analytical method for obtaining the magnitude $M(\omega) = \frac{\text{output } O(\omega)}{\text{input } I(\omega)}$ and the phase difference $\phi(\omega)$ between input and output is given in Appendix A. The result of these calculations is:

$$M(\omega) = \frac{R_4}{A}\left[\left(\frac{\omega}{\omega_n}\right)^4 + (4\delta^2 - 2)\left(\frac{\omega}{\omega_n}\right)^2 + 1\right]^{-\frac{1}{2}}$$

$$\phi(\omega) = \cos^{-1}\left\{\left[1 - \left(\frac{\omega}{\omega_n}\right)^2\right]\left[\left(\frac{\omega}{\omega_n}\right)^4 + (4\delta^2 - 2)\left(\frac{\omega}{\omega_n}\right)^2 + 1\right]^{-\frac{1}{2}}\right\}$$

Constants appropriate to the present magnetometers are:

$G_1 = 4\frac{v}{oe}$ (tuned fluxgate)	$G_2 = 25$	$G_3 = 1$
$R_4 = 340K\Omega$	$A = 340\frac{oe}{amp}$	$R_2 = 33\ K\Omega$
$C_2 = 1.0\ \mu f$	$R_3 = 120K\Omega$	$C_3 = 0.05\mu f$

and these values result in $f_n = \frac{\omega_n}{2\pi} = 3.5$ Hz and $\delta = 0.67$.

Figure 5 shows M (*f*) and ϕ (*f*) plotted against *f* for a system with the constants given above. It should be noted that changing the value of any component used in calculation of ω_n and δ can alter the magnetometer constants greatly, and will lead to instability if δ approaches 0.

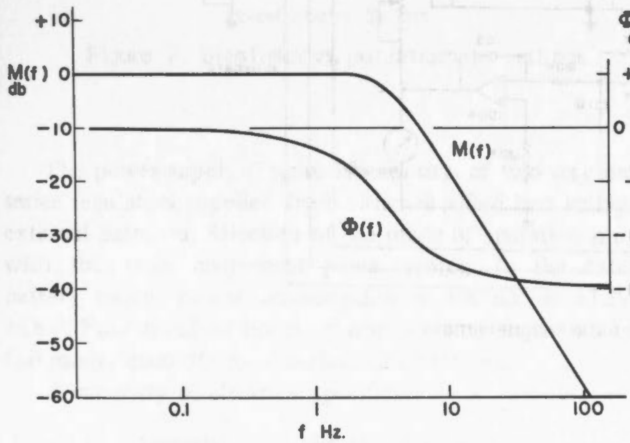

Figure 5. Theoretical frequency response.

Circuit details

A schematic of the 3-component magnetometer currently in use at the Earth Physics Branch appears in Figure 6. The three fluxgates are orthogonally mounted in a sensing head assembly, which also contains a platinum resistance thermometer. The sensing head is connected to the electronics package by means of a multi-conductor cable of any desired length up to several thousand feet.

Excitation current of approximately 100 mA rms is required by the fluxgates and is derived from a Wien-bridge oscillator circuit operating at 330±20Hz. A power booster is included within the oscillator feedback loop to provide the necessary current drive capability. The oscillator amplitude, and hence fluxgate drive current, may be varied by means of the 10KΩ potentiometer. It is of utmost importance that the second-harmonic content (660 Hz) of the drive circuit be minimized. Measured amplitudes at the output of this oscillator circuit are typically 70 db below the fundamental amplitude. Recent work by Primdahl (1970) has shown that a blocking capacitor in series with the 120KΩ resistor in the oscillator circuit lowers the second harmonic content to more than 80 db below the fundamental.

The oscillator output is full-wave rectified, then amplified and filtered by a band-pass filter tuned to the second harmonic at 660 Hz. This filter is simply an operational amplifier with a twin-T network as the feedback element. The 330KΩ shunt across the twin-T network keeps the filter Q low enough that phase shifts due to any variations of oscillator frequency do not reduce phase-sensitive detector gain enough to impair magnetometer response. The doubler output provides the reference signal at the centre-tap of each phase-sensitive detector transformer.

Each fluxgate secondary winding is tuned (Serson and Hannaford, 1956) to 660 Hz with a 0.75 μf capacitor and damped with a 2.7KΩ resistor. Second-harmonic signal from the secondary winding is amplified and filtered by a circuit similar to the doubler filter and fed to the phase-sensitive detector transformer. The output of the detector, a d.c. signal with polarity and amplitude determined by the direction and magnitude of fluxgate axial field, is integrated and fed back through the 340KΩ resistor (330KΩ plus 20KΩ variable) to the fluxgate secondary winding. This provides the negative feedback, and the magnetometer output is taken at the integrator output. It is a measure of the voltage necessary to provide sufficient feedback current through the 340KΩ resistor to produce a field in the fluxgate secondary winding just sufficient to cancel the ambient axial field at the fluxgate. If the total ambient field were to be cancelled by dynamic feedback (for example, a 60,000γ Z component), a much lower value of R_4 would be necessary, since the output voltage of the operational amplifiers is limited to about 12 volts. This means the output sensitivity R_4/A would be greatly reduced, necessitating a sophisticated recording device with a very large dynamic range (equivalent to 60,000γ) and high resolution (about 1γ). In practice, the bulk of the ambient field is

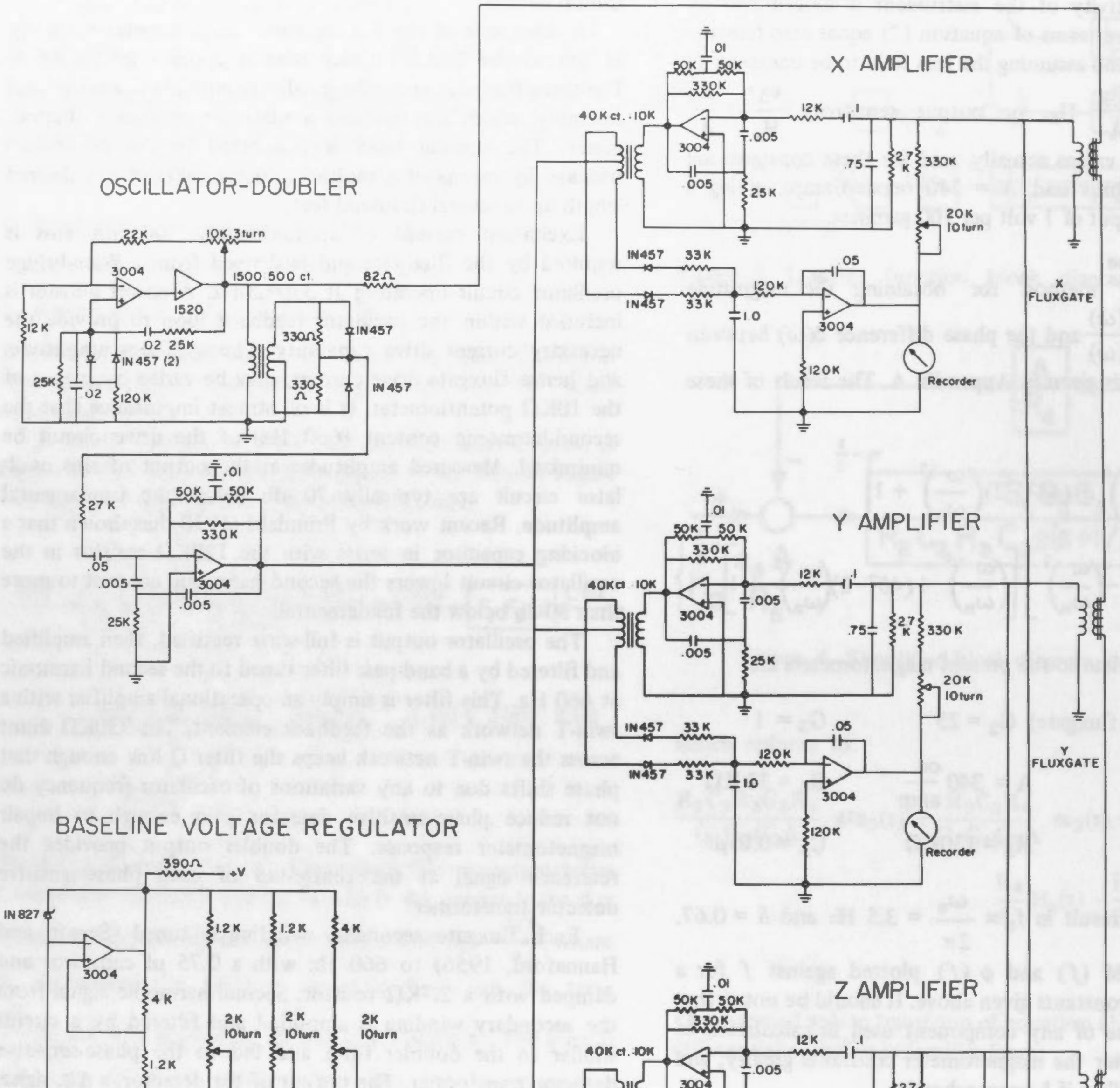

Figure 6. Circuit schematic of the magnetometer.

cancelled by a bias current in the fluxgate secondary, which is obtained from the very stable baseline voltage regulator, and the remainder of the field is then cancelled by dynamic feedback. The baseline voltage is obtained from the 1N827 temperature compensated zener diode (0.001 per cent /°C), which is operated at constant current by the action of the operational amplifier. A platinum resistance thermometer, mounted in the sensing head, provides a bias compensation for the average temperature sensitivity of the fluxgates. Three 10-turn 2KΩ precision potentiometers permit adjustment of the bias current over ranges corresponding to 0 to 20,000 gammas field in the X and Y channels and 46,000 to 67,000 gammas in the Z channel. Curves showing the bias field as a function of potentiometer setting are presented in Figure 7. No attempt has been made to provide baseline controls which are accurately calibrated.

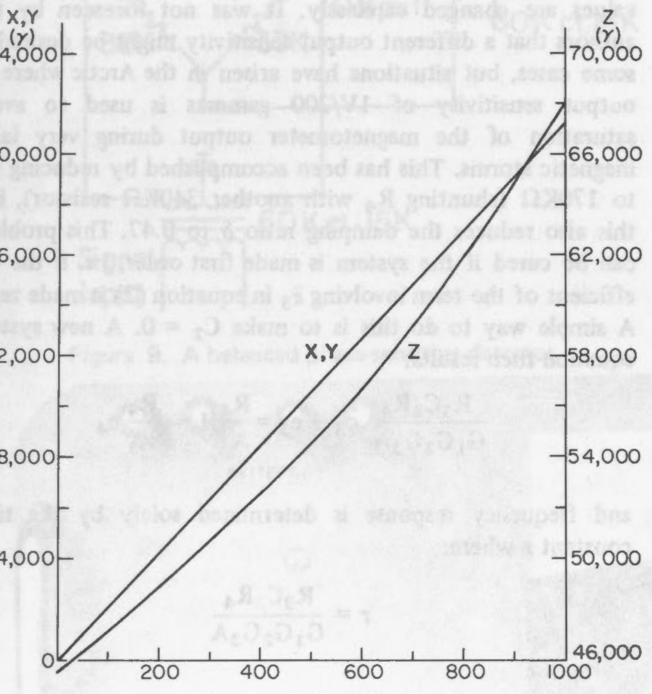

Figure 7. Bias fields vs. potentiometer settings.

The power supply (Figure 13) consists of two very simple series regulators supplied from either rectified line voltage or external batteries. Selection of the mode of operation is made with the main instrument power switch. In the external battery mode, power consumption is ±90mA at ±12V to ±18V. Four hundred hours of operation can be obtained, in this mode, from 40 lbs of carbon-zinc batteries.

A summary of electrical specifications is presented below:

Power requirements:	4W at 115V, 60 Hz or ±90mA at ±12V to ±18V
Baseline adjustment range:	X – 0 to 20,000 gammas Y – 0 to 20,000 gammas Z – 46,000 to 67,000 gammas
Sensitivity:	1V per 100 gammas
Resolution:	1 gamma
Dynamic range:	±1000 gammas (±10V) from baseline
Output impedance:	0Ω
Output current capability:	±20 mA max.
Frequency response:	-3db at 3.5 Hz.

Stability and drift

Data on long-term stability of the magnetometers has been obtained by the Ottawa magnetic observatory and is summarized in the graphs of Figure 8. Here, baseline values for the three components H, D and Z of a magnetometer are plotted against time, starting from January 3, 1969 (day 3) and ending on July 11, 1969 (day 192). The magnetometer and sensing head were located in a thermostatted room. Changes in the Z baseline values are closely correlated with the temperature of the recording room. The thermostat was changed from 22°C to 19°C between days 57 and 66 and on day 177 the temperature rose to 21°C. A temperature coefficient of 10γ per degree explains the main features of the variation in Z. The changes of D baseline are larger than expected (one minute of arc in D corresponds to 4.5γ at Ottawa), and apparently unrelated to temperature. The record from the photographic variometers indicates that the absolute observations of days 57 and 66 are probably in error by 5′. However, no explanation has been found for the fluctuation following day 130.

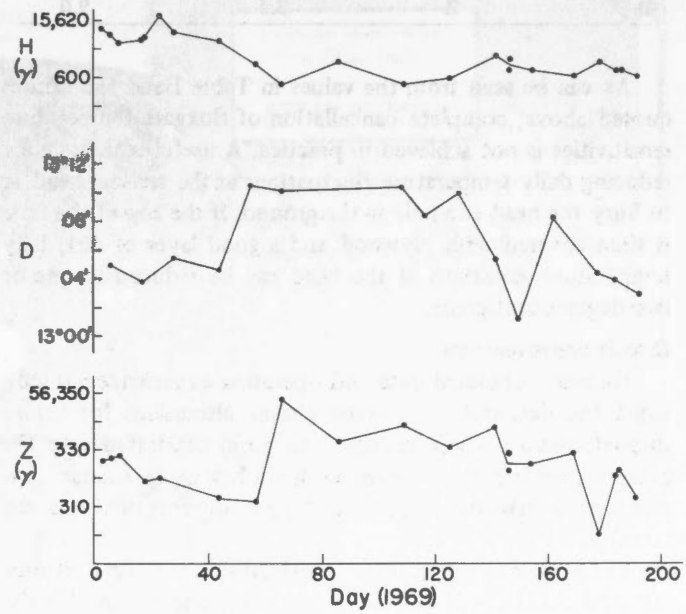

Figure 8. Drifts in component baselines from January 3, 1969 to July 11, 1969.

Tests to determine the temperature sensitivity of fluxgates were carried out by placing sensing heads in a non-magnetic oven and varying the temperature over a range from 20°C to 40°C. The head and oven were in turn mounted within a set of 3-axis Helmholtz coils (Roy *et al.*, 1969), providing an ambient field free of variations. During these tests the thermometer mounted on the sensing head was disabled so that no compensation of thermal drift took place within the magnetometer circuit. Table I presents the drift results for the 3-sensing heads so tested. These drifts are only roughly proportional to the axial field sensed by each fluxgate in the tuned operating mode. The temperature compensation network is designed to provide a change of 56 ppm/°C in bias field on the fluxgates. For the Z component at Ottawa (56,000γ) this provides a compensation of 3γ per °C. Detailed calculations of the temperature compensation network appear in Appendix B.

Table I
Temperature Sensitivity of Fluxgate Sensors

		Untuned gammas/°C	Tuned gammas/°C
Head X 11			
	D	0	1.5
	H	0.5	2.5
	Z	2.5	6.0
Head X 14			
	D	0.2	1.2
	H	0.6	2.5
	Z	3.0	6.0
Head X 26			
	D	0.75	3.0
	H	0.6	7.0
	Z	3.5	9.0

As can be seen from the values in Table I and the figures quoted above, complete cancellation of fluxgate temperature sensitivities is not achieved in practice. A useful technique for reducing daily temperature fluctuations at the sensing head is to bury the head in a hole in the ground. If the top of the hole is then covered with plywood and a good layer of dirt, daily temperature variations at the head can be reduced to one or two degrees centigrade.

Circuit improvements

Recently obtained data and operating experience has indicated the desirability of some circuit alterations for future magnetometers. These changes can be incorporated into the present magnetometer design without having to change anything other than the component layout on some of the circuit boards.

Examination of Table I indicated the first change which should be made. In every case a fluxgate operated in the tuned mode had a higher temperature sensitivity than when it was untuned. Moreover, the drifts in untuned fluxgates are very nearly proportional to the magnetic field sensed by the fluxgate, and the temperature compensation designed into the baseline voltage regulator is nearly sufficient to eliminate these drifts. Certainly a temperature sensitivity less than 1 gamma/°C should be realized in every component. A consequence of removing the tuning capacitance and shunt resistor from the fluxgate secondary circuit is that the fluxgate gain G_1 is reduced, from 4V/0e to 0.75V/0e in the present case. This effect can be compensated (in order to keep ω_n and δ constant) by increasing the a.c. amplifier gain G_2. Since the fluxgate is normally operated with all even harmonics of the output waveform nulled, the amount of fundamental and third harmonic present in the input signal will determine the maximum allowable value for G_2. Care must be taken to ensure that the phase relationship between amplifier output and the reference signal is not severely altered.

A disadvantage of the second order magnetometer system described thus far is that instability can occur if component values are changed carelessly. It was not foreseen by the authors that a different output sensitivity might be desired in some cases, but situations have arisen in the Arctic where an output sensitivity of 1V/200 gammas is used to avoid saturation of the magnetometer output during very large magnetic storms. This has been accomplished by reducing R_4 to 170KΩ (shunting R_4 with another 340KΩ resistor), but this also reduces the damping ratio δ to 0.47. This problem can be cured if the system is made first order, i.e. if the coefficient of the term involving $\ddot{e}_3$ in equation (2) is made zero. A simple way to do this is to make $C_2 = 0$. A new system equation then results:

$$\frac{R_3C_3R_4}{G_1G_2G_3A}\,\dot{e}_3 + e_3 = \frac{R_4}{A}H_a - \frac{R_4}{R_5}\,e_4$$

and frequency response is determined solely by the time constant τ where:

$$\tau = \frac{R_3C_3R_4}{G_1G_2G_3A}$$

An analysis similar to that of Appendix A results in:

$$M(\omega) = \frac{R_4}{A}(1 + \omega^2\tau^2)^{-\frac{1}{2}}$$

$$\phi(\omega) = \cos^{-1}(1 + \omega^2\tau^2)^{-\frac{1}{2}}$$

which are the magnitude ratio and phase angle for a first order system.

Since $M(\omega)$ now rolls off at 6 db/octave instead of 12 db/octave the second harmonic content in the magnetometer output will be greater in the first order case (assuming that 1st and 2nd order systems have a similar 3-db roll-off point). The magnetometer has been designed to be sensitive to second harmonic fluxgate signal so the feedback current must not contain this frequency. To prevent this, either the time constant must be increased, degrading frequency response, or a way must be found to reduce the second harmonic content at the integrator input. The present phase-sensitive detector is not a balanced type, with the result that the whole of the second harmonic reference signal appears at the integrator input when C_2 is removed. A balanced detector of the type shown in Figure 9 eliminates this high second harmonic content.

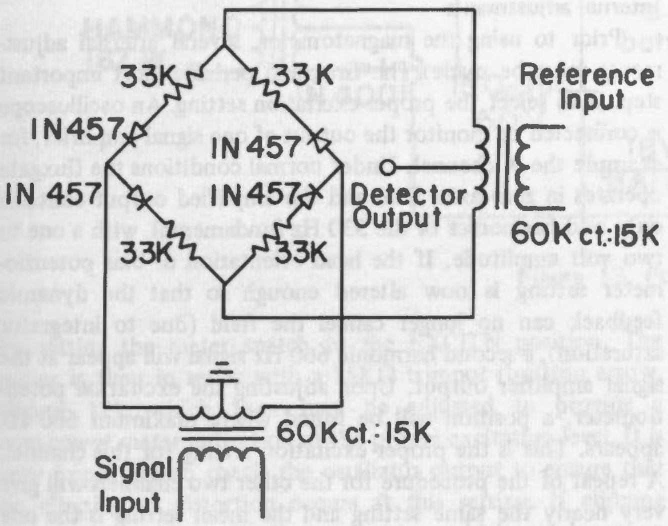

Figure 9. A balanced phase-sensitive detector.

Part II – Magnetometer controls

Figure 10 provides a view of the various magnetometer controls available on the panel. 115V line power enters via the plug mounted just above the fuse holder and alternate battery power may be provided at the four binding posts. The second and third binding posts are wired together internally to provide the electrical ground point. The meter switch has a position labelled OFF which provides a short circuit across the meter terminals, and this should not be confused with the power OFF condition. With the meter switch set at the EXCITN position the meter monitors excitation current, as described later in the Internal Adjustments section. The X, Y and Z switch positions permit the meter to measure the amount and polarity of dynamic feedback applied to the corresponding fluxgate at a scale of 500 gammas–0–500 gammas. B– and B+ switch settings enable the meter to indicate the negative and positive regulated supply voltages respectively. In this case, the numerical meter reading is 20 times the supply voltage, i.e. a meter reading of 240 indicates a regulated supply voltage of 12V. The bias field potentiometers, labelled X, Y and Z and equipped with lockable turns-counting dials, are used in conjunction with the meter switch to bring the magnetometer channels within the range of dynamic feedback operation. Immediately to the right of the 3 bias potentiometers is the excitation current adjustment potentiometer.

Wiring details and power supplies

A schematic of the chassis wiring is presented in Figure 11. The various numbers and letters refer to the labelling of

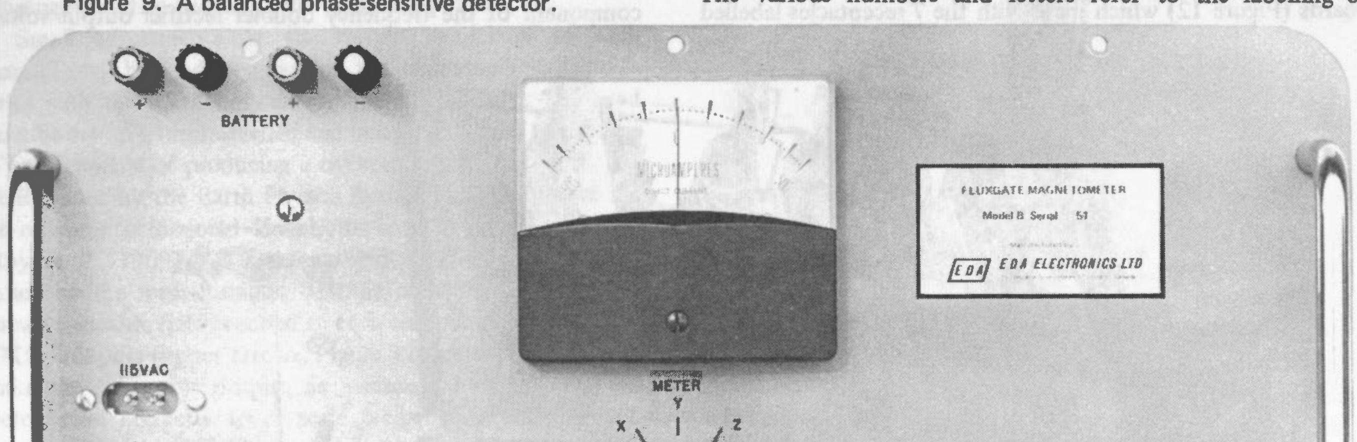

Figure 10. Magnetometer panel controls.

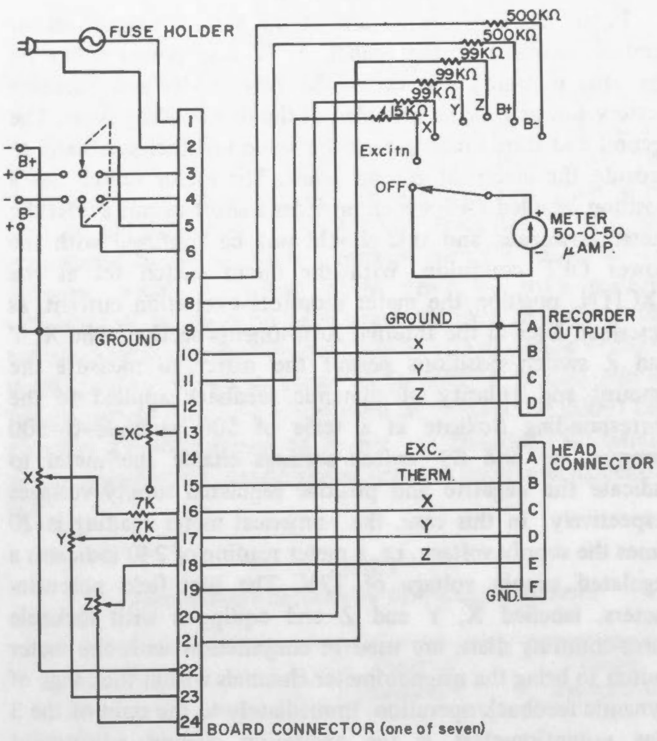

Figure 11. Chassis wiring details.

connector pins and the single 24-pin receptacle indicated in the figure represents seven such receptacles with pins wired in parallel. The electronics has been partitioned to fit on 7 circuit boards (Figure 12) which mate with the 7 receptacles labelled J1 to J7 inclusive (labelling not visible in Figure 12). Each power supply is mounted on a single card and must be mated with either J1 or J2 (right-hand receptacles in Figure 12) for proper operation. The circuits for both power supplies are given in Figure 13. The remaining circuitry partitions into X, Y and Z component amplifier cards, an oscillator-doubler card and a baseline voltage regulator card. These cards may be placed randomly in receptacles J3 to J7 inclusive. No damage will occur if all cards are placed randomly in receptacles but operation is impossible until the power supply cards are placed in J1 and J2.

Internal adjustments

Prior to using the magnetometer, several internal adjustments must be made. The first, and perhaps most important step, is to select the proper excitation setting. An oscilloscope is connected to monitor the output of one signal amplifier, for example the X channel. Under normal conditions the fluxgate operates in zero axial field and the amplified output contains only odd harmonics of the 330 Hz fundamental, with a one to two volt amplitude. If the head orientation or bias potentiometer setting is now altered enough so that the dynamic feedback can no longer cancel the field (due to integrator saturation), a second harmonic 660 Hz signal will appear at the signal amplifier output. Upon adjusting the excitation potentiometer, a position will be found where maximum 660 Hz appears. This is the proper excitation setting for this channel. A repeat of the procedure for the other two channels will give very nearly the same setting and the mean setting is the one desired. The panel meter can be made to sample the d.c. component of the frequency doubler rectifier output voltage

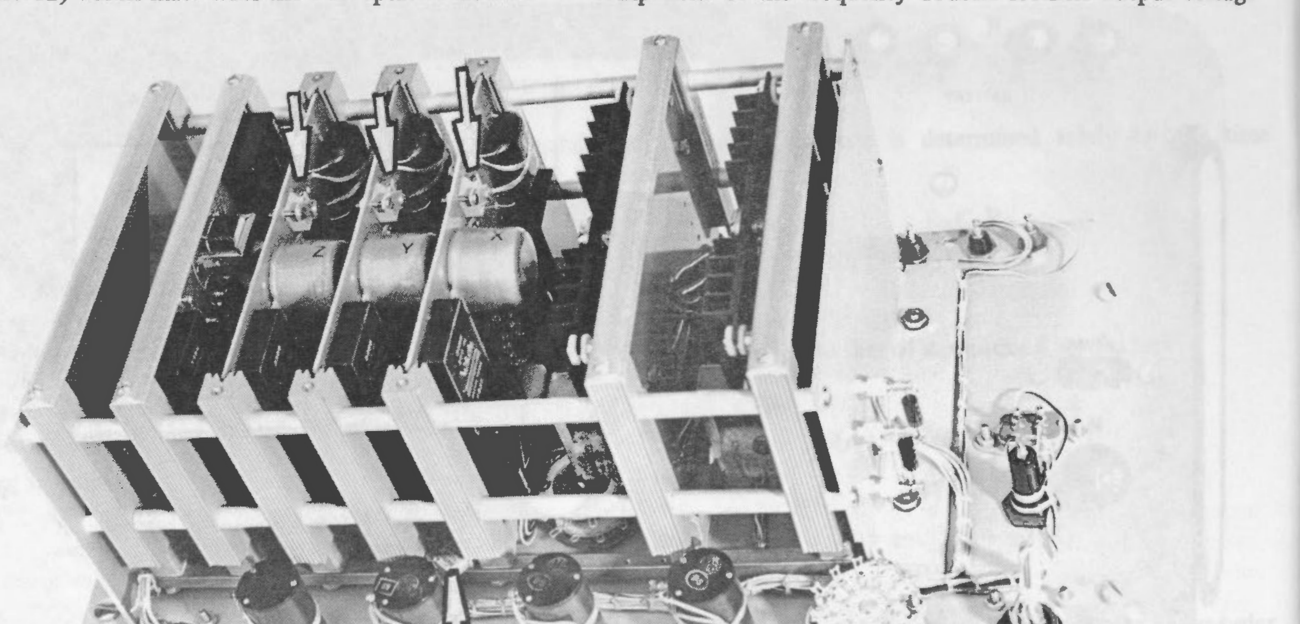

Figure 12. Location of internal potentiometers for adjustments of output sensitivities (upper arrows) and meter reading at desired excitation (lower arrow).

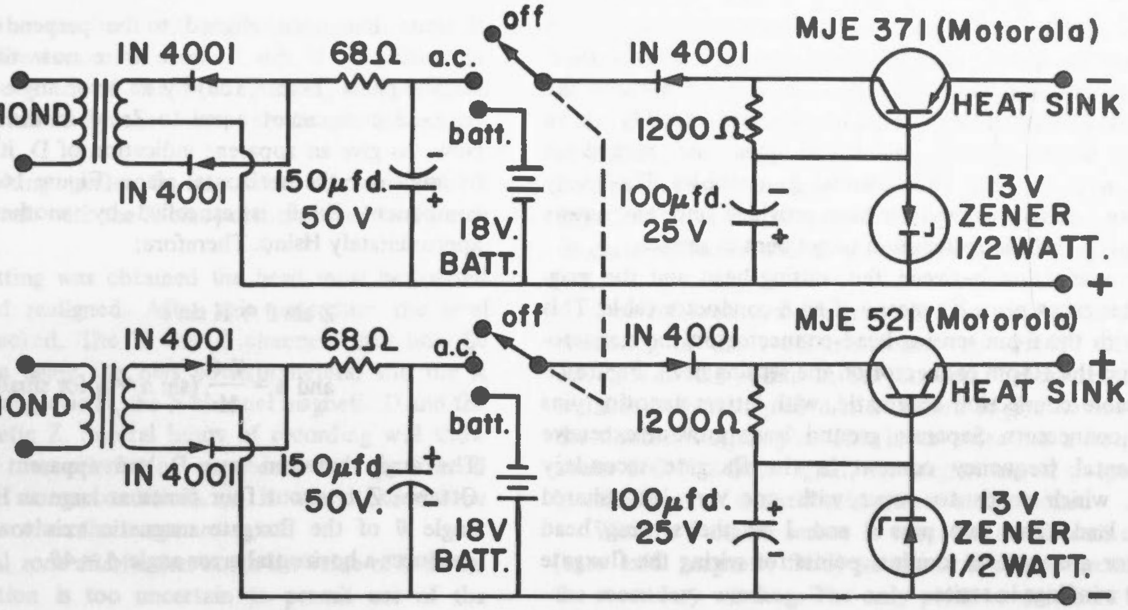

Figure 13. Power supply circuit.

by setting the meter switch to the EXCITN position. The meter is then in series with a 15KΩ trimpot (bottom arrow, Figure 12), which then may be adjusted to provide a convenient meter indication of the proper excitation level. It is very important to check the oscillator output to ensure that no clipping or distortion occurs at this setting. If clipping occurs, the highest excitation setting which produces no clipping should be chosen as the operating point.

Small adjustments of the output sensitivity of each channel may be made by varying the trimming resistance in series with the 330KΩ dynamic feedback resistor. The head must be set up within, levelled and oriented parallel to the axis of coils capable of producing a calibrated magnetic field. The facility used by the Earth Physics Branch for this purpose is a set of three orthogonal Helmholtz coils of 8 feet diameter [Roy *et al.*, 1969]. After the ambient field has been exactly nulled by the magnetometer baseline controls, an accurately known magnetic field is added to each component in turn. The 20KΩ trimpots (upper arrows, Figure 12) are then adjusted to make the integrator output, as measured by a digital voltmeter, read correctly for a scale factor of 1 volt per 100 gammas. If no such facilities are available, the same 20KΩ trimpots are adjusted to make the total dynamic feedback resistance equal to 340KΩ, under which conditions the scale factor will be 1V/100 gammas ±2 per cent.

Sensing head and cable details

The sensing head, with cover removed, is depicted in Figure 14. All components and materials used are non-magnetic. The fluxgates are locked in three accurately-machined, mutually orthogonal holes by means of nylon screws threaded into the acrylic mounting piece. Pliobond rubber adhesive is used to cement the platinum resistance thermometer to the same piece. A graduated circle with 5-degree markings is

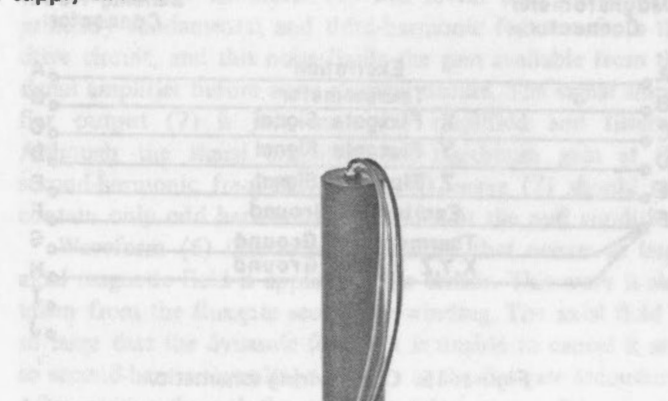

Figure 14. Sensing head with cover removed.

engraved on the baseplate and is useful in the head orientation procedures described later. A teflon gasket ensures smooth differential motion between the engraved baseplate and the upper casting with the pointer. The complete assembly can be mounted on a $1\frac{3}{8}$-inch aluminum pipe and locked in position with two large thumbscrews (not visible). Three very large brass levelling screws have been provided since any screws less than $\frac{3}{8}$-inch diameter seem to get bent in service.

Interconnection between the sensing head and the magnetometer takes place by means of an 8-conductor cable. This mates with the 6-pin sensing head connector on the magnetometer and the 10-pin connector on the sensing head. Figure 15 is the cable connection schematic, with letters denoting pins on the connectors. Separate ground leads prevent excessive fundamental frequency content in the fluxgate secondary circuits, which tends to occur with one very long shared ground lead. The two pins I and J at the sensing head connector are used as terminal points for wiring the fluxgate primary windings in series.

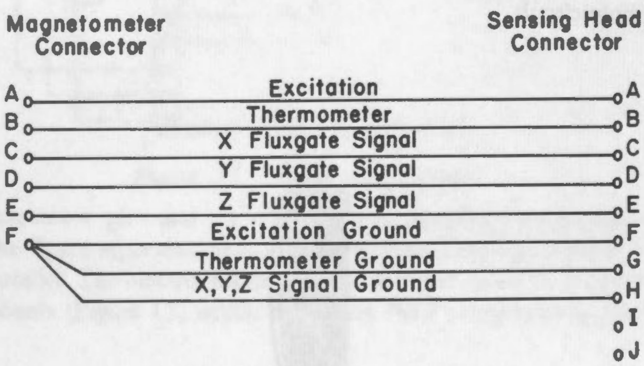

Figure 15. Cable wiring schematic.

Sensing head alignment

Experience has shown that the magnetic axis of the fluxgates differs from the physical axis by approximately 30 minutes of arc. This apparent defect is used as the basis of the head alignment procedure. The head is mounted with the "vertical" axis roughly parallel to F. Baseline controls are set at zero and the head is rotated about its axis. The magnetometer output provides a recording usually containing a large sinusoidal component as well as a d.c. level in the X and Y channel outputs. Proper adjustment of the levelling screws will eliminate the sinusoidal component of X and Y. At this point the axis of rotation is parallel to F. The remaining d.c. offset in the X and Y traces is a measure of the component of F seen by these fluxgates. It is eliminated by rotating the X and Y sensors about their own cylindrical axes. The magnetic axes of these two fluxgates then lie in a plane perpendicular to the physical axis of rotation, which is the desired alignment.

The reason for performing this adjustment becomes apparent from an examination of Figure 16. A horizontal fluxgate has been aligned to be perpendicular to H, i.e. measuring D. If this fluxgate were now tilted slightly in a vertical plane (Figure 16a) by an error angle θ, it would sense an axial component equal to $Z\sin\theta$ in the direction shown. Now, to give an apparent indication of D, it must be rotated by angle ϕ in the horizontal plane (Figure 16b) until the error component $Z\sin\theta$ is cancelled by another component of approximately $H\sin\phi$. Therefore:

$$Z \sin \theta \simeq H \sin \phi$$

$$\text{and } \phi \simeq \frac{Z\,\theta}{H} \quad (\sin\alpha \simeq \alpha \text{ for small } \alpha).$$

The angle between true D and apparent D is just ϕ. At Ottawa, Z is about four times as large as H, and so an error angle θ of the fluxgate magnetic axis towards the vertical produces a horizontal error angle $\phi \simeq 4\theta$.

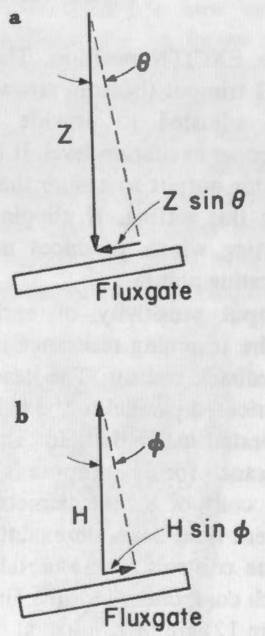

Figure 16.
(a) Error component sensed if the magnetic axis of a horizontal fluxgate sensor is tilted by an angle θ into a vertical plane
(b) Error angle ϕ necessary in the horizontal plane to compensate for the error component resulting from θ in the vertical plane.

Orientation of the head

Two head orientations are used extensively by the Earth Physics Branch. In these configurations the magnetometer measures the magnetic components D, H, Z or X, Y, Z. Orientation is relatively simple in the former case and this will be described first. To align in D, H and Z the head is levelled and the Y bias potentiometer is set to read zero. The meter switch on the magnetometer should be in the Y position. Rotation of the head about the vertical axis will bring the meter on scale and zero reading indicates the correct position or a position 180° from the correct one. Any one of three clues can be used to decide which of the two positions has been reached.

1. The pointer on the head will point to magnetic north in the correct orientation.
2. Clockwise rotation of the sensing head will result in clockwise rotation of the meter needle at the proper setting.
3. Incorrect setting makes it impossible to bring the X channel on scale with the X bias potentiometer (and meter switch at X).

If the wrong setting was obtained the head must be rotated 180 degrees and realigned. After this procedure the level should be re-checked. The X and Z channels may now be brought on scale using the bias potentiometers, and the X channel records magnetic H, the Y channel magnetic D and the Z channel magnetic Z. Several hours of recording will show whether or not the orientation procedure was performed during magnetic storm conditions. If it was, it should be repeated at a time when the traces are quiet.

In the auroral zone and further north the value of D at the time of orientation is too uncertain to permit use of the previous method. The head must then be oriented in geographical co-ordinates as determined by the position of the sun at local noon, the position of the pole star or a local survey. In those regions where the declination is east of true north, the pointer on the sensing head must point to true north. The X channel then records magnetic X, the Y channel magnetic Y and the Z channel magnetic Z. All channels can be brought on scale by using the bias potentiometers. In regions where the declination is west of true north the pointer on the sensing heads must point to true west. In this case, the X channel is used to record the Y component of the magnetic field and the Y channel is used to record the X field component.

Occasionally it is extremely difficult or impossible to determine geographical co-ordinates directly, and the following procedure may be attempted. Obtain estimated values of the magnetic components X and Y from magnetic maps or previous survey information in the area. Set the X and Y bias potentiometers to these estimated values using the bias field vs. potentiometer setting graph in Figure 7. Rotate the sensing head until the X and Y outputs come on scale. If they do not pass through zero simultaneously, increase or decrease the settings of both potentiometers by amounts proportional to their readings and repeat the procedure.

Troubleshooting

Waveforms which may be observed at eight points in the magnetometer circuit during correct operation are presented in Table II. The oscillator output (1) is taken at the output pin of the type 1520 power booster and should be a very clean sinusoidal wave of about 330 Hz frequency. Any distortion of the wave at this point means that the magnetometer is operating incorrectly and the output voltages do not accurately represent the magnetic field sensed by the associated sensor. Waveform (2) should appear at the junction of the 82-ohm resistor and the fluxgate primary winding. Although this wave looks very distorted, all even harmonics of 330 Hz are absent and so the sensor secondary windings pick up no even harmonics from the drive circuit. If there is an open circuit anywhere after the 82-ohm resistor, in either the cable or the fluxgate primaries, the wave at this point will be identical with (1).

The reference wave is generated by the full-wave rectifier consisting of the 143H transformer and 1N457 diodes. The wave (3) should appear at the junction of these 1N457 diodes and this is then amplified and filtered to give waveform (4) at the doubler output pin. This latter wave has a frequency of about 660 Hz. Once again, the magnetometer output cannot be relied upon if distortion is present at this point.

When a fluxgate sensor is operated in the null condition (zero axial magnetic field) waveform 5 will be present across the secondary winding. The only point to note here is that all even harmonics should be absent and whatever is left is noise. Examination of waveform (5) will reveal that the noise is primarily fundamental and third-harmonic fed over from the drive circuit, and this noise limits the gain available from the signal amplifier before wave-clipping occurs. The signal amplifier output (7) is just wave (5) amplified and filtered. Although the signal amplifier has maximum gain at the second-harmonic frequency (660 Hz), wave (7) should still contain only odd harmonics of 330 Hz at the null condition.

Waveform (6) illustrates the change that occurs as large axial magnetic field is applied to the sensor. This wave is also taken from the fluxgate secondary winding. The axial field is so large that the dynamic feedback is unable to cancel it and so second-harmonic voltage appears at the fluxgate secondary. After passing through the signal amplifier, where all harmonics are attenuated relative to 660 Hz the wave (8) appears at the amplifier output . Waves (6) and (8) have a high proportion of even-harmonic content.

References

Harrison, H.L. and J.G. Bollinger. 1963. Introduction to automatic controls, Chap. 6, 7, 9, *International Textbook Company*.

Primdahl, F. 1970. The fluxgate mechanism, *IEEE transactions on magnetics*, Vol. MAG-6, No. 2, 376.

Primdahl, F. 1970. A ferrite core fluxgate magnetometer, *Pub. Earth Physics Branch*, Vol. 40, No. 1.

Roy, J.L., W.A. Robertson and C. Keeping. 1969. Magnetic "field free" spaces for paleomagnetism, rock magnetism, and other studies. *Can. J. Earth Sci.*, 6, 1312.

Serson, P.H. 1957. An electrical recording magnetometer, *Can. J. Phys.*, 35, 1387.

Serson, P.H. and W.L.W. Hannaford. 1956. A portable electrical magnetometer, *Can. J. Tech.*, 34, 232.

Table II
Typical Waveforms

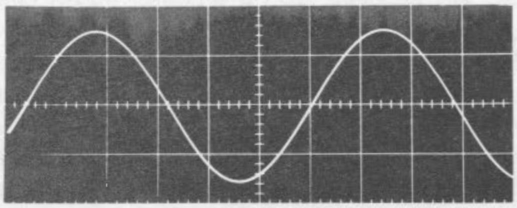

1. Oscillator Output
Hor: 0.5 ms/cm Vert: 5 v/cm

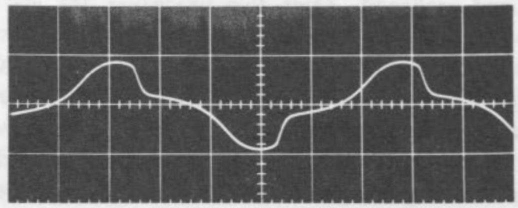

2. Fluxgate Primaries
Hor: 0.5 ms/cm Vert: 5 v/cm

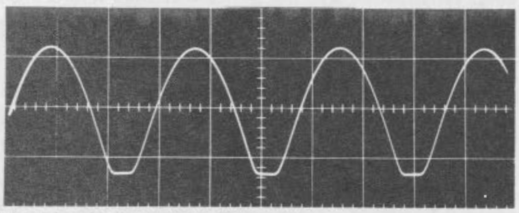

3. Rectifier Output
Hor: 0.5 ms/cm Vert: 0.5 v/cm

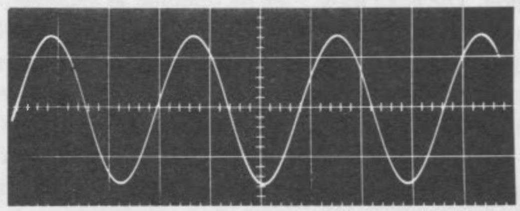

4. Doubler Output
Hor: 0.5 ms/cm Vert: 5 v/cm

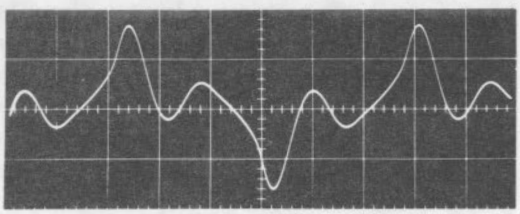

5. Fluxgate Secondary (at null)
Hor: 0.5 ms/cm Vert: 0.2 v/cm

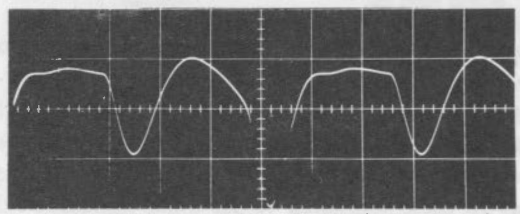

6. Fluxgate Secondary (off null)
Hor: 0.5 ms/cm Vert: 0.5 v/cm

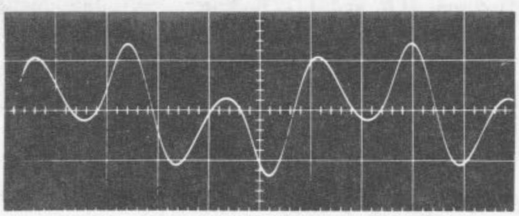

7. Amplifier Output (at null)
Hor: 0.5 ms/cm Vert: 2 v/cm

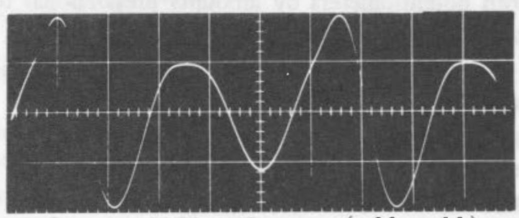

8. Amplifier Output (off null)
Hor: 0.5 ms/cm Vert: 5 v/cm

Appendix A – Calculation of frequency response

Substitute expressions for ω_n and δ into equation (1) to give:

$$\frac{s^2}{\omega_n^2}e_3 + \frac{2\delta}{\omega_n}se_3 + e_3 = \frac{R_4}{A}\left(H_a - \frac{e_4A}{R_5}\right)$$

or rearranging:

$$\frac{e_3}{H_a - \frac{e_4A}{R_5}} = \frac{R_4}{A}\cdot\frac{1}{\left(\frac{s}{\omega_n}\right)^2 + 2\delta\left(\frac{s}{\omega_n}\right) + 1} = \frac{\text{output } O(s)}{\text{input } I(s)}$$

Substituting $s = j\omega$ gives:

$$\frac{O(j\omega)}{I(j\omega)} = \frac{R_4}{A}\cdot\frac{1}{\left(\frac{j\omega}{\omega_n}\right)^2 + 2\delta\left(\frac{j\omega}{\omega_n}\right) + 1}$$

$$= \frac{R_4}{A}\cdot\frac{1}{1-\left(\frac{\omega}{\omega_n}\right)^2 + j2\delta\left(\frac{\omega}{\omega_n}\right)}$$

Multiplying numerator and denominator by conjugate of denominator:

$$\frac{O(j\omega)}{I(j\omega)} = \frac{R_4}{A}\cdot\frac{1-\left(\frac{\omega}{\omega_n}\right)^2 - j2\delta\left(\frac{\omega}{\omega_n}\right)}{\left[1-\left(\frac{\omega}{\omega_n}\right)^2 + j2\delta\left(\frac{\omega}{\omega_n}\right)\right]\left[1-\left(\frac{\omega}{\omega_n}\right)^2 - j2\delta\left(\frac{\omega}{\omega_n}\right)\right]}$$

$$= \frac{R_4}{A}\cdot\frac{1-\left(\frac{\omega}{\omega_n}\right)^2 - j2\delta\left(\frac{\omega}{\omega_n}\right)}{\left(\frac{\omega}{\omega_n}\right)^4 + (4\delta^2-2)\left(\frac{\omega}{\omega_n}\right)^2 + 1}$$

Call denominator $D = \left(\frac{\omega}{\omega_n}\right)^4 + (4\delta^2-2)\left(\frac{\omega}{\omega_n}\right)^2 + 1$

and let $X = 1 - \left(\frac{\omega}{\omega_n}\right)^2$ and $Y = -2\delta\left(\frac{\omega}{\omega_n}\right)$

Then $\frac{O(j\omega)}{I(j\omega)} = \frac{R_4}{AD}[X + jY]$

The magnitude $M(\omega)$ of $\frac{O(j\omega)}{I(j\omega)}$ is equal to $\frac{R_4(X^2+Y^2)^{\frac{1}{2}}}{AD}$

Observe that $D = X^2 + Y^2$

Therefore $M(\omega) = \frac{R_4D^{\frac{1}{2}}}{AD} = \frac{R_4D^{-\frac{1}{2}}}{A}$

$$M(\omega) = \frac{R_4}{A}\left[\left(\frac{\omega}{\omega_n}\right)^4 + (4\delta^2-2)\left(\frac{\omega}{\omega_n}\right)^2 + 1\right]^{-\frac{1}{2}}$$

The phase angle $\phi(\omega)$ between $O(j\omega)$ and $I(j\omega)$ is $\phi(\omega) = \cos^{-1}[X(X^2+Y^2)^{-\frac{1}{2}}] = \cos^{-1}(XD^{-\frac{1}{2}})$

$$\phi(\omega) = \cos^{-1}\left\{\left[1-\left(\frac{\omega}{\omega_n}\right)^2\right]\left[\left(\frac{\omega}{\omega_n}\right)^4 + (4\delta^2-2)\left(\frac{\omega}{\omega_n}\right)^2 + 1\right]^{-\frac{1}{2}}\right\}$$

Appendix B – Temperature compensation

The following equations are obtained from examination of Figure 17:

$$e_1 = e_o - e_z - i_zR_z$$

and $e_1 = i_zR_1$

Eliminating i_z:

$$e_1 = \frac{R_1}{R_1+R_z}(e_o - e_z)$$

Also,

$$e_2 = \frac{R_3+R_4}{R_2+R_3+R_4}e_o$$

where R_4 is the sum of the 100-ohm platinum resistance plus 3 ohms allowed for a 250-ft sensing head cable of #18 wire. Temperature coefficient is assumed to be +3900 ppm/°C in both cases.

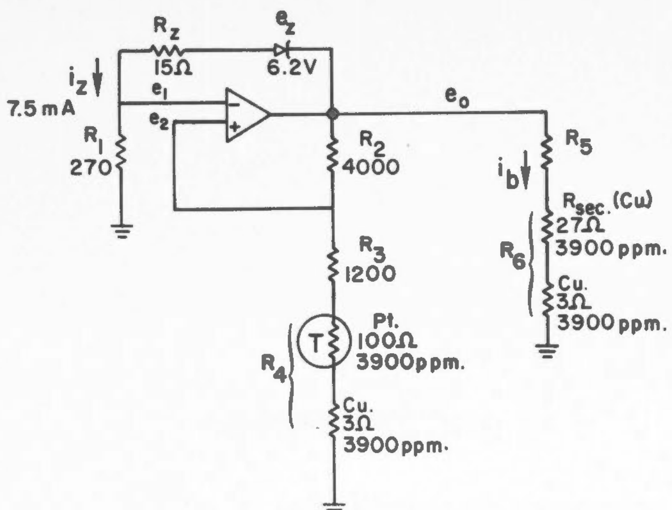

Figure 17. Schematic of the temperature compensation network.

Because of the action of the operational amplifier, $e_1 = e_2$

$$\therefore e_o = \frac{e_z}{1 - \frac{(R_3+R_4)(R_1+R_z)}{R_1(R_2+R_3+R_4)}}$$

At 0°C: $e_z = 6.2V$, $R_1 = 270\Omega$, $R_2 = 4000\Omega$, $R_3 = 1200\Omega$
$R_4 = 103\Omega$
$e_o = 8.37114$ V
At 25°C: $e_z = 6.2V$, $R_1 = 270\Omega$, $R_2 = 4000\Omega$, $R_3 = 1200\Omega$,
$R_4 = 113\Omega$
$e_o = 8.38812$ V.

$$\frac{\Delta e_o}{e_o \Delta T} = \frac{+0.01698 \text{ V}}{8.37 \times 25} = +81 \text{ ppm/°C}$$

Consequently, reference voltage increases at a rate of 81 ppm/°C.
Bias current i_b is determined by total resistance $R_5 + R_6$, and if $Z=60{,}000\gamma$:

$$R_5+R_6 = \frac{8.37\text{V} \times 340 \text{ oe}}{0.60 \text{ oe} \quad A} = 4740\Omega$$

and $R_5 = 4740\Omega - 30\Omega = 4710\Omega$

Temperature changes in bias current from the effect of R_6 will be:

$$\frac{\Delta i_b}{i_b} = \frac{-\Delta R_6}{R_6} \times \frac{R_6}{(R_5+R_6)}$$

$$\therefore \frac{\Delta i_b}{i_b} = -25 \text{ ppm/°C}$$

with the minus sign indicating a decrease in bias current with an increase in temperature (and resistance). The net temperature effect is then the sum of bias voltage coefficient and bias current coefficient due to changes in R_6.

$$\text{Net} \frac{\Delta i_b}{i_b} = 81 - 25 = 56 \text{ ppm/°C}$$

PUBLICATIONS of EARTH PHYSICS BRANCH

record of observations

PUBLICATIONS of the EARTH PHYSICS BRANCH

VOLUME 41 - NO. 6

record of observations at victoria magnetic observatory 1969

D. R. AULD and I. W. FETTERLEY

DEPARTMENT OF ENERGY, MINES AND RESOURCES

OTTAWA, CANADA 1971

Cat. No.: M70-41/6

Contents

Tables

record of observations at victoria magnetic observatory 1969

D. R. AULD and I. W. FETTERLEY

Geographic Coordinates: 48° 31′; 123° 25′
Geomagnetic Coordinates: 54.3°; 292.7°

Officer-in-Charge: B. Caner
Assistant: D.R. Auld

Introduction

The Victoria Magnetic Observatory was established in 1957, on the grounds of the Dominion Astrophysical Observatory, Royal Oak, about 10 miles north of Victoria, British Columbia. Information on the site can be found in the publication containing the record of observations for the period 1957-1958 (Caner and Loomer, 1961).

Magnetic equipment

The basic observatory equipment was unchanged from that described in the preceding publications (Caner and Perry-Whittingham, 1962; Caner *et al.*, 1963; Auld and Moseley, 1965; Auld and Andersen, 1966; Auld and Andersen, 1967; Auld and Fetterley, 1970).

The adopted scale values for Ruska magnetograms are as follows:

D: Jan. 1 to Nov. 26, 0.93 min/mm or 5.10 ± 0.02 γ/mm
Nov. 26 to Dec. 31, 0.94 min/mm or 5.15 ± 0.02 γ/mm

		(γ/mm)
H:	Jan. 1 to May 28,	2.36 ± 0.02
	May 28 to Nov. 26,	2.27 ± 0.02
	Nov. 26 to Dec. 31,	2.36 ± 0.02
Z:	Jan. 1 to May 28,	4.03 ± 0.02
	May 28 to Nov. 26,	3.93 ± 0.04
	Nov. 26 to Dec. 31,	4.09 ± 0.02

Absolute observations and baseline values

The procedures used were essentially those described by Auld and Moseley (1965) for the period following September 11, 1961 and by Auld and Fetterley (1970).

Baseline drift in all three components was negligible. The rms value of the observed minus adopted baselines is ± 0.2 minute for declination, ± 2 gammas for the horizontal component, and ± 3 gammas for the vertical component.

Magnetic reductions

The methods used were essentially those described by Auld and Holmes (1969).

Magnetic activity and disturbance indices

The procedures followed remain unchanged from those described by Caner and Loomer (1961) and by Auld and Andersen (1966).

Summary of annual mean values

The mean values listed have been corrected to the new (post-1961) location and absolute standards.

For the period 1968.5 - 1969.5, the decrease in declination was 2.0 minutes (the mean rate of decrease over the whole 14-year period being 2.5 minutes per year); the increase in horizontal intensity was 21 gammas (the mean rate of increase over the 14-year period being 18 gammas

1969 Ruska Baseline Values

Declination D	Jan. 1 (0000) – July 27 (0005)	22° 11.0′ East
	July 27 (0005) – Dec. 31 (2400)	22° 10.5′
		(γ)
Horizontal intensity H	Jan. 1 (0000) – May 28 (1545)	18831
	May 28 (1545) – Nov. 26 (1640)	18897
	Nov. 26 (1640) – Dec. 8 (1948)	18825
	Dec. 8 (1948) – Dec. 31 (2400)	18864
Temperature correction (γ/mm T)	+9 when temperature is greater than reference level −5 when temperature is less than reference level	
		(γ)
Vertical intensity Z	Jan. 1 (0000) – May 28 (1545)	53073
	May 28 (1545) – Nov. 26 (1640)	53057
	Nov. 26 (1640) – Dec. 31 (2400)	53074
Temperature correction	−2 γ/mm T	
		(mm)
Temperature reference levels	Jan. 1 (0000) – May 28 (1545)	4.2
	May 28 (1545) – Nov. 26 (1640)	12.7
	Nov. 26 (1640) – Dec. 31 (2400)	4.3

Summary of annual mean values

Year	D East		H	Z	X	Y	I		F
	°	′	γ	γ	γ	γ	°	′	γ
1956.6	23	00.2	18689	53427	17203	7303	70	43.2	56601
1957.75	22	57.1	18705	53408	17224	7294	70	41.9	56589
1958.5	22	55.2	18713	53396	17236	7288	70	41.2	56580
1959.5	22	52.8	18736	53377	17262	7284	70	39.5	56570
1960.5	22	50.3	18748	53362	17278	7277	70	38.5	56560
1961.5	22	47.8	18787	53322	17319	7279	70	35.5	56535
1962.5	22	44.4	18804	53288	17342	7268	70	33.8	56508
1963.5	22	41.4	18814	53264	17358	7257	70	32.7	56489
1964.5	22	38.6	18837	53239	17385	7252	70	30.9	56473
1965.5	22	36.0	18860	53205	17412	7248	70	28.9	56449
1966.5	22	34.2	18873	53179	17428	7244	70	27.6	56429
1967.5	22	31.7	18888	53157	17447	7237	70	26.3	56413
1968.5	22	29.4	18902	53138	17464	7230	70	25.1	56400
1969.5	22	27.4	18923	53127	17488	7228	70	23.7	56396

per year); the decrease in the vertical component was 11 gammas (the mean rate of decrease over the 14-year period being 23 gammas per year).

Acknowledgments

The help of the Director and staff of the Dominion Astrophysical Observatory is greatly appreciated.

References

Auld, D.R. and P.H. Andersen. 1966. Record of observations at Victoria magnetic observatory, 1963-1964. *Pub. Dom. Obs.* Vol. XXXII No. 8.

Auld, D.R. and P.H. Andersen. 1967. Record of observations at Victoria magnetic observatory, 1965. *Pub. Dom. Obs.* Vol. XXXV No. 6.

Auld, D.R. and P.H. Andersen. 1968. Record of observations at Victoria magnetic observatory, 1966. *Pub. Dom. Obs.* Vol. XXXVII No. 3.

Auld, D.R. and I.W. Fetterley. 1970. Record of observations at Victoria magnetic observatory, 1968. *Pub. Dom. Obs.* Vol. XXXIX No. 9.

Auld, D.R. and D.G. Holmes. 1969. Record of observations at Victoria magnetic observatory, 1967. *Pub. Dom. Obs.* Vol. XXXVIII No. 6.

Auld, D.R. and M.J. Moseley. 1965. Record of observations at Victoria magnetic observatory, 1961-1962. *Pub. Dom. Obs.* Vol. XXXI No. 6.

Caner, B. and E.I. Loomer. 1961. Record of observations at Victoria magnetic observatory, 1957-1958. *Pub. Dom. Obs.* Vol. XXIV No. 9.

Caner, B. and A. Perry-Whittingham. 1962. Record of observations at Victoria magnetic observatory for 1959. *Pub. Dom. Obs.* Vol. XXVI No. 8.

Caner, B., D.R. Auld, and D.V. Kissinger. 1963. Record of observations at Victoria magnetic observatory for 1960. *Pub. Dom. Obs.* Vol. XXVII No. 8.

HORIZONTAL INTENSITY

MEAN VALUES FOR PERIODS OF SIXTY MINUTES, UNIVERSAL TIME

TABLE 1 VICTORIA H = 18,500 GAMMA + JANUARY 1969

HOUR =	00 TO 01	01 TO 02	02 TO 03	03 TO 04	04 TO 05	05 TO 06	06 TO 07	07 TO 08	08 TO 09	09 TO 10	10 TO 11	11 TO 12	12 TO 13	13 TO 14	14 TO 15	15 TO 16	16 TO 17	17 TO 18	18 TO 19	19 TO 20	20 TO 21	21 TO 22	22 TO 23	23 TO 24	MEAN
DAY																									
1	393	396	393	399	401	399	398	397	398	399	409	406	407	404	405	411	411	406	395	393	392	392	395	401	400
2	405	406	404	402	400	409	409	409	409	411	411	415	411	410	408	407	409	401	391	388	394	399	402	405	405
3 Q	411	415	419	421	422	421	421	422	423	425	427	429	428	425	424	421	416	410	403	399	401	405	407	405	417
4	410	413	414	408	417	416	417	417	421	418	415	411	417	419	421	418	417	411	400	391	392	397	407	409	412
5	417	420	421	415	417	418	419	421	421	422	423	425	426	426	427	425	417	409	401	396	399	405	411	414	416
6 Q	419	420	420	421	419	419	417	417	418	421	423	423	426	424	423	419	413	401	392	391	395	395	412	417	414
7	422	427	427	429	429	431	431	429	421	415	415	411	425	419	418	421	415	400	381	387	401	409	408	410	416
8	413	417	416	419	409	414	417	422	415	415	414	415	417	416	415	415	413	408	397	383	383	391	396	398	409
9	414	421	421	421	425	421	419	420	419	420	417	417	419	420	417	417	412	403	393	385	385	391	398	408	412
10 Q	417	423	424	423	425	423	425	423	419	419	421	419	420	423	423	423	418	405	397	394	395	405	409	417	416
11	423	428	428	428	428	426	423	421	417	422	427	425	427	427	425	427	429	417	402	395	396	402	412	419	420
12	425	427	433	426	432	423	426	420	422	418	420	420	421	422	416	430	424	420	405	390	391	398	402	410	418
13 Q	419	421	422	421	423	420	422	418	420	420	419	418	421	423	425	423	423	416	408	400	399	405	414	418	417
14	421	409	415	413	415	415	419	417	412	414	414	419	419	421	424	424	422	417	403	395	393	391	395	406	412
15 D	406	406	413	417	411	418	418	415	415	419	417	418	419	421	424	425	427	416	379	370	395	401	401	407	411
16	414	414	418	419	419	425	415	422	419	421	418	419	416	425	425	424	430	417	405	402	405	413	412	407	417
17 D	395	409	402	409	407	396	409	414	415	429	410	416	417	418	422	418	415	402	383	392	400	392	393	394	407
18 D	391	410	421	413	405	401	411	412	409	409	414	409	423	427	420	416	416	402	396	392	396	389	395	407	408
19	403	408	420	415	418	416	416	411	415	415	411	422	414	416	420	420	421	416	392	384	388	388	399	412	410
20	420	420	418	407	412	413	409	416	415	414	418	417	419	415	423	417	422	409	404	398	398	403	403	407	412
21	418	424	414	419	424	419	425	419	420	418	419	421	423	424	425	420	418	412	405	406	410	412	416	419	418
22	422	422	425	428	427	429	425	425	420	422	424	422	425	425	425	425	423	415	408	402	400	399	411	420	420
23	423	425	427	427	425	424	421	421	421	426	425	426	428	432	429	430	429	431	423	411	406	412	421	425	424
24	432	431	430	431	430	430	427	427	428	429	429	432	432	434	436	431	430	429	408	391	372	370	391	405	420
25 D	401	378	399	408	404	404	392	387	380	395	388	398	383	414	434	418	395	384	392	364	359	382	394	401	394
26 D	371	373	408	405	410	411	413	412	414	416	413	412	412	419	424	414	413	407	399	392	385	395	395	404	405
27	412	418	415	416	408	406	407	403	399	396	404	408	413	407	422	427	412	415	398	390	387	395	398	400	407
28	405	408	408	415	420	417	419	419	416	417	419	419	420	422	418	419	420	415	402	394	393	392	396	404	412
29 Q	417	419	422	418	420	418	421	422	420	419	419	422	424	424	425	430	427	418	404	393	388	396	409	417	416
30	414	420	423	421	416	416	417	420	419	419	427	420	425	428	428	425	421	423	418	405	400	407	411	419	418
31	423	425	425	425	426	425	420	420	416	411	415	418	418	419	429	430	431	428	413	401	393	399	402	399	417
MEAN	412	415	418	417	418	417	417	417	415	417	417	418	419	421	423	422	419	412	400	393	393	398	404	409	413

DECLINATION

MEAN VALUES FOR PERIODS OF SIXTY MINUTES, UNIVERSAL TIME

TABLE 2 VICTORIA D = 22 DEG 00.0 MIN EAST + JANUARY 1969

HOUR =	00 TO 01	01 TO 02	02 TO 03	03 TO 04	04 TO 05	05 TO 06	06 TO 07	07 TO 08	08 TO 09	09 TO 10	10 TO 11	11 TO 12	12 TO 13	13 TO 14	14 TO 15	15 TO 16	16 TO 17	17 TO 18	18 TO 19	19 TO 20	20 TO 21	21 TO 22	22 TO 23	23 TO 24	MEAN
DAY																									
1	29.5	30.2	31.1	30.8	30.4	30.0	30.6	32.0	29.9	30.0	27.7	31.3	30.0	29.3	28.4	32.2	31.9	30.4	30.2	31.1	30.8	31.1	30.6	30.4	30.4
2	30.5	30.1	30.5	30.9	33.1	30.3	29.8	29.6	29.6	29.8	29.6	30.1	30.6	30.5	30.7	30.1	32.3	33.2	33.4	32.5	31.1	30.5	30.5	30.1	30.8
3 Q	29.9	30.1	30.4	30.6	30.6	30.4	30.2	30.1	30.4	30.4	30.4	30.8	30.8	31.0	31.5	32.6	33.5	33.5	32.6	31.7	31.2	30.8	30.8	30.4	31.0
4	30.0	30.0	29.8	29.6	29.8	29.6	29.6	29.4	29.4	29.8	30.7	31.1	31.8	31.8	31.4	31.4	32.0	31.8	31.6	31.7	30.3	29.0	29.4	29.2	30.4
5	29.8	29.6	29.8	30.2	30.9	28.4	27.3	28.0	28.0	27.6	28.0	28.7	28.7	28.0	29.1	30.4	30.9	31.3	31.1	30.2	29.5	28.4	27.3	27.3	29.1
6 Q	28.0	28.4	28.9	29.7	29.7	29.3	29.3	29.3	29.1	28.2	28.0	28.9	30.0	29.8	29.3	30.6	32.2	33.7	33.3	31.8	29.7	28.2	27.5	28.2	29.6
7	28.2	27.6	28.0	28.8	29.5	29.1	29.1	29.1	30.6	30.8	32.8	32.2	37.7	37.3	35.3	33.1	33.1	33.5	31.7	25.1	24.2	24.4	26.2	26.9	30.2
8	27.7	28.2	28.8	28.0	27.7	28.6	28.2	27.1	28.8	28.2	28.0	28.9	28.9	29.7	29.7	29.7	31.3	31.9	31.1	29.9	27.1	25.7	25.3	24.9	28.5
9	25.7	26.8	28.2	28.6	29.2	29.0	28.8	29.2	29.0	29.2	29.4	29.7	30.8	31.0	29.5	32.1	33.5	33.9	33.5	31.7	29.5	28.2	27.5	27.3	29.6
10 Q	28.6	29.2	29.7	30.3	30.1	30.5	30.1	30.1	30.1	29.5	30.1	31.0	29.9	31.9	32.8	33.2	33.6	33.0	32.5	30.3	28.1	27.0	27.0	27.5	30.3
11	28.1	28.5	29.2	29.7	29.9	29.6	29.7	29.4	29.6	29.6	30.3	30.6	31.4	32.1	30.1	33.0	33.9	33.4	32.7	30.5	28.8	27.5	26.8	27.0	30.1
12	28.1	28.4	28.1	28.2	28.6	28.3	28.2	28.0	27.9	29.2	29.2	30.7	31.7	32.9	29.3	31.6	33.6	30.5	30.2	29.8	29.2	27.7	27.4	27.2	29.3
13 Q	27.5	27.3	28.1	28.2	28.8	28.6	28.4	28.3	28.6	28.8	29.3	29.6	28.6	28.6	29.1	29.2	31.0	32.1	32.3	30.8	29.1	27.2	26.6	26.1	28.8
14	26.5	27.3	29.1	28.7	29.0	30.6	30.2	29.2	30.5	29.2	28.2	29.8	29.3	29.2	29.3	30.0	30.7	31.9	31.8	29.5	27.1	26.1	24.2	25.3	28.9
15 D	27.8	26.2	27.0	26.3	27.5	28.2	28.3	28.8	29.6	31.5	30.8	30.5	31.2	29.8	29.6	30.2	31.1	32.4	31.3	26.4	26.1	26.7	26.1	26.6	28.7
16	28.0	27.5	28.0	27.4	28.5	26.5	28.0	28.1	28.7	27.8	28.4	30.6	32.2	23.1	31.6	31.9	32.0	30.9	30.2	29.0	27.7	26.7	26.6	26.4	28.6
17 D	28.2	27.6	26.6	26.2	25.8	29.2	28.5	28.3	29.2	28.0	31.2	30.9	27.9	27.7	30.0	30.7	31.6	30.5	27.8	25.8	28.5	27.8	28.3	26.7	28.5
18 D	27.4	27.8	28.9	28.9	29.9	29.1	28.2	25.0	29.8	26.5	29.6	23.4	30.7	31.9	31.6	29.5	30.6	30.6	29.5	29.4	29.0	26.9	26.9	25.8	28.6
19	27.6	29.8	28.3	28.1	28.3	29.1	28.7	28.3	27.8	24.2	28.5	30.5	29.7	27.8	28.8	30.0	30.8	30.5	29.9	28.3	26.6	25.6	25.4	26.3	28.3
20	27.3	27.5	27.8	31.3	30.7	28.6	29.3	28.4	28.1	28.0	28.0	29.4	29.7	29.5	29.0	29.6	29.4	29.1	28.3	27.9	27.4	26.8	25.9	26.1	28.5
21	27.6	26.9	27.7	28.5	28.5	28.6	27.7	27.6	27.6	27.3	26.2	28.9	29.7	29.3	29.6	29.6	30.6	31.1	29.0	27.9	27.3	26.0	26.1	26.8	28.2
22	27.9	27.7	28.3	28.4	28.8	27.8	28.0	27.9	27.4	26.9	28.4	28.2	29.0	29.0	29.2	30.0	31.2	31.0	31.4	30.3	28.0	26.7	26.0	26.2	28.5
23	26.9	27.6	27.5	28.0	28.2	28.6	28.5	27.7	28.3	28.0	28.4	28.4	28.3	30.1	30.4	30.5	29.5	29.8	30.5	29.8	28.2	27.1	26.3	26.3	28.5
24	27.6	27.7	28.0	28.2	28.3	28.3	28.0	28.2	28.2	27.8	27.7	28.1	28.5	25.1	27.7	24.9	28.1	29.2	28.2	27.8	26.2	22.5	23.0	23.7	27.1
25 D	26.5	27.9	29.4	29.5	30.1	31.7	30.8	31.7	32.8	28.8	29.6	26.3	25.0	23.4	28.1	29.3	25.9	22.9	26.4	27.7	26.0	27.0	27.1	27.3	28.0
26 D	29.2	32.9	29.0	31.7	31.1	29.9	28.9	28.4	28.4	28.3	28.6	25.8	20.3	28.5	30.8	31.1	33.1	33.4	31.3	29.5	27.2	26.5	26.2	25.8	29.0
27	28.4	28.7	28.7	29.3	31.2	33.1	30.4	32.9	32.9	30.0	29.6	26.3	25.8	20.9	29.4	29.7	28.5	29.5	30.4	27.7	28.0	27.7	22.3	28.1	28.7
28	27.3	28.1	30.6	29.0	29.5	29.3	29.3	28.9	28.0	28.3	28.5	28.1	28.3	28.7	29.5	29.6	31.3	32.1	31.9	30.4	29.3	27.1	26.9	26.4	29.0
29 Q	27.4	28.3	28.8	28.7	28.9	28.7	28.7	28.1	28.2	28.1	28.0	28.0	28.0	29.1	29.5	29.7	31.5	33.1	33.1	32.0	31.2	28.2	27.1	27.0	29.1
30	27.6	27.9	28.3	28.4	29.5	29.5	28.7	28.1	28.7	32.2	29.2	30.3	29.6	28.9	28.7	29.2	31.0	31.6	31.2	30.1	28.1	26.9	26.9	27.4	29.1
31	28.0	27.4	27.9	28.2	27.9	28.1	28.1	28.3	29.7	29.7	28.6	29.3	30.1	30.9	30.5	27.3	24.8	28.4	31.5	30.9	29.7	28.8	27.6	25.9	28.6
MEAN	28.0	28.4	28.7	29.0	29.4	29.2	29.0	28.8	29.2	28.8	29.1	29.2	29.5	29.3	30.0	30.4	31.1	31.3	31.0	29.6	28.4	27.3	26.8	27.0	29.1

VERTICAL INTENSITY

MEAN VALUES FOR PERIODS OF SIXTY MINUTES, UNIVERSAL TIME

TABLE 3 VICTORIA Z = 53,000 GAMMA + JANUARY 1969

HOUR =	00 TO 01	01 TO 02	02 TO 03	03 TO 04	04 TO 05	05 TO 06	06 TO 07	07 TO 08	08 TO 09	09 TO 10	10 TO 11	11 TO 12	12 TO 13	13 TO 14	14 TO 15	15 TO 16	16 TO 17	17 TO 18	18 TO 19	19 TO 20	20 TO 21	21 TO 22	22 TO 23	23 TO 24	MEAN
DAY																									
1	105	105	106	109	112	111	111	112	114	112	109	104	108	113	115	112	116	116	115	117	121	123	122	120	113
2	120	120	122	122	124	126	124	124	124	125	123	122	120	122	124	125	130	128	126	130	132	132	130	131	125
3 Q	133	131	130	131	131	131	130	130	130	130	130	130	129	129	129	129	129	128	129	133	136	134	134	133	131
4	137	136	135	138	138	138	139	140	141	141	141	142	140	143	144	146	148	147	147	148	146	144	144	144	142
5	148	148	147	148	149	147	146	148	148	146	146	148	146	144	144	147	146	145	145	144	145	146	144	143	146
6 Q	143	142	142	142	142	142	142	145	146	143	144	143	144	142	140	141	143	144	141	140	139	140	141	142	142
7	141	138	137	136	136	137	137	139	141	141	143	142	116	130	138	141	141	140	141	140	141	143	141	139	138
8	141	140	138	140	140	143	143	139	135	138	142	142	143	141	137	140	142	142	140	138	139	142	143	141	140
9	145	145	144	144	142	143	142	144	144	146	146	145	146	146	145	146	146	142	141	141	142	147	148	149	145
10 Q	148	146	144	144	142	141	142	142	143	134	136	146	145	142	144	143	144	142	140	136	138	141	144	145	142
11	144	142	140	140	138	138	138	140	141	144	145	144	144	144	143	143	145	138	134	130	131	136	133	133	140
12	133	133	132	130	130	127	128	128	129	130	127	122	125	126	124	121	122	121	121	121	122	125	132	133	127
13 Q	133	133	134	131	131	130	128	128	127	128	126	124	126	129	128	130	134	133	130	126	122	125	127	126	129
14	127	129	132	132	133	132	131	127	120	129	125	123	128	129	130	130	129	124	123	125	124	121	121	128	127
15 D	131	131	137	140	142	140	138	138	137	135	130	131	131	129	132	134	134	128	122	120	125	125	124	127	132
16	129	131	134	133	136	138	140	137	134	130	127	125	125	107	109	121	128	127	124	123	122	125	124	122	127
17 D	125	132	136	144	149	153	150	145	138	125	114	123	123	117	126	125	128	123	125	128	128	123	127	133	131
18 D	133	138	139	137	138	139	137	124	133	130	130	103	104	118	118	125	123	120	125	126	128	125	129	129	127
19	131	137	136	136	136	135	137	137	135	122	115	122	123	121	125	127	128	126	122	129	131	129	127	130	129
20	132	132	132	132	137	135	139	139	136	133	133	132	126	124	125	124	128	123	123	121	119	122	125	129	129
21	133	133	131	133	133	133	129	129	130	130	125	127	131	129	129	130	131	129	127	126	128	131	132	132	130
22	128	130	131	132	130	129	129	129	129	125	129	131	130	129	130	130	131	131	131	130	126	126	131	129	129
23	130	134	132	132	131	130	129	131	130	131	131	130	128	127	127	130	130	128	124	125	125	127	127	124	129
24	127	129	128	128	127	125	127	127	126	128	127	128	126	118	100	95	96	100	106	114	116	128	134	137	121
25 D	146	149	155	149	145	146	139	138	120	104	91	92	81	83	98	112	119	118	126	123	130	141	144	145	125
26 D	146	162	158	153	153	145	140	137	135	134	137	125	86	102	111	128	133	132	134	134	129	134	135	134	134
27	137	140	139	139	138	138	137	134	124	119	119	115	113	104	111	124	128	134	130	131	133	135	139	139	129
28	141	143	145	145	144	140	140	138	137	135	135	135	135	135	136	138	140	135	125	124	128	130	133	137	136
29 Q	138	138	139	138	137	138	135	135	134	134	133	134	133	132	134	136	140	136	133	131	129	128	131	135	135
30	136	136	137	137	135	138	136	135	134	129	113	124	131	133	134	134	136	135	131	126	125	127	133	135	132
31	133	133	134	134	133	134	133	132	130	130	129	123	124	118	121	122	125	125	129	131	131	131	132	129	129
MEAN	135	136	136	136	137	136	135	135	133	131	129	128	126	126	127	130	132	130	129	129	130	132	133	134	132

HORIZONTAL INTENSITY

MEAN VALUES FOR PERIODS OF SIXTY MINUTES, UNIVERSAL TIME

TABLE 4 VICTORIA H = 18,500 GAMMA + FEBRUARY 1969

HOUR =	00 TO 01	01 TO 02	02 TO 03	03 TO 04	04 TO 05	05 TO 06	06 TO 07	07 TO 08	08 TO 09	09 TO 10	10 TO 11	11 TO 12	12 TO 13	13 TO 14	14 TO 15	15 TO 16	16 TO 17	17 TO 18	18 TO 19	19 TO 20	20 TO 21	21 TO 22	22 TO 23	23 TO 24	MEAN
DAY																									
1 Q	415	420	420	417	419	419	419	419	417	421	419	421	422	422	423	422	423	419	409	405	399	398	407	412	416
2 D	419	420	424	422	424	424	422	421	424	416	416	418	415	420	423	436	447	415	153	154	299	288	292	332	380
3 D	348	322	359	342	340	344	362	363	373	375	367	366	374	362	378	401	393	368	322	310	337	324	365	385	358
4	390	395	396	398	402	401	397	396	400	399	399	403	403	407	411	412	407	403	398	394	400	399	392	405	400
5	407	396	397	404	400	398	399	408	401	402	401	412	412	415	414	413	409	398	391	394	392	399	400	404	403
6	408	412	406	391	399	394	400	414	408	408	416	412	416	414	414	413	407	399	393	395	396	403	399	394	405
7	413	415	416	416	417	416	415	416	412	412	414	412	417	416	415	418	409	397	382	379	391	398	399	399	408
8	396	406	419	417	413	404	411	413	415	416	418	420	424	424	423	419	409	394	398	396	391	393	400	402	409
9 Q	420	422	418	419	423	421	421	422	417	419	418	418	420	423	421	419	419	404	396	392	394	399	407	410	414
10	419	423	423	423	422	423	420	418	424	426	421	418	419	423	423	421	407	403	397	390	385	369	376	366	410
11 D	403	394	374	395	395	384	401	412	376	374	356	352	258	324	370	307	281	274	287	308	329	324	371	392	352
12	384	390	395	399	395	397	397	398	398	396	395	396	396	398	400	399	403	397	384	383	381	379	381	365	392
13	379	389	395	404	405	404	408	400	404	404	407	410	410	410	406	417	420	411	401	397	392	383	395	404	402
14	412	411	414	400	408	411	411	411	411	412	410	415	413	412	412	410	409	401	395	396	394	398	386	381	406
15 D	399	413	409	390	413	406	406	409	413	414	416	425	423	424	421	425	417	404	380	367	385	390	390	390	405
16	394	405	411	412	411	403	407	404	417	414	417	420	421	417	418	410	400	401	396	390	389	393	402	410	407
17 Q	414	419	416	417	417	415	415	417	417	414	415	416	421	424	419	417	412	406	402	394	388	394	403	408	412
18 Q	415	418	418	421	423	422	422	421	421	424	424	424	425	428	427	423	414	410	404	398	398	402	406	416	417
19	423	422	427	425	423	425	425	428	430	430	430	433	439	439	431	426	417	405	398	394	392	389	399	409	419
20	419	425	425	419	404	409	417	424	423	426	429	427	426	430	431	430	423	413	409	396	384	384	390	393	415
21	402	413	422	422	420	413	405	412	423	423	426	426	425	427	424	424	419	409	397	387	380	386	396	408	412
22 Q	418	422	424	426	425	424	425	424	428	430	432	431	432	435	436	439	428	417	401	393	384	384	390	406	419
23	418	424	429	428	424	413	417	416	422	423	429	427	421	436	428	436	430	418	408	396	389	393	401	414	418
24	423	423	425	427	422	419	424	427	428	428	427	429	432	430	431	430	423	415	405	393	383	383	390	398	417
25	415	417	419	423	426	427	425	425	424	431	429	429	433	433	431	430	425	416	409	397	386	384	384	386	417
26	411	417	425	419	413	419	429	436	435	431	431	427	431	434	433	431	428	419	405	391	383	383	391	405	418
27 D	416	420	412	433	419	428	425	418	425	430	430	433	441	434	415	418	393	387	377	367	360	350	362	376	407
28	392	399	403	402	409	409	413	420	418	416	413	415	409	408	408	413	410	414	403	382	371	371	358	365	401
MEAN	406	409	411	411	411	410	412	414	414	415	414	416	414	417	417	416	410	401	382	376	380	380	387	394	405

DECLINATION

MEAN VALUES FOR PERIODS OF SIXTY MINUTES, UNIVERSAL TIME

TABLE 5 VICTORIA D = 22 DEG 00.0 MIN EAST + FEBRUARY 1969

HOUR =	00 TO 01	01 TO 02	02 TO 03	03 TO 04	04 TO 05	05 TO 06	06 TO 07	07 TO 08	08 TO 09	09 TO 10	10 TO 11	11 TO 12	12 TO 13	13 TO 14	14 TO 15	15 TO 16	16 TO 17	17 TO 18	18 TO 19	19 TO 20	20 TO 21	21 TO 22	22 TO 23	23 TO 24	MEAN
DAY																									
1 Q	27.5	27.7	27.9	28.4	28.3	28.2	28.1	27.6	27.9	27.9	27.8	28.2	28.2	27.8	28.2	29.2	30.8	31.3	30.0	28.6	27.8	26.3	26.9	26.6	28.2
2 D	27.4	27.3	27.7	27.7	27.9	28.0	27.9	27.8	28.6	28.9	28.8	28.9	28.4	28.6	30.5	28.0	33.7	39.5	39.3	12.0	20.9	21.6	20.4	22.4	27.6
3 D	25.4	24.3	21.8	23.2	27.5	31.4	30.4	24.0	25.7	36.5	34.4	38.5	35.4	28.7	35.1	36.6	36.5	34.6	29.8	22.1	22.8	22.3	22.3	24.8	28.9
4	27.0	28.5	29.0	29.2	29.2	29.0	28.9	29.5	29.0	28.0	29.6	29.1	30.1	29.6	30.3	30.8	32.6	32.1	30.4	29.6	27.8	25.0	24.4	24.2	28.9
5	26.1	24.2	28.4	29.1	29.1	29.3	29.4	29.1	29.1	29.1	26.4	28.3	29.9	30.6	30.6	31.9	32.7	31.9	29.1	27.1	27.1	26.6	27.6	27.9	28.8
6	28.5	28.0	28.0	33.5	32.3	29.8	30.4	27.4	28.1	26.6	26.5	29.4	28.8	29.2	29.6	30.7	31.5	31.4	30.2	28.4	27.5	24.9	25.2	25.3	28.8
7	27.2	26.7	27.8	28.3	28.0	28.2	27.8	28.9	27.3	28.2	29.2	28.8	32.3	32.2	30.3	33.2	34.6	33.5	32.0	28.4	26.2	25.5	24.3	24.1	28.9
8	24.5	25.8	27.8	28.6	29.1	29.7	29.7	28.7	28.6	28.8	28.4	29.2	28.7	29.6	30.8	31.3	33.8	31.4	28.8	28.3	26.6	25.6	25.7	26.0	28.6
9 Q	26.1	26.3	26.8	27.4	27.8	28.4	28.4	28.4	28.4	28.7	28.6	28.5	28.9	28.9	29.0	30.5	31.8	33.2	32.4	30.9	28.5	26.6	25.6	24.8	28.5
10	25.1	25.9	26.8	27.4	28.5	28.7	28.6	29.2	28.6	28.9	29.7	30.3	28.8	26.7	29.5	31.5	32.8	33.0	32.6	30.7	29.2	24.8	20.2	21.0	28.3
11 D	18.2	25.5	25.0	29.2	30.4	31.5	31.9	35.4	38.4	42.0	44.2	37.6	30.9	28.2	20.1	17.7	5.9	20.2	22.8	22.8	25.5	21.5	22.3	25.0	27.2
12	26.6	27.6	28.3	28.7	28.4	29.0	29.3	29.0	28.8	28.9	29.6	29.5	29.4	29.3	29.3	30.9	31.9	32.5	32.8	30.8	28.6	27.5	26.2	26.3	29.1
13	26.8	25.8	26.5	27.6	27.8	28.4	28.0	27.8	27.8	27.0	29.3	29.4	29.5	29.6	27.2	29.9	30.9	31.2	30.9	30.3	29.2	28.4	26.7	25.8	28.4
14	27.0	26.6	26.7	27.5	27.5	28.1	28.5	29.1	28.5	28.8	29.5	28.5	30.3	30.5	29.2	30.0	31.9	32.5	30.9	29.3	28.1	27.4	26.7	25.1	28.7
15 D	24.5	25.4	26.7	32.1	28.8	28.1	29.2	28.9	28.6	25.2	24.3	27.6	29.5	30.5	28.5	30.3	31.9	31.2	30.0	25.4	22.9	25.3	26.3	26.9	27.8
16	25.6	26.2	26.3	26.9	27.7	30.6	31.0	27.9	22.6	29.0	29.6	30.0	31.3	32.2	30.7	30.9	29.7	29.1	29.1	28.5	28.5	28.0	26.5	26.9	28.5
17 Q	27.0	27.7	27.1	27.5	27.7	27.4	27.4	27.3	27.3	28.3	29.3	29.5	29.8	29.9	29.4	30.1	30.8	31.4	31.1	30.2	29.1	27.5	24.8	25.5	28.5
18 Q	27.2	27.2	27.2	27.3	27.9	27.6	27.7	27.6	27.5	27.7	27.9	28.1	28.6	28.9	29.6	30.7	31.5	30.9	29.4	27.9	26.0	25.8	25.5	25.7	28.0
19	26.2	25.9	26.6	26.5	27.3	25.7	26.1	26.9	26.8	27.3	28.0	28.9	25.5	31.5	31.1	33.4	33.5	34.7	33.5	30.9	28.0	27.0	25.6	25.3	28.4
20	25.7	26.7	27.3	27.4	27.8	28.3	27.7	27.7	27.6	28.1	28.8	29.1	29.2	27.9	29.5	31.2	31.7	30.3	30.5	30.7	29.0	27.6	26.8	23.8	28.3
21	25.7	26.6	27.4	27.8	28.3	28.7	33.0	28.0	27.4	27.2	27.4	28.4	28.4	29.3	29.2	30.9	33.0	34.2	32.5	31.6	28.6	26.7	25.3	23.5	28.7
22 Q	25.6	26.3	26.8	27.4	27.4	27.8	27.7	27.9	27.9	27.9	27.7	28.2	27.0	27.7	29.4	31.3	32.4	33.0	32.9	32.1	29.2	26.7	24.9	24.2	28.3
23	24.9	26.3	26.6	27.6	27.7	29.1	33.6	29.9	28.1	27.8	25.7	27.5	26.5	27.4	30.7	32.1	34.4	35.3	34.3	31.8	29.7	27.1	25.8	25.0	29.0
24	25.9	27.0	27.5	27.4	27.6	28.2	28.3	28.2	27.5	28.2	28.4	28.7	28.4	28.9	29.2	31.5	34.2	34.0	33.8	32.7	30.4	27.7	25.5	23.9	28.9
25	23.5	25.0	26.8	27.1	27.7	27.7	28.1	28.2	28.4	28.2	28.1	26.6	27.9	29.1	29.3	30.6	32.2	33.0	31.5	31.7	29.3	27.0	26.0	24.6	28.2
26	25.0	25.9	26.4	28.6	27.0	28.4	28.2	29.0	33.9	31.9	30.4	31.9	29.0	28.6	30.2	30.6	32.2	34.8	30.9	28.4	27.0	25.3	25.3	25.3	28.9
27 D	26.4	26.6	28.5	26.8	26.5	27.8	27.2	31.8	29.1	27.8	28.3	28.6	27.6	28.2	26.0	16.8	23.1	25.4	29.1	30.5	28.4	27.4	27.6	27.5	27.2
28	27.9	27.7	27.7	27.6	27.6	27.4	30.6	28.5	30.0	29.7	29.8	29.8	29.7	30.2	31.2	30.0	30.6	30.3	31.8	31.1	30.6	28.2	28.1	25.8	29.2
MEAN	25.9	26.5	27.0	28.0	28.2	28.6	29.0	28.6	28.5	29.0	29.1	29.5	29.2	29.3	29.4	30.1	31.2	32.0	31.2	28.7	27.6	26.1	25.3	25.1	28.5

VERTICAL INTENSITY

MEAN VALUES FOR PERIODS OF SIXTY MINUTES, UNIVERSAL TIME

TABLE 6 VICTORIA Z = 53,000 GAMMA + FEBRUARY 1969

HOUR =	00 TO 01	01 TO 02	02 TO 03	03 TO 04	04 TO 05	05 TO 06	06 TO 07	07 TO 08	08 TO 09	09 TO 10	10 TO 11	11 TO 12	12 TO 13	13 TO 14	14 TO 15	15 TO 16	16 TO 17	17 TO 18	18 TO 19	19 TO 20	20 TO 21	21 TO 22	22 TO 23	23 TO 24	MEAN
DAY																									
1 Q	132	131	132	131	132	131	132	132	131	130	130	130	131	129	131	134	136	135	126	128	126	125	130	130	131
2 D	131	130	129	130	131	129	131	131	129	125	127	124	123	126	128	131	129	117	84	79	98	113	131	169	124
3 D	179	174	201	210	225	215	197	171	128	138	141	114	96	58	88	133	142	135	125	128	135	146	157	151	149
4	147	145	146	143	145	145	145	149	150	146	147	146	145	142	140	142	138	141	139	139	133	129	133	137	142
5	141	140	146	146	144	144	146	145	141	143	136	133	134	135	137	139	140	137	138	141	142	139	138	138	140
6	141	143	141	144	147	150	155	151	145	140	126	136	141	139	139	140	140	142	139	142	142	142	138	139	142
7	145	143	142	139	138	139	138	139	138	141	141	134	130	134	137	138	139	141	136	136	139	140	140	141	139
8	140	142	144	144	141	143	144	143	143	141	142	142	139	138	137	139	139	136	136	135	134	135	136	138	140
9 Q	142	142	140	139	138	137	137	136	138	138	138	138	137	137	135	136	138	138	133	131	129	128	130	133	136
10	136	138	137	137	137	136	135	135	134	127	128	129	131	131	134	138	137	137	137	133	130	125	132	137	134
11 D	156	188	176	164	154	152	141	109	92	47	-42	-52	-139	-85	-9	-35	-38	34	82	113	136	153	158	163	76
12	156	155	154	153	149	149	147	147	146	145	145	145	144	144	144	145	147	146	143	144	141	137	135	139	146
13	148	150	150	151	151	148	146	148	146	138	135	140	140	140	129	128	134	134	133	135	135	133	132	137	140
14	141	141	143	142	143	143	143	143	141	140	137	130	126	129	134	138	141	138	136	136	132	127	122	127	136
15 D	135	140	142	146	149	146	149	149	145	137	123	129	134	134	134	135	133	129	128	129	131	129	125	130	136
16	135	137	139	141	141	145	145	145	126	133	136	134	122	121	128	131	133	132	133	133	135	132	129	130	134
17 Q	131	134	133	135	135	136	137	137	136	136	135	137	135	135	134	137	141	143	141	140	137	132	130	130	136
18 Q	132	132	133	133	134	134	134	136	135	135	134	135	133	133	134	134	135	132	134	133	130	126	127	132	133
19	134	135	135	134	135	138	138	139	136	136	134	134	121	110	117	125	129	132	130	125	122	125	128	129	130
20	133	132	132	131	133	136	137	137	135	134	133	131	127	126	127	133	130	124	117	111	108	111	116	125	127
21	130	134	136	134	131	132	134	134	136	135	134	133	132	131	133	134	132	127	120	121	122	122	123	126	130
22 Q	131	131	131	131	131	131	131	131	132	131	131	130	129	127	126	132	130	129	124	120	119	119	120	123	128
23	128	131	131	131	130	131	134	131	132	131	127	120	119	116	121	131	130	123	112	109	110	115	118	126	124
24	135	133	132	131	130	130	132	131	127	124	128	130	129	130	130	133	134	132	131	128	124	121	120	122	129
25	131	133	135	134	133	129	128	129	128	128	129	128	126	127	129	131	129	123	121	118	119	120	124	128	128
26	132	135	136	135	138	139	138	135	127	123	129	132	129	129	129	132	129	121	113	109	114	119	124	130	128
27 D	131	132	133	136	135	136	133	137	130	131	130	129	127	125	116	98	88	98	103	116	126	130	134	137	125
28	141	144	143	144	145	146	150	133	133	136	136	138	133	132	131	131	126	121	118	110	108	115	124	135	132
MEAN	139	141	142	142	142	142	141	139	134	132	128	126	121	120	125	127	127	128	125	126	127	128	131	135	132

HORIZONTAL INTENSITY

MEAN VALUES FOR PERIODS OF SIXTY MINUTES, UNIVERSAL TIME

TABLE 7 VICTORIA | H = 18,500 GAMMA + | MARCH 1969

HOUR =	00 TO 01	01 TO 02	02 TO 03	03 TO 04	04 TO 05	05 TO 06	06 TO 07	07 TO 08	08 TO 09	09 TO 10	10 TO 11	11 TO 12	12 TO 13	13 TO 14	14 TO 15	15 TO 16	16 TO 17	17 TO 18	18 TO 19	19 TO 20	20 TO 21	21 TO 22	22 TO 23	23 TO 24	MEAN
DAY																									
1	382	405	407	407	409	412	411	415	416	416	418	416	416	419	419	419	406	384	398	399	387	385	385	380	405
2	376	391	406	406	400	410	413	413	414	415	417	416	415	420	416	415	413	405	397	389	381	380	387	396	404
3 Q	409	415	417	419	416	419	418	420	421	424	421	424	424	426	425	421	415	408	395	384	379	384	392	404	412
4 Q	413	417	419	421	422	420	420	422	422	423	425	427	426	427	428	425	419	409	402	391	391	393	393	405	415
5	414	423	425	423	424	427	430	430	432	433	430	435	430	428	428	431	427	413	394	383	386	394	405	420	419
6	412	422	427	420	423	426	423	430	423	421	427	425	428	427	427	424	417	399	396	392	380	379	390	405	414
7	409	413	401	404	420	404	409	416	418	423	426	427	425	439	431	435	425	403	380	387	382	389	387	396	410
8	400	409	406	415	412	409	412	412	415	416	416	415	421	426	425	424	417	405	394	389	387	386	386	378	407
9	402	413	414	416	416	415	423	424	427	415	418	427	423	426	422	419	419	417	398	392	392	393	394	407	413
10 Q	421	420	425	424	417	422	419	419	423	424	422	425	426	428	430	435	436	433	423	406	404	398	399	404	420
11	416	425	420	426	428	421	419	413	409	406	406	416	410	423	417	416	417	412	402	352	349	365	382	380	405
12 D	385	402	389	382	370	379	386	373	374	388	382	408	409	405	401	397	385	378	381	385	389	392	400	402	389
13	406	409	409	408	413	411	414	413	415	416	417	420	417	416	416	417	408	402	397	391	389	384	389	400	407
14	410	410	406	406	413	415	415	421	420	422	425	421	422	423	419	414	410	405	387	383	379	374	396	407	408
15	418	409	401	409	406	406	402	395	408	395	405	415	413	417	416	418	423	405	393	391	392	386	389	403	405
16	409	412	415	419	410	403	404	396	390	398	417	422	422	419	421	423	412	401	389	386	384	391	405	415	407
17 D	434	410	381	396	398	376	390	409	410	414	415	411	389	416	413	405	378	380	386	381	364	369	386	396	396
18	406	414	414	409	401	400	410	386	398	417	420	423	420	422	423	423	413	399	402	393	385	374	390	391	406
19	414	421	419	419	419	420	420	417	412	417	427	430	430	430	430	428	416	407	395	391	397	397	386	399	414
20	398	413	364	389	403	402	403	406	404	413	420	417	414	413	413	412	398	382	394	396	382	374	366	378	398
21	388	390	401	407	405	400	407	427	410	418	422	422	425	426	425	422	412	397	389	367	367	367	379	395	403
22	410	413	410	403	408	418	424	420	416	408	408	413	431	422	418	418	416	404	385	379	374	380	387	385	406
23 D	402	410	414	421	418	422	425	426	425	424	431	431	432	432	432	421	423	414	348	332	321	290	347	402	402
24 D	405	423	600	395	354	390	376	260	165	155	60	125	373	387	369	364	365	361	355	360	365	370	419	422	342
25 D	375	376	384	382	384	385	393	380	383	390	395	393	389	381	374	395	391	380	367	369	377	376	373	377	382
26	390	393	399	399	401	401	405	403	410	409	413	416	412	409	403	405	403	389	378	374	374	381	380	381	397
27 Q	392	399	405	406	402	405	407	413	418	418	419	421	423	420	420	418	416	406	396	390	389	387	393	399	407
28 Q	407	411	418	414	415	416	419	420	426	429	430	429	429	431	423	425	416	411	412	405	404	403	408	412	417
29	422	425	425	422	420	422	414	418	410	413	420	425	421	424	416	413	416	412	407	392	382	387	387	391	412
30	399	400	415	416	408	413	414	419	423	429	423	423	425	424	422	422	409	378	364	375	388	394	399	414	408
31	411	421	402	417	426	427	427	430	432	433	434	440	435	430	426	430	424	398	366	380	379	377	385	402	414
MEAN	404	410	414	410	408	410	411	408	405	407	407	412	419	421	418	417	411	400	389	383	381	381	389	398	405

DECLINATION

MEAN VALUES FOR PERIODS OF SIXTY MINUTES, UNIVERSAL TIME

TABLE 8 VICTORIA D = 22 DEG 00.0 MIN EAST + MARCH 1969

DAY	00 TO 01	01 TO 02	02 TO 03	03 TO 04	04 TO 05	05 TO 06	06 TO 07	07 TO 08	08 TO 09	09 TO 10	10 TO 11	11 TO 12	12 TO 13	13 TO 14	14 TO 15	15 TO 16	16 TO 17	17 TO 18	18 TO 19	19 TO 20	20 TO 21	21 TO 22	22 TO 23	23 TO 24	MEAN
1	25.4	25.9	26.9	27.7	27.7	28.1	28.0	28.3	28.0	28.2	28.6	29.1	29.1	28.7	30.1	31.1	30.3	26.1	24.9	27.0	25.3	25.5	25.0	26.0	27.5
2	25.7	25.6	29.1	26.8	27.9	27.4	27.4	28.3	28.2	28.7	29.0	26.0	24.3	26.8	29.9	31.7	32.5	32.7	31.3	30.2	29.2	28.3	27.2	26.6	28.4
3 Q	27.1	27.3	27.2	27.7	27.4	27.6	27.5	27.7	27.5	28.1	28.0	28.4	28.1	28.8	28.9	30.4	31.5	33.1	32.4	31.1	28.2	25.9	24.6	24.6	28.3
4 Q	25.8	26.6	27.0	27.4	27.2	27.6	27.7	27.6	28.0	27.9	27.8	28.0	28.3	28.0	29.4	30.8	32.2	32.3	31.2	27.7	25.8	22.9	21.6	22.1	27.5
5	25.5	26.7	27.2	27.5	27.9	27.4	27.2	27.4	27.3	27.4	28.0	28.8	30.5	31.5	32.2	32.1	32.5	34.0	33.0	31.5	28.2	25.6	24.1	23.4	28.6
6	25.4	25.7	25.4	26.8	27.0	27.4	27.5	28.4	28.7	28.4	28.7	31.3	30.0	29.8	30.4	29.7	30.4	29.6	29.9	29.7	27.6	25.4	24.0	24.1	28.0
7	24.5	25.3	26.7	27.1	26.5	28.3	28.9	28.7	29.9	27.9	27.3	28.7	29.1	25.7	26.1	30.5	33.1	32.4	28.7	26.8	24.3	23.7	25.2	23.6	27.5
8	24.6	24.8	25.7	27.1	28.9	27.9	27.9	28.7	28.8	28.4	29.9	29.2	26.5	29.2	29.8	31.7	32.5	33.1	31.3	30.2	27.6	27.1	25.7	24.1	28.4
9	24.3	24.7	25.2	25.4	25.9	27.6	28.5	28.4	30.1	31.8	30.3	29.7	30.5	29.5	32.1	31.6	31.0	33.6	31.4	30.7	29.6	27.9	26.8	25.5	28.8
10 Q	24.9	25.4	26.1	25.5	26.6	26.6	27.4	27.9	28.8	30.5	28.8	28.4	28.4	28.3	29.2	30.5	31.5	33.1	33.5	31.7	29.3	27.7	26.8	25.1	28.4
11	25.0	24.9	25.9	26.6	26.6	26.2	29.4	28.8	33.6	33.4	31.9	33.8	37.2	32.7	31.4	30.3	31.9	33.3	32.2	29.6	23.7	22.8	21.9	21.7	28.9
12 D	24.2	25.9	25.1	28.9	24.8	28.8	27.1	33.8	39.0	31.8	29.3	29.9	28.7	29.1	27.3	28.5	25.6	30.1	31.7	30.4	28.7	26.8	24.5	24.4	28.5
13	25.5	29.6	27.5	27.0	27.2	27.5	29.0	28.5	28.0	28.7	28.8	29.1	28.4	29.4	30.4	32.0	32.7	32.4	31.1	28.9	26.2	24.4	23.0	23.3	28.3
14	24.5	23.7	23.4	24.8	26.6	26.9	27.4	27.7	28.1	28.5	28.8	29.9	29.5	29.6	31.1	32.0	32.9	33.6	31.0	28.7	26.5	23.8	21.1	21.2	27.6
15	22.0	22.4	26.2	24.0	25.3	29.2	28.0	29.7	29.5	34.5	31.2	32.0	32.9	32.8	32.7	29.3	31.1	34.5	29.5	27.8	26.6	25.7	25.2	24.8	28.6
16	26.6	27.1	27.0	26.6	28.2	33.6	24.9	32.6	32.5	34.9	34.9	31.2	31.8	32.6	30.6	31.5	33.2	34.5	33.1	31.7	28.3	25.9	24.6	24.2	30.1
17 D	22.2	20.5	20.9	26.3	25.6	31.3	27.6	27.6	27.8	27.6	31.3	30.7	24.1	32.1	32.4	35.5	35.1	24.5	24.5	26.5	26.2	23.8	24.8	25.6	27.3
18	26.5	27.1	27.6	29.9	29.6	29.2	32.6	32.3	32.2	28.3	28.3	28.8	29.0	29.6	30.7	32.0	33.5	31.8	32.1	32.4	29.5	27.2	25.7	26.6	29.7
19	26.4	26.9	27.1	27.3	27.5	27.3	27.3	32.5	30.8	29.0	27.7	28.0	28.6	29.4	31.2	33.7	35.7	35.9	33.6	29.9	27.4	24.2	20.1	16.3	28.5
20	20.8	18.2	23.6	26.7	27.9	27.7	28.1	33.8	27.5	28.7	28.4	29.0	28.9	30.2	30.0	33.1	33.0	30.3	26.9	26.5	24.3	22.8	19.8	20.6	26.9
21	23.8	24.6	24.3	26.2	27.1	27.9	31.1	31.9	30.3	29.0	27.7	26.1	27.5	28.6	30.4	32.7	35.1	35.8	34.8	32.5	26.2	23.1	22.0	22.0	28.4
22	22.2	23.1	23.9	27.8	26.6	27.5	27.7	28.4	34.6	32.8	32.8	29.8	29.0	29.2	29.8	31.3	33.7	36.2	36.2	30.7	26.0	23.2	21.9	20.2	28.5
23 D	23.3	25.0	26.4	27.4	27.4	27.6	27.9	28.3	28.2	28.4	28.2	28.8	28.9	29.8	30.7	32.2	32.7	36.2	40.7	35.8	37.0	31.5	20.8	17.0	29.2
24 D	15.5	17.9	17.9	19.1	22.8	24.2	29.9	31.7	37.7	48.8	53.9	34.2	28.4	30.4	30.4	32.1	33.2	33.2	31.5	30.1	28.8	27.9	28.0	27.7	29.8
25 D	27.9	27.9	28.2	28.6	29.0	29.4	29.0	34.8	36.6	34.1	32.7	30.9	31.5	30.1	28.8	32.3	33.2	33.2	30.4	27.5	27.1	27.3	27.5	27.7	30.2
26	27.5	28.2	27.1	27.1	27.9	27.7	27.5	27.9	31.5	28.4	27.5	27.5	29.4	29.7	27.9	29.0	32.8	31.5	32.8	30.1	28.8	26.3	24.2	23.9	28.4
27 Q	23.5	24.6	25.0	26.1	26.3	26.5	26.1	26.5	27.9	27.7	27.9	27.5	27.7	27.7	27.9	30.1	32.6	34.1	32.8	31.2	29.4	27.1	26.1	24.6	27.8
28 Q	24.4	24.4	25.7	26.1	26.8	27.7	27.1	27.5	27.5	27.9	27.7	27.5	28.4	28.6	29.0	30.4	32.6	32.7	32.8	31.9	29.2	27.3	25.7	23.9	28.0
29	23.9	24.5	25.0	26.5	26.6	27.0	27.5	31.0	30.9	30.5	31.2	29.1	26.3	27.2	26.5	27.7	30.7	31.2	32.3	32.8	31.7	28.4	25.2	24.5	28.3
30	22.4	24.7	26.0	27.6	29.2	28.1	27.8	28.1	26.5	28.3	28.5	28.7	28.6	28.8	30.4	32.7	35.1	36.2	30.2	26.8	26.0	25.2	23.6	23.6	28.0
31	25.5	26.1	27.8	28.5	26.7	27.3	26.9	28.0	27.3	27.0	26.9	27.9	27.9	27.1	30.9	34.4	36.3	36.8	33.9	28.6	26.9	26.6	25.6	25.0	28.6
MEAN	24.4	25.0	25.7	26.7	27.1	27.9	28.0	29.4	30.1	30.2	30.1	29.3	29.0	29.4	30.0	31.4	32.6	32.8	31.7	29.9	27.7	25.8	24.3	23.7	28.4

VERTICAL INTENSITY

MEAN VALUES FOR PERIODS OF SIXTY MINUTES, UNIVERSAL TIME

TABLE 9 VICTORIA Z = 53,000 GAMMA + MARCH 1969

HOUR =	00 TO 01	01 TO 02	02 TO 03	03 TO 04	04 TO 05	05 TO 06	06 TO 07	07 TO 08	08 TO 09	09 TO 10	10 TO 11	11 TO 12	12 TO 13	13 TO 14	14 TO 15	15 TO 16	16 TO 17	17 TO 18	18 TO 19	19 TO 20	20 TO 21	21 TO 22	22 TO 23	23 TO 24	MEAN
DAY																									
1	136	137	137	137	137	139	137	136	136	133	132	134	132	132	131	134	132	130	127	120	116	118	122	130	131
2	137	144	151	153	152	148	142	141	138	136	136	128	116	119	128	137	139	139	137	136	135	135	137	137	138
3 Q	140	138	137	136	135	137	136	136	134	134	133	133	133	131	133	135	138	141	136	131	128	125	124	130	134
4 Q	132	134	134	135	140	138	138	139	137	136	135	135	133	132	133	136	136	133	125	117	117	121	121	124	132
5	128	129	130	129	128	128	129	129	128	127	125	118	108	114	120	124	124	124	123	122	119	118	121	123	124
6	124	127	129	130	131	133	132	131	128	130	120	110	119	123	125	128	127	124	122	118	113	113	119	126	124
7	128	132	136	139	144	148	144	146	145	138	130	131	129	122	96	99	107	106	107	110	116	121	123	127	126
8	133	135	140	144	144	143	141	139	138	131	131	130	123	129	131	134	133	131	131	125	124	126	130	129	133
9	133	140	140	139	140	144	140	138	135	130	135	134	130	119	109	118	123	125	121	119	121	120	124	127	129
10 Q	133	133	133	132	131	133	135	135	136	130	131	132	132	132	132	133	130	131	126	123	123	122	122	127	130
11	130	133	134	135	135	134	139	140	135	132	127	110	101	114	118	125	130	128	117	105	114	128	137	157	127
12 D	176	177	185	189	180	181	111	126	132	106	60	111	135	134	132	129	122	121	127	127	126	129	134	136	137
13	139	146	145	143	140	140	138	139	137	138	136	135	131	134	137	138	138	135	132	131	124	128	136	140	137
14	143	142	143	144	145	144	141	141	139	137	134	133	134	134	133	135	135	132	126	122	119	118	124	129	134
15	139	143	151	157	158	159	154	154	123	116	116	99	111	117	115	110	109	115	112	119	119	125	134	140	129
16	139	136	133	136	140	146	138	133	116	100	85	123	129	133	138	136	133	130	126	121	116	116	121	130	127
17 D	146	154	163	156	163	184	171	152	146	132	126	128	78	86	130	139	130	115	108	114	116	131	136	138	135
18	141	139	140	142	147	149	141	130	137	131	118	123	128	132	136	138	136	133	131	127	121	124	131	133	134
19	135	138	137	135	133	133	132	134	124	130	132	133	131	130	131	132	131	126	118	116	110	112	111	116	128
20	141	169	196	169	151	147	147	153	149	146	127	137	136	135	133	131	125	122	118	118	117	127	135	148	141
21	156	152	155	154	152	153	152	135	128	132	125	122	123	131	133	137	139	136	129	121	119	116	124	129	136
22	137	142	142	147	148	144	140	141	138	128	128	127	121	117	122	121	125	123	113	105	104	114	120	128	128
23 D	136	136	137	138	136	135	135	136	135	135	133	133	133	132	132	131	125	119	104	103	103	111	206	269	137
24 D	308	334	381	310	273	250	248	159	85	-47	-152	-125	55	150	167	174	176	173	171	173	173	173	173	170	165
25 D	165	162	161	156	154	153	157	151	124	112	146	152	147	144	128	143	142	135	138	133	142	150	161	172	147
26	175	170	160	150	148	142	144	146	148	144	140	129	134	139	135	138	144	140	132	136	140	141	153	158	145
27 Q	157	155	151	151	145	145	144	143	142	140	141	138	139	141	142	143	145	141	135	135	137	137	142	143	143
28 Q	148	148	148	146	144	140	140	139	139	138	136	136	137	138	136	137	138	134	129	124	124	127	127	132	137
29	131	134	138	137	136	137	138	137	135	132	129	135	131	128	132	128	134	133	136	129	126	130	135	145	134
30	157	151	154	151	150	148	145	147	141	136	135	138	138	139	140	145	142	130	126	127	127	126	125	130	140
31	133	142	145	149	143	141	140	140	133	129	126	127	127	129	129	138	137	125	118	121	121	123	125	133	132
MEAN	147	150	154	151	148	148	144	140	134	125	118	120	124	129	130	133	133	130	126	123	123	126	133	141	135

HORIZONTAL INTENSITY

MEAN VALUES FOR PERIODS OF SIXTY MINUTES, UNIVERSAL TIME

TABLE 10 VICTORIA H = 18,500 GAMMA + APRIL 1969

HOUR =	00 TO 01	01 TO 02	02 TO 03	03 TO 04	04 TO 05	05 TO 06	06 TO 07	07 TO 08	08 TO 09	09 TO 10	10 TO 11	11 TO 12	12 TO 13	13 TO 14	14 TO 15	15 TO 16	16 TO 17	17 TO 18	18 TO 19	19 TO 20	20 TO 21	21 TO 22	22 TO 23	23 TO 24	MEAN
DAY																									
1 D	419	427	430	425	415	423	426	425	427	426	431	430	418	426	429	417	387	351	345	329	345	369	381	400	404
2	413	410	411	417	419	420	418	423	424	425	429	427	424	427	424	415	386	364	381	373	344	356	366	385	403
3	395	396	403	401	397	405	406	414	414	415	415	418	418	418	417	411	393	375	356	346	351	357	370	393	395
4	401	406	408	428	412	407	420	417	418	420	418	415	418	424	423	418	408	387	369	360	363	368	380	405	404
5	409	409	416	421	418	419	430	407	405	406	412	421	420	422	425	422	408	395	390	386	379	377	391	405	408
6	418	420	425	421	417	419	425	420	431	428	429	432	431	431	430	429	427	409	390	376	378	393	383	394	415
7	411	410	408	407	411	391	386	413	406	411	417	420	422	414	413	415	403	389	369	375	392	397	398	410	404
8	410	417	416	415	415	419	423	421	425	425	428	426	424	428	428	431	428	416	406	393	390	390	396	402	416
9	418	418	426	429	424	413	413	417	423	422	423	419	412	416	422	412	404	398	383	377	387	398	401	410	411
10 Q	408	418	422	426	427	431	419	419	421	424	423	423	426	426	424	421	408	400	399	403	394	396	400	410	415
11	417	416	428	425	428	426	431	419	406	412	418	424	434	435	428	416	405	393	392	394	397	404	407	411	415
12	419	421	424	423	423	427	423	426	430	430	433	433	438	435	435	432	421	405	410	412	417	422	416	441	425
13 D	434	416	407	423	429	439	431	437	429	434	432	432	417	404	407	408	390	355	352	361	364	378	396	416	408
14	427	449	399	405	409	416	414	417	422	421	422	416	418	424	425	411	402	381	368	365	368	383	392	401	406
15	406	396	412	414	422	421	422	429	434	424	414	427	423	422	418	415	405	389	382	385	394	401	405	407	411
16	417	424	425	421	418	419	429	412	423	426	426	422	424	427	421	412	402	382	389	389	386	393	401	418	413
17 D	405	425	397	405	418	422	413	418	405	414	422	415	420	414	405	383	386	378	361	365	375	379	395	418	402
18	420	414	418	413	406	416	420	414	418	420	426	419	414	422	420	415	405	393	387	383	389	404	396	393	409
19 Q	414	412	425	421	424	423	425	426	429	429	432	433	434	430	431	426	412	397	392	400	401	407	409	410	418
20	423	415	419	422	425	427	426	426	429	430	430	436	436	434	434	436	427	417	411	403	405	401	404	404	422
21 Q	406	413	415	422	425	426	428	424	428	430	435	434	438	441	446	445	436	421	411	408	402	409	411	412	424
22	432	445	453	455	456	466	457	431	436	437	441	444	440	437	444	449	440	425	418	417	408	404	409	415	436
23 Q	425	429	427	431	430	429	431	436	436	443	439	440	443	436	438	445	434	427	419	413	408	408	412	420	429
24	429	432	419	426	430	435	429	437	439	440	441	440	442	447	453	454	442	432	424	414	418	421	421	425	433
25	441	412	428	434	429	427	434	437	436	436	441	440	442	438	435	435	435	419	404	405	410	411	426	425	428
26 Q	431	431	432	435	433	431	431	436	435	438	441	440	440	438	441	433	429	420	409	405	416	412	409	418	429
27	430	424	412	421	427	420	424	423	431	434	439	438	438	441	435	440	432	415	408	412	410	424	433	439	427
28 D	447	445	446	456	454	467	419	401	379	403	379	415	407	373	398	412	396	405	404	404	410	417	415	420	416
29	413	419	413	412	413	409	414	425	422	415	418	418	421	423	423	410	410	415	413	390	396	401	409	393	412
30 D	401	410	429	411	389	411	399	408	416	427	418	420	413	402	402	386	394	385	379	381	398	405	409	425	405
MEAN	418	419	420	422	421	423	422	422	423	425	426	427	427	425	426	422	412	398	391	387	390	396	401	411	415

DECLINATION

MEAN VALUES FOR PERIODS OF SIXTY MINUTES, UNIVERSAL TIME

TABLE 11 VICTORIA   D= 22 DEG 00.0 MIN EAST +   APRIL 1969

HOUR =	00 TO 01	01 TO 02	02 TO 03	03 TO 04	04 TO 05	05 TO 06	06 TO 07	07 TO 08	08 TO 09	09 TO 10	10 TO 11	11 TO 12	12 TO 13	13 TO 14	14 TO 15	15 TO 16	16 TO 17	17 TO 18	18 TO 19	19 TO 20	20 TO 21	21 TO 22	22 TO 23	23 TO 24	MEAN
DAY																									
1 D	25.3	25.4	26.2	26.4	27.1	25.5	26.7	28.0	28.0	27.2	27.5	32.5	33.3	31.6	32.0	34.3	37.7	31.4	31.6	25.7	20.5	22.1	25.0	22.7	28.1
2	24.1	26.1	27.0	26.4	27.0	27.3	27.1	27.5	28.0	28.3	29.1	31.1	28.8	29.0	32.6	35.0	34.5	30.2	28.5	31.1	28.4	23.3	22.0	20.0	28.0
3	20.5	24.4	24.2	25.3	26.8	27.2	28.5	28.8	27.4	28.3	28.2	28.6	28.2	30.0	32.0	35.7	37.6	36.9	34.5	32.8	27.6	25.5	23.4	22.9	28.6
4	23.0	24.5	26.6	30.4	28.3	27.2	28.2	27.9	26.7	27.6	29.8	26.0	25.9	28.3	31.6	33.0	35.1	36.7	35.5	32.2	28.8	25.7	23.6	22.9	28.6
5	23.3	24.8	26.1	27.2	27.5	28.9	27.7	31.6	31.0	31.1	30.7	29.6	29.7	29.6	30.4	31.6	34.5	33.6	31.8	30.9	28.1	25.8	24.3	22.5	28.8
6	22.7	23.9	24.8	24.9	24.9	27.0	26.8	27.9	30.6	28.6	27.8	28.1	28.5	28.9	30.9	32.8	34.2	35.8	34.0	30.2	25.2	23.4	21.9	19.8	27.6
7	20.5	22.7	22.3	26.0	26.4	28.0	32.7	29.5	31.8	29.4	28.0	27.9	27.2	29.4	30.4	32.6	32.2	31.3	29.0	26.2	24.5	24.1	23.4	21.8	27.4
8	23.0	23.4	24.8	27.2	27.4	27.5	27.4	28.0	28.4	29.2	28.6	28.1	28.5	28.0	28.9	29.9	30.8	31.7	31.6	29.9	28.7	26.1	24.3	24.8	27.8
9	24.0	24.7	25.2	26.2	26.6	25.3	28.0	28.4	29.6	32.2	32.8	34.6	32.9	32.9	33.5	32.1	31.5	31.8	29.1	26.0	24.8	24.1	24.8	23.1	28.5
10 Q	25.2	25.1	25.6	26.8	26.7	26.8	27.0	26.3	29.9	30.3	28.8	31.6	30.6	30.3	31.7	32.6	34.3	30.0	28.6	27.4	26.2	24.5	23.1	22.0	28.0
11	22.7	24.7	25.0	25.9	25.1	26.0	25.2	27.6	31.4	32.2	32.4	30.9	31.8	33.1	33.3	33.2	33.7	32.5	29.1	26.8	26.2	25.7	25.7	25.0	28.5
12	24.7	24.5	25.6	26.4	27.0	26.8	26.8	27.2	26.9	28.6	27.9	27.5	28.7	29.8	31.2	32.4	33.5	34.0	30.3	28.9	27.6	27.4	23.9	24.4	28.0
13 D	20.2	21.2	22.5	24.2	24.8	25.0	28.7	25.9	25.0	26.0	27.8	28.7	29.4	30.4	35.1	37.5	38.0	36.6	26.7	25.0	25.6	24.4	23.7	23.9	27.3
14	22.5	22.2	27.3	26.3	26.8	26.9	27.1	27.4	27.6	27.8	28.7	28.0	27.9	31.2	32.8	34.5	35.1	34.9	32.7	28.6	26.5	24.1	21.5	20.2	27.9
15	21.2	22.6	25.1	27.5	30.6	29.4	26.6	28.4	29.0	28.9	28.8	28.4	33.1	33.3	34.6	35.6	36.3	34.8	31.0	27.9	25.6	24.3	23.3	23.1	28.7
16	22.7	23.2	24.8	25.0	25.1	26.0	25.0	26.7	29.6	28.1	28.9	27.8	25.3	31.9	34.2	35.4	36.1	36.4	30.6	27.9	26.2	21.6	21.0	18.7	27.4
17 D	20.3	20.6	21.3	25.9	26.6	27.2	21.1	29.6	31.8	27.2	24.0	27.9	32.3	31.7	32.5	31.3	31.6	32.4	28.9	23.6	22.9	21.9	21.1	21.2	26.5
18	21.5	21.4	26.1	28.1	26.6	31.5	28.2	30.6	28.3	27.6	27.3	26.1	25.4	27.2	30.3	31.8	33.2	34.0	31.5	28.8	25.5	23.0	21.3	20.8	27.3
19 Q	22.1	25.0	25.9	26.6	26.9	27.1	27.2	27.2	27.3	27.4	27.2	28.0	27.8	28.4	31.1	34.4	36.0	35.2	32.3	28.7	25.8	23.3	21.6	20.8	27.6
20	21.0	23.8	24.9	26.3	26.8	27.0	28.7	28.1	27.9	27.9	28.2	28.0	28.6	30.1	31.7	34.2	36.9	37.1	34.4	31.9	28.2	25.1	23.4	23.4	28.5
21 Q	23.6	24.4	26.0	26.7	27.7	27.5	27.7	27.6	27.7	27.4	27.6	27.5	28.3	29.1	30.4	32.6	34.9	35.3	33.4	29.5	26.4	23.3	21.9	20.9	27.8
22	20.3	21.6	23.0	24.1	23.9	24.0	24.9	28.5	28.8	29.1	27.0	25.2	29.9	30.0	31.6	33.5	35.4	36.3	35.3	31.8	28.1	24.7	23.1	22.3	27.6
23 Q	23.0	24.9	26.2	26.4	27.5	27.5	28.4	27.6	27.3	27.1	27.6	27.0	26.1	27.4	30.1	32.5	34.6	35.0	31.8	30.0	27.0	24.0	22.2	21.0	27.6
24	21.9	23.3	25.3	27.0	26.9	26.9	29.6	27.3	27.0	27.2	27.5	28.0	28.6	29.8	30.8	32.4	33.8	34.7	32.6	30.1	27.1	25.5	24.7	23.9	28.0
25	22.9	26.3	25.6	26.8	26.4	27.7	30.4	28.9	27.0	26.8	26.9	27.0	27.5	28.4	29.8	31.8	33.0	33.5	30.4	26.4	24.2	23.8	23.3	23.6	27.4
26 Q	24.2	26.2	28.5	27.0	26.3	27.0	27.2	27.3	27.1	27.1	27.3	28.0	27.9	30.9	32.0	33.7	34.2	33.8	32.4	27.9	25.2	24.0	23.0	22.2	27.9
27	23.7	25.0	28.2	29.2	29.5	28.2	28.9	28.8	28.0	27.4	28.3	30.7	28.8	29.7	30.2	33.2	33.5	33.3	31.0	27.0	24.7	22.6	21.8	22.1	28.1
28 D	23.2	24.0	24.7	24.9	24.0	28.5	26.0	40.3	25.1	34.2	37.3	36.5	39.0	36.9	33.9	33.4	36.0	33.1	28.6	26.6	25.6	25.4	26.0	24.7	29.9
29	26.4	25.5	26.2	26.3	26.0	26.6	27.6	27.1	27.7	28.4	28.6	29.5	30.1	32.2	33.7	35.0	33.7	32.5	30.6	27.6	24.5	23.3	22.2	21.5	28.0
30 D	22.6	22.6	26.2	26.3	28.5	27.6	31.0	29.2	27.5	25.6	28.0	28.7	29.2	23.4	26.0	27.6	30.2	29.3	27.7	23.4	21.2	21.1	21.7	22.0	26.1
MEAN	22.7	23.9	25.4	26.5	26.7	27.2	27.5	28.5	28.3	28.5	28.6	28.9	29.3	30.1	31.6	33.2	34.4	33.8	31.2	28.4	25.9	24.1	23.1	22.3	27.9

VERTICAL INTENSITY

MEAN VALUES FOR PERIODS OF SIXTY MINUTES, UNIVERSAL TIME

TABLE 12 VICTORIA   Z = 53,000 GAMMA +   APRIL 1969

HOUR =	00 TO 01	01 TO 02	02 TO 03	03 TO 04	04 TO 05	05 TO 06	06 TO 07	07 TO 08	08 TO 09	09 TO 10	10 TO 11	11 TO 12	12 TO 13	13 TO 14	14 TO 15	15 TO 16	16 TO 17	17 TO 18	18 TO 19	19 TO 20	20 TO 21	21 TO 22	22 TO 23	23 TO 24	MEAN
DAY																									
1 D	141	139	137	142	143	145	151	152	149	136	114	123	123	134	140	143	135	117	109	119	131	137	151	139	135
2	145	143	143	143	142	142	142	141	141	139	136	133	132	128	131	138	134	129	128	127	125	136	144	156	137
3	171	193	174	166	158	153	150	148	143	144	144	143	136	137	140	141	137	133	130	133	134	137	138	143	147
4	149	154	156	156	150	152	150	146	139	123	120	117	109	115	134	138	138	134	130	129	131	131	131	134	136
5	139	140	144	144	142	144	135	124	139	138	137	139	137	137	137	138	140	135	131	127	124	124	128	130	136
6	139	142	146	146	145	146	143	143	138	138	138	137	135	135	132	131	131	122	118	119	120	123	123	132	134
7	152	158	159	168	164	160	163	149	147	147	143	140	127	115	118	129	129	120	116	126	137	140	140	143	141
8	148	152	152	151	147	144	143	143	143	143	134	137	137	134	130	130	126	125	121	122	124	127	131	130	136
9	135	135	141	144	142	147	152	150	147	137	123	120	120	119	114	104	97	97	100	107	122	131	129	134	127
10 Q	134	137	138	140	138	137	140	133	136	138	133	126	131	134	133	136	137	128	124	122	118	120	124	128	132
11	136	137	142	142	142	140	142	145	139	135	137	133	123	130	137	134	131	122	119	120	127	134	133	132	134
12	135	137	140	139	137	137	137	137	138	136	137	135	135	136	139	138	141	136	130	128	129	129	127	133	135
13 D	144	158	162	154	148	153	155	153	149	147	140	133	124	116	106	104	101	102	103	109	120	139	159	172	135
14	178	199	182	157	148	150	145	143	143	141	139	134	127	134	140	141	136	129	123	124	128	138	143	140	144
15	151	150	150	155	158	152	148	148	125	119	121	112	102	127	134	141	140	128	119	119	126	129	127	129	134
16	132	139	142	145	148	155	141	125	138	140	136	126	113	122	128	129	127	119	113	110	111	126	137	140	131
17 D	148	166	164	156	150	153	131	131	132	134	119	111	107	99	96	99	99	101	105	110	123	132	139	147	127
18	163	166	180	166	155	151	129	130	138	140	137	135	125	126	131	132	133	130	128	121	120	123	126	129	138
19 Q	140	144	150	143	141	139	139	138	137	138	137	137	136	131	131	136	132	125	119	119	120	126	127	123	134
20	137	138	143	139	138	139	139	139	139	138	137	136	134	131	132	133	132	124	115	103	105	110	114	120	130
21 Q	127	135	134	136	137	135	135	134	135	133	133	132	132	132	131	132	128	122	116	115	107	104	109	115	127
22	126	130	131	128	127	126	128	132	134	131	131	123	120	129	130	130	125	119	117	110	102	102	110	118	123
23 Q	124	130	131	131	131	131	131	131	129	132	130	131	130	123	124	124	122	111	108	111	116	116	115	119	124
24	125	134	138	138	137	135	132	134	133	131	131	130	133	132	132	132	130	125	115	108	107	111	112	117	127
25	137	137	139	137	132	132	131	127	129	131	132	131	126	126	129	132	131	127	116	114	118	123	130	136	129
26 Q	138	140	139	136	131	129	129	130	130	129	130	127	130	132	131	133	134	128	125	121	123	120	119	123	129
27	134	143	145	139	137	137	138	136	135	132	122	113	126	130	126	121	123	114	113	111	108	110	113	120	126
28 D	129	129	131	133	132	139	125	115	-5	88	50	91	97	56	86	136	145	139	135	138	138	139	142	140	115
29	141	140	140	138	136	135	137	138	136	134	134	135	137	136	138	131	124	115	110	112	119	124	133	143	132
30 D	148	153	164	165	170	151	136	144	137	105	110	120	117	101	95	102	114	121	122	123	129	132	140	140	131
MEAN	142	147	148	146	144	143	140	138	133	133	129	128	125	125	127	130	128	123	119	119	121	126	130	134	132

HORIZONTAL INTENSITY

MEAN VALUES FOR PERIODS OF SIXTY MINUTES, UNIVERSAL TIME

TABLE 13 VICTORIA H = 18,500 GAMMA + MAY 1969

HOUR =	00 TO 01	01 TO 02	02 TO 03	03 TO 04	04 TO 05	05 TO 06	06 TO 07	07 TO 08	08 TO 09	09 TO 10	10 TO 11	11 TO 12	12 TO 13	13 TO 14	14 TO 15	15 TO 16	16 TO 17	17 TO 18	18 TO 19	19 TO 20	20 TO 21	21 TO 22	22 TO 23	23 TO 24	MEAN
DAY																									
1	431	424	425	420	431	414	419	431	427	420	417	418	423	420	419	413	402	387	391	393	406	410	410	420	415
2 D	421	429	420	409	422	414	420	430	426	434	426	429	426	426	426	427	403	422	370	398	396	400	406	420	417
3	422	426	426	424	422	434	410	416	422	416	422	422	418	427	414	404	400	390	389	390	390	390	406	406	412
4	428	434	428	433	420	428	424	428	428	425	429	426	424	427	425	422	411	406	396	402	401	403	399	415	419
5	423	426	429	432	424	430	431	435	432	428	430	436	428	431	440	431	418	405	398	394	389	403	403	406	421
6	413	424	431	435	429	445	431	424	426	430	428	428	428	431	432	427	417	405	398	402	407	411	407	414	422
7 Q	431	427	428	422	418	421	429	428	431	434	429	432	433	437	435	436	433	432	427	427	423	421	417	416	428
8	452	428	431	431	427	430	428	425	434	434	436	441	444	451	449	450	445	430	433	433	435	432	431	416	435
9	428	437	438	434	422	419	423	433	429	423	431	435	434	441	438	432	432	422	410	406	408	428	415	426	427
10	429	421	427	415	410	416	426	440	439	440	445	437	431	436	437	433	423	409	409	407	408	406	404	417	424
11 Q	440	435	433	430	440	440	442	443	441	451	447	449	449	458	454	449	437	432	432	425	416	419	420	430	438
12	424	431	426	429	431	435	437	438	437	445	444	445	449	453	452	446	441	438	439	424	429	428	429	430	437
13 D	440	450	410	426	419	418	409	377	400	417	402	394	405	406	400	395	371	359	397	392	397	405	426	441	407
14 D	439	443	410	387	411	424	404	408	417	426	423	421	422	416	397	389	394	409	405	372	337	406	458	441	411
15 D	427	405	502	444	379	367	358	368	369	330	398	351	322	350	322	295	276	268	302	308	308	354	414	439	361
16 D	457	440	434	421	394	370	377	379	404	408	401	403	404	425	418	410	404	399	394	387	395	398	400	408	405
17	410	401	403	403	393	395	391	410	415	414	422	424	422	422	415	408	392	383	373	376	390	401	395	402	403
18	454	426	420	412	410	420	438	412	420	420	415	423	428	429	421	426	414	403	399	392	393	404	411	411	417
19	427	424	430	427	420	427	432	432	432	436	437	438	439	437	438	442	433	425	417	403	393	403	415	426	426
20	432	435	436	425	426	431	430	431	427	428	433	441	441	438	447	452	449	437	422	428	422	411	412	422	432
21	424	432	430	413	408	410	406	418	419	435	419	404	415	429	427	443	443	423	411	401	396	394	408	424	418
22	439	433	434	429	430	428	432	429	436	441	439	424	426	432	423	429	441	439	421	412	411	409	415	427	428
23	438	437	428	423	427	430	430	430	429	434	431	430	425	434	435	427	419	408	414	419	417	417	424	432	427
24	449	445	445	443	451	438	422	431	431	438	438	440	443	433	430	440	431	420	418	421	420	427	444	451	435
25	455	442	427	418	423	427	429	432	435	440	438	441	443	445	439	431	418	401	403	411	417	417	420	425	428
26 Q	433	431	427	431	430	433	435	437	440	444	444	445	444	447	444	438	427	418	413	418	420	423	433	435	433
27 Q	441	440	441	442	438	439	439	440	440	439	439	434	441	442	444	447	439	432	424	420	430	438	446	442	438
28	443	442	442	444	439	446	439	436	425	427	420	432	435	436	432	427	419	408	402	403	406	406	415	409	426
29 Q	423	429	433	432	429	429	432	431	435	431	429	431	430	430	432	423	418	418	414	421	420	413	429	428	427
30	426	433	432	433	433	426	425	434	436	427	430	436	431	430	427	410	392	410	399	398	396	403	413	413	421
31	436	428	420	430	427	423	416	426	417	416	423	429	430	420	419	420	407	410	411	405	403	404	417	429	419
MEAN	433	431	431	426	422	423	421	424	426	427	428	427	427	430	427	423	414	408	404	403	403	409	417	423	421

DECLINATION

MEAN VALUES FOR PERIODS OF SIXTY MINUTES, UNIVERSAL TIME

TABLE 14 VICTORIA D = 22 DEG 00.0 MIN EAST + MAY 1969

HOUR =	00 TO 01	01 TO 02	02 TO 03	03 TO 04	04 TO 05	05 TO C6	06 TO 07	07 TO 08	08 TO 09	09 TO 10	10 TO 11	11 TO 12	12 TO 13	13 TO 14	14 TO 15	15 TO 16	16 TO 17	17 TO 18	18 TO 19	19 TO 20	20 TO 21	21 TO 22	22 TO 23	23 TO 24	MEAN
DAY																									
1	23.0	26.3	27.1	27.2	31.3	28.4	27.7	27.2	28.1	29.6	28.9	29.1	29.3	30.0	32.1	32.8	33.7	34.6	30.0	25.6	24.7	22.9	23.2	23.5	28.2
2 D	23.4	23.3	24.0	26.9	27.6	27.4	27.6	26.7	26.0	26.4	30.7	29.1	29.5	28.4	30.2	25.3	27.6	30.9	33.5	22.2	21.6	21.1	21.8	22.9	26.4
3	24.7	26.9	27.3	27.8	30.9	39.7	33.5	26.7	28.9	30.9	29.1	30.7	30.9	29.3	30.4	32.2	33.8	32.2	29.3	25.8	24.0	23.3	21.4	21.4	28.8
4	23.7	24.7	26.3	27.3	30.6	26.8	26.3	26.7	28.1	27.5	27.6	28.6	28.9	30.6	30.9	31.5	33.9	32.8	29.4	27.3	26.2	25.3	23.5	21.1	27.7
5	21.9	23.8	25.2	26.6	26.6	26.7	26.8	27.3	27.5	26.9	26.5	25.8	25.4	26.3	31.4	35.5	36.3	34.4	29.2	25.5	22.4	21.6	21.0	21.4	26.7
6	22.6	23.4	25.4	26.8	28.3	28.2	32.1	29.7	27.1	27.0	27.1	27.4	28.3	29.9	31.4	34.2	33.9	33.7	31.2	28.0	25.8	23.1	22.1	21.6	27.8
7 Q	21.7	22.4	23.9	24.9	26.3	26.8	27.1	27.7	24.5	28.5	28.4	28.0	28.8	30.1	31.0	32.6	32.5	32.9	30.9	29.3	27.2	25.6	24.4	23.4	27.5
8	23.5	23.4	24.7	25.5	25.8	26.3	26.7	27.2	26.9	27.4	28.0	27.9	29.2	29.7	29.9	33.6	33.1	32.7	29.2	26.8	25.5	25.2	24.1	24.8	27.4
9	24.4	24.3	25.5	27.3	29.1	27.6	28.1	28.6	34.6	31.0	29.4	28.1	29.1	30.6	31.4	33.0	34.0	34.4	31.9	29.0	26.0	24.4	23.5	22.4	28.7
10	22.0	22.5	24.1	26.9	28.5	28.0	28.3	27.8	28.0	28.7	27.6	25.8	28.3	29.8	31.6	33.1	34.0	32.9	28.5	26.1	24.0	23.8	24.0	23.1	27.4
11 Q	23.5	25.3	26.1	26.2	27.4	27.4	27.4	28.0	29.0	30.0	28.6	28.0	28.9	30.2	31.1	33.2	34.0	35.0	31.7	29.0	26.3	24.1	21.8	21.4	28.1
12	22.8	24.7	26.2	26.7	26.2	26.3	27.2	27.6	28.1	28.1	27.7	27.3	28.2	30.4	32.4	34.1	35.2	35.3	32.9	30.4	26.4	26.5	23.9	21.1	28.2
13 D	20.7	19.2	23.8	24.6	29.2	28.0	29.1	29.2	34.3	32.1	34.7	33.6	26.1	36.7	37.5	36.5	35.3	32.8	27.9	24.5	23.4	21.9	20.2	22.9	28.5
14 D	20.7	28.1	26.1	26.1	30.7	31.9	28.1	26.8	28.7	27.1	25.5	27.7	29.0	30.8	31.7	30.4	30.0	30.7	28.1	30.9	22.2	19.0	12.6	12.2	26.5
15 D	12.9	13.6	13.9	32.6	25.8	25.9	25.1	27.7	29.9	43.7	29.3	32.1	24.3	24.8	32.4	33.0	22.4	27.2	23.9	25.5	22.7	23.4	23.3	23.5	25.8
16 D	31.4	25.6	30.7	35.5	34.9	31.8	31.9	21.1	28.9	28.4	25.3	27.8	26.6	29.8	32.2	34.5	34.1	34.8	31.9	27.8	25.9	24.4	22.9	22.8	29.2
17	24.0	25.5	27.8	27.1	28.2	30.0	25.2	28.6	30.6	31.0	27.8	28.1	27.8	30.6	33.5	34.4	33.8	33.2	30.0	25.8	22.8	20.7	19.5	19.7	27.7
18	19.0	23.4	25.2	24.8	25.0	26.1	25.0	28.6	27.2	31.0	31.2	29.5	29.4	31.8	35.0	37.8	36.5	37.4	30.6	26.3	26.1	24.2	21.9	22.0	28.1
19	23.0	24.8	25.8	27.0	27.2	27.1	27.3	27.2	27.5	27.3	26.6	27.0	26.3	29.2	30.1	33.4	34.3	33.9	30.7	28.9	26.2	23.1	21.7	20.8	27.3
20	23.0	25.2	27.8	26.6	26.8	28.9	30.1	28.4	27.8	27.3	26.4	26.6	28.2	30.6	31.6	34.3	34.2	33.7	29.9	25.7	24.8	23.9	23.5	23.3	27.9
21	24.1	25.0	28.3	30.1	29.7	31.7	34.1	30.6	29.7	27.2	30.6	29.6	30.4	31.2	27.9	34.0	35.5	35.7	32.6	30.0	27.4	24.4	21.9	22.3	29.3
22	22.3	23.3	25.0	28.7	27.2	26.2	26.7	27.5	28.0	27.4	28.9	32.4	32.8	33.9	32.9	31.3	33.3	33.3	32.2	28.5	26.4	24.3	22.2	21.9	28.2
23	23.2	24.5	25.8	26.9	26.9	26.4	27.7	31.2	31.6	28.0	30.5	28.0	29.9	33.3	32.0	34.9	35.1	34.3	31.7	29.7	26.4	25.1	23.4	22.6	28.7
24	23.4	24.9	25.5	26.0	26.3	28.9	28.2	27.3	26.9	28.3	27.9	28.0	28.4	28.4	29.1	31.1	33.8	32.1	28.1	25.2	22.1	22.0	20.3	21.4	26.8
25	23.3	26.7	27.8	28.3	25.9	25.7	26.3	26.3	26.4	26.2	26.3	27.1	28.6	31.0	33.1	34.1	33.8	33.0	27.9	24.9	22.9	22.5	22.0	22.4	27.2
26 Q	24.9	26.2	27.3	27.5	26.2	25.7	26.0	26.1	26.5	26.4	26.7	27.8	29.0	31.0	32.7	33.6	33.2	32.0	29.1	26.2	24.8	23.8	22.4	23.0	27.4
27 Q	23.7	24.3	24.8	24.8	25.5	25.7	26.2	26.4	27.1	27.4	28.1	28.8	29.3	30.5	30.7	32.5	33.0	32.1	31.3	29.3	25.8	23.9	22.9	22.4	27.4
28	23.1	23.5	24.5	25.3	26.0	26.7	25.0	26.7	29.0	28.3	30.4	31.5	31.2	32.1	34.9	35.8	31.0	28.4	25.8	25.3	24.4	23.2	22.1	22.2	27.3
29 Q	23.0	24.5	24.9	25.8	26.2	26.5	26.8	26.7	27.6	27.2	28.0	27.0	29.0	31.4	34.0	34.4	34.6	32.9	30.2	26.2	24.6	22.6	21.6	21.3	27.4
30	22.7	23.7	24.8	25.0	25.6	25.7	25.8	25.9	28.6	29.5	27.0	25.6	28.0	32.3	34.1	35.6	31.4	28.0	26.8	24.8	23.6	22.1	22.1	22.7	26.7
31	22.2	23.1	25.0	25.0	29.2	34.0	27.7	27.1	30.7	28.9	27.2	27.3	27.2	31.3	33.2	31.2	31.2	29.5	29.3	29.3	26.7	23.8	22.2	21.9	27.7
MEAN	22.8	24.1	25.5	27.0	27.8	28.1	27.8	27.4	28.5	28.9	28.3	28.4	28.6	30.5	32.0	33.4	33.2	32.8	29.9	27.1	24.8	23.4	22.0	21.9	27.7

VERTICAL INTENSITY

MEAN VALUES FOR PERIODS OF SIXTY MINUTES, UNIVERSAL TIME

TABLE 15 VICTORIA

Z = 53,000 GAMMA +

MAY 1969

HOUR =	00 TO 01	01 TO 02	02 TO 03	03 TO 04	04 TO 05	05 TO 06	06 TO 07	07 TO 08	08 TO 09	09 TO 10	10 TO 11	11 TO 12	12 TO 13	13 TO 14	14 TO 15	15 TO 16	16 TO 17	17 TO 18	18 TO 19	19 TO 20	20 TO 21	21 TO 22	22 TO 23	23 TO 24	MEAN
DAY																									
1	145	149	149	149	144	139	139	128	120	121	127	130	131	131	133	131	131	124	114	114	121	123	126	131	131
2 D	134	135	134	137	136	135	137	132	132	119	123	130	128	120	108	110	112	114	106	120	126	132	137	140	127
3	139	142	140	137	138	134	124	121	108	123	122	116	118	123	110	112	115	117	120	122	124	120	130	130	124
4	137	140	136	138	140	136	134	135	134	134	130	128	129	130	131	130	125	123	116	119	124	123	122	126	130
5	138	144	140	138	136	135	135	135	135	134	133	130	118	109	113	118	119	115	106	101	106	113	118	127	125
6	132	137	145	149	144	130	126	130	136	135	135	134	130	129	128	129	125	120	117	119	125	125	120	125	130
7 Q	135	141	149	151	149	148	146	146	135	123	133	136	137	136	135	135	129	122	116	114	115	111	113	120	132
8	128	134	136	140	140	141	143	143	142	142	139	141	140	141	136	134	128	125	124	118	119	123	129	135	134
9	141	144	144	145	145	147	149	147	137	134	137	140	140	143	142	142	138	131	120	113	120	124	123	131	137
10	131	130	126	138	140	136	136	115	109	114	114	112	113	113	110	112	110	108	110	115	118	120	124	127	120
11 Q	142	143	144	141	138	136	136	135	134	127	123	128	133	136	137	138	134	129	119	118	115	113	115	120	131
12	129	140	143	142	138	135	133	132	132	131	130	129	134	137	141	143	138	127	121	117	117	112	118	129	131
13 D	140	167	171	160	174	160	161	127	122	110	87	92	53	77	91	90	96	104	112	120	134	145	163	204	128
14 D	211	245	206	184	171	148	145	139	141	121	106	119	131	137	132	127	118	116	108	103	106	131	148	207	146
15 D	250	226	290	338	306	220	190	187	190	121	31	23	-99	-53	-86	-53	-22	36	84	134	160	197	219	221	130
16 D	264	238	243	211	180	204	132	90	134	110	66	103	86	132	138	146	147	147	142	139	134	128	126	137	149
17	148	160	171	189	195	194	156	135	149	148	142	138	132	133	136	144	143	142	136	134	137	138	142	149	150
18	192	197	182	170	165	160	135	137	145	127	122	136	148	155	153	150	139	132	123	130	136	139	146	147	149
19	163	159	156	151	149	151	152	153	152	152	150	145	131	129	128	134	132	129	122	119	120	127	137	146	141
20	159	159	161	152	148	148	138	143	142	144	145	147	146	146	149	150	146	139	126	129	131	129	131	144	144
21	160	165	170	165	164	160	158	149	147	142	126	111	126	130	110	113	120	117	118	120	124	128	141	151	138
22	156	155	154	150	146	146	144	148	145	134	117	101	105	108	118	122	131	136	132	124	122	121	130	142	133
23	146	153	151	149	147	144	145	142	143	141	134	138	132	137	137	142	140	133	127	126	130	136	137	142	140
24	146	146	145	141	145	148	145	148	142	138	138	140	139	131	124	119	121	118	110	104	111	118	132	148	133
25	164	171	159	151	144	141	141	141	139	137	136	139	141	141	138	137	131	126	125	121	118	123	132	143	139
26 Q	147	149	145	141	137	137	136	135	136	135	134	127	133	136	136	133	128	113	99	95	100	109	116	125	128
27 Q	132	136	135	130	130	128	128	130	128	129	130	130	132	131	128	125	120	112	110	109	107	107	120	121	125
28	133	134	133	133	131	130	131	132	131	132	129	130	132	133	130	127	115	118	108	101	105	113	121	125	125
29 Q	137	140	142	140	135	134	133	134	134	132	131	129	132	131	132	129	124	111	101	97	101	78	109	132	125
30	137	143	141	139	138	137	137	136	129	117	126	129	112	119	126	124	113	109	104	105	107	117	123	130	125
31	142	147	147	148	147	131	133	138	134	130	133	133	121	115	121	126	123	125	123	116	118	127	129	135	131
MEAN	153	157	158	156	153	148	141	137	137	130	124	125	119	123	121	123	122	120	116	117	120	124	132	142	133

HORIZONTAL INTENSITY

MEAN VALUES FOR PERIODS OF SIXTY MINUTES, UNIVERSAL TIME

TABLE 16 VICTORIA H = 18,500 GAMMA + JUNE 1969

HOUR =	00 TO 01	01 TO 02	02 TO 03	03 TO 04	04 TO 05	05 TO 06	06 TO 07	07 TO 08	08 TO 09	09 TO 10	10 TO 11	11 TO 12	12 TO 13	13 TO 14	14 TO 15	15 TO 16	16 TO 17	17 TO 18	18 TO 19	19 TO 20	20 TO 21	21 TO 22	22 TO 23	23 TO 24	MEAN
DAY																									
1	425	430	430	430	420	415	415	423	423	426	426	424	420	423	427	424	414	403	393	401	400	405	408	417	418
2	426	434	437	437	422	415	421	434	425	425	430	434	431	428	425	413	407	399	395	405	410	417	419	418	421
3	423	414	418	420	425	429	430	431	430	433	434	435	434	432	429	422	416	402	407	410	419	432	432	416	424
4	417	419	428	433	417	423	430	439	429	427	432	431	426	424	426	426	415	409	411	410	397	401	408	415	421
5	427	431	434	424	428	431	429	429	438	435	437	433	435	432	433	429	421	415	413	417	415	416	420	427	427
6 Q	433	434	430	429	431	433	436	437	438	440	437	438	440	440	441	432	429	427	416	416	420	420	426	432	431
7	437	430	421	427	434	434	436	439	444	443	440	428	437	438	429	418	413	417	423	420	415	413	419	428	428
8	425	430	430	426	426	450	450	451	457	462	457	457	462	465	459	452	436	420	444	434	418	416	408	413	440
9	423	430	429	440	431	432	435	434	438	439	436	429	421	426	429	413	402	399	415	410	403	397	416	430	423
10	410	425	417	412	416	426	416	417	427	421	415	416	420	423	427	417	394	389	400	403	401	407	416	422	414
11	421	427	419	419	421	427	429	435	440	428	430	433	431	433	438	437	425	413	403	405	410	415	432	410	424
12 D	432	446	458	446	407	422	409	416	421	402	410	412	420	421	417	418	404	398	386	400	409	418	415	418	417
13 D	431	435	435	434	426	423	414	423	425	423	424	422	413	418	421	423	405	380	386	402	415	403	401	432	417
14 D	428	438	425	422	447	444	439	441	424	433	435	438	427	450	427	414	423	426	421	414	411	402	409	404	427
15	419	428	434	430	423	423	425	431	429	434	440	427	424	431	438	438	435	418	419	417	416	420	413	415	426
16 D	419	434	419	422	420	418	422	432	439	430	438	442	445	444	432	439	434	433	428	421	424	425	417	411	429
17 D	426	444	444	433	416	422	430	427	425	434	449	441	440	442	442	437	424	399	385	412	422	415	411	414	426
18 Q	421	422	428	428	426	427	428	428	431	429	432	433	437	442	440	437	421	413	426	423	417	416	423	426	427
19	426	433	429	432	430	430	432	437	438	437	425	434	438	442	449	447	448	438	422	406	402	412	414	416	430
20	439	440	425	428	426	436	413	425	438	423	425	427	430	440	447	448	440	429	422	413	407	414	428	433	429
21	439	440	437	432	432	431	430	425	429	431	431	428	432	432	436	436	434	431	426	424	412	412	420	428	430
22 Q	431	433	434	432	431	430	431	432	432	432	437	434	439	447	447	442	432	418	412	413	413	417	423	436	430
23	445	444	438	439	439	439	434	435	437	438	435	439	442	441	442	436	439	444	438	433	433	428	425	426	437
24	425	431	441	439	426	434	429	427	422	420	423	425	426	422	415	420	411	416	424	433	425	424	422	427	425
25	437	437	432	424	426	437	435	430	433	435	433	429	427	426	425	423	407	404	424	416	415	413	422	427	426
26	438	422	422	434	431	434	436	433	436	435	435	432	425	423	428	423	419	410	402	408	410	413	418	422	425
27	420	426	431	425	422	430	433	431	430	433	432	426	426	431	430	425	425	418	416	417	419	414	415	418	425
28 Q	430	431	428	432	434	432	437	435	438	440	441	439	438	439	437	436	432	429	427	428	424	415	410	424	432
29 Q	433	438	433	443	433	435	438	439	440	437	433	433	435	441	442	436	420	401	403	406	411	424	432	437	430
30	435	432	433	435	433	436	440	438	437	439	439	442	448	454	447	444	436	422	425	434	434	433	438	447	438
MEAN	428	432	431	430	427	430	429	432	433	432	433	432	432	435	434	430	422	414	414	415	414	415	419	423	427

DECLINATION

MEAN VALUES FOR PERIODS OF SIXTY MINUTES, UNIVERSAL TIME

TABLE 17 VICTORIA — D = 22 DEG 00.0 MIN EAST + — JUNE 1969

HOUR =	00 TO 01	01 TO 02	02 TO 03	03 TO 04	04 TO 05	05 TO 06	06 TO 07	07 TO 08	08 TO 09	09 TO 10	10 TO 11	11 TO 12	12 TO 13	13 TO 14	14 TO 15	15 TO 16	16 TO 17	17 TO 18	18 TO 19	19 TO 20	20 TO 21	21 TO 22	22 TO 23	23 TO 24	MEAN
DAY																									
1	22.9	23.7	26.6	27.0	25.9	27.0	27.1	26.5	26.5	27.1	27.2	27.4	27.6	28.1	30.9	32.8	33.0	32.5	29.0	27.5	25.6	24.6	23.9	22.6	27.2
2	24.8	25.6	25.7	26.6	28.9	26.7	26.1	27.1	27.5	27.5	27.0	27.2	28.7	31.9	33.1	35.1	34.4	34.2	30.3	25.4	22.1	20.5	21.5	22.3	27.5
3	21.5	23.0	24.1	25.7	24.5	26.5	25.3	25.4	25.5	26.4	26.1	26.6	28.4	28.8	30.4	31.4	31.8	31.5	28.0	26.3	23.2	21.8	19.1	20.3	25.9
4	21.5	23.7	25.7	27.0	24.8	25.4	25.1	28.2	28.5	25.7	26.2	27.2	29.9	31.6	33.9	35.6	32.8	35.1	30.1	28.4	25.3	23.9	22.8	21.8	27.5
5	22.6	24.0	26.5	27.5	26.0	26.5	26.3	25.5	25.4	26.7	26.3	27.1	29.1	30.9	33.4	34.6	34.5	33.4	30.8	27.2	24.8	22.7	22.4	22.1	27.3
6 Q	23.5	25.2	26.7	27.3	27.3	27.2	26.8	26.1	26.1	26.3	26.9	27.6	29.7	32.2	34.3	36.3	37.3	32.4	29.3	26.0	22.2	20.7	19.5	19.7	27.4
7	21.6	23.9	25.2	24.0	24.8	25.1	25.7	25.8	25.7	25.4	27.1	29.5	24.8	32.1	34.9	37.0	35.6	33.6	29.0	26.1	24.5	23.1	21.9	21.6	27.0
8	23.8	25.0	27.0	27.5	27.7	25.8	25.6	27.1	26.9	26.5	28.0	27.7	31.1	33.3	36.1	38.6	38.2	34.7	27.4	28.5	24.0	20.4	20.0	20.3	28.0
9	22.0	22.5	24.7	27.1	25.9	25.7	24.8	25.5	25.8	25.6	25.8	28.1	27.7	30.8	35.0	35.2	33.2	30.6	25.2	22.0	20.8	19.3	19.0	20.6	26.0
10	23.9	24.7	26.7	26.0	25.8	24.7	28.1	26.3	27.9	28.1	26.7	26.6	26.2	30.4	33.4	34.8	36.5	34.5	31.4	27.4	23.2	21.4	21.5	21.1	27.4
11	22.8	25.4	27.4	26.7	25.7	28.0	27.4	26.2	27.1	30.0	27.6	27.8	28.9	30.3	31.6	33.1	34.5	34.9	31.5	27.0	24.2	22.2	20.1	21.0	27.6
12 D	20.5	21.8	20.3	22.3	27.8	34.6	28.2	26.2	29.1	27.4	25.3	21.1	24.7	27.0	29.5	31.1	31.8	30.2	27.4	20.7	20.2	20.3	21.8	22.9	25.5
13 D	23.4	23.7	24.0	24.0	33.5	31.9	26.6	25.3	25.3	25.9	26.9	28.6	27.6	29.1	33.3	34.3	35.3	33.3	28.3	23.6	23.1	21.3	18.7	18.2	26.9
14 D	19.5	20.1	23.7	27.8	28.2	26.3	26.7	28.1	28.2	25.4	25.0	26.0	22.8	33.9	36.8	36.2	38.5	34.7	32.2	30.0	26.6	24.1	22.5	22.5	27.7
15	23.2	24.2	25.8	27.7	27.6	26.1	25.8	26.3	29.3	26.8	25.0	24.9	26.4	30.5	34.2	35.6	35.7	35.0	31.6	26.3	24.3	23.4	23.5	23.6	27.6
16 D	24.7	25.6	27.2	27.5	26.8	29.2	31.7	28.4	31.1	34.1	27.1	26.0	27.7	30.7	31.9	34.0	35.6	33.5	31.6	28.1	24.8	23.4	22.4	21.8	28.5
17 D	22.0	24.2	30.5	28.6	25.2	25.2	30.8	33.8	26.0	24.7	26.8	26.6	29.3	31.6	33.6	34.3	38.1	37.8	30.9	25.7	25.5	25.3	24.0	23.6	28.5
18 Q	25.1	25.3	26.2	26.7	26.7	26.2	26.4	27.1	26.9	26.9	26.9	27.6	28.6	29.2	30.7	32.7	33.1	31.6	27.1	25.0	24.5	23.3	22.3	22.1	27.0
19	24.1	25.0	26.3	27.1	26.1	26.3	26.3	26.5	28.2	29.0	28.9	27.7	29.3	30.1	31.3	31.6	32.4	32.0	30.4	26.5	23.9	21.5	21.4	21.6	27.2
20	22.9	26.0	27.5	28.2	31.6	31.0	28.8	26.7	30.5	27.7	28.9	27.7	28.9	30.0	33.7	35.5	36.2	33.7	28.0	25.1	22.7	21.3	20.5	21.2	28.1
21	24.1	25.7	26.7	26.9	27.2	28.4	30.6	27.9	26.4	25.3	27.6	28.8	30.2	30.0	32.3	35.9	35.8	33.2	30.8	27.9	26.3	24.1	22.1	22.3	28.2
22 Q	24.5	26.0	27.5	28.0	27.0	26.7	26.5	26.2	26.4	26.4	26.4	27.5	29.2	30.1	30.7	33.0	33.2	32.3	30.9	27.4	25.2	24.1	23.1	22.8	27.5
23	23.6	24.7	25.7	25.6	25.5	25.4	25.8	26.4	26.1	26.6	27.7	28.7	28.4	30.1	31.7	32.8	32.5	30.6	28.8	26.7	25.5	23.2	22.1	22.3	26.9
24	23.4	23.5	26.9	28.8	26.7	29.3	29.0	27.9	28.8	27.3	26.7	26.1	27.8	29.8	31.1	30.4	32.5	30.1	28.6	25.2	24.7	22.8	21.6	21.7	27.1
25	23.6	24.3	25.9	26.2	26.2	26.3	27.1	27.1	26.0	27.2	27.7	27.6	29.1	26.4	30.3	33.3	34.4	30.5	25.2	23.6	22.2	20.5	20.0	19.3	26.2
26	19.7	22.4	24.9	25.4	26.4	26.8	26.2	26.3	26.6	26.1	27.4	25.5	27.0	28.4	29.2	30.3	30.6	31.7	29.5	26.4	24.0	23.1	22.5	21.5	26.2
27	22.4	23.2	25.3	27.2	26.5	25.9	27.1	26.8	26.6	26.6	26.4	27.5	27.9	30.3	31.7	31.9	31.3	31.0	28.3	25.7	23.8	23.3	22.1	21.9	26.7
28 Q	23.1	23.8	24.8	25.9	26.3	26.4	26.9	26.6	26.8	26.9	26.5	26.7	27.9	29.4	31.0	32.6	34.0	32.1	29.8	25.8	23.5	21.3	20.8	20.9	26.7
29 Q	22.2	23.7	25.6	26.5	26.2	26.2	25.7	26.4	26.9	27.2	27.6	27.9	30.1	30.9	31.6	33.5	35.2	33.0	29.0	25.4	22.9	21.3	20.7	21.2	27.0
30	23.8	25.9	26.8	26.3	25.7	25.7	26.7	26.8	26.7	26.1	26.5	27.5	28.9	29.6	32.1	33.4	34.4	33.2	27.4	22.7	19.7	18.4	18.7	19.0	26.3
MEAN	22.9	24.2	25.9	26.6	26.8	27.1	27.0	26.9	27.2	27.0	26.9	27.1	28.1	30.2	32.5	33.9	34.4	32.9	29.3	26.0	23.8	22.2	21.4	21.5	27.2

VERTICAL INTENSITY

MEAN VALUES FOR PERIODS OF SIXTY MINUTES, UNIVERSAL TIME

TABLE 18 VICTORIA   Z = 53,000 GAMMA +   JUNE 1969

HOUR =	00 TO 01	01 TO 02	02 TO 03	03 TO 04	04 TO 05	05 TO 06	06 TO 07	07 TO 08	08 TO 09	09 TO 10	10 TO 11	11 TO 12	12 TO 13	13 TO 14	14 TO 15	15 TO 16	16 TO 17	17 TO 18	18 TO 19	19 TO 20	20 TO 21	21 TO 22	22 TO 23	23 TO 24	MEAN
DAY																									
1	136	143	145	147	140	140	140	139	136	135	133	131	134	130	131	134	131	124	113	111	120	128	128	126	132
2	137	140	139	141	140	139	139	123	121	129	131	131	126	126	129	130	123	113	104	103	103	106	108	118	125
3	128	137	143	138	131	138	132	132	131	133	133	133	133	129	129	127	119	120	114	114	102	107	108	123	126
4	133	139	145	145	133	136	135	133	123	130	133	131	127	122	128	130	118	99	83	83	91	104	116	125	123
5	133	138	147	139	131	130	131	129	130	131	131	128	134	130	128	128	125	120	115	114	119	118	116	125	128
6 Q	135	137	135	133	131	128	130	129	128	129	130	132	134	134	130	122	116	111	100	97	106	113	122	131	125
7	141	144	143	136	137	136	138	135	132	131	129	126	114	111	116	115	113	107	103	104	108	112	119	129	124
8	143	150	155	148	139	142	146	144	142	139	137	136	141	142	140	135	115	97	97	91	98	108	119	134	131
9	140	151	148	151	140	136	131	131	130	131	129	129	128	122	125	123	118	103	99	97	116	129	147	166	130
10	162	166	166	158	144	142	142	142	132	128	124	133	136	136	143	145	134	118	115	118	120	117	117	129	136
11	141	148	147	140	135	137	138	136	128	125	132	134	136	136	137	140	136	131	123	120	116	118	132	130	133
12 D	137	136	165	184	190	171	143	145	127	121	127	125	127	134	133	127	124	111	103	111	117	126	130	134	135
13 D	143	150	157	162	174	156	152	150	145	142	141	142	136	125	119	115	110	105	90	89	98	113	128	146	133
14 D	148	150	148	148	149	142	146	143	120	137	139	141	129	95	112	122	123	115	105	105	107	114	131	137	129
15	142	146	153	149	146	140	137	138	136	137	136	125	110	116	116	124	127	122	110	97	112	121	120	127	129
16 D	136	150	154	152	152	151	150	144	133	112	126	132	136	134	125	116	114	103	95	98	94	100	108	127	127
17 D	145	167	191	177	150	143	141	133	134	135	125	125	137	139	140	133	126	112	97	94	104	107	111	118	133
18 Q	133	140	141	136	132	131	132	132	133	135	137	135	136	136	136	136	131	121	115	105	103	104	115	126	128
19	134	138	137	135	132	131	132	133	132	128	130	134	136	135	130	126	125	119	108	103	101	106	114	128	126
20	138	149	146	144	144	140	134	139	125	107	118	125	130	135	134	131	126	120	111	111	117	122	128	133	129
21	143	147	144	135	132	133	134	132	134	130	124	124	129	126	124	125	124	120	116	118	121	122	126	136	129
22 Q	137	140	140	132	131	127	129	128	129	129	130	131	135	133	133	131	116	110	112	109	108	115	119	128	126
23	138	138	134	133	129	128	125	127	129	123	126	128	130	128	130	122	120	118	119	110	111	115	128	139	126
24	144	147	152	152	139	139	127	132	131	128	132	133	123	129	130	126	122	119	114	112	116	116	122	131	130
25	144	144	142	136	130	131	133	131	130	127	128	127	128	120	115	110	104	100	99	98	104	107	117	124	122
26	136	144	142	139	134	133	131	128	128	125	124	119	114	115	107	102	100	102	96	98	97	99	104	115	118
27	125	131	143	143	137	133	131	130	129	127	125	121	121	125	130	130	130	122	120	118	119	118	121	126	127
28 Q	134	137	137	133	133	131	131	129	128	126	123	123	125	127	128	125	119	117	112	108	105	97	100	111	122
29 Q	123	131	130	133	130	128	127	127	126	123	122	124	124	125	128	129	126	112	97	96	96	96	110	118	120
30	126	130	134	131	127	126	127	128	125	126	125	127	128	129	128	124	113	102	97	95	95	106	115	116	120
MEAN	138	144	147	144	140	137	135	134	130	129	129	130	129	127	128	126	121	113	106	104	107	112	119	129	127

HORIZONTAL INTENSITY

MEAN VALUES FOR PERIODS OF SIXTY MINUTES, UNIVERSAL TIME

TABLE 19 VICTORIA H = 18,500 GAMMA + JULY 1969

HOUR =	00 TO 01	01 TO 02	02 TO 03	03 TO 04	04 TO 05	05 TO 06	06 TO 07	07 TO 08	08 TO 09	09 TO 10	10 TO 11	11 TO 12	12 TO 13	13 TO 14	14 TO 15	15 TO 16	16 TO 17	17 TO 18	18 TO 19	19 TO 20	20 TO 21	21 TO 22	22 TO 23	23 TO 24	MEAN
DAY																									
1 D	458	459	444	446	454	452	455	437	416	431	437	434	434	442	453	450	436	414	399	401	407	418	422	422	434
2	438	441	432	424	429	434	434	437	435	438	433	432	436	440	444	437	429	410	394	389	394	408	430	437	427
3	441	440	435	435	436	436	436	437	440	440	440	442	445	447	447	437	423	415	411	411	417	422	427	429	433
4 Q	428	430	435	439	441	442	442	441	440	442	442	442	445	448	448	448	444	431	413	402	411	422	429	442	435
5 Q	445	447	443	442	442	444	440	442	441	441	440	443	441	444	446	437	430	422	421	420	425	427	427	428	437
6	439	442	442	443	445	444	448	447	447	447	450	454	456	459	452	445	454	454	448	439	430	424	426	427	444
7	441	462	454	447	450	442	442	445	447	444	443	442	448	445	448	449	436	427	421	427	427	423	416	418	439
8	428	434	434	436	443	438	443	441	439	441	438	439	443	440	444	446	439	423	410	410	410	414	426	417	432
9	426	437	427	428	434	429	436	437	434	431	431	430	431	430	429	422	414	409	407	400	409	421	429	433	426
10	428	438	431	432	424	426	429	431	434	437	431	427	431	432	427	419	421	420	424	426	425	425	423	421	428
11	417	428	434	436	435	439	445	442	446	446	446	445	446	446	443	435	436	432	427	416	412	414	414	419	433
12	438	442	438	431	421	416	424	426	442	433	438	444	452	465	466	465	450	430	424	412	416	422	393	415	433
13 D	435	444	433	435	432	430	426	429	442	440	437	440	453	464	462	461	450	423	395	367	390	397	412	421	430
14 D	425	421	432	436	426	427	430	429	435	431	436	440	443	453	458	444	424	402	394	391	388	394	410	417	424
15	423	431	427	432	434	434	434	435	437	439	436	436	441	445	447	445	431	421	409	399	397	401	408	420	428
16	430	435	438	426	431	435	432	435	439	443	448	437	444	452	448	442	424	426	404	405	420	426	419	426	432
17	436	434	426	435	433	429	435	437	437	440	440	441	442	446	443	438	425	413	403	407	408	411	418	430	429
18	439	439	435	435	436	437	438	439	437	439	435	430	439	438	444	442	435	423	419	420	418	430	427	429	433
19 Q	432	434	433	434	434	439	440	441	437	443	441	443	442	447	446	440	429	420	415	411	412	415	419	425	432
20 Q	436	437	439	433	435	437	439	444	445	444	448	452	465	468	469	464	457	447	439	433	421	424	437	442	444
21	438	437	438	439	441	444	445	453	455	459	460	462	461	463	455	443	432	431	430	433	432	433	434	425	443
22	423	428	422	430	439	441	425	430	425	433	436	439	438	438	434	434	430	426	423	428	430	425	425	426	430
23	438	438	441	437	435	439	439	442	443	443	445	441	442	443	441	432	424	408	409	419	429	432	430	414	434
24	415	426	432	435	437	437	438	433	433	436	438	439	438	443	443	444	443	438	436	438	439	435	431	428	436
25	430	438	439	429	426	431	433	432	437	438	438	439	440	439	440	433	424	410	403	414	427	435	437	425	431
26 D	433	429	438	427	431	436	440	442	447	448	446	450	464	456	458	458	462	456	448	442	438	444	440	461	446
27 D	489	462	418	394	376	378	388	395	382	404	412	403	406	411	411	400	388	378	372	375	393	401	407	421	403
28	417	420	414	416	417	421	422	430	421	423	425	426	430	433	433	431	428	423	418	414	414	416	420	423	422
29 Q	425	429	431	431	427	428	432	431	432	433	434	435	437	440	439	436	428	424	424	420	418	419	425	429	429
30	435	424	432	433	436	441	438	444	446	445	446	451	450	457	460	464	444	400	385	412	414	413	422	434	434
31	424	423	430	434	427	434	436	436	439	441	440	437	437	441	444	442	431	417	408	405	405	413	418	424	429
MEAN	434	436	434	433	432	434	435	436	436	438	439	439	443	446	446	441	433	422	414	412	415	419	423	427	432

DECLINATION

MEAN VALUES FOR PERIODS OF SIXTY MINUTES, UNIVERSAL TIME

TABLE 20 VICTORIA D = 22 DEG 00.0 MIN EAST + JULY 1969

HOUR =	00 TO 01	01 TO 02	02 TO 03	03 TO 04	04 TO 05	05 TO 06	06 TO 07	07 TO 08	08 TO 09	09 TO 10	10 TO 11	11 TO 12	12 TO 13	13 TO 14	14 TO 15	15 TO 16	16 TO 17	17 TO 18	18 TO 19	19 TO 20	20 TO 21	21 TO 22	22 TO 23	23 TO 24	MEAN
DAY																									
1 D	21.0	23.8	25.5	25.0	24.1	23.3	24.3	25.8	28.9	26.0	26.9	28.6	29.7	33.6	35.6	36.6	37.0	34.4	29.9	25.4	23.2	21.1	20.6	20.9	27.1
2	23.3	24.9	25.9	27.7	26.7	27.0	26.0	26.1	25.8	26.3	26.5	27.2	29.2	30.4	32.2	32.9	33.7	33.6	30.6	27.1	23.7	19.5	19.6	21.5	27.0
3	24.1	25.5	26.5	26.9	26.6	26.4	26.3	26.0	26.2	26.4	27.0	28.4	30.1	31.8	33.0	35.9	36.9	33.8	29.6	23.8	21.4	21.3	21.9	22.7	27.4
4 Q	24.0	24.7	25.1	25.0	25.5	26.1	26.0	26.3	26.3	26.4	27.2	27.4	28.6	30.7	32.3	33.7	34.2	33.2	30.5	26.6	22.3	19.3	19.1	20.1	26.7
5 Q	22.4	24.3	25.9	26.4	26.6	26.4	25.4	26.3	26.1	26.6	27.4	27.1	28.3	30.5	32.3	34.4	35.9	34.3	31.0	26.5	22.3	19.7	18.8	19.5	26.8
6	20.4	22.3	24.7	25.4	25.4	25.5	25.7	25.4	25.7	26.6	27.4	28.2	29.2	30.5	33.0	34.9	34.5	34.5	33.4	29.2	26.0	23.3	21.2	20.9	27.2
7	19.9	21.0	23.7	25.7	26.7	26.2	26.1	25.9	26.3	27.1	28.3	28.6	31.7	32.0	33.3	33.2	37.0	35.7	31.9	27.9	23.6	19.6	17.8	18.2	27.0
8	19.9	23.0	24.9	25.4	25.2	26.2	25.4	26.0	26.5	26.9	27.7	28.2	28.4	30.0	32.4	34.3	35.0	33.9	30.7	25.9	23.6	21.2	19.7	21.1	26.7
9	22.3	23.9	25.3	25.6	26.6	26.5	25.6	27.2	28.2	26.5	27.3	28.7	30.0	30.3	30.9	33.6	35.6	33.6	28.9	23.0	20.0	17.9	18.9	21.9	26.6
10	24.5	24.8	27.2	27.4	25.3	25.4	25.0	25.4	25.1	26.4	26.3	27.2	28.2	29.3	30.3	29.6	32.4	30.5	27.3	24.3	20.7	19.8	19.9	20.7	26.0
11	23.4	24.7	26.6	27.0	26.3	26.1	26.2	27.0	27.8	27.2	27.1	27.7	28.5	30.2	31.1	33.9	35.0	31.9	27.9	23.7	22.6	21.5	20.8	21.7	26.9
12	23.7	24.6	25.5	26.2	26.5	27.3	27.7	26.8	27.8	28.5	26.9	27.5	28.8	31.5	33.2	35.9	37.2	36.3	32.3	29.0	26.8	25.0	23.1	22.6	28.4
13 D	23.8	25.7	27.1	27.1	27.1	29.0	27.8	26.6	29.7	31.5	28.5	27.5	27.4	30.4	32.5	34.6	34.1	32.8	31.6	26.4	19.7	18.5	19.3	20.8	27.5
14 D	24.0	26.6	27.9	29.7	35.7	28.4	27.1	31.0	29.9	28.1	27.1	26.0	27.2	30.6	33.5	35.0	35.5	34.0	28.5	24.8	22.2	22.1	21.9	23.1	28.3
15	24.8	27.3	28.0	27.1	26.3	26.0	26.0	26.6	28.5	27.6	24.9	24.3	26.1	29.9	33.2	35.8	35.9	35.2	32.5	28.2	24.6	22.9	22.4	23.4	27.8
16	24.3	26.9	27.7	29.6	29.2	27.4	26.7	26.3	25.2	25.7	25.3	29.4	29.2	31.7	33.3	34.9	35.0	31.5	31.0	25.8	23.9	24.5	24.2	24.6	28.1
17	25.3	26.6	27.0	27.5	27.6	28.2	26.3	26.3	26.0	26.6	26.2	27.4	28.2	29.0	32.0	32.9	32.5	31.9	28.9	25.6	23.5	22.5	21.6	21.9	27.1
18	22.4	23.8	24.8	25.7	25.9	26.6	26.6	27.0	27.4	27.5	26.5	28.1	28.6	27.6	30.0	32.2	34.0	34.1	30.3	27.4	25.5	24.6	24.8	24.5	27.3
19 Q	24.8	25.3	25.8	25.9	26.7	26.9	28.1	27.4	27.3	26.9	26.8	27.2	27.8	29.2	30.4	32.3	32.5	31.3	26.2	23.1	22.1	21.8	21.2	21.7	26.6
20 Q	22.6	24.4	25.4	26.1	26.3	27.1	26.7	26.6	26.5	26.6	26.9	27.0	27.9	30.0	32.1	34.9	35.4	33.7	30.7	27.0	23.8	22.1	21.1	22.0	27.2
21	24.1	25.3	25.8	26.2	25.8	25.6	26.0	25.8	25.7	25.9	26.4	27.2	27.7	29.4	32.1	33.1	32.7	32.0	25.6	22.3	19.8	20.0	21.4	23.5	26.2
22	24.8	24.7	25.2	25.4	25.1	25.1	26.2	26.8	27.4	26.9	26.7	27.7	28.8	30.6	31.5	31.7	32.6	31.8	28.0	26.9	25.8	24.7	23.7	22.6	27.1
23	24.0	24.7	24.0	24.6	25.3	26.1	26.3	26.5	26.6	26.9	26.4	27.3	28.1	29.6	30.1	30.7	31.0	29.7	25.1	22.9	22.8	22.5	21.6	22.6	26.1
24	23.4	24.3	24.5	25.1	25.7	26.4	26.6	27.8	26.9	26.8	27.1	28.1	28.7	29.6	31.3	32.9	32.5	32.1	29.9	27.7	26.7	26.7	25.3	25.5	27.6
25	25.9	25.2	25.6	25.7	26.0	27.1	27.6	27.1	26.4	27.0	27.7	28.6	28.9	29.2	30.6	30.7	31.3	30.8	27.9	23.9	22.4	21.6	21.0	23.1	26.7
26 D	23.9	24.7	24.8	24.9	26.9	24.9	24.8	25.6	26.2	27.0	27.5	27.8	28.4	30.1	28.2	35.2	35.2	34.6	31.4	28.8	26.8	25.3	24.1	22.0	27.5
27 D	19.4	21.6	25.5	38.1	31.7	35.9	32.6	31.0	34.1	30.4	28.4	28.1	28.4	31.0	33.9	35.2	35.0	33.7	30.1	27.1	23.2	21.5	21.7	23.7	29.2
28	25.8	26.3	27.2	26.6	26.1	26.4	27.0	25.2	25.6	26.8	26.7	27.5	28.5	29.8	30.6	31.5	32.4	32.0	29.9	27.7	25.1	24.7	24.8	23.8	27.4
29 Q	25.4	25.6	25.6	25.9	26.0	26.3	26.1	27.2	26.5	26.7	27.0	27.7	29.0	30.3	32.4	34.7	35.1	33.0	29.2	26.2	22.9	22.3	22.2	21.8	27.3
30	22.6	24.4	24.6	24.9	25.0	25.1	25.1	24.9	25.5	26.2	26.3	27.3	26.7	27.4	28.8	33.4	36.0	36.5	28.5	22.9	19.6	18.7	20.4	21.5	25.9
31	24.2	24.6	24.9	26.6	25.6	26.0	25.2	25.5	25.5	26.8	26.5	27.2	29.1	29.8	31.8	33.4	34.2	33.8	30.9	27.3	24.6	22.3	20.9	21.0	27.0
MEAN	23.4	24.7	25.7	26.7	26.6	26.7	26.4	26.6	27.0	27.1	26.9	27.6	28.6	30.2	31.9	33.7	34.4	33.2	29.7	25.9	23.3	21.9	21.5	22.1	27.2

VERTICAL INTENSITY

MEAN VALUES FOR PERIODS OF SIXTY MINUTES, UNIVERSAL TIME

TABLE 21 VICTORIA — Z = 53,000 GAMMA + — JULY 1969

HOUR = DAY	00 TO 01	01 TO 02	02 TO 03	03 TO 04	04 TO 05	05 TO 06	06 TO 07	07 TO 08	08 TO 09	09 TO 10	10 TO 11	11 TO 12	12 TO 13	13 TO 14	14 TO 15	15 TO 16	16 TO 17	17 TO 18	18 TO 19	19 TO 20	20 TO 21	21 TO 22	22 TO 23	23 TO 24	MEAN
1 D	124	131	127	128	125	126	132	100	109	123	122	124	119	129	132	126	114	109	98	101	104	104	109	122	118
2	139	142	143	139	137	132	129	119	123	124	125	126	129	131	132	129	123	114	106	97	103	106	112	121	124
3	132	137	137	131	131	127	127	127	127	127	128	129	132	131	131	127	123	115	106	99	91	94	109	113	122
4 Q	123	128	128	126	126	124	124	124	124	126	126	126	128	130	129	127	122	117	111	104	101	98	104	117	121
5 Q	126	132	131	128	126	125	123	123	124	123	124	127	123	123	125	124	121	116	104	96	99	97	100	107	119
6	114	121	125	122	122	120	120	119	119	121	123	124	125	125	127	124	123	120	111	106	100	98	106	116	118
7	120	121	123	123	123	123	122	120	120	122	119	119	121	122	124	117	107	104	103	101	99	99	106	115	116
8	126	129	125	124	124	123	121	120	119	118	118	119	121	122	124	125	116	108	99	96	99	103	117	125	118
9	133	143	144	148	143	139	135	130	125	124	124	125	125	122	120	121	117	110	106	100	98	101	117	125	124
10	128	138	139	140	132	130	128	125	125	122	116	117	122	121	124	115	117	117	113	112	111	115	120	127	123
11	132	139	143	138	131	126	128	126	125	123	121	124	124	126	127	126	117	105	99	99	102	106	114	128	122
12	142	152	159	158	157	151	146	139	116	120	126	128	132	135	135	139	135	130	121	107	108	113	116	129	133
13 D	140	147	148	143	144	135	138	137	127	109	116	123	127	137	143	146	144	133	120	106	110	121	131	139	132
14 D	148	151	150	154	159	142	136	132	126	117	121	126	130	129	139	139	133	124	111	103	105	109	119	129	131
15	140	147	144	140	135	132	130	129	128	124	123	119	124	129	133	135	127	120	111	106	104	108	117	126	126
16	137	143	144	140	139	136	134	132	131	130	116	110	124	130	130	132	129	126	118	117	117	123	124	127	129
17	133	137	132	133	133	130	129	129	128	127	124	126	127	129	129	130	126	121	112	111	113	120	122	127	126
18	130	132	130	130	128	127	127	126	127	126	124	118	126	126	124	126	124	118	114	111	112	115	118	124	123
19 Q	125	128	129	127	124	125	125	123	122	122	119	124	124	126	126	124	122	111	102	108	113	120	120	124	121
20 Q	129	130	129	126	124	125	122	123	122	123	124	125	127	127	126	126	124	117	108	109	112	104	109	119	121
21	128	128	128	124	121	123	120	122	122	122	121	123	123	127	122	117	108	106	108	106	106	116	124	127	120
22	130	136	133	130	128	127	129	132	131	131	128	128	129	130	126	122	119	116	108	107	107	108	116	120	124
23	130	128	124	122	121	121	120	120	121	121	120	118	118	122	123	121	119	108	105	113	116	122	124	126	120
24	131	134	133	129	127	125	124	124	122	122	122	124	124	127	127	129	120	114	107	109	107	110	115	116	122
25	117	124	126	127	129	131	126	125	124	124	124	124	124	124	126	124	118	114	104	103	113	120	124	125	122
26 D	130	132	136	137	140	136	131	127	126	125	123	125	127	126	117	103	104	107	108	108	107	102	107	133	122
27 D	174	243	237	230	198	179	171	80	96	129	136	137	129	127	141	145	138	127	120	126	132	133	132	138	150
28	138	144	142	141	138	136	136	126	122	128	131	132	134	135	134	133	133	132	131	131	131	126	128	132	133
29 Q	137	134	134	133	133	131	132	133	131	132	129	129	126	127	127	129	129	121	110	105	102	104	112	117	125
30	128	127	127	125	126	126	126	129	128	127	126	126	126	126	128	129	122	107	108	110	114	121	126	135	124
31	140	140	137	134	129	130	128	131	131	130	128	125	129	129	130	128	123	114	109	105	111	115	119	127	126
MEAN	132	139	138	136	134	131	130	124	123	124	123	124	126	127	128	127	122	116	109	107	108	111	117	124	124

HORIZONTAL INTENSITY

MEAN VALUES FOR PERIODS OF SIXTY MINUTES, UNIVERSAL TIME

TABLE 22 VICTORIA H = 18,500 GAMMA + AUGUST 1969

HOUR =	00 TO 01	01 TO 02	02 TO 03	03 TO 04	04 TO 05	05 TO 06	06 TO 07	07 TO 08	08 TO 09	09 TO 10	10 TO 11	11 TO 12	12 TO 13	13 TO 14	14 TO 15	15 TO 16	16 TO 17	17 TO 18	18 TO 19	19 TO 20	20 TO 21	21 TO 22	22 TO 23	23 TO 24	MEAN
DAY																									
1 Q	437	439	439	440	436	436	437	442	442	443	442	438	441	442	444	441	429	410	391	383	389	399	419	428	429
2	432	435	436	437	437	436	439	440	442	444	446	448	452	459	457	457	447	425	412	403	403	406	426	442	436
3 D	450	454	456	445	437	444	448	450	451	441	438	440	441	441	439	436	425	415	398	413	422	413	416	410	434
4	407	410	410	408	425	433	431	432	434	440	429	421	431	433	430	417	396	387	386	392	405	416	435	435	418
5	437	435	434	425	426	429	430	433	434	434	439	436	438	441	443	434	424	417	412	409	406	413	417	424	428
6	434	440	428	428	428	434	436	438	438	441	441	438	437	441	442	436	429	417	409	419	426	434	439	443	433
7	441	444	448	447	442	443	444	445	442	452	452	457	453	453	446	446	438	426	412	402	407	419	432	427	438
8	433	425	426	433	438	439	443	448	442	437	443	443	442	446	441	433	417	404	407	413	415	416	418	434	431
9	430	427	437	418	429	435	437	441	438	442	444	450	449	447	453	453	440	426	424	425	424	425	429	432	436
10	438	434	429	427	428	424	425	431	434	445	435	438	438	441	443	435	420	409	399	397	400	411	422	435	427
11 Q	440	441	437	436	440	439	441	442	444	447	444	446	445	455	457	451	437	431	430	429	431	433	443	446	441
12 D	451	455	423	428	428	431	439	436	446	438	437	431	435	444	444	436	415	400	423	434	439	435	426	427	433
13	430	436	429	433	435	427	433	437	446	439	434	436	437	438	437	426	407	392	397	419	426	422	436	436	429
14	437	431	434	439	436	434	436	438	437	436	441	434	438	443	441	436	425	410	399	404	411	415	425	430	430
15	436	437	438	440	442	440	440	436	439	437	437	441	447	448	450	442	435	425	422	421	424	428	425	426	436
16	431	435	439	441	442	440	442	442	446	446	450	448	447	449	454	445	430	421	421	430	427	420	423	430	437
17	436	438	430	429	423	422	431	425	433	430	438	442	443	446	442	432	418	402	395	397	407	415	420	432	426
18	433	434	427	433	440	442	443	445	446	449	449	453	450	444	442	449	441	429	423	420	417	422	433	438	438
19 D	450	436	433	428	436	435	435	438	450	460	462	450	442	445	446	434	410	406	393	390	404	407	415	426	430
20	431	424	423	427	425	425	433	436	426	433	433	432	433	430	434	425	404	393	396	400	403	409	423	433	422
21	438	432	424	428	435	437	438	438	440	439	439	439	439	433	431	421	410	417	415	412	419	422	422	427	429
22	422	434	434	438	441	441	443	445	447	448	450	451	448	449	446	439	429	417	416	418	423	423	437	448	437
23	452	440	439	450	435	426	438	443	440	442	450	447	441	437	435	424	416	411	408	401	398	401	423	442	431
24	440	427	429	432	435	438	439	445	443	441	443	438	438	444	451	444	430	411	410	406	408	414	429	438	432
25 Q	437	439	436	442	435	437	438	441	441	440	442	441	443	444	442	429	411	401	403	408	410	417	422	430	430
26 D	440	443	444	442	447	448	449	449	448	451	475	457	457	463	459	439	420	412	411	414	425	441	430	453	442
27 D	445	456	427	422	404	414	427	431	432	440	423	426	435	434	431	419	411	401	382	383	406	420	430	436	422
28	431	430	427	420	428	437	425	428	429	430	433	433	434	437	435	426	410	398	382	390	401	406	410	421	421
29 Q	434	441	444	441	440	442	441	445	444	443	442	441	446	445	445	437	425	411	397	385	383	391	404	419	429
30 Q	432	437	440	440	443	444	442	435	442	443	444	446	447	447	446	444	431	419	404	393	394	398	419	435	432
31	449	448	446	443	443	445	448	444	438	434	437	440	442	443	441	430	408	398	389	392	398	404	416	431	429
MEAN	437	437	434	434	434	435	438	439	440	441	442	441	442	444	443	436	422	411	405	407	411	416	425	433	431

DECLINATION

MEAN VALUES FOR PERIODS OF SIXTY MINUTES, UNIVERSAL TIME

TABLE 23 VICTORIA D = 22 DEG 00.0 MIN EAST + AUGUST 1969

HOUR =	00 TO 01	01 TO 02	02 TO 03	03 TO 04	04 TO 05	05 TO 06	06 TO 07	07 TO 08	08 TO 09	09 TO 10	10 TO 11	11 TO 12	12 TO 13	13 TO 14	14 TO 15	15 TO 16	16 TO 17	17 TO 18	18 TO 19	19 TO 20	20 TO 21	21 TO 22	22 TO 23	23 TO 24	MEAN
DAY																									
1 Q	22.3	24.2	25.6	26.5	26.3	26.3	26.8	26.4	26.3	26.3	26.7	27.2	27.5	28.6	32.2	34.5	35.5	36.2	32.8	29.6	24.9	21.5	20.2	21.0	27.3
2	22.6	23.9	25.7	26.3	26.1	26.3	26.0	26.3	26.0	26.0	26.8	27.1	28.8	30.7	31.9	35.4	36.2	37.0	31.8	24.8	18.8	16.6	17.2	18.7	26.5
3 D	21.1	23.1	24.2	23.2	24.2	24.9	25.0	25.2	25.5	29.1	28.0	27.3	29.2	32.4	34.5	36.0	37.0	34.8	27.0	23.2	20.8	18.7	17.3	18.8	26.3
4	20.5	21.2	24.3	28.9	27.3	28.0	25.5	25.5	24.9	25.4	27.0	28.8	27.7	30.3	31.7	33.3	33.8	30.4	28.1	23.7	21.7	22.1	22.1	22.9	26.5
5	23.7	24.9	25.5	29.7	27.5	30.7	26.1	25.6	25.9	26.8	26.8	26.3	27.2	30.9	33.1	35.3	36.7	33.2	29.1	24.7	22.8	22.1	22.9	23.8	27.6
6	24.2	24.6	26.7	25.7	27.0	28.2	27.0	25.9	25.9	26.4	26.6	27.2	28.5	29.2	30.8	33.3	33.4	31.7	26.3	22.3	19.0	18.2	19.5	20.4	26.2
7	22.2	23.9	24.3	24.7	25.3	26.8	29.2	28.3	27.6	26.5	27.4	27.7	29.5	30.4	31.4	33.4	33.5	33.1	30.2	25.5	22.2	20.2	21.5	24.3	27.0
8	25.6	27.6	26.9	25.2	25.0	25.1	25.3	27.5	30.6	29.1	26.5	25.9	30.8	32.7	35.0	34.9	33.7	29.8	26.3	24.0	23.6	23.2	22.2	23.2	27.5
9	24.9	25.9	26.4	28.0	26.2	24.6	25.2	27.2	29.9	27.6	26.6	26.2	27.6	29.6	30.9	32.3	32.6	30.1	28.5	25.9	25.4	25.0	24.8	25.5	27.4
10	26.1	26.3	26.9	26.7	27.4	26.8	26.2	26.8	26.3	26.4	27.9	27.3	28.7	31.4	31.7	33.1	34.1	33.6	29.8	26.7	24.4	23.1	22.5	23.3	27.6
11 Q	24.4	25.2	25.6	25.8	25.5	25.5	25.7	26.2	26.4	26.2	26.8	27.9	29.2	30.5	31.4	34.2	33.9	32.8	28.3	25.5	24.0	23.2	23.5	24.3	27.2
12 D	24.4	24.1	25.1	25.9	26.9	32.6	27.2	26.2	27.4	28.9	25.5	27.4	31.2	29.6	31.2	34.7	33.7	27.4	22.1	22.1	22.0	22.9	25.0	25.8	27.1
13	25.7	25.7	25.4	26.8	25.9	26.3	25.6	25.6	22.7	24.5	26.7	26.6	28.6	30.0	31.1	31.2	33.1	32.1	26.1	22.0	20.2	20.5	21.9	23.9	26.2
14	25.5	26.8	25.9	25.7	25.3	26.0	26.5	26.4	26.9	25.5	27.6	27.9	26.4	29.1	32.0	33.9	33.9	31.6	28.2	23.6	21.3	21.6	22.3	23.0	26.8
15	24.5	25.5	25.6	25.6	25.5	25.4	25.8	26.4	26.5	26.5	26.9	27.5	27.5	29.0	30.1	31.7	32.1	31.6	28.8	25.4	23.2	22.3	22.8	24.3	26.7
16	25.7	25.7	25.6	25.9	26.0	25.9	26.1	26.2	26.4	27.0	25.6	27.9	27.5	28.6	29.9	32.1	33.3	32.9	26.9	22.0	21.4	21.4	21.9	23.6	26.5
17	25.4	25.1	25.6	23.9	22.8	25.0	24.9	26.4	26.0	27.0	26.4	26.8	27.9	29.6	31.0	32.8	33.1	32.4	28.4	24.7	22.0	21.3	21.6	22.2	26.3
18	23.6	24.6	26.4	25.0	25.0	25.2	25.6	25.7	25.6	25.9	27.2	26.6	26.9	28.4	27.2	32.0	34.3	32.3	28.2	24.5	23.0	22.8	22.8	24.4	26.4
19 D	24.4	24.8	25.9	24.6	24.4	28.6	28.0	26.8	26.4	26.3	24.2	28.6	29.4	30.4	32.4	34.5	33.6	29.0	25.3	21.2	19.4	17.5	20.8	23.1	26.2
20	24.1	25.3	26.0	27.5	26.1	26.1	28.0	27.8	29.6	27.9	28.6	27.8	28.4	27.9	31.2	32.7	33.4	31.5	28.3	25.0	23.1	21.9	21.0	22.3	27.1
21	24.1	25.2	25.2	25.4	30.1	25.9	25.7	25.8	26.1	26.4	26.9	27.3	28.2	28.5	29.7	32.3	31.6	28.4	29.3	26.8	24.9	24.5	23.6	22.8	26.9
22	24.5	23.7	23.8	24.3	25.1	25.4	25.5	26.1	26.5	26.7	27.1	28.1	28.9	29.9	31.9	32.8	33.4	31.6	26.8	22.9	20.5	20.3	20.7	21.0	26.1
23	20.6	22.1	23.2	22.6	22.0	23.4	24.6	27.3	26.8	25.3	24.3	29.2	29.9	32.4	32.2	32.6	31.4	30.0	27.7	24.6	22.1	21.5	21.9	22.0	25.8
24	23.7	24.6	25.5	26.6	25.5	25.1	25.5	25.3	26.2	27.2	27.8	30.4	30.2	31.2	33.9	35.0	35.7	34.9	30.4	26.2	23.8	22.4	21.3	21.8	27.5
25 Q	23.9	26.1	26.9	25.2	24.8	24.8	25.4	25.6	26.3	27.0	27.2	27.5	28.0	28.8	31.0	33.5	35.6	34.2	30.0	25.4	23.5	22.5	21.9	22.7	27.0
26 D	23.9	24.9	25.5	25.0	24.9	24.4	25.1	26.1	26.0	24.1	25.6	30.8	28.2	31.5	34.2	35.8	36.8	33.3	27.3	23.4	21.5	20.0	21.7	21.3	26.7
27 D	20.8	17.6	19.9	24.4	35.2	27.5	23.8	23.9	27.0	34.7	31.7	27.5	27.7	29.9	31.1	30.8	30.3	30.5	25.1	20.3	21.0	21.7	22.6	24.1	26.2
28	25.8	26.7	26.1	24.2	27.5	27.9	26.7	26.6	26.3	26.0	26.6	27.6	28.6	29.8	31.4	33.4	34.8	33.5	29.1	22.5	22.9	22.8	22.9	24.5	27.3
29 Q	25.1	26.1	26.1	25.5	25.7	25.3	25.9	25.7	26.1	26.4	27.1	27.4	28.6	29.8	32.4	34.7	36.9	34.8	30.3	25.4	22.1	20.6	20.8	22.5	27.1
30 Q	24.7	25.5	25.6	25.1	25.8	25.9	26.8	26.7	25.8	26.5	27.0	27.2	27.9	27.5	31.0	33.4	36.1	35.1	31.6	26.9	23.2	20.9	20.8	21.8	27.0
31	23.5	25.0	25.2	25.2	25.8	26.0	26.4	28.5	29.0	27.5	27.3	27.0	28.2	29.5	32.1	35.6	36.6	32.8	28.7	23.4	20.6	19.6	19.7	20.4	26.8
MEAN	23.9	24.7	25.4	25.6	26.1	26.3	26.0	26.3	26.6	26.9	26.9	27.6	28.5	29.9	31.7	33.6	34.2	32.3	28.3	24.3	22.2	21.4	21.7	22.7	26.8

VERTICAL INTENSITY

MEAN VALUES FOR PERIODS OF SIXTY MINUTES, UNIVERSAL TIME

TABLE 24 VICTORIA Z = 53,000 GAMMA + AUGUST 1969

HOUR =	00 TO 01	01 TO 02	02 TO 03	03 TO 04	04 TO 05	05 TO 06	06 TO 07	07 TO 08	08 TO 09	09 TO 10	10 TO 11	11 TO 12	12 TO 13	13 TO 14	14 TO 15	15 TO 16	16 TO 17	17 TO 18	18 TO 19	19 TO 20	20 TO 21	21 TO 22	22 TO 23	23 TO 24	MEAN
DAY																									
1 Q	139	135	134	130	126	126	128	128	129	130	126	125	125	122	120	121	121	115	109	105	100	100	112	125	122
2	127	130	129	128	125	125	126	126	125	128	127	128	131	130	128	126	129	126	111	99	96	99	109	116	122
3 D	125	127	130	126	120	121	122	123	124	125	126	124	119	116	118	115	106	91	89	91	91	90	111	130	115
4	141	152	160	154	146	136	127	131	128	128	106	111	124	131	136	133	129	120	110	116	122	125	132	132	130
5	139	138	137	144	140	136	128	130	128	128	130	127	115	119	125	125	121	115	107	102	104	115	121	129	125
6	142	148	147	140	136	132	129	129	128	128	127	129	129	133	133	129	123	115	111	103	99	96	101	109	125
7	119	127	126	126	123	125	125	123	121	126	124	127	125	129	126	126	122	114	101	92	90	101	119	130	119
8	140	142	138	130	128	126	126	126	125	124	126	110	113	122	122	120	115	105	100	98	97	102	112	121	120
9	128	133	141	141	137	131	128	127	126	125	125	125	124	123	122	125	123	112	111	113	117	115	125	130	125
10	139	133	132	133	134	134	135	134	126	105	113	122	122	121	118	115	114	107	104	108	113	118	123	127	122
11 Q	129	130	127	127	126	126	125	125	125	124	123	123	124	127	126	127	126	117	109	96	97	105	108	114	120
12 D	119	129	128	135	140	138	134	131	116	120	120	90	95	113	116	121	118	106	99	102	100	102	110	118	117
13	122	127	123	127	128	128	125	126	111	97	108	117	121	124	125	126	127	120	108	110	115	122	132	133	121
14	139	133	131	131	127	127	128	117	120	122	108	110	111	110	114	120	119	111	103	101	104	108	114	115	118
15	126	125	124	121	123	120	122	124	123	122	123	123	123	124	125	128	127	118	113	110	116	121	121	123	122
16	126	124	120	120	120	120	119	122	122	121	117	113	119	123	125	125	117	102	94	93	101	106	113	121	116
17	130	136	141	142	142	145	139	136	134	130	131	129	128	128	128	126	119	111	109	112	114	116	122	127	128
18	131	132	132	127	124	124	123	123	123	122	120	122	121	122	116	109	112	102	95	100	109	115	119	124	119
19 D	129	128	128	127	127	129	126	126	124	112	98	105	111	116	119	119	118	109	99	100	110	121	132	136	119
20	129	127	127	135	134	135	131	109	115	119	119	124	128	125	123	126	120	111	107	107	112	117	120	128	122
21	134	132	126	128	129	126	124	124	122	124	124	124	125	123	121	118	117	110	105	102	107	112	119	126	121
22	127	129	126	125	123	123	122	121	120	121	121	120	118	117	119	119	120	115	105	98	97	99	105	115	117
23	127	122	122	125	132	130	127	127	127	125	105	98	102	111	119	119	115	109	108	106	115	120	127	132	119
24	136	134	133	131	129	126	125	123	122	123	122	120	124	125	127	127	127	115	106	106	109	110	110	117	122
25 Q	123	129	129	128	126	124	125	121	119	118	120	119	120	120	123	124	120	109	103	103	106	105	109	115	118
26 D	125	127	127	125	125	125	125	123	126	121	84	94	99	102	113	119	113	104	102	97	97	98	101	117	112
27 D	127	139	149	181	154	150	142	134	129	116	104	109	113	124	126	126	127	117	103	104	118	128	131	137	129
28	141	140	139	137	139	127	129	133	132	129	127	129	129	128	128	124	124	119	110	105	112	116	121	126	127
29 Q	134	130	130	126	126	126	126	127	126	125	125	124	124	125	128	130	127	119	110	105	103	106	112	119	122
30 Q	127	126	123	121	124	123	126	127	127	125	125	125	124	124	126	130	128	125	118	115	109	109	117	122	123
31	131	127	121	121	121	120	122	120	115	119	121	123	124	124	125	123	120	109	97	98	108	114	120	126	119
MEAN	131	132	132	132	130	129	127	126	124	122	119	118	120	122	123	123	121	112	105	103	106	110	117	124	121

HORIZONTAL INTENSITY

MEAN VALUES FOR PERIODS OF SIXTY MINUTES, UNIVERSAL TIME

TABLE 25 VICTORIA H = 18,500 GAMMA + SEPTEMBER 1969

HOUR =	00 TO 01	01 TO 02	02 TO 03	03 TO 04	04 TO 05	05 TO 06	06 TO 07	07 TO 08	08 TO 09	09 TO 10	10 TO 11	11 TO 12	12 TO 13	13 TO 14	14 TO 15	15 TO 16	16 TO 17	17 TO 18	18 TO 19	19 TO 20	20 TO 21	21 TO 22	22 TO 23	23 TO 24	MEAN
DAY																									
1 Q	433	443	443	442	436	437	441	440	443	442	443	445	448	449	448	441	426	406	398	404	415	421	426	430	433
2 Q	437	443	445	444	444	447	447	444	441	443	446	447	446	449	448	443	428	410	395	397	410	422	432	440	435
3	448	450	451	449	450	448	448	452	450	449	452	451	448	448	445	435	421	415	415	416	421	425	436	438	440
4	437	436	438	434	434	441	442	444	448	454	454	452	454	450	446	434	421	412	413	422	436	442	442	438	439
5	441	442	445	450	450	450	454	452	449	450	455	462	464	453	420	428	409	401	393	386	411	433	431	416	435
6 D	395	415	413	406	416	413	434	424	432	430	433	426	436	434	433	422	415	402	400	405	418	409	416	429	419
7	436	427	424	431	433	433	434	433	423	415	430	435	436	435	433	418	404	397	390	394	406	412	409	415	421
8	414	428	420	419	417	420	410	397	380	408	427	426	428	427	426	421	404	391	391	398	409	421	432	435	415
9	435	427	423	429	431	433	446	434	437	439	442	441	427	424	436	425	404	403	398	396	401	406	415	420	424
10	427	433	433	423	426	432	436	438	439	440	439	441	437	434	431	426	413	401	395	402	410	410	429	439	426
11	442	413	409	409	418	419	418	421	412	422	430	433	434	430	435	430	420	410	409	409	423	432	435	439	423
12	441	428	434	435	425	444	436	436	438	442	441	441	441	440	436	426	416	408	405	404	412	420	431	439	430
13 Q	439	438	436	435	433	433	438	437	442	444	440	445	440	441	441	432	417	407	402	407	417	427	433	441	432
14	446	442	436	433	440	441	442	446	449	448	450	449	447	450	451	443	428	423	416	408	407	409	423	434	436
15	434	406	400	403	412	418	427	428	413	409	414	415	415	423	435	417	393	389	386	368	374	390	408	423	408
16	423	425	424	420	422	420	413	423	423	429	431	432	429	435	433	430	421	413	408	409	420	429	434	440	424
17	443	442	442	443	444	444	445	447	450	450	452	446	443	451	441	439	434	421	404	409	427	427	428	434	438
18 D	442	440	439	440	439	433	444	439	437	438	444	444	449	453	441	434	418	382	395	415	414	415	423	425	431
19	437	428	421	431	444	438	440	438	438	439	442	443	441	439	434	425	418	411	400	404	411	417	424	433	429
20	440	437	439	440	437	433	434	432	437	436	437	441	437	438	436	421	417	393	406	407	411	418	428	438	429
21	446	440	438	441	443	441	442	443	447	445	447	447	446	444	439	428	419	412	414	419	423	427	435	435	436
22 Q	434	436	439	438	437	443	453	446	447	445	446	448	445	448	446	438	426	417	413	415	425	433	440	441	437
23	440	440	442	445	443	444	448	448	451	453	455	458	459	455	449	445	439	422	418	414	407	406	420	433	439
24	438	441	439	442	437	436	437	434	439	443	440	442	443	443	440	432	417	400	396	402	413	426	439	440	432
25	442	432	438	436	417	433	447	439	441	442	443	443	444	441	439	422	417	416	404	401	400	406	428	432	429
26 Q	440	440	440	438	439	441	442	438	437	441	444	442	444	445	442	436	425	415	407	404	409	414	428	436	433
27	447	447	447	449	449	449	451	451	453	455	456	457	459	457	456	448	435	430	421	413	408	429	443	453	444
28 D	459	445	454	455	457	461	456	462	457	455	450	505	493	447	433	430	422	392	377	401	403	401	420	424	440
29 D	430	430	430	428	438	450	439	441	413	388	410	404	435	418	361	380	429	407	400	386	399	416	389	370	412
30 D	404	396	407	370	395	384	386	373	308	323	340	290	296	403	389	394	379	373	354	376	385	411	421	422	374
MEAN	436	433	433	432	434	435	438	436	432	434	438	438	439	440	435	428	418	406	401	403	411	418	427	431	428

DECLINATION

MEAN VALUES FOR PERIODS OF SIXTY MINUTES, UNIVERSAL TIME

TABLE 26 VICTORIA D = 22 DEG 00.0 MIN EAST + SEPTEMBER 1969

HOUR =	00 TO 01	01 TO 02	02 TO 03	03 TO 04	04 TO 05	05 TO 06	06 TO 07	07 TO 08	08 TO 09	09 TO 10	10 TO 11	11 TO 12	12 TO 13	13 TO 14	14 TO 15	15 TO 16	16 TO 17	17 TO 18	18 TO 19	19 TO 20	20 TO 21	21 TO 22	22 TO 23	23 TO 24	MEAN
DAY																									
1 Q	23.6	25.0	25.5	25.6	25.5	25.3	25.7	25.5	26.0	25.8	26.2	26.6	27.1	28.6	31.4	34.2	36.3	35.1	30.2	24.1	20.5	20.0	20.9	23.0	26.6
2 Q	24.5	24.7	24.7	25.1	25.7	25.4	25.3	24.8	25.5	26.5	26.9	27.3	28.2	28.8	31.4	33.7	36.1	34.7	29.8	25.2	22.2	21.3	21.2	22.3	26.7
3	24.0	24.8	25.0	25.1	25.8	25.9	26.2	26.1	26.3	26.6	27.0	28.3	30.0	30.4	32.6	33.9	34.7	31.6	26.9	24.0	23.2	23.2	23.0	22.9	27.0
4	23.2	23.4	22.9	23.2	23.6	25.4	25.7	26.1	26.2	26.4	26.9	27.8	28.4	29.1	31.1	33.1	34.7	31.0	26.2	21.9	20.7	21.2	23.7	25.7	26.1
5	26.7	25.6	24.5	24.4	25.0	25.5	25.7	26.2	27.1	28.2	28.6	27.1	27.0	26.5	19.3	30.9	27.4	27.4	26.0	21.6	20.2	21.8	22.4	23.5	25.4
6 D	25.0	25.8	25.5	30.6	26.4	33.8	33.3	29.2	27.6	28.0	29.6	28.7	28.3	29.2	31.7	32.9	31.2	30.4	26.3	23.0	22.7	22.6	22.3	23.4	27.8
7	24.9	24.9	24.9	25.5	25.8	25.8	26.4	27.6	33.0	33.3	27.0	23.1	27.5	30.8	31.3	32.3	33.5	29.9	24.7	22.2	20.7	21.7	23.0	23.8	26.8
8	25.0	26.3	28.0	30.0	26.5	24.0	23.0	23.6	30.8	34.1	31.2	28.4	28.7	30.6	30.2	30.0	32.7	31.1	27.7	24.2	21.9	21.5	23.2	24.9	27.4
9	26.4	27.2	26.2	26.0	25.5	26.4	24.4	26.4	26.1	26.8	27.3	25.5	24.9	25.0	29.4	32.5	32.9	30.3	25.7	24.0	23.2	22.8	23.1	24.1	26.3
10	27.6	28.5	26.6	27.0	27.0	24.9	24.7	25.2	25.8	26.5	26.9	27.2	28.0	28.8	28.7	30.4	31.5	30.1	24.2	22.0	21.5	22.0	23.4	24.8	26.4
11	25.2	26.6	26.5	26.5	25.0	25.5	25.9	27.7	29.8	29.1	28.0	27.7	28.1	26.6	29.0	31.8	32.0	30.3	27.0	21.4	20.2	21.5	23.7	25.4	26.7
12	26.1	27.2	26.2	26.1	26.6	28.6	25.9	25.0	25.9	24.9	27.3	26.8	27.9	29.1	30.8	32.8	33.1	31.3	28.1	25.2	23.5	22.7	23.7	24.9	27.1
13 Q	26.3	26.9	26.6	26.0	25.9	25.6	25.5	25.7	25.0	25.3	27.5	27.8	29.3	29.7	31.1	32.9	34.2	32.0	28.6	25.2	23.1	22.3	23.0	24.2	27.1
14	25.4	26.3	26.1	27.1	26.6	25.8	25.8	25.6	26.1	26.8	24.9	28.6	29.3	30.2	32.0	34.4	35.6	30.6	27.1	25.3	20.7	19.2	19.7	21.7	26.7
15	19.4	23.0	31.1	30.1	27.4	25.4	30.5	26.6	28.0	28.9	29.6	30.7	32.1	32.9	34.7	31.1	24.5	22.2	24.3	24.6	22.9	21.4	21.2	21.9	26.9
16	25.2	26.1	27.4	32.5	27.5	28.7	28.1	27.2	28.0	27.4	27.0	28.6	29.1	29.4	31.2	32.1	32.6	31.8	30.5	28.7	26.0	24.3	24.5	24.8	28.3
17	24.9	25.1	25.4	25.3	25.9	25.9	25.8	25.9	26.2	26.9	28.3	33.6	35.1	33.0	34.9	34.2	33.5	32.7	32.0	24.0	22.2	22.0	22.8	23.9	27.9
18 D	23.3	23.0	25.0	24.5	23.9	25.9	25.7	26.3	26.5	27.1	26.4	24.2	25.7	29.4	31.3	30.7	30.9	27.4	21.9	21.2	21.8	21.2	21.8	22.5	25.3
19	23.8	23.0	25.2	26.2	29.8	28.4	26.2	25.8	26.4	26.1	26.9	27.8	26.7	27.7	29.9	30.8	31.5	30.4	29.9	27.7	25.5	24.3	23.5	23.3	26.9
20	23.9	25.0	25.9	27.1	26.4	27.3	28.4	27.5	27.5	29.9	28.1	28.0	27.2	26.7	29.7	30.0	29.1	29.8	27.5	25.7	24.0	22.4	23.1	24.1	26.8
21	24.2	24.6	24.7	24.9	26.2	26.2	26.2	25.8	24.6	26.4	26.9	27.8	28.1	28.5	29.5	30.3	29.7	29.6	27.1	26.0	24.7	24.0	24.3	24.3	26.4
22 Q	24.9	24.8	24.5	24.9	25.4	25.8	24.6	26.2	27.2	27.4	27.9	29.1	29.1	28.7	29.4	30.8	31.6	31.1	29.2	26.4	24.6	24.3	24.5	25.3	27.0
23	25.5	24.8	24.7	24.7	25.5	25.7	25.6	25.2	26.3	26.6	27.1	27.6	28.4	26.8	27.1	31.6	31.0	28.0	25.5	24.2	24.0	21.7	22.6	24.0	26.0
24	25.5	25.2	24.5	25.2	25.2	26.2	25.1	25.7	26.8	27.7	29.3	29.8	29.4	29.2	30.5	31.9	33.2	33.1	30.2	27.0	24.0	23.2	23.4	24.7	27.3
25	24.6	25.3	24.8	25.7	28.6	26.0	26.5	26.0	25.8	26.3	27.3	27.7	28.5	29.3	29.9	29.2	28.5	29.5	28.6	25.4	22.2	21.0	21.5	22.8	26.3
26 Q	25.0	25.0	25.7	25.8	25.9	25.9	26.1	29.2	26.9	24.2	28.7	28.0	28.2	29.0	30.1	32.1	33.5	32.9	30.8	27.6	25.2	23.9	22.9	23.3	27.3
27	24.1	25.0	25.7	26.1	26.3	26.5	26.3	26.1	25.9	26.1	26.1	26.5	26.5	27.0	28.3	30.1	31.4	30.3	28.3	26.3	22.8	19.2	18.1	18.6	25.7
28 D	19.6	20.6	24.5	25.0	25.0	24.7	24.3	25.0	25.7	27.9	27.4	25.7	40.7	36.8	29.6	32.3	34.1	33.7	27.6	24.6	22.5	20.6	20.6	22.8	26.7
29 D	24.9	26.2	26.2	29.4	28.1	24.7	24.5	26.5	20.6	22.7	37.9	32.2	26.8	31.1	29.9	27.3	30.1	31.5	27.9	25.0	25.8	23.9	22.1	23.2	27.0
30 D	18.4	26.4	33.1	33.5	30.0	29.0	28.9	22.4	13.6	44.0	45.0	33.6	31.0	26.1	22.7	25.9	26.9	25.8	28.3	26.9	27.0	25.6	25.3	25.7	28.1
MEAN	24.4	25.2	25.9	26.6	26.3	26.3	26.2	26.1	26.2	27.8	28.5	28.1	28.8	29.2	30.0	31.5	31.9	30.5	27.6	24.7	23.0	22.2	22.6	23.7	26.8

VERTICAL INTENSITY

MEAN VALUES FOR PERIODS OF SIXTY MINUTES, UNIVERSAL TIME

TABLE 27 VICTORIA Z = 53,000 GAMMA + SEPTEMBER 1969

HOUR =	00 TO 01	01 TO 02	02 TO 03	03 TO 04	04 TO 05	05 TO 06	06 TO 07	07 TO 08	08 TO 09	09 TO 10	10 TO 11	11 TO 12	12 TO 13	13 TO 14	14 TO 15	15 TO 16	16 TO 17	17 TO 18	18 TO 19	19 TO 20	20 TO 21	21 TO 22	22 TO 23	23 TO 24	MEAN
DAY																									
1 Q	129	129	126	124	122	122	122	122	121	120	122	121	123	124	126	125	120	110	100	96	99	107	115	117	118
2 Q	122	123	123	122	121	120	119	120	122	123	125	123	123	124	123	121	117	103	97	98	101	107	113	117	117
3	123	124	122	121	120	117	118	117	118	118	120	117	114	120	122	120	113	104	98	97	101	103	106	111	114
4	117	121	122	124	125	125	124	122	122	121	121	120	121	121	122	119	110	100	91	93	102	112	118	119	116
5	123	119	120	121	120	119	119	119	121	122	121	119	102	85	57	41	65	84	88	98	118	128	137	145	108
6 D	148	144	148	150	143	141	117	124	131	128	113	87	115	120	127	128	128	122	117	116	116	118	126	124	126
7	128	129	129	127	128	125	127	126	121	113	124	110	110	114	123	126	128	118	108	106	121	126	130	141	122
8	141	145	143	146	148	150	140	82	73	99	123	133	135	134	130	132	137	130	124	122	127	128	132	133	129
9	133	134	128	130	131	129	117	114	125	126	127	123	112	102	104	104	107	108	105	110	117	122	128	131	119
10	136	141	135	132	134	132	129	129	127	126	126	126	124	125	124	123	119	109	107	106	115	121	128	128	125
11	134	132	140	143	142	138	135	131	125	126	131	130	128	125	127	130	131	128	123	122	126	130	131	135	131
12	135	127	126	126	128	127	123	125	126	122	123	123	121	124	123	123	122	119	117	116	116	119	125	126	123
13 Q	128	124	123	124	124	125	125	125	125	118	119	121	118	122	125	127	125	120	112	109	112	116	123	127	122
14	128	123	123	124	125	125	125	126	126	123	114	116	119	120	123	123	115	105	98	97	106	118	133	140	120
15	153	165	185	164	153	145	150	141	143	139	132	131	131	125	123	110	93	91	93	102	115	126	138	143	133
16	147	141	138	138	137	138	138	137	135	136	134	130	131	134	135	138	138	138	136	134	134	135	136	136	136
17	133	129	126	126	125	126	125	126	127	127	129	116	122	125	121	121	117	113	110	112	114	114	119	121	122
18 D	125	127	131	132	131	136	128	131	130	128	126	122	111	118	109	114	110	103	108	112	115	121	127	134	122
19	141	140	139	139	138	125	125	127	127	126	121	124	125	125	125	125	123	124	119	114	114	118	121	122	126
20	129	127	127	127	127	126	127	125	117	108	119	123	121	118	116	116	115	110	114	110	111	116	117	123	120
21	131	127	128	128	129	127	128	125	119	118	121	121	123	123	123	124	122	120	117	118	119	122	126	128	124
22 Q	128	127	129	128	128	128	122	118	119	121	122	121	122	122	125	127	128	124	122	118	120	124	124	119	124
23	118	122	123	124	123	124	124	123	123	123	122	122	121	119	109	111	109	110	113	116	118	123	129	133	120
24	129	127	126	126	130	132	130	131	130	128	123	122	122	123	127	128	127	122	118	117	119	124	124	123	125
25	124	120	125	127	130	133	130	121	127	125	126	124	123	123	123	121	120	116	113	114	117	124	131	129	124
26 Q	127	126	125	127	127	126	127	128	128	120	117	123	122	122	124	127	124	118	110	107	113	118	121	120	122
27	125	124	123	123	123	122	121	121	121	121	120	119	118	116	117	118	115	113	114	111	111	113	115	117	118
28 D	125	120	124	123	122	120	122	121	121	121	121	95	45	55	74	84	91	95	95	98	107	113	127	129	106
29 D	135	138	137	135	137	137	135	120	63	19	43	85	83	83	47	33	72	89	99	106	122	132	134	166	102
30 D	229	239	323	268	187	181	181	137	-7	42	0	-57	-57	41	90	106	114	121	131	150	153	153	148	144	126
MEAN	134	134	137	135	132	131	128	124	117	116	116	113	111	114	115	115	115	112	110	111	116	121	126	129	121

HORIZONTAL INTENSITY

MEAN VALUES FOR PERIODS OF SIXTY MINUTES, UNIVERSAL TIME

TABLE 28 VICTORIA H = 18,500 GAMMA + OCTOBER 1969

HOUR =	00 TO 01	01 TO 02	02 TO 03	03 TO 04	04 TO 05	05 TO 06	06 TO 07	07 TO 08	08 TO 09	09 TO 10	10 TO 11	11 TO 12	12 TO 13	13 TO 14	14 TO 15	15 TO 16	16 TO 17	17 TO 18	18 TO 19	19 TO 20	20 TO 21	21 TO 22	22 TO 23	23 TO 24	MEAN
DAY																									
1 D	434	400	404	415	416	415	413	408	406	417	401	417	413	435	431	419	407	413	410	405	397	390	402	415	412
2 D	415	415	409	422	421	430	406	388	373	380	393	407	421	442	403	378	398	406	395	392	398	400	404	406	404
3 D	409	414	407	409	411	406	417	421	419	429	425	423	421	433	421	420	416	405	389	400	416	417	422	422	416
4	423	419	425	425	427	426	425	426	429	432	432	426	434	435	431	432	425	402	406	417	413	415	419	423	424
5	423	426	434	433	432	432	434	436	442	441	433	434	439	440	435	430	425	418	406	405	407	417	425	429	428
6 D	431	431	426	427	420	422	425	425	428	435	440	438	438	431	435	430	409	392	389	395	401	413	421	426	422
7	428	433	427	413	423	428	428	438	431	434	435	433	435	436	432	430	426	421	410	404	404	410	416	424	425
8 Q	432	434	435	438	437	437	441	443	446	443	444	445	446	443	441	441	440	429	416	415	417	421	423	427	435
9	431	433	436	435	435	433	436	435	437	439	442	443	442	440	439	435	432	432	428	433	422	420	437	449	435
10 D	449	450	434	416	421	427	424	432	431	430	422	430	431	437	442	437	433	422	400	386	390	398	416	421	424
11	424	417	421	428	430	417	420	419	426	432	432	442	437	440	440	432	418	409	406	411	412	412	423	435	424
12	440	431	423	434	435	432	431	442	426	431	435	436	441	446	436	432	430	416	406	407	409	421	431	436	429
13	434	438	437	438	435	431	434	441	437	440	449	440	441	444	440	436	428	423	417	416	421	423	429	432	434
14 Q	439	444	448	445	444	444	443	444	447	449	447	450	448	445	443	438	428	417	411	412	413	422	429	435	437
15 Q	439	443	443	442	441	440	447	437	441	440	448	452	451	452	451	443	433	421	413	415	421	429	436	440	438
16	441	441	443	444	443	444	453	450	449	451	453	453	453	450	445	435	422	427	430	426	422	428	429	429	440
17	427	434	440	441	439	437	438	438	441	444	448	449	452	452	451	447	440	432	428	423	419	420	414	414	436
18	418	426	433	436	438	438	434	430	425	436	432	451	446	443	444	440	433	427	423	424	431	443	440	446	435
19	454	450	446	450	455	453	445	451	445	442	440	442	443	444	441	437	424	413	411	413	421	427	429	430	438
20	434	435	442	443	443	445	444	445	443	446	446	449	450	450	447	441	435	429	420	421	417	419	428	436	438
21	441	443	447	449	449	450	448	450	454	441	445	446	445	447	445	433	429	424	424	422	431	436	435	439	441
22	442	441	441	442	441	439	436	441	441	445	447	449	444	440	443	437	425	410	410	413	424	430	433	437	435
23	440	445	443	442	442	444	444	448	445	449	451	451	452	451	448	443	436	432	428	427	423	421	430	434	440
24	438	443	434	425	431	437	437	430	424	439	447	447	453	449	447	441	432	426	418	417	423	434	433	441	435
25	450	454	448	439	433	435	438	441	442	446	447	448	449	449	450	449	441	432	424	419	418	416	427	431	439
26 Q	438	442	446	444	444	442	443	441	435	443	447	447	448	449	449	448	441	431	424	417	422	428	433	436	439
27	447	449	454	451	449	447	448	446	443	445	447	446	449	449	451	451	441	429	418	411	390	394	413	423	437
28	437	433	433	432	439	440	442	441	438	441	444	448	449	448	447	439	429	425	417	410	402	409	423	429	433
29	432	439	439	440	444	446	445	445	445	447	448	449	450	449	448	444	433	422	412	406	416	422	427	433	437
30 Q	440	444	444	447	446	447	446	446	445	445	445	445	446	446	447	441	433	424	417	416	424	433	441	445	440
31	447	451	448	440	439	436	430	430	428	436	437	448	435	443	446	443	435	424	410	404	408	416	422	434	433
MEAN	435	435	435	435	436	435	435	436	434	438	439	441	442	444	441	436	428	420	413	412	414	419	425	431	432

DECLINATION

MEAN VALUES FOR PERIODS OF SIXTY MINUTES, UNIVERSAL TIME

TABLE 29 VICTORIA D = 22 DEG 00.0 MIN EAST + OCTOBER 1969

HOUR =	00 TO 01	01 TO 02	02 TO 03	03 TO 04	04 TO 05	05 TO 06	06 TO 07	07 TO 08	08 TO 09	09 TO 10	10 TO 11	11 TO 12	12 TO 13	13 TO 14	14 TO 15	15 TO 16	16 TO 17	17 TO 18	18 TO 19	19 TO 20	20 TO 21	21 TO 22	22 TO 23	23 TO 24	MEAN
DAY																									
1 D	26.9	28.2	29.6	27.8	28.6	29.0	27.8	29.3	29.8	26.5	25.8	26.9	22.4	28.2	30.7	31.8	32.2	27.6	27.3	30.0	29.8	28.4	26.4	25.3	28.2
2 D	25.1	32.4	25.9	25.9	26.8	32.2	32.2	35.2	39.3	34.5	33.0	28.3	23.0	28.0	21.2	18.1	20.5	26.9	29.3	28.1	27.7	27.3	26.6	26.3	28.1
3 D	26.7	27.2	33.4	32.3	28.0	28.6	27.8	28.3	27.5	25.3	26.5	27.9	20.8	21.9	18.6	18.5	23.2	30.4	26.3	26.8	25.6	25.3	26.0	26.3	26.2
4	26.7	27.2	27.2	26.9	27.3	27.5	28.3	27.8	27.5	24.8	28.1	27.7	27.0	27.8	27.5	29.1	31.3	30.0	28.5	28.0	26.6	26.1	25.2	25.1	27.5
5	26.9	25.5	25.9	26.3	26.2	28.1	28.1	26.8	28.3	29.0	29.1	29.1	27.5	27.2	28.2	30.4	31.0	32.1	31.7	26.9	24.6	23.0	23.4	23.7	27.5
6 D	24.5	25.7	26.2	30.3	26.3	27.1	28.3	27.4	26.7	27.3	23.2	26.9	26.6	26.7	24.8	26.9	27.4	23.9	20.6	20.2	21.2	21.5	23.7	24.7	25.3
7	25.2	25.4	25.1	30.3	26.0	26.8	27.7	25.9	25.7	26.2	27.1	27.6	26.3	27.1	28.5	29.2	29.4	29.4	29.2	27.9	25.2	23.0	22.6	23.3	26.7
8 Q	24.4	25.1	25.8	26.0	26.1	26.0	26.3	26.1	27.7	26.6	26.6	26.9	26.9	27.1	27.0	28.3	28.9	29.4	28.9	26.0	24.2	22.7	22.4	23.0	26.2
9	24.3	25.1	25.5	25.8	26.1	26.6	25.8	26.5	26.1	26.6	26.4	26.9	27.0	27.8	27.7	28.7	30.6	29.8	28.7	26.0	24.6	20.8	22.8	24.0	26.3
10 D	24.5	24.4	25.1	27.0	26.7	28.0	28.9	26.6	28.1	33.8	30.7	34.0	27.9	26.2	29.9	29.4	27.5	27.0	29.0	25.7	23.8	22.9	23.8	24.5	27.3
11	25.1	25.6	26.0	25.7	25.9	28.7	28.8	28.0	27.3	26.3	23.1	27.6	30.2	27.5	31.4	30.5	31.2	30.7	27.7	25.3	23.3	22.8	24.1	24.4	27.0
12	24.6	25.6	27.6	26.0	26.1	25.9	26.1	22.2	26.8	29.0	30.0	30.5	29.9	32.6	29.3	26.9	28.2	29.6	29.2	27.1	25.2	23.9	24.0	24.5	27.1
13	25.5	26.1	26.0	26.4	26.2	26.9	25.8	26.1	25.3	26.3	26.3	29.1	28.8	28.9	29.0	30.9	30.8	29.9	28.6	26.8	24.0	23.5	23.7	24.2	26.9
14 Q	24.7	25.3	26.0	26.4	26.4	26.3	26.3	26.1	26.1	26.0	26.4	27.0	26.9	27.8	28.8	30.5	31.6	30.6	27.1	23.9	22.2	22.2	23.1	24.1	26.3
15 Q	24.8	25.8	26.4	26.6	26.6	26.6	25.7	25.5	26.0	27.0	27.3	26.8	29.8	30.1	30.0	31.0	31.7	31.5	30.0	28.1	26.1	25.2	25.0	25.6	27.5
16	25.7	25.3	25.5	26.1	25.5	25.7	24.3	25.4	26.0	26.1	26.7	27.0	27.2	27.9	28.9	30.6	31.4	26.5	24.0	23.1	21.1	21.2	22.1	23.4	25.7
17	24.6	24.9	25.3	26.0	26.0	26.2	26.1	26.2	26.2	26.7	27.0	27.2	26.9	27.5	28.3	30.2	31.5	31.8	29.6	27.3	24.6	22.5	21.3	22.1	26.5
18	23.4	23.9	25.8	26.0	26.2	26.3	29.9	27.3	27.5	28.6	25.5	27.5	27.8	27.3	27.6	28.8	29.4	30.1	27.9	24.4	22.9	22.4	23.7	23.9	26.4
19	23.8	23.6	24.1	24.5	24.6	25.1	25.8	27.9	27.5	27.2	27.8	29.6	26.8	30.5	28.3	29.2	30.4	30.1	26.7	23.8	22.3	21.8	23.1	24.0	26.2
20	24.5	25.3	25.1	25.4	25.6	26.2	25.9	26.5	26.8	26.9	27.1	26.9	27.0	27.3	28.0	29.1	30.2	31.0	29.7	26.9	24.1	23.4	23.5	24.7	26.5
21	24.1	24.3	24.9	25.5	25.7	26.0	26.2	26.7	28.0	30.1	29.6	27.8	27.6	28.1	28.7	29.8	28.7	29.0	26.0	23.5	22.5	23.0	24.7	25.5	26.5
22	25.9	25.2	25.4	25.9	25.7	27.8	25.0	26.1	26.3	26.6	27.1	28.4	29.3	27.9	27.2	29.7	30.9	31.9	29.5	26.8	25.2	25.6	26.0	25.5	27.1
23	25.9	24.6	25.5	25.9	26.2	26.5	26.8	26.0	26.2	26.5	26.7	26.8	27.0	27.1	27.6	28.7	29.8	30.3	28.5	26.1	23.9	24.2	23.9	24.5	26.5
24	24.1	25.2	25.8	26.3	26.9	31.4	28.4	30.6	30.0	30.0	27.8	28.9	29.9	28.0	29.6	30.4	29.2	29.0	28.1	25.9	25.1	25.1	25.8	24.9	27.8
25	24.6	25.2	25.6	26.1	26.5	29.0	25.7	26.2	26.1	26.6	27.2	27.5	27.2	27.3	27.7	29.3	30.0	30.9	30.5	27.5	25.1	25.2	24.1	24.9	26.9
26 Q	25.0	25.3	25.4	25.9	25.9	26.0	27.9	28.8	27.8	26.6	26.6	26.9	27.0	27.4	27.6	29.1	30.2	30.9	29.7	28.2	24.8	23.3	23.2	23.9	26.8
27	24.5	25.1	25.7	26.1	26.0	26.1	26.0	26.3	26.8	28.0	27.7	27.6	27.3	26.7	27.6	30.0	31.9	32.6	30.9	28.7	25.8	22.8	21.0	22.3	26.8
28	22.1	23.3	23.9	24.9	25.8	26.5	26.5	27.3	27.2	27.5	26.1	26.4	26.5	27.4	28.2	29.7	30.7	30.7	30.8	26.6	23.5	21.7	22.6	23.7	26.2
29	25.2	25.5	25.6	26.8	27.4	26.3	26.3	26.2	26.2	26.2	26.4	26.6	26.8	27.0	27.6	28.9	30.0	30.7	29.6	25.8	22.4	22.0	22.6	24.5	26.4
30 Q	24.7	25.5	25.8	26.1	26.5	26.5	27.0	26.3	25.7	25.8	26.2	26.5	26.8	27.4	28.0	29.0	30.3	31.9	30.1	27.1	24.5	23.9	23.6	24.2	26.6
31	24.7	25.1	26.2	27.0	27.8	26.4	27.0	28.1	29.3	29.0	27.4	26.8	28.1	27.5	27.9	28.5	28.8	30.9	29.7	27.9	25.4	24.4	23.9	24.0	27.2
MEAN	24.9	25.5	26.0	26.6	26.4	27.2	27.1	27.1	27.5	27.5	27.2	27.8	27.1	27.7	27.8	28.7	29.6	29.9	28.5	26.3	24.4	23.6	23.8	24.4	26.8

VERTICAL INTENSITY

MEAN VALUES FOR PERIODS OF SIXTY MINUTES, UNIVERSAL TIME

TABLE 30 VICTORIA Z = 53,000 GAMMA + OCTOBER 1969

HOUR =	00 TO 01	01 TO 02	02 TO 03	03 TO 04	04 TO 05	05 TO 06	06 TO 07	07 TO 08	08 TO 09	09 TO 10	10 TO 11	11 TO 12	12 TO 13	13 TO 14	14 TO 15	15 TO 16	16 TO 17	17 TO 18	18 TO 19	19 TO 20	20 TO 21	21 TO 22	22 TO 23	23 TO 24	MEAN
DAY																									
1 D	151	150	151	151	149	148	134	125	132	133	106	97	78	115	127	127	133	134	129	130	133	135	137	137	131
2 D	143	152	148	143	142	135	122	122	93	55	38	60	52	89	81	71	90	123	134	135	139	141	146	145	112
3 D	148	147	147	144	144	140	135	135	133	127	124	117	92	81	72	78	87	98	103	102	110	118	127	131	118
4	132	134	136	134	134	129	131	131	132	124	123	123	123	125	129	134	134	129	127	126	124	125	131	133	129
5	137	138	137	137	136	135	136	133	131	126	121	124	128	128	132	135	133	132	129	128	124	127	125	127	131
6 D	131	135	137	138	140	143	142	139	140	134	120	117	117	118	120	122	124	121	118	114	117	123	125	128	128
7	131	135	137	141	144	141	140	127	126	125	125	126	127	128	131	132	130	131	126	118	112	113	118	124	129
8 Q	131	130	131	131	130	131	131	130	129	128	126	126	127	125	125	127	127	123	119	114	109	111	117	122	125
9	128	128	130	131	131	131	129	128	131	130	129	127	128	127	129	131	132	126	115	112	106	110	118	123	125
10 D	123	128	128	140	143	147	143	141	130	124	95	101	104	101	117	122	120	121	120	118	120	123	125	130	124
11	136	136	139	140	137	138	138	137	138	138	118	121	121	109	109	120	128	125	115	112	116	123	128	130	127
12	132	133	137	136	134	134	134	116	111	125	123	122	110	100	96	101	105	113	116	118	120	124	126	129	121
13	128	128	129	128	128	131	130	127	128	130	124	107	115	120	125	128	128	127	122	116	117	118	124	127	124
14 Q	128	128	128	129	127	128	127	129	128	129	128	128	127	127	128	129	132	128	124	119	119	121	125	128	127
15 Q	129	130	129	128	127	128	125	124	127	127	128	122	121	123	125	126	128	127	124	120	117	124	125	127	125
16	127	126	126	127	126	125	119	119	125	127	126	127	125	125	123	126	127	120	115	114	117	122	122	125	123
17	130	130	129	128	127	127	127	127	129	128	127	128	128	126	126	130	130	128	119	116	116	120	121	130	126
18	136	138	137	136	133	134	133	132	134	133	129	122	127	130	130	131	134	132	118	114	116	122	127	128	129
19	129	130	129	129	128	127	127	130	120	128	130	129	114	108	120	128	133	130	121	120	124	129	126	124	126
20	131	131	131	134	132	132	129	131	128	127	128	128	127	127	127	132	133	133	125	117	118	124	126	127	128
21	130	129	131	130	130	128	127	128	125	118	124	127	128	127	127	130	128	125	120	118	122	126	126	126	126
22	127	128	127	128	128	131	132	131	129	127	121	125	121	123	127	130	130	129	122	117	117	120	118	118	125
23	121	124	126	127	126	127	127	127	126	126	126	125	123	124	124	127	129	125	121	114	112	117	119	120	123
24	124	128	128	131	136	138	139	139	141	136	131	128	114	114	120	124	124	124	117	117	116	119	120	123	126
25	124	125	123	124	126	129	129	130	128	128	124	125	125	125	126	129	130	131	121	109	109	115	117	120	124
26 Q	124	127	125	127	125	127	128	128	128	129	128	128	125	125	126	129	129	130	122	109	110	117	118	122	124
27	125	125	126	126	125	125	126	129	128	129	123	125	124	122	120	128	130	130	128	122	112	119	124	126	125
28	130	131	130	132	132	131	132	131	131	132	130	129	127	125	127	129	130	129	123	117	113	118	122	123	127
29	127	127	127	129	130	129	127	127	127	128	127	126	126	125	126	127	129	126	119	112	114	116	122	128	125
30 Q	129	128	127	128	125	126	125	125	124	124	125	125	125	125	125	126	128	128	121	117	120	124	122	122	125
31	124	126	124	124	124	126	126	127	121	123	119	105	101	108	115	118	122	125	122	119	119	120	123	126	120
MEAN	131	132	132	133	132	132	131	129	128	126	121	120	117	119	120	123	126	126	121	117	117	121	124	127	125

HORIZONTAL INTENSITY

MEAN VALUES FOR PERIODS OF SIXTY MINUTES, UNIVERSAL TIME

TABLE 31 VICTORIA H = 18,500 GAMMA + NOVEMBER 1969

HOUR =	00 TO 01	01 TO 02	02 TO 03	03 TO 04	04 TO 05	05 TO 06	06 TO 07	07 TO 08	08 TO 09	09 TO 10	10 TO 11	11 TO 12	12 TO 13	13 TO 14	14 TO 15	15 TO 16	16 TO 17	17 TO 18	18 TO 19	19 TO 20	20 TO 21	21 TO 22	22 TO 23	23 TO 24	MEAN
DAY																									
1 Q	436	435	437	440	441	441	442	443	444	446	445	447	448	447	449	449	441	430	409	409	409	418	425	432	436
2	435	437	441	438	441	441	439	442	442	444	448	447	448	450	444	432	427	432	425	407	416	418	425	423	435
3 D	422	424	431	436	432	432	415	416	422	431	440	441	440	439	437	431	440	436	422	412	400	404	414	423	427
4	435	440	438	424	431	437	438	440	440	438	444	439	443	443	443	445	442	434	418	409	404	410	417	423	432
5	429	430	435	440	443	437	437	440	440	449	446	453	450	451	447	444	447	451	440	433	430	435	439	448	441
6 Q	450	451	448	448	446	447	447	450	450	451	451	450	450	449	448	442	436	433	427	425	431	432	441	454	444
7	456	458	443	443	435	426	424	427	433	438	446	443	452	445	448	450	447	439	427	423	418	420	424	430	437
8	433	437	438	435	432	432	437	435	439	442	442	443	445	448	451	446	446	419	412	405	414	412	415	418	432
9 D	428	437	440	439	426	413	411	415	416	374	413	440	419	422	391	400	429	417	414	414	418	426	435	441	420
10 D	445	437	437	432	424	430	447	425	432	434	441	432	435	429	436	428	417	407	384	356	372	405	412	424	422
11	434	434	435	435	432	432	434	436	437	434	432	433	442	444	437	423	428	421	409	399	404	414	430	437	429
12	430	424	441	442	442	443	438	438	439	441	440	439	442	440	440	437	427	410	414	412	411	417	424	430	432
13	442	445	446	446	444	442	443	441	442	438	438	441	445	445	444	444	438	428	419	414	414	420	426	433	437
14 Q	442	443	442	443	440	442	439	438	442	442	441	443	444	444	442	440	435	427	416	412	418	426	432	435	436
15 Q	441	445	446	446	446	446	444	444	445	445	447	449	448	448	447	444	438	434	429	424	424	426	432	440	441
16	447	452	451	453	452	450	450	448	447	448	448	451	452	452	453	452	449	439	433	427	426	429	437	446	446
17	451	456	455	454	456	455	452	451	450	450	450	450	449	449	448	448	444	438	436	428	429	436	437	442	446
18	447	449	453	451	450	453	449	447	448	451	451	450	450	450	451	449	440	428	430	432	424	421	427	436	443
19	443	449	450	450	450	449	444	444	444	448	450	451	449	452	451	449	444	437	431	431	417	414	420	421	441
20	430	439	438	440	441	445	441	442	444	445	445	444	445	447	447	446	448	446	443	438	433	431	434	438	441
21 Q	448	448	445	445	446	445	443	445	449	451	450	452	452	451	448	446	447	441	430	425	423	426	433	439	443
22	444	447	449	451	453	446	441	445	451	451	454	456	457	454	454	454	449	443	429	421	424	435	443	441	446
23	445	449	451	450	448	450	448	449	450	453	452	453	455	455	454	447	436	426	418	410	407	417	429	436	441
24	443	448	444	444	443	442	442	444	447	446	451	452	451	454	452	452	447	435	429	422	410	416	427	436	441
25	446	450	452	452	450	450	442	441	439	442	445	449	453	452	448	444	439	438	430	422	416	416	423	428	440
26	438	439	432	430	435	439	443	439	441	444	445	446	450	446	445	455	452	463	436	422	409	411	421	433	438
27 D	441	441	440	437	412	408	407	417	414	419	430	420	426	443	434	421	432	415	406	407	407	407	408	397	420
28	410	417	420	425	421	422	422	424	422	437	437	438	437	437	436	443	438	428	428	425	406	404	401	418	425
29	427	430	431	437	435	433	426	422	422	432	434	435	433	430	441	438	430	416	394	388	375	379	399	399	420
30 D	406	399	407	410	423	421	415	418	411	426	426	430	430	431	433	428	423	418	415	399	398	398	405	414	416
MEAN	437	440	441	441	439	438	437	437	438	440	443	444	445	445	443	441	439	431	422	415	413	417	425	431	435

DECLINATION

MEAN VALUES FOR PERIODS OF SIXTY MINUTES, UNIVERSAL TIME

TABLE 32 VICTORIA D = 22 DEG 00.0 MIN EAST + NOVEMBER 1969

HOUR =	00 TO 01	01 TO 02	02 TO 03	03 TO 04	04 TO 05	05 TO 06	06 TO 07	07 TO 08	08 TO 09	09 TO 10	10 TO 11	11 TO 12	12 TO 13	13 TO 14	14 TO 15	15 TO 16	16 TO 17	17 TO 18	18 TO 19	19 TO 20	20 TO 21	21 TO 22	22 TO 23	23 TO 24	MEAN
DAY																									
1 Q	24.1	25.1	26.0	26.3	26.2	26.2	26.1	26.1	26.1	26.2	26.1	26.5	26.4	27.0	27.5	29.3	32.0	33.0	31.3	29.5	26.4	25.1	24.4	24.1	27.0
2	24.7	23.6	25.5	26.1	26.3	26.4	26.4	26.8	28.2	28.7	25.8	27.0	26.5	26.3	24.8	23.4	23.0	26.6	30.6	29.5	26.5	25.2	23.9	24.7	26.1
3 D	25.1	24.4	25.7	26.3	26.5	29.3	29.6	30.9	26.3	27.0	26.7	27.0	26.8	25.2	26.1	24.7	26.5	30.2	30.2	28.2	28.0	25.6	24.8	24.6	26.9
4	24.3	25.0	25.4	26.5	26.4	26.5	26.6	28.4	27.8	25.8	26.0	27.9	25.8	25.7	26.1	27.9	28.8	30.3	28.7	26.7	25.9	24.3	23.4	23.6	26.4
5	23.7	24.7	25.9	25.9	26.6	26.4	26.0	26.6	26.8	27.2	26.1	26.5	27.0	27.1	26.4	25.2	27.7	30.0	28.4	27.2	26.0	25.3	24.7	24.6	26.3
6 Q	25.2	25.6	26.0	26.4	26.4	26.3	26.2	26.3	25.6	26.1	26.0	26.5	26.3	26.9	27.4	29.0	30.5	30.2	28.5	27.3	25.4	24.6	24.6	23.8	26.5
7	24.1	23.9	26.6	25.4	25.0	26.8	27.2	28.6	28.0	31.4	27.6	26.9	27.3	28.3	29.0	30.0	29.5	29.7	26.6	25.7	23.9	24.2	24.0	25.3	26.9
8	25.9	26.1	26.8	26.7	27.8	26.5	28.4	26.5	25.9	25.8	25.3	25.7	26.7	27.3	26.4	23.1	30.0	30.5	24.9	25.7	23.7	22.1	23.4	24.6	26.1
9 D	25.3	26.2	26.8	26.8	26.3	28.0	41.1	33.9	30.5	18.7	22.7	30.7	28.0	25.6	19.6	22.6	27.4	31.6	26.3	22.6	23.7	24.2	24.7	25.3	26.6
10 D	24.8	26.7	27.1	27.2	27.7	25.4	37.2	29.5	26.1	23.8	26.1	25.2	24.5	23.6	30.5	32.2	31.7	30.2	28.1	22.4	20.9	24.5	24.3	25.5	26.9
11	25.4	26.6	26.6	27.1	28.0	27.7	27.0	25.8	26.8	25.3	26.9	24.4	26.6	27.6	26.7	26.3	29.9	31.3	29.6	27.8	26.8	25.5	24.4	24.7	26.9
12	24.5	27.1	26.8	26.6	28.1	28.0	26.6	26.5	26.3	25.1	26.5	27.0	26.9	26.5	27.2	29.7	32.1	31.3	28.4	26.6	25.3	24.2	24.0	23.7	26.9
13	24.8	25.1	26.6	26.5	27.0	26.8	26.7	26.4	26.6	27.1	26.8	26.9	27.4	27.7	27.8	29.9	30.2	28.9	26.7	25.8	25.1	23.9	24.0	24.1	26.6
14 Q	24.2	24.6	25.6	26.3	26.3	26.6	26.6	26.3	26.5	26.2	26.4	26.7	26.7	27.6	27.7	28.9	29.9	30.2	29.1	27.5	25.8	24.5	24.2	24.5	26.6
15 Q	25.0	25.5	26.3	26.7	26.7	26.7	26.6	26.5	26.5	26.4	26.6	26.2	26.8	27.1	27.5	28.7	30.2	30.5	28.7	26.9	25.4	24.9	24.3	23.8	26.7
16	24.1	25.5	26.0	26.4	26.6	26.6	26.6	26.7	26.3	26.2	26.2	26.4	26.4	27.0	27.5	28.4	30.5	31.7	29.3	28.2	25.6	24.8	24.5	25.0	26.8
17	24.9	25.0	25.6	25.9	26.3	26.5	26.4	26.8	26.5	26.7	26.9	26.8	27.0	27.4	27.0	28.8	30.6	30.9	28.1	27.9	25.8	24.0	24.1	24.3	26.7
18	25.1	25.0	25.1	26.1	26.3	26.6	26.4	27.1	27.2	26.8	27.9	27.8	27.8	27.4	27.4	28.8	30.4	31.7	27.8	26.7	26.5	26.1	24.9	24.3	27.0
19	24.8	25.2	25.7	25.7	26.0	26.2	26.9	26.5	27.0	26.7	26.6	27.4	26.5	24.8	27.1	28.5	29.3	29.4	27.0	25.6	25.6	23.4	25.3	25.8	26.4
20	24.8	25.9	26.8	26.2	26.4	26.5	26.5	27.0	26.6	27.4	27.5	27.1	26.8	27.1	27.3	27.6	28.0	28.6	28.4	27.8	27.0	26.5	25.1	25.0	26.8
21 Q	25.2	25.7	26.0	26.3	26.6	26.4	26.1	26.2	26.6	26.6	26.7	26.7	26.6	27.4	27.1	27.7	28.8	30.1	29.5	28.1	26.9	25.0	24.2	24.6	26.7
22	25.6	25.9	26.0	25.7	24.9	24.2	25.4	25.0	25.1	25.1	25.7	26.4	26.7	27.7	27.4	28.3	29.3	30.8	28.6	26.6	23.9	22.6	24.1	25.0	26.1
23	25.2	25.6	26.3	26.4	26.5	26.1	26.1	25.9	25.8	25.9	26.2	26.3	26.6	27.2	27.9	29.2	30.5	30.7	28.0	25.7	23.4	23.6	24.3	24.6	26.4
24	25.5	26.2	26.8	26.7	26.4	26.4	26.5	26.0	26.2	23.0	24.7	26.6	27.1	27.8	26.2	28.9	30.3	30.0	28.4	27.3	26.2	24.4	23.8	24.7	26.5
25	25.3	26.0	26.6	26.9	26.6	26.7	27.9	28.3	27.4	26.8	26.7	25.8	27.1	29.5	28.7	29.1	29.4	31.9	28.4	27.9	25.8	24.3	22.6	21.8	27.0
26	22.6	24.2	24.6	24.7	26.9	27.9	27.1	27.2	26.3	26.3	26.4	26.9	27.4	27.1	27.5	30.0	29.7	25.0	23.6	23.4	24.9	24.8	24.5	24.9	26.0
27 D	26.1	26.8	27.5	27.3	29.3	39.0	30.4	29.5	27.6	27.0	30.2	29.0	19.0	24.9	26.4	25.3	28.5	30.2	26.7	23.3	24.9	24.9	24.3	24.8	27.2
28	25.7	26.0	26.2	27.5	28.6	27.9	28.7	31.8	25.3	24.4	25.9	26.3	26.3	24.5	26.2	27.7	28.9	29.3	30.2	26.1	22.6	21.7	22.8	23.0	26.4
29	24.9	25.1	26.3	27.0	27.3	27.6	28.6	34.1	28.1	26.5	24.0	23.4	26.3	19.7	25.2	27.9	27.8	29.9	30.7	28.7	26.5	24.3	23.5	23.3	26.5
30 D	24.9	28.2	27.7	28.7	28.4	27.8	26.6	26.9	26.5	26.2	25.6	26.0	26.8	26.6	26.3	24.8	20.3	22.7	25.1	27.4	26.6	25.5	25.4	24.8	26.1
MEAN	24.9	25.5	26.2	26.5	26.8	27.2	27.8	27.7	26.7	26.1	26.3	26.7	26.5	26.5	26.9	27.7	29.1	29.9	28.2	26.7	25.4	24.5	24.2	24.4	26.6

VERTICAL INTENSITY

MEAN VALUES FOR PERIODS OF SIXTY MINUTES, UNIVERSAL TIME

TABLE 33 VICTORIA Z = 53,000 GAMMA + NOVEMBER 1969

HOUR =	00 TO 01	01 TO 02	02 TO 03	03 TO 04	04 TO 05	05 TO 06	06 TO 07	07 TO 08	08 TO 09	09 TO 10	10 TO 11	11 TO 12	12 TO 13	13 TO 14	14 TO 15	15 TO 16	16 TO 17	17 TO 18	18 TO 19	19 TO 20	20 TO 21	21 TO 22	22 TO 23	23 TO 24	MEAN
DAY																									
1 Q	126	126	128	128	125	125	123	124	124	124	125	124	124	125	125	127	128	126	121	118	114	116	119	123	124
2	129	128	128	128	128	126	125	125	124	120	119	120	122	125	124	122	119	121	119	118	120	121	122	124	123
3 D	136	139	138	134	136	134	138	137	125	118	126	127	127	128	124	124	128	133	129	131	129	130	130	132	131
4	131	132	132	132	135	135	132	130	127	120	110	110	120	124	125	132	131	130	126	126	126	126	128	130	127
5	131	132	133	134	134	134	132	129	127	126	126	126	125	125	125	123	122	122	116	115	116	117	118	120	125
6 Q	122	125	124	125	124	123	122	122	121	120	121	120	121	121	122	124	125	122	116	115	113	113	116	118	121
7	120	120	120	123	124	125	125	127	116	114	116	111	105	110	122	128	128	126	124	124	126	127	131	130	122
8	132	132	131	130	129	129	125	119	121	119	116	118	121	125	125	119	122	122	116	107	117	122	127	136	123
9 D	137	135	133	132	133	122	120	126	124	67	41	70	83	99	79	95	118	127	115	111	119	126	130	130	111
10 D	127	126	131	136	142	151	133	138	137	135	128	109	89	102	124	133	131	128	122	129	139	139	139	141	130
11	138	137	134	134	132	133	132	128	124	124	121	123	127	126	126	126	133	130	125	124	127	126	129	130	129
12	128	130	133	131	131	132	130	130	130	127	123	127	128	128	128	133	133	129	127	128	126	126	128	128	129
13	130	132	130	129	127	128	128	127	126	125	128	128	130	128	126	128	127	124	122	122	127	131	133	131	128
14 Q	131	131	128	129	128	127	127	128	128	128	128	128	128	127	127	129	129	129	128	126	127	128	128	130	128
15 Q	132	131	130	128	127	127	125	125	126	127	126	127	126	126	126	127	129	126	124	124	127	128	128	128	127
16	131	129	128	128	125	125	124	123	123	123	122	124	124	125	126	126	128	128	124	119	122	125	127	125	125
17	127	129	127	126	125	125	123	124	123	123	124	124	124	125	124	127	129	127	125	122	119	119	116	120	124
18	123	126	126	125	123	123	122	122	121	123	122	122	121	121	121	125	123	123	123	119	116	115	116	119	122
19	124	124	125	125	124	125	125	126	124	124	123	123	121	117	117	119	119	118	113	110	109	111	117	122	120
20	123	131	133	133	131	129	127	127	127	124	124	123	123	124	124	124	124	122	116	112	112	112	115	118	123
21 Q	119	121	122	123	122	123	122	123	121	123	120	121	120	119	120	121	123	121	122	120	120	117	120	119	121
22	121	122	122	124	125	127	128	129	125	125	122	122	121	119	117	117	119	121	117	113	113	119	120	118	121
23	122	122	123	123	121	123	123	123	122	121	120	120	120	119	119	123	126	127	122	118	118	122	125	123	122
24	125	125	125	124	124	123	123	124	122	116	110	116	117	119	119	120	122	122	122	123	123	124	124	122	121
25	122	125	125	124	124	124	124	125	124	125	124	120	113	117	119	123	121	120	115	114	116	117	118	122	121
26	126	132	130	134	135	137	134	133	131	130	128	128	126	125	125	129	128	126	115	106	108	113	118	121	126
27 D	122	123	124	122	125	132	127	114	94	68	63	94	84	68	83	89	108	109	106	106	112	117	122	125	106
28	133	136	135	134	133	133	131	129	124	116	122	124	123	121	121	125	128	124	121	113	106	116	123	126	125
29	131	133	132	130	128	127	126	122	123	124	123	122	122	109	113	121	124	120	121	127	128	129	135	134	125
30 D	142	148	147	145	143	139	122	119	111	113	126	132	131	133	131	130	122	116	115	119	123	127	130	133	129
MEAN	128	129	129	129	129	129	127	126	123	119	118	119	119	119	120	123	125	124	120	119	120	122	124	126	124

HORIZONTAL INTENSITY

MEAN VALUES FOR PERIODS OF SIXTY MINUTES, UNIVERSAL TIME

TABLE 34 VICTORIA   H = 18,500 GAMMA +   DECEMBER 1969

HOUR =	00 TO 01	01 TO 02	02 TO 03	03 TO 04	04 TO 05	05 TO 06	06 TO 07	07 TO 08	08 TO 09	09 TO 10	10 TO 11	11 TO 12	12 TO 13	13 TO 14	14 TO 15	15 TO 16	16 TO 17	17 TO 18	18 TO 19	19 TO 20	20 TO 21	21 TO 22	22 TO 23	23 TO 24	MEAN
DAY																									
1	422	423	430	431	431	431	427	428	432	431	429	427	437	436	434	434	433	430	420	408	398	401	410	422	425
2	431	432	434	432	428	425	427	429	438	434	435	434	432	436	441	430	435	436	427	413	406	409	416	424	429
3	430	433	432	432	428	425	428	431	435	435	435	432	434	436	434	437	436	437	426	412	407	410	415	425	429
4	447	442	442	445	450	450	446	446	442	443	439	445	441	433	441	451	441	435	428	423	424	430	430	436	440
5 D	442	440	440	440	436	427	440	439	439	438	450	427	448	448	452	447	442	436	437	423	407	403	418	421	435
6 D	420	423	405	417	424	399	420	424	425	427	429	429	434	429	420	437	440	435	423	413	407	415	420	426	423
7	436	436	438	437	435	433	428	432	433	434	439	439	440	442	440	440	441	440	435	425	422	419	425	432	434
8	440	441	437	439	436	434	434	434	435	440	439	442	440	441	442	439	438	441	433	426	419	426	431	428	436
9 D	430	435	431	441	439	442	438	439	439	443	440	443	438	441	439	438	437	439	434	422	417	419	423	431	435
10	435	440	437	436	435	433	430	432	433	436	436	440	436	439	438	442	440	440	431	421	404	400	402	409	430
11	413	431	437	433	432	432	437	442	434	434	435	438	445	446	444	442	439	429	420	418	414	421	427	437	433
12	444	441	437	427	432	430	426	429	431	433	435	435	436	441	440	440	439	434	427	414	412	420	428	439	432
13 Q	448	449	446	443	445	440	440	440	439	441	443	444	446	447	445	448	443	434	425	416	417	425	435	442	439
14	446	448	450	448	447	448	444	443	443	440	441	443	441	443	440	441	440	427	417	410	411	420	427	435	437
15	445	447	447	448	447	447	446	442	444	441	449	446	447	448	446	446	443	431	421	410	410	420	429	432	439
16 D	430	421	436	438	437	437	429	433	428	431	431	431	435	440	441	432	431	429	414	412	409	414	417	429	429
17	434	426	432	440	440	442	441	441	438	438	434	434	438	438	437	442	439	441	429	417	409	418	422	429	433
18	431	436	437	440	441	442	441	443	440	442	439	439	440	440	441	442	441	437	428	419	418	424	430	435	436
19	444	447	443	442	440	440	439	440	440	441	439	446	444	444	444	441	442	439	429	432	430	438	443	444	440
20 Q	452	451	451	454	449	448	447	447	446	448	448	447	446	448	445	449	446	442	431	424	426	434	437	441	444
21 Q	452	449	445	446	445	445	447	448	445	446	445	445	447	447	446	445	445	444	437	430	428	428	433	436	443
22	450	451	450	451	448	449	441	431	430	437	439	440	440	453	451	451	456	450	441	436	430	428	431	435	442
23 D	442	448	446	443	433	432	432	428	432	437	429	434	436	436	423	440	440	433	422	427	421	423	419	420	432
24	420	413	429	436	437	437	435	433	434	436	438	438	443	439	436	437	434	436	428	418	417	411	420	428	431
25	434	438	435	435	430	438	428	429	427	427	432	437	438	433	436	429	431	427	421	415	420	424	425	429	430
26	434	437	438	435	435	432	433	441	433	434	437	442	445	448	442	448	436	446	432	417	408	415	427	427	434
27	427	429	422	428	438	438	435	432	434	431	439	438	439	440	439	438	432	426	415	410	413	415	417	430	429
28	439	439	440	440	437	438	439	440	438	441	441	441	441	441	440	442	446	435	430	426	421	424	429	434	437
29	430	438	440	441	442	439	438	438	443	440	439	439	438	442	446	447	443	439	431	425	422	424	427	433	437
30 Q	443	445	444	441	442	440	442	445	442	443	445	444	444	444	448	449	451	443	432	424	426	427	431	437	441
31 Q	450	447	447	445	441	444	443	442	440	440	445	444	444	444	444	449	449	441	436	431	423	420	427	440	441
MEAN	437	438	438	439	438	437	436	437	437	437	439	439	440	441	440	442	440	437	428	420	416	420	425	431	435

DECLINATION

MEAN VALUES FOR PERIODS OF SIXTY MINUTES, UNIVERSAL TIME

TABLE 35 VICTORIA D = 22 DEG 00.0 MIN EAST + DECEMBER 1969

HOUR =	00 TO 01	01 TO 02	02 TO 03	03 TO 04	04 TO 05	05 TO 06	06 TO 07	07 TO 08	08 TO 09	09 TO 10	10 TO 11	11 TO 12	12 TO 13	13 TO 14	14 TO 15	15 TO 16	16 TO 17	17 TO 18	18 TO 19	19 TO 20	20 TO 21	21 TO 22	22 TO 23	23 TO 24	MEAN
DAY																									
1	25.8	26.1	26.5	26.4	26.9	27.0	26.6	26.6	26.4	26.6	26.5	24.3	24.2	26.0	26.9	27.4	27.9	29.3	30.5	29.8	28.1	25.8	24.8	24.5	26.7
2	24.9	25.4	25.8	26.1	26.7	27.0	26.7	26.7	25.1	25.8	25.8	25.9	25.7	26.5	26.9	26.9	29.0	30.1	29.1	28.6	25.9	23.8	23.4	23.9	26.3
3	24.7	25.5	26.1	26.3	26.4	26.7	26.4	26.7	26.1	26.1	26.1	26.1	26.0	26.4	26.9	27.9	29.8	30.6	29.7	27.9	26.3	23.9	23.0	22.2	26.4
4	24.4	25.1	25.5	26.2	25.7	25.2	25.9	26.3	26.0	26.4	25.5	24.8	26.1	26.2	26.2	29.5	28.7	28.8	28.4	27.0	25.7	25.2	24.2	24.3	26.1
5 D	25.3	25.7	26.1	26.5	26.7	27.0	28.4	26.7	25.0	25.5	25.1	25.8	26.7	28.5	25.6	28.2	28.9	19.7	21.1	22.9	23.0	23.1	24.6	23.1	25.4
6 D	24.8	25.5	28.9	27.0	29.1	33.5	30.1	28.9	26.6	23.7	24.1	24.6	27.3	25.7	19.7	24.0	28.8	29.8	28.6	28.4	26.2	25.5	24.8	25.4	26.7
7	25.7	26.3	26.8	26.7	26.5	26.3	27.1	26.4	26.1	24.1	23.6	26.4	26.9	27.5	26.9	27.4	27.1	28.3	28.0	27.4	26.4	25.5	25.6	25.6	26.4
8	25.4	26.1	27.1	26.8	26.5	27.4	26.3	26.1	26.1	25.9	26.1	26.4	26.5	26.9	26.7	26.8	26.7	28.6	28.7	28.3	26.9	25.9	25.2	25.2	26.6
9 D	25.3	25.8	27.2	28.4	26.1	26.3	26.7	26.4	26.4	25.9	26.4	26.5	26.8	26.9	27.6	28.8	28.4	27.5	27.5	27.1	26.1	25.3	24.4	24.3	26.6
10	24.7	26.0	26.4	26.8	26.7	26.7	26.4	26.4	26.3	26.0	25.9	26.1	26.1	26.8	26.8	27.7	28.5	27.6	26.6	27.2	25.3	24.0	23.2	22.2	26.1
11	23.4	24.6	25.8	27.2	26.9	27.5	29.1	28.5	27.0	25.4	26.9	27.1	27.1	28.8	30.4	29.7	31.1	31.3	30.5	28.2	25.7	23.7	23.0	22.7	27.1
12	24.1	25.3	25.1	26.5	26.7	27.2	27.0	27.3	26.2	25.8	26.1	26.8	25.2	26.3	27.1	27.4	28.8	30.1	29.6	27.4	25.1	23.7	23.4	23.7	26.3
13 Q	24.0	25.1	25.9	26.4	26.7	27.2	27.0	26.1	26.0	25.5	25.5	26.2	26.4	26.8	27.1	27.0	28.6	29.9	29.9	28.5	26.3	24.8	23.6	23.3	26.4
14	24.7	24.9	25.8	26.4	26.6	26.5	26.5	26.6	26.1	26.3	26.2	26.2	26.4	26.9	27.6	26.9	29.9	30.7	29.4	28.3	25.8	23.9	22.8	22.5	26.4
15	24.1	24.8	25.5	26.5	26.6	26.8	26.2	26.5	26.2	25.5	25.3	26.6	27.0	26.3	27.0	27.4	29.7	32.0	29.0	27.8	25.5	24.1	23.1	23.1	26.4
16 D	24.0	24.5	25.0	26.7	27.1	27.1	27.0	31.4	25.3	26.9	26.2	26.2	25.7	25.8	26.9	26.5	26.8	30.7	30.0	28.2	25.5	23.8	23.6	23.9	26.4
17	24.3	24.7	25.5	26.1	26.7	26.9	26.8	26.7	26.6	26.8	27.2	26.5	26.8	26.8	26.5	27.2	27.7	29.3	28.8	28.2	26.8	25.9	25.1	24.7	26.6
18	24.7	25.3	25.8	26.2	26.2	26.4	26.3	26.2	26.2	26.5	26.0	26.3	26.3	26.6	26.1	26.9	27.2	28.7	28.8	27.8	25.5	24.6	23.7	23.7	26.2
19	24.6	25.5	25.7	26.2	26.2	26.6	26.0	26.1	26.1	26.7	26.5	26.9	27.4	26.8	26.8	27.5	28.0	29.2	28.6	27.8	26.4	25.4	24.5	23.6	26.5
20 Q	24.1	24.8	25.3	26.0	25.9	26.3	26.2	26.3	26.1	26.1	26.2	26.7	27.0	26.4	26.4	26.8	27.3	28.9	27.9	26.9	25.5	24.5	24.5	23.5	26.1
21 Q	23.9	24.5	25.3	26.0	26.4	25.9	25.6	26.0	26.0	26.0	26.2	26.2	26.2	26.4	26.4	26.8	27.2	28.6	28.7	28.1	26.4	26.0	25.0	24.7	26.2
22	24.3	25.6	25.7	26.0	26.0	25.9	24.2	27.6	27.4	25.8	26.0	27.1	26.5	26.8	28.2	29.1	28.6	28.8	27.0	26.5	26.2	25.5	25.3	25.6	26.5
23 D	25.6	26.1	26.7	26.6	27.0	26.2	26.8	26.1	26.2	25.8	29.6	28.1	28.6	26.8	21.8	26.6	28.8	26.9	22.1	24.1	23.7	24.1	25.6	26.0	26.1
24	25.5	27.0	28.2	27.5	26.6	26.2	25.7	26.4	26.1	26.3	26.3	25.0	27.7	27.5	28.7	29.0	28.3	28.6	27.5	26.5	24.3	24.1	23.9	24.9	26.6
25	26.0	26.6	26.5	27.0	29.5	30.1	27.4	26.8	23.7	27.5	25.9	26.9	27.5	26.5	25.2	27.2	27.4	27.3	25.9	24.7	23.8	23.8	24.0	24.6	26.3
26	26.0	26.3	26.4	26.3	26.4	26.7	26.9	26.5	26.4	26.1	25.4	25.0	27.7	27.9	28.0	28.3	26.1	26.2	28.5	26.5	23.3	23.7	24.3	24.8	26.2
27	27.6	27.6	26.6	28.6	27.3	28.5	27.4	27.0	25.7	26.2	21.0	26.7	27.4	28.0	27.5	27.7	28.9	30.2	30.0	29.1	27.4	26.6	25.6	25.8	27.3
28	26.2	26.0	25.9	26.3	26.6	26.7	26.3	26.4	26.1	26.2	25.3	25.8	26.6	26.9	26.7	27.5	28.5	29.0	28.1	27.5	26.0	25.1	24.8	24.6	26.5
29	25.0	25.9	26.3	26.7	26.7	26.6	26.4	26.4	25.7	25.9	26.2	26.6	26.4	26.8	26.7	26.8	27.5	29.3	29.3	27.7	26.8	26.1	25.3	24.9	26.6
30 Q	24.9	25.5	25.9	26.1	26.8	26.0	26.1	26.4	26.3	26.3	25.6	26.6	26.1	26.4	26.0	26.4	28.0	29.8	30.3	29.1	27.4	26.3	25.0	24.3	26.6
31 Q	25.1	25.3	26.1	26.2	26.2	26.3	26.1	26.1	26.1	26.0	26.0	26.7	25.7	26.1	26.0	26.2	28.1	28.9	28.4	28.7	27.7	26.2	24.2	24.4	26.4
MEAN	24.9	25.6	26.2	26.6	26.7	27.0	26.7	26.8	26.1	26.0	25.8	26.2	26.6	26.8	26.6	27.4	28.3	28.9	28.3	27.5	25.8	24.8	24.3	24.2	26.4

VERTICAL INTENSITY

MEAN VALUES FOR PERIODS OF SIXTY MINUTES, UNIVERSAL TIME

TABLE 36 VICTORIA Z = 53,000 GAMMA + DECEMBER 1969

HOUR =	00 TO 01	01 TO 02	02 TO 03	03 TO 04	04 TO 05	05 TO 06	06 TO 07	07 TO 08	08 TO 09	09 TO 10	10 TO 11	11 TO 12	12 TO 13	13 TO 14	14 TO 15	15 TO 16	16 TO 17	17 TO 18	18 TO 19	19 TO 20	20 TO 21	21 TO 22	22 TO 23	23 TO 24	MEAN
DAY																									
1	137	137	135	135	132	131	130	129	130	127	129	125	119	123	124	126	126	124	124	122	122	127	129	130	128
2	134	133	132	132	130	130	129	128	123	126	126	128	127	125	123	120	120	119	119	126	122	122	121	126	126
3	129	131	131	129	128	128	127	125	125	125	125	126	125	126	127	126	130	128	122	121	119	119	123	126	126
4	128	127	130	132	131	132	129	128	127	126	124	121	119	120	113	120	119	117	112	112	112	115	118	121	122
5 D	127	127	127	126	127	125	127	122	123	122	113	96	91	96	100	107	117	108	102	104	110	116	126	127	115
6 D	129	136	139	143	141	135	144	139	133	123	118	122	123	124	108	108	119	122	123	123	124	125	127	127	127
7	129	131	129	128	128	128	128	126	127	123	118	119	122	125	124	126	129	129	128	126	126	125	123	123	126
8	129	130	128	130	128	130	129	129	127	128	125	125	125	125	126	127	129	128	127	123	122	123	123	119	126
9 D	125	126	127	132	128	127	126	127	126	127	124	123	119	120	118	121	125	127	125	124	123	120	118	121	124
10	126	125	125	125	124	126	126	127	125	126	124	125	123	123	124	126	127	126	126	122	122	121	123	127	125
11	133	135	134	133	131	134	134	119	127	131	131	132	129	125	120	124	125	121	114	110	109	114	118	124	125
12	125	123	123	123	128	129	128	128	127	128	125	125	122	121	121	123	125	122	119	118	117	120	121	123	124
13 Q	127	126	123	122	123	121	122	122	123	123	124	124	123	122	121	122	122	122	120	118	118	123	125	124	123
14	126	129	129	128	126	124	124	123	123	123	123	123	124	123	122	124	123	122	117	117	121	125	124	125	124
15	128	126	126	125	125	124	122	121	120	120	113	117	120	121	120	123	124	125	123	120	121	124	127	125	123
16 D	129	128	133	132	129	128	126	125	122	123	126	126	124	124	123	120	120	118	115	114	108	112	117	123	123
17	126	130	131	131	129	129	127	126	125	125	123	123	125	126	126	127	128	125	119	116	119	122	123	125	125
18	127	130	129	128	129	127	126	124	122	123	122	123	124	124	124	124	123	122	119	118	113	114	116	118	123
19	124	125	125	124	125	124	122	123	123	122	122	123	122	122	123	124	124	123	119	120	124	124	122	117	123
20 Q	121	121	122	121	121	123	121	122	121	120	120	120	119	120	120	120	122	121	117	122	122	122	117	116	120
21 Q	122	124	124	126	126	124	125	123	122	121	120	120	120	120	120	121	122	122	122	123	124	123	121	120	122
22	123	123	123	124	122	125	123	122	129	128	124	124	121	116	118	117	119	115	115	116	117	117	113	114	120
23 D	119	119	118	120	119	120	120	121	119	108	100	101	108	111	100	110	115	114	113	116	117	121	120	122	115
24	125	127	133	130	126	124	124	124	122	122	120	117	100	105	112	117	120	118	117	115	116	114	115	119	119
25	122	123	122	122	123	125	122	127	121	120	124	125	123	117	114	121	123	123	121	122	124	124	125	124	122
26	127	125	123	123	123	123	123	121	119	121	120	117	119	120	121	122	123	115	111	115	116	123	127	127	121
27	129	128	128	131	128	128	126	125	123	116	110	100	111	118	121	123	126	128	126	127	126	124	122	126	123
28	125	126	124	124	122	124	123	124	123	123	123	121	121	121	123	123	124	121	123	123	123	122	121	122	123
29	126	129	127	125	124	123	123	122	121	117	115	117	121	123	122	123	123	121	120	120	118	118	117	119	121
30 Q	126	124	123	123	123	122	123	124	122	124	124	122	122	122	121	123	126	125	123	125	124	123	122	121	123
31 Q	124	122	121	121	120	120	120	118	119	119	117	116	115	118	119	121	121	120	122	123	119	118	117	119	120
MEAN	127	127	127	127	126	126	126	125	124	123	121	120	120	120	119	121	123	122	119	119	119	121	121	123	123

MEAN VALUES OF MAGNETIC ELEMENTS

HORIZONTAL INTENSITY (GAMMAS) (ALL DAYS)

TABLE 37 VICTORIA H = 18,500 GAMMA + 1969

U.T.	JAN	FEB	MAR	APR	MAY	JUN	JUL	AUG	SEP	OCT	NOV	DEC	YEAR	SUMMER	EQUINOX	WINTER
0- 1	412	406	404	418	433	428	434	437	436	435	437	437	426	433	423	423
1- 2	415	409	410	419	431	432	436	437	433	435	440	438	428	434	424	426
2- 3	418	411	414	420	431	431	434	434	433	435	441	438	428	433	426	427
3- 4	417	411	410	422	426	430	433	434	432	435	441	439	427	431	425	427
4- 5	418	411	408	421	422	427	432	434	434	436	439	438	427	429	425	427
5- 6	417	410	410	423	423	430	434	435	435	435	438	437	427	431	426	426
6- 7	417	412	411	422	421	429	435	438	438	435	437	436	428	431	427	426
7- 8	417	414	408	422	424	432	436	439	436	436	437	437	428	433	426	426
8- 9	415	414	405	423	426	433	436	440	432	434	438	437	428	434	424	426
9-10	417	415	407	425	427	432	438	441	434	438	440	437	429	435	426	427
10-11	417	414	407	426	428	433	439	442	438	439	443	439	430	436	428	428
11-12	418	416	412	427	427	432	439	441	438	441	444	439	431	435	430	429
12-13	419	414	419	427	427	432	443	442	439	442	445	440	432	436	432	430
13-14	421	417	421	425	430	435	446	444	440	444	445	441	434	439	433	431
14-15	423	417	418	426	427	434	446	443	435	441	443	440	433	438	430	431
15-16	422	416	417	422	423	430	441	436	428	436	441	442	430	433	426	430
16-17	419	410	411	412	414	422	433	422	418	428	439	440	422	423	417	427
17-18	412	401	400	398	408	414	422	411	406	420	431	437	413	414	406	420
18-19	400	382	389	391	404	414	414	405	401	413	422	428	405	409	399	408
19-20	393	376	383	387	403	415	412	407	403	412	415	420	402	409	396	401
20-21	393	380	381	390	403	414	415	411	411	414	413	416	403	411	399	401
21-22	398	380	381	396	409	415	419	416	418	419	417	420	407	415	404	404
22-23	404	387	389	401	417	419	423	425	427	425	425	425	414	421	411	410
23-24	409	394	398	411	423	423	427	433	431	431	431	431	420	427	418	416
MEAN	413	405	405	415	421	427	432	431	428	432	435	435	423	428	420	422

MEAN VALUES OF MAGNETIC ELEMENTS

DECLINATION (MINUTES) (ALL DAYS)

TABLE 38 VICTORIA D = 22 DEG 00.0 MIN EAST + 1969

U.T.	JAN	FEB	MAR	APR	MAY	JUN	JUL	AUG	SEP	OCT	NOV	DEC	YEAR	SUMMER	EQUINOX	WINTER
0- 1	28.0	25.9	24.4	22.7	22.8	22.9	23.4	23.9	24.4	24.9	24.9	24.9	24.4	23.3	24.1	25.9
1- 2	28.4	26.5	25.0	23.9	24.1	24.2	24.7	24.7	25.2	25.5	25.5	25.6	25.3	24.4	24.9	26.5
2- 3	28.7	27.0	25.7	25.4	25.5	25.9	25.7	25.4	25.9	26.0	26.2	26.2	26.2	25.6	25.8	27.0
3- 4	29.0	28.0	26.7	26.5	27.0	26.6	26.7	25.6	26.6	26.6	26.5	26.6	26.9	26.5	26.6	27.5
4- 5	29.4	28.2	27.1	26.7	27.8	26.8	26.6	26.1	26.3	26.4	26.8	26.7	27.1	26.8	26.6	27.8
5- 6	29.2	28.6	27.9	27.2	28.1	27.1	26.7	26.3	26.3	27.2	27.2	27.0	27.4	27.1	27.1	28.0
6- 7	29.0	29.0	28.0	27.5	27.8	27.0	26.4	26.0	26.2	27.1	27.8	26.7	27.4	26.8	27.2	28.1
7- 8	28.8	28.6	29.4	28.5	27.4	26.9	26.6	26.3	26.1	27.1	27.7	26.8	27.5	26.8	27.8	28.0
8- 9	29.2	28.5	30.1	28.3	28.5	27.2	27.0	26.6	26.2	27.5	26.7	26.1	27.7	27.3	28.0	27.6
9-10	28.8	29.0	30.2	28.5	28.9	27.0	27.1	26.9	27.8	27.5	26.1	26.0	27.8	27.4	28.5	27.5
10-11	29.1	29.1	30.1	28.6	28.3	26.9	26.9	26.9	28.5	27.2	26.3	25.8	27.8	27.3	28.6	27.6
11-12	29.2	29.5	29.3	28.9	28.4	27.1	27.6	27.6	28.1	27.8	26.7	26.2	28.0	27.7	28.5	27.9
12-13	29.5	29.2	29.0	29.3	28.6	28.1	28.6	28.5	28.8	27.1	26.5	26.6	28.3	28.4	28.6	27.9
13-14	29.3	29.3	29.4	30.1	30.5	30.2	30.2	29.9	29.2	27.7	26.5	26.8	29.1	30.2	29.1	28.0
14-15	30.0	29.4	30.0	31.6	32.0	32.5	31.9	31.7	30.0	27.8	26.9	26.6	30.0	32.0	29.8	28.2
15-16	30.4	30.1	31.4	33.2	33.4	33.9	33.7	33.6	31.5	28.7	27.7	27.4	31.2	33.6	31.2	28.9
16-17	31.1	31.2	32.6	34.4	33.2	34.4	34.4	34.2	31.9	29.6	29.1	28.3	32.0	34.1	32.1	29.9
17-18	31.3	32.0	32.8	33.8	32.8	32.9	33.2	32.3	30.5	29.9	29.9	28.9	31.7	32.8	31.8	30.5
18-19	31.0	31.2	31.7	31.2	29.9	29.3	29.7	28.3	27.6	28.5	28.2	28.3	29.6	29.3	29.7	29.6
19-20	29.6	28.7	29.9	28.4	27.1	26.0	25.9	24.3	24.7	26.3	26.7	27.5	27.1	25.8	27.3	28.1
20-21	28.4	27.6	27.7	25.9	24.8	23.8	23.3	22.2	23.0	24.4	25.4	25.8	25.2	23.5	25.3	26.8
21-22	27.3	26.1	25.8	24.1	23.4	22.2	21.9	21.4	22.2	23.6	24.5	24.8	23.9	22.2	23.9	25.7
22-23	26.8	25.3	24.3	23.1	22.0	21.4	21.5	21.7	22.6	23.8	24.2	24.3	23.4	21.6	23.4	25.2
23-24	27.0	25.1	23.7	22.3	21.9	21.5	22.1	22.7	23.7	24.4	24.4	24.2	23.6	22.0	23.5	25.2
MEAN	29.1	28.5	28.4	27.9	27.7	27.2	27.2	26.8	26.8	26.8	26.6	26.4	27.4	27.2	27.5	27.6

MEAN VALUES OF MAGNETIC ELEMENTS

VERTICAL INTENSITY (GAMMAS) (ALL DAYS)

TABLE 39 VICTORIA Z = 53,000 GAMMA + 1969

U.T.	JAN	FEB	MAR	APR	MAY	JUN	JUL	AUG	SEP	OCT	NOV	DEC	YEAR	SUMMER	EQUINOX	WINTER
0- 1	135	139	147	142	153	138	132	131	134	131	128	127	136	139	139	132
1- 2	136	141	150	147	157	144	139	132	134	132	129	127	139	143	141	133
2- 3	136	142	154	148	158	147	138	132	137	132	129	127	140	144	143	134
3- 4	136	142	151	146	156	144	136	132	135	133	129	127	139	142	141	134
4- 5	137	142	148	144	153	140	134	130	132	132	129	126	137	139	139	134
5- 6	136	142	148	143	148	137	131	129	131	132	129	126	136	136	139	133
6- 7	135	141	144	140	141	135	130	127	128	131	127	126	134	133	136	132
7- 8	135	139	140	138	137	134	124	126	124	129	126	125	131	130	133	131
8- 9	133	134	134	133	137	130	123	124	117	128	123	124	128	129	128	129
9-10	131	132	125	133	130	129	124	122	116	126	119	123	126	126	125	126
10-11	129	128	118	129	124	129	123	119	116	121	118	121	123	124	121	124
11-12	128	126	120	128	125	130	124	118	113	120	119	120	123	124	120	123
12-13	126	121	124	125	119	129	126	120	111	117	119	120	121	124	119	122
13-14	126	120	129	125	123	127	127	122	114	119	119	120	123	125	122	121
14-15	127	125	130	127	121	128	128	123	115	120	120	119	124	125	123	123
15-16	130	127	133	130	123	126	127	123	115	123	123	121	125	125	125	125
16-17	132	127	133	128	122	121	122	121	115	126	125	123	125	122	126	127
17-18	130	128	130	123	120	113	116	112	112	126	124	122	121	115	123	126
18-19	129	125	126	119	116	106	109	105	110	121	120	119	117	109	119	123
19-20	129	126	123	119	117	104	107	103	111	117	119	119	116	108	118	123
20-21	130	127	123	121	120	107	108	106	116	117	120	119	118	110	119	124
21-22	132	128	126	126	124	112	111	110	121	121	122	121	121	114	124	126
22-23	133	131	133	130	132	119	117	117	126	124	124	121	126	121	128	127
23-24	134	135	141	134	142	129	124	124	129	127	126	123	131	130	133	130
MEAN	132	132	135	132	133	127	124	121	121	125	124	123	127	126	128	128

MEAN VALUES OF MAGNETIC ELEMENTS

HORIZONTAL INTENSITY (GAMMAS) (QUIET DAYS)

TABLE 40 VICTORIA H = 18,500 GAMMA + 1969

U.T.	JAN	FEB	MAR	APR	MAY	JUN	JUL	AUG	SEP	OCT	NOV	DEC	YEAR	SUMMER	EQUINOX	WINTER
0- 1	417	416	408	417	434	430	433	436	437	438	443	449	430	433	425	431
1- 2	420	420	412	421	432	432	435	439	440	441	444	448	432	435	429	433
2- 3	421	419	417	424	432	431	436	439	441	443	444	447	433	435	431	433
3- 4	421	420	417	427	431	433	436	440	439	443	444	446	433	435	432	433
4- 5	422	421	414	428	431	431	436	439	438	442	444	444	433	434	431	433
5- 6	420	420	416	428	432	431	438	440	440	442	444	443	433	435	432	432
6- 7	421	420	417	427	435	434	439	440	444	444	443	444	434	437	433	432
7- 8	420	421	419	428	436	434	440	441	441	442	444	444	434	438	433	432
8- 9	420	420	422	430	437	436	439	443	442	443	446	442	435	439	434	432
9-10	421	422	424	433	440	436	441	443	443	444	447	444	436	440	436	434
10-11	422	422	423	434	438	436	441	443	444	446	447	445	437	440	437	434
11-12	422	422	425	434	438	435	443	442	445	448	448	445	437	440	438	434
12-13	424	424	426	436	439	438	446	444	445	448	448	445	439	442	439	435
13-14	424	426	426	434	443	442	449	447	446	447	448	446	440	445	438	436
14-15	424	425	425	436	442	441	450	447	445	446	447	446	439	445	438	436
15-16	423	424	425	434	439	437	445	440	438	442	444	448	437	440	435	435
16-17	419	419	420	424	431	427	438	427	424	435	439	447	429	431	426	431
17-18	410	411	413	413	426	418	429	414	411	424	433	441	420	422	415	424
18-19	401	402	406	406	422	417	422	405	403	416	422	432	413	417	408	414
19-20	395	396	395	406	422	417	417	400	405	415	419	425	409	414	405	409
20-21	396	393	393	404	422	417	417	401	415	419	421	424	410	414	408	409
21-22	401	395	393	406	423	418	421	408	423	427	426	427	414	418	412	412
22-23	410	403	397	408	429	423	427	421	432	432	433	433	421	425	417	420
23-24	415	410	405	414	430	431	433	432	438	437	440	439	427	432	424	426
MEAN	416	416	414	423	433	430	435	432	434	438	440	441	429	433	427	428

MEAN VALUES OF MAGNETIC ELEMENTS

DECLINATION (MINUTES) (QUIET DAYS)

TABLE 41 VICTORIA D = 22 DEG 00.0 MIN EAST + 1969

U.T.	JAN	FEB	MAR	APR	MAY	JUN	JUL	AUG	SEP	OCT	NOV	DEC	YEAR	SUMMER	EQUINOX	WINTER
0- 1	28.3	26.7	25.1	23.6	23.4	23.7	23.8	24.1	24.9	24.7	24.7	24.4	24.8	23.7	24.6	26.0
1- 2	28.7	27.0	25.7	25.1	24.5	24.8	24.9	25.4	25.3	25.4	25.3	25.0	25.6	24.9	25.4	26.5
2- 3	29.2	27.2	26.2	26.4	25.4	26.2	25.6	26.0	25.4	25.9	26.0	25.7	26.3	25.8	26.0	27.0
3- 4	29.5	27.6	26.6	26.7	25.8	26.9	25.9	25.6	25.5	26.2	26.4	26.1	26.6	26.0	26.2	27.4
4- 5	29.6	27.8	26.9	27.0	26.3	26.7	26.2	25.6	25.7	26.3	26.4	26.4	26.7	26.2	26.5	27.6
5- 6	29.5	27.9	27.2	27.2	26.4	26.5	26.6	25.6	25.6	26.3	26.4	26.3	26.8	26.3	26.6	27.5
6- 7	29.3	27.9	27.2	27.5	26.7	26.5	26.5	26.1	25.4	26.6	26.3	26.2	26.8	26.4	26.7	27.4
7- 8	29.2	27.8	27.4	27.2	27.0	26.5	26.8	26.1	26.3	26.6	26.3	26.2	26.9	26.6	26.9	27.3
8- 9	29.3	27.8	27.9	27.9	26.9	26.6	26.5	26.2	26.1	26.7	26.3	26.1	27.0	26.6	27.1	27.4
9-10	29.0	28.1	28.4	27.9	27.9	26.7	26.6	26.5	25.8	26.4	26.3	26.0	27.1	26.9	27.1	27.3
10-11	29.2	28.3	28.0	27.7	28.0	26.9	27.1	27.0	27.4	26.6	26.4	25.9	27.4	27.2	27.4	27.4
11-12	29.7	28.5	28.0	28.4	27.9	27.5	27.3	27.4	27.8	26.8	26.5	26.5	27.7	27.5	27.7	27.8
12-13	29.5	28.5	28.2	28.1	29.0	29.1	28.3	28.2	28.4	27.5	26.6	26.3	28.1	28.7	28.0	27.7
13-14	30.1	28.6	28.3	29.2	30.6	30.4	30.1	29.0	29.0	28.0	27.2	26.4	28.9	30.0	28.6	28.1
14-15	30.4	29.1	28.9	31.1	31.9	31.7	31.9	31.6	30.7	28.3	27.4	26.4	29.9	31.8	29.7	28.3
15-16	31.1	30.4	30.4	33.2	33.3	33.6	34.0	34.1	32.7	29.6	28.7	26.6	31.5	33.7	31.5	29.2
16-17	32.4	31.5	32.1	34.8	33.5	34.6	34.6	35.6	34.3	30.5	30.3	27.8	32.7	34.6	32.9	30.5
17-18	33.1	32.0	33.1	33.9	33.0	32.3	33.1	34.6	33.2	30.9	30.8	29.2	32.4	33.2	32.7	31.3
18-19	32.8	31.2	32.5	31.7	30.6	29.2	29.5	30.6	29.7	29.2	29.4	29.0	30.5	30.0	30.8	30.6
19-20	31.3	29.9	30.7	28.7	28.0	25.9	25.9	26.6	25.7	26.7	27.9	28.3	28.0	26.6	27.9	29.3
20-21	29.9	28.1	28.4	26.1	25.7	23.7	22.7	23.5	23.1	24.4	26.0	26.7	25.7	23.9	25.5	27.7
21-22	28.3	26.6	26.2	23.8	24.0	22.1	21.0	21.7	22.4	23.5	24.8	25.6	24.2	22.2	24.0	26.3
22-23	27.8	25.5	25.0	22.4	22.6	21.3	20.5	21.4	22.5	23.5	24.3	24.5	23.4	21.5	23.3	25.5
23-24	27.8	25.4	24.1	21.4	22.3	21.3	21.0	22.5	23.6	24.2	24.2	24.0	23.5	21.8	23.3	25.3
MEAN	29.8	28.3	28.0	27.8	27.5	27.1	26.9	27.1	26.9	26.7	26.7	26.3	27.4	27.2	27.4	27.8

MEAN VALUES OF MAGNETIC ELEMENTS

VERTICAL INTENSITY (GAMMAS) (QUIET DAYS)

TABLE 42 VICTORIA Z = 53,000 GAMMA + 1969

U.T.	JAN	FEB	MAR	APR	MAY	JUN	JUL	AUG	SEP	OCT	NOV	DEC	YEAR	SUMMER	EQUINOX	WINTER
0- 1	139	134	142	133	139	132	128	130	127	128	126	124	132	132	133	131
1- 2	138	134	142	137	142	137	130	130	126	129	127	123	133	135	134	131
2- 3	138	134	141	138	143	137	130	129	125	128	126	123	133	135	133	130
3- 4	137	134	140	137	141	133	128	126	125	129	127	123	132	132	133	130
4- 5	137	134	139	136	138	131	127	126	124	127	125	123	130	131	132	130
5- 6	136	134	139	134	137	129	126	125	124	128	125	122	130	129	131	129
6- 7	135	134	139	135	136	130	125	126	123	127	124	122	130	129	131	129
7- 8	136	134	138	133	136	129	125	126	123	127	124	122	129	129	130	129
8- 9	136	134	138	133	133	129	125	125	123	127	124	121	129	128	130	129
9-10	134	134	136	134	129	128	125	124	120	127	124	121	128	127	129	128
10-11	134	134	135	133	130	128	124	124	121	127	124	121	128	127	129	128
11-12	135	134	135	131	130	129	126	123	122	126	124	120	128	127	129	128
12-13	135	133	135	132	133	131	126	123	122	125	124	120	128	128	129	128
13-14	135	132	135	130	134	131	127	124	123	125	124	120	128	129	128	128
14-15	135	132	135	130	134	131	127	125	125	126	124	120	129	129	129	128
15-16	136	135	137	132	132	129	126	126	125	127	126	121	129	128	130	130
16-17	138	136	137	131	127	122	124	124	123	129	127	123	128	124	130	131
17-18	137	135	136	123	117	114	116	117	115	127	125	122	124	116	125	130
18-19	135	132	130	118	109	107	107	110	108	122	122	121	118	108	120	128
19-20	133	130	126	118	107	103	104	105	106	116	121	122	116	105	117	127
20-21	133	128	126	117	108	104	105	103	109	115	120	121	116	105	117	126
21-22	134	126	126	117	104	105	105	105	114	119	120	122	116	105	119	126
22-23	135	127	127	119	115	113	109	112	119	121	122	120	120	112	122	126
23-24	136	130	131	122	124	123	117	119	120	124	124	120	124	121	124	128
MEAN	136	133	135	129	128	124	121	121	120	125	124	122	127	124	127	129

MEAN VALUES OF MAGNETIC ELEMENTS

HORIZONTAL INTENSITY (GAMMAS) (DISTURBED DAYS)

TABLE 43 VICTORIA H = 18,500 GAMMA + 1969

U.T.	JAN	FEB	MAR	APR	MAY	JUN	JUL	AUG	SEP	OCT	NOV	DEC	YEAR	SUMMER	EQUINOX	WINTER
0- 1	393	397	400	421	437	427	448	447	426	428	428	433	424	440	419	413
1- 2	395	394	404	425	433	439	443	449	425	422	428	433	424	441	419	413
2- 3	409	396	434	422	435	436	433	437	429	416	431	432	426	435	425	417
3- 4	410	396	395	424	417	431	428	433	420	418	431	436	420	427	414	418
4- 5	407	398	385	421	405	423	424	430	429	418	423	434	416	421	413	416
5- 6	406	397	390	432	399	426	425	434	428	420	421	427	417	421	418	413
6- 7	409	403	394	418	394	423	428	440	432	417	419	432	417	421	415	416
7- 8	408	405	370	418	392	428	426	441	428	415	418	433	415	422	408	416
8- 9	407	402	351	411	403	427	424	445	409	411	419	433	412	425	396	415
9-10	414	402	354	421	403	424	431	446	407	418	417	435	414	426	400	417
10-11	408	397	337	416	410	431	434	447	415	416	430	436	415	431	396	418
11-12	411	399	354	422	400	431	433	441	414	423	433	433	416	426	403	419
12-13	411	382	398	415	396	429	440	442	422	425	430	438	419	427	415	415
13-14	420	393	404	404	405	435	445	445	431	436	433	439	424	433	419	421
14-15	425	401	398	408	393	428	448	444	411	426	426	435	420	428	411	422
15-16	418	397	396	401	383	426	443	433	412	417	422	439	416	421	407	419
16-17	413	386	388	391	370	418	432	416	413	413	428	438	409	409	401	416
17-18	402	370	383	375	371	407	415	407	391	408	419	434	398	400	389	406
18-19	390	304	367	368	374	401	402	401	385	397	408	426	385	395	379	382
19-20	382	301	365	368	371	410	395	407	397	396	398	419	384	396	382	375
20-21	387	342	363	378	367	416	403	419	404	400	399	412	391	401	386	385
21-22	392	335	359	390	393	413	411	423	410	404	408	415	396	410	391	388
22-23	396	356	385	399	421	411	418	423	414	413	415	419	406	418	403	397
23-24	403	375	400	416	430	416	428	430	414	418	420	425	415	426	412	406
MEAN	405	380	382	407	400	423	427	433	415	416	421	431	412	421	405	409

MEAN VALUES OF MAGNETIC ELEMENTS

DECLINATION (MINUTES) (DISTURBED DAYS)

TABLE 44 VICTORIA D = 22 DEG 00.0 MIN EAST + 1969

U.T.	JAN	FEB	MAR	APR	MAY	JUN	JUL	AUG	SEP	OCT	NOV	DEC	YEAR	SUMMER	EQUINOX	WINTER
0- 1	27.8	24.4	22.6	22.3	21.8	22.0	22.4	22.9	22.2	25.5	25.2	25.0	23.7	22.3	23.2	25.6
1- 2	28.5	25.8	23.4	22.8	22.0	23.1	24.5	22.9	24.4	27.5	26.5	25.5	24.7	23.1	24.5	26.6
2- 3	28.2	25.9	23.7	24.2	23.7	25.1	26.2	24.1	26.9	28.0	27.0	26.8	25.8	24.8	25.7	27.0
3- 4	28.5	27.8	26.1	25.5	29.1	26.0	29.0	24.6	28.6	28.7	27.3	27.0	27.4	27.2	27.2	27.7
4- 5	28.9	28.2	25.9	26.2	29.6	28.3	29.1	27.1	26.7	27.3	27.6	27.2	27.7	28.5	26.5	28.0
5- 6	29.6	29.4	28.3	26.8	29.0	29.4	28.3	27.6	27.6	29.0	29.9	28.0	28.6	28.6	27.9	29.2
6- 7	28.9	29.3	28.3	26.7	28.4	28.8	27.3	25.8	27.3	29.0	33.0	27.8	28.4	27.6	27.8	29.8
7- 8	28.4	29.6	31.2	30.6	26.3	28.4	28.0	25.6	25.9	29.4	30.1	27.9	28.5	27.1	29.3	29.0
8- 9	30.0	30.1	33.9	27.5	29.6	27.9	29.8	26.5	22.8	30.3	27.4	25.9	28.5	28.4	28.6	28.3
9-10	28.6	32.1	34.1	28.0	31.5	27.5	28.6	28.6	29.9	29.5	24.5	25.6	29.1	29.1	30.4	27.7
10-11	30.0	32.0	35.1	28.9	29.1	26.2	27.7	27.0	33.3	27.8	26.3	26.3	29.1	27.5	31.3	28.6
11-12	27.4	32.2	30.9	30.9	30.1	25.7	27.6	28.3	28.9	28.8	27.6	26.2	28.7	27.9	29.9	28.4
12-13	27.0	30.4	28.3	32.6	27.1	26.4	28.2	29.1	30.5	24.1	25.0	27.0	28.0	27.7	28.9	27.4
13-14	28.3	28.8	30.3	30.8	30.1	30.5	31.1	30.8	30.5	26.2	25.2	26.7	29.1	30.6	29.5	27.3
14-15	30.0	28.0	29.9	31.9	32.8	33.0	32.7	32.7	29.0	25.0	25.8	24.3	29.6	32.8	29.0	27.0
15-16	30.2	25.9	32.1	32.8	31.9	34.0	35.3	34.4	29.8	24.9	25.9	26.8	30.3	33.9	29.9	27.2
16-17	30.5	26.2	32.0	34.7	29.9	35.9	35.4	34.3	30.6	26.2	26.9	28.3	30.9	33.8	30.9	28.0
17-18	30.0	30.2	31.4	32.6	31.3	33.9	33.9	31.0	29.8	27.2	29.0	26.9	30.6	32.5	30.2	29.0
18-19	29.3	30.2	31.8	28.7	29.1	30.1	30.3	25.4	26.4	26.5	27.3	25.9	28.4	28.7	28.3	28.1
19-20	27.8	22.6	30.1	24.9	26.2	25.6	26.5	22.0	24.1	26.2	24.8	26.1	25.6	25.1	26.3	25.3
20-21	27.4	24.1	29.6	23.2	23.2	24.0	23.0	20.9	24.0	25.6	24.8	24.9	24.6	22.8	25.6	25.3
21-22	27.0	23.6	27.5	23.0	22.0	22.9	21.7	20.2	22.8	25.1	24.9	24.4	23.7	21.7	24.6	25.0
22-23	26.9	23.8	25.1	23.5	20.2	21.9	21.5	21.5	22.4	25.3	24.7	24.6	23.4	21.3	24.1	25.0
23-24	26.4	25.3	24.5	22.9	20.9	21.8	22.1	22.6	23.5	25.4	25.0	24.5	23.7	21.8	24.1	25.3
MEAN	28.6	27.7	29.0	27.6	27.3	27.4	27.9	26.5	27.0	27.0	26.7	26.2	27.4	27.3	27.6	27.3

MEAN VALUES OF MAGNETIC ELEMENTS

VERTICAL INTENSITY (GAMMAS) (DISTURBED DAYS)

TABLE 45 VICTORIA Z = 53,000 GAMMA + 1969

U.T.	JAN	FEB	MAR	APR	MAY	JUN	JUL	AUG	SEP	OCT	NOV	DEC	YEAR	SUMMER	EQUINOX	WINTER
0- 1	136	146	186	142	200	142	143	125	152	139	133	126	148	153	155	135
1- 2	142	153	193	149	202	151	161	130	154	142	134	127	153	161	160	139
2- 3	145	156	205	152	209	163	160	132	173	142	135	129	158	166	168	141
3- 4	145	157	190	150	206	165	158	139	162	143	134	131	157	167	161	142
4- 5	145	159	181	149	193	163	153	133	144	144	136	129	152	161	155	142
5- 6	145	156	181	148	173	153	144	133	143	143	136	127	148	151	154	141
6- 7	141	150	164	140	153	146	142	130	137	135	128	129	141	143	144	137
7- 8	136	139	145	139	135	143	115	127	127	132	127	127	133	130	136	132
8- 9	133	125	124	112	144	132	117	124	88	126	118	125	122	129	113	125
9-10	126	116	88	122	116	129	121	119	88	115	100	121	113	121	103	116
10-11	120	96	63	107	83	132	124	106	81	97	97	116	102	111	87	107
11-12	115	89	80	116	93	133	127	104	66	98	106	114	103	114	90	106
12-13	105	68	110	114	60	133	126	107	59	89	103	113	99	107	93	97
13-14	110	72	129	101	83	125	130	114	83	101	106	115	106	113	104	101
14-15	117	91	138	105	77	126	134	118	89	103	108	110	110	114	109	107
15-16	125	92	143	117	84	123	132	120	93	104	114	113	113	115	114	111
16-17	127	91	139	119	90	119	127	116	103	111	121	119	115	113	118	115
17-18	124	103	133	116	103	109	120	105	106	119	123	118	115	109	119	117
18-19	126	104	130	115	110	98	111	98	110	121	117	116	113	104	119	116
19-20	126	113	130	120	123	99	109	99	116	120	119	116	116	108	122	119
20-21	128	125	132	128	132	104	112	103	123	124	124	116	121	113	127	123
21-22	130	134	139	136	147	112	114	108	127	128	128	119	127	120	133	128
22-23	132	141	162	146	159	122	120	117	132	132	130	122	134	130	143	131
23-24	134	150	177	148	182	132	132	128	139	134	132	124	143	144	150	135
MEAN	130	122	144	129	136	131	130	118	116	123	121	121	127	129	128	124

THREE-HOUR RANGE INDICES

VICTORIA 1969

TABLE 46

JANUARY					FEBRUARY				
DAY	D	H	Z	K	DAY	D	H	Z	K
1	0134 2211	1112 1111	1002 0010	1134 2211	1	0000 0222	0011 0122	0000 0011	0011 0222
2	0300 2100	1110 1000	0000 0000	1310 2100	2	0022 2574	0021 2684	0011 1354	0022 2684
3	0000 0000	0000 0000	0000 0000	0000 0000	3	4465 6443	4363 5344	3354 5323	4465 6444
4	0001 1111	1012 1112	0001 0000	1012 1112	4	2032 3322	2122 2223	1011 2222	2132 3323
5	0301 1000	0111 1101	0010 0000	0311 1101	5	3123 1011	3233 1012	2112 0011	3233 1012
6	0011 0000	1011 0011	0000 0000	1011 0011	6	2433 0122	3332 0012	1223 0011	3433 0122
7	1123 4232	1122 2012	1002 3001	1123 4232	7	1033 3222	0012 1012	0003 1011	1033 3222
8	1242 0100	1231 0111	1021 0000	1242 0111	8	2121 1221	3221 1111	1000 0000	3221 1221
9	1100 0010	1111 0001	0000 0000	1111 0011	9	0000 0110	0100 0100	0000 0000	0100 0110
10	0001 2000	0110 2000	0000 0000	0111 2000	10	1033 3124	1132 1114	0011 1022	1133 3124
11	0020 2211	0021 1210	0000 0100	0021 2211	11	6356 6633	5255 7534	5356 6652	6356 7634
12	1023 4300	1121 3100	0001 1000	1123 4300	12	2101 0221	2110 0113	1000 0012	2111 0223
13	0001 1001	0000 1001	0000 0000	0001 1001	13	2123 2312	2222 2212	0012 2100	2223 2312
14	1333 1123	2122 1002	0022 0000	2333 1123	14	0202 2122	1301 1113	0002 1012	1302 2123
15	1213 2232	2212 2231	1001 0000	2213 2232	15	1424 3232	2322 2132	1213 1111	2424 3232
16	1333 5311	1222 3311	0011 3200	1333 5311	16	2352 2212	2232 2111	1031 2101	2352 2212
17	2424 3232	3324 2222	2223 2111	3424 3232	17	0011 1101	1111 1000	0000 0001	1111 1101
18	2455 4222	2442 2222	1134 3101	2455 4222	18	0000 0110	0000 0001	0000 0000	0000 0111
19	3134 3111	3223 2111	1013 0010	3234 3111	19	0211 4211	0122 2111	0000 3110	0222 4211
20	1322 2222	1221 2222	0100 0011	1322 2222	20	0112 3332	0321 2221	0101 1222	0322 3332
21	1123 1211	2211 0011	0001 0000	2223 1211	21	1140 1210	2231 1100	1010 0100	2241 1210
22	0132 0110	0011 0000	0011 0000	0132 0110	22	0021 2312	0021 2102	0000 0100	0021 2312
23	0012 2110	0000 1112	0000 0000	0012 2112	23	2343 4222	2322 3112	1012 2111	2343 4222
24	0000 4332	1001 3222	0000 3212	1001 4332	24	0121 1101	1221 0002	0021 0011	1221 1102
25	2344 4442	4233 5332	2133 4321	4344 5442	25	2012 1110	3121 0000	1000 1000	3122 1110
26	4325 5222	5312 3222	3213 3321	5325 5222	26	1343 2220	3232 2121	2132 1100	3343 2221
27	0334 5222	1133 3211	0021 310	1334 5222	27	1341 4532	2332 4432	1121 3330	2342 4532
28	2111 0110	1212 0000	0000 0000	2212 0110	28	1241 2323	2331 1213	0230 1112	2341 2323
29	0001 0101	0000 0001	0000 0000	0001 0101					
30	0114 2100	1112 1100	0003 0000	1114 2100					
31	0013 3322	0022 3211	0001 1110	0023 3322					

THREE-HOUR RANGE INDICES

VICTORIA 1969

TABLE 47

MARCH

DAY	D	H	Z	K
1	1000 2333	3121 2233	0000 0122	3121 2333
2	4303 3111	4301 2001	2212 2000	4303 3111
3	0000 1110	1000 0001	0000 0000	1000 1111
4	0000 1023	0000 0023	0000 0011	0000 1023
5	1002 2222	2122 2112	0003 2001	2122 2222
6	3223 1221	2122 1222	1013 1111	3223 1222
7	2332 4333	3321 2332	1212 3210	3332 4333
8	2323 2212	2322 2013	1102 1001	2323 2213
9	1223 3322	2223 1111	0011 3100	2223 3322
10	2222 0120	2211 1011	0001 0000	2222 1121
11	2243 4333	2222 3243	0013 3123	2243 4343
12	5655 2421	4454 2211	4445 1100	5655 2421
13	3122 1211	2101 0103	2000 0011	3122 1213
14	1211 1222	1211 1113	0001 0001	1211 1223
15	4443 2332	3243 2323	2143 2122	4443 2333
16	1554 3211	1334 2121	1244 1000	1554 3221
17	4534 5531	5433 4333	3433 5312	5534 5533
18	0333 2212	1243 1222	0233 1011	1343 2222
19	0032 2234	2122 1034	0021 0022	2132 2234
20	4253 2323	5433 1333	5323 1212	5453 2333
21	2254 3122	2243 1123	1132 2012	2254 3123
22	1343 2321	2322 3121	2211 2122	2343 3321
23	0002 2355	1112 2256	0000 0146	1112 2356
24	7588 5321	9587 6213	6587 7101	9588 6323
25	1153 4122	3243 3123	2045 3112	3253 4123
26	1133 3311	3121 2122	2112 1101	3133 3322
27	1121 2100	2221 2011	1100 0000	2221 2111
28	1211 2221	1121 2212	0000 0011	1221 2222
29	1133 3333	1123 3323	0011 1222	1133 3333
30	3233 1233	3222 0224	2011 0112	3233 1234
31	3222 3321	3322 2332	2121 1110	3322 3332

APRIL

DAY	D	H	Z	K
1	1224 2453	2322 2332	1013 3222	2324 2453
2	3113 3342	3121 2443	2001 1112	3123 3443
3	4221 3222	3221 1122	3211 1100	4221 3222
4	3443 3221	2332 2122	2232 3000	3443 3222
5	2252 1212	3242 1112	1030 0000	3252 1212
6	2231 2222	2231 2223	1020 0112	2231 2223
7	3532 2321	3442 2112	3232 2010	3542 2322
8	2112 2211	2212 1112	1101 1000	2212 2212
9	2243 2222	2233 2122	1123 1121	2243 2222
10	0043 2321	1221 1221	0022 0000	1243 2321
11	1142 2110	2233 2011	1021 2000	2243 2111
12	0012 2233	1112 1134	0000 0022	1112 2234
13	4253 3432	5332 3433	3223 3123	5353 3433
14	4113 3332	5322 3322	4302 2112	5323 3332
15	2343 3332	3333 2222	2233 4111	3343 3332
16	2353 4222	2343 2223	2243 3012	2353 4223
17	3263 4332	4342 3333	3243 3111	4363 4333
18	5453 2111	3342 2113	3331 1000	5453 2113
19	2000 2111	2011 1022	2000 1001	2011 2122
20	1020 2122	3221 1112	2000 0011	3221 2122
21	2000 0121	2122 2022	2000 0011	2122 2122
22	1134 2210	3342 2121	1122 2111	3344 2221
23	0121 3211	1221 2212	1000 1001	1221 3212
24	2231 1222	3331 2222	2220 0011	3331 2222
25	3232 2221	4222 1222	2110 1001	4232 2222
26	2211 2132	2111 1212	1100 0001	2211 2232
27	2333 1231	3222 2232	2003 1111	3333 2232
28	2685 5432	3576 4433	2476 5311	3686 5433
29	2221 2323	3331 2334	2110 1112	3331 2334
30	3443 4322	3443 3333	2433 3211	3443 4333

THREE-HOUR RANGE INDICES

VICTORIA 1969

TABLE 48

MAY

DAY	D	H	Z	K
1	3422 1111	2431 0112	1231 0000	3432 1112
2	1324 3462	2223 3453	0012 3241	2324 3463
3	2553 3212	2332 2223	0232 3101	2553 3223
4	1322 1221	2311 1222	1101 0011	2322 1222
5	2113 3221	2212 2222	2002 2110	2213 3222
6	2331 2111	2331 1102	2310 1001	2331 2112
7	1133 0000	2221 0001	2032 0000	2233 0001
8	1111 1211	1222 2112	0000 0010	1222 2212
9	1243 2233	2222 2234	0022 0122	2243 2234
10	1333 2212	3332 2112	2131 1000	3333 2212
11	0123 2110	2112 1121	1002 0000	2123 2121
12	0011 1132	1111 1133	1100 0022	1111 1133
13	4564 5433	5453 3433	4364 4334	5564 5433
14	5543 1354	5432 3355	5423 2135	5543 3355
15	6656 6653	7656 6445	7747 5654	7656 6655
16	5574 3221	4563 3123	4565 5002	5574 3223
17	1353 2111	3342 1123	3242 1013	3353 2123
18	3344 2342	4343 1233	3133 1221	4344 2343
19	2113 3221	3222 2222	1111 2112	3223 3222
20	2332 2120	2322 2132	2210 0022	2332 2132
21	2343 4121	3233 3223	2224 3212	3343 4223
22	1323 3321	2123 2322	2104 2212	2323 3322
23	1233 3331	3222 2231	2112 2120	3233 3331
24	1432 2222	2432 2223	1320 3012	2432 2223
25	3311 1111	4221 1112	3200 0001	4321 1112
26	0201 0100	1222 0111	1102 1100	1222 0111
27	0001 2100	0111 2112	0000 0001	0111 2112
28	1333 2311	2233 1313	1101 0111	2333 2313
29	0012 2221	1111 1223	0000 0101	1112 2223
30	1134 4311	2232 2313	1032 2101	2234 4313
31	1533 3221	3332 2233	1321 2001	3533 3233

JUNE

DAY	D	H	Z	K
1	2211 2220	3221 2122	2100 0010	3221 2222
2	0331 2121	2332 1212	0130 1001	2332 2222
3	1111 0221	2211 1213	2100 1021	2211 1223
4	1131 2211	2221 1101	2221 1100	2231 2211
5	1213 2120	2221 1120	2200 0111	2223 2120
6	0011 1211	2110 1212	1000 0000	2111 1212
7	2213 5210	3223 3121	1011 3000	3223 5221
8	1332 3332	2432 2343	2211 0211	2432 3343
9	2223 4243	3312 2244	2200 1023	3323 4244
10	2233 3210	3332 2221	2332 2101	3333 3221
11	1233 2132	3231 2124	2132 0012	3233 2134
12	3544 2231	2432 2222	3332 2111	3544 2232
13	2522 3132	3422 2234	2320 3122	3522 3234
14	3343 5421	3444 4323	2242 4212	3444 5423
15	1333 3221	3223 2222	2203 2031	3333 3222
16	1355 3222	3333 3223	2133 2112	3355 3223
17	5453 2331	4433 2332	4422 1110	5453 2332
18	1000 1121	2211 1222	1100 0011	2211 1222
19	0222 2122	1223 3123	0001 1011	1223 3123
20	3332 3111	4332 3122	2233 1000	4332 3122
21	1233 3110	2121 1121	1101 0000	2233 3121
22	0102 0210	1101 2110	0000 0110	1102 2210
23	0112 2110	2332 1212	0111 0101	2332 2212
24	3323 3322	3422 2223	2311 1001	3423 3323
25	0132 3221	2322 1233	0100 0011	2332 3233
26	2113 3211	3212 1212	2102 2000	3213 3212
27	1221 2102	2212 1112	2200 1010	2222 2112
28	1011 0010	2211 0112	1000 0001	2211 0112
29	0111 1211	2211 2122	1100 0011	2211 2222
30	0212 2211	2111 2122	0000 0001	2212 2222

THREE-HOUR RANGE INDICES

VICTORIA 1969

TABLE 49

JULY

DAY	D	H	Z	K
1	1242 3321	3252 3222	1051 2112	3252 3322
2	2330 0000	3222 2002	2120 0000	3332 2002
3	0000 0110	2110 0011	0000 0011	2110 0111
4	0000 0000	1000 1012	0000 0001	1000 1012
5	0001 1000	1100 0001	1100 0000	1101 1001
6	1001 2111	2111 2212	0000 0001	2111 2212
7	0102 2321	2211 1222	1000 0100	2212 2322
8	0100 1221	2200 1122	1000 0101	2200 1222
9	1132 2212	3221 1222	1220 1001	3232 2222
10	2303 2211	3212 1123	1201 0101	3313 2223
11	0120 1221	2110 0222	1200 0011	2120 1222
12	2242 2121	3332 2124	2242 0021	3342 2124
13	0434 2231	4332 3232	2332 2021	4434 3232
14	1533 3222	2422 3222	0322 2010	2533 3222
15	0223 3001	2122 2012	1100 1000	2223 3012
16	0323 2230	2223 2333	1103 1010	2323 2333
17	1321 1110	3211 1121	1100 0000	3321 1121
18	0012 3000	1012 2011	0001 1000	1012 3011
19	0121 0000	1121 1001	0000 0000	1121 1001
20	0211 2000	2223 1111	0000 0011	2223 2111
21	1000 1220	2121 1212	1000 0001	2121 1222
22	2122 1211	2332 1112	1100 0001	2332 1212
23	0002 0210	1211 0122	1000 0000	1212 0222
24	0010 1100	1120 1011	0000 0000	1120 1111
25	1220 1121	1220 0112	0010 0011	1220 1122
26	1203 3212	2314 3223	1112 3103	2314 3223
27	6563 3110	6342 2122	6562 2010	6563 3122
28	0130 0100	2231 1100	0030 0000	2231 1100
29	0020 0000	1110 0000	0000 0000	1120 0000
30	0001 2342	2222 2444	0000 0122	2222 2444
31	1211 2210	2211 1111	1100 0000	2211 2211

AUGUST

DAY	D	H	Z	K
1	0012 1100	2111 0001	1000 0000	2112 1101
2	0000 2212	1001 2122	0000 0000	1001 2222
3	2213 2333	3323 1333	2201 1122	3323 2333
4	3322 1311	4423 2212	2303 1000	4423 2312
5	1413 3110	3322 2101	1201 2000	3423 3111
6	2221 0000	3211 0011	1200 0000	3221 0011
7	1331 2120	3212 1122	2100 0001	3332 2122
8	2034 2212	2112 1223	2003 2001	2134 2223
9	1332 3221	3312 2122	2200 0001	3332 3222
10	0234 1000	2232 1000	0032 0000	2234 1000
11	0001 1211	0112 2222	0000 0010	0112 2222
12	2534 3331	4333 3323	2234 3211	4534 3333
13	2233 0100	3232 0122	1132 0000	3233 0122
14	1143 3220	2232 3110	1123 1000	2243 3220
15	0020 2211	0022 2103	0000 0001	0022 2213
16	0002 0100	1011 1112	0001 0000	1012 1112
17	2331 0000	3222 0001	1010 0000	3332 0001
18	2002 2101	2212 2112	0000 1000	2212 2112
19	1433 2212	2233 2222	0023 1102	2433 2222
20	3342 2110	2231 1012	1031 0000	3342 2112
21	0400 2211	2300 0212	1100 0000	2400 2212
22	1101 2212	2001 1222	1000 0000	2101 2222
23	2224 3212	4423 2213	2203 2111	4424 3213
24	1303 2221	3213 2113	1101 0001	3313 2223
25	2110 0000	3110 0001	1000 0000	3110 0001
26	0126 4113	1224 2013	0004 2002	1226 4113
27	3644 3211	4423 1112	3433 2000	4644 3212
28	1321 1100	2311 0002	1200 0000	2321 1102
29	0001 1110	1011 0000	0000 0000	1011 1110
30	0031 2100	0121 1011	0000 0010	0131 2111
31	1032 1110	2021 0111	1010 0000	2032 1111

THREE-HOUR RANGE INDICES

VICTORIA 1969

TABLE 50

SEPTEMBER					OCTOBER				
DAY	D	H	Z	K	DAY	D	H	Z	K
1	0020 0100	1110 0000	1000 0000	1120 0100	1	2234 4321	4244 4222	1034 4211	4244 4322
2	0112 0000	0111 1001	0000 0000	0112 1001	2	4446 5511	3245 4421	2345 4400	4446 5521
3	0002 0120	1011 1022	0001 0000	1012 1122	3	4333 4312	3222 3211	1213 3210	4333 4312
4	2200 1111	1211 1012	0000 0000	2211 1112	4	3333 2123	2212 1012	0102 0000	3333 2123
5	0023 5332	1113 4223	0000 5432	1123 5333	5	2223 1120	2122 1011	0001 0010	2223 1121
6	1654 2211	3442 0213	2344 2001	3654 2213	6	2334 3221	2321 3221	0113 1110	2334 3221
7	1045 3221	3123 1222	1023 2001	3145 3222	7	1441 1100	2332 0000	1130 0000	2442 1100
8	3564 2220	3354 1110	1264 1000	3564 2220	8	0020 1110	0020 0001	0010 0000	0020 1111
9	0343 3210	2332 2212	1032 2000	2343 3212	9	0111 1322	1110 1132	0000 0000	1111 1332
10	3300 2121	2200 1022	1000 0000	3300 2122	10	2435 5321	4333 2213	2324 3110	4435 5323
11	3232 3121	4232 1111	1121 0000	4232 3121	11	1334 3201	2332 2012	0013 3100	2334 3212
12	1413 1100	3312 0000	1201 0000	3413 1100	12	3042 3210	3242 3100	1031 3100	3242 3210
13	0022 1000	0122 0001	0001 0000	0122 1001	13	0033 0100	0023 1000	0013 1000	0033 1100
14	1214 1333	2212 1323	0002 0212	2214 1333	14	0000 0100	0010 1111	0000 0000	0010 1111
15	5453 3530	4332 3422	4322 2200	5453 3532	15	0122 1000	0032 0000	0011 0000	0132 1000
16	2422 1001	2331 1012	2111 0001	2432 1012	16	0120 0211	0210 0011	0010 0000	0220 0211
17	0004 3332	1013 2223	1002 2111	1014 3333	17	0002 0111	0011 0012	0000 0000	0012 0112
18	2334 4322	3232 3323	1022 2111	3334 4323	18	1044 1011	1023 1002	0012 0001	1044 1012
19	2423 2212	3411 1113	1301 0001	3423 2213	19	1132 3222	2232 2112	0021 3001	2232 3222
20	1243 2211	2222 2121	0032 1110	2243 2221	20	0000 0111	1001 0011	0000 0000	1001 0111
21	0121 0100	1121 0001	0010 0000	1121 0101	21	0023 1312	1022 1112	0012 0100	1023 1312
22	0021 1100	1220 0000	0020 0001	1221 1100	22	2312 3211	2112 2010	1001 1000	2312 3211
23	0000 3221	0011 2222	0000 2111	0011 3222	23	1120 0101	1010 0001	0000 0000	1120 0101
24	1222 1112	1222 0102	1101 0001	1222 1112	24	2432 3223	3323 1003	1212 2101	3433 3223
25	1330 1302	2330 1212	1120 0101	2330 1312	25	1310 0002	3200 0002	0000 0001	3310 0002
26	0033 0001	1112 0011	0002 0000	1133 0011	26	0020 1000	0121 0011	0000 0000	0121 1011
27	0000 1213	0000 1003	0000 0002	0000 1213	27	0002 2311	0011 1022	0001 1110	0012 2322
28	3225 5533	3335 5424	1214 4323	3335 5534	28	2122 0202	1201 0111	0000 0010	2222 0212
29	1456 5544	2454 6535	0255 5524	2456 6545	29	0201 0110	0201 0001	0000 0000	0201 0111
30	6576 5321	6566 6332	8777 7332	6576 6332	30	0020 0000	0000 0000	0000 0000	0020 0000
					31	1234 3201	1233 2101	0013 2100	1234 3201

THREE-HOUR RANGE INDICES

VICTORIA 1969

TABLE 51

NOVEMBER

DAY	D	H	Z	K
1	0000 0000	0000 0000	0000 0000	0000 0000
2	2023 3211	1121 0222	0000 0000	2123 3222
3	2443 3321	2333 2222	1132 1100	2443 3322
4	0233 1110	2212 0001	0003 0000	2233 1111
5	1102 2200	1212 1201	0000 0100	1212 2201
6	0020 0001	1010 0001	0000 0000	1020 0001
7	2233 3231	3232 3312	1021 3110	3233 3332
8	0232 3343	1221 2342	0020 0232	1232 3343
9	1455 5441	2436 5532	0336 4531	2456 5542
10	1365 5332	2354 4232	1343 4220	2365 5332
11	1123 2221	1122 1312	0011 0100	1123 2322
12	1212 0000	3111 0110	1001 0000	3212 0110
13	0012 1211	0012 0101	0000 0000	0012 1211
14	1000 0000	0100 0000	0000 0000	1100 0000
15	0000 0000	0000 0000	0000 0000	0000 0000
16	0000 0110	1011 0011	0000 0000	1011 0111
17	0000 0111	1000 0011	0000 0010	1000 0111
18	0002 0211	1110 0121	0000 0000	1112 0221
19	0031 3111	0011 1021	0000 1000	0031 3121
20	1001 0000	1111 0000	0000 0000	1111 0000
21	0001 0101	0010 1001	0000 0000	0011 1101
22	1321 1221	3322 1011	1100 0010	3322 1221
23	0000 0211	0000 0012	0000 0001	0000 0212
24	0013 2211	1012 1111	0002 0000	1013 2211
25	0032 3212	0022 0111	0001 1000	0032 3212
26	2331 1332	2321 1331	1010 0110	2331 1332
27	1545 4332	1333 3332	0234 3310	1545 4332
28	1252 3112	2122 0112	1022 1011	2252 3112
29	0044 4222	1021 2222	0011 3111	1044 4222
30	4342 2421	3333 2221	2232 0100	4343 2421

DECEMBER

DAY	D	H	Z	K
1	0013 3210	0022 1000	0001 1000	0023 3210
2	0121 1110	0020 0000	0010 0000	0121 1110
3	0010 0013	0000 0013	0000 0001	0010 0013
4	2213 3210	2222 2200	0001 2100	2223 3210
5	0234 4433	0233 3323	0013 2212	0234 4433
6	3543 4322	3422 3322	2322 3201	3543 4322
7	1023 1101	1121 1100	0001 0000	1123 1101
8	1110 1110	1110 0111	0000 0000	1110 1111
9	3301 2211	1211 1101	0100 1000	3311 2211
10	0011 0222	0011 0112	0000 0000	0011 0222
11	2142 2221	2232 1110	0030 2100	2242 2221
12	1211 2000	1211 1000	0000 0000	1211 2000
13	0020 1100	1110 0000	0000 0000	1120 1100
14	0000 1311	0001 1100	0000 0000	0001 1311
15	0002 1211	0012 0111	0001 0000	0012 1211
16	1052 2321	3131 2311	1010 0010	3152 2321
17	1002 1100	2001 0000	0000 0000	2002 1100
18	0000 0010	0000 0000	0000 0000	0000 0010
19	0001 2111	1001 1111	0000 0001	1001 2111
20	0000 0111	0000 0010	0000 0011	0000 0111
21	1000 0001	2000 0101	0000 0000	2000 0101
22	1042 3321	1031 3211	0010 1101	1042 3321
23	0224 4332	1223 3222	0002 2200	1224 4332
24	3204 3221	3112 2021	2002 2000	3214 3221
25	0432 3222	0222 2111	0111 1100	0432 3222
26	1032 1322	0022 0312	0010 0101	1032 1322
27	3334 2110	2323 0101	0113 2000	3334 2111
28	0002 1110	0001 0201	0000 0100	0002 1211
29	0012 0110	1021 1000	0000 0000	1022 1110
30	0201 0000	0100 1000	0000 0000	0201 1000
31	0002 0001	0102 0011	0000 0010	0102 0011

PUBLICATIONS of the EARTH PHYSICS BRANCH

VOLUME 41-NO. 7

determining mean hourly values by electronic integration

W. R. DARKER

DEPARTMENT OF ENERGY, MINES AND RESOURCES

OTTAWA, CANADA 1971

Cat. No.: M70-41/7

determining mean hourly values by electronic integration

W. R. DARKER

Abstract. An electronic integrator with a time constant of one hour has been constructed for the purpose of determining, in real time, the mean hourly values of the magnetic field. After calibration, the error in output did not exceed 5 mv for an input voltage of 1 volt. Temperature drift, referred to the output, is 0.2 per cent/degree C. Used with a fluxgate magnetometer giving a signal of 10 mv/γ, the integrator should produce mean hourly values accurate to 1γ.

Résumé. Un intégrateur électronique fonctionnant avec une constante de temps d'une heure a été construit afin de déterminer, en temps réel, les valeurs horaires moyennes du champ magnétique. Après l'étalonnage de l'intégrateur, l'erreur de sortie n'a pas dépassé 5mV pour une tension d'entrée de 1 volt. La variation de température reliée à la sortie est de 0.2 p. 100 par degré centigrade. Utilisé avec un magnétomètre à noyau saturable émettant un signal de 10mV/γ, l'intégrateur devrait donner des valeurs horaires moyennes d'une précision de 1γ.

Introduction

The two basic outputs of a geomagnetic observatory are the *magnetogram*, a sheet of photographic paper on which the variations of three elements of the earth's magnetic field have been recorded throughout a 24-hour period, and *mean hourly values*, tables of figures giving the average value of the elements from the beginning of one Greenwich hour to the beginning of the next, for each hour of the day. The mean hourly values (MHV) provide the basis for studies of the diurnal variation of the geomagnetic field, solar and lunar tidal effects on the ionosphere, secular change, and other long-period phenomena. The magnetograms are used to study variations with periods of a few minutes to a few hours.

At all but a few magnetic observatories, mean hourly values are obtained by manual scaling of the magnetograms. A transparent scale with a line parallel to the time-axis is placed over the magnetogram and adjusted until the areas between the trace and the line are equal, above and below the line (Figure 1). The mean ordinate for the hour is then read, in millimetres from the baseline, and recorded. It is of course equivalent to the integral of the instantaneous ordinate, divided by the averaging interval of 60 minutes.

Even when a computer is used to process the manually scaled values, the work is tedious, and it requires great care to avoid errors, especially when the traces are disturbed by a magnetic storm. Semi-automatic machines have been designed to compute hourly means from the magnetograms (Caner and Whitham, 1962), or alternatively, to digitize the magnetograms at closely spaced points, so that means may be calulated by a computer (Nelson, 1967).

The approach adopted here is to compute mean hourly values in real time, as the observations are in progress. When the observatory possesses an instrument, such as a fluxgate magnetometer, whose output is three electrical voltages proportional to three components of the geomagnetic field, the averaging can be done by electronic integrators. The integral is set to zero at the beginning of the hour. The integrator is then allowed to operate for 60 minutes, the integral is read by a digital voltmeter and recorded on punched tape, the integrator is reset to zero, and the process is repeated

In the past, it has been difficult to build electronic integrators which will operate accurately over time intervals longer than one minute. The recent development of operational amplifiers with low input currents and offset voltages, and the development of plastic film capacitors with low leakage currents now make it possible to construct integrators which will operate over intervals of an hour or more with acceptable accuracy.

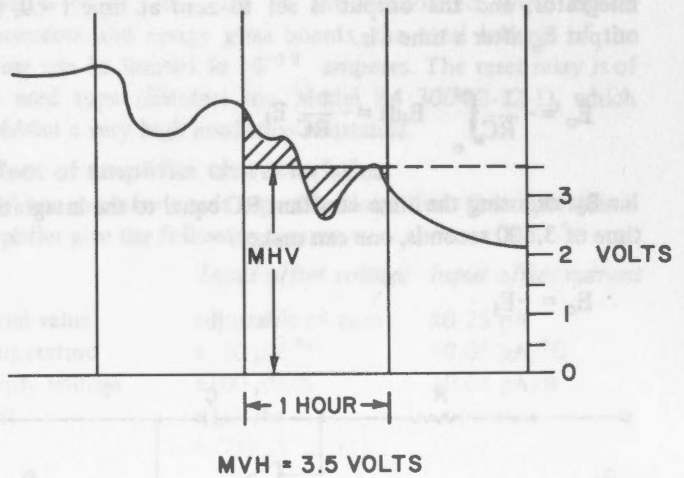

Figure 1. Scaling mean hourly values.

Design requirements

The overall aim is to produce mean hourly values accurate to $\pm 1\gamma$ (10^{-5} gauss). The fluxgate magnetometer output consists of three voltages, with respect to ground, proportional to the variations of three orthogonal magnetic components from preset baseline values, at a scale of 1 volt = 100γ (Trigg *et al.*, 1970). The range of the magnetometer is $\pm$10 volts, corresponding to $\pm 1000\gamma$.

The scale and range of the integrator output, after integration over 60 minutes, may conveniently be the same as the magnetometer. The error of the integrator output should be less than 1γ, or 0.01 volt. The magnetometer baselines are adjusted so that the quantities being integrated are of the order 100γ or 1 volt on the average, except during large magnetic disturbances, when signals averaging several volts over the hour must be integrated.

The ideal integrator

Figure 2 shows the basic integrator circuit with ideal components. It is assumed that the amplifier has zero input current and infinite gain, so that the voltage at the input terminal must be zero. Summing currents at the input terminal,

$$\frac{e_i}{R} + C\frac{de_o}{dt} = O \qquad \ldots .1$$

$$\frac{de_o}{dt} = \frac{1}{RC}e_i \quad \text{and} \qquad \ldots .2$$

$$e_o = -\frac{1}{RC}\int e_i dt \qquad \ldots .3$$

If a constant voltage E_i is applied to the input of the integrator, and the output is set to zero at time $t=0$, the output E_o after a time t is

$$E_o = -\frac{1}{RC}\int_o^t E_i dt = -\frac{t}{RC}E_i \qquad \ldots .4$$

By choosing the time constant RC equal to the integrating time of 3,600 seconds, one can make

$$E_o = -E_i \cdot$$

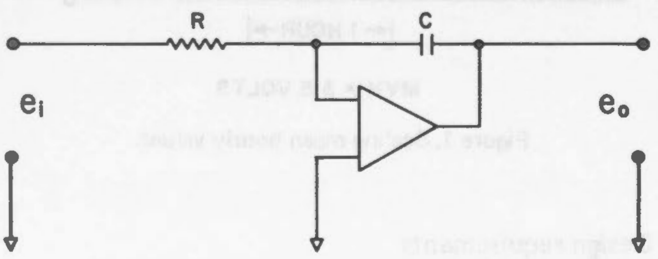

Figure 2. Basic integrator circuit with ideal components.

The practical integrator

Unfortunately, practical components do not meet the above ideal specifications, and it is necessary to examine their limitations and evaluate their effects.

In the design of a long-period integrator, the most critical departure from the ideal is that for an amplifier to give zero output voltage, it must be supplied with an input offset current i_{os}, and an input offset voltage e_{os}. Moreover, its voltage gain will not be infinite, but will have some value G. The practical circuit is shown in Figure 3. Some current will also leak through the dielectric and the case of the capacitor, as represented by the leakage resistance R_c.

Summing currents at the input terminal of the amplifier,

$$\frac{e_i - e_2}{R} + i_{os} + C\frac{d(e_o - e_2)}{dt} + \frac{e_o - e_2}{R_c} = 0 \qquad \ldots .5$$

$$e_o = -G\,e_3 = -G(e_2 + e_{os}) \qquad \ldots .6$$

Eliminating e_2 from Equations 5 and 6, we obtain

$$\frac{de_o}{dt} = -\frac{1}{(1+\frac{1}{G})RC}\left[e_i + Ri_{os} + (1+\frac{R}{R_c})e_{os}\right] - \frac{de_{os}}{dt}\left[\frac{1}{(G+1)RC} + \frac{1}{R_cC}\right]e_o \qquad \ldots .7$$

Integrating with respect to t,

$$e_o = -\frac{1}{(1+\frac{1}{G})RC}\int\left[e_i + Ri_{os} + (1+\frac{R}{R})e_{os}\right]dt - e_{os} - \left[\frac{1}{(G+1)RC} + \frac{1}{R_cC}\right]\int e_o dt \qquad \ldots .8$$

In comparison with Equation 3, four types of errors may be identified:

(a) The time constant RC is increased by the factor $(1+\frac{1}{G})$. In practice, G is greater than 10,000, so that the resulting scale error is less than 0.01 per cent. In any case, a constant scale error will be compensated in the overall calibration of the system.

(b) Errors proportional to the current offset and voltage offset of the amplifier input are in effect added to the input

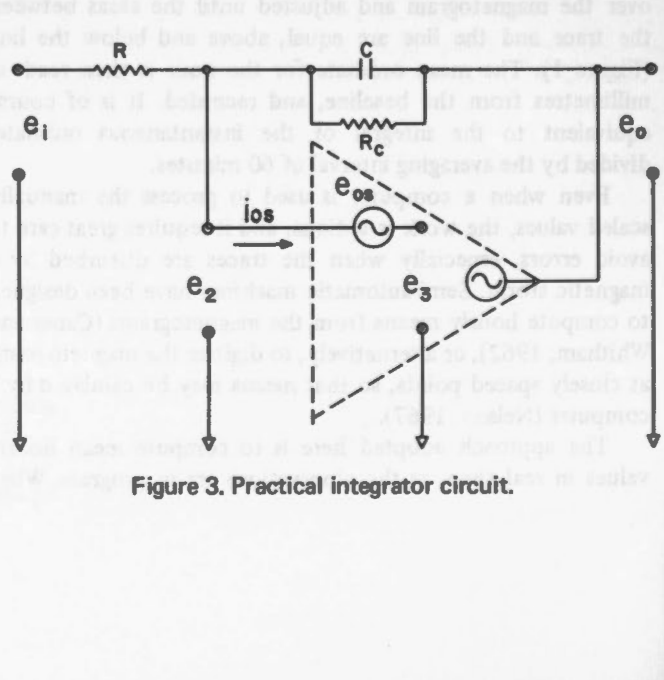

Figure 3. Practical integrator circuit.

signal e_i. The result of the offsets can thus be estimated easily.

(c) The integrator output is displaced by the voltage $-e_{os}$.

(d) The integrator output is reduced by a term containing the integral of e_o. The effect of this term is examined by considering the case of a constant input E_i, neglecting for the moment the scale error (a) and the offset errors (b) and (c). Equation 8 becomes

$$e_o = -\frac{1}{RC}\int_0^t E_i dt - \left[\frac{1}{(G+1)RC} + \frac{1}{R_cC}\right]\int_0^t e_o dt \quad \ldots 9$$

Since the last term is small, we may substitute from Equation 4, to a good approximation

$$e_o = -\frac{t}{RC}E_i, \text{ for any t during the integrating interval,}$$

$$\text{and} \int_0^t e_o dt = -\frac{E_i}{2RC}t^2 \quad \ldots 10$$

The equation analogous to Equation 4 is

$$E_o = -\frac{t}{RC}\left[1 - \left(\frac{1}{(G+1)RC} + \frac{1}{R_cC}\right)\frac{t}{2}\right]E_i \quad \ldots 11$$

The percentage error from this source is thus proportional to the integrating time.

An integrator with a time constant of one hour

The circuit diagram of the integrator built by the author is shown in Figure 4. The input resistor $R_1 = 3.6 \times 10^9$ ohms is vacuum-sealed in a glass envelope (Welwyn type M51). The capacitor C_1 x 1.0 μf has a polystyrene film dielectric (West-Cap WR 94W1105). The leakage current of the capacitor

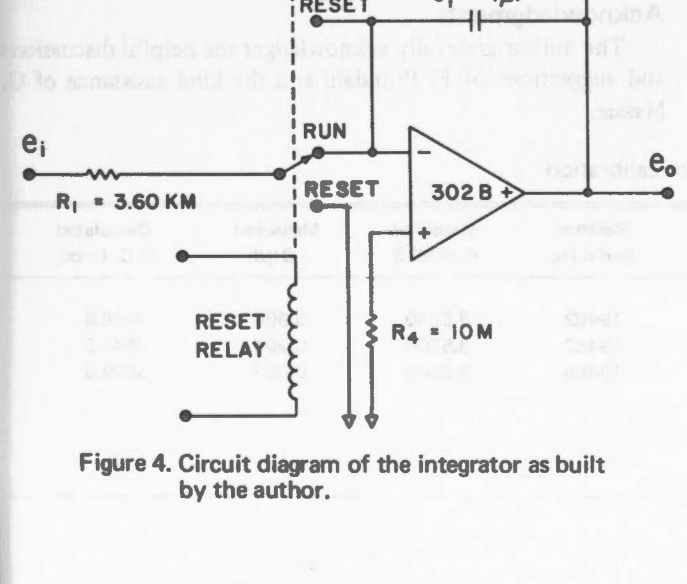

Figure 4. Circuit diagram of the integrator as built by the author.

was measured to be 1 pA at 1.0 volt, corresponding to $R_c = 10^{12}$ ohms. A parametric operational amplifier (Analog Devices type 302B) was chosen as the active device for the integrator, chiefly because of its small input bias current (0.25×10^{-12} A).

At the beginning of the hour, the reset relay is closed for about 1 second, removing the input signal and connecting R_3 across the capacitor. Since the input impedance of the amplifier is greater than R_4, which is 10 megohms, the capacitor discharges through R_3 with a time constant of .01 second, if the left-hand end of R_2 is open-circuited. The voltage on the condenser will thus be reduced to 0.1 per cent of its initial value in .07 second, and e_o is quickly brought to the value $-e_{os}$. The output voltage e_o is then recorded by the digital recording system, thus providing a record of the amplifier offset voltage e_{os}. If it is desired to reset the integrator to a voltage different from zero, the free end of R_2 may be connected to a suitable voltage source.

It will be appreciated that the avoidance of leakage currents at the input of the amplifier is of the greatest importance. With an input resistor of 3.6×10^9 ohms, a leakage current of 10^{-12} amperes will cause an error of 3.6 millivolts, or 0.36γ. It is estimated that with careful layout of the power supply leads, the use of teflon-insulated wire, teflon connectors and epoxy glass boards, the total leakage of the wiring can be limited to 10^{-13} amperes. The reset relay is of the reed type (Electrol Inc. Model R4 3004-2-12-1), which possesses a very high insulation resistance.

Effect of amplifier characteristics

The manufacturer's specifications for the operational amplifier give the following figures:

	Input offset voltage	*Input offset current*
initial value	adjustable to zero	±0.25 pA
temperature	± 30 μV/°C	±0.05 pA/°C
supply voltage	±100 μV/%	±0.01 pA/%
drift	±7μV/hr or ± 200 μV/month	not stated

For a temperature range of ±10°C, and a supply voltage range of ±0.1 per cent, over a period of one month the input offset voltage should remain within the range ±500 μV, and the input offset current should not exceed ±1 pA.

From the specifications it is difficult to predict the amplifier performance over longer intervals of time, but it is unlikely that a drift rate of 200 μv/month in the offset voltage would continue for many months in the same direction. The above figures of ±500 μV and ±1 pA will therefore be assumed as a reasonable estimate of long-term performance.

Inserting e_{os} = 500 μV and i_{os} = 1 pA in Equation 8, we find that the error in the integrator output at the end of the integration period will be

$$-Ri_{os} - \left(1 + \frac{R}{R_c}\right)e_{os} + e_{os} = -4.6 \text{ mV}$$

corresponding to 0.46γ.

Stability of the integrator scale constant

The integrator time constant RC will be affected by the variations with temperature of R and C. The temperature coefficient of the input resistor is −0.15 per cent/°C and the temperature coefficient of the feedback capacitor is −0.01 per cent/°C. The main effect of temperature on the scale constant of the integrator t/RC will be due to the resistor, amounting to +0.16 per cent/°C.

The amplifier gain G will depend on temperature, but may be assumed to remain greater than 10,000 in normal operating conditions. The effect of temperature on the factor $(1+\frac{1}{G})$ may thus be ignored.

It was shown above in Equation 11 that there is an additional scale-constant error, a factor of the order

$$1-\left[\frac{1}{(G+1)RC}+\frac{1}{R_cC}\right]\frac{t}{2}$$

where t is the integration time (3,600 seconds).

With $R_c = 10^{12}$ ohms, the error amounts to −0.18 per cent. However, the capacitor leakage increases rapidly with increasing temperature, so that at 40°C, $R_c= 0.5 \times 10^{12}$ ohms, and the error would be doubled for a 20° rise in temperature.

In summary, the scale constant of the integrator would be expected to have a temperature coefficient of −0.12 per cent/°C. If the signal being averaged is 1 volt, or 100γ; the temperature variation of the output will be −1.2 mv/°C, or −0.12γ/°C.

Calibration tests

Table I shows the results of calibration tests carried out over an interval of nine months. Three integrators were allowed to run for a period of 3600 ±1 seconds with a constant input of 1.00000 volt. At the end of the hour, the output was read, the integrator was reset, and the cycle was repeated. The standard deviation for each integrator was 0.0017 volt or 0.2 per cent.

If the integrator scale constants were exactly one, the output voltages should equal the constant input voltage. The measured outputs deviated by less than 2 per cent, which is the tolerance of the input resistors.

The effective time constants RC determined on January 23, 1970, agreed to within 0.1 per cent with the values of RC calculated from individual measurements of the resistors and capacitors. There was no significant change in the effective time constants over the nine-month interval.

Temperature tests

One integrator operating with a constant input voltage of 1.00000 volt and averaging intervals of one hour was tested over a temperature range of 30°C. The measured output changed by −54 mV, or −1.8 mV/°C. This result is in satisfactory agreement with the predicted temperature effect.

Linearity tests

To check the long-term error calculated in Equation 11, an integrator was operated for 12 hours with a constant input voltage of 1.00000 volt. According to Equation 11, the predicted output voltage at the end of 12 hours will be 2.2 per cent smaller than the ideal response.

The measured error at the end of 12 hours was 0.4 per cent, indicating that the leakage resistance R_c is considerably larger than 10^{12} ohms.

As part of the long-term test, the integrators were allowed to run to saturation. This occurred at an output of ±14.4 volts.

Conclusions

It is practical to derive mean hourly values of an electrical signal using a capacitive feedback integrator constructed with modern components. Assuming that the system is calibrated, to take into account the tolerances of the resistor and capacitor, the error in the output after integrating for one hour due to drift, voltage offset and current offset of the amplifier does not exceed 5 mv, over a temperature range of ±10°C. The error in the output due to temperature variation of the integrating resistor and capacitor does not exceed 0.2 per cent of the output /°C.

Applied to a fluxgate magnetometer giving a signal of 10 mv/γ, the integrator should produce mean hourly values accurate to 1γ, in a laboratory environment, provided the average magnetometer output is not greater than 1 volt, corresponding to 100γ.

Acknowledgments

The author gratefully acknowledges the helpful discussions and suggestions of F. Primdahl and the kind assistance of G. Massie.

Table I. Integrator calibration

Date	Unit No.	Volts in ±1x10^{-6}	Volts out ±0.002	Apparent R.C. (secs)	Resistor Serial No.	Measured R (KMΩ)	Measured C (μf)	Calculated R.C. (secs)
Jan. 23	1	1.00000	1.005	3589.2	19462	3.5940	0.998	3586.8
1970	2	1.00000	1.015	3546.7	19463	3.5700	0.994	3548.5
	3	1.00000	0.990	3636.3	19465	3.6500	0.997	3639.0
Apr. 23	1	1.00000	1.007					
1970	2	1.00000	1.016					
	3	1.00000	0.990					

References

Caner, B., and K. Whitham. 1962. A semi-automatic magnetogram reader, *J. Geophys. Res.*, Vol. 67, No. 13, pp. 5362-5364.

Conant, R. 1968. How to select R and C for minimum drift, *Analog Dialogue*, 2, No. 1, pp. 10-11, Analog Devices Inc., Cambridge, Mass.

Nelson, J.H. A magnetogram scaling machine, U.S. Coast and Geodetic Survey, ESSA, Rockville, Maryland, 12 pp.

Philbrick Research Corpn., Computing Amplifiers, *Philbrick Applications Manual*, 2nd ed., June 1966, 45 pp.

Strata, R. 1968. Minimizing Integrator Errors, *Electrotechnology*, Oct., 1968, pp. 46-50.

Terman, F.E. 1966. Electronic and radio engineering, Fourth ed., pp 621-624, McGraw-Hill, New York.

Trigg, D.F., P.H. Serson, and P.A. Camfield. 1971. A solid-state electrical recording magnetometer, Pub. Earth Physics Branch, Vol. 41, No. 5.

[illegible]

Attention [illegible] considering the [illegible] output [illegible] [illegible] of the [illegible] the output

[illegible]

where t is the integration time, [illegible] seconds.

With $R_L = 10^{13}$ ohms, the error amounts to [illegible] per cent. However, the capacitor leakage increases rapidly with increasing temperature, so that at 60°C, R_L = [illegible] $\times 10^{12}$ ohms, and the error would be doubled for a 20° rise in temperature.

In summary, the scale constant of the integrator would be [illegible] to have a temperature coefficient of [illegible] per cent/°C. If the signal being averaged is 1 volt, or 100γ, the [illegible] variation of the output will be [illegible] °C, or [illegible]

Integration tests

Table 1 shows the results of calibration tests carried out over an interval of [illegible] months. Three integrators were [illegible] to [illegible] for a period of 3600 [illegible] seconds with a constant input of 1.00000 volt. At the end of the hour, the output was read, the integrator was reset, and the cycle was repeated. The standard deviation for each integrator was [illegible] per cent.

If the integrator scale constants were exactly one, the output voltage should equal the [illegible] input voltage. The [illegible] by less than [illegible] per cent, which is [illegible]

[illegible]

[illegible] than measurements of the [illegible] [illegible] there was no significant change in the effective [illegible]

References

Cook, [illegible] and [illegible], [illegible]. [illegible], *J. Geophys. Res.*, Vol. 67, No. 13, pp. [illegible]

Counts, [illegible] 1966. How to select R and C for integrating [illegible] [illegible], pp. [illegible]. Boston [illegible]

[illegible] Survey, [illegible] Maryland, [illegible] pp.

Philbrick Research Corp. Computing Amplifiers. [illegible] Applications Manual, 2nd ed., June 1966, 45 pp.

[illegible] agreement with the predicted temperature effect.

Linearity tests

To check the nonlinear error calculated in Equation 11, an integrator was operated for 12 hours with a constant input voltage of 1.00000 volt. According to Equation 11, the predicted output voltage at the end of 12 hours will be 2.2 per cent smaller than the ideal response.

The measured error at the end of 12 hours was 0.4 per cent, indicating that the leakage resistance R_L is considerably larger than 10^{13} ohms.

As part of the long-term test, the integrators were allowed to run to saturation. This occurred at an output of [illegible] volts.

Conclusions

It is practical to derive mean hourly values of an electrical signal using a capacitive feedback integrator constructed with modern components. Assuming that the system is calibrated to take into account the tolerances of the resistor and capacitor, the error in the output after integrating for one hour due to drift, voltage offset and current offset of the amplifier does not exceed 5 [illegible] over a temperature range of ±10°C. The error in the output due to temperature variation of the integrating resistor and capacitor does not exceed [illegible] per cent of the output /°C.

Applied to a fluxgate magnetometer giving a signal of [illegible] mV/γ, the integrator should produce mean hourly values accurate to [illegible] γ in a laboratory environment, provided the average magnetometer output is not greater than 1 volt, corresponding to 100γ.

Acknowledgements

The author gratefully acknowledges the helpful discussions and suggestions of [illegible] and the kind assistance of [illegible]

Table 1. Integrator calibration

[illegible]	[illegible]	[illegible]	[illegible]	[illegible]	[illegible]	Standard [illegible]	Calculated R.C. [illegible]
[illegible]	[illegible]	[illegible]	[illegible]	[illegible]	[illegible]	[illegible]	[illegible]
[illegible]	[illegible]	[illegible]	[illegible]	[illegible]	[illegible]	[illegible]	[illegible]
[illegible]	[illegible]	[illegible]	[illegible]	[illegible]	[illegible]	[illegible]	[illegible]

PUBLICATIONS of the EARTH PHYSICS BRANCH

VOLUME 41 – NO. 8

problems in the development of a mirror transit telescope at ottawa

R. W. TANNER

DEPARTMENT OF ENERGY, MINES AND RESOURCES

OTTAWA, CANADA 1971

Cat. No.: M70-41/8

Contents

problems in the development of a mirror transit telescope at ottawa

R. W. TANNER

Abstract. In order to assist other observatories working on improvements in meridian circle techniques, some of the difficulties encountered at the Dominion Observatory in its Mirror Transit Circle program are described. Some satisfactory aspects of the design, applicable perhaps to other instruments, are noted. An outline is given of the circumstances leading to abandonment of the project.

Résumé. Afin d'apporter une aide à d'autres observatoires dans leurs travaux d'amélioration de la technique du cercle méridien, l'auteur décrit quelques difficultés auxquelles l'Observatoire fédéral a dû faire face dans son programme relatif au télescope des passages. Il mentionne quelques aspects satisfaisants de l'instrument susceptibles d'être appliqués à d'autres. Il décrit brièvement les circonstances qui ont amené l'abandon des travaux.

Introduction

In 1954 plans were initiated for the replacement of the Ottawa meridian circle, installed in 1905, whose performance, particularly in declination, was falling increasingly behind modern standards. A proposed mirror transit-circle (Atkinson, 1947) offered among other advantages, much greater freedom from flexure, a fundamental control of any variation of collimation with altitude, the possibility of increasing aperture and scale, and greater facility for incorporating automated impersonal methods of registration. The disadvantages noted by Atkinson (double the effect of circle errors on the declination, increase in the effect of pivot errors on the right ascensions, difficulty of providing azimuth marks, and others) did not appear decisive.

Design considerations

Because of favourable experience with our photographic zenith tube of 25-cm aperture at f/17, the same dimensions were chosen, permitting the observation of PZT stars and asteroids. Photographic registration was intended, but as it was not certain that the instrumental constants could be so determined, provision was made for visual observations also. To minimize the circle reading disadvantage, a 76-cm-diameter circle and six long-focus microscopes rather elaborately mounted were specified. Observing slit and room refraction problems were to be obviated by nearly open-air operation. Atkinson's idea for observing all contributions to effective pivot errors was followed. Control of systematic errors down to ±0″.10 or better was aimed at; accidental errors two or three times as large could be tolerated as still superior to our meridian circle. If these last two goals could be achieved, a valuable contribution could be made to fundamental astronomy.

Brief history of the project

Construction, begun by 1959 on a temporary site adjacent to the observatory made available for 10 years, was almost completed by 1961. Brealey (1961) provides a good description, with additional detail in Brealey (1963). Fulfilment of the meridian circle commitment to AGK3R at the end of 1962 freed enough staff to commence operations in 1963. It soon became clear that the circle graduations were much too ill-defined for our requirements. The United States Naval Observatory undertook to regraduate the circle; while this was being done, a series of test observations in right ascension of stars selected from FK4 was begun in August 1963. Observations in both co-ordinates were resumed in February 1965 on this list supplemented by Ottawa zenith stars and several high polars ($\delta > 89°$). This work was halted in 1967 because of an increasingly evident instability of the axis. A right ascension list involving a few fundamental stars, repeated high polars, and doubled observations of zenith stars before and after transit was substituted for it. This program, intended to show as directly as possible the effects of the modifications undertaken, continued until suspension of activity in 1969.

Some of the problems encountered

An enumeration of some of the principal scientific problems encountered during these efforts follows.

1. The systematic accuracy of ±0″.05 required of the divided circle was not attained. The graduations, at 3′ intervals on a gold band, although greatly superior to the originals and closely similar to ones found quite satisfactory at USNO, were seen to shift in apparent position when illumination and exposure were varied. The six cameras in regular use (two 45° above, two 45° below the horizontal pair) made it possible to determine the relative division errors of four diameters at 45° in the course of the numerous regular readings at settings 0°, 45°, 90° etc., made for determining the instrumental constants. These relative errors were found to differ by amounts of the order of ±0″.10 (on the circle) in changing from the circle west set of cameras to circle east. These discrepancies were not removed by a fairly elaborate regulation of the obvious variables, and therefore a fuller determination of division errors was never undertaken.

Further complications probably resulted from the fact that the gold background of the filled graduations was not of a uniform aspect all around the circle. The automatic measuring engine for the circle films, on the other hand, could only be got to give properly repeatable results on a rather narrow range of film density. Visual measurement was found to be too inaccurate, and of course very tedious. Mechanical film-processing and photo-electric control of exposures were introduced to get satisfactory automatic measuring. It might be mentioned that the investigation of circle problems was made easier by the great stability (order of 0."10 relative motion over a six-hour session) of the long microscope tubes with 5X magnification. Even changing the film magazines would alter the pointing by only a few seconds of arc.

2. The long horizontal air path, over 13 m from north to south collimator prime focus, about 1.5 m above grade, led to generally poor local "seeing". This was evident both in the millisecond duration exposures for instrumental constants, where successive images of the same graticule were often displaced by a second of arc (20μ), and on the repeated 15- to 30-second exposures of the high polars for azimuth, where the star images were not infrequently similarly displaced.

In the special series of observations of zenith stars twice per transit, where nearly all variables except a minimum of seeing can be eliminated, the typical discordance in right ascension (which includes the relatively small photographic and measurement errors) was 40 ms for two 40-second exposures with centres one minute apart. This corresponds to a typical seeing displacement of about 0."30 in a single image. A strictly comparable figure for the nearby PZT with 20-second exposures is 0."20. In the case of the PZT this is halved by the four exposures available; for the mirror transit the seeing errors increase with zenith distance, are worse in the declination co-ordinate, and multiple exposures on a single transit are not generally feasible. The effect on the instrumental constants other than azimuth can be reduced by multiplying the readings, and the azimuth uncertainty reduced by using more stars in its determination, but with an evident loss of efficiency.

Various combinations of building and tube fans were tried, and insofar as their use could mitigate the temperature differences displayed by the thermistors at the central section and the collimators, with beneficial result. But the observers often found this impossible; it was often necessary to close the building to get a readable set of the instrumental constants taken every hour.

3. The above difficulty was obviously compounded by the almost open-air operation. Rolling away the roof and walls exposed the whole instrument to a near-hemisphere of sky, with subsequent radiative cooling, and to the passage, with the breeze, of inhomogeneous parcels of air close to the ground. Collimation readings were usually taken at the half aperture above and below the mirror (directed at the zenith then the nadir for this purpose), and these often differed systematically by over 1" in the vertical plane. A more striking phenomenon was the occasional doubling of the return image at auto-collimation or nadir. Both were ascribed to layering of the air in the proximity of the massive central section.

Ventilation, radiative shielding and thermal lagging were tried; the "over-under" difference was never wholly eliminated, thus casting doubt on the reliability of the declinations deduced. From the practical point of view, the roof opening mechanism was among the most vulnerable of the many subsystems of the mirror transit, and many months of observing were lost by failures in it.

4. A perplexing instability in the azimuth of the mirror axis, which became increasingly evident after 1966 (although perhaps not entirely absent previously) was not wholly removed. Variations of over 100 ms during the night (corresponding to relative motion of 7μ at the vees) were found eventually to correlate roughly with temperature changes. At the same time the level of the axis as well as the line of collimation between north and south telescopes would remain constant to 10 ms, barely above the error in their determination. As the old meridian circle had never displayed such symptoms, the mode of attachment of the superstructures was suspect first. Modifications to attach the massive base plates more directly and firmly to the reinforced concrete piers did not remove the fault. The portions of the piers above ground were heavily insulated as well as the superstructure, with rudimentary thermostatting around the base plates; these steps brought about some improvement as the experiments ended. It should be mentioned that changes in the line of collimation in the vertical plane, consonant with vertical motion in the independent north-south piers, were also evident, so that changes would have had to be made there too if measures in declination had been resumed.

The foregoing problems prevented the attainment of the goals mentioned earlier. Although several hundred nights of observations of fundamental and zenith stars were made, no useful positions have resulted; in declination for want of division corrections, in right ascension because of the dispersion. This could rarely be brought down to 20 ms secδ even in a differential reduction of the results of a single session, so that the number of satisfactory observations of even the most frequently observed stars was too small to be valuable.

Some satisfactory features of the design

Turning now to features of the Ottawa design found useful, the following are noted.

1. On the whole, photographic registration of stars and constants worked well. Visual observations were made only for such purposes as checking the focus, seeing or adjustment. The system of flashing the graticule at known five-second intervals during transit did away with any need of a chronograph, ensured that the star image was always close to a reference mark, and allowed the accuracy of tracking to be verified. Normally 40 s exposures gave well-measurable images of tenth magnitude stars. All stars were screened to appear between seventh and tenth magnitude; this range apparently caused no difficulty. The dimensional stability of the 35 mm film (Estar base) during exposure, processing and measuring was generally better than 1/1000, and observations were made so that the distances to be measured were usually under 1 mm. The overall contribution of film and measuring errors was about ±0."10 (±2μ) for the best defined

images. The fact of not working at the prime focus seemed to introduce no problems, probably because of the narrowly differential method of measurement. It is regrettable that no way was found to image all the stars of an observing session together in a common frame as is done with the PZT.

2. The lateral collimators advocated by Atkinson for measuring the effective pivot errors were incorporated in the design at 75 mm aperture, f/24. The consequent enlargement of the hollow pivots was not found to be detrimental, nor was the use of "ears" cemented to the sides of the main mirror. The first tests of the lateral collimators revealed clearly the presence of an oscillation of 15° period and several microns amplitude at the pivot, the result of chatter in the grinding of the latter. After this had been lapped off, the only remaining departure of the normal to the main mirror from a conical path on rotation was less than 15 ms, from a slight pivot ellipticity. The systematic accuracy attained in the course of a repeated series of measurements for this departure was about ±3 ms, but continuous monitoring of the mirror to such accuracy would have been impractical, had it been necessary, as the lateral collimators had hourly drifts several times as large. It was found desirable to align the "ear" normals very closely with the axis of rotation to reduce the excursions of the autocollimated test ray to a minimum.

3. The main mirror, on a simple six-point support held in by springs, showed no detectable flexure or motion in its cell with changes in orientation or temperature. Instead of attempting to maintain a constant pressure of the mirror on its supports by a system of counterpoises, the pressure was made several times what gravity would provide, so that its proportional variation on rotating the axis would be small. The central axis had been designed to be very stiff, and the location of the counterpoising with respect to the vees chosen to minimize flexure at the mirror supports. It was gratifying, then, that no evidence of lateral flexure was found with the autocollimators; that is, it could not have exceeded a few milliseconds. The figure of the mirror could be examined directly at nadir and autocollimation by Foucault testing; no change could be seen after the 45° rotation. While no direct evidence could be got for non-rotation of the mirror in its cell about an east-west axis, the constancy of Atkinson's β_1 (the angle between the plane of the mirror and the axis of rotation), to within the error of observation of a few milliseconds, over periods of months, was reassuring.

4. High polars (specifically BD 89°01, 02, 03, 38, plus Polaris and λUMi) furnished satisfactory azimuth control. Two or three were usually in the extended field (±20′) at all times, and three or four exposures could be made in a few minutes. Since these stars were allowed to trail, measurability depended on their speed as well as magnitude; 89°02, at $10^{m}.8$ with about 30′ polar distance, was generally unusable. A more careful determination of the scale of the photographs (from the known scale of the graticule markings) was necessary in these frames, where the star, up to 25 mm off the optical axis, might be 5 mm from the nearest fiducial mark. The north-south collimators were sufficiently stable to be used as short-term azimuth marks, but the necessity of altering their focal settings from month to month precluded their use as long term controls.

5. The remote-control, servo-setting features of the design were eventually made to work well and reliably. With observing largely reduced to pushing buttons, and the subsequent drudgery of film measurement greatly reduced by automation, no questions of personal equation, or of the effects of the proximity of the observer on the instrument could arise. There was some concern about some of these mechanisms as heat sources close to the instrument, but no difficulties were in fact encountered.

Circumstances leading to abandonment

The final section of this paper outlines the circumstances leading to the abandonment of the project. The disappointingly slow progress in solving the remaining difficulties was discouraging, but no serious flaws in the mirror transit principles had been found. Plausible solutions can be suggested for each problem: a glass circle with direct photo-electric read-out; much taller piers thermostatted throughout; evacuation or helium filling of the collimators; much better isolation of all parts from ambient fluctuations, and so on.

But the time was approaching to vacate the temporary site. Two men closely connected with instrumental development had been sent to the Dominion Astrophysical Observatory, Victoria, to work on the Queen Elizabeth II telescope project. It was hoped that they would resume their first task when the mirror transit was relocated in British Columbia as part of an intended Institute for Astronomy. The Institute plan was rejected, and the Observatories Branch, faced with the prospect of a costly local re-installation of an instrument needing a good deal more time, money and expertise than were available to ensure its success, suspended the operation.

Although there was some thought of storing components to await a more favorable time for resuming the program, subsequent reorganization of the federal government's responsibilities in astronomy, and re-evaluation of all Branch projects, led to the dismantling of the instrument and the dispersal of its constituents in 1970.

References

Atkinson, R. d'E. 1947. A proposed "mirror transit-circle". *Mon. Not. R.A.S.*, 107, 3, pp. 291-307.

Brealey, G.A. 1961. The Ottawa mirror transit telescope. *Sky and Telescope*, 21, 4, pp. 205-209.

Brealey, G.A. and R.W. Tanner, 1963. Photographic registration of transits and reduction of observations on the Ottawa mirror transit telescope. *Dom. Obs. Pub.* Ottawa, XXV, 3.

problems ... [illegible] ... the importance of atmospheric convolution of ... nabula ... [illegible] ... bance isolation of all parts from seismic fluctuations, and so on.

But the time was approaching for vacating the temporary site. Two events closely connected with instrumental development had been sent to the Dominion Astrophysical Observatory, Victoria, to work on the Queen Elizabeth II telescope project. It was hoped that they would sooner than last such as the mirror transit was relocated in British Columbia as part of an intended Institute for Astronomy. The Institute plan was rejected, and the Observatory's Branch faced with the prospect of a costly installation of an instrument needing a good deal more time, money and expertise than were available to ensure its success, suspended the operations.

Although there was some favourable time for completing the assessment measurements of the lateral engagements ... [illegible] ...

... should be got, the uncertainty of current in the coil ... [illegible] ... the constancy of Atkinson's ... constant between the plane of the mirror and the axis of rotation, to within the error of the mirror of a few milliseconds, over periods of months, was maintained.

4. High points (respectively, BD 89 ...), 02, 03, 3?, plus Polaris and ... bracketed collimation azimuth control. Two of these were usually in the extended field ... at all times, and three or four exposures could be made in a few minutes. Since these stars were allowed to trail, measurability depended on their speed as well as on magnitude. 89°03', at 10^h·6 with about 30' polar distance, was generally unusable. A more careful determination of the scale of the photographs (from the known scale of the graticule markings) was necessary in these frames, where the star, up to 25 mm off the optical axis, might be 5 mm from the nearest fiducial mark. The north-south collimators were sufficiently stable to be used as short-term azimuth marks, but the necessity of altering their focal settings from month to month precluded their use as long-term controls.

5. The ... [illegible] ... features of the design were generally made to work well ... [illegible] ...

images. The lack of pin marking at the pivot point seemed to introduce no problems, probably because of the narrowly differential method of measurement. It is noteworthy that no way was found to image all the stars of an observing season together in a common frame as is done with the PZT.

2. The lateral collimators advocated by Atkinson for measuring the effective pivot errors were incorporated in the design of 75 mm aperture. The consequent enlargement of the hollow pivots was not found to be detrimental, nor was the use of "ears" suspended to the sides of the main mirror. The first tests of the lateral collimators revealed clearly the presence of an oscillation of 15' period and several microns amplitude at the pivot, the result of chatter in the clamping of the latter. After this had been stopped out, the only remaining departure of the normal to the main mirror from a conical path on rotation was less than 15 ms, from a right pivot ... The systematic accuracy attained in the course of a repeated series of measurements for this departure was about 25 ms, but continuous monitoring of the mirror to such accuracy would have been impractical, had it been necessary, as the lateral collimators had slowly drifts several times at times. It was found desirable to align the "ear" normals very closely with the axis of rotation to reduce the excursions of the autocollimated test ray to a minimum.

3. The main mirror, on a simple six-point support held in by springs, allowed an appreciable degree of motion in its cell with changes in orientation or temperature. Instead of attempting to ... a constant pressure of the mirror on its support by a system of counterpoises, the pressure was made ... than that gravity would provide, so that the proportional variation on rotation ... axis would be small. The ... been designed ... [illegible]

PUBLICATIONS of the EARTH PHYSICS BRANCH

VOLUME 41–NO. 9

seismological detection and identification of underground nuclear explosions

P. W. BASHAM and K. WHITHAM

DEPARTMENT OF ENERGY, MINES AND RESOURCES

OTTAWA, CANADA 1971

Cat. No.: M70-41/9

Contents

seismological detection and identification of underground nuclear explosions

P. W. BASHAM and K. WHITHAM

An assessment of world-wide seismological capabilities in detecting and identifying underground nuclear explosions based on information submitted by co-operating countries in accordance with the United Nations General Assembly Resolution 2604A (XXIV).

Évaluation à l'échelle mondiale des possibilités de détection et d'identification des explosions nucléaires souterraines fondée sur les renseignements fournis par les pays participants conformément à la résolution 2604A (XXIV) de l'Assemblée générale des Nations Unies.

Preface

As a first step in clarifying what seismological resources would be available for world-wide exchange purposes to facilitate a comprehensive test ban prohibiting underground nuclear explosions, Canada proposed a resolution asking the Secretary-General of the United Nations to circulate to governments a request that they supply information concerning seismograph stations from which they would be prepared to supply records on the basis of guaranteed availability. This resolution (2604A) was adopted at the 1836th plenary meeting of the Twenty-Fourth United Nations General Assembly on December 16, 1969.

Following receipt by the Secretary-General of the solicited seismograph station summary information, the next logical step in clarification was an assessment of the significance of the guaranteed station data for purposes of detecting and identifying underground nuclear explosions. The Arms Control and Disarmament Division of the Department of External Affairs requested the Earth Physics Branch of the Department of Energy, Mines and Resources to prepare such a technical assessment. A preliminary assessment was completed and distributed at the Conference of the Committee on Disarmament (CCD) in early August 1970, prior to an informal meeting on August 12, 1970, of the CCD on a Comprehensive Test Ban. At the time of preparation of the preliminary assessment, the returns to the Secretary-General's questionnaire were incomplete, the assessment being made on the basis of returns from 54 countries, only 33 of which reported information concerning seismograph stations on their territory. The report for which this preface is being written is the final version of the assessment and is based on returns from 75 countries received by the Secretary-General to August 15, 1970, 45 of the countries reporting information on seismograph stations.

These assessments, both the preliminary and final versions, present conceptual seismological schemes whereby existing seismological facilities throughout the world are applied to a test ban situation. It is necessary in such a hypothetical study to neglect all feasibility problems and financial consequences, and to examine the theoretical capability without prejudice to the necessity or otherwise of implementing such a scheme in any test ban situation. In reality, however, the analysis attempts to answer the following question: for country A, an event is either known or reported or thought to have occurred at approximately a certain time in country B; using world-wide data guaranteed by governments, what is the possibility that country A can form an opinion as to whether the event took place, and whether it was an earthquake or an underground nuclear explosion, and how does this capability for country A deteriorate as the size of an underground explosion is reduced? To answer this question, there is a requirement only for availability on demand of a limited amount of seismological data for this ad hoc purpose. However, the analysis does attempt to answer the further question: if some agency, international or national, had access to the daily abstracted seismological data that is guaranteed, to what levels of earthquake magnitude or explosion yield could an event be determined to occur, to what levels could the event be identified as either an earthquake or an explosion, and to what accuracy could it be located?

In our assessment, country A and country B described above are entirely general. This approach could, of course, be extended in a variety of ways working from the world-wide ensemble of stations. If country A is concerned about the possibility of clandestine testing in countries B, C and D only, for example, the problem of the minimum additional information required to meet certain levels of guarantee is, in our opinion, solvable by similar analyses. The general problem we have studied is, in many ways, the most difficult. Another example of the application of such a dialectic approach would arise in considering the application of this analysis to "verification by challenge": the approach used allows calculation of the limits of the effectiveness of a refutation of a challenge by the provision of seismological information. Extension to stations not reported in the UN returns is, in principle, straightforward for country A with a country B, C, D problem, or for the general case.

It may be of value to explain here briefly how this final assessment differs in content and format from the preliminary analysis distributed and discussed in the CCD in August, 1970. The principal reason for preparing a second edition is to include in the analysis all seismograph station data received by the Secretary-General after completion of the earlier preliminary analysis. We have, in addition, made other changes, the most important of which are as follows.

(1) On the basis of new information received the effective sensitivities of two long period arrays have been increased.

(2) A more elegant method of defining detection probabilities of events on the basis of station sensitivities is employed.

(3) All global detection and identification capabilities are defined at the 90 per cent probability level.

(4) All formal calculations are made using conceptual global networks of fixed numbers of stations.

(5) Explosion thresholds are stated in both equivalent earthquake magnitudes and explosive yields.

(6) Additional published and unpublished research results are discussed.

This paper is long because we felt it important to describe unequivocally at each state in the developing theme exactly what assumptions are made, giving our rationale for them. We have, perforce, needed to make a number of scientific judgments at different points in the development, and these we have attempted to explain fully so that any of our colleagues who read this paper can more easily form their own professional judgment about them. In addition, in a serious attempt to make the scientific significance of this document understandable to readers outside the seismological community, we have judged it useful to labour some points that would be simply appreciated by seismologists. However, of necessity, the entire document is couched in seismological terminology. So that the results of the analysis may be more comprehensible to a wider audience of readers, we present here a brief, non-technical summary of the basic procedures and conclusions. To do so we must retain three basic seismological terms; these are: "magnitude" (m), the logarithmic scale that is employed to define the size of both earthquakes and underground explosions (the reader is referred to Table VIII in the text for an easily understood equivalence between m and explosion yield), "P wave", the first arriving seismic wave which propagates through the body of the earth, and "Rayleigh wave", the most important (in this study) seismic wave that propagates around the surface of the earth. The summary follows.

Using data quoted in the UN returns and published in the open literature, the capability of each conventional and array station is described in terms of its ability to detect P waves and Rayleigh waves as a function of distance from the event. All such stations are reduced to two conceptual global networks, one that is used for global P wave detection calculations and the other for global Rayleigh wave detection calculations. The basic formally calculated results are global contours of m values for which there will be a 90 per cent probability of detection, by a certain number of stations, of P waves and Rayleigh waves from earthquakes and explosions. These are defined as the *thresholds of detection.*

The detection thresholds are m4.2 for explosion and earthquake P waves in Europe and North America, deteriorating to m4.5 for Asian coverage and further to m5.0 in parts of the southern hemisphere (all capabilities are much poorer in the southern hemisphere and any further discussion of this half of the earth is omitted here). The thresholds are m4.8 for Rayleigh waves from earthquakes in North America and northern Europe, deteriorating to m5.1 for generally complete Asian coverage. The thresholds are one magnitude unit larger for Rayleigh waves from correspondingly located explosions. A number of important empirical results from the seismological literature are cited to illustrate that these formally calculated detection thresholds can be considered conservative.

The most generally applicable identification criterion, the relative excitation of P and Rayleigh waves, has a threshold of application equal to the threshold of detection of explosion Rayleigh waves, i.e., m5.8 – m6.0 in much of the northern hemisphere. This rather high explosion identification threshold can be reduced in a number of ways. (a) By employing special processing of Rayleigh wave data from one or two of the highest sensitivity stations, the average northern hemisphere threshold can be reduced to m5.6 – m5.8. (b) By taking advantage of highly efficient Rayleigh wave propagation over purely continental paths, the threshold has been reduced to m5.0 in North America, but an equal reduction remains unproven for other continental areas. (c) By employing identification criteria that rely only on P wave data, the criteria can, in theory, be applied near the lower P wave detection threshold. One such criterion is proven successful for one station-region combination at an identification threshold of m4.9; all other documented attempts have resulted in overlapping populations of earthquakes and explosions at all magnitudes. (d) By employing the absence of recorded waves, for example, long period Rayleigh waves, to identify explosions, on the basis that had the event concerned been an earthquake the waves in question would have been observed, the threshold of identification can be reduced. Illustrations are presented to show that existing thresholds can be reduced by m0.5 by accepting these criteria. (e) By employing more than one imperfect criterion, analyses can result in statistical probabilities (rather than certainty) that an event in question falls into an earthquake or explosion category.

A very brief and oversimplified summary of the results and conclusions of this assessment is that the global system of stations produces proven detection, location and identification of underground nuclear explosions down to yields of about 60 kilotons in hardrock in most of the northern hemisphere: the threshold is 10-20 kilotons for certain test sites only, and this lower threshold cannot be reached on a global basis with this ensemble of stations. We complete the study by making a number of recommendations, which, with very little financial commitment, will provide some basic data required to define existing capabilities better and that may significantly improve them.

The problems of evasion are not treated in great depth in this analysis. In principle, a potential violator of a Comprehensive Test Ban could attempt either to reduce the size of the seismic signals from a clandestine explosion of a given yield by suitable choice and artificial modification, if necessary, of the variables of the emplacement medium, or attempt to simulate an earthquake-like seismic signal by multiple firing techniques, or depend on major simultaneous natural earthquake signals to obscure the artificial event, or events, of interest. The advantages and disadvantages, limits of feasibility, etc., in these different techniques are not analyzed in this document, which treats all explosion yields in terms of their hardrock equivalents.

We are indebted to many colleagues, both in Canada and abroad, who, after a careful study of our preliminary assessment, have made valuable suggestions for improvements for incorporation in this final edition.

However, we accept sole responsibility for the interpretations we have placed on the data in the UN returns, and for the scientific contents and judgments contained in the paper.

P. W. Basham
K. Whitham

1. Introduction

1.1 The General Assembly resolution

At the Twenty-Fourth United Nations General Assembly, Canada proposed a resolution, 2604A, which was adopted at the 1836th plenary meeting on December 16, 1969, by a vote of 99 to 7, with 13 abstentions. In summary form, the resolution requested the United Nations Secretary-General tó circulate to governments a request that they supply information concerning seismological stations from which they would be prepared to supply records on the basis of guaranteed availability and to provide certain information about each of such stations. This resolution, which had been proposed and discussed in the Conference of the Committee on Disarmament (CCD) in Geneva in 1969, was designed to assist in clarifying what resources would be available for the eventual establishment of an effective world-wide exchange of seismological information which would facilitate the achievement of a comprehensive test ban.

Very simply, therefore, the aim of the resolution was to achieve a limited first step of clarification. This modest proposal is a first step in any process whereby seismology could assist in clarifying for national states the implications of the essentially political decision involved in any form of test ban treaty.

Pursuant to Resolution 2604A, the Secretary-General circulated on January 30, 1970, a note soliciting responses to the questionnaire appended to the resolution, which specified the details concerning conventional seismograph stations and array stations that governments were invited to submit to the Secretary-General.

At the time of preparation of this analysis of the returns, 75 countries had replied to the Secretary-General's note*: 45 countries reporting information for seismograph stations on their territory, 22 countries reporting no operational seismograph stations on their territory, and eight countries indicating that in their view the purposes of the resolution were unnecessary or preferring to maintain a voluntary form of seismological data exchange and including no data on seismograph stations in their returns. The national states in each of these categories are listed in Table I.

1.2 Usable data in the UN returns

For purposes of compiling this assessment, the authors examined all data in all returns submitted by countries listed in Table I(a). These included the summary documents, A/7967 to A/7967/Add.5, circulated by the Secretary-General, together with all additional diagrammatic and tabular data deposited in the archives of the United Nations.

The returns containing seismograph station data varied considerably in general format and in the form and contents of tabular and diagrammatic material. The data required for this study were for each seismograph station, the geographic co-ordinates, the magnification of any operational short-period vertical (SPZ) seismograph at a period of 1 second, and the magnification of any operational long-period vertical (LPZ) seismograph at a period of 15 or 20 seconds. Thus, we required, in addition to data on array stations (see section 2.2), the fundamental operating gain of all available vertical component seismographs which we have defined as "conventional".

A great variety of types of seismographs are in operation throughout the world and have been listed by the

* This includes all returns available up to and including Document A/7967/Add.5. Numerous UN member countries remain which have submitted no return of any type (positive or negative) to the Secretary-General. Although it will be important to assess the significance of any late returns which may yet be received, based on other sources of information concerning world seismograph stations, we believe no late returns will contain station data which will significantly alter the conclusions of this assessment.

Table I. Countries submitting returns in response to UN Secretary-General's questionnaire

(a) Countries reporting information for seismograph stations on their territory:

Australia, Austria, Belgium, Brazil, Canada, Ceylon, China, Colombia, Denmark, Ethiopia, Finland, Germany (Fed. Rep.), Greece, India, Indonesia, Iran, Ireland, Israel, Italy, Jamaica, Japan, Korea (Rep. of), Luxembourg, Madagascar, Malawi, Mexico, Monaco, Morocco, Netherlands, New Zealand, Norway, Pakistan, Philippines, Portugal, Spain, Sweden, Switzerland, Thailand, Turkey, United Arab Republic, United Kingdom, United States of America, Venezuela, Vietnam (Rep. of), Yugoslavia

(b) Countries reporting no operational seismograph stations on their territory:

Burundi, Cambodia, Cameroon, Costa Rica, Cyprus, Dahomey, Ghana, Guyana, Kuwait, Laos, Malaysia, Mali, Malta, Nauru, Niger, Nigeria, San Marino, Singapore, Sudan, Tanzania, Uganda, Zambia

(c) Countries replying to the circular of the Secretary-General preferring to retain a bilateral and voluntary form of seismological data exchange, and which so indicated in their UN return, including no data on seismograph stations:

Bulgaria, Byelorussian Soviet Socialist Republic, Czechoslovakia, Hungary, Mongolia, Romania, Ukrainian Soviet Socialist Republic, Union of Soviet Socialist Republics

host countries in their returns. The primary decision for inclusion of a particular seismograph station in this analysis rested in all cases on our ability to define from the information available the operational magnification at the required period. In numerous cases a secondary decision was made to exclude a particular station (which we choose to call a "special station"), if it was judged that the overall response characteristics were not suitable to general teleseismic recording of the short- and long-period seismic waves to be considered, or if, even though defined, the magnification at the required period was so low as to make a negligible contribution in the world-wide context. For example, in the former category high frequency microearthquake seismographs were excluded, and in the latter, low magnification "strong-motion" seismographs.

The selection of the stations to be included required considerable judgment. We are aware that either our ignorance concerning particular seismograph types or our misinterpretation of the available data may have contributed errors and omissions; we apologize at the outset to any country whose data may have been so treated.

1.3 Scope and purposes of present study

This study is made with the basic assumption that the identification of underground nuclear explosions as such is possible in principle for any event, provided that the seismic signals generated by it can be detected with a suitable signal-to-noise ratio at an appropriate number of stations at suitable distances. We largely neglect the possibility of seismic signals from an event of potential interest being obscured by a very large natural earthquake, although we dwell briefly on this subject in Chapter 6.

In Chapter 2, the information provided on the conventional and array seismograph stations is summarized. Chapter 3 outlines one method of reducing this heterogeneous information on station capabilities to obtain a single sensitivity parameter which can be applied in Chapters 4 and 5 to P wave and Rayleigh wave detection calculations. The total of 300 available independent seismograph stations is reduced for purposes of detection calculations to two conceptual world-wide networks, one for P wave detection calculations and the other for Rayleigh wave detection calculations. In choosing to define the world-wide capabilities of conceptual networks of stations rather than of isolated individual stations, or station sub-sets, we are assuming that, in an effective world-wide exchange of seismological information (of either an ad hoc or continuous nature), the combined seismological resources of all participating nations can, in theory, be applied to the problem at hand.

In Chapters 4 and 5, using an explicitly defined detection probability calculation, we present in terms of the P wave magnitude the capabilities of the networks in detecting earthquake P and Rayleigh waves originating at any point on the earth. In Chapter 6 we present some illustrations of situations on the real earth which can alter the capabilities derived in the formal calculations; these include advantages gained from lateral inhomogeneities in the earth, special propagation paths, and special instrumental and signal processing capabilities, as well as disadvantages resulting from global seismicity patterns and interference effects. The general conclusion of Chapter 6 is that the formal calculations can be considered conservative.

Chapter 7 relates the results of Chapters 4 and 5 directly to the problem of the detection of underground explosions. To do so we characterize underground explosions as a fixed source of P wave energy, i.e., as equivalent P wave magnitude earthquakes. However, we do present all formal and empirical detection and identification thresholds for explosions in terms of both P wave magnitude and equivalent hardrock explosion yield.

Chapter 8 is a generalized discussion of the suite of possible identification criteria with particular reference to both published and unpublished results obtained from the data recorded at conventional and array stations included in the returns. The purposes are to define identification thresholds on the basis of the formal detection calculations and to clarify some of the interacting possibilities of improving the identification thresholds. These include the use of short-period discriminants which are intrinsically of great appeal, if they will work adequately, certain highly efficient Rayleigh wave propagation paths, where proven to occur, and the use of combinations of many imperfect discrimination criteria.

In the final chapter we give the specific and general conclusions that can be drawn from this study, and make some recommendations which, with a modest investment of effort and finances, can both better define and significantly improve earthquake-explosion discrimination capabilities.

2. Seismograph stations

2.1 Conventional stations

All seismograph stations for which the host country will guarantee access to seismological data, a total of 300 stations, are listed in Table II. The stations, each designated by its three-letter international code (ESSA, 1970a), are listed alphabetically by country, and within each country alphabetically by station code.

A conventional station is defined as one which, at a minimum, has either an SPZ seismograph with a known magnification at 1 second, or an LPZ seismograph with a known magnification near 20 seconds. An LPZ magnification quoted within the range 15-30 seconds is accepted. The remaining stations in Table II are either array stations (see section 2.2) or special stations (see section 1.2) which have a "YES" entered in the last column. Some of the conventional stations in Table II are listed as containing additional special seismographs. The magnifications in Table II are quoted in K (thousands).

2.2 Array stations

Seven SPZ arrays and five LPZ arrays considered in this study are listed in Tables III and IV, respectively. For an array station to be considered for our purposes as such, it must have three or more SPZ or LPZ sensors with an aperture adequate to produce a signal-to-noise improvement ideally equal to the square root of the number of sensors following delayed-sum signal processing, and have the sensors connected to a central location with either on-line or off-line (preferably digital) elementary delay-and-sum (phasing) facilities. Alternatively, the signal-to-noise gains from processing modes must have been published. Some of the array stations contain, or have associated with them, horizontal SP and LP seismographs; these are noted in the last column of Table III.

Four countries indicated possession of SPZ arrays which are not included as such in this study; these are listed in the lower part of Table III with the reason for omission stated in the "Comments" column.

3. Sensitivities of stations assumed in this study

3.1 SPZ conventional stations

Each country was asked to specify in its UN return the operational magnification of any reported short-period seismograph at a period of 1 second. These values, where available, are listed in Table II and are the only data, except for some special cases for which additional data has appeared in the literature, from which a judgment can be made of the operational sensitivities of the SPZ stations.

The standard short-period or hot-pen (helicorder) record or seismogram is normally of one-day duration with a speed of 60 mm per minute, 15 minutes of data per line, and thus 2.5 mm between adjacent lines. It is the usual practice to have the operational seismograph magnification set to yield a certain background noise amplitude appropriate to this trace spacing. In order to define the detection capabilities of the Stations, the basic assumption we have made is that the noise levels, and thus the operational magnifications, are such that a P wave signal will be identified on the records 50 per cent of the time if it reaches a trace amplitude of 1 mm. There are a number of known cases for which this assumption will yield conservative estimates of station sensitivities; Canadian stations, particularly, with which we are most familiar, will be discussed in section 6.2.

A further complication is that in the UN returns, there are also cases of stations where the quoted magnification is believed by us to be a maximum rather than the normal operational value; in these cases resulting sensitivities will be too large.

However, in order to proceed further, the 1 mm, 50 per cent signal detection assumption is applied to all stations without consideration of possible exceptions, and is believed to be realistic, if slightly conservative.

The formula relating P wave signal displacement with P wave magnitude is

$$m = \log(A/T) + Q(\Delta,h) \qquad \ldots 1$$

where A is the vertical ground displacement in microns, T is the

Table II. World seismograph stations

	Latitude ° '	Longitude ° '	Country	SPZ Mag. (K)	LPZ Mag. (K)	Horizontal SP	Horizontal LP	Special
ADE	34 58 S	138 43 E	AUSTRALIA	25.	.8	N,E	N,E	
AGE	8 49 S	148 05 E	AUSTRALIA	3.				
AVO	22 35 S	150 37 E	AUSTRALIA	33.				
BOV	36 48 S	147 14 E	AUSTRALIA	17.8				
BRS	27 24 S	152 47 E	AUSTRALIA	70.		N,E	N,E	
CAB	35 56 S	146 26 E	AUSTRALIA					YES
CAN	35 19 S	149 00 E	AUSTRALIA	54.5	9.	N,E	N,E	YES
CLV	33 41 S	136 30 E	AUSTRALIA					YES
CTA	30 05 S	146 15 E	AUSTRALIA	100.	3.	N,E	N,E	
DAR	12 25 S	130 49 E	AUSTRALIA	13.				
DLN	34 43 S	149 11 E	AUSTRALIA	17.				
ESA	09 44 S	150 49 E	AUSTRALIA	38.		N,E		YES
GRK	6 04 S	145 24 E	AUSTRALIA	5.				
HLA	33 32 S	150 55 E	AUSTRALIA	32.				
HTT	33 26 S	138 56 E	AUSTRALIA			N		YES
INV	34 58 S	149 40 E	AUSTRALIA	10.				
JIN	36 26 S	148 36 E	AUSTRALIA					YES
JNL	33 50 S	150 01 E	AUSTRALIA	58.				
KDB	9 28 S	147 10 E	AUSTRALIA	10.				
KET	4 20 S	152 02 E	AUSTRALIA	*N/A		N,E		
KHA	36 13 S	148 08 E	AUSTRALIA					YES
KLG	30 47 S	121 27 E	AUSTRALIA	50.		N,E		
KOA	6 13 S	155 37 E	AUSTRALIA	39.8				
LAE	6 43 S	146 59 E	AUSTRALIA	10.		N,E		
LMT	41 37 S	146 09 E	AUSTRALIA	50.				
MAW	67 36 S	62 53 E	AUSTRALIA	35.				YES
MCQ	54 30 S	158 57 E	AUSTRALIA	N/A				
MEA	34 13 S	148 24 E	AUSTRALIA	N/A				
MEK	26 37 S	118 33 E	AUSTRALIA					YES
MOM	2 04 S	127 25 E	AUSTRALIA	N/A				
MOO	42 27 S	147 11 E	AUSTRALIA	50.				
MTV	38 24 S	146 34 E	AUSTRALIA	N/A				
MUN	31 59 S	116 12 E	AUSTRALIA	25.	.4	N,E	N,E	YES
NIA	29 03 S	167 58 E	AUSTRALIA	10.				
PNA**	32 00 S	138 10 E	AUSTRALIA					YES
PMG	9 25 S	147 09 E	AUSTRALIA	50.	3.	N,E	N,E	YES
RAB	4 12 S	152 10 E	AUSTRALIA	12.5	.8	N,E	N,E	YES
RAL	4 13 S	152 12 E	AUSTRALIA					YES
RIV	33 50 S	151 10 E	AUSTRALIA	12.5	.8	N,E	N,E	
SAV	41 43 S	147 11 E	AUSTRALIA	50.				
SFF	42 20 S	146 18 E	AUSTRALIA	50.				
SUL	4 13 S	152 12 E	AUSTRALIA					YES
SNL**	33 53 S	138 38 E	AUSTRALIA	N/A				
TAO**	35 37 S	148 17 E	AUSTRALIA	N/A				
TAU	42 55 S	147 19 E	AUSTRALIA	25.	.8	N,E	N,E	
TAV	4 14 S	152 13 E	AUSTRALIA					YES
TBL	4 06 S	145 01 E	AUSTRALIA	1.7				
TOO	37 34 S	145 29 E	AUSTRALIA	25.	N/A	N,E	N,E	
TRR	42 18 S	146 27 E	AUSTRALIA	50.				
UMB**	30 14 S	139 08 E	AUSTRALIA	N/A				

Table II (Cont'd)

Code	Latitude ° ′	Longitude ° ′	Country	SPZ Mag. (K)	LPZ Mag. (K)	Horizontal SP	Horizontal LP	Special
VUL	4 17 S	152 09 E	AUSTRALIA					YES
WAB	5 30 S	143 44 E	AUSTRALIA	25.		N,E		
WAM	36 12 S	148 53 E	AUSTRALIA					YES
WAN	4 12 S	152 11 E	AUSTRALIA					YES
WER	33 57 S	150 35 E	AUSTRALIA	35.		N,E		
WRA	19 57 S	134 20 E	AUSTRALIA	(ARRAY,SEE TABLE 3)				
VIE	48 15 N	16 22 E	AUSTRIA					YES
VKA	48 16 N	16 19 E	AUSTRIA	5.		N,E		
DOU	50 06 N	4 36 E	BELGIUM	300.	3.	N,E	N,E	
GIP	50 36 N	5 58 E	BELGIUM					YES
UCC	50 48 N	4 22 E	BELGIUM					YES
WRM	49 50 N	5 23 E	BELGIUM	4.				YES
RDJ	22 54 S	43 13 W	BRAZIL		N/A		N,E	
ALE	82 29 N	62 24 W	CANADA	60.	3.7	N,E	N,E	
BLC	64 19 N	96 01 W	CANADA	26.	3.8	N,E	N,E	
FBC	63 44 N	68 28 W	CANADA	32.	2.6	N,E	N,E	
FCC	58 46 N	94 05 W	CANADA	36.	4.1	N,E	N,E	
FFC	54 43 N	101 59 W	CANADA	39.	4.2	N,E	N,E	
FSJ	54 26 N	124 15 W	CANADA	29.	2.0	N,E	N,E	
GWC	55 17 N	77 45 W	CANADA	28.	4.0	N,E	N,E	
INK	68 17 N	133 30 W	CANADA	68.	3.1	N,E	N,E	
LHC	48 25 N	89 16 W	CANADA	23.	2.8	N,E	N,E	
MBC	76 14 N	119 22 W	CANADA	72.	3.6	N,E	N,E	
OTT	45 24 N	75 43 W	CANADA	24.	3.2	N,E	N,E	
PHC	50 42 N	127 26 W	CANADA	14.	1.9	N,E	N,E	
PNT	49 19 N	119 37 W	CANADA	50.***	2.6	N,E	N,E	
RES	74 41 N	95 54 W	CANADA	60.	3.2	N,E	N,E	
SCH	54 49 N	66 47 W	CANADA	29.	3.0	N,E	N,E	
SES	50 24 N	111 02 W	CANADA	42.	3.5	N,E	N,E	
SFA	47 07 N	70 50 W	CANADA	21.	1.8	N,E	N,E	
STJ	47 34 N	52 44 W	CANADA	8.4	.9	N,E	N,E	
VIC	48 31 N	123 25 W	CANADA	22.	1.9	N,E	N,E	
YKA	62 30 N	114 36 W	CANADA	(ARRAY,SEE TABLE 3 AND 4)				
YKC	62 29 N	114 29 W	CANADA	44.	2.2	N,E	N,E	
COC	6 54 N	79 52 E	CEYLON					YES
ALS	23 31 N	120 48 E	CHINA					YES
ANP	25 11 N	121 31 E	CHINA	6.3	.8	N,E	N,E	
CHY	23 30 N	120 25 E	CHINA					YES
HEN	22 00 N	120 45 E	CHINA					YES
HSI	23 06 N	121 22 E	CHINA					YES
HSN	24 48 N	120 58 E	CHINA					YES
HWA	23 58 N	121 37 E	CHINA					YES
ILA	24 46 N	121 45 E	CHINA					YES
KAU	22 37 N	120 16 E	CHINA					YES
LAY	22 02 N	121 33 E	CHINA					YES
PNG	23 32 N	119 33 E	CHINA					YES
TAI	23 00 N	120 13 E	CHINA					YES
TAP	25 02 N	121 31 E	CHINA					YES
TAW	22 21 N	120 54 E	CHINA					YES
TCU	24 09 N	120 41 E	CHINA					YES

Table II (Cont'd)

Code	Latitude ° '	Longitude ° '	Country	SPZ Mag. (K)	LPZ Mag. (K)	Horizontal SP	Horizontal LP	Special
TTN	22 45 N	121 09 E	CHINA					YES
YUS	23 29 N	120 57 E	CHINA					YES
BOG	4 37 N	74 04 W	COLOMBIA	12.5	3.0	N,E	H	
CHN	4 58 N	75 37 W	COLOMBIA	N/A			N,E	
FUQ	5 28 N	73 44 W	COLOMBIA					YES
GAL	10 47 N	75 16 W	COLOMBIA	N/A			N,E	
COP	55 41 N	12 26 E	DENMARK	12.5	.8	N,E	N,E	YES
GDH	69 15 N	53 32 W	DENMARK	25.	1.5	N,E	N,E	
KTG	70 25 N	21 59 W	DENMARK	12.5	.8	N,E	N,E	
NOR	81 36 N	16 41 W	DENMARK	5.	.8	N,E	N,E	
AAE	9 02 N	38 46 E	ETHIOPIA	50.	1.5	N,E	N,E	
HEL	59 14 N	24 55 E	FINLAND	18.				
JOE	62 39 N	29 42 E	FINLAND	33.				
KEV	69 45 N	27 01 E	FINLAND	25.	1.5	N,E	N,E	
KJN	64 06 N	27 42 E	FINLAND	46.		N,E		
NUR	60 31 N	24 39 E	FINLAND	25.	1.5	N,E	N,E	YES
OUL	65 05 N	25 54 E	FINLAND	200.	1.5			
SOD	67 22 N	26 38 E	FINLAND	47.				YES
GRF	49 42 N	11 13 E	GERMANY(FD.REP)	50.	15.	N,E	N,E	
ARG	36 13 N	28 8 E	GREECE					YES
ATH	37 58 N	23 43 E	GREECE	12.5	1.5	N,E	N,E	
JAN	29 39 N	20 51 E	GREECE					YES
PLG	40 22 N	23 27 E	GREECE					YES
PRK	39 15 N	26 16 E	GREECE					YES
VAM	35 24 N	24 12 E	GREECE					YES
VLS	38 11 N	20 35 E	GREECE					YES
GBA	13 36 N	77 26 E	INDIA		1.2	(SEE TABLE 3)		
DJA	6 11 S	106 50 E	INDONESIA					YES
DNP	8 39 S	115 12 E	INDONESIA					YES
LEM	6 50 S	107 37 E	INDONESIA	25.	.8	N,E	N,E	
MED	3 33 N	98 41 E	INDONESIA					YES
MKA**	5 04 S	119 38 E	INDONESIA					YES
TNG	6 11 S	106 30 E	INDONESIA					YES
KER	34 21 N	47 06 E	IRAN	6.		N,E		
MJL**	36 46 N	49 23 E	IRAN	80.		N,E		
MSH	36 19 N	59 35 E	IRAN	12.5	1.5	N,E	N,E	
SHI	29 31 N	52 32 E	IRAN	100.	1.5	N,E	N,E	
SRI	36 46 N	49 23 E	IRAN					YES
TAB	38 04 N	46 20 E	IRAN	12.5	1.5	N,E	N,E	
TEH	35 44 N	51 23 E	IRAN	10.	.3	N,E	N,E	
VAL	51 56 N	10 15 W	IRELAND	12.5	.8	N,E	N,E	
EIL	29 5 N	35 0 E	ISRAEL	N/A	N/A	N,E	N,E	
HAF	32 48 N	35 1 E	ISRAEL	N/A				
JER	31 46 N	35 11 E	ISRAEL	N/A	N/A	N,E	N,E	
AQU	41 21 N	13 24 E	ITALY	N/A	N/A	N,E	N,E	
FIR	43 47 N	11 15 E	ITALY					YES
MES	38 12 N	15 33 E	ITALY	4.8		N,E		YES
RMP	41 49 N	12 42 E	ITALY	N/A	N/A	N,E	N,E	YES
TRI	45 43 N	13 46 E	ITALY	50.	3.	N,E	N,E	YES
HOJ	18 00 N	76 45 W	JAMAICA	10.				

Table II (Cont'd)

Code	Latitude ° ′		Longitude ° ′		Country	SPZ Mag. (K)	LPZ Mag. (K)	Horizontal SP	Horizontal LP	Special
PRJ	17 56	N	76 51	W	JAMAICA	N/A				
STH	18 05	N	76 49	W	JAMAICA	3.4				
DDR	36 00	N	139 12	E	JAPAN	36.	.8	N,E	N,E	YES
IHR	33 41	N	133 28	E	JAPAN					YES
KYS	35 12	N	140 09	E	JAPAN	11.		N,E		
MAT	36 33	N	138 13	E	JAPAN	100.	3.	N,E	N,E	
MTJ	36 13	N	140 07	E	JAPAN	42.	.7	N,E	N,E	YES
OIS	34 06	N	135 19	E	JAPAN					YES
SHK	34 32	N	132 41	E	JAPAN	10.2	1.4	N,E	N,E	YES
SRY	35 37	N	139 16	E	JAPAN	45.		N,E		
TSK	36 12	N	140 07	E	JAPAN	14.				YES
URS	33 32	N	133 29	E	JAPAN					YES
WKU	34 11	N	135 10	E	JAPAN					YES
WMY	33 39	N	133 41	E	JAPAN					YES
SEO	37 34	N	126 58	E	KOREA (REP)	50.	1.5	N,E	N,E	
LUX	49 36	N	6 08	E	LUXEMBOURG					YES
TAN	18 55	S	47 33	E	MADAGASCAR	75.9				YES
CLK	15 41	S	34 59	E	MALAWI	20.		N,E		
CHH	28 38	N	106 05	W	MEXICO					YES
COM	16 15	N	92 08	W	MEXICO	20.				YES
GUM	20 41	N	103 19	W	MEXICO					YES
LCG	21 09	N	101 42	W	MEXICO	17.5		N,E		
LNM	21 07	N	101 40	W	MEXICO					YES
MAZ	23 11	N	106 24	W	MEXICO					YES
MER	20 57	N	89 37	W	MEXICO					YES
MNZ	19 03	N	104 20	W	MEXICO					YES
OAX	17 01	N	96 46	W	MEXICO					YES
OXM	19 18	N	99 43	W	MEXICO	120.				
PBJ	16 29	N	95 25	W	MEXICO	48.				YES
PIM	18 16	N	101 53	W	MEXICO	170.				YES
PMM	17 14	N	93 33	W	MEXICO	82.				YES
PPM	19 04	N	98 38	W	MEXICO	120.				
TAC	19 24	N	99 12	W	MEXICO					YES
TMM	25 45	N	100 12	W	MEXICO	50.		N,E		
TPM	18 59	N	99 04	W	MEXICO	120.				
UNM	19 20	N	99 11	W	MEXICO	6.3	1.5	N,E	N,E	
VCM	19 12	N	96 08	W	MEXICO					YES
VHM	17 09	N	96 47	W	MEXICO	67.				
MON	43 44	N	7 26	E	MONACO	N/A	N/A			
AVE	33 18	N	7 25	W	MOROCCO	30.		N,E		
IFR	33 31	N	5 08	W	MOROCCO	80.		N,E		
RBA	34 01	N	6 50	W	MOROCCO		1.0			
RBZ	33 56	N	6 50	W	MOROCCO	30.				
TIO	30 57	N	7 16	W	MOROCCO	50.				
DBN	52 06	N	5 11	E	NETHERLANDS		.5		N,E	YES
HEE	50 53	N	5 59	E	NETHERLANDS					YES
RSB	50 53	N	5 50	E	NETHERLANDS					YES
WIT	52 49	N	6 40	E	NETHERLANDS	6.5				YES
AFI	13 55	S	171 47	W	NEW ZEALAND	12.5	.8	N,E	N,E	
KRP	37 56	S	175 32	E	NEW ZEALAND	35.		N,E		

Table II (Cont'd)

Code	Latitude ° '	Longitude ° '	Country	SPZ Mag. (K)	LPZ Mag. (K)	Horizontal SP	Horizontal LP	Special
MJZ	43 59 S	170 28 E	NEW ZEALAND	30.		N,E		
MNG	40 37 S	175 29 E	NEW ZEALAND	49.				
MSZ	44 40 S	167 55 E	NEW ZEALAND	53.				
RAR	21 13 S	159 46 W	NEW ZEALAND	6.3	.4	N,E	N,E	
SBA	77 51 S	166 45 E	NEW ZEALAND	6.3	.8	N,E	N,E	
WEL	41 17 S	174 46 E	NEW ZEALAND	6.3	.8	N,E	N,E	
BER	60 23 N	5 20 E	NORWAY		6.		N,E	
KHS	78 55 N	11 55 E	NORWAY	25.	1.5	N,E	N,E	
KON	59 39 N	9 38 E	NORWAY	50.	1.5	N,E	N,E	
NOS**	60 49 N	10 50 E	NORWAY	(ARRAY,SEE TABLE 3 AND 4)				
TRO	69 38 N	18 56 E	NORWAY	50.		N,E		
NIL	33 39 N	73 15 E	PAKISTAN	100.	3.0	N,E	N,E	
QUE	30 11 N	66 57 E	PAKISTAN	200.	6.0	N,E	N,E	
BAG	16 25 N	120 35 E	PHILIPPINES	25.	3.0	N,E	N,E	
DAV	7 08 N	125 37 E	PHILIPPINES	6.3	3.0	N,E	N,E	
MAN	16 40 N	121 05 E	PHILIPPINES	12.5	1.5	N,E	N,E	
COI	40 12 N	8 26 W	PORTUGAL	8.				
CNG	26 18 S	32 11 E	PORTUGAL	N/A	N/A			YES
LIS	38 43 N	9 09 W	PORTUGAL	3.5				
PDA	37 45 N	25 40 W	PORTUGAL					YES
PTO	41 08 N	8 37 W	PORTUGAL	50.	3.	N,E	N,E	
SDB	14 56 S	13 34 E	PORTUGAL	N/A	N/A			
ALI	38 21 N	0 29 W	SPAIN	8.5		N,E		
ALM	36 51 N	2 28 W	SPAIN	8.5		N,E		
FBR	41 25 N	0 09 E	SPAIN	6.3		N,E		YES
LGR	42 27 N	2 30 W	SPAIN	6.8		N,E		
MAL	36 44 N	4 25 W	SPAIN	50.	1.5	N,E	N,E	
SFS	36 28 N	6 12 W	SPAIN	2.5				YES
TEN	28 27 N	16 14 W	SPAIN	8.5		N,E		
TOL	39 53 N	4 03 W	SPAIN	25.	1.5	N,E	N,E	YES
DEL	56 28 N	13 52 E	SWEDEN	13.5				
HFS	60 08 N	13 42 E	SWEDEN	(ARRAY,SEE TABLE 3 AND 4)				
KIR	67 50 N	20 25 E	SWEDEN	13.8	1.2			YES
SKA	63 35 N	12 17 E	SWEDEN	14.5				
UDD	60 05 N	13 36 E	SWEDEN	13.0				
UME	63 49 N	20 14 E	SWEDEN	75.	5.5	N,E	N,E	
UPP	59 52 N	17 38 E	SWEDEN	40.		N,E		YES
BAS	47 32 N	7 35 E	SWITZERLAND					YES
CHU	46 51 N	9 32 E	SWITZERLAND					YES
COS**	46 12 N	8 51 E	SWITZERLAND					YES
NEU	47 00 N	6 57 E	SWITZERLAND					YES
ZUR	47 22 N	8 35 E	SWITZERLAND					YES
ANK	39 55 N	32 49 E	TURKEY	15.				
CIN	37 36 N	28 05 E	TURKEY	15.				
DMK	41 49 N	27 45 E	TURKEY	N/A				
DRB	39 35 N	28 38 E	TURKEY	N/A				
ERD	40 24 N	27 48 E	TURKEY	N/A				
ERZ	39 55 N	41 16 E	TURKEY	15.				
EZN	39 46 N	26 20 E	TURKEY	N/A				
GPA	40 17 N	30 19 E	TURKEY	N/A				

Table II (Cont'd)

Code	Latitude ° '	Longitude ° '	Country	SPZ Mag. (K)	LPZ Mag. (K)	Horizontal SP	Horizontal LP	Special
ISK	41 04 N	29 04 E	TURKEY	150.	1.5	N,E	N,E	YES
IST	41 03 N	28 59 E	TURKEY	25.	1.5	N,E	N,E	
KAS	41 22 N	33 46 E	TURKEY	18.				
RAM	37 46 N	41 18 E	TURKEY	50.	.6	N,E	N,E	
CHG	18 47 N	98 59 E	THAILAND	400.	3.0	N,E	N,E	
SNG	7 10 N	100 37 E	THAILAND	25.	3.0	N,E	N,E	
HLW	29 51 N	31 20 E	UNITED ARAB REP	50.	3.	N,E	N,E	
EKA	55 20 N	3 10 W	UNITED KINGDOM	(ARRAY,SEE TABLE 3)				
ESK	55 20 N	3 11 E	UNITED KINGDOM		5.			
WOL	51 19 N	1 13 W	UNITED KINGDOM		15.			
AAM	42 18 N	83 39 W	UNITED STATES	25.	1.5	N,E	N,E	
ALP**	65 13 N	146 00 W	UNITED STATES	(ARRAY,SEE TABLE 4)				
ALQ	34 57 N	106 28 W	UNITED STATES	200.	3.0	N,E	N,E	
ATL	33 26 N	84 20 W	UNITED STATES	50.	1.5	N,E	N,E	
BHP	8 58 N	79 33 W	UNITED STATES	12.5	.8	N,E	N,E	
BKS	37 53 N	122 14 W	UNITED STATES	25.	3.0	N,E	N,E	
BLA	37 13 N	80 25 W	UNITED STATES	50.	3.0	N,E	N,E	
BOZ	45 36 N	111 38 W	UNITED STATES	200.	3.0	N,E	N,E	
COL	64 54 N	147 48 W	UNITED STATES	100.	1.5	N,E	N,E	
COR	44 35 N	123 18 W	UNITED STATES	12.5	.8	N,E	N,E	
DAL	32 51 N	96 47 W	UNITED STATES	25.	1.5	N,E	N,E	
DUG	40 12 N	112 49 W	UNITED STATES	400.	3.0	N,E	N,E	
FLO	38 48 N	90 22 W	UNITED STATES	50.	3.0	N,E	N,E	
GEO	38 54 N	77 04 W	UNITED STATES	25.	1.5	N,E	N,E	
GOL	39 42 N	105 22 W	UNITED STATES	400.	1.5	N,E	N,E	
GSC	35 18 N	116 48 W	UNITED STATES	100.	1.5	N,E	N,E	
GUA	13 32 N	144 55 E	UNITED STATES	6.3	.8	N,E	N,E	
JCT	30 29 N	99 48 W	UNITED STATES	200.	1.5	N,E	N,E	
KIP	21 25 N	158 54 W	UNITED STATES	12.5	.8	N,E	N,E	
LAO	46 41 N	106 13 W	UNITED STATES	(ARRAY,SEE TABLE 3 AND 4)				
LON	46 45 N	121 49 W	UNITED STATES	100.	1.5	N,E	N,E	
LUB	33 35 N	101 52 W	UNITED STATES	25.	1.5	N,E	N,E	
OGD	41 04 N	74 37 W	UNITED STATES	50.	.8	N,E	N,E	
OXF	34 31 N	89 25 W	UNITED STATES	50.	3.0	N,E	N,E	
RCD	44 05 N	103 13 W	UNITED STATES	25.	1.5	N,E	N,E	
SCP	40 49 N	77 52 W	UNITED STATES	50.	3.0	N,E	N,E	
SHA	30 42 N	88 08 W	UNITED STATES	6.3	1.5	N,E	N,E	
SJG	18 07 N	66 09 W	UNITED STATES	50.	.8	N,E	N,E	
SPA	90 00 S	0 00	UNITED STATES	100.	.4	N,E	N,E	
TUC	32 19 N	110 47 W	UNITED STATES	200.	3.	N,E	N,E	
WES	42 23 N	71 19 W	UNITED STATES	50.	3.	N,E	N,E	
CAR	10 26 N	66 55 W	VENEZUELA	25.	3.	N,E	N,E	YES
CUM	10 41 N	66 22 W	VENEZUELA	4.5		N,E		
LGN	10 05 N	71 16 W	VENEZUELA	3.6				
MEV**	8 32 N	71 09 W	VENEZUELA	3.2				
NHA	12 13 N	109 13 E	VIET-NAM (REP)	75.	1.5	N,E	N,E	
LJU	46 03 N	14 32 E	YUGOSLAVIA	20.	2.5	N,E	N,E	
OHR**	41 07 N	20 48 E	YUGOSLAVIA	28.		N,E		
SKO	41 58 N	21 26 E	YUGOSLAVIA	35.	1.0	N,E	N,E	
VAY**	41 19 N	22 34 E	YUGOSLAVIA	25.		E		

Table II (Cont'd)

Footnotes:

---

* N/A (NOT AVAILABLE) INDICATES A SEISMOGRAPH IN OPERATION AT STATION BUT MAGNIFICATION COULD NOT BE DEFINED FROM INFORMATION AVAILABLE.

** CODES SO DESIGNATED ARE ADOPTED HERE AND DO NOT APPEAR IN U.S. DEPT. OF COMMERCE, ESSA PUBLICATION - SEISMOGRAPH STATION ABBREVIATIONS -, APRIL, 1970.

*** PNT SPZ MAGNIFICATION OF 25K IN THE CANADIAN SUBMISSION TO THE UNITED NATIONS WAS IN ERROR.

/ THE PHILIPPINES SPZ AND LPZ MAGNIFICATIONS FOR BAG AND DAV ARE BELIEVED BY THE AUTHORS TO HAVE BEEN INADVERTENTLY REVERSED IN THE PHILIPPINES RETURN.

Table III. SPZ array stations

Code	Latitude	Longitude	Country	Number of Elements	Effective Magnification	Other Components
GBA	13 36 N	77 26 E	India	20	210 K	See GBA in Table II
EKA	55 20 N	3 10 W	United Kingdom	22	135 K	See ESK in Table II
HFS	60 08 N	13 42 E	Sweden	3	140 K	See HFS in Table IV, LPN and LPE at one element
LAO*	46 41 N	106 13 W	United States of America	345	1250 K	All LP elements (Table IV) contain LPN and LPE
NOS*	60 49 N	10 50 E	Norway	147	1250 K	All LP elements (Table IV) contain LPN and LPE
WRA	19 57 S	134 20 E	Australia	20	300 K	None
YKA	62 30 N	114 36 W	Canada	19	400 K	See YKC in Table II and YKA in Table IV
SPZ Arrays Not Included:						Comments
GRF	49 42 N	11 13 E	Germany (Fed. Rep. of)	7		Incomplete; included as a single station (Table II)
SAA	15 38 S	47 59 W	Brazil	19		Incomplete; no magnification or noise figures given
HEL	59 14 N	24 55 E	Finland	3		No phasing facility; also conventional station (Table II)
DDR	36 00 N	139 12 E	Japan	Irregular		Microearthquake array; also conventional station (Table II)

* LAO and NOS are commonly referred to in the literature as LASA and NORSAR, respectively.

Table IV. LPZ array stations

Code	Latitude	Longitude	Country	Number of Elements	Effective Magnification
ALP	65 13 N	146 00 W	United States of America	19	120 K
HFS	60 08 N	13 42 E	Sweden	3	28 K
LAO	46 41 N	106 13 W	United States of America	17	120 K
NOS	60 49 N	10 50 E	Norway	19	120 K
YKA	62 30 N	114 36 W	Canada	3	28 K

corresponding period in seconds, and Q is the distance (Δ) and focal depth (h) calibrating function. Considering only a fixed focal depth of h = 25 km, using a fixed signal period of T = 1 sec, and making the appropriate conversion of units, the 50 per cent 1 mm seismogram signal can be converted to a 50 per cent interval probability (I.P.) magnitude detection value as follows:

$$m_{50}(\Delta) = Q(\Delta) - \log V, \qquad \ldots .\ 2$$

where V is the magnification in K at a period of 1 second. Thus each SPZ station with a known (and fixed) magnification has a 50 per cent I.P. magnitude detection capability as a function of distance only, defined by Equation 2.

3.2 SPZ array stations

It is essential when considering world-wide detection capabilities involving mixed array and conventional stations to devise a technique whereby array stations can be considered as extra-sensitive single stations with assumed *effective* magnifications which depend on the character and geometry of the array and the signal processing technique adopted. Each of the SPZ arrays must, therefore, be considered separately using all available information to decide on this effective magnification.

The U.K.-type arrays. The data available for the four U.K.-type short-period arrays (YKA, WRA, GBA and EKA; see Table III) are an approximate 50 per cent annual noise level for each of the arrays (Burch, 1969), and a well-defined detection capability for the YKA array (Anglin, 1970). The noise levels, converted to equivalent m at a distance of Δ = 60°, are m4.0, m4.1, m4.3, and m4.5 for YKA, WRA, GBA and EKA, respectively. In this calculation, Burch has assumed a unity signal-to-noise ratio for a single sensor, which is equivalent to a signal-to-noise ratio of approximately four for the phased sum. Anglin's results for YKA based on automatic array detection with digital delayed-sum and correlogram processing indicate an average 50 per cent I.P. detection capability of m_{50}4.3 at epicentral distances about 60°. The YKA capability using an automatic detection algorithm is δm_{50}0.3 poorer than the equivalent noise calculation because the algorithm assumes no prior knowledge of where to focus the beams and must limit the occurrence of false event (noise) triggers to a reasonable number. With no equivalent detection figures available for the other arrays, it is assumed that using an equivalent processing technique the δm0.3 difference would apply, and the 60° m_{50} values are converted to an effective magnification V using Equation 2. This results in the effective magnification for these arrays shown in Table III.

HFS (SPZ). No detection figures are available for HFS, but the 1-second noise is quoted as 12.5 mμ* (Swedish UN return). Assuming $\sqrt{3}$ signal-to-noise improvement using a phased sum, the signal will be detectable 50 per cent of the time with a displacement of about 7 mμ. This converts to the effective magnification of 140 K given in Table III.

LAO (SPZ). The quoted 50 per cent I.P. detection capability for LAO (SPZ) is given (SIPRI, 1968) as m3.8, using beam-forming techniques. Assuming a mid-third zone distance of 60°, this converts using Equation 2 to the effective magnification of 1250 K given in Table III.

NOS (SPZ). No noise levels, operating magnification or detection capabilities are available for NOS; this is due principally to the short period of time it has been in operation.** However, because of the importance of NOS to world-wide detection, an effective magnification has been assigned to it for purposes of this study. Although it has fewer elements than LAO (see Table III), it does have a more suitable geometry, and on this basis is assigned an effective magnification equal to that of LAO, 1250 K.***

3.3 LPZ conventional stations

Each country was asked to specify the magnification of its long-period stations at 15 or 20 seconds; the returns included values in the range from 15 to 30 seconds. Since conventional long-period seismographs usually have generally flat magnification within the range from 10 to 30 seconds, the quoted value is assumed to apply at 20 seconds; the values for LPZ are listed in Table II.

* This single sensor noise level appears unusually high in comparison to noise data available for similar environments elsewhere in the world, and is believed to include noise at periods slightly above 1 second. If this is true, a narrow band filtering of the HFS data (this is applied to the YKA data prior to automatic processing) would increase the effective magnification determined for HFS by a factor of 2 or more.

** At the time of preparation of this report, the authors understand that full array operation at NOS can be expected in the autumn of 1970. Parts of the array have been operational for some time.

*** If these assumptions concerning NOS are in error, the assumed effective magnification for this array may, in fact, be different by up to about a factor of 2; this, however, would have no important effect on P wave detection described in later chapters.

The dominant noise on conventional LPZ seismograms is commonly near 6-second periods and due to oceanic microseisms. A conventional LPZ seismograph writes one line per hour with 10 mm between adjacent lines. It is assumed for purposes of discussing the detection of 20-second Rayleigh waves that the shorter period noise level and thus the operational magnification are such that a 20-second signal will be identifiable 50 per cent of the time if it reaches a trace amplitude of 2 mm. From our experience this seems a reasonable practical criterion to adopt in order to proceed further.

There are two single LPZ stations (GRF in Germany and WOL in the U.K.) in the returns which possess magnetic tape recording facilities. This tape facility, with extra electronic filtering during recording or on playback from the magnetic tape to reject the shorter period noise, allows quotation of a magnification at least three times higher than the conventional photographic stations.

The formula adopted for relating Rayleigh wave signal to a surface wave magnitude is

$$M = \log (A/T) + 1.66 \log \Delta + 3.3 \quad \ldots\ 3$$

where A is the maximum vertical Rayleigh wave trace amplitude converted to ground displacement in microns, and T is the corresponding period in seconds. Considering a Rayleigh wave period of 20 seconds and making the appropriate units conversion, the 50 per cent detection signal level of 2 mm is related to the 50 per cent I. P. Rayleigh wave magnitude by the formula

$$M_{50}(\Delta) = 1.66 \log \Delta - \log V + 2.3 \quad \ldots\ 4$$

where V is the LPZ 20-second magnification in K. Thus each LPZ station has, for a fixed magnification, a 50 per cent I.P. Rayleigh wave detection capability as a function of distance only, given by Equation 4.

3.4 LPZ array stations

As for the SPZ array stations, the LPZ arrays can be assigned an effective magnification on the basis of available noise data and detection capabilities. The basic assumptions concerning LPZ arrays are that they include sufficient filtering capability that the 6-second noise can be ignored, and that they have a data processing facility for forming phased sums.

YKA (LPZ). An unpublished study by the authors has shown that the 50 per cent noise at YKA is about 60 $m\mu$ near 20 seconds. Assuming a $\sqrt{3}$ signal-to-noise improvement due to a phased sum and a 2.0 signal-to-noise ratio for signal detection, the 50 per cent I.P. signal will be 70 $m\mu$ which can be converted to the effective magnification of 28 K given in Table IV.

HFS (LPZ). The quoted 20-second noise for HFS (Swedish UN return) is identical to that for YKA and the effective magnification will also be 28 K.

LAO (LPZ). The quoted Rayleigh wave detection capability for LAO (Capon *et al.*, 1967b) is m4.5 at the 60 per cent I.P. level, which can be converted to m4.4 at the 50 per cent I.P. level or M3.0 (see section 3.5) at the 50 per cent I.P. level. This is for $\Delta = 85°$, but includes matched filtering. The matched filtering which yields a detection improvement of 8 db (δMO.4) will be removed here, but discussed in a later section. Following this correction, the 50 per cent I.P. for Rayleigh detection is M3.4, which converts (using $\Delta = 85°$) from Equation 4 to the effective magnification of 120 K given in Table IV.

NOS (LPZ) and ALP. No noise or detection figures are available for NOS and ALP. Although there may be a slightly higher noise level at these sites (comparable to northern Canada and Sweden) than at LAO, NOS and ALP were designed for optimum LPZ detection and on this basis are assigned effective LPZ magnifications equal to the empirically defined value for LAO, 120 K.

3.5 Rayleigh wave detection in terms of m_{50}

In order to refer to both P wave and Rayleigh wave detection in terms of a single magnitude scale, the M_{50} Rayleigh wave magnitudes determined from Equation 4 are converted to equivalent m_{50} using the equation

$$M_{50} = 1.59\ m_{50} - 3.97 \quad \ldots\ 5$$

This is the original (Gutenberg and Richter, 1956) relationship relating M and m and applies reasonably well to any world distribution of earthquakes.

The only specific study of Rayleigh wave detection which directly supports this adopted formulation is by Simons and Goforth (1967). They present Rayleigh wave detection probabilities as a function of P wave magnitude, epicentral distance and LPZ magnification using a large suite of widely distributed earthquakes recorded at five sensitive LPZ stations in the United States. Their data for equivalent m_{50} interval probability of Rayleigh wave detection versus epicentral distance for fixed magnifications agree with the formulation of Equations 4 and 5 within δm_{50}0.2 over the distance range from 35° to 90°. At nearer distances they illustrate an improvement in Rayleigh wave detection roughly equivalent to the improvements gained from continental path propagation discussed in section 6.3. Capon *et al.* (1967b) present M versus m data which, when combined as a world-wide average, support the adoption of Equation 5, but when considered on a regional basis show that variations in the M versus m relationship occur.

Thus, with the adoption of Equation 5, the P wave magnitude, m_{50}, for which there is a 50 per cent interval probability of Rayleigh wave detection, can be determined as a function of distance for any station with an available LPZ magnification.

4. Global P wave detection

4.1 Individual station detection probability functions

The basic input data for the P wave detection calculations are the individual station $m_{50}(\Delta)$ values defined in section 3.1 and 3.2. To determine the probability of detecting a given magnitude event at a given site by a group of stations with various capabilities (various m_{50}), we require a detection probability function for each station which varies with the event magnitude. Ideally, we need either the noise amplitude probability distribution or an empirically defined detection probability distribution versus m for each station. Since this type of station information is available for only a very small percentage of the stations being considered, a general approximation must be used.

The only empirically defined individual station P wave detection probabilities of which we are aware are from an unpublished study by the authors of the capabilities of the Canadian SPZ stations SES, OTT and ALE. For these stations, the magnitude range between the 10 and 90 per cent interval probabilities of detection is $\delta m0.8$ to 1.0, with the 50 per cent I.P. magnitude near the centre of the range.

Assuming that the probability of locating an event by a given network of stations is directly related to individual station probabilities of detection events, some location statistics can contribute to this problem. Some tests made by the authors on the detection capability in a number of European and Asian regions using data for 1965, published by the International Seismological Centre, give a magnitude difference $\delta m0.4$ to 0.5 between the 50 and 90 per cent capability. Evernden (1970b) has published some diagrams indicating the world-wide capability of the United States Coast and Geodetic Survey system. Our interpretation of the occurrence slopes again leads to a correction of $\delta m0.4$ to change from 50 to 90 per cent interval probability magnitudes.

Noise probabilities indicate a smaller range of equivalent magnitudes than do the actual detection probabilities given above. A study by the authors (Basham and Whitham, 1966) of short period microseismic noise on Canadian seismograms shows that the 90 per cent cumulative noise is on the average a factor of about three greater than the 10 per cent cumulative noise: a difference in equivalent magnitudes of $\delta m0.5$. We believe that the actual detection probability range is greater than this because of the requirement of a larger signal-to-noise ratio for detection in the presence of high noise than in low noise.

Statistically, the most likely shape expected for an individual station detection probability function versus magnitude would be an integrated normal curve, with each station expected to have a somewhat different effective normal variance. Since these individual station probability curves are not available, and there are other uncertainties in these calculations of equal or greater magnitude, a linear probability function, suitable to the above illustrated empirical data, of the form

$$P(m) = m - m_{50} + 0.5 \quad (0 \leq P(m) \leq 1) \qquad \ldots 6$$

will be employed; P(m) is the probability that a station with capability m_{50} (defined in section 3.1) will detect the P wave of an earthquake of magnitude m. This is simply an increase of 0.1 in detection probability for each $\delta m0.1$ increase, with the $P = 0.5$ centred on the adopted m_{50}.

4.2 90 per cent detection probabilities for an event

In order to find, for a specific point on the earth, the earthquake magnitude that will have P waves detected with a required probability by a given number of stations, we require some knowledge of the probability distribution of numbers of detections, as a function of the magnitude of the event, that can be expected from a large suite of available stations having a wide range of P wave detection capabilities. If the average number of detections is small relative to the total number of stations, the probability distribution of the number of detections can be closely approximated by the Poisson distribution for each magnitude under consideration. If one then considers at the specific point in question a range of event magnitudes, one has a family of Poisson curves. For each of these curves the procedure in section 4.1 describes how the number of detections can be calculated. How one employs this family of curves for purposes of detection probability calculations depends on the requirements of the exercise. We have chosen to define the P wave detection capability of the group of stations under consideration as the earthquake magnitude at a given site for which there will be a 90 per cent probability of detection by a minimum given number of stations (N). To do this we employ the cumulative form of the above family of Poisson distributions and calculate that earthquake magnitude for which the cumulative Poisson distribution indicates a 90 per cent probability of detection by $\geq$N stations. This computational procedure was used for all detection calculations presented in the remainder of this report.

4.3 The 46-station SPZ network

There are 199 stations in Table II (including the seven SPZ arrays) which have some degree of SPZ detection capability, i.e., a known SPZ magnification at 1 second. It will be seen in the following sections that most of the lower magnification SPZ stations will not contribute in any highly significant way to discussions of global P wave detection capabilities. The first requirement, therefore, is to reduce the total of 199 SPZ stations to a conceptual world-wide network of a manageable number of SPZ stations which can be used to discuss global P wave detection.

In sections 4.5 and 4.6, the principal P wave detection results of this study will be presented as global contour maps, the calculations for the contours being made at 146 grid points on the earth separated by 20° in both latitude and longitude. The procedure adopted to define an SPZ network was to choose for each grid point the four stations with the best P wave detection capability, i.e., with the lowest m_{50} values (see Equation 2). If, at the fourth lowest m_{50} value, there was more than one station with the same capability, the additional stations were also included. The total number of individual stations chosen by such a process was 46 (the seven SPZ array stations and 39 SPZ conventional stations). This 46-station SPZ network is shown in Figure 1 and will be used exclusively for all P wave detection calculations which follow. In addition, however, we have illustrated in Figure 1 the locations of the 30 additional stations which have SPZ magnifications $\geq$50 K. Many of these stations, although not employed in detection calculations made here, are of importance in considering regional studies and, in fact, have been used in particular research studies which will be cited in later sections. It can be noted that most of these additional stations are located in

North America and Europe. It should also be noted that a number of southern hemisphere stations selected for inclusion in the 46-station network by the procedure defined above have SPZ magnifications less than 50 K; this is due to the paucity of high SPZ magnification stations in the southern hemisphere.

Although it may appear that the 46-station SPZ network as defined will have a poorer P wave detection capability than a larger network consisting of all 199 SPZ stations, in fact, the N-station detection limit as we have defined it (see section 4.2) will not, for small values of N and for a general point on the earth's surface, be significantly different whether using the 46-station or a 199-station network.

4.4 P wave detection at specific sites

Although the principal result of this chapter will be global P wave detection contour maps, it is of value to begin with a discussion of P wave detection capabilities for events at seven specific sites: (a) as an illustration of the procedures which will be generalized to the global coverage, and (b) to define for these sites the formal detection capabilities of the 46-station SPZ network which will, in later sections, be compared with empirical detection capabilities published in the literature.

The sites chosen for examination in the light of available seismograph station data are seven of the active nuclear explosion test sites; these seven sites, each assigned a 3-letter site code, are listed in Table V, and plotted in Figure 2. It must be emphasized that the discussion at this point applies only to earthquakes, that is, to hypothetical or real (if they happen to occur) earthquakes at a depth of 25 km, at or near (say, with epicentres within about 10° of) the seven sites chosen for study. The conclusions drawn for conceivable earthquakes at these sites will, of course, be expanded in later chapters to a discussion of both the detection and identification of underground nuclear explosions at these same sites.

All presumed underground nuclear explosions have been detonated in the northern hemisphere. It is for purposes of comparing and contrasting detection capabilities at a southern hemisphere site that MUR (an atmospheric explosion test site) has been included with the six northern hemisphere sites in this study.

Table V. Nuclear explosion test sites given special consideration in this report

Site Code	Location	Latitude	Longitude
NTS	Nevada, U.S.A.	37.2 N	116.5 W
KAZ	E. Kazakh, U.S.S.R.	49.7 N	78.1 E
SAH	Southern Algeria	24.2 N	5.1 E
CHI	Northwest China	41.4 N	88.3 E
ALU	Aleutian Islands	51.4 N	179.2 E
NVZ	Novaya Zemlya	73.4 N	54.8 E
MUR	Mururoa Island	22.0 S	139.0 W

The epicentral distance range considered for P wave detection calculations is $0 \leq \Delta \leq 90°$. Although the magnitude computational formula, and therefore the P wave detection capability, is poorly defined at distances less than 20°, any reasonably sensitive seismograph station will detect P waves from quite small earthquakes at the near distances. Thus it is necessary to devise an approximation to include in the detection calculations all stations nearer than 20° to a particular site. The approximation used here is an extrapolation of the Q distance calibration function (see Equation 1) to zero distance; the empirical Q* function from Basham (1969a) is employed in the range from 12° to 20°, and a somewhat arbitrary value of Q=6.4 is employed between 0° and 12°. There are more accurate procedures for calculating P wave magnitudes at the near distances (see, for example, Evernden, 1967), but they require a regionally-dependent calibration of the appropriate P phase arrivals and amplitudes. Without such phase calibration available for a general point on the earth's surface, some approximation must be employed; the one chosen will not significantly distort the resulting P wave detection results. The 90° outer limit of epicentral distance for detection calculations is the limit of the so-called "third zone", a distance slightly less than the one at which P waves begin to be diffracted by the earth's core.

Using the detection computational procedure described in section 4.2, the P wave detection capability of the 46-station SPZ network for earthquakes at the seven specific sites are given in Table VI. The m values listed are those earthquake magnitudes for which there will be a 90 per cent probability of detection by $\geq$N stations; m values are listed for N= 4, 6, 8 and 10. The number of stations within the $0 \leq \Delta \leq 90°$ detection range for each site are also indicated.

To avoid the repeated use of a long phrase throughout this report, we will employ the wording "N-station threshold", and rely on the reader to recall the exact computational procedure as described in sections 4.1 and 4.2, and the more explicit meaning described by the table heading in Table VI. For example, from Table VI, the *4-station* P wave detection *threshold* of the 46-station network for earthquakes at the site NTS is m4.0.

Table VI. Earthquake m magnitudes at specific sites for which there is a 90 per cent probability of P wave detection by $\geq$N stations

N	NTS (22)*	KAZ (26)	SAH (22)	CHI (23)	ALU (33)	NVZ (31)	MUR (27)
4	4.0	4.2	4.3	4.3	4.2	4.1	4.5
6	4.2	4.4	4.4	4.4	4.4	4.3	4.6
8	4.3	4.5	4.6	4.6	4.5	4.4	4.7
10	4.5	4.6	4.7	4.8	4.6	4.5	4.9

* Number of stations from 46-station SPZ network within detection range ($\Delta \leq 90°$).

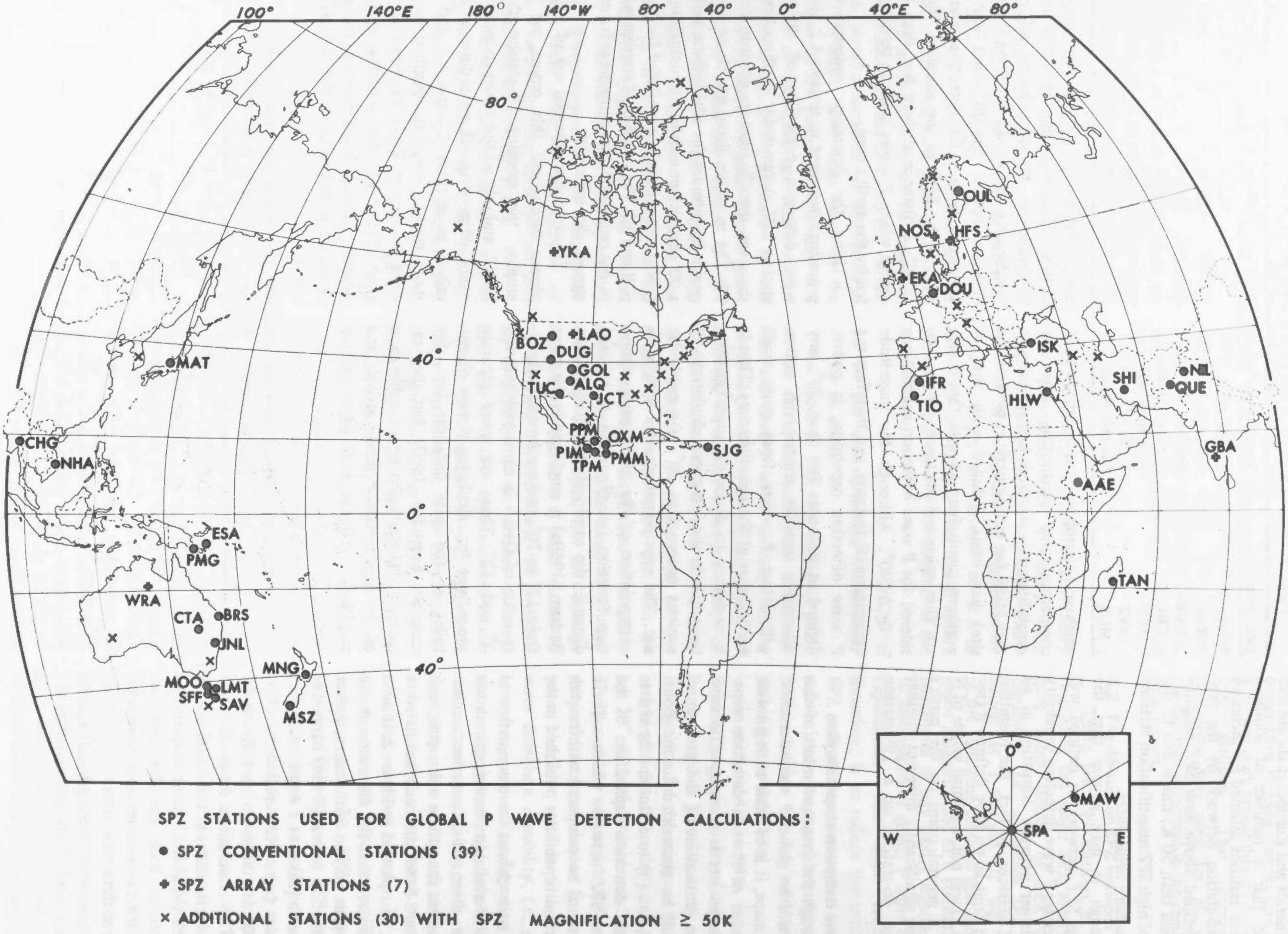

Figure 1. Conventional and array stations in the 46-station SPZ network used for global P wave detection calculations. The 30 station locations shown without station code names are all additional stations from Table II with SPZ magnification ≥ 50 K.

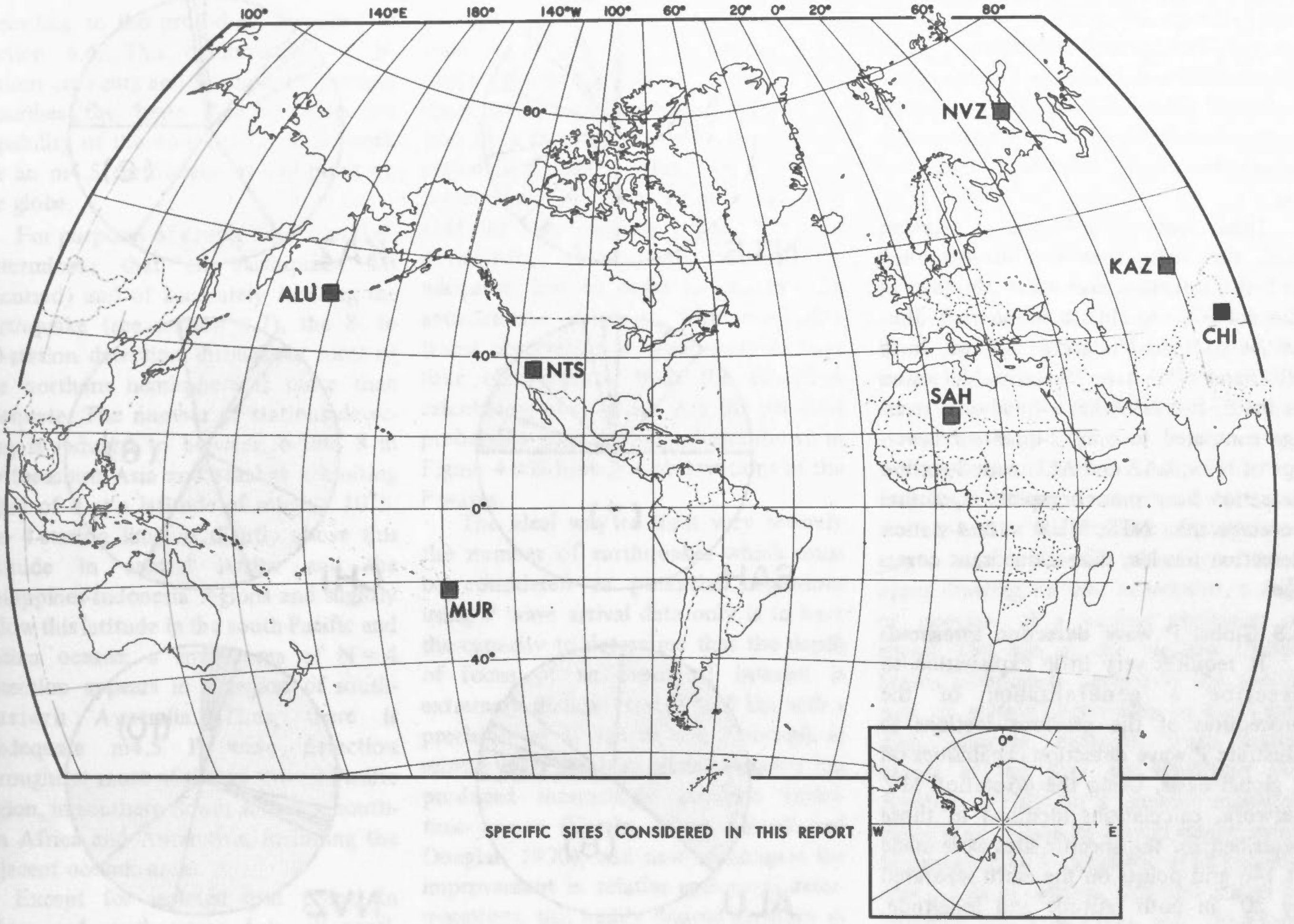

Figure 2. Nuclear explosion test sites given special consideration in this report.

A brief examination of the results of Table VI will illustrate some characteristics of P wave detection which will have general validity in the global context:

(a) The higher latitude sites (ALU and NVZ) have more stations within detection range than do mid-latitude sites in the northern hemisphere.

(b) The N-station detection thresholds are within δm0.3 of being equivalent at all northern hemisphere specific sites; the extremes within this range show NTS and NVZ thresholds to be roughly δm0.3 lower than the SAH and CHI thresholds.

(c) The N-station detection threshold for the southern hemisphere site, MUR, is approximately δm0.3 higher than the average for the northern hemisphere sites.

(d) The 10-station detection thresholds are about δm0.4 greater than the 4-station thresholds at all specific sites.

Because of asymmetries in P wave radiation patterns and for purposes of estimating epicentre location errors when using small numbers of stations (see section 4.7), it is important to define the source-to-station azimuthal coverage provided by the stations at the threshold being discussed. The threshold magnitudes derived for N stations are statistically determined on the basis of all stations of the network within detection range. However, for purposes of illustrating azimuthal coverage, it is adequate to examine the azimuthal coverage provided by the best N stations at the N-station threshold. The threshold magnitude to be examined here for P wave detection at the specific sites (and for global coverage; see section 4.6) is m4.5. Thus, we wish to examine the azimuthal coverage provided by the best N stations for which the N-station threshold is m4.5 at each site. The values of N for some sites are apparent in Table VI; for example, we will examine the azimuthal coverage provided by the best 10 stations for NTS, the best eight stations for KAZ, etc.

The P wave azimuthal coverage for m4.5 earthquakes is illustrated for the seven specific sites in Figure 3. The radial plots show both individual station azimuths from the source (solid radial lines) and a method of shading which illustrates azimuthal coverage in a more general way, the principal use of the shading to be an illustration of the global results in section 4.6. The rules adopted for the shading are as follows: (1) any quadrant (NW, SW, SE or NE) which contains more than one station is completely filled (e.g., NE and SE for NTS); (2) for a single station in a quadrant, the area between the station line and the nearest filled section is filled (e.g., part of SE for CHI); and (3) any single station separated by more than 90° in azimuth from the nearest filled section is represented by a 30° "pie-slice" (e.g., see MUR).

Thus, from Figure 3, one can examine both the number of stations detecting and the effective azimuthal coverage at the m4.5 threshold. A number of illustrative comparisons are as follows: both NVZ and NTS have 10-station detection at m4.5, but NVZ has 3-quadrant coverage compared to only 2-quadrant coverage of NTS; KAZ and ALU with 8-station detection have more complete azimuthal coverage than NTS; MUR with 4-station detection has less than 2-quadrant coverage.

4.5 Global P wave detection thresholds

It requires very little explanation to describe a generalization of the procedures of the previous sections to illustrate P wave detection capabilities on a global basis. Using the 46-station SPZ network, calculations identical to those described for the specific sites were made at 146 grid points on the earth separated by 20° in both latitude and longitude. (This equal spacing in longitude for all latitudes produces denser coverage at high latitudes, but is useful for contouring on Mercator-type map projections.)

A contour map of the 4-station P wave detection threshold is shown in Figure 4; the contour interval used is δm0.2. The broad feature of these contours is a general increase in the 4-station threshold from m4.2 in the north to m5.0 in the south. The distribution of high magnification stations produces one dominant "low" and one "high" on the map. The "low" of m4.0 in southern North America results from a concentration of sensitive stations (see Figure 1); the "high" of m5.0 in the south Atlantic Ocean results from a paucity of stations in South America and southern Africa. The station sensitivities and distribution in the northern hemisphere are sufficient to produce a broad, flat 4-station threshold at m4.2 over North America, Europe and northern Asia, deteriorating to m4.5 for virtually complete Asian and north African coverage.

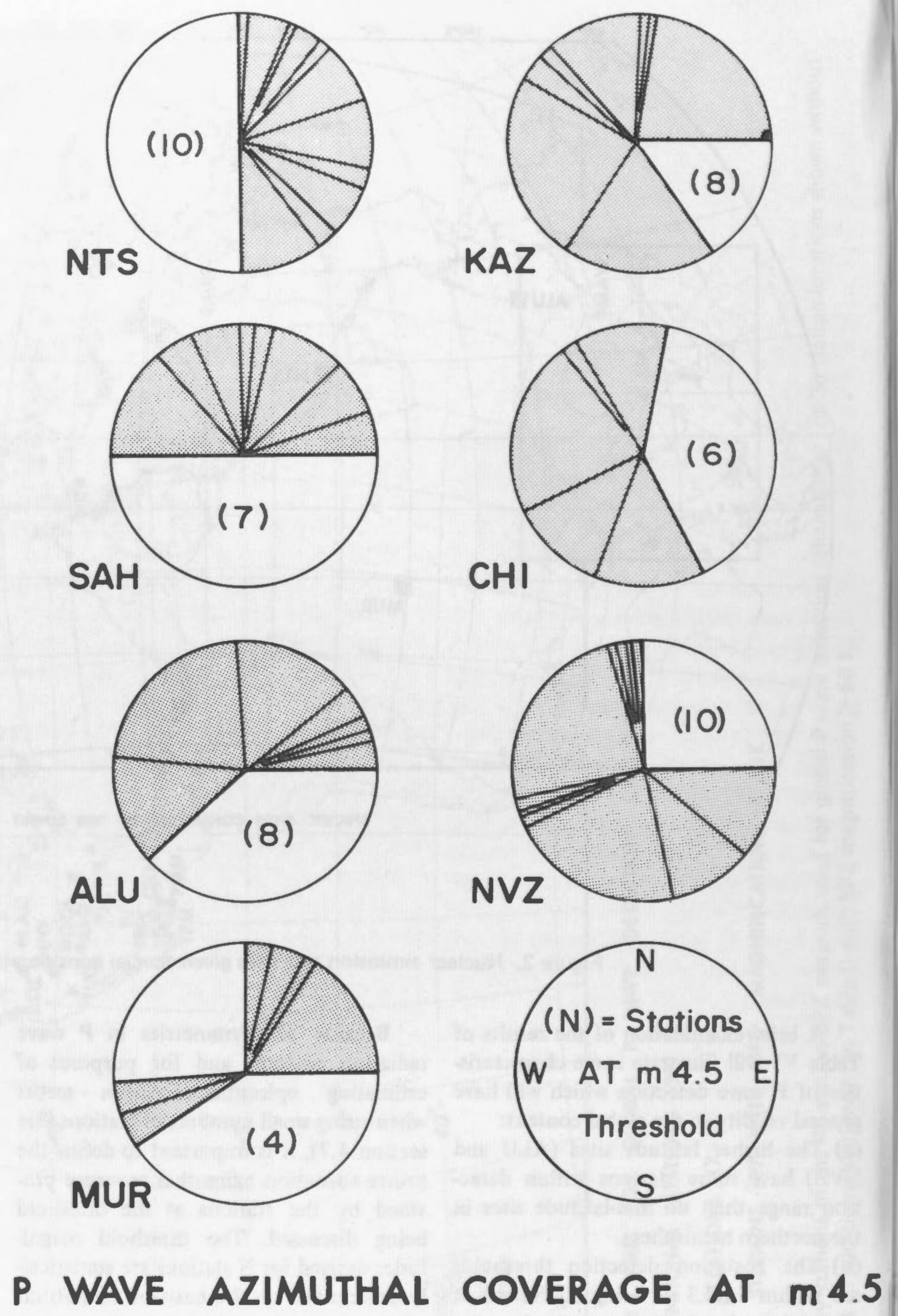

Figure 3. Number of stations detecting and azimuthal coverage provided by the 46-station SPZ network for earthquake P waves at a threshold m4.5 at the seven specific sites. See text for procedure for choosing N and representing azimuthal coverage by radial plot shading.

4.6 P wave detection and azimuthal coverage at m4.5

The number of stations detecting P waves at a threshold magnitude m4.5 is contoured in increments of 2 in Figure 5. The contour numbers are equivalent to the numbers in parentheses in each radial plot in Figure 3. Also shown in Figure 5 at each grid point for which N ≥ 4, is an azimuthal coverage radial plot drawn according to the procedure described in section 4.4. This combination of N-station contours and azimuthal coverages describes the basic P wave detection capability of the 46-station SPZ network for an m4.5 earthquake at any point on the globe.

For purposes of simple detection (i.e., determining that an earthquake has occurred) and of accurately locating the earthquake (see section 4.7), the 8- to 10-station detection throughout most of the northern hemisphere is more than adequate. The number of stations detecting is reduced to between 6 and 8 in southeastern Asia and reaches a limiting value of 4 at a latitude of roughly 10°S; the 4-station limit is slightly above this latitude in central Africa and the Philippines-Indonesia regions and slightly below this latitude in the south Pacific and Indian oceans; a small area of $N = 4$ detection appears in a region of southwestern Australia. Thus, there is inadequate m4.5 P wave detection throughout most of the southwest Pacific region, in southern South America, southern Africa and Antarctica, including the adjacent oceanic areas.

Except for isolated grid points in Africa and southeastern Asia, all continental areas which have $N \geq 4$ station detection are represented in azimuth by at least 2-quadrant coverage. The most obvious inadequate azimuthal coverage occurs in the eastern Pacific Ocean for which all detecting stations are in North America, resulting in only 1-quadrant coverage.

4.7 P wave detection and epicentral determination

Whatever assumptions are made to define adequate P wave detection capabilities, the problem of using these detected P waves to compute the epicentre and the focal depth of the earthquake must be considered. We have defined as an adequate P wave detection capability the 4-station thresholds which are illustrated in Figure 4. Assuming a known travel-time curve for regional and teleseismic distance, for detection by only a small number of stations, the depth and origin time of an event can largely be traded against each other, and so there are only three significant unknowns, latitude, longitude and origin time. A zero depth, or some other fixed depth, restraint is usually made in the epicentral calculation with P wave detection by a small number of teleseismic or regional stations, when other phase information or data from very close stations are lacking. Therefore, in principle, three observations are adequate, but in order to confirm the approximate epicentre with one additional observation it is necessary to have four observations. With the detection calculation used, there is a 90 per cent probability that the magnitudes shown in Figure 4 will have ≥ 4 observations of the P waves.

The ideal way to limit very severely the number of earthquakes which must be considered as potential explosions using P wave arrival data only is to have the capacity to determine that the depth of focus of an event of interest is extremely shallow (say, 0 to 5 km with a precision of ±1 km or so). Although in recent years much excellent research has produced increasingly accurate travel-time curves (Herrin, 1968; Lilwall and Douglas, 1970), and new techniques for improvement in relative epicentral determinations, this highly desired accuracy in focal depth determination is unattainable, even with some tens or hundreds of observations. This is because there are lateral complexities in the earth. In practice, a small number of P wave observations (say, 10 or less) cannot determine a focal depth to better than ±10 km at best.

In principle, there are two possibilities of interest with a small number of detecting stations. The first involves co-operation by nuclear testing powers in releasing publicly the times and positions of a number of suitably large explosions for each test site in order to obtain accurate empirical travel-time corrections for each testing area for the network of observing stations. The only study known to us of the effect of these corrections for a small network at one test site is one by Weichert and Newton (1970) using some NTS explosions recorded on the Canadian network. When corrections were obtained for 13 Canadian stations from publicly released data, and calculations made using the network on other NTS explosions, the focal depth could not be estimated better than ± 5 km. If the calculations are repeated with no known corrections (i.e., no master events in the public domain), the situation is impossible and errors of many tens of km in the best computed depth of focus can occur. We estimate that with a small network, reasonably adequately distributed in azimuth, but with no master event control, all events with a nominal focal depth from zero to about 50 km could be potential surface focus events–or in this context, potential explosions. A further complication is that the master event technique may not give control over a very large distance from the master event site because of the presence of crustal and upper mantle lateral inhomogeneities–again drawing on our experience, a shift of position of a nuclear explosion of about 150 km in the western United States completely destroyed the usefulness of station corrections to the Canadian network obtained from master events at the first site (Weichert and Newton, 1970). In a control situation, there is no reason to expect master event information to be available at all conceivable points of interest, although it may be available for some areas, and, therefore, we can dismiss the matter from further practical consideration in this paper.

The second possibility for improvement was well demonstrated by Evernden (1969a). A striking improvement in precision of depth of focus can be obtained when an independent estimate of the origin time can be made from time differences between certain seismic phases on the record at a small number of near stations. This, for the 46-station SPZ network under study, is impossible–insufficient stations are reported at distances of 150-1000 km from already known test sites. From conceivable test sites, the station distribution is worse, and once again we can, therefore, dismiss precision in focal depth determination as a feasible identification technique at the limits of detection by a small number of stations.

Reasoning along these lines is the summary basis for the generally accepted contention that with a finite number of sensitive stations all earthquakes with

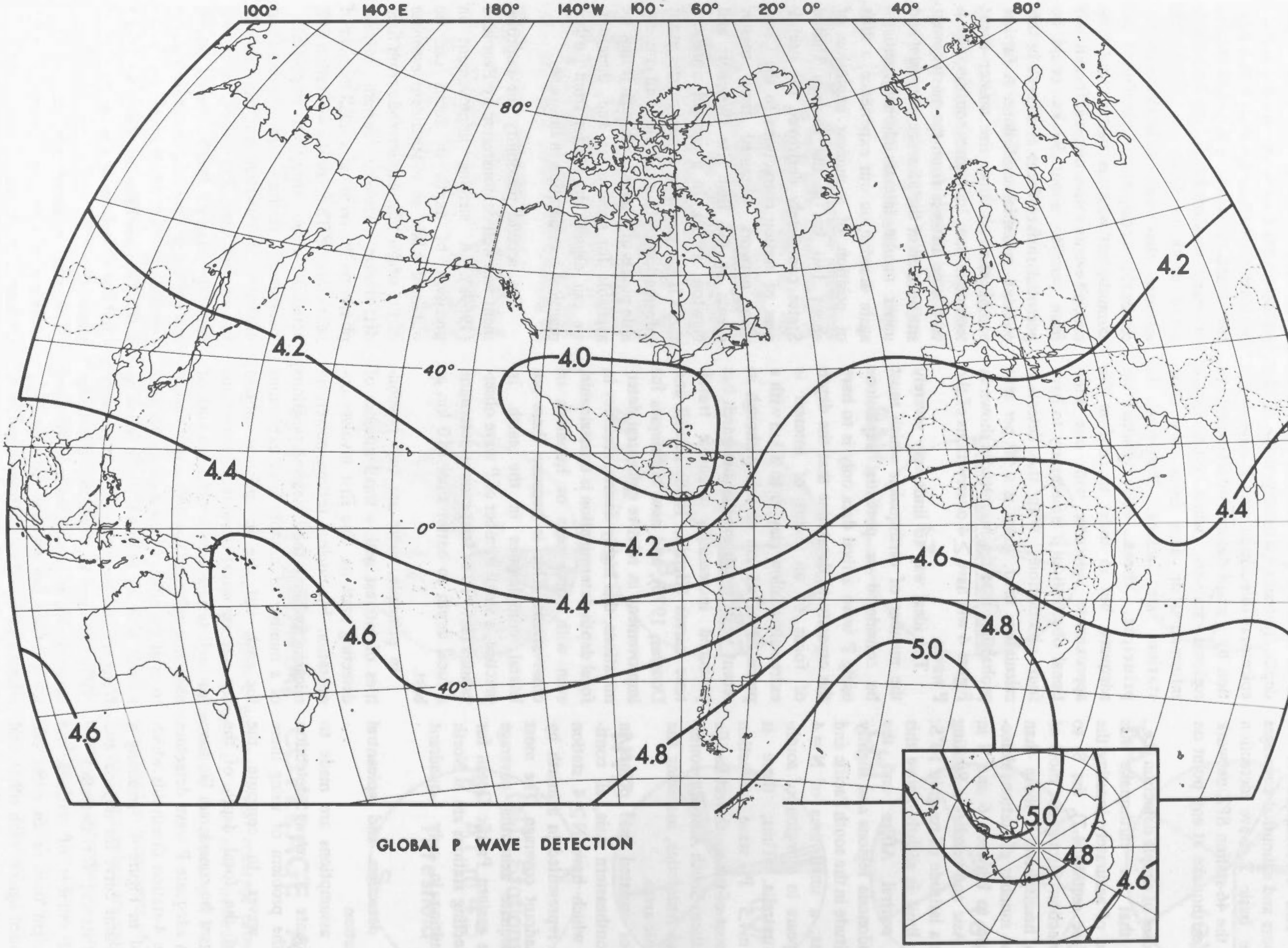

Figure 4. Global contours of the 4-station earthquake P wave detection threshold. A shallow earthquake with this P wave magnitude will have a 90 per cent probability of P wave detection by $\geq$ 4 stations of the 46-station SPZ network.

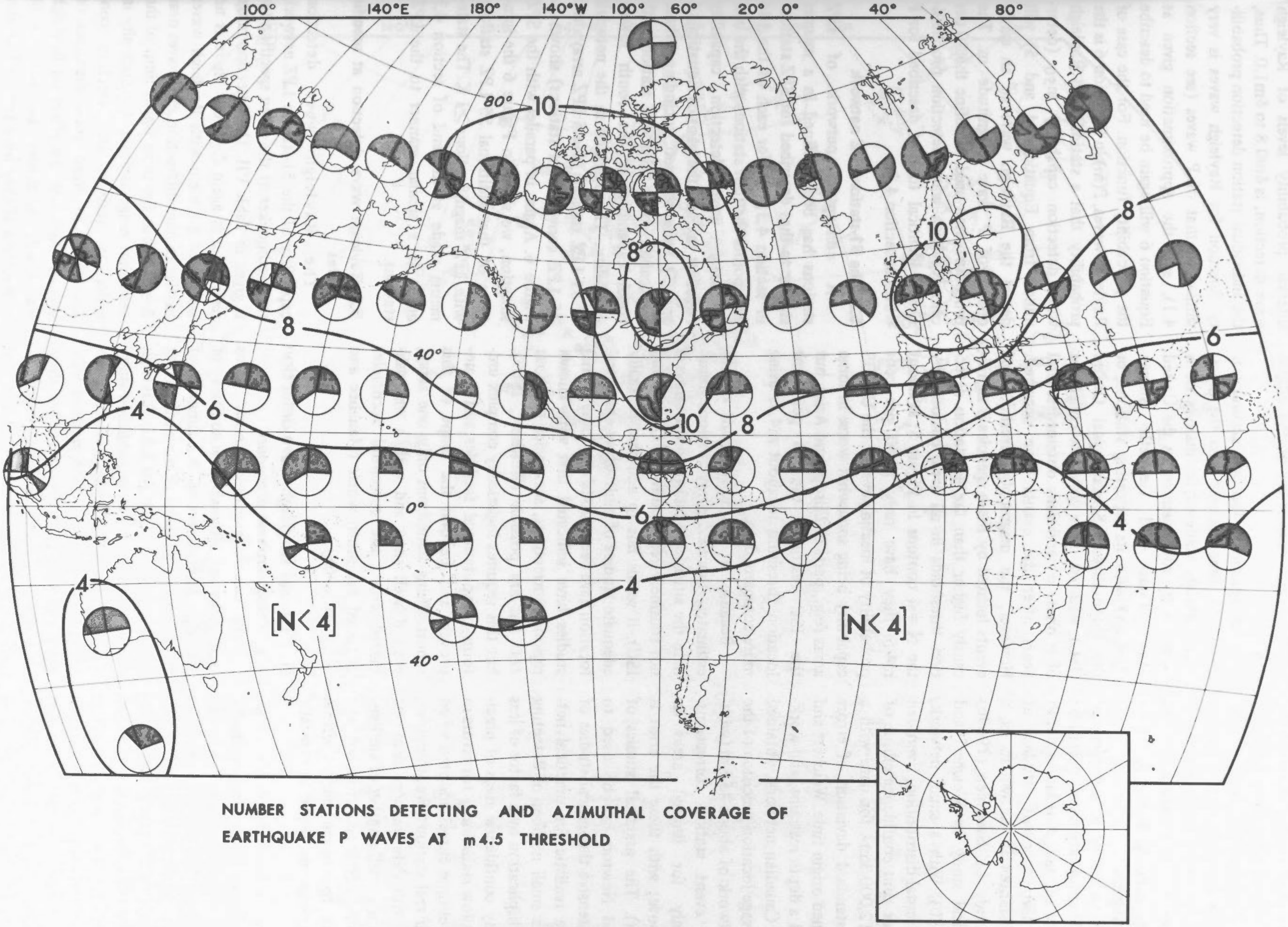

Figure 5. Number of stations detecting and azimuthal coverage provided by the 46-station SPZ network for earthquake P waves at a threshold m4.5. See text for procedure for representing azimuthal coverage by radial plot shading.

crustal depths need testing, in principle, as potential nuclear explosions against a number of identification criteria. The depth of focus derivable in the general case, in practice, with a small number of detecting stations, even if reasonably well distributed in azimuth, is too uncertain for use as a criterion.

It is now necessary to consider the question of location accuracy, accepting this ambiguity of, say, ±30 km in depth of focus. Two relevant studies at teleseismic distances are known to us, a theoretical study by Evernden (1969b) and a practical study by Weichert and Newton (1970). With a small network, and a 1-quadrantal distribution, Evernden gives a 95 per cent confidence ellipse of area about 12,000 km^2 for data with a 0.5 second standard deviation of errors and a restrained origin time. Weichert and Newton used a depth restraint, and working with the Canadian network, obtained a typical average location precision of the Canadian network of about 45 km (without master event station corrections, available only for limited areas as described above; with these the error is about 5 km). The practical studies of Weichert and Newton can be used to show the extensive theoretical studies of Evernden are realistic for practical networks with a small number of detecting stations: multiplication by a factor of less than 2 in any confidence areas of precision should allow statistically for errors in the best travel-time curves adopted when working with real stations. We, therefore, believe that with data in more than one quadrant from a small number of stations, and with no master control but the best possible travel-time curves, errors in epicentral positions should be typically 20-45 km.

Referring to the azimuthal coverage presented in Figure 5, it can be concluded that, using the 46-station network, errors in epicentral position for m4.5 events at all locations enclosed by the N = 4 contour should not exceed 20-45 km. There may be minor exceptions to this at the fringe of the N = 4 contour and at other isolated locations of poor azimuthal coverage, for which cases the 95 per cent confidence ellipses (see Evernden, 1969b) may be elongated and the exact precision would require knowledge of the ellipse shapes.

This epicentral location accuracy is about two times poorer than the precision routinely achieved for many station locations by such agencies as the United States Coast and Geodetic Survey (USCGS) with its reporting stations, or the International Seismological Centre (ISC), with its more complete collection of P phase observations obtained several years after the events have occurred. However, the magnitude thresholds of events located by these agencies is significantly higher than the 46-station detection thresholds in all areas enclosed by the N = 4 contour in Figure 5; at about m4.5 they have only a 50 per cent probability of locating events, the USCGS capability being somewhat worse in some areas (e.g., parts of Europe and Asia), but the ISC restoring the 50 per cent location threshold to about m4.5, using more complete data.

Because, at the lower limit of our estimates, the SPZ array stations dominate the situation (data from the arrays is not routinely reported to the USCGS and ISC), it seems fair to add that no really adequate studies of multi-array epicentral location have been published. Some partial studies have indicated that with known regional corrections, accuracies of about ±60 km are possible (Weichert, 1969), but this requires logistically complex uniform computational facilities and is unproven and beyond the scope of this report. Using data from only one array, even if well sited and with a well calibrated crust, the epicentral accuracies obtained are much worse (Manchee and Weichert, 1968).

5. Global Rayleigh wave detection

5.1 Computational procedure

The two data sources known to us that present interval probabilities of Rayleigh wave detection as a function of the P wave magnitudes of the earthquakes are by Lacoss (1969a) for LAO Rayleigh wave detection, and an unpublished study by the authors of Rayleigh wave detection at the Canadian LPZ stations SES, OTT and ALE. Both these studies show that the P wave magnitude range, between the 10 per cent and 90 per cent interval probability levels of Rayleigh wave detection, is δm0.8 to δm1.0. Thus, the individual station detection probability function for Rayleigh waves is very similar to that of P waves (see section 4.1), and the approximation given as Equation 6 will again be used to describe the probability function. For the case of Rayleigh waves, P(m) in Equation 6 is the probability that a station with Rayleigh wave detection capability m_{50} (determined from Equations 4 and 5) will detect the Rayleigh wave of an earthquake of P wave magnitude m. The procedure then used to define the 90 per cent Rayleigh wave detection probabilities is identical to that described for P waves in section 4.2.

5.2 The 51-station LPZ network

A conceptual network of LPZ stations has been defined in a manner similar to that described for SPZ stations in section 4.3; i.e., for each of the 146 grid points the four stations with the best Rayleigh wave detection capability (smallest m_{50} on the basis of Equations 4 and 5) were selected, including, where applicable, more than one station with equal capability at the fouth lowest capability. This resulted in the network of 51 LPZ stations (the 5 LPZ arrays and 46 LPZ conventional stations) shown in Figure 6. Again, in parallel with the SPZ situation, we show in Figure 6 the locations of the additional 55 LPZ stations with LPZ magnifications $\geq$1 K. The statements made at the end of section 4.3 apply in a similar manner to the LPZ stations.

5.3 Rayleigh wave detection at specific sites

The Rayleigh wave detection capability of the 51-station LPZ network for earthquakes at the seven specific sites is given in Table VII. The detection range restriction is again $\Delta \lesssim 90°$. There is no associated problem with Rayleigh waves similar to core diffraction of P waves near $\Delta = 90°$, but the same upper limit of the detection range is applied, principally in order to restrict all detection considerations to third zone distances or shorter. Although the effect on Rayleigh waves will, in theory, be only one of attenuation if they have travelled greater

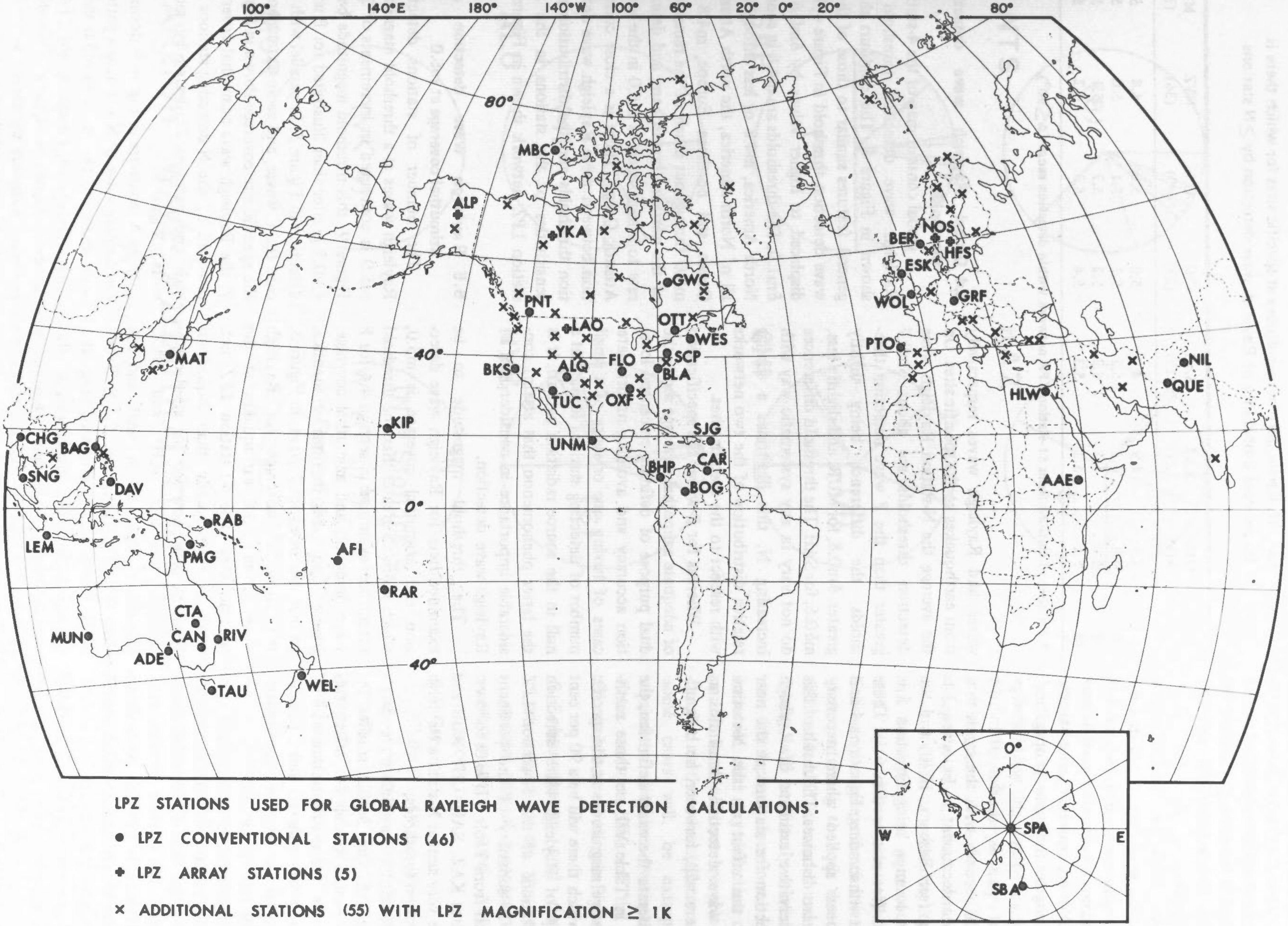

Figure 6. Conventional and array stations in the 51-station LPZ network used for global Rayleigh wave detection calculations. The 55 station locations shown without station code names are all additional stations from Table II with LPZ magnification ≥ 1 K.

distances, there would be problems at great distances of associating both the Rayleigh and P wave to a specific event for stations having both LPZ and SPZ instrumentation.

However, there is an associated problem at the near distances in that the detection equations applied, Equations 4 and 5, are known to be inaccurate at near distances. For near distances, and particularly for continental path propagation, the dominant Rayleigh wave energy appears at periods shorter than the assumed 20 seconds with the result that the distance decrement in Equation 3 is too strong (see Basham, 1970) and the conversion to m_{50} using Equation 5 is invalidated (see also section 6.3). These effects notwithstanding, Equations 4 and 5 have been applied where necessary down to zero distances. The result of this is a conservative estimate of Rayleigh wave detection for stations at the near distances; the effect on the N-station Rayleigh wave detection thresholds as defined here will, however, be insignificant.

To reiterate the exact definition, the m values in Table VII are those earthquake P wave magnitudes at the specific sites for which there will be a 90 per cent probability of Rayleigh wave detection by ≥N stations of the 51-station LPZ network. A summary of the pertinent conclusions from Table VII is as follows:
(a) the sites KAZ, SAH, CHI, ALU and NVZ have very similar N-station Rayleigh wave detection thresholds,
(b) the N-station Rayleigh wave detection thresholds are δm0.2 smaller for NTS and δm0.3 greater for MUR, this being due to the concentration of LPZ stations in North America and a paucity of stations in the southern hemisphere, respectively (see Figure 6),
(c) the high-latitude sites (ALU and NVZ) have more LPZ stations within detection range than do the mid-latitude sites,
(d) the 10-station Rayleigh wave detection thresholds are about δm0.4 greater than the 4-station thresholds.

A comparison of Tables VI and VII will illustrate the relative capabilities of the 46-station SPZ network and the 51-station LPZ network in detecting P waves and Rayleigh waves respectively from earthquakes at the specific sites. On the average the N-station Rayleigh wave detection thresholds are about δm0.7 greater than the P wave detection thresholds, the difference being slightly greater, δm0.8, for MUR, and slightly less, mδ0.6, for SAH. The threshold differences do not vary in any systematic way with increasing N; this illustrates a similar relative distribution of the two networks with respect to the specific sites.

Table VII. Earthquake m magnitudes at specific sites for which there is a 90 per cent probability of Rayleigh wave detection by ≥N stations

N	NTS (31)*	KAZ (29)	SAH (27)	CHI (27)	ALU (40)	NVZ (36)	MUR (31)
4	4.7	4.9	4.9	5.0	5.0	4.8	5.3
6	4.9	5.1	5.1	5.1	5.1	5.0	5.4
8	5.0	5.2	5.2	5.2	5.2	5.1	5.5
10	5.1	5.3	5.3	5.4	5.3	5.2	5.6

* Number of stations from 51-station LPZ network within detection range (Δ≤90°).

Whereas for P waves the specification of adequate azimuthal coverage serves the dual purpose of defining epicentral location accuracy and avoiding unfortunate cases of having one or more of a small number of detecting stations located at a null in the source radiation pattern, it is the latter phenomenon that attains considerable importance in consideration of Rayleigh wave detection.

The threshold magnitude to be examined here for Rayleigh wave detection and azimuthal coverage is m5.0, which is δm0.5 greater than the threshold magnitude examined in section 4.4 for P wave detection and azimuthal coverage. Figure 7 illustrates, in a manner identical to that described for P waves in Figure 3, the azimuthal coverage for Rayleigh waves from m5.0 earthquakes at the specific sites. The 51-station LPZ network provides greater than 2-quadrant Rayleigh wave coverage for m5.0 earthquakes at KAZ, CHI and NVZ, 2-quadrant coverage for SAH, and less than 2-quadrant coverage for NTS and ALU. Fewer than 4-station coverage at a particular threshold magnitude, in this case m5.0, is considered inadequate detection; this is the case illustrated for MUR in Figure 7.

5.4 Global Rayleigh wave detection thresholds

A global contour map of the 4-station Rayleigh wave detection threshold is shown in Figure 8. The contours show general features similar to those of the P wave detection threshold in Figure 4, but displaced to higher values by δm0.6 to δm1.0. The thresholds are m4.6 in central North America, m4.8 or less throughout all of North America, the north Atlantic Ocean and northern Europe, m4.8 to m5.0 throughout much of the remainder of the northern hemisphere, and deteriorate to a high value of m6.0 in the south Atlantic Ocean. There is a close correlation between these Rayleigh wave detection thresholds and the distribution and sensitivities of the stations in the 51-station LPZ network shown in Figure 6.

5.5 Rayleigh wave detection and azimuthal coverage at m5.0

The number of stations detecting Rayleigh waves at a threshold magnitude m5.0 is contoured in increments of 2 in Figure 9, this threshold magnitude being δm0.5 greater than illustrated for P wave detection in Figure 5. In parallel with the case for P waves, and as an extension of the specific site coverage shown in Figure 7, the Rayleigh wave azimuthal coverage provided by the N detecting stations for each grid point is illustrated by radial plots in Figure 9.

The N contours in Figure 9 down to the limiting value of N = 4 have a pattern very similar to the m4.6 to m5.0 threshold contours of Figure 8; the N = 4 contour in Figure 9 and the m5.0 contour in Figure 8 display the same basic information. The azimuthal coverage for Ray-

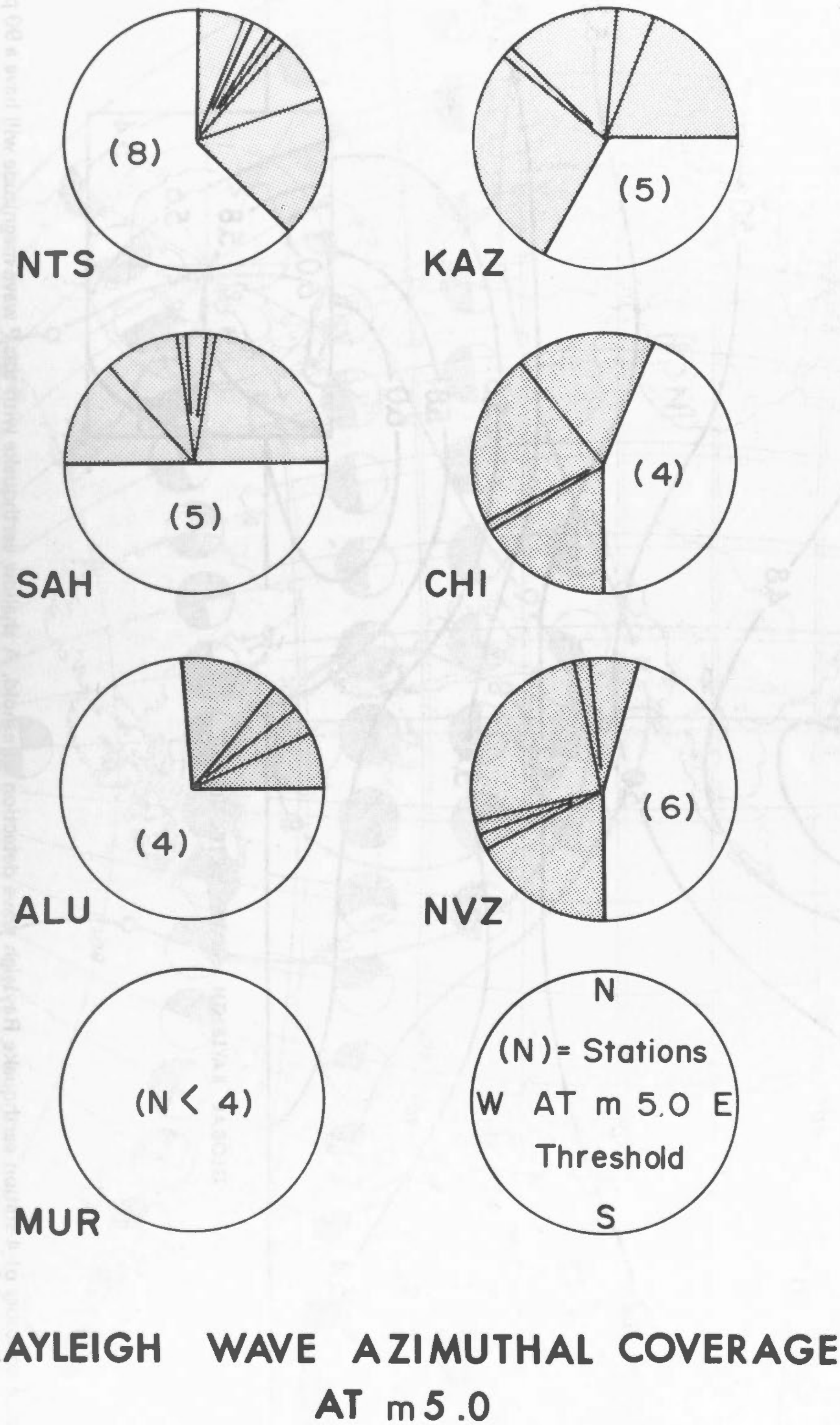

Figure 7. Number of of stations detecting and azimuthal coverage provided by the 51-station LPZ network for earthquake Rayleigh waves at a threshold m5.0 at the seven specific sites. See text for procedure for choosing N and representing azimuthal coverage by radial plot shading.

leigh waves is generally adequate, 2 or more quadrants, at all locations enclosed by the N = 6 contour, and, except for parts of northeastern and southwestern Asia, there is 2-quadrant coverage between the N = 4 and N = 6 contours.

In choosing to illustrate in Figure 9 the Rayleigh wave coverage at a threshold of m5.0, we have in effect limited consideration of Rayleigh wave detection to northern hemisphere locations. This is justified by the limited capabilities of both P and Rayleigh wave detection in the southern hemisphere illustrated on foregoing maps, which results directly from the lack of availability in the southern hemisphere of numerous sensitive SPZ and LPZ stations. Thus, in the following chapters much of the discussion, pertaining to both the conceptual SPZ and LPZ networks and published results, will be directly related to northern hemisphere locations. It follows, however, that any detection or identification thresholds we are able to define for the northern hemisphere can, and in some cases will, be extrapolated to equivalent southern hemisphere thresholds on the basis of the detection threshold contour maps in Figures 4 and 8.

6. Enhancement and degradation of detection on the real earth; special signal processing, global seismicity and interference phenomena

6.1 General

All the P and Rayleigh wave detection results presented to this point have assumed that the earth is a spherically symmetrical body for which the earth-wide radial average of its properties apply at any point. In particular, the P waves were assumed to obey everywhere the $Q(\Delta,h)$ distance-depth attenuation function and the Rayleigh waves the 1.66 log Δ distance attenuation function. The real earth is known to be quite different from this assumed average and, indeed, it has been the discovery of the numerous anomalies or vagaries in the earth that has led to understanding of important earth processes in recent years.

Many of the earth's vagaries, when sufficiently documented, can make important differences to the narrow field of

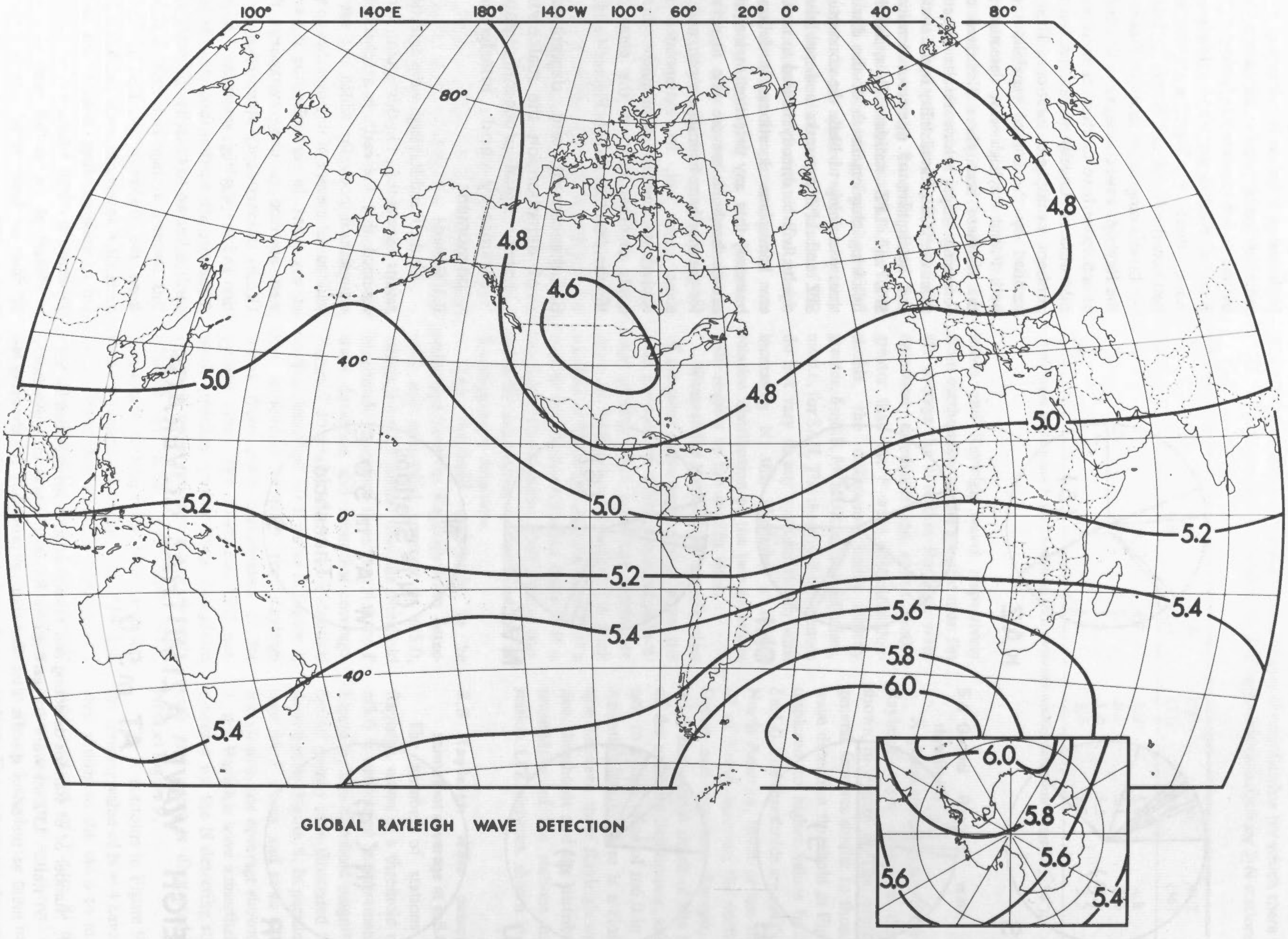

Figure 8. Global contours of 4-station earthquake Rayleigh wave detection threshold. A shallow earthquake with this P wave magnitude will have a 90 per cent probability of Rayleigh wave detection by $\geq$ 4 stations of the 51-station LPZ network.

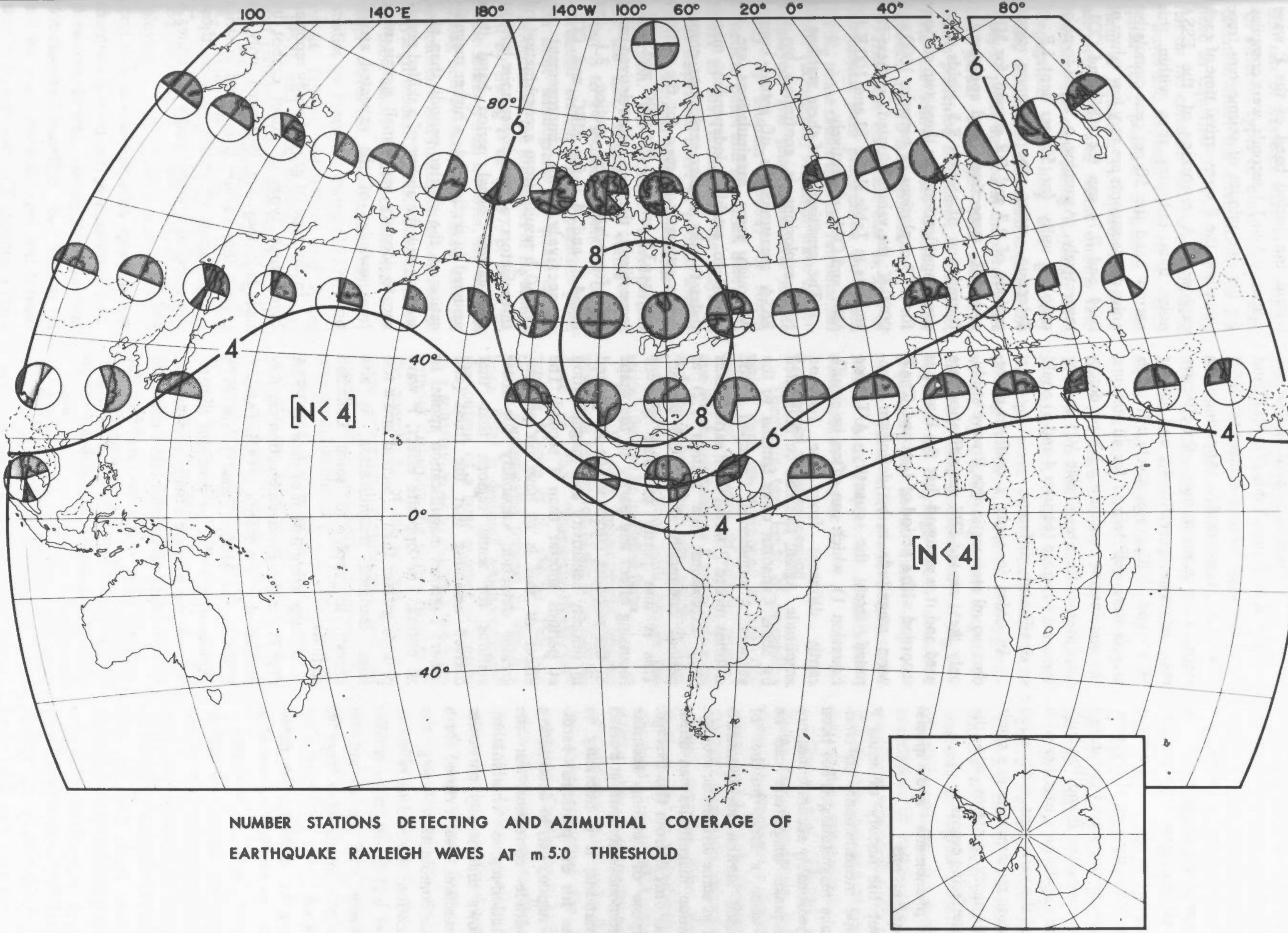

Figure 9. Number of stations detecting and azimuthal coverage provided by the 51-station LPZ network for earthquake Rayleigh waves at a threshold m5.0. See text for procedure for representing azimuthal coverage by radial plot shading.

investigation being considered here: the simple detection of P and Rayleigh waves at given stations for certain magnitude earthquakes. This chapter will deal with some of these phenomena to show how they might change the broad picture of detection so far presented. In addition, this is a useful point in the text to present any specialties of instrumental response and data processing that have been shown capable of improving the P and Rayleigh wave detection capabilities, together with a discussion of the variations in detection and identification requirements as a result of global seismicity patterns and the presence of interfering events.

6.2 P wave phenomena and special instrumental effects

Throughout the history of using P wave amplitude measurements to compute earthquake magnitudes, it has been found that a reasonably accurate measure of the earthquake magnitude can be found only when a large number of widely dispersed station measurements are combined in some arithmetic average. Individual station magnitudes can differ by as much as $\delta m 1.0$ from this average. For the purpose of defining accurate magnitudes from measurements at a small number of stations, it is necessary to calibrate these for the particular earthquake source region, i.e., to determine a station magnitude correction for the particular station-region combination. Thus, it follows that at any particular magnitude detection level defined for a station-region combination using the average Q function, the real or effective detection level will be larger or smaller than the average level by an amount equivalent to the positive or negative station correction.

There is great difficulty in determining the effect of such phenomena on the world-wide P wave detection discussed here because for only a few station-region combinations have such effects been well defined, a problem to be given some emphasis in a later chapter on recommendations. Some Canadian data can be used to illustrate the importance of station-region phenomena to P wave detection. Using two stations with large corrections from the study by Basham (1969a), it can be seen that MBC has a correction of −0.7 and VIC a correction of +0.9 for P waves originating near the test site KAZ* (see Table V). MBC and VIC have m_{50} values for this site of 4.9 and 5.5, respectively. Applying the station corrections to m_{50}, the effective m_{50} values are in reality 4.2 and 6.4 for MBC and VIC, respectively. If such effects were well defined for all stations, the conclusions concerning P wave detection at specific sites (Table VI) and for the areal coverage (Figures 4 and 5) could be significantly different.

In order to apply a uniform procedure to all stations in this P wave study, only the 1-second SPZ magnifications are used and it is assumed that the P wave is recorded with a period of 1 second. The P wave magnitude is by definition computed from the quantity A/T (see Equation 1), which can often be significantly different from the 1-second amplitude. Again, this can be illustrated by some Canadian cases familiar to the authors. A number of Canadian Arctic stations record P waves from earthquakes (and explosions; see section 7.2) at periods commonly 0.6 to 0.8 second. This is due partly to some type of focussing effect and partly to the shape of the response curves which are peaked in velocity sensitivity and magnification at periods shorter than 1 second. The effect of this is to have, in practice, greater detection capability for these stations for some regions than that derived assuming that the fixed (and lower) 1-second magnification applies to all events. The opposite effect, P wave periods greater than 1 second and a too large assumed magnification, is also known to apply to some Canadian stations.

A large compilation of data by ESSA (1967) on the P wave detection capabilities of the two stations, COL (Alaska, U.S.A.) and MBC (Canada), for NTS explosions provides an excellent illustration of the positive effects described in the preceding paragraphs. ESSA compiled detection and magnitude statistics for these two stations for 194 NTS explosions in the period, September 1961 to March 1967; in addition, noise statistics within the period band of the P wave signals, 0.5 to 1.1 seconds, were compiled for the one minute of seismogram trace preceding the P wave arrival time of each explosion. A reworking of the ESSA noise data indicates that within this narrow band the 50 per cent cumulative noise displacements are very low values of 0.34 and 0.74 mμ for MBC and COL, respectively. Assuming a signal-to-noise ratio of unity for 50 per cent I.P. of detection, using the common signal periods of 0.7 and 0.8 second for MBC and COL, respectively, and applying the formulation of section 3.1, yields effective magnifications for these two stations for NTS explosions of between 1000 and 2000 K; the values adopted for these two stations in Table II are 72 and 100 K for MBC and COL, respectively.

The sensitivities of these stations to NTS explosions is confirmed by the ESSA measurements of actual events. Although some manipulations are required to establish independent magnitudes for the smaller explosions, conservative estimates of m_{50} for the stations are $m_{50}3.9$ and 4.0 for MBC and COL, respectively; the m_{50} values derived using the formulation of section 3.1 are $m_{50}4.6$ and 4.7 for MBC and COL, respectively. This improvement of $\delta m_{50}0.7$ results from a combination of three factors: a much lower noise level in the narrow signal period band than assumed in section 3.1, a higher magnification at the shorter periods than at 1 second, and the ability of a skilled observer to identify very small signals with foreknowledge of the expected arrival times.

In the type of general study reported here, these types of effect cannot be included; they are illustrated only to suggest that caution is required in strict interpretation of results such as those presented as contour maps in Figures 4 and 5.

6.3 Rayleigh wave phenomena

The differences that the real earth can make to Rayleigh wave detection occur as a result of different propagation phenomena over different parts of the earth's surface. The two related effects

* These station corrections were determined from explosions, but are known to apply equally well to earthquakes near that region.

requiring attention are the real attenuation rate of Rayleigh waves with distance for different types of crust (i.e., possible deviation from the attenuation rate implied in Equation 3), and the effect this has on the *apparent* relative excitation of P waves and Rayleigh waves by an earthquake (i.e., possible deviations in the form of Equation 5). Equations 3 and 5 are acceptable and usable average relationships for considering Rayleigh wave propagation over long and generally mixed continental and oceanic paths, the types of paths implied in the specific site and global Rayleigh wave detection results presented in Chapter 5. However, there are known cases where neither equation 3 nor 5 is acceptable.

The most important case is that of continental path propagation for which the R_g phase rather than the fundamental mode (20-second) Rayleigh wave can be employed. The phase measured in the study by Basham (1969a) for North American paths and identified here as R_g refers to that section of the Rayleigh wave dispersion curve at periods shorter than 20 seconds which shows little or no dispersion. The dominant wave periods on the LPZ seismograms varied from about 8 to 14 seconds depending on the particular station and propagation path. On most seismograms the phase clearly conformed to the properties of R_g identified by Ewing *et al.* (1957, p. 219); on some seismograms, however, R_g was less strong and probably was mixed with the sedimentary and fundamental continental Rayleigh modes. The distinctive character of these short period continental Rayleigh waves is demonstrated in early studies by Press and Ewing (1952), Press *et al.* (1956) and Oliver and Ewing (1957), and more recently by Basham and Halliday (1969) and ESSA (1970b). The results of Basham (1970) show that R_g attenuates as $\Delta^{-0.8}$ rather than $\Delta^{-1.66}$, appropriate to 20-second waves in Equation 3. The disadvantage of employing the R_g phase is that its shorter period is much nearer the periods of the dominant oceanic microseismic band. However, Rayleigh wave detection using the R_g phase has improved on 20-second detection in both North America (Basham, 1969a; Evernden, 1970c) and Asia* (Thirlaway, see SIPRI (1968)).

Rayleigh wave magnitudes calculated from R_g are, because of larger inherent amplitudes and smaller rates of attenuation, significantly different from those calculated from 20-second Rayleigh waves; R_g magnitudes are typically 0.6 – 1.1 larger than 20-second magnitudes (Basham, 1969b, 1970; Evernden, 1970c). This difference can be considered as a correction relating R_g and 20-second Rayleigh wave magnitudes; when considering detection, however, it is approximately by this Rayleigh wave magnitude difference that measurement of R_g can improve on Rayleigh wave detection (equivalent to about δm0.4 improvement). These effects will be discussed further with respect to identification thresholds in Chapter 8.

6.4 Special signal processing

There are two kinds of processing which must be mentioned in any discussion of detection of seismic phases: one which can enhance P wave detection and the other which can enhance Rayleigh wave detection; both require the seismic data to be in digital form.

The P wave enhancement process which can be applied to digital SPZ array data is the "maximum-likelihood" process (Capon *et al.*, 1967a). This is a highly sophisticated process in which a linear filter is designed which combines the output of a large number of sensors in a subarray so as to suppress the noise without distorting the signal. Because of the complexity of the process, the computer processing requirement and the special array geometry required for maximum-likelihood processing, it can be considered for possible application at only the two large aperture SPZ arrays, LAO and NOS. However, it can make an important improvement in the P wave detection capability: the LAO improvement quoted in SIPRI (1968) is $m_{90}3.9$ for maximum-likelihood processing compared with $m_{50}3.8$ for standard beam forming. This is an m_{50} improvement of about δm0.3 (see section 4.1). However, since we consider here N-station P wave detection thresholds with $N \geq 4$, the possible application of maximum-likelihood processing at the two arrays that already have the best detection capability without the application of this special process will have little effect on our conclusions.

The process which has been used to enhance Rayleigh wave detection is the "matched filtering" process which can be applied to any long period seismic data available in digital form. The matched filtering process is simply a cross-correlation of signal plus noise with a waveform representing the pure signal. If the signal is present in the noise, it will be enhanced by this process.

Capon *et al.* (1967b), using a simple linear frequency-sweep reference waveform (to represent a dispersed Rayleigh wave) on LAO data, demonstrate an 8 db (δM0.4) detection improvement over a phased sum for Asian Rayleigh waves. Basham, in an unpublished study, has obtained, using YKA data, a similar δM0.4 detection improvement for Gulf of California earthquake Rayleigh waves by cross-correlating the full Rayleigh wavetrain (including R_g) of a large event with wavetrains of smaller events hidden by noise. Using Equation 5, the δM0.4 values can be considered equivalent to 0.2 to 0.3 improvement in m_{50}.

It is only the LPZ array facilities and possibly a few of the conventional stations that will have LPZ data readily available in digital form, and thus have the potential (it will require additional off-line digital processing) capability to apply matched filters. However, since the world-wide Rayleigh detection is strongly dominated by the LPZ arrays, the N-station Rayleigh wave detection thresholds for small values of N (say, N = 4) have the potential of being reduced by about δm0.2 using this process.

6.5 Global seismicity and interference phenomena

To this point, we have considered the thresholds of detection of P waves and

* The improvement for Asia is our interpretation of the SIPRI statement which reads in part: "When magnitude determination at 20 seconds proves impossible at near distances, Thirlaway considers 12-second period waves and applies an appropriate correction."

Rayleigh waves for the conceptual networks; for both waves we have considered azimuthal coverage provided by the detecting stations. Before proceeding further, it is important to make a number of distinctions as follows for a general approach to the identification problem. All points on the earth's surface are not conceivable locations for underground nuclear explosions for a variety of obvious reasons. However, conceivable locations (this includes test sites in present use) can be in either seismic areas, or areas with minor and often ill-defined seismic activity, or virtually aseismic areas. For each of these three situations, the problem of explosion identification is, in practice, different. The highly seismic and the virtually aseismic areas of the earth are geophysically and geographically well defined; see, for example, Barazangi and Dorman (1969). Areas of low seismicity are, however, present which have an earthquake occurrence rate and areal extent which are less well defined, and these complicate the problem.

The philosophy of identification adopted in Chapter 8 is that, given an event which requires identification, the location of that event is both a conceivable location for an underground explosion and a probable location for a natural earthquake. This is the most conservative approach, since in an aseismic region the threshold for identification is the threshold for detection with adequate location accuracy: in a region of major or minor seismicity the threshold for identification is appreciably higher as will be demonstrated later. A potential violator, in a test ban context, is assumed in this approach to have access to a seismic region in which clandestine testing may theoretically be attempted.

Some specific examples may clarify the distinction we are seeking to make. A shallow seismic event in the earth's crust beneath a highly populated area is extremely unlikely to be a clandestine underground explosion, whereas a shallow seismic event in an historically aseismic Precambrian shield area is unlikely to be a natural earthquake, and would at least be a suspicious event in a test ban context. In the former example, the requirement for identification is obviated; in the latter example there could be immediate suspicion of clandestine testing for any event above the detection threshold, even though formal identification by techniques to be described later would only be possible if the event were above the higher identification threshold.

A further assumption in our treatment of detection and identification is that events being considered are recorded in the presence of continuous natural background noise, but in the absence of other unrelated but simultaneously occurring events. Over a long time period, say, one year, some approximate assumptions concerning the number of P waves visible at a relatively sensitive station per day and the duration of the P wave signal can be used to estimate that the probability of having an interfering P wave disrupt or mask the P wave of the event under consideration will be about 1 per cent, and will, therefore, not seriously alter calculations of P wave detection probabilities. The case of interfering Rayleigh waves is somewhat more important. Some unpublished studies by the authors have shown that the probability of encountering an interfering Rayleigh wave at any point in time on an LPZ record is about 15 per cent. If it is assumed that no useful measurement can be made in the presence of an interfering event, regardless of the magnitude of the event of interest, then the interval probability of Rayleigh wave detection from an event of interest will be zero 15 per cent of the time, i.e., limited to a maximum of 85 per cent. If this were combined in a statistical approximation with the Equation 6 detection probability function, the Rayleigh wave detection probability of an individual station would be reduced by about 0.1 over the m-range covered by Equation 6. The consequent effect on the N-station Rayleigh wave detection thresholds would be an increase in the threshold of about $\delta m 0.1$. This correction will not be made, so it must be remembered that the results presented apply only in the absence of interfering Rayleigh waves.

A further complication, by a potential violator design, can arise if one anticipates the worst possible combination of the global seismicity and interference phenomena mentioned above, the phenomena of earthquake swarms and aftershock sequences. There are numerous occurrences annually of swarms of earthquakes (many earthquakes of varying magnitude occurring within a relatively small area) and sequences of earthquakes of generally diminishing number and magnitude following a large earthquake. The problems of discriminating a possible explosion from within one of these sequences would be much more severe: (a) if it were suspected at a location near the earthquake sequence, because of the great number of natural events with which it must be compared and by which it might be masked, and (b) if it were suspected at a location anywhere else on earth, because of the presence on all world seismograms of interfering P and Rayleigh waves resulting from the natural event sequence.

7. Detection of underground explosions

7.1 Assumed characteristics of the explosions

All discussions of detection to this point have assumed the P and Rayleigh waves originated from an earthquake with a focal depth of about 25 km. Here, all available information will be applied to interpret the same network detection capabilities assuming the source of the waves is an underground nuclear explosion of shallow depth.

Numerous references have appeared in the literature relating the size of the explosion (the explosive yield), the medium in which the explosion is detonated and the effects of cavity decoupling (where feasible) to the seismic magnitude; see, for example, SIPRI (1968) and Evernden (1970a). For purposes of relating the yield of an explosion to an equivalent earthquake, Table VIII presents for hardrock media the range of explosion yields in kilotons that are associated in various literature sources with specific P wave magnitudes. The formally calculated and empirically determined P wave magnitude thresholds to be discussed will, where appropriate, be equated using the data of Table VIII to equivalent hardrock yields. We note that these yield figures for any magnitude would need multiplication by a factor up to 10 for low yield explosions in, for example, dry alluvium. Decoupling factors of more than 100 have been obtained by detonating low yield explosions in suitable cavities. Since we can add nothing new in a discussion of the effects of the variables of explosion emplacement, we note the vital relevance of these problems to test ban considerations, and proceed.

Table VIII. Range of hardrock nuclear explosion yields associated with specific P wave magnitudes

P Wave Magnitude (m)	Yield Range (Kilotons)
4.0	1 – 3
4.5	3 – 10
5.0	10 – 20
6.0	100 – 200

7.2 Explosion P waves

It is the P waves which, by definition, are used to equate underground explosions to equivalent earthquakes, and any discussion of P wave detection can, in theory, apply to both explosion and earthquake sources. However, there are two effects that can make minor differences to explosion P wave detection.

The first is the $Q(\Delta,h)$ distance calibrating function used to compute P wave magnitudes. For the earthquakes, a Q for a fixed depth of 25 km was applied to computations of P wave detection. Underground explosions are confined, by engineering considerations, to a maximum depth of about 3 km, and thus the appropriate Q would be the one for this depth, or, say, for surface focus events ($h = 0$). The Q function being used has $Q(\Delta,0)$ equal to $Q(\Delta,25\text{ km})$ over 50 per cent of the 20° to 90° range, 0.1 larger than $Q(\Delta,25\text{ km})$ over 36 per cent of the range, and 0.1 smaller than $Q(\Delta, 25\text{ km})$ over the remaining 14 per cent of the range. Thus, the maximum difference for explosions at a single station can be $\delta m_{50}0.1$, but is more likely to be negligible when considering N-station thresholds.

The second factor is a characteristic of recorded explosion P waves which contributes to their identification using short period discrimination criteria, but which can also alter the ability to detect them. This is the generally impulsive character and shorter dominant periods of explosion P waves. The effects of this have been described in section 6.2 in relation to more favourable short period instrumental effects and, although the effect is important to detection at certain stations, it is difficult to include in a consideration of global coverage.

Therefore, bearing in mind the two factors discussed above, together with the other phenomena described in section 6.2, all the P wave detection results so far presented can be assumed to apply equally to earthquakes and underground explosions. The positive effects described in section 6.2 suggest that the calculations presented earlier in Table VI, for example, err on the side of being slightly conservative – in any case we believe them to be realistic and the best ones that can currently be made. Figure 5, for example, can be interpreted as showing conservatively the number of network stations detecting P waves, and the azimuthal coverage, for underground nuclear explosions of 3-10 kilotons yield, detonated in hardrock.

7.3 Explosion Rayleigh waves

The fundamental difference between an earthquake and an underground explosion is in the nature of the source and, in particular, in the geometry and size of the source. The major influence this has on the resulting seismic waves is a marked reduction in the excitation of explosion surface waves compared to a similar P wave magnitude earthquake. A review of theoretical consideration of this phenomenon has been given by Liebermann and Pomeroy (1969). This effect provides one of the most useful criteria for distinguishing between an earthquake and an underground explosion, a matter given full consideration in section 8.3. Here we shall be concerned with the effect this phenomenon has on changing the detection capabilities for explosion Rayleigh waves compared with the case for earthquakes. The problem will be attacked by determining the average amount by which explosion Rayleigh waves are reduced, and applying this to the detection results already presented for earthquakes.

The reduction in explosion Rayleigh waves will appear in a new form of Equation 5 which can be applied to explosions. It is apparent that each study of M versus m for explosion, reported in the literature, results in a different form of Equation 5; see, for example, SIPRI (1968), Liebermann and Pomeroy (1969), Capon *et al.* (1967b), Basham (1969a, 1969b) and Liebermann and Basham (1970). However, earthquake Rayleigh wave detection was computed using an earth-wide average value of M versus m given as Equation 5; it is convenient, therefore, to adopt an earth-wide average form of Equation 5 for explosions. Studies which have been based on earthquakes and explosions in the same geographic region and restricted to or adjusted to only 20-second waves (Capon *et al.*, 1967b; Basham, 1969b) show earthquake and explosion M versus m relationships nearly parallel and separated by 1.5 to 2.0 in M. Magnitudes based on R_g (Basham, 1969a; Evernden, 1970c) also show parallel relationships, but they tend to be nearer, separated by about 1.4 in M. For purposes of discussion of global explosion Rayleigh wave detection, a parallel relationship separated by 1.5 in M will be applied. Thus, Equation 5 for explosions takes the form

$$M_{50} = 1.59\ m_{50} - 5.47 \qquad \ldots .\ 7$$

Rather than present new tables and figures for explosion Rayleigh wave detection, the difference this makes can be stated quite simply. The application of Equations 4 and 7 to explosions increases all Rayleigh wave m_{50} station capabilities presented for earthquakes by about 1.0. The R_g relationships have slopes near 1.4 rather than 1.59 as in Equation 7; because they are separated by $\delta M1.4$ rather than $\delta M1.5$ to 2.0, the $m_{50}1.0$, the N-station threshold magnitudes will shift upward an equal amount. That is, Table VII and Figure 8 apply to explosion Rayleigh wave detection with the threshold magnitudes increased by 1.0, and Figure 9 applies to explosions at a threshold m6.0, or 100-200 kilotons in hardrock. It should be recalled that Figure 9 presents the situation without the gains from matched filtering, obtainable at particular stations, or from the continental path propagation, obtainable for particular station-site combinations.

At a later stage, explosion yield equivalents will be reintroduced briefly in a discussion of important new relationships between explosion yield and surface wave magnitudes (R_g and 20-second) which have recently been defined.

8. Identification of earthquakes and explosions

8.1 Identification criteria

The state-of-the-art in seismological discrimination between natural earthquakes and underground explosions to the year 1968 is presented in excellent summary form in the SIPRI (1968) document. A table in that document (p. 62) lists 10 discrimination criteria, three of which are described as "positive identifiers" above a certain threshold magnitude, and seven of which (including the positive identifiers) are described as "diagnostic aids" to identification.

A great deal of research has been published on these 10 and other discrimination criteria since 1968. The basic conclusions concerning discrimination, however, have not changed significantly from those presented in the SIPRI document: the same three "positive identifier" criteria are considered of most value in identifying underground explosions. The three criteria are listed by SIPRI as surface wave: body wave magnitude, Rayleigh wave spectra, and P wave spectra. The concept of these three criteria in total or in combination can be considered as discriminating between earthquakes and explosions on the basis of the total spectrum of seismic energy released by the two types of sources. Although some of the less useful criteria will be considered in various ways in this chapter, the majority of the discussion will be confined to these three criteria and this concept of differences in the total seismic wave spectrum between earthquakes and explosions.

The entire discussion can be confined to consideration of only shallow focus (say h < 50 km) earthquakes by assuming the capability exists, either by least-square hypocentral determination or by observation of pP phases, of accurately defining focal depths greater than 50 km and thereby positively identifying such deep events as earthquakes. Section 4.7 explains why, in the low magnitude range, all shallow focus earthquakes are potential explosions in terms of the accuracy achievable in depth of focus.

Differences in the total seismic spectra of earthquakes and explosions appear over a wide range of frequencies, and are apparent in a wide variety of both body wave and surface wave phases. They are most distinct, or most easily measured, within the short period P waves, in the relative excitation of Rayleigh and P waves and within the Rayleigh waves. These three criteria are the major topics for discussion in the next three sections.

8.2 P wave spectral ratio

The P wave spectral ratio criterion often uses a measure of the ratio of energy in two frequency bands in the P wave. The results have shown that shallow earthquakes tend to have relatively more low frequency energy in the P wave than do explosions. Results using this type of method are available from studies in the U.S.S.R. (see SIPRI, 1968), Japan (see SIPRI, 1968), United States (see Lacoss, 1969b) and Canada (see Basham *et al.*, 1970, and Weichert, 1970). Both the methods and the conclusions differ among these studies. The Japanese and U.S.S.R. methods use measurements from visual seismograms; the United States and Canadian methods use Fourier analysis of digital array data.

The conclusions of the U.S.S.R. and Japanese studies, that the frequency content of P waves of earthquakes and explosions are sufficiently different so as often to be apparent on visual seismograms, are quite valid, but the method is not sufficiently rigorous and their statistics too poorly defined to be of value to a discussion of world-wide identification. Most seismologists have observed this characteristic of earthquake and explosion P waves: we require here a rigorously defined quantitative measure of this difference in frequency content and, therefore, will confine discussion to the United States and Canadian results.

The spectral ratio used for the LAO phased beam (Lacoss, 1969b) is the ratio of energy in a high frequency band (1.45 – 1.95 Hz) to the energy in a low frequency band (0.35 – 0.85 Hz), applied to P waves of both 10 and 20 seconds duration. The process applies a strict signal-to-noise ratio criterion in each frequency band. When plotted as spectral ratio versus LAO P wave magnitude, a suite of 82 earthquakes (with h < 100 km) and 33 explosions in Asia has the two populations separated nearly completely by a decision line which is a smooth function of magnitude; the exceptions are five earthquakes which appear on the explosion side of the decision line. Four of these earthquakes can be identified as such by the application of other discrimination criteria, an important point in itself which demonstrates the multivariate nature of the discrimination problem. Thus, for the process as defined, the spectral ratio at LAO has a high (but undefined) probability of correctly identifying both earthquakes and explosions in Asia.

Lacoss (1969a) presents some data on interval probabilities that the spectral ratio can be applied to a P wave. There is a 50 per cent I.P. of applying the spectral ratio at about m4.5, which is about δm0.6 greater than the magnitude of m3.9 at which there is a 50 per cent I.P. of LAO detecting the P wave.* Here, we cannot extrapolate this LAO success to other regions or to other short period arrays and can state only that LAO has a 50 per cent I.P. of identifying Asian events at the m4.5 level. Using either the I.P. distribution of Lacoss or adapting Equation 6 for this purpose, LAO spectral ratios will have a 90 per cent I.P. of identifying Asian events at about the m4.9 level.

* Note that in section 3.2 we assumed that the 50 per cent I.P. of LAO of a P wave was m3.8, using the SIPRI reference. The difference δm0.1 is due to a greater distance to KAZ than assumed to apply at mid-third zone distances in section 3.2.

The reason that these results cannot be extrapolated to other SPZ arrays or to a general world-wide coverage is that no other P wave spectral ratio study has yet shown equal success in identification. Basham *et al.* (1970) using YKA data show complete separation between small NTS explosions and aftershock earthquakes of large NTS explosions, but the data base was very restricted (three events of each type). However, the events ranged in magnitude from m4.2 to m4.6 with the smallest of the events having a sufficiently high signal-to-noise ratio to make the spectral ratio application meaningful. It appears, therefore, that the 90 per cent I.P. threshold of application (which will not necessarily be the threshold at which the criterion is a successful discriminant) may be significantly below m4.9; this process is being tested with a large suite of NTS explosions and United States earthquakes at the time of writing.

Weichert (1970) in a comprehensive examination of the spectral ratio method applied to Asian events cannot completely separate earthquakes and explosions using YKA data. His data sample goes down to magnitude m4.5 for earthquakes and m4.8 for explosions. The best process Weichert has found, average third moments of the P wave spectra, results in about 80 per cent of the shallow earthquakes overlapping 20 per cent of the explosions, with the data regionalized. Thus, as neither the Asian P wave spectral ratio data of Weichert nor the preliminary NTS spectral ratio data (E.B. Manchee, personal communication) using YKA records result in a threshold magnitude above which the criterion can be described as a "positive identifier", the Canadian P wave spectral ratio method is simply a "diagnostic aid" with overlapping population at all magnitudes.

The threshold of application of the P wave spectral ratio method (whether at that threshold it is a positive identifier or a diagnostic aid) is much lower than the threshold of application, particularly for explosions, of the two criteria requiring measurement of Rayleigh waves (see sections 8.3 and 8.4). The method, therefore, retains considerable value for the application, in the absence of positive identification, of a multivariate analysis (the combined application of all available imperfect criteria to the problem of discrimination). This multivariate analysis can include, in addition to spectral ratio data, correlogram complexity data such as that described by Whitham *et al.* (1968), any depth of focus information, "negative" Rayleigh wave criteria (see section 8.5), etc.

8.3 Relative excitation of P and Rayleigh waves

The spectral ratio described in the previous section is confined to a narrow frequency band within the P wave signal. Similar differences between earthquakes and explosions at longer periods of the total spectrum are usually described by a measure of the relative excitation of the long period surface waves (Rayleigh) and the short period body waves (P), or as a ratio of two bands of energy within the long period waves (see section 8.4)

The simplest method of defining the relative excitation of P and Rayleigh waves is to use the straightforward phase amplitude measurements required for calculation of magnitudes from the two types of waves, i.e., by comparing earthquakes and explosions by their M versus m relationships. It is for this discrimination criterion that the greatest body of results are available; SIPRI (1968) contains all significant results achieved prior to that date; see also Capon et al. (1969), Lacoss (1969b), Liebermann and Pomeroy (1969), Basham (1969a, 1969b), Molnar *et al.* (1969), Lambert *et al.* (1969), Liebermann and Basham (1970) and Evernden (1970c) for more recent results. In 1968, arguments were still raised about the validity of this criterion at low magnitudes: we now believe that there is clear proof (see, for example, Evernden, 1970c) that, provided the appropriate waves can be detected, the method works at least down to magnitudes below those considered in this report.

The form of M versus m for earthquakes and explosions and the separation between populations when plotted in this manner have been discussed briefly in section 7.3. Although the scatter of individual events with respect to average relationships of the forms of Equations 5 and 7 is very large, and the regional variations in Rayleigh wave propagation phenomena produced large variations in the forms of Equations 5 and 7, in all studies the populations of earthquakes and explosions are sufficiently separated to allow consideration of this criteria as the most successful positive identifier of shallow earthquakes and underground explosions. It is apparent from each set of research results that the magnitude threshold above which the criterion can be applied is (in the absence of interfering Rayleigh waves) equal to the magnitude threshold at which the explosion Rayleigh wave can be detected. This occurs because, as explained in sections 5.3 and 5.4, the earthquake Rayleigh wave detection threshold is about δm0.7 higher than the P wave detection threshold and because, as explained in section 7.3, the explosion Rayleigh wave detection threshold is about δm1.0 higher than the earthquake Rayleigh wave threshold. Thus, the problem of discrimination using this technique reduces to one of detecting explosion Rayleigh waves and can be considered in the separate ways that Rayleigh wave detection has been considered in previous sections.

Consider first the six northern hemisphere specific sites in Table V, and adopt 4-station thresholds with some azimuthal variation as adequate for identification purposes. The earthquake Rayleigh wave detection thresholds of m4.7 – m5.0 (see Table VII) increase to explosion detection and identification thresholds of m5.7 to m6.0, using the gross average properties of the earth and ignoring for the moment the advantages gained by Rg continental propagation and matched filter processing. The equivalent available empirical study supports this formal calculation: Basham (1969b) demonstrates positive identification of KAZ and NVZ explosions at a threshold of about m6.0 using relatively insensitive conventional Canadian stations; this threshold can, therefore, be expected to reduce to about m5.7 using more sensitive conventional and array stations from the 51-station LPZ network.

Applying matched filters to specific site explosions, the possible threshold reduction is δ0.2 to δm0.3, assuming each of the stations involved has the capability of applying the matched filtering process (see section 6.4). The only published result is, in effect, one-station coverage for which the threshold has naturally been reduced below the 4-station requirement we have adopted. Lacoss (1969a) demonstrates that applying matched filters to LAO data for KAZ explosion Rayleigh waves yields a 90 per cent probability of detection (and, therefore, of identification) at about m5.4. This, of course, is using one of the most sensitive LPZ systems being considered in this study. It can be estimated from the above data that the 4-station matched filtering threshold, restricted to stations capable of matched filtering, is about m5.6 at the northern hemisphere specific sites.

The possible improvement using R_g and purely continental paths has been demonstrated only for NTS explosions using Canadian and United States stations* (Basham, 1969a; Evernden, 1970c). In this case the available stations are those confined to the same continental mass as the events of interest and thus there is the benefit of shorter propagation paths (maximum Δ about 40°) as well as the smaller R_g wave attenuation with distance (see Basham, 1970). An estimate of the empirical 4-station threshold of explosion R_g detection, and therefore of explosion identification, is about m5.0 using Canadian stations in the distance range 13° to 40°, and about m4.7 using United States stations as near as about 3°. Thus, the use of lower sensitivity conventional stations and taking advantage of shorter paths with purely continental propagation yields an explosion identification threshold lower than that of the most sensitive LPZ systems applying matched filtering to more distant events.

A short diversion to a discussion of some recently determined explosion yield versus Rayleigh wave magnitude relationships will clearly illustrate the proven and potential advantages of using the shorter period continental Rayleigh waves. Until recently the equivalent hardrock yield of an underground explosion has been defined only on the basis of empirically determined, but theoretically supported, relationships between yield and P wave magnitude (the relationships we are applying are shown in Table VIII). Evernden and Filson (1970), observing a similar non-linearity in m versus log-yield and M versus m, derived a new relationship between M and log-yield which has the form

$$M = 1.4 + 1.3 \log Y \qquad \ldots 8$$

where M is determined from 20-second Rayleigh waves and Y is the yield in kilotons. This linear relationship accurately represents the available yield data between yields of about 6 and 1000 kilotons, M2.5 to M5.5. Evernden and Filson also show for explosions that M_{Rg} determined from the 8 to 14 second (R_g) Rayleigh waves is equivalent to M + 1.1; this is in close agreement with the difference derived by Basham (1969b). Thus, we have

$$M_{Rg} = 2.5 + 1.3 \log Y \qquad \ldots 9$$

In an independent study using Canadian magnitude data, Ericsson* derived the relationship

$$M_{Rg} = 2.7 + 1.2 \log Y \qquad \ldots 10$$

Equations 9 and 10 can be considered equivalent; they produce the same M_{Rg} value, within 0.1, over the yield range of interest.

Consider for purposes of illustration an explosion 10-second R_g wave and an explosion 20-second Rayleigh wave recorded on a 4 K magnification LPZ seismogram with a trace amplitude of 5 mm at an epicentral distance of 20°. Using Equation 3, the M value of the explosion is 4.3. Using either Equation 3, or the more appropriate formula of Basham (1970) which is equivalent in this distance range, the M_{Rg} value is 4.6. From Equation 8 the M4.3 equivalent explosion yield is about 170 kilotons and from Equation 9 or 10 the M_{Rg} 4.6 equivalent explosion yield is about 40 kilotons. With the trace amplitude used above recorded on about 4 stations in the distance range near 20°, and using the fact that one or more of the stations (say, LPZ arrays) can have a larger effective magnification, the situation described is roughly equivalent to the (90 per cent) Rayleigh wave detection thresholds described in Chapter 5. Thus the explosion identification threshold using the R_g wave is about 40 kilotons, or a factor of about 4 in yield better than the threshold using 20-second Rayleigh waves.

Consider now the extrapolation of northern hemisphere earthquake Rayleigh wave detection thresholds (section 5.4) to explosion identification thresholds. Using the formal calculations for 20-second earthquake Rayleigh waves incremented δm1.0 to convert to explosions, the explosion identification thresholds using M versus m will be about m5.6 in central North America, m5.6 to m5.8 for the remainder of North America, the north Atlantic Ocean and northern Europe, and m5.8 to m6.0 throughout the remainder of the hemisphere; a realistic average for the northern hemisphere is about m5.8, or about 60 to 100 kilotons equivalent yield.

The Rayleigh wave detection threshold at any location in the northern hemisphere is highly influenced by the number of, and distance to, LPZ arrays within the 90° detection range. Since each of the LPZ arrays has data in a form suitable to matched filtering, the explosion identification thresholds can be reduced by about δm0.2 using this process, i.e., to about m5.4 in central North America and m5.8 in the poorest areas of the hemisphere, with a realistic average of m5.6, or about 40-60 kilotons yield in hardrock.

It is unreasonable, because of the distribution of available stations, to extrapolate to other northern hemisphere continental locations the R_g detection thresholds for NTS explosions achievable at nearby United States stations. However, the Canadian R_g results, an explosion identification threshold of about m5.0 (10-20 kilotons) for NTS at a mean distance of about 25°, may be

* All Canadian stations used by Basham (1969a) are shown in Figure 6, but only four are included in the 51-station LPZ network; Evernden (1970c) used moderate magnification Long Range Seismic Measurement stations, none of which are included in the United States UN return; however, the abundance of United States conventional stations shown in Figure 6 would have an equivalent capability.

* CCD/306, Swedish technical working paper for the Conference of the Committee on Disarmament, August 1969.

possible on any northern hemisphere continental mass, although this result remains unproven as yet outside of North America.

This 10 to 20 kiloton hardrock explosion identification threshold for NTS using Canadian stations is some three times lower than the threshold obtained above in the illustrative example used to compare R_g and 20-second wave detection. This difference between one empirical result and a theoretical study demonstrates the conservative nature of the assumptions made in defining the 50 per cent interval probability of Rayleigh wave detection at a station in section 3.3.

8.4 Rayleigh wave spectral ratio

The relative excitation of Rayleigh waves by earthquakes and explosions has been described in the previous section in relation to the P wave energy (or magnitude) of the events. Important differences between earthquakes and explosions have been shown to exist within the Rayleigh wave spectrum itself. This phenomenon was given brief coverage in the SIPRI document in diagrams illustrating the larger amount of longer period (30 seconds) Rayleigh wave energy in earthquakes compared to that in explosions. The discriminant has been quantified by Molnar *et al.* (1969) using new high-gain, long-period seismographs as a ratio of the energy in Rayleigh waves at periods of 19 to 22 seconds to the energy at periods of 40 to 60 seconds. Using special long-period seismographs installed in the eastern United States, this Rayleigh wave spectral ratio achieves complete separation of earthquakes and explosions in the western United States.

The special seismograph used by Molnar *et al.* is the first of a number of such systems planned by the United States for world-wide deployment. However, these systems have not been included in the United States UN return listing stations with guaranteed accessibility to data, and, therefore, cannot be considered as available to this study.

With further testing, the Rayleigh wave spectral ratio may prove to be an important discrimination criterion; the major difficulty apparent from the study by Molnar *et al.* is the rather high threshold of detection of the longer period Rayleigh waves, particularly for explosions. Using only the positive measurements presented by Molnar *et al.* (i.e., ignoring the noise-limited information on their figures), we estimate that using equipment of this type the thresholds of detection of Rayleigh waves are m3.6 and m4.9 for 20-second waves for earthquakes and explosions, respectively, and m3.8 and m5.3 for 40- to 60-second waves for earthquakes and explosions, respectively; this is for an epicentral distance of about 30°. The threshold of application of the Rayleigh wave spectral ratio will be at the larger set of magnitudes. Thus, the threshold of application of the positive ratio criterion is at a high magnitude, near m5.3, for explosions. However, the separation between populations in terms of the ratio or of the amplitude of the longer period waves is sufficiently great that absence of the longer period waves for explosions is a useful negative criterion (see following section) with possible application down to about m4.5. The procedure is feasible using any LPZ data capable of being bandpass filtered, and can be considered a possible discriminant using station data available to this study.

8.5 Identification by negative criteria

The explosion identification thresholds described in the previous sections are defined as being equal to the threshold of detection of explosion Rayleigh waves. The procedure to be discussed in this section is identification of explosions by the *absence* of a recorded wave on the basis that had the event been an earthquake of the same P wave magnitude, the wave in question would have been observable on the record. An associated concept is the identification of earthquakes as such by measurement of a factor which shows the event to conform to prior knowledge of earthquakes with respect to this factor.

Consider as an illustrative example the results presented by Basham (1969b) for identification of Asian events using M versus. m observations on Canadian stations. Detection of earthquakes using observed Rayleigh waves has a threshold of about m5.0; identification of explosions using observed Rayleigh waves has a threshold at about m6.0; because of the wide separation between populations, both can be considered positive identification. Because of the variation in detection thresholds due to variations in the noise levels, the largest earthquake whose Rayleigh wave can be obscured by noise is about m5.4. Thus, any event larger than m5.4 which does not have an observable surface wave (and which is known from other information to be shallow) can be identified as a probable explosion. As the magnitudes approach m6.0, the Rayleigh wave will again be observable for all events and M versus m will plot in either the explosion or earthquake population and yield positive identification. In this case, the threshold of probable identification is reduced by about δm0.6 from the threshold of positive identification by the application of a negative criterion.

The M versus m relationships of the earthquakes and explosions discussed in this example are near to the assumed world-wide averages given by Equations 5 and 7, i.e., for which earthquakes and explosions are separated by about δM1.5. Therefore, we estimate that extensive studies should demonstrate a usable negative criterion with an improvement of about δm0.5 on a world-wide basis. The general validity of this assumption, however, depends on the general scatter of populations with respect to the average trends and, for any regional application, to the closeness of the earthquake and explosion average M versus m trends. For example, the regional data for R_g for North American paths presented by Basham (1969a) shows M versus m trends separated by about δM1.4 and with data point scatter that nearly overlaps. In fact, the two sets of data in the study by Basham show a theoretical (formal) overlap at about the 2 per cent level; hence great care must be exercised in the development and application of negative criteria. However, provided precautions are taken to have information in several azimuths, and the appropriate studies are made of the probability distributions of scatter about trend lines, we can see no scientific objection to taking adavantage of this possibility in this context.

Negative criteria have been shown useful when applied to other seismic phases. Evernden (1969a) illustrates the possibilities of identification using long period S waves. He finds that earthquakes down to about m5.0 have observable long period S waves; whereas no explosions smaller than about m5.7 have observable long period S and, where explosion S waves are observed, they are about a factor of 10 smaller than those observed for similar magnitude earthquakes. Thus, the possibility of identification of explosions by absence or presence of long period S waves exists for any events greater than about m5.0. A similar criteria has been discussed by Evernden using Love and long period P waves. For the long period body phases particularly, the greatest problem is the nearness of the dominant periods of the phases to the peak in the microseismic noise spectrum and the probability of applying the discriminant (i.e., of detecting the signals in highly variable noise fields) may be small.

Although negative criteria cannot, by definition, provide positive identification of an underground explosion, the argument is substantially a tautological one. There are no sources of seismic energy of the sizes under discussion other than natural earthquakes or underground or underwater explosions; hence the certain elimination of the possibility of an earthquake origin provides a positive identification of an explosive source. Multivariate combinations of such negative criteria as the absence of the expected level of R_g, 20-second, or longer, period Rayleigh waves, long period S waves, long period P waves, and Love waves requires regionalized control data for its optimum application. Much work remains to be done with these techniques, but it seems very clear that the minimum improvements possible should be δm0.5 on existing generally applicable positive criteria such as 20-second M versus m and Rayleigh wave spectral ratios, and probably somewhat less on more restricted but more successful positive criteria such as M_{R_g} versus m.

9. Conclusions and recommendations

9.1 Summary and conclusions concerning existing capabilities

It will be apparent to the reader that the authors have relied on personal experience and on published and unpublished research results to make scientific judgments and extrapolations at many points in this assessment of global seismological detection and identification capabilities. In particular, we have in some instances extrapolated results available for North America to other parts of the world; this was necessary because for many parts of the world the required research has not been undertaken, or at any rate published. We will, therefore, present this chapter in two parts: this section will present the conclusions which can be drawn concerning the existing capabilities of the ensemble of conventional and array stations described in Chapter 2; the following section will contain some recommendations, which, for a modest investment of research effort and finances using existing facilities, may significantly improve on the currently defined capability.

The conclusions of this assessment can take the form of the P wave magnitude threshold at which existing seismological facilities have a certain capability of (a) detecting, (b) locating and (c) identifying a seismic event, and of how these capabilities can vary over the surface of the earth. For each of these functions we have defined as being adequate that threshold at which there is a 90 per cent probability of ≥4-station coverage, with adequate (2 or more quadrant) azimuthal coverage.

The lowest threshold derived is that for P wave *detection;* it is m4.5 (equivalent to 3 to 10 kiloton yield in hardrock) or lower for earthquakes or explosions occurring anywhere in the northern hemisphere, and deteriorates to a high value of m5.0 (equivalent to 10 to 20 kilotons) in part of the southern hemisphere. A fundamental conclusion of this assessment is that all extant capabilities are much poorer in the major portion of the southern hemisphere; this fact will not be emphasized further. In terms of locating the epicentres of events using detected P waves, the location accuracy will be typically better than 20-45 km for any seismic event larger than the P wave detection threshold magnitude for any region (see Figure 4) plus 0.2.

The 20-second earthquake Rayleigh wave detection threshold is about δm0.6 higher than the P wave threshold, leading to the conclusion that existing LPZ facilities are relatively less sensitive than existing SPZ facilities. The explosion Rayleigh wave detection threshold is about δm1.0 higher than the equivalent threshold for earthquakes. Thus, because of the difficulty of detecting explosion 20-second Rayleigh waves, the formally calculated threshold of explosion identification using the M versus m criterion remains at a rather high level, about m5.6 to m6.0 for the northern hemisphere. Matched filtering can reduce these values by about δm0.2. It seems reasonable, therefore, to define the network system we have investigated as having a threshold capability of identifying 60 kiloton underground explosions in hardrock in the northern hemisphere.

Using stations available in the UN returns, this threshold is reduced to m5.0 in North America by taking advantage of the efficient continental propagation of the shorter period R_g Rayleigh waves. We are hesitant to extrapolate the North American R_g results to other continental masses because equivalent success remains unproven (see section 9.2). The m5.0 threshold can be reached using 20-second Rayleigh waves only by degrading the number of observations (and hence the probability of application) and relying on the matched filtered data from one or two very high-gain long period facilities. This more restricted m5.0 capability, which is not yet proven to be generally applicable, can be regarded as explosion identification in the 10 to 20 kiloton hardrock range.

The identification threshold can be reduced below m5.0 only by employing criteria whose thresholds of application are below the explosion Rayleigh wave detection thresholds with equipment currently deployed. The criterion with greatest appeal is the P wave spectral ratio, which can in theory be applied close to the P wave detection threshold. The spectral ratio method for one station-region combination is a positive identifier at the m4.9 level; others show potential application at lower levels but result in overlapping populations.

Thus, we conclude that to consistently achieve an identification threshold below m5.0 all available identification criteria must be brought to bear as a multivariate analysis. The problem of assembling the necessary regionalized data to achieve identification below m5.0 for any conceivable test site in the northern hemisphere is a formidable one. This results, in our opinion, in a tendency to neglect the intrinsic power of the different methods, and leads naturally to the alternative concept of increasing the detection capability for explosion Rayleigh waves by a major investment in widely distributed arrays designed to achieve, for example, the capability of detecting Rayleigh waves for any m4.5 explosion.

We believe that an appropriate intermediate step, between acceptance of the existing rather limited capability as defined earlier in this chapter and commitment of extensive international resources to a widely deployed, highly sophisticated, integrated system of modern array stations, would be further definitive national assessments of existing capabilities and, where necessary, minor adjustments in facilities and techniques designed to improve modestly these capabilities. Some recommendations and suggestions for implementation of this intermediate step are given in the following section.

9.2 Recommendations for improving capabilities using existing facilities

The conclusions of this assessment that result from the formal detection calculations are closely tied to the initial assumptions required to define individual station capabilities in terms of quoted operating magnifications. The assumptions we have made, in the absence of supporting definitive empirical data, are of necessity conservative: witness the conservative assumed general P wave detection capabilities of stations MBC and COL compared with their empirically defined capability for a particular site, described in section 6.2. If, on the average, our assumptions for both SPZ and LPZ station capabilities are conservative, then additional empirical data of individual station P and Rayleigh wave detection capabilities will, when inserted into the formal calculations, improve on our assessment of existing global detection. This, among all suggestions for studies given here, is the study most easily undertaken by national agencies; it simply requires documentation of probabilities of detection of P and Rayleigh waves as a function of event magnitude for the more important stations in each country.

In addition, it is important to obtain as soon as possible empirical capabilities for the two new large aperture arrays, the Norwegian SPZ/LPZ array NOS and the Unites States LPZ array ALP.

We have illustrated a number of cases in which geophysical peculiarities of the earth are assisting the discrimination process, and a few cases in which they may hinder the process. However, we are able to employ only those peculiarities with which we are familiar, from published and unpublished research and personal experience, and which pertain particularly to the North American situation. These phenomena are very important to global discrimination and urgently require documentation for other areas. Knowledge of P wave phenomena will be a by-product of any P wave detection studies that are undertaken; the Rayleigh wave phenomenon that needs extensive study in other regions is the significant reduction in detection and identification thresholds achieved in North America using the short period R_g waves. It is recommended that other countries with conventional stations on the same continental mass with earthquake and explosion sources further test the R_g applications.

The most widely applicable discrimination criterion, the M versus m discriminant, has a threshold of application that is controlled by the threshold of detection of explosion Rayleigh waves. The LPZ arrays are able to dominate the Rayleigh detection calculations principally because the recording and/or analysis procedures can reject the dominant long period noise band. But, because there are too few LPZ arrays to provide adequate Rayleigh wave detection, some conventional stations must be employed. The total number of LPZ stations required need not exceed 20 (i.e., significantly fewer than the 51 LPZ stations we have employed in Rayleigh wave detection calculations) if the included conventional stations had an improved capability; and a significant improvement of a conventional LPZ station can be achieved with modest investment. For example, WOL and GRF (see section 3.3) are considered to have magnifications about a factor of 3 greater than standard photographic recording stations because they record on magnetic tape and have the facility to filter and reject the dominant microseismic noise band. An alternative method that can be used on photographic recording seismographs is the addition of an electronic or electro-mechanical component designed to reject periods below, say, 10 seconds.

An improvement of this type on one LPZ seismograph in each of a number of countries could significantly improve Rayleigh wave detection, considering those countries in the UN returns that possess LPZ stations in reasonably quiet locations, and also considering the locations of existing LPZ arrays. Any additional new or improved stations (LPZ or SPZ) in the southern hemisphere would, of course, be of great value.

References

Anglin,F.M., 1971. Detection capabilities of the Yellowknife seismic array and regional seismicity, *Bull. Seism. Soc. Am.*, in press.

Barazangi, M., and J. Dorman, 1969. World seismicity maps compiled from ESSA, Coast and Geodetic Survey, Epicenter Data, 1961-1967, *Bull. Seism. Soc. Am., 59:* 369.

Basham, P.W., 1969a. Canadian magnitudes of earthquakes and nuclear explosions in southwestern North America, *Geophys. J. Roy. Astrom. Soc., 17:* 1.

Basham, P.W., 1969b. Canadian detection and discrimination thresholds for earthquakes and underground explosions in Asia, *Can. J. Earth Sci., 6:* 1455.

Basham, P.W., 1969c. Station corrections for Canadian magnitudes of earthquakes and underground explosions in North America and Asia, *Seism. Series Dom. Obs.*, 1969-3.

Basham, P.W., 1970. A new magnitude formula for short period continental Rayleigh waves, *Geophys. J. Roy. Astron. Soc.*, 23, in press.

Basham, P.W., and K. Whitham, 1966. Microseismic noise on Canadian seismograph records in 1962 and station capabilities, *Pub. Dom. Obs.*, *32:* 123.

Basham, P.W., and R.J. Halliday, 1969. Canadian seismic data for Project Rulison, *Seism. Series Dom. Obs.*, 1969-4.

Basham, P.W., D.H. Weichert, and F.M. Anglin, 1970. An analysis of the Benham aftershock sequence using Canadian recordings, *J. Geophys. Res.*, *75:* 1545.

Burch, R.F., 1969. A comparison of short period seismic noise at the four UKAEA type arrays and an estimate of their detection capabilities, United Kingdom Atomic Energy Authority, *AWRE* Report No. 079/68, January, 1969.

Capon, J., R.J. Greenfield, and R.J. Kolker, 1967a. Multidimensional maximum-likelihood processing of a large aperture seismic array, *Proc. I.E.E.E.*, *55:* 192.

Capon, J., R.J. Greenfield, and R.T. Lacoss, 1967b. Long-period signal processing results for large aperture seismic array, *Technical Note* 1967-50, Lincoln Laboratory, M.I.T., Lexington, Mass.

Capon, J., L. Lande, and R.W. Ward, 1969. Seismic descrimination, *Semiannual Technical Summary*, Lincoln Laboratory, M.I.T., Lexington, Massachusetts, December, 1969.

ESSA, Environmental Science Service Administration, 1967. A compilation and analysis of explosion data collected at Mould Bay, Canada, and College, Alaska, U.S. Dept. of Commerce, National Earthquake Information Center, Rockville, Maryland, August, 1967.

ESSA, Environmental Science Service Administration, 1970a. Seismograph station abbreviations, U.S. Dept. of Commerce, National Earthquake Information Center, Rockville, Maryland, April, 1970.

ESSA, Environmental Science Service Administration, 1970b. Seismic data from Rulison, U.S. Department of Commerce, National Earthquake Information Center, Rockville, Maryland, July, 1970.

Evernden, J.F., 1967. Magnitude determinations at regional and near-regional distances in the United States, *Bull. Seism. Soc. Am.*, 57:591.

Evernden, J.F., 1969a. Identification of earthquakes and explosions by use of teleseismic data, *J. Geophys. Res.*, 74:3828.

Evernden, J.F., 1969b. Precision of epicenters obtained by small numbers of world-wide stations, *Bull. Seism. Soc. Am.*, 59:1365.

Evernden, J.F., 1970a. Magnitude versus yield of explosions, *J. Geophys. Res.*, 75:1028.

Evernden, J.F., 1970b. Study of regional seismicity and associated problems, *Bull. Seism. Soc. Am.*, 60:393.

Evernden, J.F., 1970c. Discrimination between small magnitude earthquakes and explosions, submitted for publication.

Evernden, J.F., and J. Filson, 1971. Regional dependence of M_s versus m_b. *J. Geophys. Res.*, 76:3303.

Ewing, W.M., W.S. Jardetsky, and F. Press, 1957. Elastic waves in layered media, *McGraw-Hill.*

Gutenberg, B., and C.F. Richter, 1956. Magnitude and energy of earthquakes, *Ann. Geophys.*, 9:1.

Herrin, E., 1968. 1968 seismological tables for P phases, *Bull. Seism. Soc. Am.*, 58:1193.

Lacoss, R.T., 1969a. LASA decision probabilities for M_s-m_b and modified spectral ratio, *Technical Note* 1969-40, Lincoln Laboratory, M.I.T., Lexington, Massachusetts.

Lacoss, R.T., 1969b. A large-population LASA discrimination experiment, *Technical Note* 1969-24, Lincoln Laboratory, M.I.T., Lexington, Mass.

Lambert, D.G., D.H. Von Seggern, S.S. Alexander, and G.A. Galat, 1969. The Long Shot experiment, vol. II, Comprehensive Analysis, Air Force Technical Applications Center, Washington, D.C.

Liebermann, R.C., and P.W. Pomeroy, 1969. Relative excitation of surface waves by earthquakes and underground explosions, *J. Geophys. Res.*, 74:1575.

Liebermann, R.C., and P.W. Basham, 1971. Excitation of surface waves by the Aleutian underground explosion MILROW (2 October, 1969), *J. Geophys. Res.*, 76:4030.

Lilwall, R.C., and A. Douglas, 1970. Estimation of P wave travel times using the joint Epicentre method, *Geophys. J. Roy. Astron. Soc.*, 19:165.

Manchee, E.B., and D.H. Weichert, 1968. Epicentral uncertainties and detection probabilities from the Yellowknife seismic array data, *Bull. Seism. Soc. Am.*, 58:1359.

Molnar, P., J. Savino, L.R. Sykes, R.C. Liebermann, G. Hade, and P.W. Pomeroy, 1969. Small earthquakes and explosions in western North America recorded by new high gain, long period seismographs, *Nature* 224:1268.

Oliver, J., and M. Ewing, 1957. Higher modes of continental Rayleigh waves, *Bull. Seism. Soc. Am.*, 47:187.

Press, F. and M. Ewing, 1952. Two slow surface waves across North America, *Bull. Seism. Soc. Am.*, 42:219.

Press, F., M. Ewing, and J. Oliver, 1956. Crustal structure and surface wave dispersion in Africa, *Bull. Seism. Soc. Am.*, 46:97.

Simons, R.S., and T.T. Goforth, 1967. Percentages associated with the detection of long period surface waves from low magnitude events, in *VESIAC* Report 7885-1-X, Willow Run Laboratories, University of Michigan, Ann Arbor, Michigan.

SIPRI, Stockholm International Peace Research Institute (1968). Seismic methods for monitoring underground explosions, *Stockholm Papers* Number 2, Almqvist and Wiksell, Stockholm, Sweden.

Weichert, D.H., 1969. Epicentre determination by seismic array, *Nature*, 222:155.

Weichert, D.H., 1971. Short period spectral discriminant for earthquake-explosion differentiation, *Zeits. F. Geophys.*, in press.

Weichert, D.H., and J.C. Newton, 1970. Epicentre determination from first arrival times at Canadian stations, *Seism. Series* No. 59, Earth Phys. Branch.

Whitham, K., P.W. Basham, and H.S. Hasegawa, 1968. Correlogram discrimination parameters from Yellowknife seismic array data, *Seism. Series Dom. Obs.*, 1968-5.

[illegible] Canadian [illegible] Survey [illegible], Ottawa, 1969.

Capon, J., R.J. Greenfield, and R.J. Kolker, 1967, Multidimensional maximum-likelihood processing of a large aperture seismic array, Proc. IEEE, 55, [illegible].

Capon, J., R.J. Greenfield, and R.T. Lacoss, 1967b, Long-period signal processing results for large aperture seismic array, Technical Note 1967-50, Lincoln Laboratory, M.I.T., Lexington, Mass.

Capon, J., [illegible] and [illegible], 1968, Seismic discrimination, Semiannual Technical Summary, Lincoln Laboratory, M.I.T., Lexington, Massachusetts, December 1967.

ESSA, Environmental Science Services Administration, 1967, A compilation and analysis of [illegible] U.S. Dept. of Commerce [illegible], August 1968.

[illegible] Seismic [illegible] Laboratory [illegible], Maryland, [illegible] 1970.

[illegible] U.S. Department of Commerce [illegible]

[illegible] 1971, [illegible] J. Geophys. Res., [illegible].

[illegible] 1971, Discrimination [illegible] seismic [illegible] published for publication.

[illegible] 1971, Response [illegible] J. Geophys. Res., [illegible].

[illegible] Lincoln Laboratory [illegible]

Lacoss, R.T., 1969, [illegible] Lincoln Laboratory, M.I.T., Lexington, Massachusetts.

Lacoss, R.T., 1969b, A large-population LASA discrimination experiment, Technical Note 1969-24, Lincoln Laboratory, M.I.T., Lexington, Mass.

Lambert, D.G., D.H. Von Seggern, S.S. Alexander, and G.A. Galat, 1969, The Long Shot experiment, vol. II, Comprehensive analysis, Seismic Data Laboratory [illegible]

Liebermann, R.C. and P.W. Pomeroy, 1969, Relative excitation of surface waves by earthquakes and underground explosions, J. Geophys. Res., 74, [illegible].

[illegible] 1970, [illegible] Bull. Seismol. Soc. Amer., [illegible].

[illegible] 1969, [illegible] J. Geophys. Res., [illegible].

Molnar, P., J. Savino, L.R. Sykes, R.C. Liebermann, G. Hade and P.W. Pomeroy, 1969, Small earthquakes and explosions in western North America recorded by new high gain, long period seismographs, Nature [illegible].

[illegible] 1967, [illegible] Bull. Seism. Soc. Am., [illegible].

[illegible] 1958, [illegible] wave dispersion [illegible].

[illegible] 1967, [illegible] Stockholm [illegible].

SIPRI, Stockholm International Peace Research Institute, 1968, Seismic methods for monitoring underground explosions, Stockholm Papers Number 2, [illegible], Stockholm, Sweden.

[illegible], D.H., 1969, [illegible] by seismic array, Nature, 222, 155.

Weichert, D.H., 1971, Short period spectral discriminant for earthquake-explosion differentiation, Z. Geophys., [illegible].

[illegible] 1970, [illegible] Canadian [illegible].

[illegible] 1968, A teleseismic discrimination parameter [illegible].

PUBLICATIONS of the EARTH PHYSICS BRANCH

VOLUME 41–NO. 10

magnetic substorms, december 5, 1968

E. I. LOOMER and G. JANSEN VAN BEEK

DEPARTMENT OF ENERGY, MINES AND RESOURCES

OTTAWA, CANADA 1971

Cat. No.: M70-41/10

Contents

magnetic substorms, december 5, 1968

E. I. LOOMER and G. JANSEN VAN BEEK

Abstract. Magnetograms from 26 auroral and polar cap observatories and total intensity data from Ice Island T3 were used in the analysis of an intense polar magnetic substorm which developed at 08 U.T. on December 5, 1968. The magnetic effects were interpreted as resulting from a double substorm. The changing orientation of the equivalent current vector at Thule, close to the geomagnetic pole, was found to represent very closely the time development of the storm.

Equivalent currents, calculated from both the horizontal and vertical components of the magnetic perturbation vector, supported the Akasofu model of the auroral oval for the expansion and early recovery phases of the storm. Prior to the westward surge and following the end of the substorm there was some evidence for an SD-type (two-celled) current system, but the available data were insufficient to verify this. A velocity of 1.1 km/sec for the westward surge and an expansion of the auroral oval by about 15° in the midnight sector were inferred from the magnetic effects. The direction of current flow in the oval was parallel to the auroral zone a few hours after local midnight. The poleward contraction of the oval was very rapid in the recovery phase of the storm, with the storm centre returning to a position considerably east of the local midnight meridian.

A class of intense substorms for the years 1962 – 1969 was identified from the occurrence on the Mould Bay magnetograms of indented positive H bays around local midnight. These substorms occurred mainly in the winter and equinox, and were most numerous in the years immediately preceding sunspot minimum. No clear relationship was found between the occurrence and intensity of these substorms and the Dst index.

Résumé. Des enregistrements magnétiques provenant de 26 observatoires de la zone aurorale et de la calotte polaire et les données sur l'intensité totale provenant de l'île de Galce T3 ont servi à l'analyse du sous-orage magnétique polaire intense du 5 décembre 1968 à 8 heures (heure universelle). On a interprété les effets magnétiques comme le résultat d'un sous-orage double. L'orientation changeante du vecteur du courant équivalent à Thule près du pôle géomagnétique a presque coïncidé avec l'évolution de l'orage.

Les courants équivalents calculés à partir des composantes horizontales et verticales du vecteur de perturbation magnétique sont conformes au modèle d'Akasofu de l'ovale auroral des phases d'expansion et de diminution de l'orage. Avant la poussée vers l'ouest et après le sous-orage, certaines indications portaient à croire qu'il existait un réseau de courant de type SD (à deux cellules), mais il a été impossible de procéder à une vérification en raison de l'insuffisance de données. On a déduit d'après les effets magnétiques que la poussée vers l'ouest avait une vitesse de 1.1 kilomètre à la seconde et qu'il y avait eu une expansion d'environ 15° dans le secteur de minuit de l'ovale auroral. La direction du courant dans l'ovale était parallèle à la zone aurorale quelques heures après le minuit local. La contraction de l'ovale vers le pôle a été très rapide pendant l'accalmie de l'orage dont le centre est revenu à une position considérablement à l'est du méridien local de minuit.

Une variété de sous-orages intenses entre 1962 et 1969 a été identifiée grâce à l'inversion du sens de la variation H autour du minuit local sur les enregistrements magnétiques de Mould Bay. Ces sous-orages ont eu lieu principalement l'hiver et au temps de l'équinoxe et sont plus fréquents au cours des années précédant immédiatement les périodes de faible activité solaire. On n'a trouvé aucun lien entre la fréquence et l'intensité de ces sous-orages et l'index Dst.

Introduction

One of the most spectacular features of auroral zone and higher latitude magnetograms is the frequent occurrence during the night hours of large negative bays, lasting about an hour, in the horizontal component. Detailed studies of these disturbances, known as polar substorms, or polar elementary storms in the older terminology of Birkeland, show that they occur along the belt which contains the active aurora (Akasofu, 1968). If it is assumed that the geomagnetic disturbances are due to electric currents flowing in the ionosphere, it is found that the currents generally coincide with visible aurora, in position, direction and intensity (Walker, 1964; Kim and Wang, 1967). The belt containing the active aurora is approximately an oval, eccentric about the dipole axis pole and elongated toward the equator in the local midnight sector (Feldstein, 1963). The auroral zone at 67° dipole latitude is now seen to be the locus of the midnight position of the auroral oval. The polar magnetic substorm itself is only one manifestation of the more general magnetospheric substorm which includes also auroral and ionospheric substorms, and well-defined micropulsation, cosmic noise, and x-ray disturbances.

It is probable that the currents which give rise to polar magnetic substorms are three-dimensional and flow along field lines as well as in the ionosphere (Akasofu and Meng, 1969; Bostrom, 1967). Results of a rocket-borne experiment at Fort Churchill on February 26, 1969 have been interpreted as showing the existence of field-aligned sheet currents associated with the visible auroral arc (P.A. Cloutier *et al.*, 1970). Fukushima (1969) has shown that it is not possible using only geomagnetic data observed on the ground, to determine whether the current system responsible for polar elementary storms flows only in the ionosphere or along field lines as well. However, it is useful in studying the form of the oval and its changes with time, to determine an equivalent current system in the ionosphere (not the actual current system) which could give rise to the observed magnetic effects.

Essentially two models have been used to represent the equivalent flow pattern of the auroral electrojet in the ionosphere which causes polar magnetic substorms: a modification of the Silsbee and Vestine (1947) SD current system, and the Akasofu and Feldstein models (Akasofu, Chapman and Meng, 1965; Feldstein and Zaytsev, 1965). The first is a two-celled model in which an intense electrojet flows westward along the auroral zone in the dark sector. The circuit of each electrojet is completed by return currents flowing across the polar cap toward the dawn sector. Akasofu and Feldstein represent the electrojet as flowing westward all around the oval. In Akasofu's representation, the eastward flowing currents in the afternoon and evening hours are explained as leakage currents from the westward electrojet, whereas Feldstein interprets these currents as forming an independent system. The co-existence of the auroral electrojet and the twin-vortex current in the polar region has been postulated by Iijima and Nagata (1968) and Fukushima (1969).

In view of the unresolved problems concerning the generation of polar magnetic substorms and the existence of several conflicting models of the ionospheric and field-aligned currents which give rise to the magnetic effects, it is important to study the development in time and space of many individual substorms. From such studies it may be possible to synthesize a model magnetic substorm, or at least to recognize a limited number of classes of such storms, in order to test existing theories in a more rigorous fashion. The present paper analyzes the intense substorm which developed at 08 U.T. on December 5, 1968, with particular emphasis on the observed morphology of the auroral oval.

Analysis of magnetic data

Magnetograms from 26 auroral and polar cap observatories and total intensity data from Ice Island T3 were used in this analysis. These stations are shown on the map in Figure 1. Geomagnetic co-ordinates, the angle Ψ between the geographic and geomagnetic meridians, and the Universal Time of local midnight, are listed in Table I for each station.

Deflections of H, D (X, Y) and Z from the baseline were measured at approximately nine-minute intervals from 0624 to 1339 U.T. Perturbations from the midnight level of the quiet day December 14 (or December 2 in a few cases) were then expressed in the geomagnetic co-ordinate system X′, Y′, Z. Plots of magnetic perturbation vectors ΔX′, ΔY′ ΔZ, contours of ΔZ, and equivalent line currents, calculated from the three perturbation vectors for a height of 112 km (equivalent to one degree of latitude), were drawn for a number of instants of time during the storm.

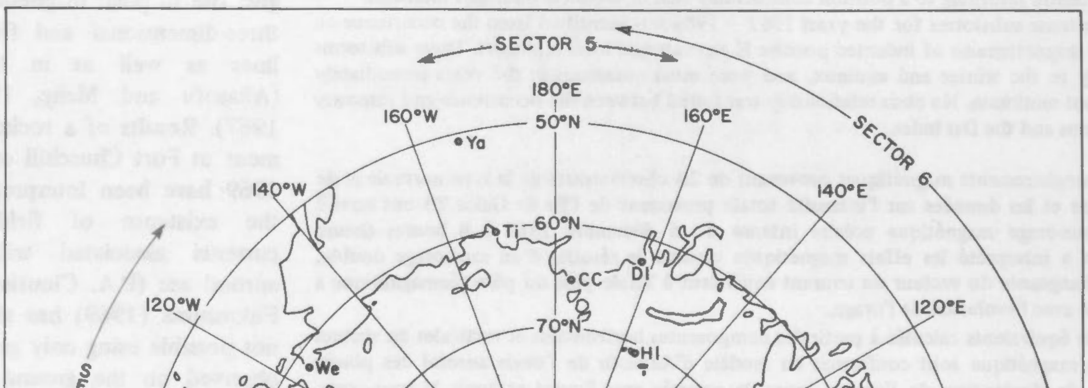

Figure 1. Map in geomagnetic co-ordinates showing the stations used for this analysis and their grouping into six sectors.

Table I

		Geomag.Co-ords. Lat.N	Long. E	ψ_E	U.T. of local midnight (hrs)			Geomag.Co-ords. Lat.N	Long.E	ψ_E	U.T. of local midnight (hrs)
Th	Thule	89.2	357.4	2.4	04.61	Ab	Abisko	65.9	115.3	330.2	22.75
Al	Alert	85.7	168.7	197.7	04.17	Co	College	64.6	256.1	27.6	09.86
RB	Resolute Bay	83.1	287.7	47.1	06.33	DI	Dixon Is.	62.8	161.7	347.0	18.63
Go	Godhavn	80.0	33.1	341.8	03.56	Le	Lerwick	62.5	89.0	336.0	00.07
MLB	Mould Bay	79.1	255.4	55.3	07.96	Me	Meanook	61.9	300.7	17.5	07.55
BL	Baker Lake	73.9	314.8	19.4	06.40	We	Welen	61.6	236.8	24.8	11.32
Na	Narssarssuaq	71.4	37.3	345.2	03.02	Ti	Tixie Bay	60.3	192.6	351.9	15.40
HI	Heiss Is.	71.1	156.3	330.0	20.13	Si	Sitka	60.0	275.0	21.8	09.02
Leir	Leirvogur	70.3	71.6	333.8	01.45	Nu	Nurmijarvi	59.6	114.4	336.4	22.36
Ch	Fort Churchill	68.8	322.5	13.8	06.27	St. J	St. John's	58.7	21.4	353.7	03.51
PB	Point Barrow	68.4	240.7	33.5	10.45	Ot	Ottawa	57.0	351.5	2.4	05.04
GWR	Great Whale River	66.8	347.2	4.5	05.18	Vi	Victoria	54.3	292.7	16.4	08.23
CC	Chelyuskin Is.	66.1	176.5	356.6	17.05	Ya	Yakutsk	50.8	193.8	5.9	15.35
						T3	Ice Island T3	79.2	209.6	84.6	09.02

Note that ψ_E, the angle between the geographic and geomagnetic meridians at a station, is measured eastward from the geographic meridian.

Calculations of ΔX, ΔY, from ΔH, ΔD, and of ΔX′, ΔY′, ΔZ, and the equivalent line current plots were programmed on the Hewlett-Packard desk calculator and plotter. In calculating the line currents, it was assumed arbitrarily that 25 per cent of the observed magnetic effect could be attributed to induction within the earth. The equivalent currents were calculated using both the horizontal and vertical components of the perturbation vector, whereas the usual practice has been to derive an overhead current density from the horizontal components only. The vertical component was included in the calculations for the sake of completeness, and to give some estimate of the position of the equivalent current north or south of the station. In a few cases, for stations near the centre of a current circulation, when very large Z effects were associated with small perturbations in the horizontal components, the current intensity and distance from the station are obviously unrealistic (e.g. Baker Lake at 0830, Figure 3). It is evident that the equivalent line currents have only limited physical validity, and precise contours of current flow were not attempted. The current plots are used as illustrations only of the development and changes in time and space of the currents flowing in and near the auroral oval.

KP indices for December 5 for the eight three-hour U.T. intervals were

3– 3o 5+ 5o 4o 3– 3+ 3–

The Dst indices had a small positive maximum of three gammas at 08 U.T. and a minimum of −48 gammas at 01 U.T. on December 6.

Auroral data for December 5, 1968

Auroral information available from the National Research Council of Canada, was unfortunately limited, as all-sky camera data were missing from the Churchill, Great Whale River and Ottawa sites owing to cloud cover.

The auroral radar at Thompson (Φ65N; Λ317.5E) recorded very intense echoes between 0330 and 0400 and around 0800 U.T. Echoes of comparable intensity were recorded at Ottawa between 0830 and 0900 and at Churchill at 0500. Slightly less intense echoes were observed at Churchill in the interval 08 – 09.

The visual observations of aurora reported for the night are as follows:

A bright rayed arc 30° above the horizon north of Saskatoon at 08 U.T.

Weak homogeneous arc (WHA) 30° above the horizon north of Cape Parry (70.2N, 124.7W) at 09 U.T. (7/10 cloud).

Series of glows and rays to SW and SE of British Arctic Expedition Ice Island (geographic co-ordinates 85N; 149.2W) at 10 U.T. No cloud, but a bright full moon was reported.

WHA 30° above the horizon north of Saskatoon at 1145.

WHA 10° above the horizon north of Regina Airport (50.4N, 104.7W) at 1200.

WHA 25° above the horizon NE of Saskatoon at 1245 U.T.

Sequence of magnetic events, December 5

The sequence of magnetic events in the night sector began with negative impulsive bays in H at Leir and Na shortly after 02 U.T. The maximum for this disturbance was recorded at BL at 0342 U.T. (-505 gammas in X).

The next magnetic event of interest was the SSC at 0633, clearly visible on all the magnetograms examined except for Ch and BL. Initial movements as high as 100 to 200 gammas were observed at Na, Leir, PB and Ab. For several hours after the SSC, Leir, Ab and Na in the early and mid-morning sector recorded strong micropulsations with periods of three to five minutes.

At 0810 very large micropulsation activity was observed on the dY/dt recording at Byrd, Antarctica (private communication, Rostoker). At about this time an intense substorm developed in the midnight sector in mid-Canada. The maximum magnetic effect was recorded at MLB (-ΔH approximately 2,000 gammas). This was followed by three less intense substorms with maxima at 1207 (Co), 1435 (Di) and 1915 (Di) U.T. respectively. The maximum perturbation in H for each of these storms was just under -800 gammas.

Polar substorm 08 – 10 U.T.

This substorm is particularly interesting because of the very intense negative bay at MLB (dp. lat. 79.1). The bay began suddenly in X and Y at 0905 U.T. with maximum deflection at 0909, suggesting the close approach to MLB of the northern edge of the oval at that time. The negative bay, which lasted about 37 minutes, followed a small negative indentation at 0836. The bay was impulsive and belongs to the class of indented positive bays discussed by Meng and Akasofu (1967). Maximum deflections from the quiet level were -1893γ in X, -1259γ in Y and 453γ in Z. It is known that the geomagnetic anomaly at Mould Bay may enhance the hourly ranges in X and Y by as much as 20 per cent and 50 per cent respectively (Whitham, 1965). An anomalous effect of this magnitude would reduce the maximum perturbations at Mould Bay to -1578γ in X and -893γ in Y. However, this amplitude is still almost twice as large as that recorded at any other observatory during the storm, and is the largest perturbation recorded at Mould Bay since observations began there in 1962.

The limited number and unequal distribution of observatories available for the analysis of polar substorms makes it impossible to accurately determine the extent in longitude and latitude of the auroral electrojet. In an attempt to estimate these parameters the stations were grouped into six sectors, as follows:

Sector	*Stations*	*Mean geomagnetic longitude*
1	Th Go Na St. J	22.3° E
2	Th BL Ch GW Ot	338.7
3	RB BL Ch Me Vi	303.7
4	RB MLB PB Co We	255.3
5	Al T3 CC Ti Ya	182.9
6	Al HI Ab Nu	138.7

Latitude profiles in ΔX′ and ΔZ were drawn during the storm for each of the six sectors.

The development of the substorm is reflected in the changing distribution of areas of maximum ΔZ, since it is only near the storm centre that the vertical component of magnetic perturbation is appreciable (Bostrom, 1967). The three stations with maximum positive and negative ΔZ for a number of instances during the storm are listed in Table II. An examination of the latitude profiles and Table II suggests that the storm can be described in three phases: an initial phase, an expansive phase, and a recovery phase. Akasofu (1968) lists an expansive and recovery phase as the two characteristic phases of the auroral substorm.

It must be emphasized that any interpretation based on the distribution of areas of maximum ΔZ may be affected by the poor distribution of observatories.

Initial phase (0800 – 0824)

The storm apparently developed in the midnight sector shortly after 0800 U.T. The bright rayed arc observed north of Saskatoon at 0800 was located immediately east and about 2° north of Me. Z bays and negative H bays were recorded around this time at all stations in and south of the auroral zone in the midnight and pre-dawn sectors (Figure 2). Times of commencement of the Z bays were often indefinite. Positive H bays were observed at Vi and Si in the return current system south of the oval in the midnight sector and at RB and MLB in the polar cap. About five minutes after the start of the bay at Me (0806), a negative bay was recorded at Co in the evening sector, when Co came under the influence of the primary electrojet. Welen recorded a slow negative H bay beginning about 0809. These bays are typical for stations in the return current regime south of the auroral oval in the evening sector (Rostoker, 1966). In the afternoon sector, positive H bays began at Ti and Di at 0820.

At 0812 the largest values of ΔZ were measured at Ch, BL and GWR in the early morning secor. The largest -ΔZ was at HI at 71.1°N in the noon sector. The current vector plot (Figure 3) indicates a strong eastward current along the auroral zone latitudes in this sector at 0812, contrary to the findings of Kamide *et al.*, 1969. At 0821 maximum positive and negative values of ΔZ were measured at GWR and Me respectively. These values were about three times larger than for 0812.

The latitude profiles (Figure 4) indicate that the electrojet was limited to the first three sectors in the initial phase of the storm, with well pronounced maxima in -ΔX′ at Na, GWR and Me at 0812. The maximum value of -ΔX′ was observed at GWR. The primary westward current flow was north of Na and Me and to the south of GWR (Figure 5).

Expansive phase (0824 – 0918)

At 0824 there is a sharp negative movement in the Z component at Co. At this time Z at PB shows a sharp positive rise followed by a negative bay which begins at 0830. A negative bay in H begins suddenly at PB at 0824, at which time a positive indentation of the -H bay is observed on the Co record (Figure 2). These magnetic effects indicate passage of a westward flowing surge north of Co at 0824 (Akasofu, 1968). The H variation at Vi and Si is typical of stations south of the oval in the midnight sector: a small positive bay beginning at 0810 followed by a negative bay. The time of beginning of the negative movements corresponds closely to the time assumed for the passage of the westward surge north of Co. At We the slow negative movement in

Table II

	Maximum +ΔZ	Maximum −ΔZ	Maximum −ΔX′	Maximum equivalent current vector x10^5 amps.
Initial phase				
0812	CH 103γ	HI −143		
	BL 99	Me −104	GWR	Ch 2.12
	GWR, Go 70	Na −101		
	(Di 60)			
0821	GWR 239	Me −286		
	BL 158	HI −151	Co	
	Ch 146	Na −105		
Expansion phase				
0830	GWR 414	Me −527		
	Ch 361	Co −222	PB	Me 8.75
	BL 191	HI −151		
0839	Ch 456	Me −358		
	GWR 379	Co −254	PB	
	BL 250	PB −206		
0848	Ch 507	Me −475		
	GWR 450	PB −296	Co	Me 8.75
	BL 407	Co −235		
0900	BL 512	Me −495		
	GWR 492	Co −209	Co	Me 11.9
	CL 404	Si −176		
0909	GWR 548	Me −515		
	CH 490	Co −266	MLB	RB 11.9
	MLB 453	Si −187		
0918	RB 496	Me −436		
	BL 407	Co −362	MLB	
	Ch 344	PB −329		
Recovery phase				
0927	RB 540	Co −273		
	MLB 348	Me −248	MLB	
	Ch 327	Si −220		
0936	RB 420	Me −183	Na −530γ	
	MLB 371	Si −176		MLB 5.88
	BL 276	Co,PB −165	Co −472γ	
0945	MLB 470	Co −222		
	RB 452	PB −185	GWR	
	BL 236	We,Si −138		
0954	MLB 470	PB −226		
	BL 341	CC −197	GWR	
	RB 300	Co −184		
1003	MLB 395	CC −222		
	BL 341	Na −189	GWR	RB 4.38
	RB 245	PB −152		
1021	BL 394	GWR −365		
	MLB 371	PB −309	GWR	GWR 6.25
	Ch 318	CC −159		

Table II (cont'd)

	Maximum +ΔZ		Maximum −ΔZ	Maximum −ΔX′	Maximum equivalent current vector x10^5 amps.
1057	Ch	211	CC −203		
	BL	210	HI −166	Ch	Ch 3.94
	MLB	151	PB −103		
	(Ti	121)			
1106	BL	171	CC −190		
	MLB	133	HI −163	Ch	GWR 4.00
	Ch	129	GWR−141		
	(Ti	111)			
New substorm begins about 1120 U.T.					
1209	Co	368	We −495		
	PB	226	Ti −194	Co	Co 5.31
	Ch	189	Si −193		
1245	CC	260	We −306		
	MLB	215	Co −273	PB	Co 4.14
	Ch	181	Ti −226		

H beginning 0809 changes abruptly at about 0823 with the development of a positive bay. From comparisons with all-sky photographs, Akasofu and Meng (1967) have shown that such positive bays to the south of the oval are associated with westward travelling surges. The bay at We appears to be an example of a class of H transition bays studied by Rostoker, 1966, who attributes the change in form to the effect of the rotation of the earth in moving a station south of the oval from the return current regime into the regime of the primary electrojet.

In the early morning sector BL moved out of the eastward return current in the polar cap into the regime of the primary electrojet at 0835, as shown by the transition in X and Y from gradual positive bays to negative bays at this time. At Ch a brief indentation of the positive Z bay reaches its maximum value at 0847, at the time of the maximum of the negative H bay. At 0857 at BL an abrupt negative movement in H is simultaneous with a negative indentation of the positive Z bay. These effects at BL and Ch are interpreted as resulting from the expansion to the north and east of the auroral oval.

An expansion to the north and west in sector 4 is indicated by the small negative indentation of the positive X bay at MLB at 0836.

Following the westward surge at 0824 the maximum amplitude of ΔZ increases by a factor of two but remains centred in the GWR, Ch and BL area until 0909. The −ΔZ maximum is strongly intensified at Me, and the Alaskan observatories, with amplitudes comparable to the postive maximum.

During the expansive phase the electrojet appeared to spread into sectors 4, 5 and 6, with the main current at 0830 flowing south of GWR, north of Me, Na, PB and HI and between T3 and CC (Figure 5). The approximate geomagnetic latitude of the main westward current (equivalent) was 72° in sector 1, 65° in sector 2, 64° in sector 3, 68° in sector 4, and 73° in the daylight sector as given by the current vector for HI. At 0835 ΔZ became positive at Na as the electrojet moved to the south about $1\frac{1}{2}°$ in sector 1. By 0900 there is a significant shift (about $1\frac{1}{2}°$) to the south in sector 6 as well. A pronounced poleward movement is evident on the 0900 plots, which show the current vector for BL at Φ~72°. −ΔX′ was maximum at PB until 0909 when the unusually large maximum in −ΔH was recorded at MLB, indicating the near approach of the northern edge of the oval to MLB at that time. This marked the extreme northward expansion of the electrojet. The current vectors for RB and MLB at 0909 were at Φ~78°.

Evidence for a double substorm

The intense perturbation at MLB about one hour after the beginning of the storm, suggests that a second substorm may have developed south of MLB at this time. (See the latitude profile for 0909 in Figure 4.) A number of observations support this interpretation.

The weak homogeneous auroral arc observed under poor conditions from Cape Parry was centred about 430 km geomagnetic southeast of MLB at 09 U.T.

The double nature of the negative H bay at Meanook could result from the conjunction of two negative bays or from a positive indentation lasting from 0831 to 0918. Such a positive indentation could be explained by the rapid northward movement of the electrojet in the midnight sector during the expansive phase (Rostoker, 1966). Assuming two negative bays, it is evident that the effects of the 0806 storm started to decay in this sector after 0831, and a second disturbance began around 0855, reaching maximum intensity at 0918.

As discussed later in this study, the rate of expansion of the 0806 storm in the direction of MLB strongly supports the argument for a double substorm.

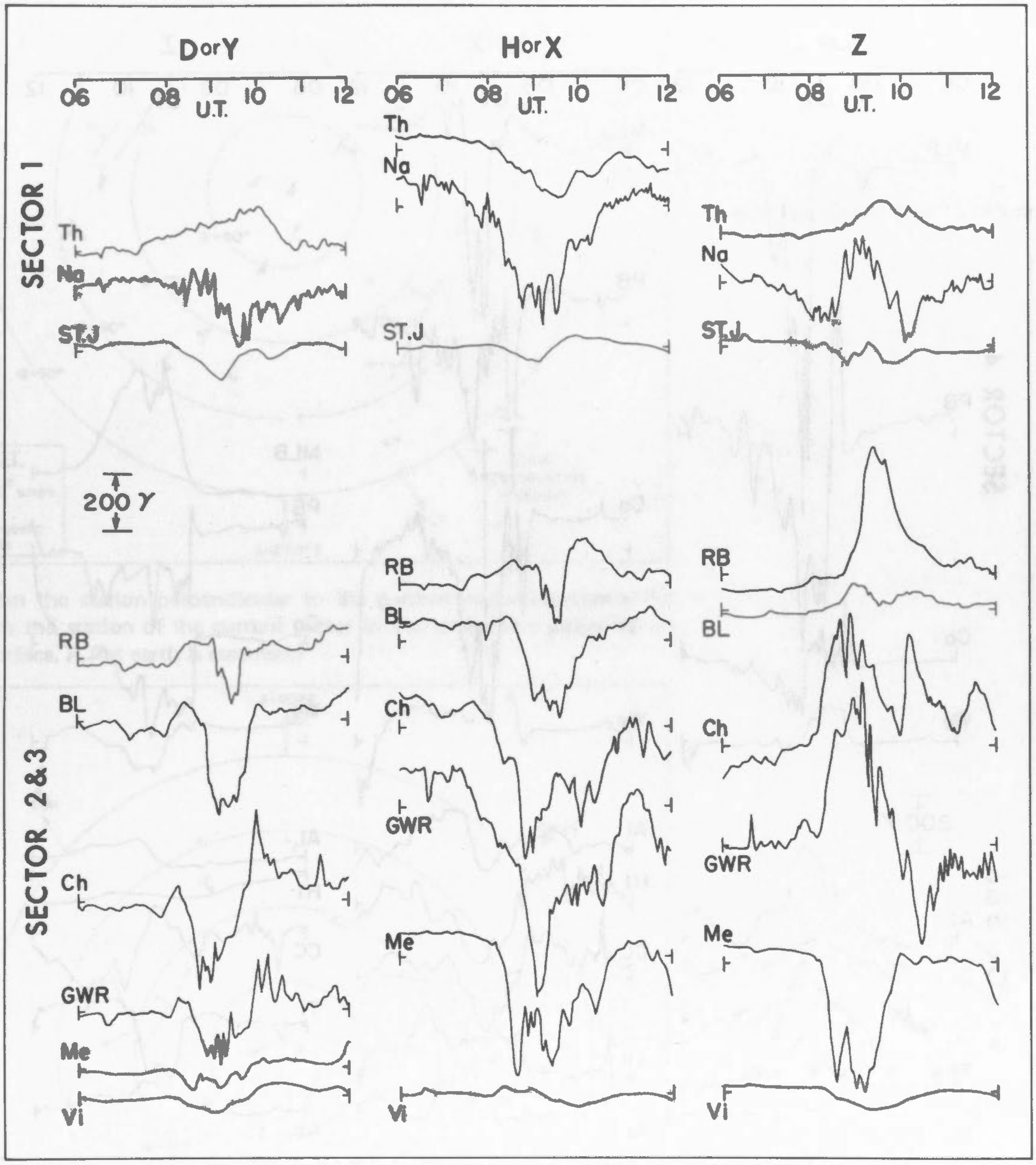

Figure 2a. H(X), D(Y), Z magnetogram traces drawn from 75 sec digitized data, for Th, Na, St. J. (section 1) RB, BL, Ch, GWR, Me, Vi (sectors 2 and 3).

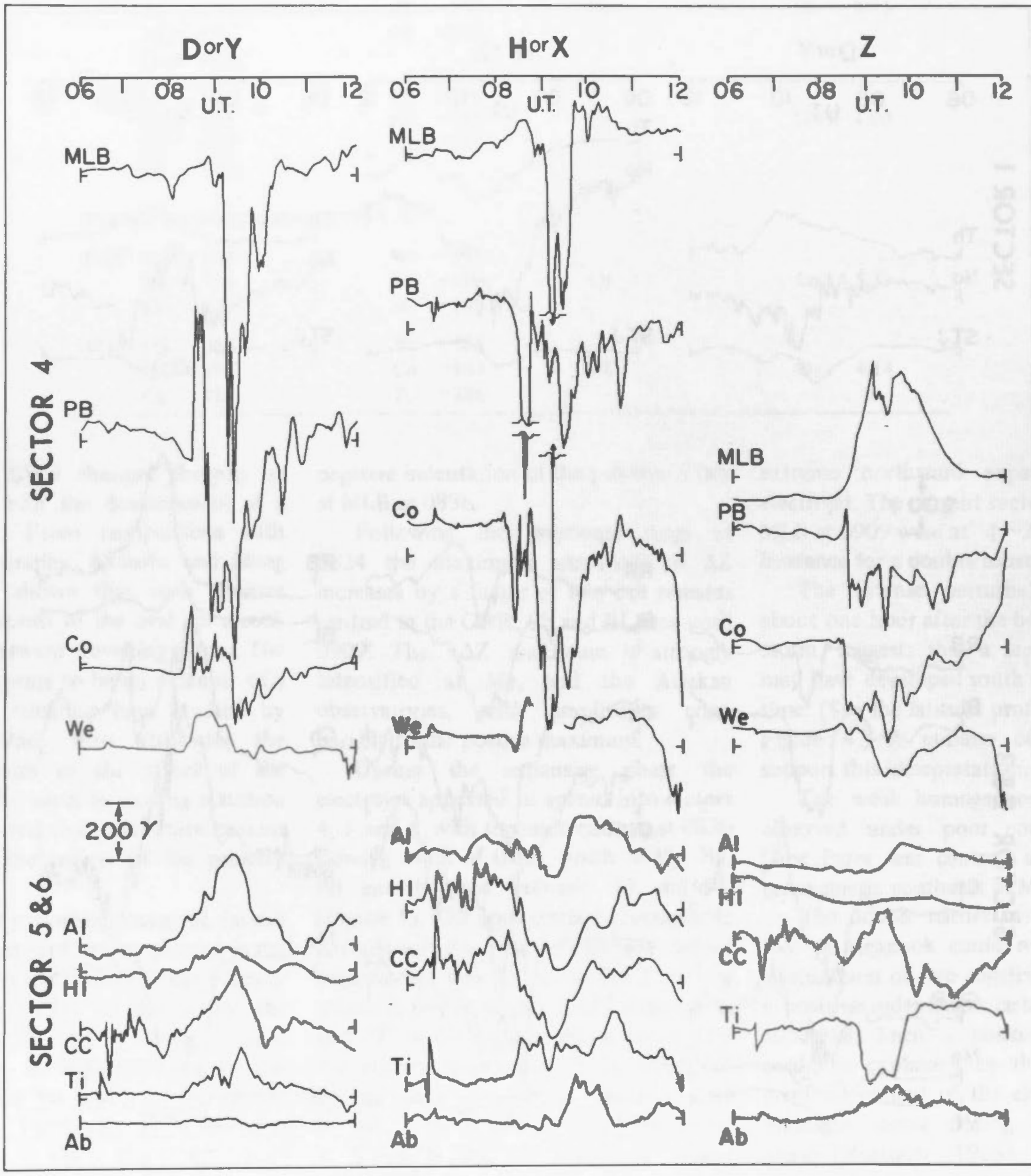

Figure 2b. H(X), D(Y), Z magnetogram traces drawn from 75 sec digitized data, for MLB, PB, Co, We (sector 4) Al, Hi, CC, Ti, Ab (sectors 5 and 6).

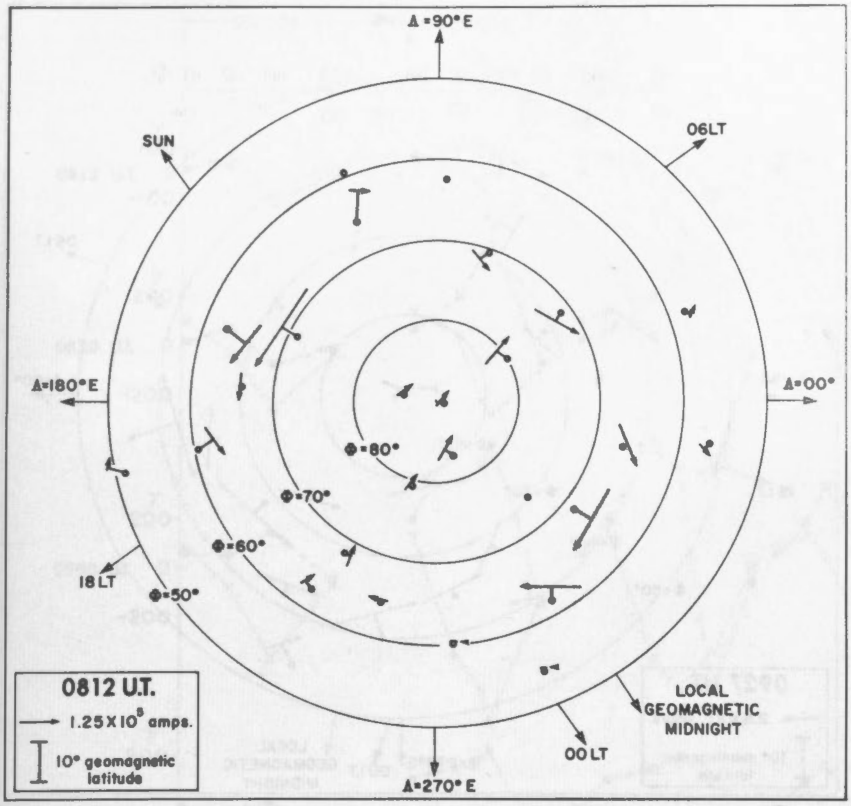

Figure 3a. Current vector plots for 0812 U.T.

(The line from the station perpendicular to the current vector represents the distance from the station of the current vector in the ionosphere projected on the earth's surface. A flat earth is assumed.)

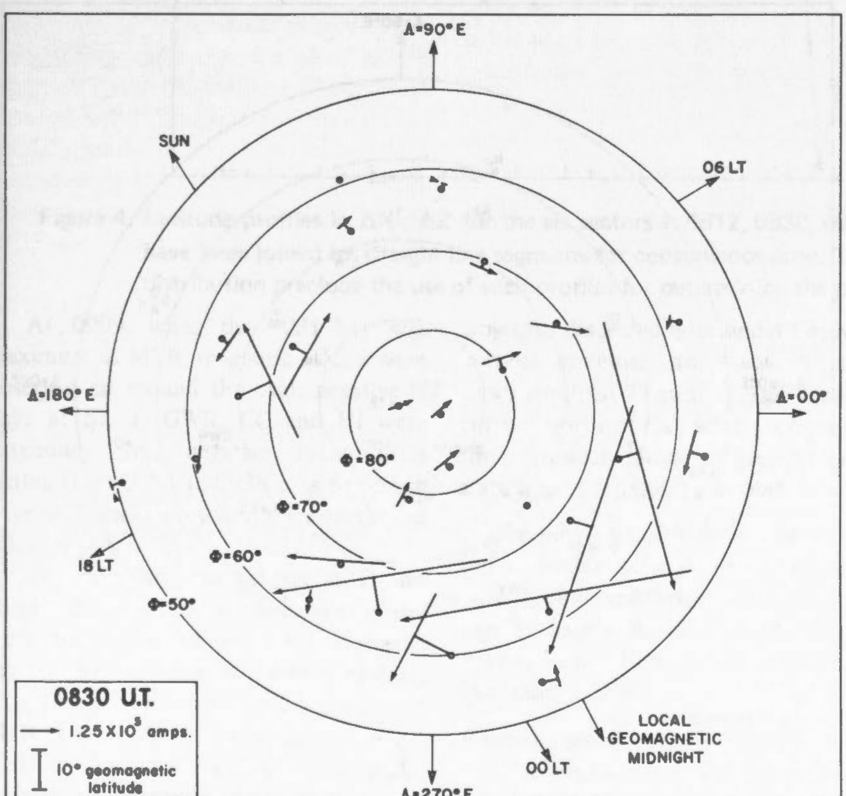

Figure 3b. Current vector plots for 0830 U.T.

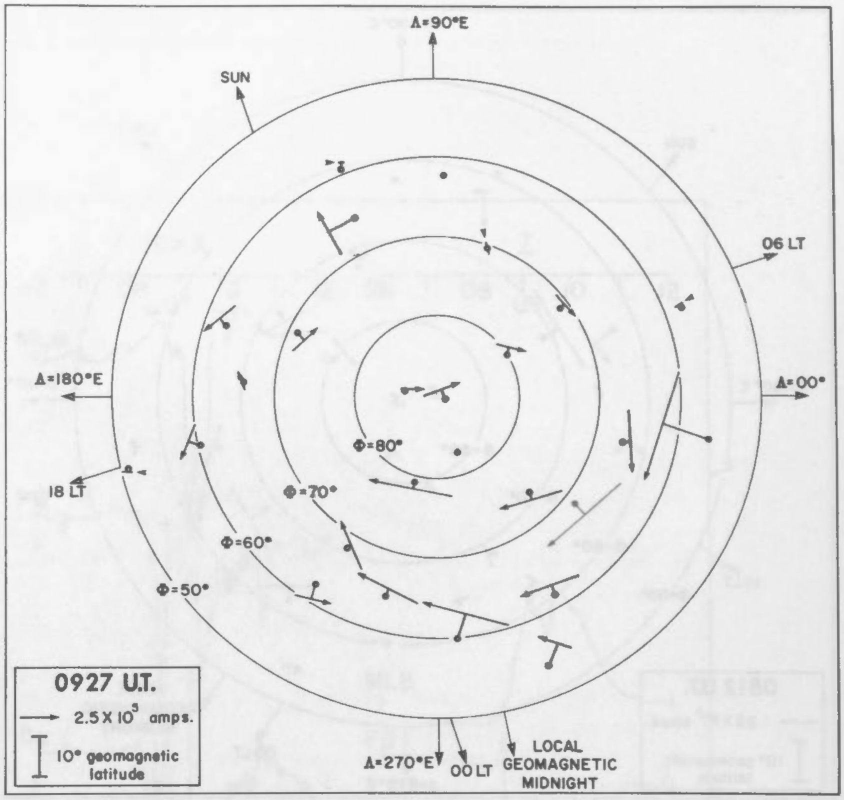

Figure 3c. Current vector plots for 0927 U.T.

(The line from the station perpendicular to the current vector represents the distance from the station of the current vector in the ionosphere projected on the earth's surface. A flat earth is assumed.)

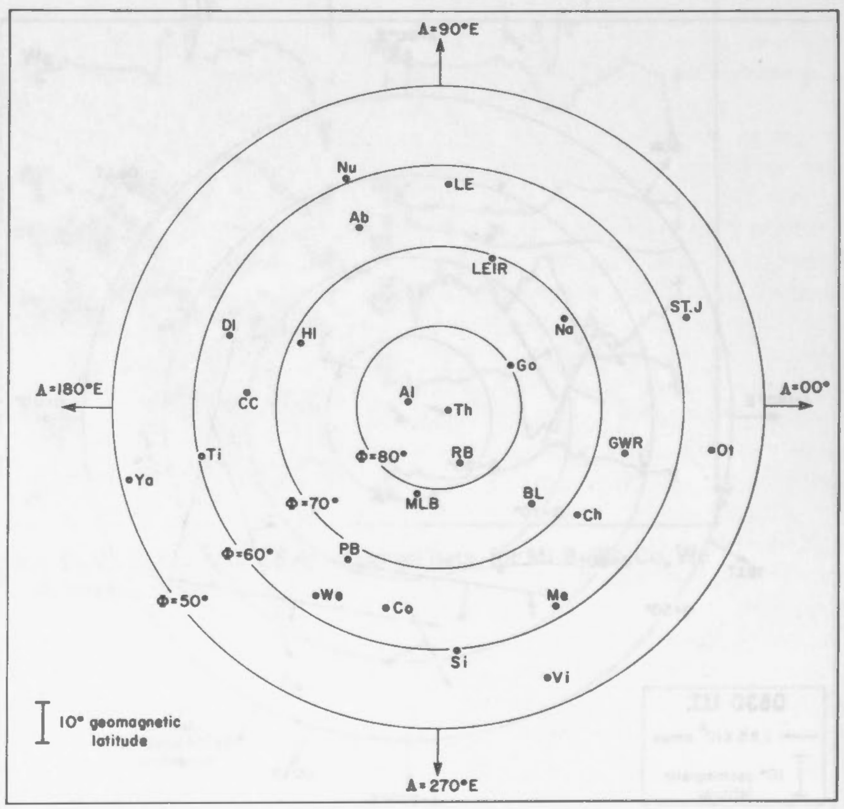

Figure 3d. Key to location of stations.

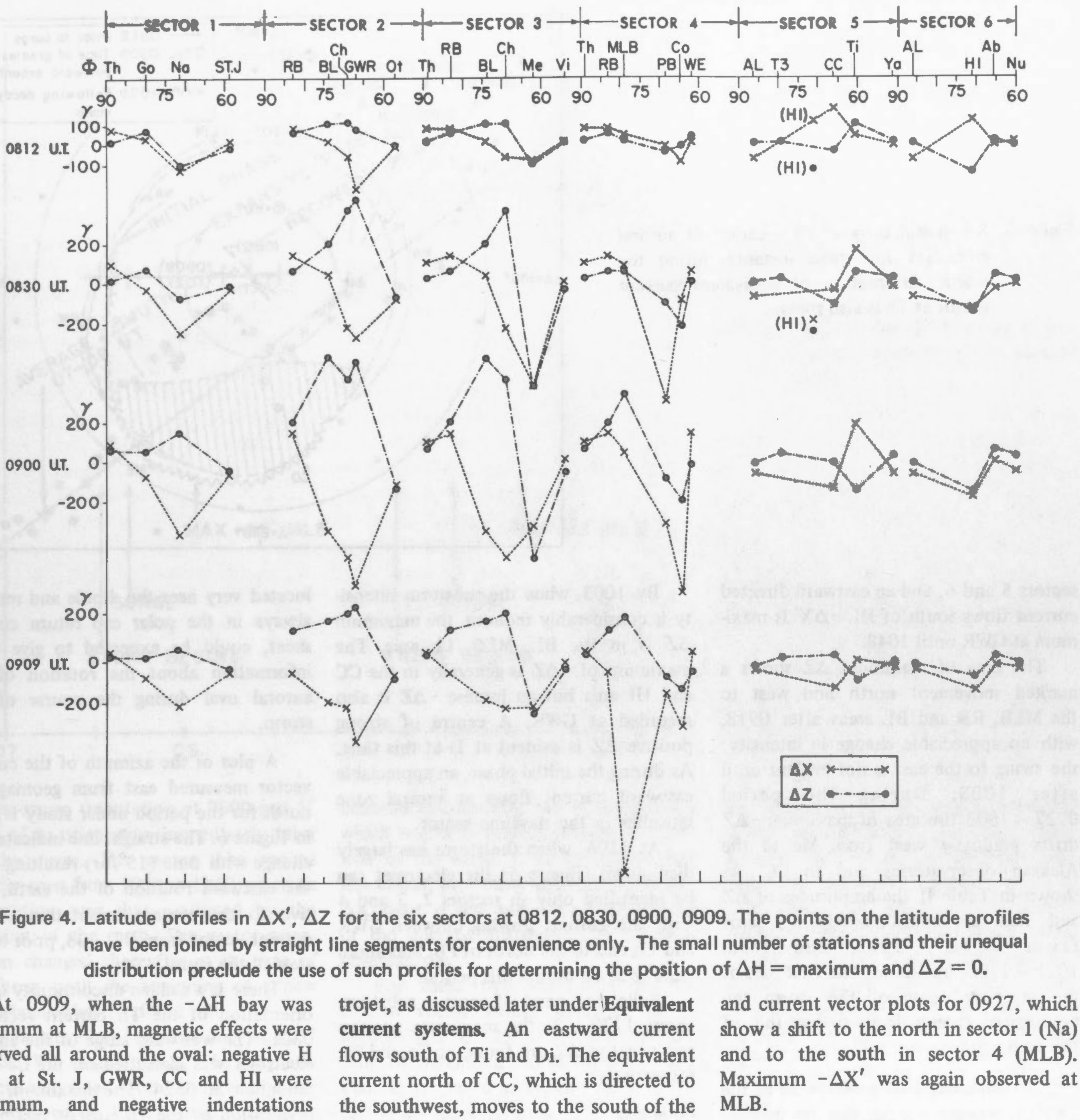

Figure 4. Latitude profiles in ΔX′, ΔZ for the six sectors at 0812, 0830, 0900, 0909. The points on the latitude profiles have been joined by straight line segments for convenience only. The small number of stations and their unequal distribution preclude the use of such profiles for determining the position of ΔH = maximum and ΔZ = 0.

At 0909, when the −ΔH bay was maximum at MLB, magnetic effects were observed all around the oval: negative H bays at St. J, GWR, CC and HI were maximum, and negative indentations lasting from 0905 to 0930 of the positive bays at Ti and Di reached their maximum value, at 0909.

The negative indentations at Ti and Di reflect the sudden enhancement of the westward electrojet and its associated return currents south of the oval resulting from the new substorm activity south of MLB around 09 U.T. During the period 0905 to 0930 Ti, Di and CC remain in the leakage current from the westward electrojet, as discussed later under Equivalent current systems. An eastward current flows south of Ti and Di. The equivalent current north of CC, which is directed to the southwest, moves to the south of the station between 0900 and 0909.

Recently Akasofu *et al.* (1970) observed a double substorm from the all-sky camera photographs and magnetic recordings at Sach's Harbour in the Canadian Arctic, and College, at 0858 U.T., December 6, 1969.

Recovery phase (0927 – 1106)

The beginning of the recovery phase is already evident on the latitude profiles and current vector plots for 0927, which show a shift to the north in sector 1 (Na) and to the south in sector 4 (MLB). Maximum −ΔX′ was again observed at MLB.

Following 0927 the oval contracted rapidly, with significant shifts of the current flow to the north in sectors 1, 2 and 6. The electrojet moved north of Na at about 0935 and north of GWR at 0954, as shown by the reversal in sign of the Z perturbations at these stations. A much smaller poleward motion was seen in sector 4 between 0945 and 0954. Little change was seen in sector 3. At 0954 the electrojet is no longer evident in

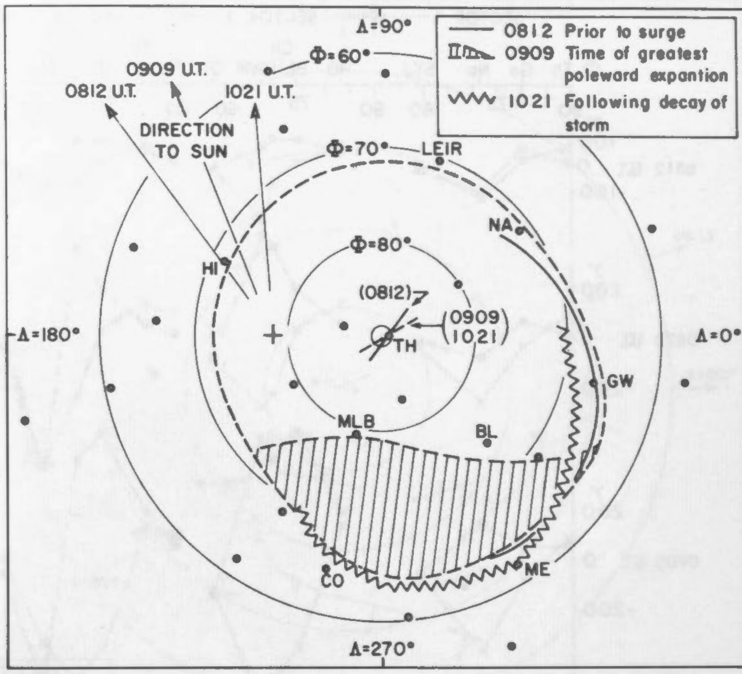

Figure 5. Schematic diagram of location of auroral electrojet for three instants during the storm. Orientation of equivalent current vector at Th is also shown.

sectors 5 and 6, and an eastward directed current flows south of HI. $-\Delta X'$ is maximum at GWR until 1048.

The area of maximum ΔZ shows a marked movement north and west to the MLB, RB and BL areas after 0918, with no appreciable change in intensity: the swing to the east is not evident until after 1003. During the period 0927 – 1003 the area of maximum $-\Delta Z$ drifts gradually west from Me to the Alaskan observatories and to CC. As shown in Table II the amplitudes of ΔZ and $-\Delta Z$ are approximately the same from 0812 – 0918 and from 1021 – 1106, but during the first part of the recovery phase of the storm the negative maximum drops to half that of the positive.

The apparent drift to the west of the area of maximum $-\Delta Z$ and its marked reduction in amplitude in the interval 0927 – 1003 must result from the lack of magnetic data around latitude $\Phi \sim 70°$ between the longitudes of Ch and PB. After the storm centre returns to its most easterly position, the amplitudes of $-\Delta Z$ and $+\Delta Z$ are again comparable. This strongly suggests that during the recovery phase the southern edge of the oval moved poleward in the early morning sector (sector 3) to about $\Phi = 70°$.

By 1003, when the substorm intensity is considerably reduced, the maximum ΔZ is in the BL, MLB, Ch area. The maximum of $-\Delta Z$ is generally in the CC and HI area but an intense $-\Delta Z$ is also recorded at GWR. A centre of strong positive ΔZ is evident at Ti at this time. As during the initial phase, an appreciable eastward current flows at auroral zone latitudes in the daytime sector.

At 1106, when the storm has largely died down (Figure 5) the electrojet can be identified only in sectors 2, 3 and 4 with the current flowing between GWR and Ch and to the north of PB. Maximum $-\Delta X'$ is at Ch during this period.

Following onset of another substorm about 1120 U.T. the maximum positive and negative ΔZ are found at Co and We respectively.

Polar cap

It has been suggested by a number of authors (e.g. Rostoker, 1966; Kamide *et al.*, 1969) that the auroral oval is fixed in space with respect to the sun-earth line. In all models of equivalent current flow, the change in orientation of the polar cap return current is related to the rotation of an idealized eccentric auroral oval about the dipole. An examination of the change with time of the geomagnetic azimuth of the current vector at Thule, which is located very near the dipole and remains always in the polar cap return current sheet, could be expected to give some information about the rotation of the auroral oval during the course of the storm.

A plot of the azimuth of the current vector measured east from geomagnetic north for the period under study is given in Figure 6. The straight line indicates the change with time (15°/hr) resulting from the eastward rotation of the earth, relative to the average orientation of the current vector from 07 – 08, prior to the start of the storm.

There is a sudden discontinuity in the orientation of the Th current vector at 0821. The westward surge of the auroral electrojet was identified on the Co magnetogram at 0824. The maximum west orientation of the Th current vector was reached at 0927. The maximum northward expansion of the double substorm, as inferred from the MLB records, was at 0909. The latitude profiles show the electrojet flowing in sector 6, at its farthest west extension, from 0830 to 0927. Following 0945 the electrojet is no longer evident in sectors 5 and 6. During the recovery phase of the storm, the Th current vector swung rapidly eastward until 1003, when it was only 16° west of

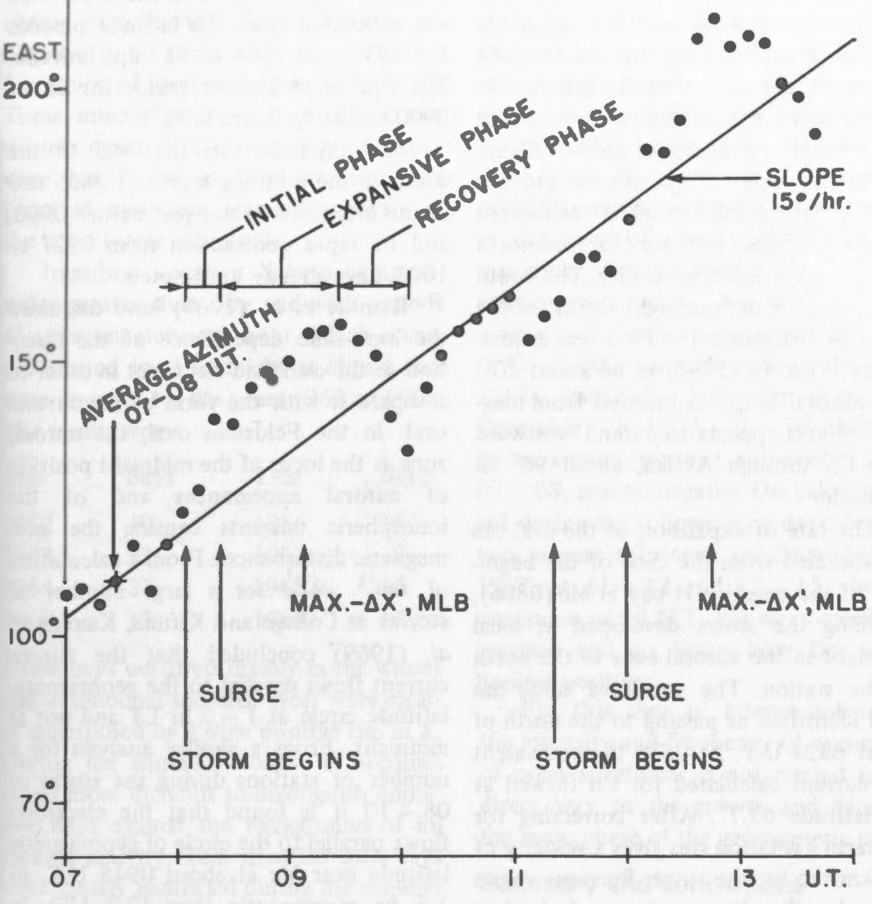

Figure 6. Graph of change with time of geomagnetic azimuth of Th current vector.

its pre-storm orientation at 0800 and 5° west of its orientation immediately prior to the surge. The vector then moved rapidly west from 1003 to 1030, when its orientation was that predicted by the rotation of the earth. The vector orientation changed thereafter at the rate of 15°/hour until the beginning of a new disturbance shortly after 1100.

A negative bay begins as early as 1107 on the We magnetogram. The magnetic effects associated with a westward surge are observed on the PB magnetogram at 1202. A negative bay begins at MLB at 1220 and $-\Delta X'$ is maximum there at 1245. It may be assumed that this marks the peak of the northward expansion (and intensity) of the 11 – 14 U.T. storm. These magnetic effects are reflected in the graph of the Th current vector, which again shows a very rapid swing to the east in the recovery phase of the storm. At 1339, the last point used in this analysis, the current vector is already oriented considerably east of the position which would be predicted from the rotation of the earth. It would appear that this effect, previously implied by the ΔZ, $\Delta X'$ data, is real and not a consequence of the unequal distribution of magnetic observatories.

For these two substorms the Th current vector swings westward at an average rate of 25° – 30°/hour to the time of maximum storm intensity, and then about twice as rapidly back to the east in the recovery phase.

Equivalent line current systems and the auroral oval

Akasofu and Meng (1969) have pointed out that it is not possible to determine an accurate equivalent current system from the present network of observatories. There is no doubt that the polar electrojet flows along the auroral oval rather than the auroral zone; however the nature of the eastward current in the afternoon and evening hours is not definitely established (Akasofu, 1967, Afonina and Feldstein, 1969). It has been suggested that such a current could be produced by an asymmetric ring current configuration (Akasofu and Meng, 1968).

Afonina and Feldstein have suggested a test to discriminate between a two-celled equivalent current system of the modified SD type, and the Feldstein-Akasofu model in which the polar electrojet flows westward at all longitudes during the substorm. The test consists essentially in determining the direction of the equivalent current at $\Phi \sim 70°$ at 20 – 22 h LT and at $\Phi \sim 75°$ at 09 – 10 LT, since at these times and locations the current directions predicted by the two models differ significantly.

Although it is difficult to apply this test rigorously to the storm of 08 – 10 U.T. owing to the unequal distribution of observatories, the equivalent current vectors for the expansion of the storm strongly support the Akasofu model. However, at 0803 and 0812, in the pre-breakup phase of the storm, the current directions can be interpreted as belonging to a two-celled system (Figure 3).

On the latitude profiles for sectors 5 and 6 (Figure 4) at 0812, a pronounced positive maximum in $\Delta X'$ ($+170\gamma$) is seen at CC ($\Phi \sim 66°$). The $\Delta X'$ value for HI was 110γ and for Ti 40γ. The corresponding ΔZ values for HI, CC, and TI were -140γ, -40γ, and 100γ respectively. These profiles are very nearly mirror images of the profiles in sector 2 at this time where $\Delta X'$, ΔZ are both maximum at GWR ($\Phi \sim 67°$) with amplitudes of -235γ and 105γ respectively. This indicates that in addition to the primary westward electrojet flowing in the dark sector, a current only slightly less intense flows eastward in the afternoon sector at $\Phi \sim 65°$. It is not possible to determine if this eastward current completes its circuit by a return current westward across the polar cap. The orientation of the current vector at Ti suggests that this may be the case.

During the expansion phase and early part of the recovery phase, the eastward currents flowing in the afternoon (Figure 3) are most readily interpreted as return currents from the westward electrojet, in agreement with the model suggested by Akasofu. As early as 0830, a strong westward current is observed just north of HI. It is likely that the electrojet flows westward all around the oval at this time.

In the latter part of the recovery phase, after 0945, the latitude profiles are similar in sectors 5, 6 to the profiles discussed for 0812: $\Delta X'$ has become positive at HI and CC. Its maximum is now at TI. The current flow at 08.5 and 09.5 LT at Leir ($\Phi \sim 70°$) is north of the station and directed to the northeast. Again, it is possible that an SD-type current exists at these times. In their study of the substorm of July 18, 1964, Kamide *et al.* (1969) found evidence for an SD-type current system only toward the end of the recovery phase of the substorm.

The current vector plot at 0927 when the storm intensity is maximum shows large equivalent line currents south of MLB, RB and BL and north of Me and Alaskan stations. Although the line currents are obviously not an adequate physical representation of the current flowing in the oval, they do indicate an expansion of the auroral oval of about 15° north in the midnight sector (Figure 5). The latitude of the auroral arc observed south of MLB at 0900 was located 12° north of the rayed arc observed north of Saskatoon one hour earlier. The width of the oval in the midnight sector for the storm of December 16, 1964 was estimated by Akasofu (1968) to be about 20°. The 'auroral bulge' as inferred from magnetic effects appears to extend westward from Ch through Alaska, about 90° in longitude.

The rate of expansion of the oval can be estimated from the time of the beginning of the negative H bay at Me (0806), assuming the storm developed at local midnight in the auroral zone to the north of the station. The westward surge has been identified as passing to the north of Co at 0824 U.T. At 0830 the equivalent line current calculated for Co flowed at dp. latitude 67.7°. After correcting for the earth's rotation this gives a velocity of 1.1 km/sec for the surge. Previous values given in the literature are 1 km/sec measured by Akasofu (1968) and 0.9 km/sec inferred by Rostoker (1970) from magnetic effects. The rate of expansion of the oval to the northwest, as given by the negative indentation of the MLB X trace at 0836, was 0.7 km/sec. The rate of expansion to the northeast indicated by the abrupt movement at BL at 0857 was 0.65 km/sec. The position of the northern edge of the oval south of MLB was estimated from the latitude profiles for 1839 and 1848 as 75° dp. latitude. The equivalent current vector for BL at 0900 was at dp. latitude 72°.

The expansion of the oval to the south in the morning sector at 0835 and in the afternoon sector just before 0900, and its rapid contraction from 0927 to 1003, have already been noted.

Kamide *et al.* (1969) have discussed the local-time dependence of the direction of the overhead electrojet in order to compare it with the form of the auroral oval. In the Feldstein oval, the auroral zone is the locus of the midnight position of auroral appearances and of the ionospheric currents causing the geomagnetic disturbances. From a calculation of $\tan^{-1} \frac{\Delta Y'}{\Delta X'}$, for a large number of storms at College and Kiruna, Kamide *et al.* (1969) concluded that the auroral current flows parallel to the geomagnetic latitude circle at 1 – 2 hr LT and not at midnight. From a similar analysis for a number of stations during the storm of 08 – 10 it is found that the electrojet flows parallel to the circle of geomagnetic latitude near Me at about 0945 U.T. or 1.5 hr geomagnetic time (2.2 LT), in good agreement with Kamide's result.

Time of occurrence of substorms

The hourly range is a convenient index for identifying large bays with periods less than one hour. The following is a list of times when the hourly range in a horizontal component exceeded 1,000 gammas at MLB.

Date	*U.T.*	*Hourly range in gammas*	*Element*
Nov. 24, 1962	8 – 9	1,580	Y
Dec. 19, 1962	8 – 9	1,090	Y
Jan. 1, 1963	9 – 10	1,430	Y
Feb. 12, 1963	8 – 9	1,400	Y
14, 1963	8 – 9	1,140	Y
Dec. 3, 1963	7 – 8	1,050	Y
Jan. 22, 1966	6 – 7	1,010	X
Dec. 10, 1967	9 – 10	1,020	X
20, 1967	11 – 12	1,080	Y
20, 1967	12 – 13	1,070	Y
Oct. 31, 1968	11 – 12	1,280	Y
Dec. 5, 1968	9 – 10	2,170	X
Sep. 28, 1969	11 – 12	1,044	Y
29, 1969	9 – 10	1,000	Y

These ranges are many times greater than the range for the hour immediately preceding or following. The deflections are negative in all cases, and occur within a few hours of local midnight (0758 U.T.). These intense bays occur usually in the winter months. Bays of this intensity were not found in 1964 or 1965, the years of minimum magnetic activity in the last 11-year solar cycle.

Impulsive negative X bays of amplitudes greater than 50γ and with periods of approximately one hour, which occurred around local midnight at Mould Bay were counted for the years 1962 to 1969. The results were:

Year	*Bays*	*Year*	*Bays*
1962	30	1966	19
1963	32	1967	9
1964	27	1968	16
1965	13	1969	18

These bays occurred mainly in the winter and equinoctial months. Most were clearly superposed on a slow positive rise in X. During the summer months it becomes much more difficult to distinguish impulsive bays against the background of increased activity. Less than 20 such bays were clearly identified during the summer months of these years.

The intensity of substorms, as measured by the poleward extension of the auroral oval in the midnight sector of Mould Bay, is greatest in the years preceding the minimum of the 11-year cycle, and not at the minimum as Meng and Akasofu (1967) had inferred from the occurrence of negative bays in the evening at Godhavn for the first three months of 1958 and 1964. The distribution of implusive negative H bays around local midnight at Baker Lake and Resolute Bay confirm the Mould Bay results. In a study of the solar cycle effect on magnetic activity, Loomer and Jansen van Beek (1969) found that magnetic activity around midnight at BL and Ch, which is clearly associated with polar substorms, was greatest about two years before sunspot minimum.

Polar substorms and Dst

Of the 26 substorms recorded at Mould Bay with amplitudes in H greater than 500 gammas, 19 were associated with the main phase of a geomagnetic storm. For the remaining seven storms, Dst was positive. The maximum Dst for the period following these intense substorms was generally small, and did not exceed −88 gammas, except for the storm of October 31, 1969, when a maximum of −211 gammas was reported. Dst values at the time of the substorm, and the maximum Dst following the substorm were approximately the same for two levels of bay intensity at MLB (500 – 1,000 gammas and greater than 1,000 gammas). For the storm of December 10, 1967 (09 – 10), Dst had its maximum positive value of 11γ at 07 – 08, and no negative Dst value occurred during the following six days. For the two intense substorms on December 20, 1967, at 11 – 12 and 12 – 13, the Dst maximum at 18 U.T. did not exceed −25 gammas and six hours later Dst values became positive.

For this class of intense substorms, the intensity and frequency of occurrence of polar substorms is not related in any direct way to the growth and decay of the main phase of the geomagnetic storm.

Summary and conclusions

Four well-defined polar substorms occurred on December 5, 1968. The second of these, at 08 – 10 U.T., believed to be a double substorm, was analyzed in some detail. Both December 4 and 5 were moderately disturbed days, with Ap's of 21 and 25. The ssc at 0633 on December 5 could be expected to enhance the conductivity in the polar region (Obayashi and Jacobs, 1957). The main phase of the geomagnetic storm which followed the ssc was small, and Dst did not exceed −48 gammas.

The storm developed around 08 U.T. with a rayed auroral arc in the midnight sector at $\Phi \sim 64°$, and negative H bays at stations in and near the auroral zone in the midnight and early morning sectors. At Byrd, Antarctica, conjugate to Great Whale River, large micropulsational activity began in dY/dt at 0810. The westward surge was identified on the Co and PB magnetograms at 0824. In the initial phase (0800 – 0824) a westward electrojet flowed in the dark sector north of Na, south of GWR and north of Me. In the daylight sector a less intense eastward current flowed at the auroral zone latitude.

In the expansive phase of the storm (0824 – 0918) a westward current apparently flowed at all longitudes, as the auroral oval expanded rapidly to the west, north and east. In the early morning sector (at Na) the oval expanded to the south at 0835. The expansion of the oval to the north and east was noted at BL at 0857. The expansion to the north in the midnight sector produced a small negative indentation on the X trace at MLB at 0836. The sharp negative H bay of 2,000 gammas recorded at MLB at 0905 is attributed to a second burst of substorm activity a few hundred km to the southeast around 09 U.T. The observed maximum of the northern expansion was at 0909, when the equivalent line currents for RB and MLB were at 78° dp. latitude. The equivalent current plots for this phase of the storm are in good agreement with the Akasofu model with the polar electrojet flowing westward all around the oval and the eastward currents in the daylight and evening sector apparently resulting from return or leakage currents from the west electrojet. Values deduced from the magnetic effects for the velocity of the westward surge (1.1 km/sec) and for the maximum width of the oval in the midnight sector of an intense substorm (15°) agree fairly closely with those found in the literature. The direction of current flow in the oval was found to be parallel to the auroral zone a few hours after local midnight, as noted previously by Kamide *et al.* (1969).

In the recovery phase of the storm the poleward contraction of the oval is very rapid (about twice the rate of the previous expansion) until 1003. All data for the recovery phase indicate that the centre of the storm had returned by 1003 to the BL-GWR area near the pre-breakup position, considerably east of the local midnight meridian. By 1030 the position of the oval relative to its position prior to the storm is that predicted by the effect of the earth's rotation.

The intensification of the storm and the movement to the west and north of the storm centre during the expansion phase are clearly reflected in the table of maximum ΔZ. The ambiguity in the maximum ΔZ data for the recovery phase of the storm is a result of the lack of magnetic data, and emphasizes the impossiblity of carrying out a precise analysis of the development of polar substorms with the existing network of magnetic observatories.

The changing orientation of the equivalent current vector at Th which was always well inside the polar cap, represents very closely the time development of the storm. The time of maximum storm intensity, and the expansion and recovery phases of both the 08 U.T. and 11 U.T. substorms, as indicated by the Th vector, are in close agreement with deductions from other data. It is concluded that the average position of the auroral oval changes with the rotation of the earth from one substorm to the next, if the substorms are separated by a few hours in time.

The Afonina-Feldstein (1969) test was not sufficient to distinguish between the two models of equivalent current flow, owing to the lack of stations in the 09 – 10 and 18 – 20 LT sectors. However, there is some indication the SD-type current systems exist prior to the westward surge and following the end of the substorm.

A class of intense substorms for the years 1962 – 1969 was identified from the occurrence on the Mould Bay ($\Phi \sim 79^\circ$) magnetograms of indented positive bays in the horizontal component during the midnight hours. As the bays have periods of 1 – 2 hours typically, the hourly range is a convenient index for identifying such magnetic substorms. These substorms occurred mainly in the winter and equinox, and were significantly most numerous in the years immediately preceding sunspot minimum. Maximum occurrence as indicated by the MLB, BL, and RB records, was in 1963.

No clear relationship was found between the Dst index and the class of substorms for which $-\Delta H$ was greater than 500 gammas at MLB. Most of these substorms were associated with the main phase of small geomagnetic storms. However the Dst index for these storms did not exceed −88 gammas except for one storm which occurred five hours after local midnight. No increase in Dst was evident in the case of two substorms which occurred within less than one hour of each other. In one case no negative value of Dst was listed for a period of six days following the substorm. These results were unexpected, and suggest an inverse relationship between the occurrence of intense polar substorms and the development of a ring-current.

Acknowledgments

Copies of magnetograms were supplied by World Data Centres A and B, University of Alaska, and Danish Meteorological Institute. Total force recordings for Ice Island T3 and the British Arctic Expedition Ice Island were obtained from the Lamont-Doherty Geological Observatory of Columbia University. Auroral information was supplied by Dr. A.G. McNamara, National Research Council of Canada. The program for the equivalent current vectors was written by Dr. P.H. Serson, Division of Geomagnetism, Ottawa. The map shown in Figure 1 was originally drawn by computer using a program developed by Dr. L. Law, Division of Geomagnetism. Mr. C. Watkiss, summer student, digitized the magnetograms and supervised the plotting for Figure 2.

References

Afonina, R.G., and Ya I. Feldstein. 1969. Form of the equivalent current system of polar geomagnetic disturbances. *Geomag. and Aeron.* Translated and produced by Scripta Technica Inc. for the A.G.U., 9:142-144.

Akasofu, S.-I. 1968. Polar and magnetospheric substorms. Astrophysics and Space Science Library, 2, D. Reidel Publishing Co., Dordrecht, Holland.

Akasofu, S.-I. *et al.* 1970. Results from a meridian chain of observatories in the Alaskan Sector (I). Preprint of *Report of Geophysical Institute*, Univ. of Alaska.

Akasofu, S.-I., S. Chapman, and C.-I. Meng. 1965. The polar electrojet. *J. Atmos. Terr. Phys.*, 27:1275-1305.

Akasofu, S.-I., and C.-I. Meng. 1967. Auroral activity in evening sector. *J. Atmos. Terr. Phys.*, 29:1015.

Akasofu, S.-I., and C.-I. Meng. 1968. Low latitude negative bays. *J. Atmos. Terr. Phys.*, 30:227.

Akasofu, S.-I., and C.-I. Meng. 1969. A study of polar magnetic substorms. *J. Geophys. Res.*, 74:293-313.

Bostrom, R. 1967. Currents in ionosphere and magnetosphere. *Birkeland Symposium on Aurora and Magnetic Storms*, 445-457. Edited by A. Egeland and J. Holtet, Paris.

Cloutier, P.A. *et al.* 1970. Detection of geomagnetically aligned currents associated with an auroral arc. *J. Geophys. Res.*, 75:2595-2600.

Feldstein, Ya. I. 1963. Some problems concerning the morphology of auroras and magnetic disturbances at high latitudes. *Geomag. and Aeron.*, 3:183.

Feldstein, Ya. I., and A.N. Zaytsev. 1965. Disturbed solar-diurnal variations at high latitudes during the IGY, *Geomag. and Aeron.*, 5:367-374.

Fukushima, N. 1969. Spatial extent of the return current of the auroral zone electrojet, Part I. *Rep. Ionos. Space Res.*, Japan, 23:209-218.

Fukushima, N. 1969. Equivalence in ground geomagnetic effect of Chapman-Vestine's and Birkeland-Alfven's electric current systems for polar magnetic storms. *Rep. Ionos. Space Res.*, Japan, 23:219-227.

Iijima, T., and T. Nagata. 1968. Constitution of polar magnetic disturbances. *Rep. Ionos. Space Res.*, Japan, 22:1-24.

Kamide, Y., T. Iijima, and N. Fukushima. 1969. Microstructure of auroral zone electrojet. *Rep. Ionos. Space Res.*, Japan, 23:185-208.

Kim, J.S., and C.S. Wang. 1967. Orientation of aurora and the concurrent magnetic disturbance. *J. Atmos. Terr. Phys.*, 29:829-837.

Loomer, E.I., and G. Jansen van Beek. 1969. The effect of the solar cycle on magnetic activity at high latitudes. *Pub. Dom. Obs.*, 37:169-180.

Meng, C.-I., and S.-I. Akasofu. 1967. Intense magnetic bays inside the auroral zone (II). *J. Atmos. Terr. Phys.*, 29:1305-1310.

Obayashi, T., and J.A. Jacobs. 1957. Sudden commencements of magnetic storms and atmospheric dynamo action. *J. Geophys. Res.*, 62:589-616.

Rostoker, G. 1966. Midlatitude transition bays and their relation to the spatial movement of overhead current systems. *J. Geophys. Res.*, 71:79-95.

Rostoker, G. *et al.* 1970. Development of a polar magnetic substorm current system. *Report of Univ. of Alberta*, Killam Earth Sciences, May 8.

Walker, J.K. 1964. Space-time associations of the aurora and magnetic disturbance. *J. Atmos. Terr. Phys.*, 26:951-958.

Whitham, K. 1965. Geomagnetic variation anomalies in Canada. *J. Geophys. Res.*, 17:481-498.

PUBLICATIONS of the EARTH PHYSICS BRANCH

VOLUME 41–NO. 11

canadian national report on geomagnetism and aeronomy

C. M. CARMICHAEL and T. R. HARTZ

DEPARTMENT OF ENERGY, MINES AND RESOURCES

OTTAWA, CANADA 1971

Cat. No.: M70-41/11

canadian national report on geomagnetism and aeronomy

C. M. CARMICHAEL and T. R. HARTZ

Foreword

This report has been prepared on behalf of the Associate Committee on Geodesy and Geophysics, National Research Council of Canada, by C.M. Carmichael, Chairman of the Geomagnetism Subcommittee, and T.R. Hartz, Chairman of the Aeronomy Subcommittee. It briefly reviews studies in geomagnetism and aeronomy by Canadian institutions for the period 1967 through 1970, and the bibliography lists published reports under appropriate headings. More complete résumés of work during this period may be found in the Canadian Geophysical Bulletin, vols. 20, 21, 22, 23, published by the National Research Council of Canada.

Avant-propos

Le présent rapport a été préparé pour le Comité mixte de géodésie et de géophysique du Conseil national de recherches du Canada, par MM. C.M. Carmichael, président du sous-comité de géomagnétisme, et T.R. Hartz, président du sous-comité de l'aéronomie. Les auteurs passent en revue brièvement les études sur le géomagnétisme et l'aéronomie menées par des institutions canadiennes entre 1967 et 1970. La bibliographie donne la liste des rapports publiés sous des rubriques appropriées. On trouvera des résumés plus complets des travaux réalisés au cours de cette période dans le *Canadian Geophysical Bulletin,* vol. 20, 21, 22, 23, publié par le Conseil national de recherches du Canada.

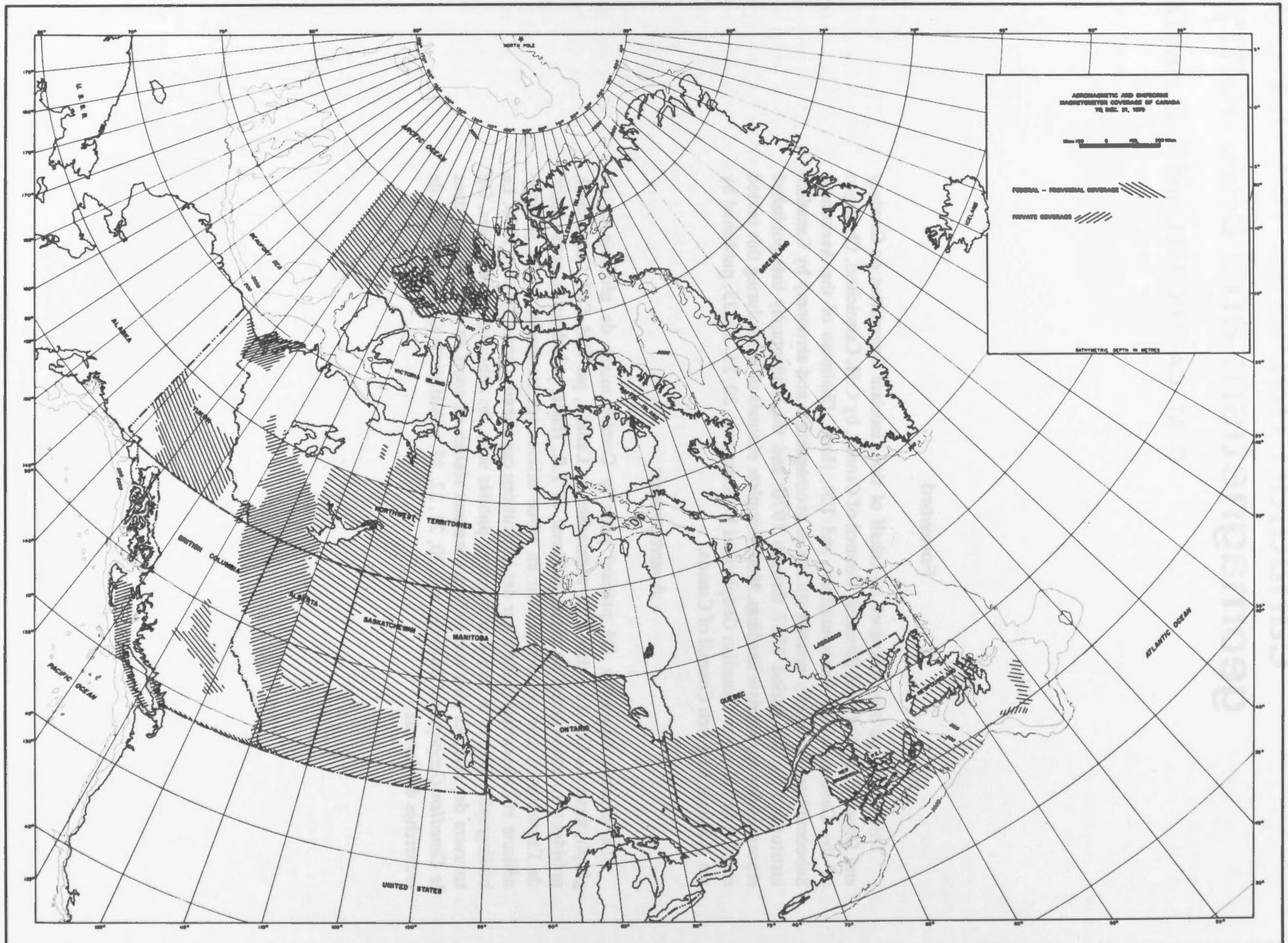

Figure 1. Detailed total-intensity surveys completed by December 31, 1970, including low-level aeromagnetic and shipborne coverage by government agencies and private industry.

Part I — Geomagnetism

Compiled by C. M. Carmichael

Department of Geophysics
The University of Western Ontario
London, Canada

1. Magnetic surveys

(a) Instruments. The development of geomagnetic instruments continued at the Earth Physics Branch (formerly the Dominion Observatory), the Geological Survey of Canada, the Defence Research Establishment Pacific (formerly the Pacific Naval Laboratories), the National Aeronautical Establishment, the University of Alberta, and the Bedford Institute of Oceanography. Significant improvements were made in the performance of fluxgate and Overhauser effect magnetometers, and the design of air-cored and high-permeability cored induction coils. Much attention was given to digital recording and data processing equipment, both for survey vehicles and for fixed stations. The development of a magnetometer capable of recording on the sea floor is in progress.

(b) Surveys. As part of a continuing study of secular change, the Earth Physics Branch observed at 95 of its repeat stations, and established six new stations. Recording instruments were operated at each station for several days.

High-level three-component airborne surveys covered the Canadian Arctic Archipelago, Northern Greenland and the Arctic Ocean up to the north pole, as well as British Columbia and an area of 1,500,000 square miles of the northeast Pacific Ocean.

Surveys of total intensity by ship have included the continental shelf on Canada's east coast, a detailed survey of the mid-Atlantic ridge at 45°N, and the path followed by the *Hudson* on its 'Around the Americas' expedition, with detailed work in the Queen Charlotte Islands region and the Beaufort Sea.

Detailed low-level airborne surveys of total intensity were carried out under the federal-provincial government plan, and by many private companies. Figure 1 shows the area of Canada covered to date by detailed total intensity surveys, including surveys by ship.

(c) Magnetic charts. During the period over 2,000 aeromagnetic maps were published on a routine basis and in addition anomaly and other charts were published for special areas. These include: anomaly charts of the Scandinavia, Greenland, Iceland region, a Z residual chart of the eastern Pacific Ocean and British Columbia, a magnetic map of Canada with the regional gradient removed, a Natural Resources chart of the magnetic data over the continental shelf and an Isogonic Chart of Canada 1970, showing lines of equal declination and its rate of change.

(d) Interpretation. The classical methods of depth-to-basement determination from isolated magnetic anomalies are still widely used, especially in ocean areas, but the period under review saw the development of several new techniques of interpretation. Downward continuation, digital filtering, and power spectra techniques have been applied by the Geological Survey of Canada and the Universities of Alberta, Dalhousie, Manitoba, and Toronto. Modelling of structures with self-adjusting computer programs has become a practical tool for interpretation at the Bedford Institute of Oceanography and the above institutions. Considerable success in correlating aeromagnetic maps with the properties of exposed rocks has been achieved by the University of Manitoba and the Geological Survey of Canada. In situ measurements of susceptibility are made, and oriented core specimens are taken for laboratory analysis.

Interest in magnetic information as an aid to understanding crustal structure on a broad scale was greatly stimulated by the publication of a magnetic anomaly map of Canada, compiled by the Geological Survey of Canada by combining 3,400 detailed total intensity map sheets. It shows striking correlations between broad-scale magnetic features which are not apparent on the original map sheets, and the boundaries between adjacent geological provinces.

2. Magnetic observatories

On April 1, 1965 the observatory at Agincourt was closed because of steadily increasing industrial interference, thus ending 70 years of records from that location, and the continuous record from the Toronto region which began in 1840. Agincourt observatory is replaced by Ottawa observatory. The observatories in St. John's, Newfoundland and Ottawa began operation in June 1968. The other eight observatories operated continuously during 1967-70: Alert, Baker Lake, Churchill, Great Whale River, Meanook, Mould Bay, Resolute Bay and Victoria. Microfilms of the magnetograms from these observatories are deposited in World Data Centres on a monthly basis, with provisional baselines and scale values. K indices and hourly ranges are reported to the appropriate commissions of IAGA. Automatic magnetic observatories are in operation at St. John's, Ottawa, Meanook and Victoria.

As part of a co-operative program with NASA, four unattended magnetic recording stations were set up in 1969 in the vicinity of the point conjugate to the synchronous satellite ATS-5 and have been kept operational since then. Three component fluxgate magnetometers with analogue records have been used at these stations.

The mu-metal cored coil magnetometers built by the Defence Research Establishment Pacific have been operated unattended over several week periods at Ralston in southern Alberta since June 1969.

The Bedford Institute of Oceanography has operated a station recording total intensity since July 1967. Monthly data reports are published, including 10-minute and hourly mean values as well as reproductions of the magnetograms. In addition several temporary stations were located by Bedford Institute during 1967-70 along the east coast of Canada for monitoring diurnal variations in this area.

The observatory operated by University of Alberta at Leduc, Alberta has been in operation since 1967. The data from the observatory, mainly high frequency magnetic and telluric variations, have been used for magnetotelluric studies.

During the summer months, the University of Alberta has operated eight magnetic recording stations, located on a geomagnetic meridian passing through Edmonton and extending from magnetic latitude 58.7°N to 77.0°N. The outputs of three-component fluxgate magnetometers are recorded on digital tape every two seconds, for studies of polar substorms and pulsations.

3. Magnetotellurics and electromagnetic induction

Experimental and theoretical studies of magnetotellurics and electromagnetic induction in the earth have been conducted by the Earth Physics Branch, the Bedford Institute of Oceanography, and the Universities of Alberta, British Columbia, Dalhousie, McGill, Memorial, Toronto, and Victoria. Areas in which experiments have been conducted include the British Columbia coast, the Rocky Mountains and southern Alberta, the Canadian Arctic Islands, the eastern continental shelf, Iceland, and Newfoundland.

The University of Alberta, in co-operation with the University of Texas, has operated an array of over 40 three-component magnetometers for several seasons across the Rocky Mountain Front, from the U.S.-Mexican border to the Trans-Canada Highway. Local conductivity anomalies as well as the broad-scale conductivity changes associated with the Rocky Mountain and Wasach Fronts have been investigated. The variation field of polar substorms have been separated by surface integral methods into parts of external and internal origin. Magnetotelluric surveys of buried rift-valley structures in southern Alberta have been completed, and the observations fitted with theoretical two-dimensional models.

The coast induction effect has been studied intensively at the Bedford Institute of Oceanography, using data from eastern Canada and from India. Equipment for magnetotelluric recording on the sea floor is being developed.

In a co-operative program, the University of British Columbia and the Earth Physics Branch have continued the mapping of conductivity anomalies in British Columbia and have published several quantitative interpretations. The Earth Physics Branch has extended its observations and interpretations of crustal induction in the Canadian Arctic. In co-operation with Cambridge University, a survey of geomagnetic variations in the British Isles has been completed.

The University of Toronto completed the analysis of its observations made in Iceland, and carried out magnetotelluric measurements across the Superior-Churchill boundary in northern Manitoba. Model studies of the distortion of a uniform electric current field by conductive bodies were completed, and applied to the Alert anomaly.

At the University of Victoria, a scaled laboratory model has been used to study the electromagnetic variations over an inhomogeneous conductor in the fields of overhead line currents, sheet currents, and vertical or horizontal magnetic dipoles. Theoretical investigations, in addition to the above models, include the development of a general theory of induction in a many-layered earth, and the computation of the magnetic fields induced by internal ocean wave movements.

4. Paleomagnetism and rock magnetism

There has been a healthy growth in Canada's activities in paleomagnetic and rock magnetic research. New laboratories have been set up at the University of Alberta and Dalhousie University. The research groups at the Earth Physics Branch and at Memorial University have moved into new quarters specifically designed for geomagnetic research. As of 1970 research groups or individuals engaged in rock magnetism and paleomagnetism are located at the Earth Physics Branch, the Geological Survey of Canada, and the following universities: Alberta, Dalhousie, Laval, Manitoba, Memorial, Toronto, and Western Ontario.

The paleomagnetic efforts of these groups have been directed toward obtaining paleodirectional data, and to a lesser extent, paleointensity data from a variety of Precambrian and Phanerozoic formations exposed in Canada. A number of these groups however, are studying material collected in other countries and have studied dredge and core material from the ocean basins with specific emphasis on mid-Atlantic Ridge material from 45°North. Two of the laboratories have also done work on lunar samples obtained in the Apollo program.

The rock magnetic investigations of these groups have involved optical and electron microscopy of the magnetic grains in some of the units which have been studied paleomagnetically. Other workers are studying the magnetic properties of pyrrhotite, single domain magnetites, pseudo single domain grains and super-paramagnetism in fine-particle hematite.

Paleomagnetic measurements made at the University of Alberta on samples from northern Labrador and a comparison with six other rock units between Labrador and Colorado suggest that the earth's field was essentially dipolar and that no large relative movements have occurred within a large part of North America in the last 1400 m.y. The high coercivity of the Michikamau anorthosite is attributed to single domain needles of magnetite.

The Earth Physics Branch concluded from measurements on samples from Canada that a significant polar drift may have occurred between the Upper Mississippian and Lower Permian, and that two geomagnetic reversals took place in the Upper Mississippian. Secondary magnetization of red beds during diagenesis was studied. An investigation of the magnetic properties of dredge and core samples from the mid-Atlantic Ridge was completed, and an explanation advanced for the spectacular remanence anomaly associated with the Median Valley. Samples collected in Vancouver Island indicate that it was not part of the continent in the early Mesozoic.

Results obtained by the Geological Survey of Canada from samples in Labrador indicate that the North American Jurassic pole position differs significantly from its Cretaceous and Triassic equivalents. Thellier's double heating technique was applied to about 100 specimens representative of basic igneous rocks across the country. This study gave an estimate of the intensity of the earth's field in the Geological past and yielded unique support for the dipole hypothesis. Magnetization measurements on samples from the Sudbury Irruptive have been published and paleointensity work is in progress. The thermomagnetic properties of banded manganiferous sediments from the mid-Atlantic Ridge have been studied. A fundamental study on synthetic pyrrhotites is under way to establish the magnetic phase relations.

A remanent magnetic study in the central and southern sectors of the Labrador Trough has been conducted at the Université Laval. The rocks are mainly iron formations of Proterozoic age belonging to the Churchill Province.

The University of Manitoba has studied the magnetic properties of samples from the Kenora area, Ontario and southeastern Manitoba to determine the nature of the magnetization associated with the regional magnetic anomaly system.

The random field demagnetization of rocks has been investigated at Memorial University. Results suggest that conversion to a steady-field method is feasible under certain restraints. Measurements on Ordovician and Cambrian rocks from Newfoundland and Labrador have been compared with results from samples in Ireland and Britain. Similar studies on Tertiary rocks in Greenland, Iceland and Baffin Island are in progress.

Measurements have been made at the University of Toronto of time effects and of magnetization and demagnetization curves for isothermal, anhysteretic and thermo remanences. A good fit to the isothermal results can be obtained if particle interactions are treated by a Preisach model. Research on the thermomagnetic properties of materials containing dispersions of very fine ferromagnetic grains has shown that the Néel theory, modified to include the effects of grain interactions can quantitatively explain nearly all experiments. An almost continuous record of the magnetic directions for a period of about .2 m.y. has been obtained from portions of the Eocene Green River Shale. In addition to the expected secular variation, there is a strong suggestion that significant transients up to 90° occur in the earth's field with a duration of a few thousand years. Lunar samples from Apollo 11 and 12 were intensively studied. Many of the iron-bearing minerals have been identified and the results suggest that a weak field of a few thousand gammas was present on the moon 3.6 x 10^9 years ago.

An outline of the paleomagnetic field intensity from 2.5 x 10^9 yrs to the present has been obtained mainly from stable basalt lavas at the University of Western Ontario. The field in the Precambrian had an intensity equal to or greater than the present value; in the early Paleozoic it is quite weak, then increased during the Mesozoic and Tertiary to present values. Paleomagnetic results from samples dredged from the mid-Atlantic Ridge indicate that the magnetic anomalies are due to a thin veneer of fine-grained basalt only a few hundred metres thick and that the remainder of the oceanic crust is relatively coarse grained, differentiated and only weakly magnetic. Studies of the middle Keweenawan in the Lake Superior region show only one reversal of magnetic polarity. The sensitivity of the conglomerate test as used in paleomagnetic studies has been statistically analyzed.

5. Geomagnetic disturbances and pulsations

Studies of geomagnetic disturbances and micropulsations have been conducted at the Universities of Alberta, British Columbia, and McGill, and at the Defence Research Establishment Pacific and the Earth Physics Branch.

The University of Alberta made detailed studies of the development and morphology of polar magnetic substorms, and of the polarization of micropulsations, using data from the array of eight special recording stations described in Section 2 above. Investigations continued of conjugate point phenomena, the propagation of VLF signals and micropulsations, and changes in the magnetic field in the magnetotail. Computer programs were developed to model current systems from observed electron densities and electric fields.

The University of British Columbia, in co-operation with other groups, has investigated natural electromagnetic noise in the sub-audible frequency range. Detailed studies of the conjugate stations Byrd and Great Whale River have revealed differences in the Pc4 and Pc5 generation mechanisms. Investigations of hydromagnetic emissions continued. The testing of a high voltage dc transmission line with ground return, connecting Vancouver Island with the mainland, was used to make a large-scale resistivity survey.

Experimental and theoretical work on the magnetic noise produced by ocean waves was carried out by the Defence Research Establishment Pacific. Micropulsations recorded at ground stations in southern Alberta and Resolute, NWT are being compared with results from an airborne caesium magnetometer survey.

The Earth Physics Branch studied the correlation of magnetic variations recorded at Byrd in the Antarctic and at five stations in an east-west line in the region conjugate to Byrd. An analysis was published of the effect of the solar cycle on diurnal and seasonal patterns of irregular magnetic activity at four high-latitude magnetic observatories. A detailed study of the intense polar substorm of 5/12/68 was based on magnetograms from 26 auroral and polar cap observatories. Micropulsations in the Pc3, 4 range recorded simultaneously at Ottawa, Meanook, Baker Lake and Resolute Bay have been analyzed for diurnal and latitudinal variation in occurrence, amplitude, and period. Special recordings in connection with the solar eclipse of March 7, 1970, revealed a pronounced decrease in the relative amplitude of magnetic fluctuations at the location of totality, compared with stations 200 km distant.

Correlations between the vertical telluric currents recorded at Mont St-Hilaire and Thetford Mines, both in Quebec, have been studied at McGill University.

6. Theoretical studies of the main field

The following studies of the main magnetic field and electromagnetic coupling in planetary interiors were carried out, at the beginning of the period under review, at the Universities of Waterloo and Western Ontario, and later, at Memorial University and the University of British Columbia.

A simplified model of electromagnetic core-mantle interaction, neglecting magnetic diffusion, predicts extremely weak damping of the Chandler wobble, in agreement with an earlier detailed study. It also shows that the accompanying core motion may be strongly damped electromagnetically.

A laboratory model of thermal convection under a central force was operated successfully. The central force is provided by an intense alternating electric field gradient acting on the dielectric fluid. With cylindrical geometry, the behaviour is similar to that of a Benard fluid layer wrapped around a cylinder. A model with spherical geometry and rotation is under construction.

Geomagnetic coupling of the earth's core-mantle system appears able to explain the observed rate of change of obliquity arising from the lunisolar precessional torque, but the simple model also predicts a nontidal deceleration of axial rotation much greater than is observed.

The electrical properties of Jupiter's interior have been inferred from changes in the rotation of the Great Red Spot, on the assumption of electromagnetic coupling between a molecular hydrogen mantle and a liquid metallic hydrogen core.

Bibliography – Geomagnetism

1. Magnetic surveys

(a) Instruments

Andersen, F., 1969. An automatic magnetic observatory (abstract). *IAGA Bull.*, 26, 106.

Barrett, D.L., 1968. Frequency modulation of a shipborne proton magnetometer signal due to the hydrodynamic instability of the towed vehicle. *J. Geophys. Res.*, 73, 5327-5334.

Gough, D.I. and J.S. Reitzel, 1967. A portable three-component magnetic variometer. *J. Geomagn. Geoelectr.*, Japan, 19, 203-216.

Hannaford, W.W., F. Andersen and P.H. Serson, 1967. A new three-component airborne magnetometer, Paper 1-9, in IAGA Symposium 'Recent developments in geoelectric and geomagnetic instrumentation', St. Gall, Switzerland. *IAGA Bull. 24.*

Hood, P., 1970. Magnetic surveying instrumentation; a review of recent advances: *Proc. Canadian Centennial Conference on Mining and Groundwater Geophysics,* Niagara Falls, October 22-27, 1967; *Mining and Groundwater Geophysics* 1967, Ed. L.W. Morley; Economic Geology Series No. 26, *Geol. Surv. Can.* 3-31.

Primdhal, F., 1970. The fluxgate mechanism. *I.E.E.E. Trans. Magnetics,* MAG-6, 376-383.

Serson, P.H., 1969. Equipment with digital recording possibilities. (Abstract only, *IAGA Bull.*, 26, 103.)

Trigg, D.F., 1967. Automatic zero suppression circuit. Paper 1-15 in IAGA Symposium 'Recent developments in geoelectric and geomagnetic instrumentation'. St. Gall, Switzerland. *IAGA Bull. 24.*

——1970. An automatic zero suppression circuit. *Review of scientific instruments.* 41, 1298-1302.

Trigg, D.F., W.W. Hannaford and L.K. Law, 1967. A portable proton precession magnetometer. Paper 1-5 in IAGA Symposium 'Recent developments in geoelectric and geomagnetic instrumentation', St. Gall, Switzerland, *IAGA Bull. 24.*

Washkurak, S., 1967. Overhauser magnetometer progress report. *Geol. Surv. Can.*, Paper 67-1B, 10.

Whitham, K., 1968. Gauss-Lamont method; elements of geomagnetic field; measurement of geomagnetic field; magnetic compass; proton precession magnetometer. *International Dictionary of Geophysics,* Pergamon Press.

(b) Surveys

Clark, J.F., 1969. Magnetic surveys at West Hawk Lake, Manitoba, Canada. (Abstract only, *"Meteoritics"* the Journal of the Meteoritical Society, 4, 268.)

Fenwick, D.B., M.J. Keen, C.E. Keen and A. Lambert, 1968. Geophysical studies of the continental margin northeast of Newfoundland. *Can. J. Earth Sci.*, 5, 483-500.

Godby, E.A., P.J. Hood and M.E. Bower, 1968. Aeromagnetic profiles across the Reykjanes Ridge southwest of Iceland. *J. Geophys. Res.*, 73, 7637-7649.

Godby, E.A., R.C. Baker, M.E. Bower and P.J. Hood, 1966. Aeromagnetic reconnaissance of the Labrador Sea. *J. Geophys. Res.*, 71, 511-517.

Hannaford, W. and G.V. Haines, 1969. A three-component aeromagnetic survey of the Nordic countries and the Greenland Sea. *Pub. Dom. Obs.* 37 No. 5.

Hood, P.J., 1967. Magnetic surveys over the North Atlantic Ocean. *Geol. Surv. Can.* Paper 67-41, 225-226.

——1967. Geophysical surveys of the continental shelf south of Nova Scotia. *Maritime Seds.*, 3, 6-11

——1967. Geologists probe Scotian Shelf. *Oilweek*, 18, 31-34.

——1967. Magnetic surveys of the continental shelves of eastern Canada. *Geol. Surv. Can.* Paper 66-15, 19-32.

Hood, P.J., M.E. Bower and E.A. Godby, 1969. Magnetic surveys in Hudson Bay: 1965 oceanographic project in earth science symposium on Hudson Bay. *Geol. Surv. Can.* Paper 68-53, 272-291.

——1968. Magnetic surveys in Hudson Bay. *Oilweek*, 19, 15.

Hood, P.J. and P. Sawatzky, 1969. Aeromagnetic investigations of the North Atlantic Ocean. *Geol. Surv. Can.* Paper 69-1, Part A, 89-90.

Hood, P.J., P. Sawatzky and M.E. Bower, 1967. Progress report on low-level aeromagnetic profiles over the Labrador Sea, Baffin Bay, and across the North Atlantic Ocean. *Geol. Surv. Can.* Paper 66-58.

——1968. Aeromagnetic investigations of Baffin Bay, the North Atlantic Ocean, and the Ottawa area. *Geol. Surv. Can.* Paper 68-1A, 79-84.

——1967. Low level aeromagnetic profiles over the Labrador Sea, Baffin Bay, and across the North Atlantic Ocean. *Geol. Surv. Can.* Paper 67-1A, 206.

Kornik, L.J., 1968. Regional magnetic susceptibility survey in Manitoba and Saskatchewan. *Geol. Surv. Can.* Paper 68-1B, 18-22.

Morley, L.W., A.S. MacLaren and P.J. Hood, 1968. Low-level aeromagnetic and ship magnetometer investigations. In *Science, History and Hudson Bay*, edited by C.S. Beals, 688, Queen's Printer, Ottawa.

Sawatzky, P., 1969. Choice of a light twin-engine aircraft for high resolution magnetometer surveying. *Geol. Surv. Can.* Topical Report, 136, 20.

Serson, P., E. Dawson, J.F. Clark and G.V. Haines, 1968. Ground and high-level aeromagnetic observations. Chapter 10, in *Science, History and Hudson Bay*, edited by C.S. Beals, 642-687, Queen's Printer, Ottawa.

Serson, P.H., 1968. Airborne magnetic surveys for Canada and Scandinavia. Presented at *IAGA–WMS Symposium* "Description of the Earth's magnetic field", Washington, D.C., October 22-25.

(c) Charts

Dawson, E., 1967. The requirement for an international reference magnetic field. Paper III-93, IAGA-146, St. Gall, Switzerland. *IAGA Bull. 24.*

——1968. A comparison of eight models proposed for an international geomagnetic reference field with Canadian data. Presented at *IAGA–WMS Symposium* "Description of the Earth's magnetic field", Washington, D.C., October 22-25.

Haines, G.V., 1967. A Taylor expansion of the geomagnetic field in the Canadian Arctic. *Pub. Dom. Obs.*, 35, No. 2.

——1968. Polynomial estimation of certain geomagnetic quantities, applied to a survey of Scandinavia. *Pub. Dom. Obs.*, 37, No. 4.

Haines, G.V., W. Hannaford and P.H. Serson, 1970. Magnetic anomaly maps of the Nordic countries and the Greenland and Norwegian seas. *Pub. Dom. Obs.*, 39, No. 5.

Sucksdorff, C., P. Serson and V. Rasanen, 1968. Magnetic charts of Finland for 1965. Studies in *Earth Magnetism*, No. 21, Finnish Meteorological Institute, Helsinki.

(d) Interpretation

Andrieux, P. and J.F. Clark, 1969. Application des méthodes électriques de prospection à l'étude du cratère d'Holleford. *Can. J. Earth Sci.*, 6, 1325-1337.

Caner, B., 1969. Long aeromagnetic profiles and crustal structure in western Canada. *Earth Planet. Sci.* Letters, 7, 3-11.

Clark, J.F., 1969. Magnetic profiles at Holleford, eastern Ontario. *Proc. Geol. Assoc. of Canada*, 20, 24-29.

Gough, D.I., 1967. Magnetic anomalies and crustal structure in the eastern Gulf of Mexico. *Bull. Amer. Assoc. Petrol. Geol.*, 51, 200-211.

Gough, D.I. and J.R. Heirtzler, 1969. Magnetic anomalies and tectonics of the Cayman Trough. *Geophys. J.*, 18, 33-49.

Gough, D.I. and H. Porath, 1970. Long-lived thermal structure under the southern Rocky Mountains. *Nature*, 226, 837-839.

Grant, A.C. and K.S. Manchester, 1970. Geophysical investigations in the Ungava Bay-Hudson Strait region of northern Canada. *Can. J. Earth Sci.*, 7, 1062-1076.

Hall, D.H. and P. Dagley, 1970. An analysis of the smoothed aeromagnetic map of Great Britain and Northern Ireland. *Institute of Geological Sciences*, Natural Environment Research Council, Rept. 70/10, 9 p. plus map.

Hood, P.J., 1967. Detectability of diabase dykes by aeromagnetic surveys. *Geol. Surv. Can.*, Paper 67-1B, 3-9.

—1967. Mineral exploration: trends and developments in 1966. *Can. Min. J.*, 88, 217-242.

Hood, P. and E. Bower, 1970. Labrador Sea: low-level aeromagnetic investigations in 1969. *Geol. Surv. Can.* Paper 70-1, Part A, 76-78.

—1970. Aeromagnetic profile from Cape Cargenholm, Baffin Island to Red Head, Greenland. *Geol. Surv. Can.* Paper 70-1, Part B, 37-39.

Hood, P.J. and D.N. Skibo, 1968. Vertical gradient studies: dipping dyke case and Euler's differential equation. *Geol. Surv. Can.*, Paper 68-1B, 14-18.

Keen, M.J., D.L. Barrett, G.N. Ewing, B.D. Loncarevic and K.S. Manchester, 1967. The continental margin of eastern Canada. *Proc. Symposium on Geology along the North Atlantic*, Gander, Newfoundland.

Kornik, L.J., 1969. Aeromagnetic extension of the Churchill-Superior Boundary in Manitoba. *Geol. Surv. Can.* Paper 69-1, Part B, 31-33.

—1969. An aeromagnetic study of the Moak Lake-Setting Lake structure in northern Manitoba. *Can. J. Earth Sci.*, 6, 373-381.

—1969. Regional magnetic susceptibility survey in Manitoba and Saskatchewan. *Geol. Surv. Can.* Paper 69-1, Part A, 92.

—1969. A magnetic interpretation of the eastern portion of the Athabasca Formation. *Geol. Surv. Can.* Paper 69-1, Part B, 29-31.

—1970. Aeromagnetic survey of the Athabasca Formation: a quantitative interpretation. *Can. Min. J.*, 91, 50-53.

MacLaren, A.S. and B.W. Charbonneau, 1968. Characteristics of magnetic data over major subdivisions of the Canadian Shield. *G.A.C. Proc.*, 19, 57-65.

McGrath, P.H., 1969. Magnetic susceptibility and natural remanent magnetization of selected rock outcrops in southern New Brunswick (21G, H, J). *Geol. Surv. Can.* Paper 69-1. Part A, 93-97.

—1968. An interpretation of the Miramichi Bay magnetic anomaly, New Brunswick. *Maritime Seds.*, 4, 11-13.

—1970. Magnetic investigations of the Charlotte and Pokiok intrusions, southern New Brunswick. *G.A.C. Proc.*, 21, 25-32.

McGrath, P.H. and D.H. Hall, 1969. Crustal structure in northwestern Ontario: Regional magnetic anomalies. *Can. J. Earth Sci.*, 6, 101-107.

McGrath, P.H. and P.J. Hood, 1968. Thin dipping dyke: a rapid graphical method of magnetic interpretation. *Geol. Surv. Can.* Paper 68-1B, 22-29.

—1969. A computerized method of magnetic interpretation for dyke anomalies. *Geol. Surv. Can.* Paper 69-1, Part B, 39-40.

—1970. The dipping dyke case: a computer curve-matching method of magnetic interpretation. *Geophysics*, 35, 831-848.

Naidu, P.S., 1968. Spectrum of the potential field due to randomly distributed sources. *Geophysics*, 33, 337-345.

—1968. An example of linear filtering in aeromagnetic interpretation. *Geophysics*, 33, 602-612.

Phillips, J.D., J.M. Woodside and C.O. Bowin, 1969. Magnetic and gravity anomalies in the central Red Sea, in "Hot brines and recent heavy metal deposits in the Red Sea," edited by E.T. Degens and D.A. Ross, Springer-Verlag, 98-113.

Ross, D.I., 1967. Magnetic and bathymetric measurements across the Pacific-Antarctic Ridge south of New Zealand. *New Zealand J. of Geology and Geophysics*, 10, 1452-1465.

Ruffman, A. and J.M. Woodside, 1970. The odd-twins magnetic anomaly and its possible relationship to the Humber Arm Klippe of western Newfoundland, Canada. *Can. J. Earth Sci.*, 7, 326-337.

Serson, P., W. Hannaford and G.V. Haines, 1968. Magnetic anomalies over Iceland, *Science*, 162, 355.

2. Magnetic observatories

Auld, D.R. and P.H. Andersen, 1967. Record of observations at Victoria magnetic observatory 1965. *Pub. Dom. Obs.*, 35, No. 6.

—1968. Record of observations at Victoria magnetic observatory 1966. *Pub. Dom. Obs.*, 37, No. 3.

Auld, D.R. and I.W. Fetterley, 1970. Record of observations at Victoria magnetic observatory 1968. *Pub. Dom. Obs.*, 39, No. 9.

Auld, D.R. and D.G. Holmes, 1970. Record of observations at Victoria magnetic observatory 1967. *Pub. Dom. Obs.*, 38, No. 6.

Cook, A.B. and G.A. Brown, 1967. Record of observations at Meanook magnetic observatory 1965. *Pub. Dom. Obs.*, 35, No. 3.

—1968. Record of observations at Meanook magnetic observatory 1966. *Pub. Dom. Obs.*, 36, No. 4.

Cook, H.E., A.B. Cook and R.G. Madill, 1967. Record of observations at Meanook magnetic observatory 1946. *Pub. Dom. Obs.*, 17C, No. 1.

—1969. Record of observations at Meanook magnetic observatory 1947-48. *Pub. Dom. Obs.*, 17C, No. 2.

Cook, H.E. and A.B. Cook, 1970. Record of observations at Meanook magnetic observatory 1951-52. *Pub. Dom. Obs.*, 17C, No. 3.

Cook, H.E., A.B. Cook and R.G. Madill, 1970. Record of observations at Meanook magnetic observatory 1949-50. *Pub. Dom. Obs.*, 17C, No. 4.

Cook, A.B. and S.J. Sprysak, 1970. Record of observations at Meanook magnetic observatory 1967. *Pub. Dom. Obs.*, 39, No. 1.

Darker, W.R. and D. McKeown, 1967. Record of observations at Agincourt magnetic observatory 1965. *Pub. Dom. Obs.*, 35, No. 9.

—1968. Record of observations at Agincourt magnetic observatory 1966. *Pub. Dom. Obs.*, 36, No. 5.

—1970. Record of observations at Agincourt magnetic observatory 1967. *Pub. Dom. Obs.* 37, No. 10.

Evans, A.E., 1970. Record of observations at Resolute Bay magnetic observatory 1967. *Pub. Dom. Obs.*, 38, No. 1.

—1970. Record of observations at Mould Bay magnetic observatory 1967. *Pub. Dom. Obs.*, 38, No. 3.

—1970. Record of observations at Alert magnetic observatory 1967. *Pub. Dom. Obs.*, 38, No. 4.

Evans, A.E., E.I. Loomer and G. Jansen van Beek, 1968. Record of observations at Alert magnetic observatory 1966. *Pub. Dom. Obs.*, 36, No. 7.

—1968. Record of observations at Baker Lake magnetic observatory 1966. *Pub. Dom. Obs.*, 36, No. 6.

—1969. Record of observations at Resolute Bay magnetic observatory 1966. *Pub. Dom. Obs.*, 36, No. 8.

Jansen van Beek, G., 1969. Record of observations at Fort Churchill magnetic variometer station 1964-65. *Pub. Dom. Obs.*, 37, No. 8.

—1970. Record of observations at Fort Churchill magnetic variometer station 1966. *Pub. Dom. Obs.*, 38, No. 5.

—1970. Record of observations at Fort Churchill magnetic variometer station 1967. *Pub. Dom. Obs.*, 39, No. 8.

—1970. Record of observations at Baker Lake magnetic observatory 1967. *Pub. Dom. Obs.*, 38, No. 2.

Loomer, E.I., 1970. Record of observations at Great Whale River magnetic observatory 1967. *Pub. Dom. Obs.*, 37, No. 9.

Loomer, E.I., A.E. Evans and G. Jansen van Beek, 1968. Record of observations at Mould Bay magnetic observatory 1966. *Pub. Dom. Obs.*, 36, No. 9.

3. Magnetotellurics and electromagnetic induction

Auld, D. and B. Caner, 1970. Telluric hourly values of DC component at Victoria for 1966/1967. *Pub. Dom. Obs.*, 39, No. 3.

Beal, H.T. and J.T. Weaver, 1970. Calculations of magnetic variations induced by internal ocean waves. *J. Geophys. Res.*, 75, 6848-6852.

Caner, B., 1970. Electrical conductivity structure in western Canada and petrological interpretation. *J. Geomagn. Geoelectr.*, Japan, 22, 113-129.

Caner, B. and R.D. Auld, 1968. Magneto-telluric determination of upper mantle conductivity structure at Victoria, B.C. *Can. J. Earth Sci.*, 5, 1209-1220.

Caner, B., P.A. Camfield, F. Andersen and E.R. Niblett, 1969. A large-scale magnetotelluric survey in western Canada. *Can. J. Earth Sci.*, 6, 1245-1261.

Caner, B., W.H. Cannon and C.E. Livingstone, 1967. Geomagnetic depth-sounding and upper mantle structure in the Cordillera region of western North America. *J. Geophys. Res.*, 72, 6335-6351.

Caner, B., G.K.C. Clarke and J.J. Lajoie, 1970. Sharp lateral discontinuities in the electrical conductivity structure of the lower crust and upper mantle (abstract). *Trans. Am. Geophys. U.*, 51, 743.

Dosso, H.W., 1969. Analogue model study of electromagnetic variations over an anisotropic conductor. *J. Geomagn. Geoelectr.*, Japan, 21, 673-679.

Dosso, H.W. and J.A. Jacobs, 1968. Analogue model measurements of electromagnetic variations in the near field of an oscillating line current. *Can. J. Earth Sci.*, 5, 23-29.

Dyck, A.V., 1968. Analogue model studies of magnetic and electric field variations over a non-homogeneous earth. *Univ. Toronto, M.Sc. Thesis.*

Gough, D.I. and J.S. Reitzel, 1969. Magnetic deep sounding and local conductivity anomalies. In "The application of modern physics to the Earth and planetary interiors", edited by S.K Runcorn, *Wiley-Interscience*, 139-153.

Hermance, J.F., 1968. Model studies of the coast effect on geomagnetic variations. *Can. J. Earth Sci.*, 5, 515-522.

Hermance, J.F. and G.D. Garland, 1968. Magneto-telluric deep-sounding experiments in Iceland. *Earth and Plan. Sci.* Letters, 4, 469-474.

——1968. Deep electrical structure under Iceland. *J. Geophys. Res.*, 73, 3797-3799.

Hyndman, R.D. and D.W. Hyndman, 1968. Water saturation and high electrical conductivity in the lower continental crust. *Earth and Plan. Sci.* Letters, 4, 427-432.

Jones, F.W. and A.T. Price, 1970. The perturbations of alternating geomagnetic fields by conductivity anomalies. *Geophys. J.*, 20, 317-334.

Lajoie, J.J. and B. Caner, 1970. Geomagnetic induction anomaly near Kootenay Lake – a strike-slip feature in the lower crust? *Can. J. Earth Sci.*, 7, 1568-1578.

Nabetani, S. and D. Rankin, 1969. An inverse method of magnetotelluric analysis for a multi-layered earth. *Geophysics*, 34, 75-86.

——1970. A method of estimation of dimensional effects on electromagnetic induction fields in the earth. *J. Min. Coll. Akita Univ.*, Sec. A., IV, 5, 15-18.

Niblett, E.R., 1968. Magnetotellurics. *International Dictionary of Geophysics*, Pergamon Press.

Niblett, E.R. and K. Whitham, 1970. Multi-disciplinary studies of geomagnetic variation anomalies in the Canadian arctic. *J. Geomagn. Geoelectr.*, Japan, 22, 99-111.

Niblett, E.R., K. Whitham and B. Caner, 1969. Electrical conductivity anomalies in the mantle and crust in Canada. In "The application of modern physics to the Earth and planetary interiors", edited by S.K. Runcorn, *Wiley-Interscience*, 155-172.

Porath, H., D.W. Oldenburg and D.I. Gough, 1970. Separation of magnetic variation fields and conductive structures in the western United States. *Geophys. J.*, 19, 236-260.

Praus, O. and V. Petr, 1969. Magnetotelluric calculations for the interaction of polarized fields with anisotropic layered media. *Can. J. Earth Sci.*, 6, 759-769.

Ramaswamy, V. and H.W. Dosso, 1969. Analogue model studies of a horizontal magnetic dipole over a conducting earth (abstract). *Trans. Am. Geophys. U.*, 50, 606.

Rankin, D. and S. Nabetani, 1969. The electromagnetic impulse response of the earth and its resistivity structure. *J. Min. Coll.*, Akita University, Sec. A., 4, 3.

Rankin, D. and I.K. Reddy, 1969. A magnetotelluric study of resistivity anisotropy. *Geophysics*, 34, 438-449.

——1970. Polarization of the magnetotelluric field over an anisotropic earth. *Pageoph.* 78, 58-65.

Reitzel, J.S., D.E. Gough, H. Porath and C.W. Anderson, 1970. Geomagnetic deep-sounding and upper mantle structure in the western United States. *Geophys. J.*, 19, 213-236.

Srivastava, S.P. 1966. Theory of the magnetotelluric method for a spherical conductor. *Geophys. J.*, 11, 373-387.

—1967. Magnetotelluric two and three-layer master curves. *Pub. Dom. Obs.*, **35**, No. 7.

Vozoff, K. and R.M. Ellis, 1966. Magnetotelluric measurements in southern Alberta. *Geophysics*, **31**, 1153-1157.

Weaver, J.T. and D.J. Thomson, 1970. The field induced in a two-layer conductor by a magnetic dipole. *Can. J. Phys.*, **48**, 71-79.

Wilhjelm J., 1968. Non-random influence of external sources on a geomagnetic induction anomaly in the northern part of Greenland. *Geophys. J.*, **16**, 259-273.

Wright, J.A., 1970. Anisotropic apparent resistivities arising from non-homogeneous, two-dimensional structures. *Can. J. Earth Sci.*, **7**, 527-531.

Yukutake, T., 1967. Electromagnetic induction in a conductor bounded by an inclined interface. *Pub. Dom. Obs.*, **35**, No. 8.

4. Paleomagnetism and rock magnetism

Brooke, J., E. Irving and J.K. Park, 1970. The mid-Atlantic Ridge near 45°N. XIII. Magnetic properties of basalt bore-core. *Can. J. Earth Sci.*, **7**, 1515-1527.

Carmichael, C.M., 1968. An outline of the intensity of the paleomagnetic field of the earth. *Earth and Plan. Sci.* Letters, **3**, 351-354.

—1970. The mid-Atlantic Ridge near 45°N. VI. Magnetic properties and opaque mineralogy of dredged samples. *Can. J. Earth Sci.*, **7**, 239-256.

Carmichael, C.M. and H.C. Palmer, 1968. Paleomagnetism of the Late Triassic, North Mountain Basalt of Nova Scotia. *J. Geophys. Res.*, **73**, 2811-2822.

Christie, K.W. and D.T.A. Symons, 1969. Apparatus for measuring magnetic susceptibility and its anisotropy. *Geol. Surv. Can.* Paper 69-41, 10.

Currie, K.L. and A. Larochelle, 1969. A paleomagnetic study of volcanic rocks from Mistastin Lake, Labrador, Canada. *Earth Planet. Sci.* Letters, **6**, 309-315.

Deutsch, E.R., J. Roy and G.S. Murthy, 1967. An improved Astatic magnetometer for paleomagnetism. *Can. J. Earth Sci.*, **4**, 1270-1273.

Deutsch, E.R. and C.R. Somayajuly, 1970. Paleomagnetism of Ordovician ignimbrites from Killary Harbour, Eire. *Earth Planet. Sci.* Letters, **7**, 337-345.

Dunlop, D.J., 1968. Experimental test of the Preisach-Neel model of interacting single domain grains. *Physics* Letters A, **27A**, 617.

—1968. Monodomain grain theory – experimental verification. *Science*, **162**, 256-257.

—1968. The remanent magnetism of rocks containing interacting single domain ferromagnetic grains. *Univ. Toronto, Ph.D. Thesis.*

Evans, M.E., 1968. Magnetization of dykes: a study of the paleomagnetism of the Widgiemooltha dyke suite, western Australia. *J. Geophys. Res.*, **73**, 3261.

Evans, M.E. and M.W. McElhinny, 1969. An investigation of the origin of stable remanence in magnetite-bearing igneous rocks. *J. Geomagn. Geoelectr.*, Japan, **21**, 757.

Evans, M.E., M.W. McElhinny and A.C. Gifford, 1968. Single domain magnetic and high coercivities in a gabbroic intrusion. *Earth Planet. Sci.* Letters, **4**, 152.

Evans, M.E. and M.L. Wayman, 1970. An investigation of small magnetic particles by means of electron microscopy. *Earth and Planet. Sci.* Letters, **9**, 365-370.

Goldstein, M.A., E.E. Larson and D.W. Strangway, 1969. Paleomagnetism of a miocene transition zone in southeastern Oregon. *Earth Planet. Sci.* Letters, **7**, 231-239.

Gough, D.I., 1967. Notes on rock sampling for paleomagnetic research. In "Methods in paleomagnetism", ed. D.W. Collinson, K.M. Creer and S.K. Runcorn, *Elsevier*, 3-7.

—1967. The spinner magnetometer at Salisbury. In "Methods in palaeomagnetism", ed. D.W. Collinson, K.M. Creer and S.K. Runcorn, *Elsevier*, 119-130.

Heirtzler, J.R., X. LePichon and J.G. Baron, 1966. Magnetic anomalies over the Reykjanes Ridge. *Deep Sea Research*, **13**, 427-443.

Hood, P., 1970. Sea-floor spreading and continental drift. *Can. Geographical J.*, **80**, 32-36.

Hood, P.J. and H. Gross, 1967. Field test of a new in situ susceptibility meter. *Geo. Surv. Can.* Paper 67-1A, 145-146.

Hood, P.J. and D.F. Sangster, 1967. The Carey Foster in situ susceptibility meter. *Geol. Surv. Can.* Paper 65-22, 17 p.

Irving, E., 1967. Evidence for paleomagnetic inclination error in sediments. *Nature*, **213**, 283-284.

—1967. Paleomagnetic evidence for shear along the Tethys. In "Aspects of Tethyan Biogeography", edited by C.G. Adams and D.V. Ager. *Systematics Association Publication*, 7, 59-76.

—1968. Measurement of polarity in oceanic basalt. *Can. J. Earth Sci.*, 5, 1319-1321.

—1970. The mid-Atlantic Ridge at 45°N. XIV. Oxidation and magnetic properties of basalt; review and discussion. *Can. J. Earth Sci.*, 7, 1528-1538.

Irving, E. and W.A. Robertson, 1968. The distribution of continental crust and its relations to ice-ages. (*NASA* Special Pub.) History of the Earth's Crust, edited by R.H. Pinney; publisher, Princeton University Press, New York.

—1969. Test for polar wandering and some possible implications. *J. Geophys. Res.*, 74, 1026-1036.

Irving, E., W.A. Robertson and F. Aumento, 1970. The mid-Atlantic Ridge near 45°N. VI. Remanent intensity, susceptibility, and iron content of dredged samples. *Can. J. Earth Sci.*, 7, 226-238.

Irving, E. and J.L. Roy, 1968. Intensité et stabilité d'aimantation des basaltes de l'Oregon et Washington et leurs applications à l'expansion du fond de l'océan et à d'autres problèmes géophysiques. *Can. J. Earth Sci.*, 5, 907-913.

Jones D.L. and M.W. McElhinny, 1967. Stratigraphic interpretation of palaeomagnetic measurements on the Waterberg red beds of South Africa. *J. Geophys. Res.*, 72, 4171-4179.

Jones, D.L., M.E.R. Walford and A.C. Gifford, 1967. A palaeomagnetic result from the Ventersdorp lavas of South Africa. *Earth Planet. Sci.* Letters, 2, 155-158.

Kristjansson, L.G., 1970. Paleomagnetism and magnetic surveys in Iceland. *Earth Planet. Sci.* Letters, 8, 101-108.

Larochelle, A., 1967. The palaeomagnetism of the Sudbury diabase swarm. *Can. J. Earth Sci.*, 4, 323-331

—1967. A re-examination of certain statistical methods in palaeomagnetism. *Geol. Surv. Can.* Paper 67-18.

—1967. Further considerations on certain statistical methods in palaeomagnetism. *Geol. Surv. Can.* Paper 67-26.

—1967. Palaeomagnetic directions of a basic sill in Prince Edward Island; preliminary data on the palaeomagnetism of the North Mountain Basalt, N.S. *Geol. Surv. Can.* Paper 67-39.

—1968. Paleomagnetism of the Monteregian Hills: New results. *J. Geophys. Res.*, 73, 3239-3246.

—1968. L'application de la statistique au paléomagnétisme, *Geol. Surv. Can.* Paper 68-59.

—1969. Paleomagnetism of the Monteregian Hills: Further new results. *J. Geophys. Res.*, 74, 2570-2575.

—1969. Preliminary results of a study of the paleomagnetism of the Sudbury Irruptive. *Geol. Surv. Can.* Paper 69-19.

—1969. A re-evaluation of the paleomagnetic data from the Manicouagan Group of Lower Triassic igneous rocks. *Geol. Surv. Can.* Paper 69-1, Part B, 33-37.

—1970. Note on the paleomagnetism of two diabase dykes of Anticosti Island. *GAC Bull.*

Larochelle, A. and K.W. Christie, 1967. An automatic 3-magnet or Biastatic magnetometer. *Geol. Surv. Can.* Paper 67-28.

Larochelle, A. and K.L. Currie, 1967. Palaeomagnetic study of igneous rocks from the Manicouagan Structure, Quebec. *J. Geophys. Res.*, 72, 4163-4169.

Larochelle, A. and E.W. Pearce, 1968. On a possible source of error in determining the remanent magnetization of cylindrical rock specimens with a Biastatic magnetometer. *Geol. Surv. Can.* Paper 68-62.

Larochelle, A. and E.J. Schwarz, 1970. Magnetic properties of lunar sample 10048-22. *Geochim. Cosmochim. Acta*, Suppl. 1, 3, 2305-2308. (Also in *Science*, 167, 700-701, 1970.)

Larson, E.E., Ozima, Mituke, Ozima, Minoru, T. Nagata and D. Strangway, 1969. Stability of remanent magnetization of igneous rocks. *Geophys. J.*, 17, 263-292.

Larson, E.E. and D.W. Strangway, 1968. Discussion of paper entitled "Correlation of petrology and natural magnetic polarity in Columbia plateau basalts" by R. Wilson and N. Watkins. *Geophys. J.*, 15, 437-441.

—1969. Magnetization of the Spanish Peaks dyke Swarm, Colorado and Shiprock dyke, New Mexico. *J. Geophys. Res.*, 74, 1505-1515.

McElhinny, M.W., J.C. Briden, D.L. Jones and A. Brock, 1968. Geological and geophysical implications of paleomagnetic results from Africa. Rev. *Geophys*, 6, 201-238.

McElhinny, M.W. and M.E. Evans, 1968. An investigation of the strength of the geomagnetic field in the early Precambrian. *Phys. Earth Planet. Interiors*, 1, 485.

McMahon, B.E. and D.W. Strangway, 1968. Stratigraphic implications of paleomagnetic data from late Paleozoic-early Triassic red beds of Colorado. *Bull. G.S.A.*, 79, 417-428.

—1968. Investigations of the Kiaman magnetic divisions in Colorado red beds. *Geophys. J.*, 15, 265-285.

Murthy, G.S., M.E. Evans and D.I. Gough, 1971. Single-domain thermoremanent magnetization in the Michikamau anorthosite. *Can. J. Earth Sci.*, 8, 361-370.

Murthy, G.S., W.F. Fahrig and D.L. Jones, 1968. The paleomagnetism of the Michikamau anorthositic intrusion, Labrador. *Can. J. Earth Sci.*, 5, 1139-1144.

Palmer, H.C., 1969. The paleomagnetism of the Croker Island complex, Ontario, Canada. *Can. J. Earth Sci.*, 6, 213-218.

—1970. Paleomagnetism and correlation of some Middle Keweenawan rocks, Lake Superior. *Can. J. Earth Sci.*, 7, 1410-1436.

Park, J.K. 1970. Acid leaching of red beds, and its application to the relative stability of the red and black magnetic components. *Can. J. Earth Sci.*, 7, 1086-1092.

Park, J.K. and E. Irving, 1970. The mid-Atlantic Ridge near 45°N. XII. Coercivity, secondary magnetization, polarity, and thermal stability of dredge samples. *Can. J. Earth Sci.*, 7, 1499-1514.

Pearce, G.W. and G.N. Freda, 1969. Magnetization of the Perry Formation of New Brunswick and the rotation of Newfoundland; discussion. *Can. J. Earth Sci.*, 6, 353-355.

Robertson, W.A. 1966. Palaeomagnetism of some Cainozoic igneous rocks from south-east Queensland. *Proc. Roy. Soc.* Queensland, 78, 87-100.

—1967. Manicouagan, P.Q. palaeomagnetic results. *Can. J. Earth Sci.*, 4, 641-649.

—1969. Magnetization directions in the Muskox Intrusion and associated dykes and lavas. *Geol. Surv. Can.* Bull., 167, 1-51.

Robertson, W.A., J.L. Roy and J.K. Park, 1968. Magnetization of the Perry Formation of New Brunswick and the rotation of Newfoundland. *Can. J. Earth Sci.*, 5, 1175-1181.

Roy, J.L., 1967. The Dominion Observatory astatic magnetometer. In Methods in Palaeomagnetism, ed. D.W. Collinson, K.M. Creer and S.K. Runcorn, *Elsevier*, Amsterdam, 69-74.

—1967. Shape and size of weakly magnetized rock specimens. In Methods in Palaeomagnetism, ed. D.W. Collinson, K.M. Creer and S.K. Runcorn, *Elsevier*, Amsterdam, 192-195.

—1967. À-propos du magnétisme des couches rouges de l'est du Canada. *Can. J. Earth Sci.*, 4, 574-577.

—1968. L'application du paléomagnétisme aux tectoniques des appalaches: résultats des couches rouges des appalaches: résultats des couches rouges de Bloomsburg (presented *Roy. Soc. of Canada* meeting, Sherbrooke, June 7).

—1969. Paleomagnetism of the Cumberland Group and other paleozoic formations. *Can. J. Earth Sci.*, 6, 663-669.

Roy, J.L., W.A. Robertson and J.K. Park, 1968. Stability of the magnetization of the Hurley Creek Formation. *J. Geophys. Res.*, 73, 697-702.

Roy, J.L., N.D. Opdyke and E. Irving, 1967. Further paleomagnetic results from the Bloomsburg Formation. *J. Geophys. Res.*, 72, 5075-5086.

Roy, J.L. and J.K. Park, 1969. Paleomagnetism of the Hopewell Group, New Brunswick. *J. Geophys. Res.*, 74, 594-604.

Roy, J.L. and W.A. Robertson, 1968. Evidence for diagenetic remanent magnetization in the Maringouin Formation. *Can. J. Earth Sci.*, 5, 275-285.

Roy, J.L., W.A. Robertson and C. Keeping, 1969. Magnetic "field-free" spaces for paleomagnetism, rock magnetism and other studies. *Can. J. Earth Sci.*, 6, 1312-1316.

Schaeffer, R.M. and E.J. Schwarz, 1970. The mid-Atlantic Ridge near 45°N. Thermomagnetics of dredged samples of igneous rocks. *Can. J. Earth Sci.*, 7, 268-273.

Schwarz, E.J., 1967. Dependence of magnetic properties on the thermal history of natural polycrystalline pyrrhotite, $Fe_{0.89}S$. *J. Geomagn. Geoelectr.*, Japan, 19, 91-101.

—1968. Magnetic phases in natural pyrrhotite $Fe_{0.89}$ and $Fe_{0.91}S$. *J. Geomagn. Geoelectr.*, Japan, 20, 67-74.

—1968. Thermomagnetic properties of banded manganiferous sediment from the mid-Atlantic Ridge. *Can. J. Earth Sci.*, 5, 1517-1518.

——1968. Investigation of Curie temperatures and susceptibilities of Precambrian rocks across a residual aeromagnetic anomaly near Haliburton, Ontario. *Geol. Surv. Can.* Paper 68-18, 30-37.

——1968. A recording thermomagnetic balance. *Geol. Surv. Can.* Paper 68-37.

——1968. Thermomagnetic analysis of some red beds. *Earth Planet. Sci.* Letters, 5, 333-338.

——1969. Thermomagnetics of pyrrhotite. *Geol. Surv. Can.* Paper 69-1, Part B, 41-45.

——1970. Thermomagnetics of lunar dust sample 84/88. *Geochim. Cosmochim Acta.*, Suppl. I, 3, 2389-2397.

——1970. A discussion of thermal and alternating field demagnetization methods in the estimation of paleomagnetic field intensities. *J. Geomagn. Geoelectr.*, Japan, 21, 669-677.

Schwarz, E.J. and K.W. Christie, 1967. Original remanent magnetization of Ontario Potsherds. *J. Geophys. Res.*, 72, 3262-3269.

Schwarz, E.J. and D.T.A. Symons, 1968. On the intensity of the paleomagnetic field between 100 million and 2,500 million years ago. *Phys. Earth Planet. Interiors*, 1, 122-128.

——1969. Geomagnetic intensity between 100 million and 2500 million years ago. *Phys. Earth Planet. Interiors*, 2, 11-18.

Stesky, R.M., 1970. The magnetism of mid-Atlantic Ridge sediments near 45°N. (unpublished M.A. Thesis, Univ. Toronto).

Strangway, D.W., 1970. Moon exploration. *Can. Mining J.*, 91, 110-111.

——1970. Possible electrical and magnetic properties of near-surface lunar materials. *NASA* Sp. Report.

——1970. What we are learning about the solar system from the lunar samples. *Science Forum*, 3, 14-18.

Strangway, D.W., R.M. Honea, B.E. McMahon and E.E. Larson, 1968. The magnetic properties of naturally occurring goethite. *Geophys. J.*, 15, 345-359.

Strangway, D.W., E.E. Larson and M. Goldstein, 1968. A possible cause of high magnetic stability in volcanic rocks. *J. Geophys. Res.*, 73, 3787-3795.

Strangway, D.W., E.E. Larson and G.W. Pearce, 1970. Magnetic properties of lunar samples. *Science*, 167, 691-693.

——1970. Magnetic studies of lunar samples – breccia and fines. Proceedings of the Apollo II Lunar Science Conference, *Geochim. Cosmochim. Acta* 3, 2435-2451.

Strangway, D.W., B.E. McMahon and J.L. Birchoff, 1969. Magnetic properties of minerals from the Red Sea thermal brines, in "Hot brines and recent heavy metal deposits in the Red Sea," edited by E.T. Degens and D.A. Ross, Springer-Verlag, 460-473.

Strangway, D.W., B.E. McMahon and E.E. Larson, 1968. Magnetic paleointensity studies on a recent basalt from Flagstaff, Arizona. *J.Geophys. Res.*, 73, 7031-7037.

Strangway, D.W. and P.R. Vogt, 1970. Aeromagnetic tests for continental drift in Africa and South America. *Earth Planet. Sci.* Letters, 7, 429-435.

Symons, D.T.A., 1969. Paleomagnetism of the late Miocene plateau basalts in the Cariboo region of British Columbia. *Geol. Surv. Can.* Paper 69-43, 16.

——1969. Paleomagnetism of four late Miocene gabbroic plugs in south-central British Columbia. *Can. J. Earth Sci.*, 6, 653-662.

——1969. Geological implications of paleomagnetic studies in the Bella Coola and Laredo Sound map-areas, British Columbia (93D and 103A). *Geol. Surv. Can.* Paper 68-72, 15.

——1970. Paleointensity study of late Miocene igneous rocks from British Columbia. *Can. J. Earth Sci.*, 7, 176-181.

5. Geomagnetic disturbances and pulsations

Gupta, J.C., 1970. Daily variability of the equatorial electrojet current system. *J. Atmosph. Terr. Phys.*, 32, 1159-1164.

Gupta, J.C., R.J. Stening and G. Jansen van Beek, 1970. Micropulsation studies in Pc3, 4 period range at four observatories in Canada. Proceedings of Upper Atmospheric Currents and Electric Fields Symposium. *ESSA ERLTM–ESL* 12, Boulder, Col.

Jacks, B.R., 1966. The origin of hydromagnetic emissions. *Earth Plan. Sci.* Letters, 1, 467-470.

Jacobs, J.A., 1968. Pi events with particular reference to conjugate point phenomena. *Radio Sci.*, 3, 539-544.

Jacobs, J.A. and T. Watanabe, 1967. Theoretical notes on whistlers and periodic emissions in the hydromagnetic regime. *Planet. Space Sci.*, 15, 799-809.

—1968. Conjugate points phenomena associated with energetic particles, magnetic observations. *Ann. Geophys.*, 24, 467-475.

Jacobs, J.A. and C.S. Wright, 1968. The 27-day period of geomagnetic activity in the auroral zones and the inactive intervals during magnetically quiet days. *Earth Plan. Sci.* Letters, 3, 394-398.

—1968. Some features of geomagnetic micropulsations observed during the recent quiet solar years, with particular reference to data obtained at the near conjugate stations Great Whale River and Byrd. *Geophys. J.*, 15, 53-67.

Kakuta, C., 1970. Polar motion and hydromagnetic oscillation in a compressible earth's core. *Publ. Astron. Soc.*, Japan 22, 223-234.

Kitamura, T. and J.A. Jacobs, 1967. Ray paths of Pc 1 waves in the magnetosphere. *Univ. British Columbia Inst. Earth Sci.*, Scientific Report No. 14.

—1967. Determination of magnetospheric plasma density by the use of long period geomagnetic micropulsations. *Univ. Brit. Columbia Inst. Earth Sci.*, Scientific Report No. 17.

—1968. Determination of the magnetosphere plasma density by the use of long period geomagnetic micropulsations. *J. Geomagn. Geoelectr.*, Japan, 20, 33-44.

—1968. Ray paths of Pc 1 waves in the magnetosphere. *Planet. Space Sci.*, 16, 863-879.

Kitamura, T., J.A. Jacobs, T. Watanabe and R.B. Flint Jr., 1968. Investigation of quasi-periodic VLF emissions and their relation to geomagnetic micropulsations. *Nature*, 220, 360-361.

Krishan, S., 1968. Coupling of plasma oscillations and ion-sound waves. *Plasma Physics*, 10, 201.

Krishan, S. and S.S. Rao, 1967. Plasma oscillations of an inhomogeneous cylindrical plasma column. *Nuovo Cimento*, 50, 129-136.

Krishan, S. and A.A. Selim, 1968. Interaction between longitudinal and transverse plasma waves. *Can. J. Physics.* 46, 39.

Lewis, T.J., 1967. The association of phase changes of ionospheric-propagating radio waves and geomagnetic variations. *Can. J. Phys.*, 45, 1549-1563.

Loomer, E.I. and G. Jansen van Beek, 1969. The effect of the solar cycle on magnetic activity at high latitudes. *Pub. Dom. Obs.*, 37, No. 6.

Rankin, D. and I.K. Reddy, 1968. Polarization of micropulsation sources. *Earth and Planet. Sci.* Letters, 3, 347-350.

Rostoker, G., 1967. The polarization characteristics of Pi-2 micro-pulsations and their relation to the determination of possible source mechanisms for the production of nighttime impulsive micropulsation activity. *Can. J. Phys.*, 45, 1319-1334.

—1967. A determining factor in the form of the equivalent current system for geomagnetic bays. *Earth Planet. Sci.* Letters, 2, 119-133.

—1967. The frequency spectrum of Pi-2 micropulsation activity and its relationship to planetary magnetic activity. *J. Geophys. Res.*, 72, 2032-2039.

—1968. A critical study of the possible modes of propagation of Pi 2 micropulsation activity over the earth's surface. *Ann. Geophys.* 24, 253-260.

—1968. The macrostructure of geomagnetic bays. *J. Geophys. Res.*, 73, 4217-4229.

—1968. Relationship between the onset of a geomagnetic bay and the configuration of the interplanetary magnetic field. *J. Geophys. Res.*, 73, 4382-4387.

Rostoker, G. and C.-G. Falthammar, 1967. Relationship between changes in the interplanetary magnetic field and variations in the magnetic field at the earth's surface. *J. Geophys. Res.*, 72, 5853-5863.

Thomson, D.J. and H.W. Dosso, 1968. Analogue model studies of electromagnetic variations in the near field of a vertical magnetic dipole. *C.A.P.* Congress.

Walker, J.K., 1967. Spatial extent of geomagnetic events conjugate to Byrd. *Radio Sci. J.*, 3, 745-750.

—1968. Current densities and field aligned current flow in the aurora. Proceedings of Upper Atmospheric Currents and Electric Fields Symposium, *ESSA, ERLTM–ESL* 12, Boulder, Col.

Watanabe, T., 1968. Conjugate points phenomena associated with energetic particles, magnetic observations. *Ann. Geophys.*, 24, 467-475.

Wright, C.S. and J.A. Jacobs, 1969. Micropulsation activity in recent years with particular reference to data obtained at the near conjugate stations of Great Whale River and Byrd. Publication No. 3, *Killam Memorial Earth Sciences Scientific Series*, Univ. Alberta.

6. Theoretical studies of the main field

Jacobs, J.A., 1967. The Earth's magnetic field. *Tenth Intern. Conf. Cosmic Rays*, Proc. Part A, 235-268.

——1968. The structure of the Earth's core. *Phys. Earth Planet. Int.*, 1, 196-197.

Jacobs, J.A. and G. Atkinson, 1967. Planetary modulation of geomagnetic activity. *Magnetism and the Cosmos*, 402-414, Oliver and Boyd.

Lilley, F.E.M. Magnetoelastic effects in a non-uniform field. Ph.D. Thesis, *Univ. Western Ontario Library*, London, Canada.

Lilley, F.E.M. and C.M. Carmichael, 1968. Electromagnetic damping of elastic waves; experimental results. *Can. J. Earth Sci.*, 5, 825.

——1970. Electromagnetic damping of elastic waves: a simple theory. *Can. J. Earth Sci.*, 7, 1304-1307.

Lilley, F.E.M. and D.E. Smylie, 1968. Elastic wave motion and a non-uniform magnetic field in electrical conductors. *J. Geophys. Res.*, 73, 6527-6533.

Rochester, M.G., 1968. Pertubations in the Earth's rotation and geomagnetic core mantle coupling. *J. Geomagn. Geoelectr.*, Japan, 20, 387-402.

——1970. Core-mantle interactions: geophysical and astronomical consequences. In Earthquake Displacement Fields and the Rotation of the Earth, ed. A.E. Beck, L. Mansinha and D.E. Smylie (D. Reidel, Dordrecht) 136-148.

Thomson, D.J. and J.T. Weaver, 1968. Theoretical calculations of the field induced in the earth by a vertical magnetic dipole. *C.A.P.* Congress.

Thomson, D.J., J.T. Weaver and H.W. Dosso, 1969. Analogue model studies of the separation of a local geomagnetic field into its external and internal parts. National Fall Meeting *AGU.*

Weaver, J.T., 1967. The quasi-static field of an electric dipole embedded in a two-layer conducting half-space. *Can. J. Phys.*, 45, 1981.

——1968. The magnetic field induced by an ocean swell formed from two wave trains. *Def. Res. Est. Pac. Tech.* Memo 68-12, Victoria, B.C.

——1969.The field of a dipole in a non-uniform conducting medium. Proceedings of the Discussion on the Analysis of Magnetic Fields. Eng. Rep. Nos. 17/18, Univ. Nevada.

Part II — Aeronomy

Compiled by T. R. Hartz
Communications Research Centre, Ottawa

1. Airglow

Investigations of the airglow are being carried out in Canada with increased vigour, the number of stations where these studies are being made having increased during the past four years. Impetus for these studies has been provided by the increased availability of rockets and satellites; however, ground-based observations continue to make an important contribution. Much inspiration for both aurora and airglow studies resulted from the Summer Advanced Study Institute "Aurora and Airglow", which was organized by Dr. B.M. McCormac, and held at Queen's University in Kingston, Ontario, in 1970.

Ground-based measurements at the University of Saskatchewan have revealed the pre-dawn enhancement of 6300 Å emissions were successfully made on April 23, 1970 at Fort Churchill.

The twilight decay of the (0-1) band of the infra-red atmospheric system of O_2 $[^1\Delta_g - ^3\Sigma_g^-]$ at 1.58μ has been observed using a Fabry-Perot interferometer. This band has also been observed in the dayglow, the brightness in the zenith at local noon being about 600 kilorayleighs. Height profiles for $[O_2(^1\Delta_g)]$ have been calculated.

Rocket measurements at Churchill of $[O_2(^1\Delta_g)]$ at 1.27μ have revealed a large maximum near 50 km, and also the existence of another layer at 85 km.

1.27μ emissions were measured during day and night using a grating spectrometer and also a filter wheel radiometer fitted with a PbS detector. The exponential time constant for evening decay declined from 50 minutes in January to 31 minutes in May over New Mexico.

Measurements of the relative intensities of the (0-0) and (0-1) bands of O_2 at 1.27μ and 1.58μ gave a value of 46 photon units.

The rate of the reaction:

$$O_2(^1\Delta_g) + O_3 \rightarrow 2O_2 + O$$

has been measured and the rate constant obtained was 4.5 x 10^{-11} exp [−5620/KT] $cm^3 sec^{-1}$ molecule $^{-1}$ with energy units in cal/mole.

Measurements of the deactivation of O_2 ($^1\Delta_g$) by oxygen, nitrogen, argon, water vapour, and carbon dioxide show that oxygen is the only significant quencher of $O_2(^1\Delta_g)$. There appears to be a $T^{\frac{1}{2}}$ temperature dependence.

Recent work on the ozone-oxygen photochemical system at 2537 Å has shown that O_2 ($^1\Delta_g$) is produced entirely by photolysis and the O_2 ($^1\Sigma_g^+$) entirely by energy transfer from O (^{1}D). Measurements of the relative intensities of these two species suggest that the efficiency of O_2 ($^1\Sigma_g^+$) production from the quenching of O (^{1}D) is high (at least 75 per cent).

The rate of the reaction of O(^{1}D) with O_2 was found to be 1.4 times faster than the corresponding reaction with nitrogen. These results indicate that about 25 – 30 per cent of the O (^{1}D) atoms formed by solar photodissociation of ozone will produce $O_2(^1\Sigma_g^+)$ in the atmosphere.

A laboratory source has been used to study the band structure of the O_2 atmospheric system. With this source a spectrum of the (0-0) band at 1.27μ has been obtained at a resolution of 2 Å.

Ground-based observations of the (4-1) and (5-2) bands of OH in the nightglow have been made with a spectrometer having an (S-1) response, and working at 6 Å spectral resolution. A temperature structure in the hydroxyl emitting region has been shown to exist at all seasons with a variation which is in phase with the atmospheric temperature in the same region.

Using a balloon-borne grating spectrometer to monitor the (1-0) band at 2.8μ a diurnal variation of intensity of OH emission was observed over a 24-hour period (extending over two days). A pronounced drop in intensity occurred at sunrise, followed by a slow recovery during the morning to roughly the night-time value.

Some rocket flights have shown that OH emission in the evening twilight apparently exists down to altitudes of 55 km. It can therefore be suggested that the collisional quenching of the vibrationally excited OH molecules is relatively slow. Balloon data also support this conclusion.

Ground-based twilight lithium observations made with a birefringent photometer have shown that unusual enhancements of the red emission occur infrequently throughout the year, the zenith intensity reaching values of about 150 rayleighs during these times. The times of the enhancements do not seem to be correlated with the times of release of lithium vapour into the atmosphere by rockets so that lithium may be deposited into the atmosphere from a natural source. The height of maximum density of the lithium layer appears to be between 90 and 95 km.

A study of the seasonal variation of the height of the twilight sodium layer has suggested an evening-morning effect in which the morning heights appear to be lower than the evening heights, the difference amounting to about 5 km near the times of the equinoxes and 1 km or less near the times of the solstices. The same effect has been noted for twilight lithium. The scale height of free atomic sodium above the layer maximum seems to have a value between 3 and 4 km. Comparisons between twilight sodium abundances at Saskatoon and Victoria, with stratospheric temperatures at several Canadian stations show a high correlation with Arctic stratospheric warmings for Saskatoon sodium but a low correlation with Victoria sodium suggesting that Victoria lies outside the Arctic circulation regime at 90 km.

The identity of the potassium emission in the twilight airglow has been definitely established by using a potassium vapour cell to show that the emission could be completely absorbed.

Studies of He emission at 1.083μ, using a 12 cm spatially scanned Fabry-Perot interferometer have shown that different twilight decays occur during magnetically active, magnetically quiet, and auroral conditions.

An analysis of spectra of the night airglow in the spectral region between 3 and 8 microns has been carried out.

Curves of growth for the R branches of the ν_3 carbon dioxide band at 4.26μ, and the ν_3 methane band at 3.31μ found in solar spectra were prepared from the best known absorption line parameters.

Atmospheric carbon dioxide and methane concentrations in the lower stratosphere derived from recorded solar spectra indicate near uniform mixing over latitudes from 10°N to 75°N.

2. Atmospheric dynamics

The principal centres for studies in atmospheric dynamics include the Universities of Toronto, McGill, Saskatchewan, Victoria and Western Ontario and the Meteorological Branch, Department of the Environment, Toronto.

Theoretical and analytical studies of wave motions including atmospheric tides and shorter period gravity waves have been performed at the Physics Department of the University of Toronto; and in particular, sources of gravity waves, their propagation through realistic atmospheres and their influence upon the momentum and energy balance of the mesosphere and thermosphere have been studied. At the Department of Meteorology, McGill University, model calculations and analytical studies of the propagation of planetary scale waves to heights above 30 km have been performed. The atmospheric dynamics group in the Physics Department, University of Saskatchewan, is investigating coupling between the stratosphere and ionosphere on a seasonal time scale, using radio waves at Saskatoon and meteorological rockets at Cold Lake (Alberta) as probes. The influence of planetary, tidal and gravity waves are involved. Model calculations and analytical studies of dynamical effects upon radio wave reflection processes and ionization changes have been made. The Institute of Space and Atmospheric Studies, University of Saskatchewan and the University of Victoria are conducting co-operative studies of seasonal variations in the twilight sodium emissions, and in particular, are making correlation studies with stratospheric temperatures. The Centre for Radio Science, Western Ontario is making meteor wind measurements.

The Meteorological Branch, Toronto, is conducting theoretical and experimental studies of the interaction between the dynamics and photochemistry of the mesosphere and lower thermosphere. A network for observations of noctilucent clouds has been established. Studies are also made of the effect of density and temperature variations ($\simeq$30–100 km) upon aerospace vehicles.

3. Aurora

3.1 Optical studies of the aurora

Ground based optical studies of the aurora are being conducted by the Universities of Calgary, Saskatchewan, and York and by the National Research Council of Canada. Auroral research of a continuing nature at Churchill ceased in 1970 with the transfer of the scientific staff to Ottawa. A number of field operations have been carried out there, however, and at such locations as Thompson, Gillam, Resolute Bay and Cold Lake to obtain specific auroral measurements associated with balloon, rocket or satellite measurements or for studies of particular auroral phenomena.

Auroral photometers have been operated at the near conjugate stations of Great Whale and Byrd in a National Research Council of Canada project beginning in 1967 and automatic photometers are being installed there. Photoelectric measurements of the auroral spectrum between 1 and 2μ are being made at Calgary and a high speed image intensifier TV system has been developed and used for investigating pulsating aurora.

A chain of patrol spectrograph stations covering the latitude range 55-78° N magnetic has been used to investigate proton and electron precipitation. The spectra show that the region of proton precipitation lies a few degrees equatorward of the electron oval of precipitation before midnight, crossing to the poleward side after 0100 hours. A study of the observed H_β intensity relative to the N_2^+ 4709 Å band has also been made yielding values of less than 0.2 for normal aurora and up to about 3.0 for proton aurora. Spectrometric measurements of Type B red aurora have been carried out and show the intensity of O_2^+ system enhanced by a factor of 2-3 relative to the N_2 1PG, although subsequent independent measurements do not confirm this.

3.2 Radio studies of the aurora

A number of centres have been actively investigating auroral phenomena by radio techniques. Auroral radars have been operated continuously by the National Research Council of Canada at Ottawa, Thompson, Churchill and Great Whale for the study and detailed examination of radio aurora. A bistatic VHF radio system operated in eastern Canada by the University of Western Ontario for the past decade has been used for a study of the rate of occurrence of radio aurora and its diurnal and seasonal characteristics. It has been established that there are two or more fundamentally different types of radio aurora, with ion-acoustic waves generated by the auroral electrojet being responsible for the observed signal amplitudes in the morning hours.

Auroral backscatter recordings from a 42 MHz transmitter were made by the University of Saskatchewan to measure the fading rates and to determine the relation between the scatter bursts and pulsating electron influx.

A study of auroral absorption events in relation to visual aurora and satellite particle measurements has been carried out by the Communications Research Centre using data from a chain of riometer stations in the latitude range 67° – 76° invariant.

3.3 Rocket, balloon and satellite studies

Rockets launched from the Churchill Rocket Range have been used increasingly in auroral studies. The National Research Council of Canada has been a major participant in this area while the Universities of Calgary, Montreal, Saskatchewan, York and Western Ontario have also participated actively.

The general characteristics of particle precipitation during various types and phases of ionospheric disturbances have been determined. Electron energy spectra and angular distributions have been measured in a variety of auroral protons and α-particles yielding evidence for a direct solar wind origin of auroral ions. Extensive measurements of plasma densities and temperature in visual aurora have been obtained.

Balloon borne detectors have been employed to investigate the association between auroral X-rays and particular types of aurora.

The latest ISIS satellite launched in March 1971 includes two auroral photometer experiments measuring 6300 Å and 3914/5577 Å emissions respectively, in addition to the energetic particle experiments of the type included in the ISIS-A and Alouette satellites. Rocket borne photometers too have been used to obtain measurements of the intensity and luminosity profiles of a number of auroral emissions in both the visible and ultraviolet regions. H_β luminosity profile measurements have been used to deduce the nature of the incoming proton spectrum.

4. Cosmic rays and particle physics

Cosmic ray and energetic particle measurements have continued at ground stations and in rockets and satellites. The National Research Council of Canada maintains stations at Ottawa, Resolute and at Churchill (jointly with the University of Texas at Dallas, Texas). The Atomic Energy of Canada Limited maintains a station at Deep River, Ontario and jointly with the National Research Council of Canada is responsible for the stations at Alert and Inuvik in the Arctic Islands and at

Goose Bay, Labrador. The University of Calgary maintains the Sulphur Mountain Station (near Banff, Alberta) and a station at Calgary and the University of Victoria maintains a station at Victoria. The University of Manitoba, Winnipeg has a number of meson telescopes, each telescope consisting of two large ($\sim$ 1.5m) scintillation counters, separated by a distance of several metres.

Most of these stations have a counter or scintillation telescope in addition to the neutron monitor. With the exception of Ottawa, the neutron monitors register rates of the order of a million counts per hour. Data from these stations are distributed to the World Data Centre on a routine basis and exchanged with various groups. The monthly Solar Geophysical Data put out by ESSA Research Laboratories (presently re-named NOAA), US Department of Commerce publishes the data from Churchill, Deep River, Alert, and Calgary and Sulphur Mountain (as of January 1, 1971).

The Division of Physics at the National Research Council of Canada, Ottawa, has recently completed a study of the daily variation of cosmic ray intensity and its relation to the interplanetary magnetic field. The Atomic Energy of Canada Limited has made an extensive cosmic ray latitude survey, which has resulted in a number of publications.

Studies of the low energy part of the particle spectrum including the particles trapped in the magnetosphere and Cosmic Ray studies have been conducted using data from some of the US satellites like Mariners 2, 4, 5, Explorers 33 and 35, and Imp-Ogo series, in collaboration with the US institutions. The cosmic ray gradient in the interplanetary space for protons and alphas, ($E > 50$ MeV) is negative, that is, it increases in going towards the sun. This indicates the solar contribution at low energies and also shows that it is not possible to determine the gradient of galactic cosmic rays even at the time of solar minimum. Study of a number of Solar Cosmic ray events during 1968-1969 is in progress. This is collaborative work between the University of Iowa and the University of Calgary. The data from Explorer 33 and 35 and the neutron monitor data from Calgary and Sulphur Mountain are used. Of particular interest is the low energy alphas and protons ($\sim$ 1 MeV/nucleon) and nuclei of $Z > 2$. The variability of the ratios of these from event to event are being studied with reference to propagation effects.

Nuclear emulsions are also flown on high altitude balloons by the University of Calgary to study primary cosmic rays, particularly in identification of solar neutrons. An excess of 2.2×10^{-2} neutrons/cm^2 sec in the energy range 20-160 MeV was observed from the direction of the sun. Balloon borne counter telescopes are also used by Calgary to study the energy spectra of different charge components of the primary cosmic radiation at different levels of solar activity to study solar controlled modulation processes. Apparatus for the measurement of energy spectrum of primary cosmic ray electrons using balloons at high geomagnetic latitudes is under construction at Calgary. Radio emissions from air showers have been investigated by the University of Calgary at the site of the Dominion Radio-Astrophysical Observatory at Penticton, British Columbia. Of particular interest are the production mechanisms and lateral dependence of the intensity of the radio signal as a function of frequency and its dependence on primary energy.

The time variation of the total detected cosmic radiation as well as that of the cosmic rays of different energies as inferred from the multiplicities of neutrons evaporated from the lead, are studied at the University of Victoria. The University of Manitoba is interested in the study of primaries of energy > 100 GeV. Apart from studies of daily variation, solar as well as sidereal, they are also interested in detecting the elusive quarks, if any are around. A watch is kept, for this purpose, over one of the telescopes.

5. The ionosphere

Studies of the ionosphere are carried on at a number of institutions on Canada. The Defence Research Telecommunications Establishment (DRTE), which has been the primary centre of such studies, was transferred in 1969 to the newly-created Department of Communications and is now called the Communications Research Centre (CRC). Ionospheric research is also done at the National Research Council of Canada, the Universities of Saskatchewan, Western Ontario, British Columbia, and Laurentian, and at RCA Ltd. in Montreal.

The Department of Transport has had responsibility for the standard vertical incidence ionosonde operation and data reduction. In 1969, these functions were transferred to the new Department of Communications.

5.1 Ionospheric sounding

Alouette-I, Alouette-II, and ISIS-I topside sounders continue to operate. A variety of studies are carried out with the data, both in Canada and internationally since the data are available through the World Data Centres. Particular attention has been given in Canada to high latitude effects. Investigations include the high latitude trough, F-region disturbances, and the equatorial anomaly. New analysis techniques have been developed to permit derivation of extremely low electron densities from the topside sounder data.

The third satellite, ISIS-I, was launched on 30 January, 1969 and is operating successfully. Six of the 10 experiments are Canadian. The addition of an onboard tape recorder to this satellite permits the acquisition of data on a much greater geographical scale.

ISIS-II was launched successfully on 31 March, 1971.

Partial reflection sounders for the D-region using 2.66 MHz transmitters have been in operation at Ottawa, Churchill, and Resolute. More recently, a second frequency of 6.275 MHz has been added. These sounders permit daily monitoring of the electron density profiles from 60 to 90 km in quiet conditions and 50 to 80 km in disturbed conditions. The technique provides a very sensitive indicator of solar disturbances.

Partial reflection observations at Saskatoon are directed toward the dynamics of the high atmosphere. Investigations include the effects of magnetic activity, particle precipitation, motions, and the detailed examination of the partial reflection mechanism.

5.2 Transmission of radio waves through the ionosphere

Radio wave absorption data are obtained from a number of riometer stations. In addition, forward scattered signals from meteor trails are employed for absorption measurement and for ionospheric wind and diffusion studies. Beacon transmitters on a number of satellites are analyzed for Faraday rotation, differential absorption, and antenna phase scintillations, to yield data on ionospheric densities, horizontal structure, absorption, and travelling waves. Similarly, beacon transmitters have been ejected from rockets at Churchill to measure auroral ionization and absorption at E-region heights.

5.3 Direct measurements of the ionosphere

In the interval 1967-70, 45 rockets were flown from Churchill by which direct ionospheric measurements were made using Langmuir probes and retarding potential analyzers. These measurements were made in auroral and in quiet ionospheric conditions, and have yeilded high resolution values of electron density, electron temperature, and ionization macro- and micro-structure. Other experiments have measured soft electron fluxes and the fluxes of high energy ionizing particles. Spin stabilized ejected probes have been released from rockets to measure the electric and magnetic fields in the ionosphere.

In addition to Churchill launches, six rocket experiments have been flow from Resolute, in the region of the north magnetic pole, to obtain electron densities by Langmuir probe and radio propagation techniques.

5.4 Radio wave scatter measurements

VHF auroral radars have been operated on a continuous basis for auroral backscatter studies at Ottawa, Thompson, Churchill, and Great Whale. VHF continuous wave bistatic experiments between Ottawa and London, Ontario, have also been used for similar purposes. Positive evidence has been obtained of scatter from ion acoustic waves in aurora, and other mechanisms appear to be present also. The polarization and fading characteristics of backscatter have been examined in detail from Saskatoon. Measurements of radio aurora at UHF were made at the Prince Albert Radar Laboratory, but this installation was closed in 1967.

Incoherent scatter measurements were made at Prince Albert, and more recently Arecibo radar data has been used to obtain ionospheric composition and temperatures.

5.5 Radio noise

Broad-band VLF and swept-frequency LF and HF receivers in the Alouette and ISIS satellites are used to study various noise emissions. Latitudinal and diurnal analyses of 200 KHz whistler-mode signals have shown a correlation with parts of the auroral oval and with the energetic electron fluxes detected on the satellite. Radio noise measurements on rockets launched from Churchill have been made in conjunction with energetic particle detectors. The antennas used for these experiments show interesting impedance variations and amplitude and harmonic modulation of the noise signals which are dependent on the $V \times B$ potential generated.

5.6 The 1970 total solar eclipse

Four rockets were flown from East Quoddy, Nova Scotia, in the path of totality of the 1970 solar eclipse on 7 March. The rockets carried Langmuir probe experiments and a 2.66 MHz radio receiver for electron density measurements in the D and E-regions. Lyman-α and X-ray experiments were provided by the R.S.R.S. (Slough) for the determination of the primary ionizing radiation levels. A 2.66 MHz ground-based partial reflection sounder was installed at the launch site to monitor the D-region electron density variations. A control measurement was obtained by the continuous operation of the 2.66 MHz partial reflection sounder at Ottawa where the eclipse was partial.

6. Laboratory studies

A well attended "Symposium on Laboratory Measurements of Aeronomic Interest" was held at York University in September 1968 under IAGA sponsorship.

The measurement of absolute band strengths using the methods of emission and absorption spectroscopy as well as the interferometric hook method has continued, principally at York University. Absolute band strengths are now available for selected band systems of NO, O_2, CO, SO_2 and NO_2. An extensive recalculation of Franck-Condon factors of over 100 important diatomic molecular band systems including all those of aeronomic importance has been made using realistic potential functions derived from experimental wavelengths. Theoretical studies relating to the factors important in the computation of molecular band intensities continues.

A considerable amount of laboratory work has concerned the problems related to the production and removal of the excited singlet states of atomic and molecular oxygen. Rate constants for the collisional deactivation of O_2 ($^1\Delta$) by N_2, O_2, O_3, N_2O, CO_2, H_2O and Ar have been obtained and the temperature dependence of the deactivation by O_2 and O_3 measured. It has been shown that the photolysis of O_3 at 2537 Å yields O_2 ($^1\Delta$) but not O_2 ($^1\Sigma$) whereas energy transfer from O(^{1}D) leads to $O_2(^1\Sigma)$ but not $O_2(^1\Delta)$. The results show that the quantum efficiency of $O_2(^1\Sigma)$ formation from O(^{1}D) is greater than 60 per cent and, further, that it is approximately equal to the quantum efficiency of $O_2(^1\Delta)$ formation in the photolysis of ozone. The relative rates of destruction of O(^{1}D) in O_2, N_2, O_3 and H_2O were measured.

At the R.C.A. Limited Research Laboratories work of aeronomic interest has included theoretical studies on wave-plasma interactions with a major emphasis on the ionosphere, and on antennas; experimental work on electromagnetic wave propagation in plasmas, with the source exterior, and within (antennas) the plasma; and experiments with flowing plasma used for simulation studies.

In the simulation studies the interaction of a flowing plasma with a magnetic dipole to simulate the boundary region between the earth's magnetosphere and the solar wind produced a boundary width less than, or comparable to, an ion gyro radius. It appears that the large scale features of the boundary can be simulated, but details such as a separate detached shock were not observed. The simulation of spacecraft-environment interactions using a plasma flow provided information that was successfully applied to the Alouette II and ISIS A spacecraft.

The experimental work carried out with electromagnetic waves in plasmas includes the reflection of circularly polarized waves from a plasma, antenna radiation properties at arbitrary angles of incidence, strong field interactions where nonlinear effects become evident, and the radar return from turbulent media.

There has been a continuing effort in the study of antennas in plasmas. A large, uniform, anisotropic plasma has been used to study antenna problems such as impedance, for antennas (short, long and loops) under various plasma conditions. A steady theoretical effort has been maintained on wave-plasma interactions, and on spacecraft-plasma interactions.

7. Magnetospheric disturbances

A number of studies are being carried out on magnetospheric dynamics that are based on a detailed examination of substorm data. While much of this involves magnetic data, energetic particles, aurora and other data are also being studied in close association with substorms and a number of equipment developments have been made to facilitate the gathering of better data.

At the National Research Council of Canada studies have continued of the energetic particle fluxes, based on data from the Alouette and ISIS satellites as well as from several rocket flights. The high latitude flux of electrons and protons in association with substorms has been investigated, in relation to the fluxes in the magnetotail and with regard to acceleration mechanisms. Studies of alpha particles have also been made in order to obtain evidence for a direct entry of solar wind particles. Data have also been studied for direct neutral point entry and neutral point acceleration mechanisms.

The study of ionospheric absorption during substorms has continued at the Communications Research Centre (formerly the Defence Research Telecommunications Establishment) in order to determine the scale and morphology of particle precipitation, and thus the magnetospheric scale of the substorm.

At the Churchill Research Range studies have been made of the auroral electrojet behaviour during substorms using a network of four magnetometers.

At the University of Calgary research is continuing into the characteristics of X-rays, detected with balloon-borne equipment, that are generated during magnetospheric substorm activity, and into their relationship to the aurora and other features of the substorm.

At the University of Alberta digital recording systems have been built for use in recording magnetic data at frequencies up to 0.3 Hz with a sensitivity of $\pm 1\gamma$ over the range $\pm 1000\gamma$. A line of fluxgate magnetometers with such digital recording systems was set up along the geomagnetic meridian from Calgary to Cambridge Bay. The data have been used to study the dependence of P_c micropulsations on latitude, and the results appear consistent with an origin in the Kelvin-Helmholtz instability at the magnetospheric boundary. The data have also been used in a detailed study of magnetic substorms, including such features as the intensification of the southern border of the electrojet, the quasi-periodic bursts of activity at the northern border, multi-current systems, and the broad eastward electrojet in the post-noon sector. In another study using an array of 42 magnetometers, the phase of the D-component was investigated during a substorm and related to the westward travelling surge. A co-operative study with the Royal Institute of Technology, Sweden, has been made on three-dimensional model current systems, and another with the University of Saskatchewan has been undertaken on electric and magnetic field data from a rocket launch into an auroral breakup. Satellite (IMP-1, -2, and -3) magnetometer data have been studied for dynamic effects in the magnetotail during substorms that can be related to distinct phases of the substorm.

Studies have been carried out on the use of hydromagnetic whistlers as a diagnostic tool in the study of the ambient magnetospheric plasma, and densities have been estimated using both cold and warm plasma approximations. Pcl micropulsation characteristics have been studied, and theoretical investigations are underway of wave-particle and wave-wave interactions.

At the University of British Columbia studies are going on of various geomagnetic phenomena. A theoretical investigation of the magnetodynamic approximation for waves in the magnetosphere was carried out, as was an analysis of plasma waves propagating across a steep density gradient. In a collaborative study with the University of California, the relationship between magnetotail field perturbations and Pi micropulsations was studied.

At the Department of Energy, Mines and Resources research into long period micropulsations has been carried out, and Pc3 activity was shown to be strongly correlated with Kp while Pc4 activity was poorly correlated with Kp. A study of the polar electrojet is underway with reference to conditions during substorms.

At Victoria Magnetic Observatory a new micropulsation recording system has been developed using air-core induction coils which produces accurately calibrated data for frequencies up to 10 Hz.

At the University of Saskatchewan rocket released probes have been developed to measure electric and magnetic fields in the ionosphere, and digital recording systems are being built for magnetometer studies.

8. Meteors

The major centres for meteor research are at the National Research Council of Canada, Ottawa, through its Upper Atmosphere Research Section and Springhill Meteor Observatory, and at London, the Centre for Radio Science of the University of Western Ontario. Research which was formerly carried out at the Dominion Observatory and its field stations is now under the auspices of the National Research Council of Canada.

The continuing program of the spectrographic and radio recording of meteors has been supplemented by photo-electric techniques, particularly through the use of television-type systems and image-intensifier devices. Some cases of individual fireballs were studied and meteoroid orbits examined. The Leonid meteor shower has been studied in some detail since several strong returns have occurred in the past decade. A network of cameras covering 7×10^5 square kilometres has been established on the Canadian prairies to patrol the skies for bright meteors. Photographic records will be used to study the influx of these objects and to provide data for rapid recovery of meteorite falls.

The determination of meteoroid mass distribution from radio measurements yielded a discrepancy in results obtained at London by forward-scatter equipment and at Ottawa by back-scatter techniques. Continuous-wave forward-scatter systems have also been used to measure meteor ionization profiles to clarify the ablation and ionization processes in the atmosphere. The effects of upper atmosphere winds on meteor trails have been investigated. Conversely, radar data on meteors have been used to measure winds and to study ionospheric absorption. Concomitant theoretical studies have been carried out.

Various models of micrometeoroid detectors were flown on 17 rockets to determine the flux and distribution of these particles in the upper atmosphere. Two of the payloads, flown during the Geminid meteor shower, included different types of detectors supplied by a number of scientists from other countries.

9. Sun–Earth relations and magnetospheric physics

During late 1969, the University of Alberta, Edmonton and the University of California, Berkeley, had a co-operative study of magnetospheric electric fields; the former provided ground based magnetometer data at a number of launch sites, while the latter were responsible for the balloons equipped with electric field probes.

The University of Alberta is also studying perturbations in the magnetotail associated with polar magnetic substorms. The analysis of magnetic field data from IMP-1 and IMP-2 in the magnetotail suggests a relaxation of sections of magnetotail to a more dipole configuration. There is strong evidence for a magnetotail geometry during substorms which is consistent with magnetic field merging at an X-type neutral point. A joint study of the VELA satellite energetic particle data by University of Alberta and the Los Alamos Scientific Laboratory (University of California) is underway.

A study of the magnetic data from IMP-3 when inside the magnetotail, has shown that there is a thick sheet of magnetic field depression surrounding the neutral sheet and that low frequency magnetodynamic noise appears to propagate preferentially along the magnetic lines of force in the magnetotail.

A study of the relationship between fluctuations in the interplanetary magnetic field and geomagnetic activity has shown that the strength of the geomagnetic activity is a function of the direction of the interplanetary magnetic field in the ecliptic plane; being higher when the interplanetary field is directed away from the sun than when it points towards it.

Hydromagnetic whistlers have been used as a diagnostic tool to determine plasma parameters in the ambient magnetospheric plasma. During a study of the propagation characteristics of ion cyclotron waves in a warm plasma it has been found that the temperature of the plasma is an important variable when the frequency of the hydromagnetic whistler is close to the ion gyro frequency. Plasma densities estimated using the cold plasma approximation are approximately 10-20 per cent lower than those obtained for a warm plasma when the ratio of the thermal velocity of the protons to the Alfven velocity is 0.1.

Theoretical studies at the University of Calgary are concerned with the mechanism and a detailed model of the heating of the outer layers of the sun by shock waves. The study leads to the production of the solar wind in the same formalism. Theoretical work is currently in progress to investigate hydro-magnetic oscillations of the magnetospheric tail to examine possible effects on wave propagation, geomagnetic pulsations, convection and particle precipitation.

The study of Solar Terrestrial Relationships including the problem of the region of modulation of Cosmic Ray variations has led into the quest of solar planetary relationships. The collaborative studies of Calgary and NASA-Goddard Space Flight Center (High Energy Astrophysics Division) have shown solar cycle variation in (a) the intensity of the Great Red Spot of Jupiter and (b) the luminosities of the planets Jupiter, Saturn, Uranus and Neptune. Thus there is direct indication of the observation of solar cycle variation up to 30 AU. The changes in the luminosities are attributed to the EUV from the sun.

The University of Calgary and the Applied Physics Laboratory/Johns Hopkins University, Maryland, USA have completed a study of the differential energy spectra of trapped low energy protons (0.3 to 1.8 Mev) using a year's data of Iowa Satellite Injun V. The study reveals the existence of a quasi-persistent peak in the differential spectrum in the L range 2.0 to 2.6 and the energy range of $\sim$0.38 to 0.72 Mev. The study is also concerned with changes in spectra correlated with geomagnetic activity, and also adds to the general body of evidence favouring diffusion from the solar wind as the primary mechanism for populating the radiation belts.

The Division of Physics, NRC, Ottawa has made use of data from the Alouette II satellite to carry out further studies of the entry of solar particles into the inner part of the earth's magnetosphere. Latitude profiles of solar protons and electrons have been studied and compared with recent cut-off rigidity calculations and with the location of the high latitude boundary of 35 keV outer zone electrons. It has been found that the latitude knee for solar electrons lies 5° to 8° above the knee for low energy (∿ 1 Mev) solar protons and that the location of the electron knee agrees approximately with the 35 keV outer zone boundary. The measurements indicate that a field model could be chosen to give agreement between trajectory calculations and measured knee latitudes for 100 Mev solar protons and 35 keV solar electrons but that lower energy protons penetrate more deeply into the magnetic field than can be accounted for on the basis of these calculations. In some cases intensity changes, not associated with the knee latitude, occur in the lower energy proton distributions at latitudes which coincide approximately with the calculated cut-offs.

Data processing for the ISIS-I satellite has started and some initial studies have begun. ISIS-II was launched on March 31, 1971.

At York University theoretical studies of the effects of superimposed electric fields on particle precipitation into the magnetosphere have been made.

Bibliography Aeronomy

1. Airglow

Bunn, F.E. and H.P. Gush, 1970. Spectrum of the airglow between 4 and 8 microns. *Can. J. Phys.*, 48, 98.

Cogger, L.L. and G.G. Shepherd, 1969. Observations of a magnetic conjugate effect in the OI 6300 Å airglow at Saskatoon. *Planet. Space Sci.*, 17, 1857.

Evans, W.F.J., D.M. Hunten, E.J. Llewellyn and A. Vallance Jones, 1968. Altitude profile of the infrared system of oxygen in the dayglow. *J. Geophys. Res.*, 73, 2885.

Evans, W.F.J., E.J. Llewellyn and A. Vallance Jones, 1969. Balloon observations of the temporal variation of the infrared atmospheric oxygen bands in the airglow. *Planet. Space Sci.*, 17, 933.

Evans, W.F.J. and E.J. Llewellyn, 1970. Molecular oxygen emissions in the airglow. *Ann. Geophys.*, 26, 167.

Evans, W.F.J., H.C. Wood and E.J. Llewellyn, 1970. The transmission of the infrared oxygen emission at 1.27μ in the atmosphere. *Can. J. Phys.*, 48, 747.

Evans, W.F.J., H.C. Wood and E.J. Llewellyn, 1970. Ground-based photometric observations of the 1.27μ band of O_2 in the twilight airglow. *Planet. Space Sci.*, 18, 1065.

Gault, W.A. and H.N. Rundle, 1969. Twilight observations of upper atmospheric sodium, potassium and lithium. *Can. J. Phys.* 47, 85.

Gattinger, R.L., 1968. Observation and interpretation of the O_2 ($^1\Delta_g$ - $^3\Sigma^-_g$) airglow emissions. *Can. J. Phys.*, 46, 1613.

——1969. Observations of the $O_2(^1\Delta_g - {}^3\Sigma^-_g)$ 0,1 band in the day airglow. *Can. J. Phys.*, 47, 367.

——1969. Interpretation of airglow emissions – OH emissions. *Ann. Geophys.*, 25, 825.

Harrison, A.W., 1969. Some observations of twilight He (1.083μ) emission. *Can. J. Phys.*, 47, 1377.

——1969. Helium emission (1.083μ) in sunlit aurora. *Planet. Space Sci.*, 17, 1213.

——1969. The night airglow spectrum 1.02μ – 1.13μ. *Planet. Space Sci.*, 17, 173.

——1970. Altitude profile of airglow hydroxyl emission. *Can. J. Phys.*, 48, 2231.

——1970. Behaviour of hydroxyl emission during aurora. *J. Geophys. Res.*, 75, 1330.

Harrison, A.W., E.J. Llewellyn and D.C. Nicholls, 1970. Night airglow hydroxyl rotational temperatures. *Can. J. Phys.*, 48, 1766.

Haslett, J.C., L.R. Megill and H.I. Schiff, 1969. Rocket measurements of $O_2(^1\Delta_g)$. *Can. J. Phys.*, 47, 2351.

Hunten, D.M., H.N. Rundle, G.G. Shepherd and A. Vallance Jones, 1967. Optical upper atmospheric investigations at the University of Saskatchewan. *Applied Optics*, 6, 1609.

Landshoff, R.K.M., J.L. Magee (Editors) with B.H. Armstrong, D.R. Churchill, B.E. Freeman, S.A. Hagstrom, R.K.M. Landshoff, R.W. Nicholls and O.R. Platas, 1969. Thermal radiation phenomena Volume I, radiative properties of air, pp. xvi + 648, *The Plenum Press*, New York.

Lowe, R.P., 1969. Interferometric spectra of the Earth's airglow from 1.2 to 1.6 microns. *Phil. Trans. Roy. Soc.*, A, 264, 163.

MacDonald, R., H.L. Buijs and H.P. Gush, 1968. Spectrum of the night airglow between 3 and 4 microns. *Can. J. Phys.*, 46, 2575.

Millman, P.M., 1968. A brief survey of upper-air spectra. *Physics and Dynamics of Meteors,* Edited by Kresak and Millman, 84-90.

Moreels, G., W.F.J. Evans, J.E. Blamont and A. Vallance Jones, 1970. A balloon-borne observation of the intensity variation of the OH emission in the evening twilight. *Planet. Space Sci.*, 18, 637.

Neo, Y.P. and H.N. Rundle, 1969. An identification of twilight helium 10,830Å emission with increased resolution and preliminary photometric measurements. *Planet. Space Sci.,* 17, 715.

Shah, G.M., 1969. Enhanced twilight glow caused by the volcanic eruption on Bali Island in March and September, 1963. *Tellus,* 21, 636.

——1969. Study of aerosols in the atmosphere by twilight scattering. *Tellus,* 22, 82.

Shepherd, G.G., 1967. Applications of the Fabry-Perot spectrometer to upper atmospheric spectroscopy. *Journal de Physique,* 28, C2-301. (Colloque C2 Supplement au no. 3-4.)

——1969. Spectroscopic measurements of auroral and airglow temperatures. *Ann. Geophys.,* 25, 666.

——1969. Airglow spectroscopic temperatures. *Atmospheric Emissions,* Edited by B.M. McCormac and A. Omholt, Van Nostrand Reinhold Co., New York.

Speer, R.J., W.R.S. Garton, F.J. Morgan, R.W. Nicholls, L. Goldberg, W.H. Parkinson, E.M. Reeves, T.J.L. Jones, H.J. Baxter, D.B. Shenter and R. Wilson, 1970. Rocket UV flash spectra from the solar eclipse March 7, 1970. *Nature,* 226, 249.

Sullivan, H.M., 1970. Some unusual red twilight emissions. *Ann. Geophys.,* 26, 161.

Sullivan, H.M. and M.G. Roberts, 1968. Height of the twilight sodium layer; evening-morning effect observed at Victoria, British Columbia, from February 1967 to February 1968. *Nature,* 220, 361.

Ticketin, S., G. Spindler and H.I. Schiff, 1967. The production of excited OH ($A\ ^2\Sigma^+$) molecules by the association of ground state oxygen and hydrogen atoms. *Discussions of the Faraday Society,* 55, Toronto.

Vallance Jones, A., 1966. Abundance of metallic atoms in the atmosphere. *Ann. Geophys.,* 22, 189.

Wallis, D.D. and C.D. Anger, 1968. High-altitude observations of a luminous wake behind two Black Brant II rockets. *Can. J. Phys.,* 46, 2753.

Wood, H.C., W.F.J. Evans, E.J. Llewellyn and A. Vallance Jones, 1970. Summer daytime height profiles of the O_2 ($^1\Delta$) concentration at Fort Churchill. *Can. J. Phys.,* 48, 862.

2. Atmospheric dynamics

Belrose, J.S. 1967. The "Berlin" warming. *Nature,* 214, 660.

Chimonas, G., 1969. Wind driven instability in the lower E region. *J. Geophys. Res.,* 74, 4091.

——1970. The equatorial electrojet as a source of long period travelling ionospheric disturbances. *Planet. Space Sci.,* 18, 583.

——1970. Infrasonic waves generated by auroral currents. *Planet. Space Sci.,* 18, 591.

Chimonas, G. and C.O. Hines, 1970. Atmospheric gravity waves launched by auroral currents. *Planet. Space Sci.,* 18, 565.

Chimonas, G. and W.R. Peltier, 1970. The bow wave generated by an auroral arc in supersonic motion. *Planet. Space Sci.,* 18, 599.

Christie, A.D., 1969. Noctilucent clouds in North America. *Progress in Astronautics and Aeronautics,* 22, 241, Academic Press, New York.

——1970. D-region winter anomaly and transport near the mesopause. *J. Atmos. Terr. Phys.,* 32, 35.

Einaudi, F. and C.O. Hines, 1970. WKB approximation in application to acoustic-gravity waves. *Can. J. Phys.,* 48, 1458.

Gregory, J.B., 1968. Solar influences and their variations. American Meteorological Society, *Meteorological Monograph,* 9, 19.

Gregory, J.B. and A.H. Manson, 1969. Seasonal variations of electron densities below 100 km at mid-latitudes. I. Differential absorption measurements. *J. Atmos. Terr. Phys.,* 31, 683.

——1969. Seasonal variations of electron densities below 100 km at mid-latitudes. II. Electron densities and atmospheric circulation. *J. Atmos. Terr. Phys.,* 31, 703.

——1970. Seasonal variations of electron densities below 100 km at mid-latitudes. III. Stratospheric-ionospheric coupling. *J. Atmos. Terr. Phys.,* 32, 837.

Hines, C.O., 1968. A possible source of waves in noctilucent clouds. *J. Atmos. Sci.,* 25, 937.

——1968. Tidal oscillations, shorter period gravity waves and shear waves. *Meteorological Monographs,* 9, 114.

—1968. Some consequences of gravity-wave critical layers in the upper atmosphere. *J. Atmos. Terr. Phys.*, 30, 837.

—1968. An effect of molecular dissipation in upper atmospheric gravity waves. *J. Atmos. Terr. Phys.*, 30, 845.

—1968. An effect of ohmic losses in upper atmospheric gravity waves. *J. Atmos. Terr. Phys.*, 30, 851.

—1968. Applications of gravity-wave theory to upper atmospheric studies. In 'Winds and Turbulence in Stratosphere, Mesosphere and Ionosphere', *North-Holland Publishing Co.*, Amsterdam, p. 364.

—1968. Gravity waves in the presence of winds, shears and dissipative processes. In 'Winds and Turbulence in Stratosphere, Mesosphere and Ionosphere', *North-Holland Publishing Co.*, Amsterdam, p. 356.

—1970. Eddy diffusion coefficients due to instabilities in internal gravity waves. *J. Geophys. Res.*, 75, 3937.

—1968. Motion in the Ionosphere. In 'International Dictionary of Geophysics', Pergamon Press.

Hines, C.O. and W.H. Hooke, 1970. Discussion of ionization effects on the propagation of acoustic-gravity waves in the ionosphere. *J. Geophys. Res.*, 75, 2563.

Johnston, T.W., 1967. Atmospheric gravity wave instability? *J. Geophys. Res.*, 72, 2972.

Manson, A.H., 1968. Coupling effects between the ionosphere and stratosphere in Canada (45°N, 75°W), 1962-1966. *J. Atmos. Terr. Phys.*, 30, 627.

—1969. The effect of solar corpuscular radiation on the 1963 final spring warming in the Antarctic. *J. Atmos. Sci.*, 26, 587.

Pakiam., J.W. and D.W. Johnson, 1967. The effects of particle radiation from a disturbed sun on atmospheric electricity. *Can. J. Phys.* 45, 1337.

Vincent, R.A., 1969. A criterion for the use of the multilayer approximation in the study of acoustic-gravity wave propagation. *J. Geophys. Res.*, 74, 2996.

Whitehead, J.D., 1970. On the reflection of internal gravity waves. *Can. J. Phys.*, 48, 1830.

Wright, J.W. and L.S. Fendor, 1967. Comparison of ionospheric drift velocities by the spaced receiver technique with neutral winds from luminous rocket trails. Space Research VII, *North-Holland Publishing Co.*, Amsterdam, pp. 68-72.

Wright, J.W., C.H. Murphy and G.V. Bull, 1967. Profiles of winds in the lower thermosphere by the gun-launched probe technique and their relation to ionospheric sporadic E. Space Research VII, *North-Holland Publishing Co.*, Amsterdam, pp. 113-122.

3. Aurora

Anger, C.D., 1967. Review of rocket auroral measurements. *Aurora and Airglow*, Reinhold, New York, p. 211.

Catchpoole, J.R., 1970. Auroral ionization and incident magnetospheric electrons. *Can. J. Phys.*, 48, 2537.

Clark, T.A. and C.D. Anger, 1967. Morphology of electron precipitation during auroral substorms. *Planet. Space Sci.*, 15, 8.

Clark, T.A. and D.L. Matthews, 1968. Simultaneous observation of electron fluxes, ionization and luminosity in an aurora. *Can. J. Phys.*, 46, 201.

Cresswell, G.R., 1968. Fast auroral waves. *Planet. Space Sci.*, 16, 1453.

—1969. Flaming auroras. *J. Atmos. Terr. Phys.*, 31, 179.

Forsyth, P.A., 1968. Auroral energy input rates from radio scintillation measurements. *Can. J. Phys.*, 46, 1841.

—1968. Radio-Aurora (A review of research in radio-aurora for the period 1963-1967) *Ann. Geophys.*, 24, 555.

—1969. The rate of occurrence of VHF radio-aurora over an eleven-year period. *J. Atmos. Terr. Phys.*, 31, 313.

—1970. The lunar influence on radio aurora. *J. Atmos. Terr. Phys.*, 32, 251.

Harris, F.R. and A. Kavadas, 1970. Latitude variation of radar aurora with local substorm activity. *Can. J. Phys.*, 48, 1411.

Harrison, A.W., 1969. Recent observations of the auroral spectrum between 1.02μ and 1.13μ. *Can. J. Phys.*, 47, 599.

Hartz, T.R., 1968. The general pattern of auroral particle precipitation and its implications for high latitude communication systems. Ionospheric Radio Communications, K. Foldestad (ed.), *Plenum Press*, New York, p. 9.

Hartz, T.R. and N.M. Brice, 1967. The general pattern of auroral particle precipitation. *Planet. Space Sci.*, 15, 301.

Hofstee, J. and P.A. Forsyth, 1969. Ion-acoustic waves in the auroral plasma. *Can. J. Phys.*, 47, 2797.

Jelly, D.H., 1968. Apparent poleward motion of onsets of auroral absorption events. *Can. J. Phys.*, 46, 33.

——1970. On the morphology of auroral absorption during substorms. *Can. J. Phys.*, 48, 335.

Jones, A.V., 1968. Auroral Spectroscopy. Atmospheric Emissions. *Proc. NATO Advanced Study Instit.*, Norway, July 29 – August 9, 1968, pp. 47-62.

——1969. Spectroscopic morphology of aurora. *Annals of the IQSY*, Vol. 4, Solar-Terrestrial Physics: Solar Aspects.

Lin, W.C., I.B. McDiarmid and J.R. Burrows, 1968. Electron fluxes at 1,000 km altitude associated with auroral substorms. *Can. J. Phys.*, 46, 80.

Lyon, G.F. 1968. Some evidence concerning the distribution of irregularities responsible for radio aurora. *Planet. Space Sci.*, 16, 449.

McDiarmid, D.R., 1970. Ion-acoustic waves and radio aurora. *Can. J. Phys.*, 48, 1863.

McDiarmid, D.R. and A.G. McNamara, 1967. V.H.F. radio aurora: simultaneous observation of auroral ionization by two separated radars. *Can. J. Phys.*, 45, 3009.

McDiarmid, D.R. and A.G. McNamara, 1969. A physical model of a radio aurora event. *Can. J. Phys.*, 47, 1271.

McDiarmid, I.B. and E.E. Budzinski, 1968. Search for low-altitude acceleration mechanisms during an auroral substorm. *Can. J. Phys.*, 46, 911.

McDiarmid, I.B., E.E. Budzinski, B.A. Whalen and N. Sckopke, 1967. Rocket observations of electron pitch-angle distributions during auroral substorms. *Can. J. Phys.*, 45, 1755.

McNamara, A.G., 1969. Rocket measurements of plasma densities and temperatures in visual aurora. *Can. J. Phys.*, 47, 1913.

Miller, J.R. and G.G. Shepherd, 1969. Rocket measurements of H Beta production in a hydrogen aurora. *J. Geophys. Res.*, 74, 4987.

——1969. Photometric rocket measurements in hydrogen auroras. Space Research X. *North-Holland Publishing Co.*, Amsterdam, p. 876.

Millman, P.M., 1968. The Canadian visual auroral program. *Ann. Geophys.*, 24, 1.

Montbriand, L.E. and A.V. Jones, 1966. Studies of auroral hydrogen emissions in west-central Canada. *Can. J. Phys.*, 44, 3259.

Müller, J.R. and G.G. Shepherd, 1968. Auroral measurements using rocket-borne photometers. *Ann. Geophys.*, 24, 1.

Oliven, N.M., D. Venkatesan and K.G. McCracken, 1968. Microburst phenomena. 2. Auroral Zone Electrons. *J. Geophys. Res.*, 73, 2345.

Palmer, F.H. and D.R. Moorcroft, 1970. Correlation analysis of radio-auroral scatter signals. *Can. J. Phys.*, 48, 1716.

Pilkington, G.R., C.D. Anger and T.A. Clark, 1968. Auroral X-rays and their association with rapidly changing auroral forms. *Planet. Space Sci.*, 16, 815.

Scourfield, M.W.J., G.R. Cresswell, G.R. Pilkington and N.R. Parsons, 1970. Auroral pulsations – Television image and X-ray correlations. *Planet. Space Sci.*, 18, 495.

Scourfield, M.W.J. and N.R. Parsons, 1969. An image intensifier-vidicon system for auroral cinematography. *Planet. Space Sci.*, 17, 75.

Scourfield, M.W.J. and N.R. Parsons, 1969. Auroral pulsations and flaming – Some initial results of a cinematographic study using an image intensifier. *Planet. Space Sci.*, 17, 1141.

Shemansky, D.E. and A.V. Jones, 1968. Type-B red aurora; the O_2^+ first negative system and the N_2 first positive system. *Planet. Space Sci.*, 16, 1115.

Shepherd, G.G., 1969. Spectroscopic measurements of auroral and airglow temperatures. *Ann. Geophys.*, 25, 666.

Shepherd, G.G. and E.V. Pemberton, 1968. Characteristics of auroral brightness fluctuations. *Radio Science*, 3, 650.

Sofko, G.J. and A. Kavadas, 1969. Periodic fading in 42 MHz auroral backscatter. *J. Geophys. Res*, 74, 3651.

Spitz, A.L., 1968. A method for plotting all-sky camera data in geomagnetic co-ordinates. *Arctic Institute of North America Research* Paper No. 43.

Staniforth, A., 1969. A remote data-recording station. *Can. J. Phys.*, 47, 2303.

Venkatesan, D., M.N. Oliveń, P.J. Edwards, K.G. McCracken, and M. Steinback, 1968. Microburst phenomena. 1. Auroral Zone X-rays. *J. Geophys. Res.*, 73, 2333.

Whalen, B.A. and I.B. McDiarmid, 1968. Direct measurement of auroral Alpha particles. *J. Geophys. Res.*, 73, 2307.

Whalen, B.A. and I.B. McDiarmid, 1969. Summary of rocket measurements of auroral particle precipitation. *Atmospheric Emissions*, Edited by B.M. McCormac and A. Omholt, Reinhold Book Corp.

——1970. Temporal behaviour of energetic particle precipitation during an auroral substorm. *J. Geophys. Res.*, 75, 123.

Whalen, B.A., I.B. McDiarmid and E.E. Budzinski, 1967. Rocket measurements in proton aurora. *Can. J. Phys.*, 45, 3247.

Whalen, B.A., J.R. Miller and I.B. McDiarmid, 1971. Energetic particle measurements in a pulsating aurora. *J. Geophys. Res.*, 76, 978.

Whalen, B.A., J.R. Miller and I.B. McDiarmid, 1971. Evidence for a solar wind origin of auroral ions from low-energy ion measurements. *J. Geophys. Res.*, 76, 2406.

Wiens, R.H. and A.V. Jones, 1969. Studies of auroral hydrogen emissions in west-central Canada. III. Proton and electron auroral ovals. *Can. J. Phys.*, 47, 1493.

Wilson, B.G., A.J. Baxter, and D.W. Green, 1969. Low-energy bremsstrahlung X-ray spectra from a stable auroral arc. *Can. J. Phys.*, 47, 2427.

4. Cosmic rays and particle physics

Balasubrahmanyn, V.K. and D. Venkatesan, 1970. Solar activity, 27-day variation and long term modulation of cosmic ray intensity. *Solar Physics*, 11, 151.

Baxter, A.J., B.G. Wilson and D.W. Green 1969. Low-energy cosmic ray measurements. *Can. J. Phys.*, 47, 2651.

Bercovitch, M., 1965. The day by day correction of the meson diurnal variation for atmospheric effects. *Proc. Int. Conf. on Cosmic Rays*, London, 1, 495.

——1966. Atmospheric contribution to the diurnal variation of the cosmic ray meson intensity at Deep River. *Can. J. Phys.*, 44, 1329.

——1967. Atmospheric effects on cosmic ray monitors. *Proc. 10th Int. Conf. on Cosmic Rays*, Invited and Rapporteur Papers, 269.

——1970. Determination of the heliocentric cosmic ray density gradient using neutron monitor data. *Proc. 11th. Int. Conf. on Cosmic Rays*, Budapest, 1969, Acta Physica Academiae Scientiarum Hungaricae, 29, Suppl. 2, 453.

Bercovitch, M. and B.C. Robertson, 1965. Meteorological factors affecting the counting rate of neutron monitors. *Proc. Int. Conf. on Cosmic Rays*, London, 1, 489.

Bland, C.J. 1967. The charge composition of cosmic ray electrons. *Planet. Space Sci.*, 15, 398.

Bland, C.J. and G. Cioni, 1968. Geomagnetic cut-off rigidities in non-vertical directions. *Earth and Planet. Sci. Letters*, 4, 339.

Bland, C.J. *et al.*, 1968. Measurements of cosmic ray electrons. *Nuovo Cimento*, Ser. X, 55A, 451.

Briggs, R.M., R.B. Hicks and S. Standil, 1969. Periodic solar-time variations in the cosmic ray muon component near sea-level. *J. of Phys. A* (Proc. Phys. Soc. A) 2, 584.

Briggs, R.M., R.B. Hicks and S. Standil, 1969. Removal of meteorological effects from meson-telescope data. *Can. J. Phys.*, 47, 1429.

Briggs, R.M., R.B. Hicks and S. Standil, 1969. Pronounced diurnal variation in cosmic ray intensity as seen by inclined meson telescopes. *J. Geophys. Res.*, 74, 4196.

Briggs, R.M., R.B. Hicks and S. Standil, 1970. Sidereal-time variations in the cosmic ray intensity. *Nuovo Cimento B.* 66b, No. 1, 97.

Carmichael, H., 1968. Cosmic ray (Instruments). *Annals of the IQSY*, 1, Chap. 13.

——1969. The ground-level solar proton event of 7 July, 1966 recorded by neutron monitors. *Annals of the IQSY*, 3, 245.

——1969. The Forbush decrease associated with the proton event of 7 July, 1966 as recorded by neutron monitors. *Annals of the IQSY*, 3, 376.

——1969. Ground-based synoptic observations of cosmic rays. *Annals of the IQSY*, 4, 141.

Carmichael, H. and M. Bercovitch, 1969. II – Cosmic ray latitude survey in Canada in December 1965. *Can. J. Phys.*, 47, 2051.

——1969. V – Analysis of IQSY cosmic-ray survey measurements. *Can. J. Phys.*, 47, 2073.

Carmichael, H., M. Bercovitch, M.A. Shea, M. Magidin, R.W. Peterson, 1968. Attenuation of neutron monitor radiation in the atmosphere. *Can. J. Phys.*, 46, S1006.

Carmichael, H., M. Bercovitch and J.F. Steljes, 1965. Introduction of meteorological corrections into meson monitor data. *Proc. Int. Conf. on Cosmic Rays*, London, 1, 492.

——1967. Introduction of meteorological corrections into meson monitor data. *Tellus*, 19, 143.

Carmichael, H., M. Bercovitch, J.F. Steljes and M. Magidin, 1965. Latitude survey in North America. *Proc. Ninth Int. Conf. on Cosmic Rays*, London, 1, 553.

Carmichael, H., M. Bercovitch, J.F. Steljes, and M. Magidin, 1969. I – Cosmic ray latitude survey in North America in Summer 1965. *Can. J. Phys.*, 47, 2037.

Carmichael, H., M.A. Shea and R.W. Peterson, 1969. III – Cosmic ray latitude survey in western USA and Hawaii in Summer 1966. *Can. J. Phys.*, 47, 2057.

Carmichael, H., M.A. Shea, D.F. Smart and J.R. McCall, 1969. IV – Geographically smoothed geomagnetic cutoffs. *Can. J. Phys.*, 47, 2067.

Chin, F.K. and S. Standil, 1968. Barometric effect for the cosmic ray photon component deep in the atmosphere. *Planet. Space Sci.*, 16, 7.

——1968. Solar diurnal variation of the cosmic ray photon component deep in the atmosphere. *Planet. Space Sci.*, 16, 15.

Green, D.W., J. Skirrow and B.G. Wilson, 1968. Cosmic X-ray measurements at Resolute. *Can. J. Phys.*, 46, S470.

Hashim, A., T. Thambyahpillai, D.M. Thomson and T. Mathews, 1968. East-West measurements of cosmic ray solar daily variation at an equatorial station. *Can. J. Phys.*, 46, S801.

Kamata, K., S. Shibata, O. Saavedra, V. Domingo, K. Suga, K. Murakami, Y. Toyoda, M. Lapointe, J. Gaebler and I. Escobar, 1968. Predominantly electromagnetic showers of energy 10^{14} ev to 10^{16} ev., *Can. J. Phys.*, 46, 10.

Kim, C.Y., 1968. A search for high energy solar neutrons. *Can. J. Phys.*, 46, S753.

——1970. Solar neutron flux in the energy range 20-160 MeV. *Can. J. Phys.*, 48, 2155.

Krimigis, S.M. and D. Venkatesan, 1969. The radial gradient of interplanetary radiation measured by Mariners 4 and 5. *J. Geophys. Res.*, 74, 16, 4129.

Mathews, T. and G.G. Sivjee, 1967. Response of mu-meson detectors deep in the atmosphere to primary cosmic ray particles of magnetic rigidity between 10 and 25 GV. *Can. J. Phys.*, 45, 1643.

Mathews, T., J.B. Mercer and D. Venkatesan, 1968. Anisotropy in cosmic ray intensity associated with Forbush decreases. *Can. J. Phys.*, 46, S855.

Mathews, T. and B.G. Wilson, 1968. The cosmic ray solar flare increase of 28 January, 1967. *Can. J. Phys.*, 46, S776.

Mathews, T., D. Venkatesan and B.G. Wilson, 1969. Pronounced variation in cosmic ray intensity. *J. Geophys. Res.*, 74, 1218.

Mathews, T., J. Quenby and J. Sear, 1971. Mechanism for cosmic ray modulation. *Nature*, 229, 246.

Mercer, J.B. and B.G. Wilson, 1968. Morphology of the March 23, 1966 Forbush decrease. *Can. J. Phys.*, 46, S849.

Prescott, J.R., G.G.C. Palumbo, J.A. Galt and C.H. Costain, 1968. Radio signals from showers at 22 MHz. *Can. J. Phys.*, 46, S246.

Sauder, T., 1970. Remarks on the modulation of low rigidity particles in cosmic radiation. *Can. J. Phys.*, 48, 744.

Shibata, S., O. Saavedra, K. Kamata, M. Lapointe, B. Rennex, K. Uchino, M. Nagano and K. Suga, 1968. Fine structure air shower cores observed with a spark chamber at 5200 m altitude. *Can. J. Phys.*, 46, 60.

Sreenivasan, S.R. and R.H. Johnson, 1968. Solar wind modulation of cosmic rays. *Can. J. Phys.*, 46, S954.

Swinson, D.B. and J.R. Prescott, 1968. The density spectrum of extensive air showers at 1575 m and 4300 m. *Can. J. Phys.*, 46, S292.

Venkatesan, D. and T. Mathews, 1968. The enhanced daily variation in cosmic ray intensity. *Can. J. Phys.*, 46, S794.

White, G.M. and J.R. Prescott, 1968. Instrumental effects in the measurement of particle densities in extensive air showers. *Can. J. Phys.*, 46, S287.

Wilson, B.G., T. Mathews and R.H. Johnson, 1967. Intercomparison of neutron monitors during solar-flare increases. *Physics Review Letters*, 18, 675.

5. Ionosphere

Austin, G.L. and A.H. Manson, 1969. On the nature of the irregularities that produce partial reflections of radio waves from the lower ionosphere (970-100 km). *Radio Science,* 4, 35.

Balmain, K.G. and G.A. Oksiutik, 1969. R.F. probe admittance in the ionosphere theory and experiment. Plasma Waves in Space and Laboratory, Vol. 1, Edited by J.O. Thomas and B.J. Landmark, *Edinburgh University Press,* pp. 247-261.

Barrington, R.E., 1969. Ionospheric ion composition deduced from VLF observations. *Proc. IEEE,* 57, 1036.

——1969. A preliminary rocket investigation of very low frequency ionospheric resonances. Space Research IX, *North-Holland Publishing Co.,* Amsterdam, p. 279.

——1969. Satellite observations of VLF resonances. Plasma Waves in Space and in the Laboratory, Vol. 1, *Edinburgh University Press,* p. 361.

Barrington, R.E. and T.R. Hartz, 1968. Satellite ionosonde records: Resonance below the cyclotron frequency. *Science,* 160, 181.

——1969. Resonances observed by the Alouette topside sounders. Plasma Waves in Space and in the Laboratory, Vol. 1, Edited by J.O. Thomas and B. Landmark, *Edinburgh University Press,* pp. 55-79.

Barrington, R.E. and D.J. McEwen, 1966. Ion composition from VLF phenomena observed by Alouette I and II. Space Research VII, *North-Holland Publishing Co.,* Amsterdam, pp. 625-633.

Belrose, J.S., 1967. The lower ionosphere: A review. MF, LF, and VLF radio propagation. *I.E.E. Conference* Publication No. 36.

——1968. Low and very low frequency radio propagation. AGARD Lecture Series XXIX: Radio Wave Propagation. *AGARD* Publications.

——1970. Radio wave probing of the ionosphere by the partial reflection of radio waves (from heights below 100 km). *J. Atmos. Terr. Phys.,* 32, 567.

Belrose, J.S., I.A. Bourne and L.W. Hewitt (editorial committee), 1967. Ground-based radio wave propagation studies of the lower ionosphere (Vols. I, II), Conference proceedings. Queen's Printer, Ottawa.

——1967. A preliminary investigation of diurnal and seasonal changes in electron distribution over Ottawa, Churchill and Resolute Bay. *Proc. conference on ground-based radio wave propagation studies of the lower ionosphere.* Queen's Printer, Ottawa.

——1967. A critical review of the partial reflection experiment. *Proc. Lower Ionosphere.* Queen's Printer, Ottawa.

Belrose, J.S., L.W. Hewitt and R. Bunker, 1969. The partial reflection experiment as a tool for synoptic D-region research: and results of recent studies related to winter variability. Meteorological and Chemical Factors in D-Region Aeronomy – *Record of Third Aeronomy Conference,* (Edited by C.F. Sechrist) Aeronomy Report No. 32, University of Illinois.

——1970. Regular and irregular diurnal variations of electron number density in the lower ionosphere over Resolute Bay. The Polar Ionosphere and Magnetospheric Processes, (Edited by G. Skovli), Gordon Breach Pub. Co., New York, pp. 285-298.

Belrose, J.S., A.G. McNamara, J.E. Hall, L.R. Bode, R. Bunker and D.B. Ross, 1970. Changes in the lower ionosphere during the eclipse. A preliminary report of the Canadian program. *Nature,* 226, 1100.

Belrose, J.S., and L. Thomas, 1968. Ionization changes in the middle latitude D-region associated with geomagnetic storms. *J. Atmos. Terr. Phys.,* 30, 1397.

Bourne, I.A. and L.W. Hewitt, 1968. The dependence of ionospheric absorption of MF radio waves at mid-latitudes on planetary magnetic activity. *J. Atmos. Terr. Phys.,* 30, 1381.

Boyd, G.M. and H.J. Duffus, 1969. Doppler observations of associated ionospheric and magnetic fluctuations. *Can. J. Phys.,* 47, 1585.

Brice, N.M., 1967. Ion effects observed in radio wave propagation in the ionosphere. Electromagnetic Wave Theory: Proceedings of a Symposium held at Delft, the Netherlands, Sept. 1969. Pergamon Press, Oxford, pp. 197-209.

Buckmaster, H.A. and J.D. Skirrow, 1968. VLF phase anomaly induced by a nuclear explosion. *Nature,* 218, 155.

Chapman, J.H., 1966. Radio waves in the ionosphere and plasma resonances. *Trans. Roy. Soc. Canada,* Vol. IV, Series IV, p. 205.

Chapman, J.H., P.A. Forsyth, P.A. Lapp and G.N. Patterson, 1967. Upper atmosphere and space programs in Canada. Queen's Printer, Ottawa.

Chapman, J.H. and E.S. Warren, 1968. Topside soundings of the earth's ionosphere. *Space Science Reviews,* 8, 846, D. Reidel Publishing Company, Dordrecht-Holland.

Chimonas, G., 1969. Ion separation in temperate zone sporadic E and the layer shape. *J. Geophys. Res.,* 74, 4189.

Collins, C. and L.A. Maynard, 1968. Simultaneous VHF riometer and forward-scatter observations of the disturbed lower ionosphere. *Ionospheric Radio Communications,* K. Folkestad (ed.), Plenum Press, New York, p. 155.

Dixon, A.F. and P.A. Forsyth, 1970. Measurements of the shape of ionospheric irregularities using satellite transmissions. *Can. J. Phys.,* 48, 2097.

Duffus, H.J. and G.M. Boyd, 1968. The association between ULF geomagnetic fluctuations and doppler ionospheric observations. *J. Atmos. Terr. Phys.,* 30, 481.

Florida, C.D., 1969. The development of a series of ionospheric satellites. *Proc. IEEE,* 57, 867.

——1970. The ISIS series of ionospheric satellites. *Proc. Eighth International Symposium on Space Technology and Science,* Tokyo, Japan.

Franklin, C.A., R.J. Bibby and N.S. Hitchcock, 1969. A data acquisition and processing system for mass producing topside ionograms. *Proc. IEEE,* 57, 929.

Franklin, C.A. and M.A. Maclean, 1969. The design of swept-frequency topside sounders. *Proc. IEEE,* 57, 897.

Fraser, G.J. and R.A. Vincent, 1970. A study of D-region irregularities. *J. Atmos. Terr. Phys.,* 32, 1591.

Gregory, J.B., 1968. Solar influences and their variations. *Meteorological Monographs,* 9, 19.

——1968. Radio wave scattering from the ionospheric D-region. Agardograph, *AGARD* CP No. 37., Part 1, p. 28-1.

Gregory, J.B. and A.H. Manson, 1967. Mesospheric electron number densities at 35°S latitude. *J. Geophys. Res.,* 72, 1073.

Gregory, J.B. and A.H. Manson, 1968. Discussion of letter by A.J. Ferraro and H.S. Lee, 'Capability of a high-power wave interaction facility'. *J. Geophys. Res.,* 73, 7540.

Gregory, J.B., A.H. Manson and D.T. Rees, 1970. Radiowave absorption at an auroral latitude. *Can. J. Phys.,* 48, 809.

Gregory, J.B. and R.A. Vincent, 1970. Structure of partially reflecting regions in the lower ionosphere. *J. Geophys. Res.,* 75, 6387.

Hagg, E.L., 1967. Electron densities of 8-100 electrons cm^{-3} deduced from Alouette II high-latitude ionograms. *Can. J. Phys.,* 45, 27.

Hagg, E.L., E.J. Hewens and G.L. Nelms, 1969. The interpretation of topside sounder ionograms. *Proc. IEEE,* 57, 949.

Hagg, E.L. and D.B. Muldrew, 1970. A novel spike observed on Alouette II ionograms. Plasma Waves in Space and in the Laboratory, Vol. 2, p. 69, Edinburgh University Press.

Hartz, T.R., 1968. Summary of sessions, Ionospheric Radio Communications, K. Folkestad (ed.), Plenum Press, New York, p. 433.

——1968. Radio noise within and above the ionosphere. *U.R.S.I.* Information Bulletin No. 167, pp. 91-98.

——1969. Radio noise levels within and above the ionosphere. *Proc. IEEE,* 57, 1042.

——1970. Low frequency noise emissions and their significance for energetic particle processes in the polar ionosphere. The Polar Ionosphere and Magnetospheric Processes (edited by G. Skovli), Gordon Breach Pub. Co., New York, pp. 151-160.

Hartz, T.R. and R.E. Barrington, 1969. Nonlinear plasma effects in the Alouette recordings. *Proc. IEEE,* 57, 1108.

Herzberg, L. and G.L. Nelms, 1969. Ionospheric conditions following the proton flare of 7 July, 1966 as deduced from topside soundings. *Annals of IQSY,* Vol. 3, The Proton Flare Project (The July 1966 Event), MIT Press.

Herzberg, L., G.L. Nelms and P.L. Dyson, 1969. Topside observation of electron density variations (G condition) at times of low magnetic activity. *Can. J. Phys.,* 47, 2683.

Hewitt, L.W., 1969. Ionization increases associated with the small solar proton events of 5 February, 1965 and 16 July, 1966. *Can. J. Phys.,* 47, 131.

Holbrook, J.A.D. and G.F. Lyon, 1969. Irregularities in the lower ionosphere deduced from beacon satellite observations. *J. Atmos. Terr. Phys.,* 31, 71.

Horita, R.E. and T. Watanabe, 1969. Electrostatic waves in the ionosphere excited around the lower hybrid resonance frequency. *Planet. Space Sci.*, 17, 61.

Jackson, J.E. and E.S. Warren, 1969. Objectives, history, and principal achievements of the topside sounder and ISIS programs. *Proc. IEEE*, 57, 861.

Jelly, D.H., 1967. Some remarks on the valley between the F-layer and thick E_s (night E) determined from simultaneous bottomside and topside ionograms. *Proc. conference on ground-based radio wave propagation studies of the lower ionosphere*, Queen's Printer, Ottawa.

Jelly, D.H. and L.E. Petrie, 1969. The high latitude ionosphere. *Proc. IEEE*, 57, 1005.

Jull, G.W., 1967. Short-term and averaged characteristics of nonreciprocal HF ionospheric paths. *IEEE Transactions on Antennas and Propagation*, AP-15, 268.

Lockwood, G.E.K., 1969. A computer-aided system for scaling topside ionograms. *Proc. IEEE*, 57, 986.

——1970. A modified iteration technique for use in computing electron density profiles from topside ionograms, *Radio Science*, 5, 575.

Lyon, G.F., 1967. Some closely spaced frequency Faraday rotation satellite observations. *J. Atmos.* Terr. Phys., 29, 871.

Lyon, G.F. and J.A.D. Holbrook, 1969. An isolated field-aligned irregularity. *J. Geophys. Res.*, 74, 4193.

Manson, A.H. and M.W.J. Merry, 1970. Particle influx and the "winter anomaly" in the mid-latitude (L = 2.5 - 3.5) lower ionosphere. *J. Atmos. Terr. Phys.*, 32, 1169.

Manson, A.H., M.W.J. Merry and R.A. Vincent, 1969. Relationship between the partial reflection of radio waves from the lower ionosphere and irregularities as measured by rocket probes. *Radio Science*, 4, 955.

Mar J. and T. Garrett, 1969. Mechanical design and dynamics of the Alouette spacecraft. *Proc. IEEE*, 57, 882.

Mason, K.H., E.H. Tull and P.A. Forsyth, 1967. Rocket studies of isolated ionospheric irregularities. *Can. J. Phys.*, 45, 3056.

McEwen, D.J. and R.E. Barrington, 1967. Some characteristics of the lower hybrid resonance noise bands observed by the Alouette I satellite. *Can. J. Phys.*, 45, 13.

McEwen, D.J. and R.E. Barrington 1968. Ion composition below 3000 km derived from ion whistler observations. Space Research VIII, *North-Holland Publishing Co.*, Amsterdam.

Meek, J.H., 1968. Physical problems of particular relevance to Arctic communications. Ionospheric Radio Communications, K. Folkestad (ed.), *Plenum Press*, New York, p. 81.

Moorcroft, D.R., 1969. Nighttime topside ionic composition and temperature over Arecibo, Puerto Rico. *J. Geophys. Res.*, 74, 315.

Muldrew, D.B., 1967. MF conjugate echoes observed on topside sounder data. *Can. J. Phys.*, 45, 3935.

——1967. Delayed generation of an electromagnetic pulse in the topside ionosphere. *J. Geophys. Res.*, 72, 3777.

——1968. Interference patterns in HF signals backscattered from ocean waves. *AGARD* Conference Proceedings No. 37, Scatter Propagation of Radio Waves, Part 1, p. 8-1 and 19-2.

——1969. Nonvertical propagation and delayed-echo generation observed by the topside sounders. *Proc. IEEE*, 57, 1097.

——1970. Preliminary results of ISIS-A concerning electron density variations ionospheric resonances and Cerenkov radiation. Space Research X, *North-Holland Publishing Co.*, Amsterdam.

Muldrew, D.B. and E.L. Hagg, 1969. Properties of high-latitude ionospheric ducts deduced from Alouette II two-hop echoes. *Proc. IEEE*, 57, 1128.

Muldrew, D.B. and E.L. Hagg, 1970. Stimulation of ionospheric-resonance echoes by the Alouette II satellite. Plasma Waves in Space and in the Laboratory, Vol. 2, p. 55, *Edinburgh University Press.*

Muldrew, D.B., M.D. Litwack and P.L. Timleck, 1967. Interpretation of the statistics of occurrence of Alouette I earth echoes. *Planet. Space Sci.*, 15, 611.

Murphy, C.H. and G.V. Bull, 1967. Nighttime variation of ionospheric winds over Barbados, West Indies. *J. Geophys. Res.*, 72, 4831.

——1968. Ionospheric winds over Yuma, Arizona, measured by gun-launched projectiles. *J. Geophys. Res.*, 73, 3005.

Murphy, C.H., G.V. Bull and J.W. Wright, 1967. Motions of an electron-ion cloud released at 100 kilometres from a gun-launched projectile. *J. Geophys. Res.*, 72, 3511.

Narayana Rao, N., G.F. Lyon and J.A. Klobuchar, 1969. Acoustic waves in the ionosphere. *J. Atmos, Terr. Phys.*, 31, 539.

Nelms, G.L. and G.E.K. Lockwood, 1966. Early results from the topside sounder in the Alouette II satellite. Space Research VII, *North-Holland Publishing Co.*, Amsterdam, pp. 604-623.

Osborne, F.J.F., F.H.C. Smith, R.E. Barrington and W.E. Mather, 1967. Plasma-induced interference in satellite v.l.f. receivers. *Can. J. Phys.*, 45, 47.

Paghis, I., C.A. Franklin and J. Mar, 1967. Alouette I – The first three years in orbit. *DRTE* Report No. 1159.

Palmer, F.H., J.W. Doan and P.A. Forsyth, 1970. Ionospheric propagation experiments using rockets and satellites. *Can. J. Phys.*, 48, 554.

Petrie, L.E., 1966. Preliminary results on mid and high latitude topside spread F. AGARDOGRAPH 95, Spread F and its Effects upon Radiowave Propagation and Communications. *Technivision Publishing Co.*, pp. 67-77.

——1968. Developments of HF predictions for the Arctic. Ionospheric Radio Communications. K. Folkestad (ed.), *Plenum Press*, New York, p. 263.

Petrie, L.E., E.L. Hagg and E.S. Warren, 1966. The influence of focussing upon the apparent reflection coefficient of the F region. AGARDOGRAPH 95, Spread F and its Effects upon Radiowave Propagation and Communications. *Technivision Publishing Co.*, pp. 103-119.

Petrie, L.E. and G.E.K. Lockwood, 1969. On the prediction of F-layer penetration frequencies. *Proc. IEEE*, 57, 1026.

Petrie, L.E. and E.S. Warren, 1968. The propagation of high frequency waves on the Winnipeg-Resolute Bay oblique sounder circuit. Ionospheric Radio Communications, K. Folkestad (ed.), *Plenum Press*, New York, p. 242.

Stevens, E.E., 1968. The significance of sporadic E propagation in determining the MUF. Ionospheric Radio Communications, K. Folkestad (ed.), *Plenum Press*, New York, p. 289.

Timleck, P.L. and G.L. Nelms, 1969. Electron densities less than 100 electron CM^{-3} in the topside ionosphere. *Proc. IEEE*, 57, 1164.

Vincent, R.A., 1969. Short period phase height oscillations in the E-region. *J. Atmos. Terr. Phys.*, 31, 607.

Warren, E.S., 1969. The topside ionosphere during geomagnetic storms. *Proc. IEEE*, 57, 1029.

Warren, E.S. and E.L. Hagg, 1968. Observation of electrostatic resonances of the ionospheric plasma. *Nature*, 220, 466.

Wrenn, G.L. and G.G. Shepherd, 1969. A conjugate point effect observed for electron temperatures in the 1,000-2,500 km height range. *J. Atmos. Terr. Phys.*, 31, 1383.

Wright, J.W., C.H. Murphy and G.V. Bull, 1967. Sporadic E and the wind structure of the E region. *J. Geophys. Res.*, 72, 1443.

6. Laboratory studies

Anketell, J. and R.W. Nicholls, 1970. The afterglow and energy transfer mechanisms of active nitrogen. *Reports on progress in physics*, 33, 269.

Arnold, S.J. and E.A. Ogryzlo, 1967. Some reactions forming $O_2(^1\Sigma_g^+)$ in the upper atmosphere. *Can. J. Phys.*, 45, 2053.

Bachynski, M.P. and B.W. Gibbs, 1968. Antenna pattern distortion by an isotropic plasma slab. *IEEE Trans.*, AP-16, 583.

——1968. Antenna radiation properties in presence of anisotropic plasmas. *Radio Science*, 3, 920.

——1969. Effect of electrostatic field on propagation of electromagnetic waves in an anisotropic plasma. *Phys. Fluids*, 12, 2447.

——1969. Propagation of strong-field electromagnetic waves through plasmas near the electron cyclotron frequency. *Phys. Rev. Letters*, 22, 583.

——1969. Plasma density measurement by electromagnetic wave propagation at small angles to magnetic field. *Phys. Fluids*, 12, 467.

Bachynski, M.P., B.W. Gibbs and K.A. Graf, 1967. Reflection of circularly polarized electromagnetic waves from an anisotropic plasma. *Radio Science*, 2, 881.

Brocklehurst, B. and R.W. Nicholls, 1969. Pink afterglow of nitrogen. *Nature*, 223, 824.

Chandraiah, G. and G.G. Shepherd, 1968. Intensity measurements in emission of 18 Vegard-Kaplan bands of N_2. *Can. J. Phys.*, 46, 221.

Chen, S.L. and J.M. Goodings, 1968. Ion current to a Langmuir probe in very low density flowing plasmas for electron density determinations. *J. Appl. Phys.*, 39, 3300.

Degen, V., S.H. Innanen, G.R. Herbert and R.W. Nicholls, 1968. Identification atlas of molecular spectra. 6. The $O_2A^3\Sigma_u^+ - X^3\Sigma_g^-$ Herzberg I System. Report from York University Centre for Research in Experimental Space Science, November.

Degen, V. and R.W. Nicholls, 1968. The oxygen-argon afterglow as a source of the $O_2(A^3\Sigma_u^+ - X^3\Sigma_g^-)$ Herzberg I band system. *J. Phys. B.* (Proc. Phys. Soc.) Ser. 2, Vol. 1, 983.

——1969. Intensity measurements of the O_2 Herzberg I band system. *J. Phys. B.*, 2, 1240.

Drake, J. and R.W. Nicholls, 1969. A study of the r-centroid approximation. *Chem. Phys. Letters*, 3, 457.

Dugan, C.H., 1967. Metastable molecules in a nitrogen afterglow. *J. Chem. Phys.*, 47, 1512.

Findlay, F.D., 1969. Relative band intensities in the atmospheric and infrared atmospheric system of molecular oxygen. *Can. J. Phys.*, 47, 687.

Findlay, F.D., C.J. Fortin and D.R. Snelling, 1969. Deactivation of $O_2(^1\Delta)$. *Chem. Phys. Letters*, 3, 204.

Fung, P.C.W., 1969. Interaction of a highly relativistic helical electron stream and a cold magnetospheric plasma. *Can. J. Phys.*, 47, 161.

Gauthier, M. and D.R. Snelling. Formation of singlet molecular oxygen from the ozone photochemical system. *Chem. Phys. Letters*, 5, 93.

Gauthier, M. and D.R. Snelling, 1970. Formation of singlet molecular oxygen from the ozone photolysis at 2537Å. *Ann. N.Y. Acad. Sci.*, 171, 220.

Harris, F.R., R.N. Peterson and D.T. Bradley, 1970. Relative intensities of the O_2^+ 1NG and N_2 1PG band systems in normal and type-B aurora. *Can. J. Phys.*, 48, 2283.

Harrison, A.W., C. Hansen and D. Will, 1970. A simple digital near infrared spectrometer. *App. Optics*, 9, 1610.

Hasson, V., G.R. Hebert and R.W. Nicholls, 1970. Transition probabilities for bands of the Schumann-Runge band system of O_2. *J. Phys. B.*, 3, 1188.

Hasson, V., R.W. Nicholls and V. Degen, 1970. Absolute intensity measurements on the Herzberg I system of O_2. *J. Phys. B.*, 3, 1192.

Hebert, G.R., S.H. Innanen and R.W. Nicholls, 1967. Identification atlas of molecular spectra. 4. The $O_2B^3\Sigma_u^- - X^3\Sigma_g^-$ Shumann-Runge system. *CRESS*, York University Report, January.

Hebert, G.R. and R.W. Nicholls, 1969. Franck-Condon factors for the V1=O progression of the N_2 fourth positive band system. *J. Phys. B.*, 2, 626.

Henderson, W.R. and H.I. Schiff, 1970. A simple sensor for the measurement of atomic oxygen height profiles in the upper atmosphere. *Planet. Space Sci.*, 18, 1527.

Jarmain, W.R. and R.W. Nicholls, 1967. A theoretical study of the $v'' = 0, 1, 2$ progressions of bands and adjoining photodissociation continua of the O_2 Herzberg I system. *Proc. Phys. Soc.*, 90, 545.

Jassby, D.L. and M.P. Bachynski, 1969. Laboratory measurements of the impedance and radiation pattern of antennas in an isotropic plasma. Plasma Waves in Space and Laboratory, J.O. Thomas and B.J. Landmark, editors, Vol. 1, pp. 285-302, *Edinburgh University Press.*

Johnston, T.W., 1969. Plane wave dispersion in gyrotropic media. *Radio Science*, 4, 729.

——1969. A review of plasma resonances. Plasma Waves in Space and Laboratory, J.O. Thomas and B.J. Landmark, editors, Vol. 1, pp. 109-122, *Edinburgh University Press.*

Kasha, M.A. and T.W. Johnston, 1967. Laboratory simulation of a satellite-mounted plasma diagnostic experiment. *J. Geophys. Res.*, 72, 4028.

Kavadas, A. and D.S. Campbell, 1968. Attitude determination of rocket-released probes from polarization measurements. *Can. J. Phys.*, 46, 2347.

Kavadas, A. and J.A. Koehler, 1969. A stabilized rocket-released magnetometer. *Can. J. Phys.*, 47, 1517.

Koehler, J.A. and A. Kavadas, 1969. A rocket-released magnetometer probe for upper atmospheric measurements. *Can. J. Phys.*, 47, 1529.

Murphy, C.H. and G.V. Bull, 1966. A review of project HARP. *Annals of the New York Academy of Sciences*, 140, Art. 1, 337.

Nicholls, R.W., 1969. Aeronomically important transition probability data. *Can. J. Chem.* 47, 1847.

——1968. Franck-condon factors for ionizing transitions of O_2, CO, NO, H_2 and the NO^+ (A–X) band system. *J. Phys. B.*, 1, 1192.

Osborne, F.J.F. and M.A. Kasha, 1967. The VXB interaction of a satellite with its environment. *Can. J. Phys.*, 45, 263.

Osborne, F.J.F., F.H.C. Smith, R.E. Barrington and W.E. Mather, 1967. Plasma induced interference in satellite V.L.F. receivers. *Can. J. Phys.*, 45, 47.

Seshadri, S.R. and K.L. Bhatnagar, 1967. Effect of ion sheath on radiation in a magnetoionic medium. II. Source current perpendicular to the magnetostatic field. *Can. J. Phys.*, 45, 279.

Shepherd, G.G. and L. Paffrath, 1967. A moire fringe method of Fabry-Perot spectrometer scanning. *Applied Optics*, 6, 1659.

Shkarofsky, I.P., 1968. Nonlinear mixing of waves in a plasma with velocity-dependent collisions. *Plasma Physics*, 10, 169.

——1968. Higher order cyclotron harmonic resonances and their observation in the laboratory and in the ionosphere. *J. Geophys. Res.*, 73, 4859.

——1968. Dipole and quadrupole bremsstrahlung and the damping of electron plasma oscillations for any degree of ionization. *Phys. Fluids*, 11, 2454.

——1969. Upper hybrid resonances detected by satellites. Plasma Waves in Space and Laboratory, J.O. Thomas and B.J. Landmark, editors, Vol. 2, pp. 105-110, *Edinburgh Univ. Press.*

——1969. Detection of upper hybrid resonance by satellites. Plasma Waves in Space and Laboratory, J.O. Thomas and B.J. Landmark, editors, Vol. 2, pp. 159-167, *Edinburgh Univ. Press.*

Sicha, M. and M.G. Drouet, 1968. Study of moving striations in plasmas. III. The fast type "r" and the determination of the ionization frequency dependance on the electron beam energy. *Can. J. Phys.*, 46, 2491.

Smith, F.H.C. and T.W. Johnston, 1966. Dielectric resonance probes and double probes compared. *J. Appl. Phys.*, 37, 4997.

Snelling, D.R. and E.J. Bair, 1968. Deactivation of O(^{1}D) by molecular oxygen. *J. Chem. Phys.*, 48, 5737.

Whitlow, S.H. and F.D. Findlay, 1967. Single and double electronic transitions in molecular oxygen. *Can. J. of Chemistry*, 45, 2087.

Young, R.A., 1967. The possibility of deducing a value for $[NO^+]^2/[NO]$ from measurements of atomic nitrogen in the upper atmosphere. *J. Geophys. Res.*, 72, 420.

——1969. Chemiluminescent reaction in the airglow. *Can. J. Chem.*, 47, 1927.

Young, R.A. and G. Black, 1967. Deactivation of O(^{1}D). *J. Chem. Phys.*, 47, 2311.

Young, R.A., G. Black and T.G. Slanger, 1968. 4000-8000A emission from far ultraviolet photolysis of N_2O, NO, CO, CO_2. *J. Chem. Phys.*, 48, 2067.

Young, R.A. and G.A. St. John, 1968. Experiments on $N_2(A^3\Sigma u^+)$. I. Reactions with N. *J. Chem. Phys.*, 48, 895.

——1968. Experiments on $N_2(A^3\ \Sigma u^+)$. II. Excitation of NO. *J. Chem. Phys.*, 48, 898.

——1968. Experiments on $N_2(A^3\ \Sigma u^+)$. III. Excitation of Hg. *J. Chem. Phys.*, 48, 2572.

7. Magnetospheric disturbances

Bonnevier, B., R. Boström, and G. Rostoker, 1970. A three-dimensional model current system for polar magnetic substorms. *J. Geophys. Res.*, 75, 107.

Boyd, G.M. and H.J. Duffus, 1968. The association between ULF geomagnetic fluctuations and Doppler ionospheric observations. *J. Atmos. Terr. Phys.*, 30, 481.

Camidge, F.P. and G. Rostoker, 1970. Magnetic field perturbations in the magnetotail associated with polar magnetic substorms. *Can. J. Phys.*, 48, 2002.

Gupta, J.C., R.J. Stening and G. Jansen van Beek, 1971. Micropulsations in the Pc3 to Pc4 period range at four Canadian observatories. *J. Geophys. Res.*, 76, 933.

Harvey, R.W., 1969. Evidence of electrostatic proton cyclotron harmonic waves from Alouette 2 satellite data. *J. Geophys. Res.*, 74, 3969.

Higuchi, Y. and J.A. Jacobs, 1970. Plasma densities in the thermal magnetosphere using hydromagnetic whistlers. *J. Geophys. Res.*, 75, 7105.

Horita, R.E. and T. Watanabe, 1968. Electrostatic waves in the ionosphere excited around the lower hybrid resonance frequency. *Planet. Space Sci.*, 17, 61.

——1969. Some remarks on the origin of lower hybrid resonance noise in the ionosphere. *Space Research IX*, 309.

Hruska, A., 1968. Interaction of plasma waves and particles in the non-uniform magnetosphere and acceleration of auroral particles. *Planet. Space Sci.*, 16, 1297.

——1968. The magnetodynamic toroidal waves. *Planet. Space Sci.*, 16, 1305.

——1969. On the interpretation of some observed features of geomagnetic pulsations. *Planet. Space Sci.*, 17, 1937.

——1969. Two-dimensional model of the neutral sheet in the earth's magnetotail. *Planet. Space Sci.*, 17, 665.

——1970. An idealized problem illustrating the effect of the ionosphere on toroidal waves. *Planet. Space Sci.*, 18, 315.

Hruska, A. and J. Hruskova, 1969. Long time scale magnetodynamic noise in the geomagnetic tail. *Planet. Space Sci.*, 17, 1497.

Hruska, A. and J. Hruskova, 1970. Transverse structure of the Earth's magnetotail and fluctuations of the tail magnetic field. *J. Geophys. Res.*, 75, 2449.

Hruska, A., J. Hruskova and J.A. Jacobs, 1970. Dependence of geomagnetic activity on the polarity of the interplanetary magnetic field. *Can. J. Phys.*, 48, 2447.

Jacobs, J.A., 1968. Pi events with particular reference to conjugate point phenomena. *Radio Science*, 3, 539.

——1970. Geomagnetic micropulsations. Vol. 1, Physics and Chemistry in Space, Springer-Verlag, p. 179.

Jacobs, J.A. and G. Atkinson, 1967. Planetary modulation of geomagnetic activity. In Magnetism and the Cosmos (ed. W.R. Hindmarsh et al.) Oliver and Boyd, p. 402.

Jacobs, J.A. and Y. Higuchi, 1969. Cyclotron amplification of geomagnetic micropulsations for pc 1 in the magnetosphere. *Planet. Space Sci.*, 17, 2009.

Jacobs, J.A. and T. Watanabe, 1967. Theoretical notes on whistlers and periodic emissions in the hydromagnetic regime. *Planet. Space Sci.*, 15, 799.

——1968. Conjugate points phenomena, associated with energetic particles, magnetic observations. *Ann. Geophys.*, 24, 467.

Jacobs, J.A. and C.S. Wright, 1968. The 27-day period of geomagnetic activity in the auroral zones and the inactive intervals during magnetically quiet days. *Earth Planet. Sci. Letters*, 3, 394.

——1968. Some features of geomagnetic micropulsations observed during the recent quiet solar years, with particular reference to data obtained at the near conjugate stations of Great Whale River and Byrd. *Geophys. J.*, 15, 53.

Jelly, D., 1970. Substorm aspects of auroral absorption and other effects of the upper part of the auroral particle spectrum. *Proc. ESRO Coll.* on Substorm Events, 1970.

Kitamura, T. and J.A. Jacobs, 1968. Ray paths of Pc 1 waves in the magnetosphere. *Planet. Space Sci.*, 16, 863.

——1968. Determination of the magnetosphere plasma density by the use of long period geomagnetic micropulsations. *J. Geomag. Geoelect.*, 20, 33.

Kitamura, T., J.A. Jacobs, T. Watanabe and R.B. Flint, 1968. An investigation of quasi-periodic VLF emissions and their relation to geomagnetic micropulsations. *Nature*, 220, 360.

——1969. An investigation of quasi-periodic VLF emissions. *J. Geophys. Res.*, 74, 5652.

Krishan, S. and A.A. Selim, 1968. Generation of transverse waves by non-linear wave-wave interaction. *Plasma Physics*, 10, 931.

——1968. Interaction between longitudinal and transverse plasma waves. *Can. J. Phys.*, 46, 39.

Rankin, D. and R. Kurtz, 1970. A statistical study of micropulsation polarization. *J. Geophys. Res.*, 75, 5444.

Rankin, D. and I.I. Reddy, 1968. Polarization of micropulsation sources. *Earth Planet. Sci. Letters*, 3, 347.

Rostoker, G., 1967. The polarization characteristics of Pi 2 micropulsations and their relation to the determination of possible source mechanisms for the production of nighttime impulsive micropulsation activity. *Can. J. Phys.*, 45, 1319.

——1967. The frequency spectrum of Pi 2 micropulsation activity and its relationship to planetary magnetic activity. *J. Geophys. Res.*, 72, 2032.

—1967. A determining factor in the form of the equivalent current system for geomagnetic bays. *Earth Planet. Sci. Letters*, 2, 119.

—1968. A critical study of the possible modes of propagation of Pi 2 micropulsation activity over the earth's surface. *Ann. Geophys.*, 24, 253.

—1969. Classification of polar magnetic disturbances. *J. Geophys. Res.*, 74, 5161.

Rostoker, G., C.W. Anderson, III, D.W. Oldenburg, P.A. Camfield, D.I. Gough and H. Porath, 1970. Development of a polar magnetic substorm current system. *J. Geophys. Res.*, 75, 6318.

Watanabe, T. and J.A. Jacobs, 1968. Conjugate points phenomena associated with energetic particles, magnetic observations. *Ann. Geophys.*, 24, 467.

8. Meteors

Folinsbee, R.E., L.A. Bayrock, G.L. Cumming and W.G.W. Smith, 1969. Vilna meteorite – camera, visual, seismic and analytic records. *J. Roy. Astron. Soc. Can.*, 63, 61.

Gault, W.A., 1970. Decay of the OI λ5577 line in meteor wakes. *Can. J. Phys.*, 48, 1017.

Gorjup, M. and I.I. Glass, 1967. Laboratory calibration of a micrometeoroid impact gauge. *CASI* Journal 13, No. 5, May.

Griffin, A.A., 1968. The fireball of April 25, 1966. II, photographic observations and orbit determination. *J.Roy. Astron. Soc. Can.*, 62, 55.

Halliday, I., 1966. The bolide of September 17, 1966. *J. Roy. Astron. Soc. Can.*, 60, 257.

—1968. The influence of exposure duration and trail orientation on photographic meteor spectra. Physics and Dynamics of Meteors, edited by L. Kresak and P. M. Millman, D. Reidel Pub. Co., Dordrecht-Holland, 91.

—1969. A study of ultraviolet meteor spectra. *Pub. Dom. Obs.*, 25, 315.

Jones, J., 1968. The mass distributions of meteoroids and asteroids. *Can. J. Phys.*, 46, 1101.

—1968. On the apparent mass distribution of underdense radio meteors. *Can. J. Phys.*, 46, 2669.

—1969. Measurement of radio-meteor ionization profiles. *Can. J. Phys.*, 47, 1467.

—1969. The reflection of radio waves from irregularly ionized meteor trains. *Planet. Space Sci.*, 17, 1519.

—1970. On the variation of the ambipolar diffusion coefficient with height. *Planet. Space Sci.*, 18, 1836.

Jones, J. and J.G. Collins, 1970. On the mass distribution of faint sporadic meteors. *Can. J. Phys.*, 48, 2584.

Maynard, L.A., 1968. Meteor burst communications in the Arctic. Ionospheric radio communications. K. Folkestad (ed.), *Plenum Press*, New York, p. 165.

McIntosh, B.A., 1966. The determination of meteor mass distribution from radar echo counts. *Can. J. Phys.*, 44, 2729.

—1967. Path of the fireball of June 14, 1967. *J. Roy. Astron. Soc. Can.*, 61, 191.

—1967. Further data concerning the 1963 anomalous increase in radar meteor rates. *Smithsonian Contr. Ap.*, 11, 201.

—1967. Radar echo duration as a function of meteoroid mass. *Can. J. Phys.*, 45, 3419.

—1968. Meteor mass distribution from radar observations. Physics and Dynamics of Meteors, edited by L. Kresak and P.M. Millman. D. Reidel Pub. Co., Dordrecht-Holland, p. 343.

—1969. The effects of wind shear on the decay constant of meteor echoes. *Can. J. Phys.*, 47, 1337.

—1970. On the end-point height of fireballs. *J. Roy. Astron. Soc. Can.*, 64, 267.

McIntosh, B.A. and J.A.V. Douglas, 1967. The fireball of April 25, 1966, I, Canadian visual observations. *J. Roy. Astron. Soc. Can.*, 61, 159.

McIntosh, B.A. and P.M. Millman, 1970. The Leonids by radar. *Meteoritics*, 5, 1.

McIntosh, B.A. and M. Simek, 1969. Mass distribution of meteoroids as determined by radar observations of underdense meteor trails. *Can. J. Phys.*, 47, 7.

Millman, P.M., 1966. Meteor news, 1966. *J. Roy. Astron. Soc. Can.*, 60, 151, 242.

—1967. Meteor news, 1967. *J. Roy. Astron. Soc. Can.*, 61, 89, 151.

—1967. Some characteristics of the major meteor showers. *Smithsonian Contr. Ap.*, 11, 105.

—1967. Radar meteor echoes. *Smithsonian Contr. Ap.*, 11, 151.

—1967. Observational evidence of the meteoritic complex. The Zodiacal Light and the Interplanetary Medium, edited by J.L. Weinberg, *NASA* SP-150, Washington, D.C., 399-407.

—1968. Meteor news, 1968. *J. Roy. Astron. Soc. Can.*, 62, 387.

—1968. The radar meteor echo. Physics and Dynamics of Meteors, edited by L. Kresak and P.M. Millman, D. Reidel Pub. Co., Dordrecht-Holland, 3-13.

—1968. A brief survey of upper-air spectra. Physics and Dynamics of Meteors, edited by L. Kresak and P.M. Millman, D. Reidel Pub. Co., Dordrecht-Holland, 84-90.

—1969. Astronomical information on meteorite orbits. Meteorite Research, edited by P.M. Millman, D. Reidel Pub. Co., Dordrecht-Holland, 541-551.

—1970. Meteor news, 1970. *J. Roy. Astron. Soc. Can.*, 64, 55, 114, 187, 251, 371.

—1970. Meteor showers and interplanetary dust. *Space Research*, 10, 260.

Millman, P.M. and D.W.R. McKinley, 1967. Stars fall over Canada. *J. Roy. Astron. Soc. Can.*, 61, 277.

Neale, M.J., 1967. An instrument to aid visual meteor observation. *J. Roy. Astron. Soc. Can.*, 61, 353.

Park, F.R. and B.A. McIntosh, 1967. A bright fireball observed photographically, by radar and visually. *J. Roy. Astron. Soc. Can.*, 61, 25.

Simek, M., 1968. The influence of ambipolar diffusion on the shape of radio echoes from meteors. *Can. J. Phys.*, 46, 1563.

Simek, M. and B.A. McIntosh, 1968. Meteor mass distribution from underdense trail echoes. Physics and Dynamics of Meteors, edited by L. Kresak and P.M. Millman, D. Reidel Pub. Co., Dordrecht-Holland, 362-372.

Stohl, J., 1968. Seasonal variation in the radiant distribution of meteors. Physica and Dynamics of Meteors, edited by L. Kresak and P.M. Millman, D. Reidel Pub. Co., Dordrecht-Holland, 298-303.

9. Sun–Earth relations and magnetospheric physics

Balasubrahmanyan, V.K. and D. Venkatesan, 1970. Solar activity and the great red spot of Jupiter. *Astrophysical Letters*, 6, 123.

Burrows, J.R. and I.B. McDiarmid, 1968. Local time asymmetries near the high latitude boundary of the outer radiation zone. Earth's Particles and Fields, *Proc. of the NATO Adv. Study Instit.* held at Freising, Germany, July 31 – August 11, 1967. Reinhold Book Corp.

Burrows, J.R., I.B. McDiarmid and M.D. Wilson, 1969. On the high-latitude limit of closed geomagnetic field lines. *Proc. IEEE*, 57, 1051.

Carmichael, H., 1968. Disturbances in the interplanetary magnetic field. ICSU Inter-Union Commission on Solar-Terrestrial Physics, STP Notes, No. 1, 55.

Carpenter, D.L., F. Walter, R.E. Barrington and D.J. McEwen, 1968. Alouette 1 and 2 observations of abrupt changes in whistler rate and of VLF noise variations in the plasmapause. A satellite-ground study. *J. Geophys. Res.*, 73, 2929.

Catchpoole, J.R., 1969. Superimposed electric fields and the magnetic moment of spiralling particles. *J. Atmos. Terr. Phys.*, 31, 615.

—1969. Electric field modification of precipitation spectra. *Australian J. of Phys.*, 22, 733.

—1969. Shell splitting modification by superimposed electric fields. *J. of Geomagnetism and Geoelectricity*, 21, 615.

—1969. Effects of a longitudinal electric field on particle motion in an asymmetrical magnetosphere. *J. of Geomagnetism and Geoelectricity*, 21, 723.

—1970. Longitudinal and transverse electric field effects in magnetospheric precipitation. *Australian J. of Phys.*, 23, 155.

Clark, T.A. and C.D. Anger, 1967. Morphology and electron precipitation during auroral substorms. *Planet. Space Sci.*, 15, 1287.

Fritz, T.A., 1970. Study of the high-latitude outer-zone boundary region for $\geq$40 kev electrons with satellite Injun 3. *J. Geophys. Res.*, 75, 5387.

Hartz, T.R., 1969. Type III solar radio noise bursts at hectometer wavelengths. *Planet. Space Sci.*, 17, 267.

Jelly, D.H. and N. Brice, 1967. Changes in Van Allen radiation associated with polar substorms. *J. Geophys. Res.*, 72, 5919.

McDiarmid, I.B. and J.R. Burrows, 1967. Dependence on the position of the outer radiation zone intensity maxima on electron energy and magnetic activity. *Can. J. Phys.*, 45, 2873.

——1968. Local time asymmetries in the high-latitude boundary of the outer radiation zone for the different electron energies. *Can. J. Phys.*, 46, 49.

——1969. Relation of solar proton latitude profiles to outer radiation zone electron measurements. *J. Geophys. Res.*, 74, 6239.

——1970. Latitude profiles of low-energy solar electrons. *J. Geophys. Res.*, 75, 3910.

McDiarmid, I.B., J.R. Burrows and M.D. Wilson, 1969. Morphology of outer radiation zone electron ($E > 35$ keV) acceleration mechanisms. *J. Geophys. Res.*, 74, 1749.

——1969. Dawn-dusk asymmetries in the outer radiation zone at magnetically quiet times. *J. Geophys. Res.*, 74, 3554.

McDiarmid, I.B. and M.D. Wilson, 1968. Dependence of the high latitude electron ($E > 35$ keV) boundary of the orientation of the geomagnetic axis. *J. Geophys. Res.*, 73, 3237.

Paghis, I., 1966. The Earth's outermost atmosphere. *RASC Jour.*, 60, 261.

Paulson, K.V., 1968. The polarization and spectral characteristics of some high-latitude irregular geomagnetic micropulsations. *Annales de Géophysique*, 24, 1.

Paulson, K.V., G.G. Shepherd and P. Graystone, 1967. A note on "Auroral-type" fluctuations in the earth's electromagnetic field. *Can. J. Phys.*, 45, 2813.

Rostoker, G., 1968. Macrostructure of geomagnetic bays. *J. Geophys. Res.*, 73, 4217.

——1968. Relationship between the onset of a geomagnetic bay and the configuration of the interplanetary magnetic field. *J. Geophys. Res.*, 73, 4382.

Sreenivasan, S.R., 1970. Amplification of magnetic fields, Int. Symposium on Solar Magnetic Fields, Paris, France, Aug. 1970. *Proc. IAU Symposium*, No. 43.

——1970. Force free fields and Beltrami flow in astrophysics. *J. Roy. Astron. Soc. (Canada)*, 64, 179.